

The Society of Fire Protection Engineers Series

Kevin LaMalva  
Danny Hopkin *Editors*

# International Handbook of Structural Fire Engineering



# **The Society of Fire Protection Engineers Series**

## **Series Editor**

Chris Jelenewicz, Society of Fire Protection Engineers, Gaithersburg, MD, USA

The Society of Fire Protection Engineers Series provides rapid dissemination of the most recent and advanced work in fire protection engineering, fire science, and the social/human dimensions of fire.

The Series publishes outstanding, high-level research monographs, professional volumes, contributed collections, and textbooks.

More information about this series at <http://www.springer.com/series/16784>

Kevin LaMalva • Danny Hopkin  
Editors

# International Handbook of Structural Fire Engineering

 Springer

**SFPE**  
  
*Engineering A Fire Safe World*

*Editors*

Kevin LaMalva  
U.S. Consultancy  
Warringtonfire  
Boston, MA, USA

Danny Hopkin  
U.K. Consultancy  
OFR Consultants  
Manchester, UK

ISSN 2731-3638

ISSN 2731-3646 (electronic)

The Society of Fire Protection Engineers Series

ISBN 978-3-030-77122-5

ISBN 978-3-030-77123-2 (eBook)

<https://doi.org/10.1007/978-3-030-77123-2>

© Springer Nature Switzerland AG 2021

This work is subject to copyright. All rights are reserved by the Publisher, whether the whole or part of the material is concerned, specifically the rights of translation, reprinting, reuse of illustrations, recitation, broadcasting, reproduction on microfilms or in any other physical way, and transmission or information storage and retrieval, electronic adaptation, computer software, or by similar or dissimilar methodology now known or hereafter developed.

The use of general descriptive names, registered names, trademarks, service marks, etc. in this publication does not imply, even in the absence of a specific statement, that such names are exempt from the relevant protective laws and regulations and therefore free for general use.

The publisher, the authors, and the editors are safe to assume that the advice and information in this book are believed to be true and accurate at the date of publication. Neither the publisher nor the authors or the editors give a warranty, expressed or implied, with respect to the material contained herein or for any errors or omissions that may have been made. The publisher remains neutral with regard to jurisdictional claims in published maps and institutional affiliations.

This Springer imprint is published by the registered company Springer Nature Switzerland AG  
The registered company address is: Gewerbestrasse 11, 6330 Cham, Switzerland

# Contents

<b>1</b>	<b>Foreword and Introduction</b> . . . . .	<b>1</b>
	Danny Hopkin and Kevin LaMalva	
<b>2</b>	<b>The Fire-Resistive Principle</b> . . . . .	<b>9</b>
	Kevin LaMalva, John Gales, Anthony Abu, and Luke Bisby	
<b>3</b>	<b>Keys to Successful Design</b> . . . . .	<b>45</b>
	Martin Feeney, Kevin LaMalva, and Spencer Quiel	
<b>4</b>	<b>Design Fires and Actions</b> . . . . .	<b>75</b>
	Danny Hopkin, Ruben Van Coile, Charlie Hopkin, Kevin LaMalva, Michael Spearpoint, and Colleen Wade	
<b>5</b>	<b>Heat Transfer to Structural Elements</b> . . . . .	<b>115</b>
	Kevin LaMalva, Cristian Maluk, Ann Jeffers, and Allan Jowsey	
<b>6</b>	<b>Concrete Structures</b> . . . . .	<b>145</b>
	Thomas Gernay, Venkatesh Kodur, Mohannad Z. Naser, Reza Imani, and Luke Bisby	
<b>7</b>	<b>Steel and Composite Structures</b> . . . . .	<b>189</b>
	Anthony Abu, Ruoxi Shi, Mostafa Jafarian, Kevin LaMalva, and Danny Hopkin	
<b>8</b>	<b>Timber Structures</b> . . . . .	<b>235</b>
	Daniel Brandon, Danny Hopkin, Richard Emberley, and Colleen Wade	
<b>9</b>	<b>Uncertainty in Structural Fire Design</b> . . . . .	<b>323</b>
	Ruben Van Coile, Negar Elhami Khorasani, David Lange, and Danny Hopkin	

**10 Advanced Analysis** ..... 413  
Thomas Gernay and Panos Kotsovinos

**11 Reinstatement of Fire-Damaged Structures** ..... 469  
Tom Lennon and Octavian Lalu

**Index** ..... 517

# About the Editor

**Kevin LaMalva** has 14 years of experience as a fire/structural consultant with dual registration in both fire protection engineering and civil engineering. Aside from faithfully serving clients, Kevin is a member of numerous industry committees (ASCE/SEI, SFPE, ICC, NIST, NFPA, and others) that conduct research and develop standards for structural fire safety. Notably, Kevin led a group of over 50 engineers to develop a first-of-its-kind ASCE/SEI Exemplar Design Guide for structural fire engineering. For his efforts in advancing structural fire safety, Kevin was awarded the distinction of ENR Newsmaker for serving the “best interests of the construction industry and the public.”

**Danny Hopkin** is a chartered engineer, fellow of the Institution of Fire Engineers (IFE), fellow of the Institution of Mechanical Engineers (IMechE), and professional member of the Society of Fire Protection Engineers (SFPE). He studied structural engineering before completing a doctorate in structural fire safety. Danny is the Technical Director of OFR Consultants in the UK and a Visiting Professor in structural fire safety at the University of Sheffield. He has delivered specialist structural fire input on high profile projects, including the Google HQ in London. He has also undertaken research in the fields of performance-based structural fire design, reliability, and mass/engineered timber structures. Danny was the chairman of the committees overseeing the revision of PD 7974-1 and PD 7974-3, while contributing to PD 7974-7 and the ongoing revision of Eurocode 5, part 1.2.



# Chapter 1

## Foreword and Introduction



Danny Hopkin and Kevin LaMalva

### 1.1 The Handbook and Target Audience

This handbook is intended to provide the readers with an understanding of structural performance in the event of fire. It has been written to mirror the anticipated workflow of a structural (fire) engineering consultancy by encouraging consideration of project goals, likely fires that might develop, manifestation and estimation of thermal boundary conditions and structural element temperatures, and material and element response to heating. Separate chapters are provided in support of specific considerations, namely for those interested in reliability-based analysis of structures in the event of fire, advanced calculation methods for fire-exposed structures, and inspection/reinstatement of fire-damaged structures. The handbook has called upon the input of global experts to deliver a resource that brings together a significant volume of material on the topic of structural performance in the event of fire. The book is primarily written for practicing consulting engineers. However, it is foreseen that it can be a useful resource for students of structural engineering who wish to develop a deeper understanding of structural performance in the event of fire, as well as building authorities to assist with review of such alternative designs.

The coverage of fire science and fire safety engineering in this handbook is limited, with readers encouraged to review alternative established texts in this space, such as the SFPE Handbook [1] and Drysdale [2].

---

D. Hopkin  
OFR Consultants, Manchester, UK  
e-mail: [danny.hopkin@ofrconsultants.com](mailto:danny.hopkin@ofrconsultants.com)

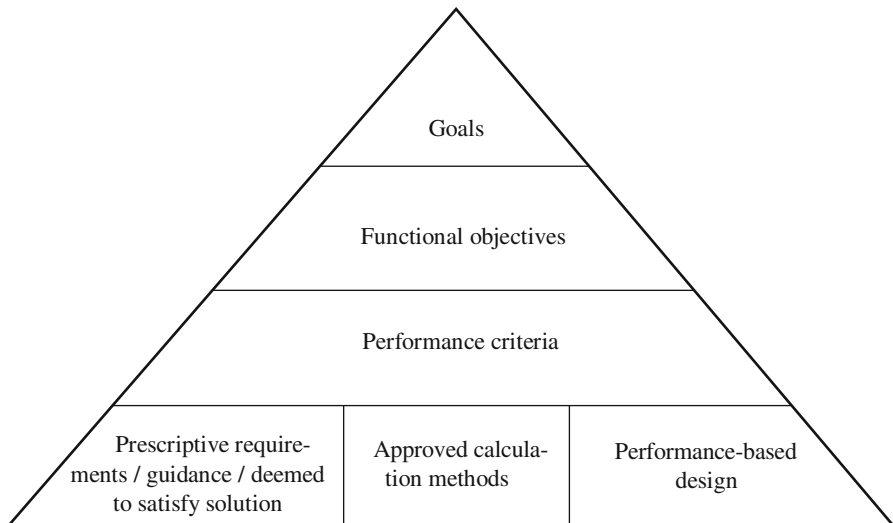
K. LaMalva (✉)  
Warringtonfire, Boston, MA, USA  
e-mail: [kevin.lamalva@warringtonfire.com](mailto:kevin.lamalva@warringtonfire.com)

## 1.2 Introduction

Sweeping and highly destructive built environment fires are now infrequent. However, this was not always the case, with, for example, the United States suffering on average one conflagration per annum in the nineteenth century [3]. To the layman, this change in fortunes is likely attributed to improvements in firefighting and fire prevention. Whilst being important factors, these have not been the sole considerations in a downturn in both sweeping and destructive building fires. The nature of the building stock and their design has played a part since the emergence of so-called fireproof materials and practices [3] which has served to both reduce damage and mitigate fire spread.

In the built environment as we experience today, building codes and regulations around the world typically impose minimum construction requirements intended to provide satisfactory structural performance in the event of fire, under a life safety purview. Even those cases, e.g., single-family dwellings, where the fire-induced structural failure consequences are limited, there may be an expectation of some structural robustness in the event of fire. The common vocabulary in this regard has centered on structural fire resistance which, on the one hand, could be said to have broad meaning, i.e., “the power not to be affected by something” (in this case, fire) (Oxford [4]), but on the other has grown to have a specific definition, as given in numerous testing codes and standards, e.g., EN 13501-2 [5]. The emergence of the fire-resistive principle is covered in greater detail in Chap. 2.

The form of these regulatory obligations enacted through codes and regulations varies between jurisdictions, but in general terms can be conveyed as per Fig. 1.1, adapted from Buchanan and Abu [6]:



**Fig. 1.1** Possible hierarchy of traditional design approaches adapted from Buchanan and Abu [6]

In some cases, the design approach/solution is the free choice of the engineer; for example, in England the legal obligation for structural performance in the event of fire is expressed through Regulation B3(1) of Part B of Schedule 1 of the Building Regulations, which requires that [7]:

The building shall be designed and constructed so that, in the event of fire, its stability will be maintained for a reasonable period.

This statement would be considered a functional objective, under the goal of an adequate level of life safety. The satisfaction of this statement can take many forms, from affording individual structural elements' fire resistance ratings according to complementary regulatory guidance, e.g., Approved Document B [8, 9], through to a full performance-based assessment, as evidence presented by UK fire engineers in many case studies [10–12].

In other jurisdictions, the legal requirement may be the attainment of prescribed fire resistance ratings to load-bearing elements of construction; for example, a beam shall achieve 60-min fire resistance, as defined/classified in EN 13501-2. That is, no goal, functional objective, or performance criteria are defined; it is simply the case that a requirement must be followed.

Whilst there may not always be commonality in how design solutions for structural fire performance manifest between jurisdictions, i.e., some are more open to performance-based solutions than others, there is a universal need to use materials more effectively to combat a climate crisis. As Bisby [13] notes: “Given the enormous impact of structural engineering decisions on carbon emissions, it is clear that structural engineers have a moral obligation to urgently take action to address the climate emergency.” This will invariably mean that demands are placed on engineers to be more efficient in their choice of materials/solutions and to adopt new approaches and technologies, which can “bring with them new hazards” or “at least partially invalidate experience as a means of having confidence in our designs.”

Supporting the innovation necessary for a solution to a climate crisis has seen, and will likely see, a greater uptake in performance-based regulatory systems, where engineers are afforded greater freedom to demonstrate the adequate safety of their designs. Whilst giving opportunities to rationalize designs, as is often mooted as a benefit of structural fire safety consultancy, the invalidation/erosion of experience that is a by-product of innovation necessitates that adequate safety be demonstrated and not be assumed [14, 15]. This is where structural fire safety input can prove valuable more generally and as a key facet of a higher proportion of future structural designs as they become increasingly innovative and deviate from the established status quo.

### 1.3 Fire Resistance and the Status Quo

Within the construction community, “fire resistance” is conventionally defined in the context of the performance (in a furnace test) of an isolated construction element, relative to specific performance criteria (integrity, insulation, and load-bearing), under defined furnace heating, e.g., ISO 834 [16]. Performance (i.e., fire resistance) is typically measured in terms of time taken (in minutes) to breach any one or all the given performance criteria, depending on the nature of the construction element tested, when subject to the furnace time–temperature curve. The specific heating curve and performance criteria vary subtly between different countries and are defined in a variety of standards permitted for use in differing jurisdictions [17]. Building codes, regulations, or guidance will then advise/require that elements achieve a fire resistance time having due regard to the building’s height and use (and in some instances, form of construction).

Whilst fire resistance is the common language/metric for expressing some level of structural fire safety, the motivations for structures achieving a level of fire resistance can span multiple indeterminate objectives. For buildings where the fire-induced failure consequences are lesser, the functional objective of the structure may be to remain stable for long enough to facilitate means of escape and early fire brigade intervention. In cases where the fire-induced failure consequences are more significant, e.g., because both evacuation and fire service intervention are protracted, the functional objective may shift to that of the structure having sufficient likelihood of withstanding the full duration of a fire. This bifurcation of objectives is not always transparent when speaking in the common language of fire resistance, with the metric used as a proxy for delivering levels of structural fire safety that are deemed to satisfy, depending upon the failure consequences to a certain extent [18].

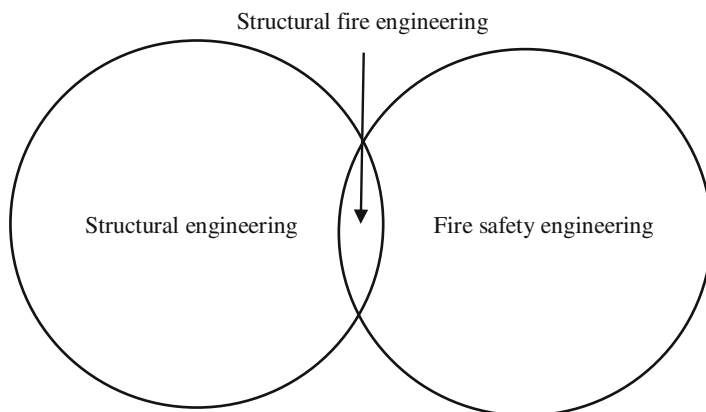
Once an appropriate fire resistance rating has been determined, having due regard to building height and use, structural elements which are largely designed without any cognizance of the impact of fire accidents are then retrospectively protected/insulated to conform to the required fire resistance rating. In the case of steel elements, passive fire protection is applied in the form of an insulation. For concrete, elements are sized with sufficient cover to reinforcement so as to mitigate substantial increases in temperature. For timber, sacrificial material is introduced to offset that consumed as structural elements combust. It is then presumed that a structural system formed of elements with defined fire resistance ratings achieves the objective, be that some adequate duration of stability or some adequate likelihood of surviving the fire. Many would argue that whilst evidence exists for this process leading to adequate performance levels, few if any could quantify the level of safety that is provided within this framework [13]. More likely, the actual level of structural fire safety is variable from building to building, subject to coincidental structural design decisions for other hazards (and then retrospectively protected/insulated).

## 1.4 Structural Design for Fire Safety

Structural design for fire safety is often mooted as a discipline that lies at the interface between structural engineering and fire safety engineering (Fig. 1.2), whilst others simply consider it as structural engineering, with fire an accidental load case. Irrespective of whether it is a discipline in its own right or a subset of another, the process and outcomes are the same. As defined by Buchanan and Abu [6], structural design for fire safety requires:

1. The definition of goals, objectives, and performance criteria.
2. The identification and description of design fires that could credibly occur.
3. The expression of these fires as a thermal boundary condition to structural elements.
4. The development of temperature within/through structural elements.
5. Characterization of material degradation and fire effects (e.g., restrained thermal expansion) as a result of high temperatures.
6. Evaluation of the structure considering material degradation and fire effects.

The design for fire workflow can be integrated into the general (ambient) structural design, allowing for the optimum design solution to be achievable by considering the demand placed on the structure under normal service conditions and the consequent relationship with fire performance/extent of subsequent passive fire protection required. In this context, potential sensitivities or failure modes that become apparent in the event of fire can be elucidated and adequately mitigated. For cases where the safety level requires estimation/quantification, quantitative risk-based methods have emerged which can be utilized to benchmark failure likelihoods against reliability-based safety targets.



**Fig. 1.2** Interface between structural engineering and fire safety engineering [6]

## 1.5 Handbook Structure

This handbook has been structured to mirror the workflow identified in Sect. 1.4, with chapters as follows:

**Chapter 2:** The Fire-Resistive Principle—K. LaMalva, J. Gales, A. Abu & L. Bisby.

**Chapter 3:** Keys to Successful Design—M. Feeney, K. LaMalva & S. Quiel.

**Chapter 4:** Design Fires and Actions—D. Hopkin, R. Van Coile, C. Hopkin, K. LaMalva, M. Spearpoint & C. Wade.

**Chapter 5:** Heat Transfer to Structural Elements—K. LaMalva, C. Maluk, A. Jeffers & A. Jowsey.

**Chapter 6:** Concrete Structures—T. Gernay, V. Kodur, M. Naser, R. Imani & L. Bisby.

**Chapter 7:** Steel and Composite Structures—A. Abu, R. Shi, M. Jafarian, K. LaMalva & D. Hopkin.

**Chapter 8:** Timber Structures—D. Brandon, D. Hopkin, R. Emberley & C. Wade.

**Chapter 9:** Uncertainty in Structural Fire Design—R. Van Coile, N. Elhami-Khorasani, D. Lange & D. Hopkin.

**Chapter 10:** Advanced Analysis—T. Gernay & P. Kotsovinos.

**Chapter 11:** Reinstatement of Fire-Damaged Structures—T. Lennon & O. Lalu.

## References

1. Hurley, M., Gottuk, D., Hall, J., Harada, K., Kuligowski, E., Puchovsky, M., Torero, J., Watts, J., Jr., & Wieczorek, C. (Eds.). (2016). *SFPE handbook of fire protection engineering* (5th ed.). Springer.
2. Drysdale, D. (2011). *An introduction to fire dynamics* (3rd ed.). Wiley. <https://doi.org/10.1002/9781119975465.ch1>
3. Wermiel, S. E. (2000). *The fireproof building: Technology and public safety in the nineteenth-century American city, studies in industry and society*. Johns Hopkins University Press.
4. Oxford Dictionary. (2020). *Oxford Dictionary entry: Resistance*. Oxford Learner's Dictionaries.
5. BSI. (2008). BS EN 13501-2:2007+A1:2009 Fire classification of construction products and building elements. Classification using data from fire resistance tests, excluding ventilation services. BSI, London.
6. Buchanan, A. H., & Abu, A. (2017). *Structural design for fire safety* (2nd ed.). Wiley.
7. HM Government. (2010). *The building regulations 2010*. Ministry for Housing, Communities & Local Government.
8. Ministry of Housing, Communities and Local Government. (2020a). *Approved document B: Fire safety - volume 1*. RIBA Publishing.
9. Ministry of Housing, Communities and Local Government. (2020b). *Approved document B: Fire safety - volume 2*. RIBA Publishing.
10. Block, F., Yu, C., & Butterworth, N. (2010). The practical application of structural fire engineering on a retail development in the UK. *Journal of Structural Fire Engineering*, 1, 205–218. <https://doi.org/10.1260/2040-2317.1.4.205>

11. Hopkin, D., Anastasov, S., Illingworth, D., McColl, B., Loughlin, E. O., & Taylor, A. (2018). A structural fire strategy for an exposed weathering steel-framed building. *The Structural Engineer/The Journal of the Institution of Structural Engineers*, 96, 60–66.
12. Kotsovinos, P., Rackauskaite, E., & Deeny, S. (2020). The role of transfer beams on the global structural fire response of tall steel framed buildings. *Fire Safety Journal*, 103172. <https://doi.org/10.1016/j.firesaf.2020.103172>
13. Bisby, L. A. (2021). Structural fire safety when responding to the climate emergency. *The Structural Engineer/The Journal of the Institution of Structural Engineers*, Vol. 99, Issue 2, London, UK.
14. Hopkin, D., Van Coile, R., & David, L. (2017). Certain uncertainty-demonstrating safety in fire engineering design and the need for safety targets. *SFPE Europe, Issue 7*, Society of Fire Protection Engineers, Gaithersburg, MD, USA.
15. Van Coile, R., Hopkin, D., Lange, D., Jomaas, G., & Bisby, L. (2019). The need for hierarchies of acceptance criteria for probabilistic risk assessments in fire engineering. *Fire Technology*, 55, 1111–1146. <https://doi.org/10.1007/s10694-018-0746-7>
16. ISO. (1999). *ISO 834-1:1999 fire-resistance tests — Elements of building construction — Part 1: General requirements*. International Organization for Standardization.
17. Wilkinson, P., Hopkin, D., & McColl, B. (2019). *Chapter 12: Fire resistance, structural robustness in fire and fire spread*, in: *CIBSE guide E: Fire safety engineering*. The Lavenham Press Ltd.
18. Hopkin, D., Spearpoint, M., Gorksa, C., Krenn, H., Sleik, T., & Milner, M. (2020). Compliance road-map for the structural fire safety design of mass timber buildings in England. *SFPE Europe, Q4*, Society of Fire Protection Engineers, Gaithersburg, MD, USA.

# Chapter 2

## The Fire-Resistive Principle



Kevin LaMalva, John Gales, Anthony Abu, and Luke Bisby

### 2.1 Time Domain

Standard fire resistance design is based on the time domain. Standard fire testing serves as the basis of standard fire resistance design. Accordingly, fire resistance is defined as an hourly rating based on the results of standard fire testing.

Standard fire testing exhibits a mock-up fire-resistant assembly to a relatively intense fire exposure by means of furnace apparatus. This test method is predicated on the assumption that the test assembly is representative of actual field construction to a certain extent. However, the size limitation of furnaces restricts assembly sizes. For instance, floor assemblies are typically tested at spans no greater than 17 ft. (5.2 m), whereas an actual floor span may be much greater.

Each standard fire test uses the same temperature history that continually rises in temperature, to heat the test assembly with an established set of failure criteria [1]. Fire resistance directories provide a list of fire resistance-rated assemblies that

---

K. LaMalva (✉)  
Warringtonfire, Boston, MA, USA  
e-mail: [kevin.lamalva@warringtonfire.com](mailto:kevin.lamalva@warringtonfire.com)

J. Gales  
Department of Civil Engineering, York University, Toronto, Canada  
e-mail: [jgales@yorku.ca](mailto:jgales@yorku.ca)

A. Abu  
Civil & Natural Resources Engineering Department, University of Canterbury, Christchurch,  
New Zealand  
e-mail: [anthony.abu@canterbury.ac.nz](mailto:anthony.abu@canterbury.ac.nz)

L. Bisby  
Civil and Environmental Engineering Department, University of Edinburgh, Edinburgh,  
Scotland, UK  
e-mail: [Luke.Bisby@ed.ac.uk](mailto:Luke.Bisby@ed.ac.uk)



have been qualified in accordance with standard fire testing [2]. These listings describe the process or details of construction that are commensurate with mock-up assemblies that have been qualified through testing. Within this framework, evaluation of structural fire protection reduces to the selection of qualified assemblies from available listings to meet prescribed levels of fire resistance.

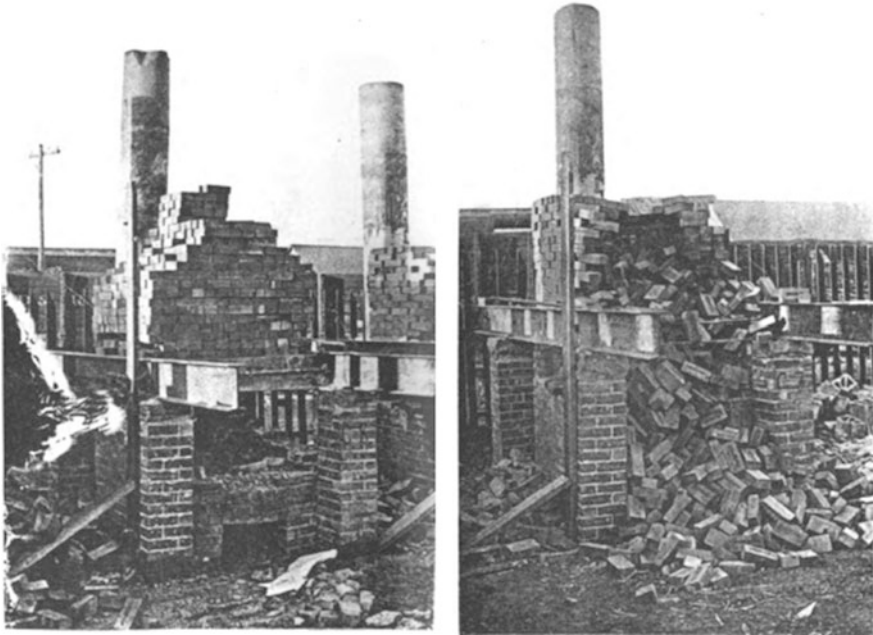
### ***2.1.1 Origins of Fire Resistance***

There exists a reference to the history of the subject of fire resistance evaluation [1]. Below is additional information that is meant to expand upon that resource. Digitization efforts in the last decade have made additional papers available in the public domain.

The origins of contemporary fire resistance began in the late nineteenth century in the aftermath of various city conflagrations, such as Chicago in 1872 and Boston in 1874. The outcome of these severe fires led to a surge in ad hoc fire tests of building elements. These tests primarily considered new reinforced concrete elements (beams and slabs). Between 1870 and 1890, the terminology called “fireproof” was adopted in practice. Fireproofing is strictly defined as incombustible construction [3]. These fireproof tests were qualitative in nature. Tests were often performed as a public demonstration of a building element constructed by a material manufacturer, supported on stilts, and burned using timber logs in random placement. They often were unloaded. Measurements (temperature and deflection) were often not recorded. Confidence in the building element was achieved by the nonappearance of “failure-collapse” with little science to validate manufacturer claims. Tests were published in newspapers as spectacles and there existed little scientific articling or reports that survive today.

In the 1890s, ad hoc testing was considered unacceptable through the eyes of architects when assigning competing assemblies for design that were claimed to be fireproof [4]. This led to the concept of fire resistance. From this point, testing considered quantitative performance—actual measurement and record keeping of the tests. Tests of building elements were compared using a more careful and rationalized test control method. Measurement of deformation of the building elements was made to define failure criteria—though collapse was often deemed being defined as failure.

One of the first “fire-designed” buildings using early principles of fire resistance was the Denver Equitable Building. The architects were faced with choosing three competing flooring (arch) systems made of terra-cotta, which were said to be fireproof [4]. The manufacturers of these competing flooring systems each argued that each of their products was superior. A demonstration-style test defined by the architectural firm Andrews, Jaques and Rantoul was organized for each flooring system. The test utilized the same target temperature of assault (gas temperatures of approximately 600 °C) and the flooring systems were ranked accordingly. Note that



**Fig. 2.1** Denver equitable building fire tests

these tests were extensively documented when performed in 1890 having a 17-photo set of loading and failure conditions; see Fig. 2.1.

In 1896 and 1897, two very different test series were organized by the New York Department of Buildings, led by researchers from the Mechanical and Mining Engineering Department at Columbia University. One test series utilized a controlled furnace for various building elements (led by Sylvanus Reed) [3], while the other utilized a testing procedure similar to the aforementioned Denver tests specifically for floors (led by Ira Woolson) [5].

The element testing by Reed established principles very similar to the ASTM standard fire that would follow in 1918 as well as some contemporary themes argued today for fire testing. Reed's tests relied on using a gas-fueled furnace to take advantage of the control of temperature. Reed documented various limitations for establishing test simplicity despite the broad objective of his test: "*steel or iron columns, girders, and beams, must be made on a full working scale and under the actual conditions, as far as possible, which would be obtained in a fire.*" Three different fire severities, based on occupancy type, were established as the metric for this series. The test parameters were defined accordingly by consultation from a committee. The objective was: "*To be a standard it must contemplate all fire possibilities, even the most remote, pertaining to those conditions . . . to establish a datum level from which allowable variations may be determined.*" The fire, he specified, would be run in a furnace as one of the three cases: (1) 1371 °C for 6 h—warehouses; (2) 648 °C for 1 h—commercial store; or (3) 371 °C for 30 min—office

building or house. All tests were under an applied service load. Temperatures were measured using a pyrometer. Reed justified that all buildings should be expected to resist a conflagration, as to quantify what expected damage state would occur. This was to inform the insurance industry. His tests were documented in the Journal of the Franklin Institute and are readily available to the interested reader [3].

At this time, engineers debated and attempted to influence the creation of these early tests. Abraham Himmelwright publically advocated that *“The object of all tests of building materials should be to determine facts and develop results that may be of practical value in future designing. In order that such facts and results may have real value, three conditions are necessary: first, that the materials tested shall be identical with what is commercially available in the open market; second, that the conditions, methods, and details of constructions conform exactly to those obtainable in practice; third, that the tests be conducted in a scientific manner.”* [6] He also stated that the design of structures had to resist thermal loading caused by fire: *“The actual and relative expansion of the materials due to heat and deflections caused by unequal heating must receive careful consideration . . . The limit of safety is in some cases dependent upon temperature and in other cases upon expansion.”*

Of note, both Reed and Woolson studied under Frederick Hutton of Columbia University. Hutton was an expert of furnace design [7]. While Woolson would start using wood-stocked furnaces, he would eventually advocate the use of a gas furnace by the inception of the standard fire test.

The tests performed by Reed were largely intended to be for informing the insurance industry and public. They were not meant as proprietary testing. Although this is not explicitly stated as the reason Reed’s tests ceased, the lack of funding may have contributed. It is interesting that Ira Woolson’s tests were more aligned to ranking proprietary systems where the material manufacturer often paid to test their systems. Ira Woolson’s tests would eventually form the basis of contemporary fire resistance as defined by qualification (standard) fire tests as per below.

Ira Woolson oversaw the second test series. His tests considered primarily flooring systems at first. The original test criterion called for a steady-state temperature of 1093 °C. The test temperature was defined in 1896 by the engineer Gus Henning, chief engineer of the New York Department of Buildings. Temperatures were reached by feeding a wood fire furnace which was beneath the loaded flooring assembly and the duration of heating was meant to be held for over 5 h (Fig. 2.2).

After Ira Woolson’s initial tests in 1896–1897, it was decided to specify a less severe fire exposure. The new test standard [8] called for a sustained “average” gas-phase temperature equivalent to 927 °C (1700 °F) for 4 h (with peaks still at 1093 °C (2000 °F)), hose stream cooling, and finally residual testing to higher loads (four times the sustained fire service load) for a further 24 h. If after this test the floor’s deflection did not exceed 1.4% of its span, the element was assumed to have “passed.” The test still used a wood-stocked furnace. The thermal scenario was intended to be more severe than a real fire. Woolson at the time advocated that *“no ordinary room would have enough inflammable material in it to maintain a 1700°F fire for more than 30 minutes.”* The basis for this heating regime was firefighters’ qualitative experience in New York. A complete catalogue of nearly 80 flooring

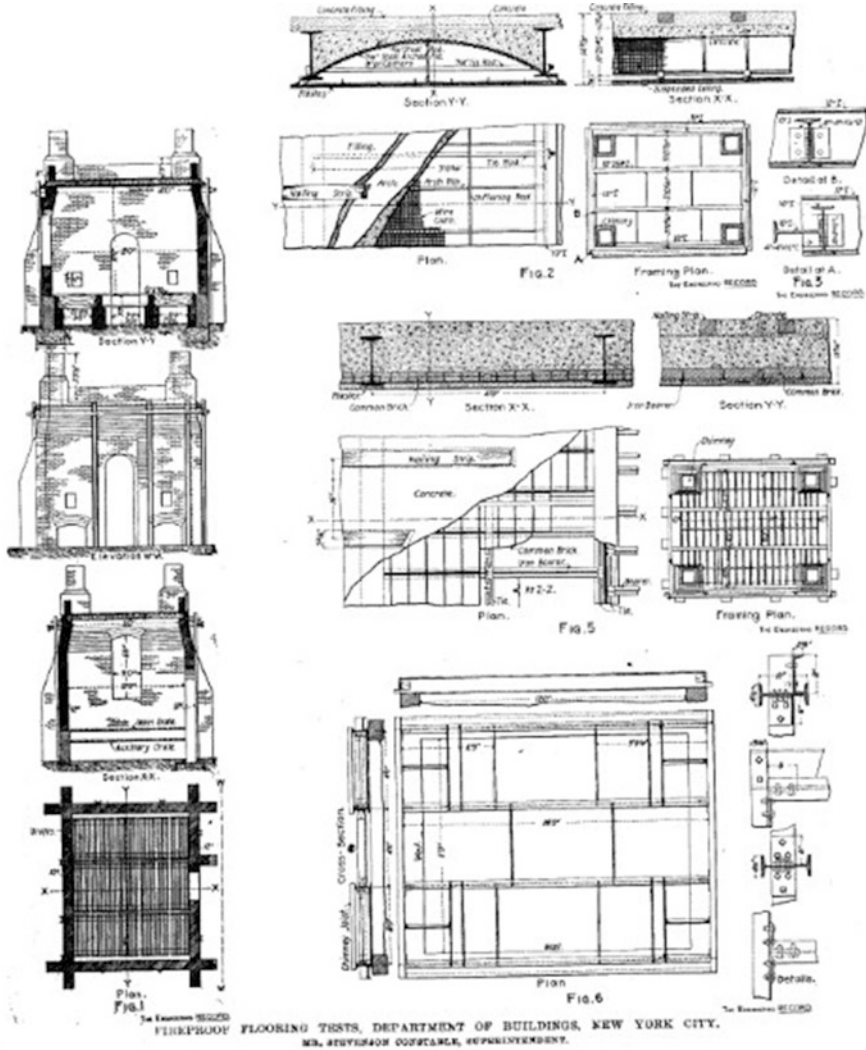


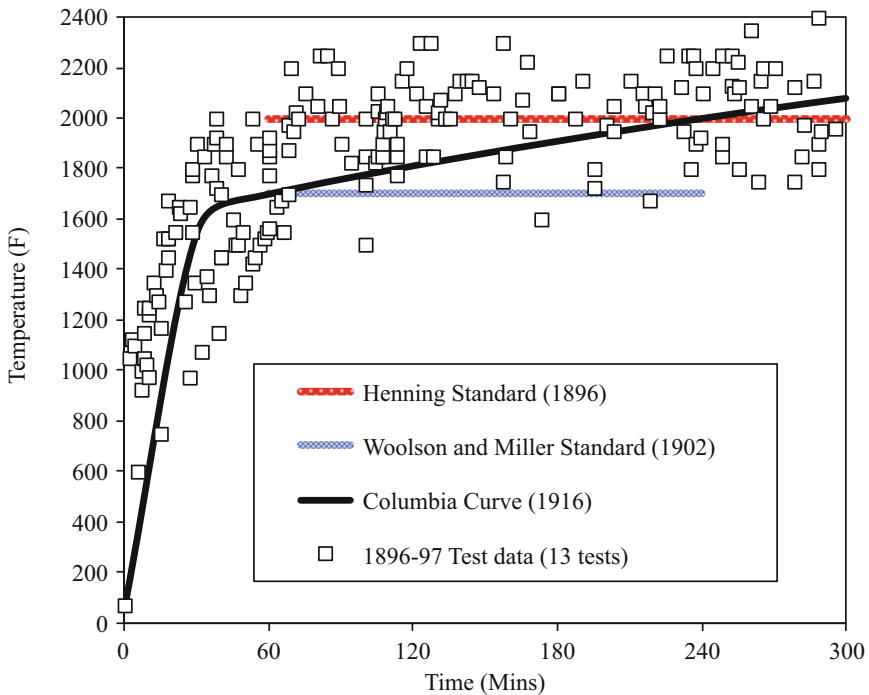
Fig. 2.2 1897 New York fire tests by the Department of Buildings [5]

systems was published by Woolson at the International Association for Testing Materials Conference in 1912 [9].

These early standard fire tests by Woolson were often criticized during this period of time [9–11]. Formerly the tests were not standardized at this time, and not widely adopted outside of New York. They were the subject of the Mazet Inquiry of 1899 which alleged corruption in the tests. These tests were followed by decreased influence of the city in the tests, and more control by research bodies to ensure their integrity. In response to the change in leadership of the test series, Gus Henning

in 1905 penned an open editorial in the New York Times where he publically criticized the current test procedure by Woolson: “*Other fakes I desire to call attention to are the fire tests now being made in New York City at temperatures of only 1,700 °F. I herewith wish to declare fire tests of materials made at average temperature of 1700°F as shams and frauds. They do in no sense of the word determine the fire proof qualities of materials.*” Henning’s reference to 1700 °F (927 °C—the 1-h mark used in the standard fire today) was in relation that real fires have more severity and that materials would behave differently under this severe heating. Following criticism towards the New York building structure fire test series, various construction material agencies lobbied for change [9]. This effort was mobilized by Ira Woolson at the American Society of Testing of Materials (ASTM). A new fire test standard evolved and was proposed in 1916. The intention was to shift away from floors and to consider columns.

There is no publically available documentation that explicitly defines the origins of the standard fire curve that was created in 1916 and actually still used today to assess fire resistance. Examination of data appears more of a compromise of the Henning 1897 and Woolson 1902 standard. Careful plotting of test data from the 1897 tests illustrates that the standard fire curve intercepts these points, as well as achieves a linear fit between 1 and 4 h of the Woolson curve adopted in 1902 and the Henning curve from 1897. This is plotted in Fig. 2.3 for the interested reader and requires continued research to definitively answer.

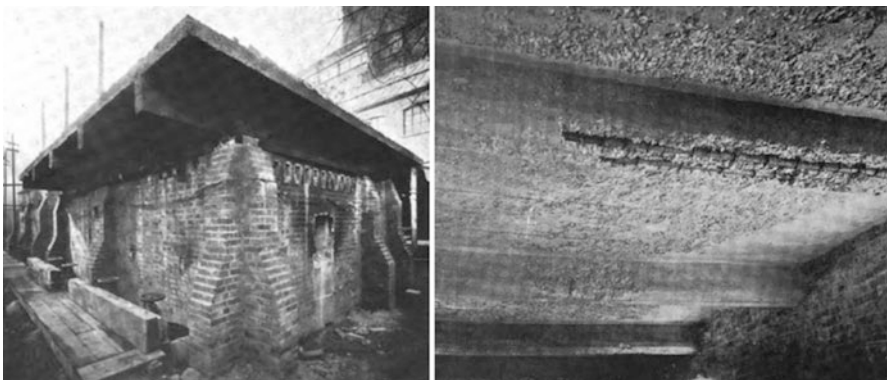


**Fig. 2.3** Evolution of fire time-temperature curves as adopted in the USA

The 1916 curve was used for the first time to test a series of timber, steel, and concrete columns. The criterion for the test was published by Simon Ingberg in the 1921 document: *Fire Tests of Building Columns* [12]. The test procedure used was very similar albeit with technological advances to the modern ASTM E119 fire test standard [1]. The tests in brevity considered using a controlled fire-time curve on loaded columns using gas-controlled furnaces. Gas furnaces could better control the time-temperature curve in linear fashions (except for timber which gave off its own heat). Even in the 1920s however, it was widely known that the standard fire was by no means indicative of a real fire. Ingberg reported that *“it is necessary to assume maximum probable conditions both with regard to building contents and air supply, as considered with respect to intensity and duration of a possible fire. Compensations and adjustments between intensity and duration may be necessary under some conditions in order to approximate a fire duration having intensity equivalent to that of the exposure of the fire test.”*

Efforts principally by Simon Ingberg [13] began to correlate a fire severity—using measurements from real burnout compartment tests—to the standard fire curve based on the “equal area concept.” Other researchers continued with the development of new concepts of equivalent fire severity based on other severity metrics (“maximum temperature concept,” “minimum load capacity concept,” and “time-equivalent formulae”). Buildings could then be reclassified, not only by fire activation risk, but also by functions of fuel load, and “equivalent” standard fire resistance times could then be specified for building elements.

Changes to the standard time-temperature curve were made through the years in various iterations of ASTM standards (though with increasingly less emphasis on residual capacity of the elements after a fire and to exploit technological advances for test control). The fire community has largely followed the original testing procedure for construction materials and elements under fire. Careful examination of literature will show similar initiatives that were underway in Europe (see Fig. 2.4); however, the momentum for developing standardized fire testing would not appear until BS 476 was adopted, which largely mirrored the ASTM fire standard. BS 476 would



**Fig. 2.4** Reinforced concrete floor tested by Edwin Sachs, 1906 [14]

later evolve into ISO 834. Further information on European background may be found elsewhere [15].

By the early 1980s, overreliance on standard fire testing was widely recognized as limiting innovation in architecture and construction, and technical papers began to appear which openly questioned the applicability of these tests [8]. Fire engineering researcher David Jeanes commented in 1982 [16]: *“although the traditional approach of assigning time for a given structural element or assembly allowed for a comparative measure between different types of construction; it is hard pressed to represent actual structural performance in a real fire due factors of restraint, redistribution of loads, moment resistance, as these are difficult to quantify and duplicate in tests.”* The standards today recognize fire resistance as the time duration that a “mock-up” assembly is able to withstand furnace heating based upon standard fire testing requirements and acceptance criterion defining test end.

### 2.1.2 Qualification Testing

Building elements can be tested under controlled conditions in a standard fire test, also known as qualification tests. Standardized tests are jurisdiction dependent and include multiple similarities as they typically originate from the ASTM standard. To date, the more popular standards referenced are ASTM E119 and ISO 834. The goal of qualification testing is to determine a time-based fire resistance rating. The test is intended to allow comparison between various assemblies used nationally. This test uses the standard fire curve (time-temperature curve) which continually rises in temperature with time. In the testing furnace, burners are controlled in order for the temperature inside the furnace to follow the designed time-temperature curve. Table 2.1 illustrates the current specified control temperatures of the test.

Control of temperatures can be very accurately defined in modern furnaces and has strict tolerances as defined in the standards. Tests typically are conducted for

**Table 2.1** Time and temperature values for ASTM E119 and ISO 834

Time (min)	ASTM E119 temperature (°C)	ISO 834 temperature (°C)
0	20	20
5	538	576
10	704	678
30	843	842
60	927	945
120	1010	1049
240	1093	1153
480	1260	1257

walls, floors, beams, columns, penetrations, and junctions. The test is intended to consider as-built construction; the assembly is placed in a rigid frame and positioned inside, next to, or over the standard testing furnace depending on the member type. Once placed a likely service load is applied. The load is maintained as the standard time-temperature curve is applied. The test is continued until a failure criterion is reached (Sect. 2.1.3).

Standard fire testing does not account for physical parameters governing fire behavior such as fuel load or ventilation. Moreover, furnace size limitations impact the size of assemblies that can be tested, as well as impact the restraints and loads acting on a test specimen. Therefore, standard fire testing is not representative of conditions in real fires. This is stated in a disclaimer in ASTM E 119 as “*this standard is used to measure and describe the response of materials, products, or assemblies to heat and flame under controlled conditions, but does not by itself incorporate all factors required for fire hazard or fire risk assessment of the materials, products or assemblies under actual fire conditions.*” [1] However, the principles of the test form the basis of many global jurisdictions’ hourly fire ratings given to various infrastructure. The reasoning is defined as above through the contextual history of the test.

There are certain limitations of assembly qualifications that the practitioner should consider, and these largely deal with the realism of the test. Many practitioners have subsequently advocated the use of consistently crude approaches for structural fire testing. In the case of qualification testing, it is largely appropriate for building elements only. When taken out of this context, there are limitations in its interpretation to reality (method of construction, appropriate element size, loading configuration, thermal boundary, cooling, etc.). Lastly, important consideration should be made regarding reproducibility. While advances in furnace control have been made through the avocation of plate thermometers, no one furnace is strictly the same from laboratory to laboratory.

### 2.1.3 Testing Criteria

Deflection, specimen temperatures, and sometimes strains are monitored during standard fire testing. The performance of an assembly is measured as the period of resistance to a standard fire before failure (Fig. 2.5). Failure criterion is denoted as either stability, integrity, or insulation. For all assemblies, some criteria are not applicable (see Table 2.2). Stability references that an assembly should not collapse (or in some cases limited to how much or how fast deflection can be). Notably, the load-bearing capacity of columns in the latter can be defined by a limiting axial contraction of  $h/100$  (mm), and a limiting rate of axial contraction of  $3 h/1000$  (mm/min). ASTM E119 does not mention a limiting value for axial contraction. However, deflection criteria for beams under both standards mentioned are given as maximum total deflection of  $L^2/400d$  (mm or in) and maximum deflection rate per minute of  $L^2/9000d$  (mm/min or in/min) after the maximum total deflection has been





**Fig. 2.5** Conclusion of a standard fire test of a wooden floor (photo by Gales)

**Table 2.2** Typical failure criteria by assembly type

	Stability	Integrity	Insulation
Partition/door		x	x
Floor/ceiling/wall	x	x	x
Beam/column	x		

exceeded. Deflection criteria (as defined above) derive from concrete and steel tests performed in the 1950s [17]; they are generally defined as limitations to prevent failure of the slab into the furnace that can cause significant damage. Integrity references to the ability of the specimen to not allow the passage of flame. The mechanism used to assess this is typically the ignition of cotton waste on the unexposed surface. Lastly insulation is the ability of the assembly to not allow excessive heat transfer. Depending on the standard this is considered less than 180 °C.

### 2.1.4 “Restrained vs. Unrestrained”

For certain fire resistance listings, the designer must judge whether a “restrained” or “unrestrained” classification is appropriate for the application. It is common for architects to task fire protection engineers or structural engineers to make such judgments. Many listings permit less applied fire protection to achieve a certain fire resistance rating if a “restrained” classification is adopted, as compared to an “unrestrained” classification.

ASTM first introduced the “restrained vs. unrestrained” concept in the 1970s [18], based on the notion that thermal restraint provided by the furnace enclosure generally enhances the performance of fire-resistant assemblies. For instance, the thrust forces generated by restrained thermal expansion can help to reduce the

deflection of steel beams under heating. Since beam deflection is an acceptance criterion of the test method, this effect is usually beneficial as it pertains to fire resistance. An assembly is considered “restrained” if it bears directly against the edges of the furnace at the outset of the test [19]. For reference, the UL Fire Resistance Directory states that the furnace enclosure boundaries provide approximately 850,000 kip-in. of flexural stiffness [20], which is significantly higher than that provided in situ in most cases.

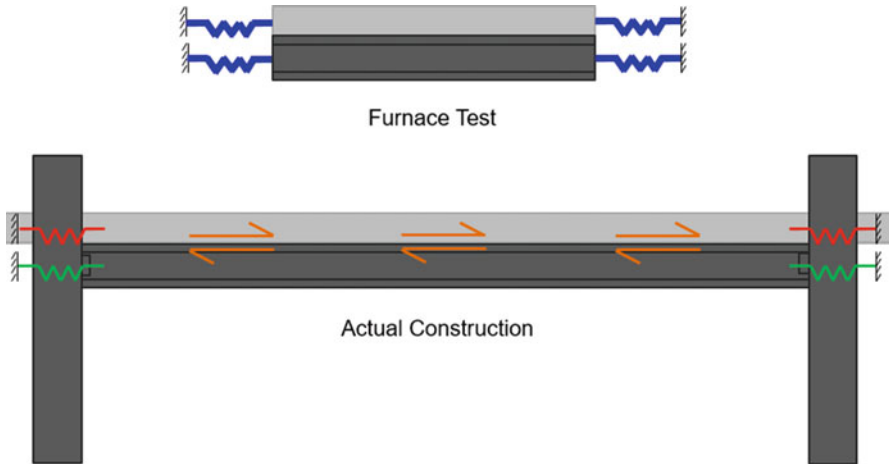
The UL Directory [20], the American Institute of Steel Construction (AISC) 360 standard [21], and certain publications provide guidance on determining restraint conditions, but the classification of an assembly as either “restrained” or “unrestrained” is ultimately governed by the judgment of the designer. Since standard furnace testing does not consider structural system response, but only the response of components, this judgment is often inconsistent among designers.

The effect of thermal restraint must be carefully evaluated since it may dominate the behavior of a structural system under fire exposure [22]. Complicating matters, it is known that a multitude of factors influence restraint conditions (e.g., varying spring stiffness), and these factors may *increase or decrease* structural system endurance under fire exposure. For instance, thermal restraint may generate forces sufficient to cause yielding or fracture of connections (as illustrated in Fig. 2.6), perhaps precipitating structural collapse. Alternatively, thermal restraint may limit the deflection of structural members and provide added stability.

The conditions of restraint differ between standard fire testing and in situ conditions. In actual building construction, restraint of structural assemblies occurs when the surrounding structural system resists their thermal expansion when exposed to



**Fig. 2.6** Steel beam flange buckling



**Fig. 2.7** Thermal restraint (furnace test vs. actual construction) [23]

heating. During standard fire testing, restraint is provided by the furnace enclosure. Furthermore, a steel beam and concrete slab would be restrained equally during a furnace test. In actual building construction, the beam would typically have less resistance to thermal expansion as compared to the slab, resulting in differential longitudinal movement under fire exposure (as illustrated in Fig. 2.7). Due to the differences between test conditions and actual construction, there continues to be ongoing confusion and debate concerning this concept.

Several organizations have conducted furnace testing to better understand the influence of restraint on the level of fire resistance achieved. AISC funded furnace testing of steel floor assemblies, which found that restraint of the furnace frame provided no fire resistance benefit [24]. The National Institute of Standards and Technology (NIST) performed furnace testing of steel trusses (Fig. 2.8) and found that an unrestrained assembly achieved a higher fire resistance when compared to an equivalent restrained assembly [25]. These test results demonstrate that the effect of restraint varies among different structural systems.

The ASCE/SEI 7 standard [26] provides guidance on how designers should consider thermal restraint generally. Specifically, ASCE/SEI 7 Section E.2 states that thermal restraint is entirely dependent on adjacent structural framing and connection details, which are not contemplated in standard fire resistance design. Accordingly, Section CE.2 states that furnace testing does not provide the information needed to predict the actual performance of a structural system under fire exposure, since furnace testing qualifies assemblies in isolation without interconnectivity or interaction with the surrounding structural system.

When structural fire engineering is employed, analysis of structural system response inherently considers the amount of structural restraint actually present. However, when standard fire resistance design is used, the degree of restraint is left to the judgment of the designer, for building codes (e.g., IBC) do not provide specific



**Fig. 2.8** NIST testing of steel trusses [25]

prescriptive classification. Hence, the designer is forced to make a somewhat conflicted judgment.

Recently, the industry has begun to reexamine the “restrained vs. unrestrained” concept in order to better serve designers going forward [23]. Many designers believe that clarification/reform of the “restrained vs. unrestrained” concept is needed. For instance, an industry consensus that is clearly stated in the IBC would relieve designers of the obligation to make uncertain judgments within standard fire resistance design. Such judgments are better reserved when employing structural fire engineering.

Until an industry consensus is included in building codes, designers may choose to take a conservative approach when classifying restraint conditions within standard fire resistance design [27]. Notably, IBC Section C703.2.3 states that in situ conditions should be considered unrestrained unless structural documentation is provided that demonstrates a restrained condition in actual construction [28]. In all cases, the authority having jurisdiction may be consulted as to the proper interpretation for a given project.

### ***2.1.5 Empirical Calculation Methods***

Assemblies that are qualified through standard fire testing are published in directories such as the UL Fire Resistance Directories [20], which contain hourly ratings for beams, floors, roofs, columns, walls, and partitions. These listings have very specific construction requirements that are commensurate with the test mock-up.

Even though fire resistance directories are quite lengthy, the ability of designers to achieve project goals is routinely inhibited by this empirical framework, especially when unique or nonconventional architecture is proposed.

Standard fire tests can be very costly to conduct (e.g., US\$100,000 to administer a single test). When members or assemblies and their passive fire protection are similar to those already tested, industry-accepted empirical calculation methods may be employed to determine the fire resistance rating. Generally, these empirical calculation methods only interpolate between established test data, for extrapolation would not be proper given the empirical nature of standard fire testing.

Chapter 7 of the International Building Code [29] is a common reference for industry-accepted empirical calculation methods. This chapter includes table lookups and equations to determine the fire resistance of generic construction materials that have been thoroughly tested. For instance, independent of a fire resistance directory, it can be derived via a table lookup that a 5 in. solid wall thickness of siliceous aggregate concrete provides 2 h of fire resistance. Similar to Chapter 7 of the IBC, ASCE/SEI/SFPE 29 [30] is a commonly used standard that exclusively provides empirical equations for use in standard fire resistance design.

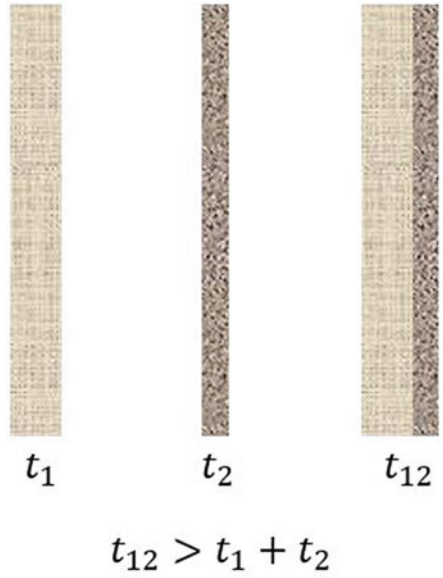
### ***2.1.6 Equivalence Methods***

Equivalence is a term used within standard fire resistance design, which can be defined as having equal or better fire resistance as compared to a tested assembly. The evaluation of equivalence must be conducted within the context of the standard fire test methodology and its specific acceptance criteria, and not be linked to actual structural systems and actual fire exposures. In other words, for a proposed fire-resistant assembly to be deemed as equivalent to a previously qualified assembly, it must be demonstrated that such an assembly would perform equally or better if exhibited to a hypothetical standard fire test. Equivalence may be demonstrated using either qualitative or quantitative approaches.

Qualitative approaches harness relatively simple logic to contemplate the anticipated performance of a given assembly as compared to another. Most notably, the “Rules of Harmathy” can be used to perform a quick assessment of fire resistance when fire test data are not available [31]. Harmathy’s Rules that are pertinent to standard fire resistance design include the following:

- Parallel insulating layers perform equal to or better than the sum of each individual layer tested separately (Fig. 2.9).
- Adding insulating layers does not decrease the fire resistance.
- Adding an air gap within parallel insulating layers does not decrease the fire resistance (Fig. 2.10).
- The further an air gap is located from the exposed surface, the higher the fire resistance.
- Increasing the width of an air gap has negligible effect on fire resistance.

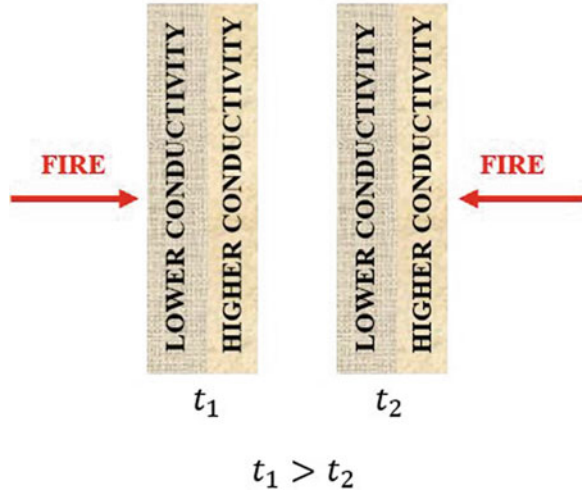
**Fig. 2.9** Harmathy's rules  
(parallel layers)



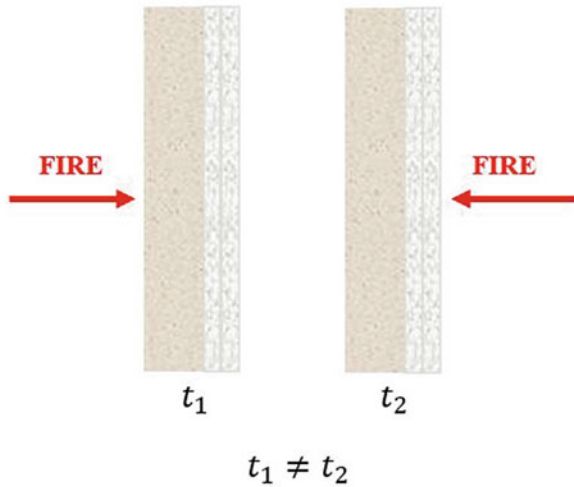
**Fig. 2.10** Harmathy's rules  
(air gaps)



**Fig. 2.11** Harmathy's rules  
(layer thermal conductivity)



**Fig. 2.12** Harmathy's rules  
(side of fire exposure)



- Locating insulating layers with a lower thermal conductivity towards the exposed side provides higher fire resistance with all else equal (Fig. 2.11).
- For a given set of insulating layers, the fire resistance achieved for fire exposure on one side does not necessarily equal that if the fire exposure is from the other side (Fig. 2.12).
- If the construction is not susceptible to explosive spalling, the presence of moisture in the insulating layers increases the fire resistance.

Quantitative approaches seek to explicitly simulate the performance of a test specimen during a standard fire test. In this case, the designer would represent the

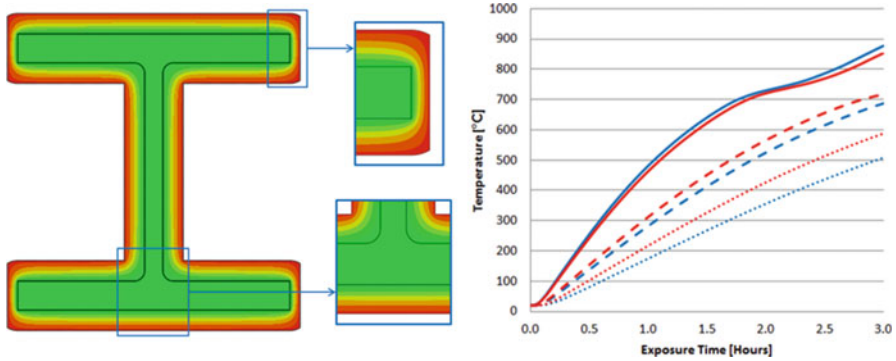


Fig. 2.13 Thermal model of an unloaded column test

span length characteristic of a furnace (e.g., 17 ft.) and expose the specimen to standard furnace heating. Also, the fire resistance of the specimen would be qualified per the acceptance criteria. This type of approach usually requires the use of finite element modeling that has been validated against similar furnace testing results. For instance, Fig. 2.13 shows the results of a 2D thermal model used to understand the heating of a protected steel column during an unloaded column test. In this example, the effect of reduced insulation thickness at the column flange tips is studied.

## 2.2 Strength Domain

Structural fire engineering is based on the strength domain. Principles of structural engineering serve as the basis of structural fire engineering (see Sect. 2.2.1). Accordingly, structural fire engineering explicitly evaluates all aspects of demand and capacity of structural systems under fire exposure. Within this framework, the demand on a structural system under fire exposure can be reduced by means of rationally allocated structural insulation (e.g., applied protective insulation), control of fuel loads, and/or other fire exposure mitigation techniques. Also, the capacity of a structural system to endure fire exposure can be increased by means of specific member sizing, connection detailing, and/or other measures to enhance structural robustness [32].

Figure 2.14 illustrates the difference in controllable design variables between standard fire resistance design (time domain) and structural fire engineering (strength domain).

### 2.2.1 Structural Engineering

Structural design in the USA primarily uses the load and resistance factor design (LRFD) method. This method employs a statistical based approach for predicting



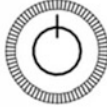



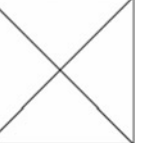
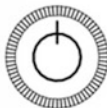
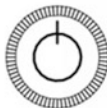
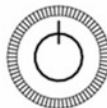
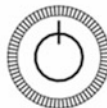
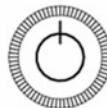
	INSULATION	FUEL LOAD CONTROL	STRUCTURAL DESIGN	STRUCTURAL DETAILING	OTHER MITIGATION
STANDARD FIRE RESISTANCE DESIGN					
STRUCTURAL FIRE ENGINEERING DESIGN					

Fig. 2.14 Controllable design variables [27]

loads and material strengths. Within this paradigm, a load effect is defined as the force in a member or an element (axial force, shear force, bending moment, or torque) due to the nominal load (e.g., self-weight, snow weight, wind pressure, seismic inertia). Each member and element has specific structural capacities (e.g., flexural capacity) to withstand load effects. A limit state is reached when a specific capacity or capacities of a member or element no longer fulfill the relevant design criteria (e.g., flexural yielding). Accordingly, to qualify the safety of a conventional design, structural engineers must calculate the demand-to-capacity ratio (DCR) for each applicable limit state. The selection of applicable limit states is based in part on a designer’s ability to identify all conceivable modes of failure or mechanisms in which the structural system could conceivably fail.

LRFD criteria reduce the probability of the load effect exceeding a capacity to an acceptable level. Accordingly, this method results in members and elements that are sized to withstand all considered load effects during the design life of the structural system, with an appropriate level of reliability for each relevant limit state. For instance, steel beams designed to withstand gravity loads have a probability of exceeding their flexural limit state on the order of 0.005 to 0.0005 on a 50-year basis, corresponding to reliability indices of approximately 2.5–3.3 [33]. Specific limit states that have a higher consequence of failure typically have higher target reliability. For instance, brittle failure modes, such as concrete column crushing, occur with little warning and usually inhibit load redistribution.

LRFD results in a more consistent degree of reliability across different design scenarios, as compared to preceding deterministic approaches, such as allowable stress design (ASD). For instance, consider two roof structures: a reinforced concrete beam/slab and a reinforced concrete plate, designed for the same snow load using the same allowable stresses per ASD. The first structure has considerably higher dead load as compared to the second. Since the dead load can be estimated with much more precision than the snow load, the roof having the high ratio of dead to snow load would have a lower probability of failure than the lighter structure. Accordingly, LRFD accounts for the variability of individual loads through load effect

factors. In Europe, the Eurocodes adopt a similar approach by utilizing concepts of limit states and associated design factors. Also, the ISO 13824 standard, which is adopted by a number of countries across the world, provides guidance for risk-informed design of structural systems [34].

The determination of structural load effects in the USA is primarily conducted in accordance with the ASCE/SEI 7 standard [26]. This standard requires that structural members and elements be designed considering certain load combinations, which comprise individual load effects multiplied by specific load factors. The load combinations used for conventional structural engineering design pertain to those resulting from dead (i.e., self-weight), live (i.e., movable weights), snow, rain, wind, and seismic nominal load effects. Nominal loads are frequently defined with reference to a probability level (e.g., 50-year mean recurrence interval wind speed).

The nominal dead, live, and snow loads provided in ASCE/SEI 7 are based on a combination of measured data and engineering judgment. Thus, there is a small but finite probability that a nominal load per this design method will be exceeded in a given year. For instance, stochastic models of typical building operations were used to develop nominal live loads based on the occupancy or use. Based on the principles of mechanics, the nominal loads produce load effects that are used in the load combinations. If the relation between the nominal load and the resulting load effect is linear (which is typically the case in conventional design), the designer may apply the load effect factor to the nominal load for convenience when performing a structural analysis. The sum of a load combination produces the demand for DCR calculations.

In the USA, the determination of structural capacity is primarily conducted in accordance with standards produced by material organizations (e.g., AISC 360 [35]). Material organizations specify strength reduction factors that are typically less than unity, which are applied to nominal strength parameters used in structural calculations (e.g., yield strength, modulus of rupture). These factors are based on uncertainties associated with the strength of members and elements (e.g., material composition, dimensional tolerances) and the consequence of the failure limit state (e.g., concrete crushing). Also, strength reduction factors are intentionally set lower for structural connections as compared to structural members, reflecting the higher consequence of connection failures. For a given limit state, multiplying the strength reduction factor by the nominal strength parameter produces the capacity in DCR calculations.

Since independent material organizations govern the composition of corresponding material standards (and the load effect factors in ASCE/SEI 7 are constant irrespective of the material of construction used), the underlying reliability of structural designs varies across different building materials (e.g., steel, concrete, wood, masonry). Notwithstanding, the average reliability index  $[\beta]$  of a structural design using ASCE/SEI 7 load effect combinations involving dead, live, and snow loads is approximately 3.0. For wind and seismic loads, the average reliability index is approximately 2.5 and 1.8, respectively [36].

## 2.2.2 *Relevant Standards*

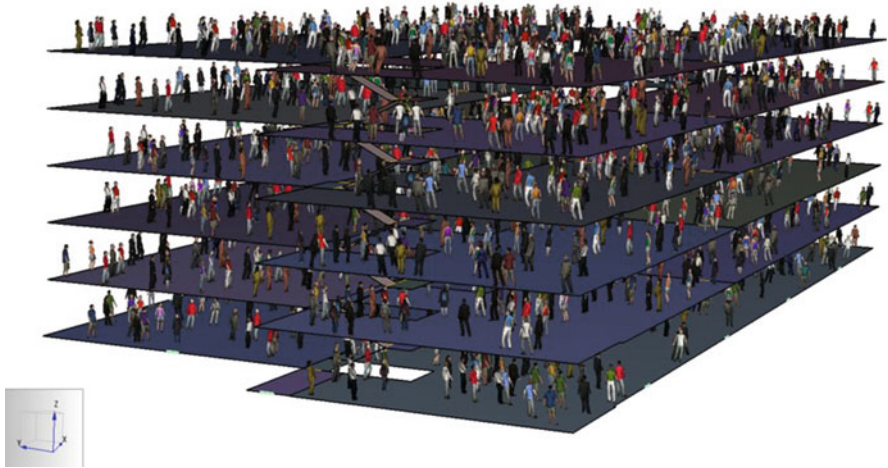
Since standard fire resistance design does not contemplate structural system performance or explicit performance objectives, there exists no practical method for a designer to quantitatively compare the level of safety provided by a structural fire engineering design to that provided by a standard fire resistance design. Furthermore, it is not reasonable to require that a structural fire engineering design be “equivalent” to a standard fire resistance design, which does not provide any affirmative quantification of structural fire safety. Hence, the industry consensus embodied in industry standards is absolutely essential for successful implementation of structural fire engineering [37].

The use of structural fire engineering constitutes an alternative methodology to meet project design objectives, as permitted by the alternative materials, design, and methods of construction provision in building codes, such as the IBC. Acceptance of structural fire engineering designs is elective and subject to approval by the authority having jurisdiction.

The SFPE Engineering Guide to Performance-Based Fire Protection [38] outlines the process for using a performance-based approach for building fire safety, which is applicable to structural fire engineering design. Notably, this standard provides guidance for creating a design brief, which serves as a memorialized agreement of the assumptions, performance expectations, etc. Also, this standard describes the role of various stakeholders. Unlike standard fire resistance design in which the architect typically serves as the responsible party for satisfying code requirements for structural fire resistance, structural fire engineering usually requires a team consisting of structural engineers, fire protection engineers, and possibly other design professionals.

In addition to designers, the involvement of the owner, building authority, and possibly peer reviewers would need to be addressed when employing structural fire engineering. If required, a third-party peer review is conducted independently by persons with appropriate expertise and experience to evaluate compliance of the proposed design with industry standards (e.g., ASCE/SEI 7-16), and any other requirements of the building official. The SFPE Guideline for Peer Review in the Fire Protection Design Process provides guidance on the peer review process [39].

ASCE/SEI 7 serves as the parent standard for structural engineering in the IBC. The current edition of this standard includes a new Chap. 1 section (Fire Resistance). In addition to being the first time that fire resistance has ever been addressed in this standard, this section commences a new industry consensus standard of care for structural fire protection practice in the USA, and other adopting jurisdictions [40]. The default option is for the designer to strictly adhere to the requirements and restrictions of standard fire resistance design per the applicable building code. The only permitted alternative to standard fire resistance design is structural fire engineering, as constituted in the standard’s new Appendix E section (Performance-Based Design Procedures for Fire Effects on Structures). Notably, the inclusion of



**Fig. 2.15** Occupant evacuation simulation

Appendix E in ASCE/SEI 7 marks the first time that fire effects are considered as an explicit design load in a US structural engineering standard [32].

ASCE/SEI 7-16 Appendix E is organized into six sections with associated commentary. Notably, Section E.4 specifies mandatory and discretionary performance objectives for structural systems under fire exposure. The mandatory performance objectives uphold the intended functionality of occupant egress systems. In all cases, the designer must explicitly demonstrate that the structural system would allow for a safe and complete evacuation of building occupants to a public right of way (e.g., roadway) in the event of an uncontrolled fire. This necessitates an ASET (Available Safe Egress Time) vs. RSET (Required Safe Egress Time) analysis, in which the determination of RSET involves consideration of occupant egress times (Fig. 2.15). The SFPE Guide to Human Behavior in Fire provides guidance on how to calculate RSET [41].

In addition to occupant evacuation, the designer must demonstrate that structural elements that support building refuge areas within the building (e.g., refuge floors) would remain stable during and after an uncontrolled fire event. Beyond the mandatory performance objectives, all other relevant performance objectives are classified as discretionary within ASCE/SEI 7-16.

Per ASCE/SEI 7-16, discretionary performance objectives may address issues such as tolerable levels of structural damage, structural support of ingress routes for firefighters, structural support of fire resistance-rated assemblies, and others. For instance, ASCE/SEI 7-16 Section CE.4.2 recommends tolerable levels of structural damage under fire exposure based upon the building's Risk Category assuming that all of the mandatory performance objectives are satisfied. For buildings that meet Risk Category I criteria (e.g., storage buildings), structural collapse from fire exposure is permissible if the collapse does not damage surrounding properties, including

buildings and infrastructure systems. For the majority of buildings which can be classified as either Risk Category II or III, the primary structural system (i.e., columns, structural elements having direct connections to columns, and lateral bracing elements) should remain stable under fire exposure and subsequent cooling. As such, damage to structural elements or assemblies that does not compromise the stability of the primary structural system or continuity of the load path is permissible. For buildings which are classified as Risk Category IV (e.g., hospitals), the entire structural system (including secondary structural elements) should remain stable under fire exposure and subsequent cooling which would allow for rapid reoccupation of areas not directly affected by fire exposure.

The need for and the scope of discretionary performance objectives must be agreed upon by project stakeholders, and this agreement should be memorialized within a Design Brief document. Even if discretionary performance objectives are not explicitly analyzed for a given project, fulfilment of the mandatory performance objectives may enhance structural performance in these respects (e.g., added structural robustness of stairways used by firefighters).

ASCE/SEI 7-16 Appendix E Section E.5 provides requirements for evaluating the heating of structural systems under fire exposure with reference to the NFPA 557 [42], SFPE S.01 [43], and SFPE S.02 [44] standards. The NFPA 557 standard establishes a basis for estimating building fuel loads. The SFPE S.01 standard provides requirements for evaluating thermal boundary conditions from fire exposure. Lastly, the SFPE S.02 standard provides requirements for heat transfer calculations based on the thermal boundary conditions. ASCE/SEI 7-16 requires that “structural design fires” be analyzed, defined as those that are uncontrolled by active measures, such as automatic fire sprinklers or firefighting activities.

The NFPA 557 standard provides a reliability-based method for calculating either localized or distributed fuel loads for use in fire exposure calculations. For enclosure-type fire exposures, the design distributed fuel load would be applicable. Unless the distributed fuel loads contained in a particular building are explicitly surveyed, the occupancy-based method in this standard should be used. The occupancy-based method involves calculating a fuel load risk factor that reflects the likelihood of an uncontrolled fire occurring based on National Fire Incident Reporting System (NFIRS) data, and a target  $\beta$ -value of approximately 5.0. The distributed fuel load risk factor is a function of the following:

- Occupancy type (e.g., educational).
- Construction characteristics (e.g., protected noncombustible).
- Presence or absence of active fire protection systems.
- Level of inherent and applied fire protection present.

Based on specific fuel load surveys and studies vetted by the NFPA, this standard specifies average and standard deviation values of the distributed fuel load for different occupancy types. These values reflect a 99% upper confidence bound. The design distributed fuel load is calculated as a function of these statistical values and the fuel load risk factor.

The Eurocode provides a similar framework for determination of fuel load density, which is a function of the nominal fuel load and specific risk factors per Annex E [45]. Notably, there is a risk factor that accounts for the presence or absence of active fire protection measures (including manual suppression). The Eurocode treats the nominal fuel load as a variable parameter with a Gumbel distribution, and suggests the use of an 80% upper confidence interval. These risk factors (as stated in the Eurocode background documents) were determined considering the  $\beta$ -value to be approximately 5.0 for a building design life of 55 years. Notably, some countries of Europe (e.g., UK) have not adopted the risk factors as presented in the Eurocode (with the exception of the reduction factor for the presence or absence of a fire sprinkler system).

The survey-based method in NFPA 557 serves as an alternative approach and involves the manual accounting of anticipated fuel masses and their respective combustion properties. Generally, a survey-based approach would only be used in cases where justification of a lower fuel load density (as compared to that calculated using the occupancy-based method) is warranted by special circumstances. Otherwise, there would be limited justification for the effort involved.

Based upon the fuel load, ignition(s), and arrangement of compartments and ventilation openings, structural design fires are often characterized as either an enclosure fire or a localized fire. Accordingly, the SFPE S.01 standard provides methods to determine time-dependent thermal boundary conditions on a structural system due to either an enclosure or a localized fire. Similarly, the Eurocode Annex A provides equations for parametric fire curves. However, the Eurocode allows for the use of the standard fire curve (used for furnace testing), which is unlike ASCE/SEI 7. Exterior fire exposures and traveling fires are also discussed for which design guidance is comparatively less robust. In special circumstances, it may be necessary to perform fire modeling which should be substantiated according to the SFPE G.06 standard [46].

The NFPA 557 standard specifies the extent of a structural design fire as either the entire building or that portion of the building that is bounded by exterior walls and/or by fire-rated boundaries that are capable of containing a fire for the entire duration through burnout. If a given floor of a building has no fire-rated boundaries, the entire extent of the floor must be assumed to be involved in fire. The SFPE S.01 standard currently specifies the extent of fire exposure similar to NFPA 557. Neither NFPA 557 nor SFPE S.01 currently provides specific guidance on the number of building stories that should be considered as involved in fire.

Based upon the time-dependent thermal boundary conditions from fire exposure, the thermal response of a structural system can be determined based upon the principles of heat transfer in accordance with the SFPE S.02 standard. Additionally, key sources for temperature-dependent thermal properties of conventional construction materials are identified in ASCE/SEI 7-16 Section E.5.

Based on the results of thermal response calculations, ASCE/SEI 7-16 Section E.6 provides requirements for subsequent structural response calculations. This section requires consideration of all heated members of a structural system, and those unheated members that induce thermal restraint forces. Additionally, the effect

of material strength and stiffness degradation must be considered, which may result in high deflections and deformations. Specifically for steel structures, AISC 360 Appendix 4 (Structural Design for Fire Conditions) provides added relevant guidance for designers [21]. However, AISC 360 Appendix 4 should not be relied upon exclusively for structural fire engineering designs since it lacks critical over-arching and material-neutral requirements. Notably, structural analysis scope and other baseline requirements are left undefined/open-ended. In such cases, ASCE/SEI 7-16 Appendix E requirements would govern.

Unlike standard fire resistance design, ASCE/SEI 7-16 Section E.6 requires that structural analyses include portions of the structural system that are subject to fire effects with consideration of unheated portions of the structural system that provide thermal restraint (see Sect. 2.1.4). A single-member analysis is permitted in cases where only a single member is affected by a fire without consequential effects from surrounding members. Otherwise, a systems approach that evaluates thermal expansion of heated sections and restraint by cooler adjacent framing is necessary. Additionally, analyses of structural system response to fire exposure must always consider the performance of structural connections.

Unlike conventional structural engineering design, ASCE/SEI Section E.6 allows for consideration of alternative sources of load-carrying capacity and load paths that are capable of being maintained following structural damage or degradation due to fire exposure (e.g., catenary action). Moreover, Section E.6 includes discussion of specific design considerations and critical failure modes for columns, floor systems, connections, and other structural components. Lastly, this section discusses proper transfer of results from heat transfer analyses to subsequent structural analyses, and key sources for temperature-dependent mechanical properties.

ASCE/SEI 7-16 Section E.6 requires the use of load combinations for extraordinary events to evaluate structural performance under fire exposure. For a structural system that has been conventionally designed, the following additional load combination is used to analyze its ability to endure uncontrolled fire exposure:

$$1.2D + A_k + 0.5L + 0.2S$$

$A_k$ : load effect from fire.

$D$ : load effect from dead load.

$L$ : load effect from live load.

$S$ : load effect from snow load.

The force in structural components due to fire effects has a load factor of 1.0. The live load factor of 0.5 included in the extraordinary event load combinations is intended for typical occupancies and arbitrary point-in-time live loads that will likely exist during an uncontrolled fire [47]. It is noteworthy that this live load factor represents a philosophical difference from the approach used in standard fire testing in which the assembly is loaded to its design limit for member stress, representing application of the full dead and live load. Also, this load combination excludes hurricane wind and seismic event consideration due to the negligible probability of joint occurrence with an uncontrolled fire. Granted, fire following earthquake would

have a higher probability of occurrence, and such an event has not yet been explicitly addressed within ASCE/SEI 7, or any other relevant standards.

The applicable load combination in the Eurocode includes wind loading. However, such considerations may be identified as a discretionary performance objective within the framework of Appendix E if deemed necessary by stakeholders. Since the relation between the nominal fire load (i.e., temperature at a given time) and the resulting fire load effect is usually nonlinear, the designer must apply the load factor only to the fire load effect itself, and not the nominal fire load (i.e., temperature). Conveniently, the current fire load effect factor specified in ASCE/SEI 7 is unity, so there is no procedural impact.

As it applies to uncontrolled fire exposure, the input into the load combination shown above would be the axial force, shear force, bending moment, and torque induced from restrained thermal expansion and contraction of structural members and elements. The nominal fire load (i.e., temperature at a given time) must be determined for the specific design condition (e.g., fuel load, enclosure characteristics). Hence, a trivial application of the standard fire curve (used for furnace testing) is not permitted. Currently, ASCE/SEI 7 specifies that the selection of structural design fire scenarios is within the purview of the designer. Similarly, the Eurocode does not provide specific requirements for the selection of structural design fires. However, the industry is currently developing standards that may soon assist in this selection process, and relieve some of the onus on designers in this respect. In Europe, it is relatively common for this selection to be based on some form of risk analyses, which varies from country to country and project to project. Moreover, it is typically assumed that structural design fires involve only one fire compartment of a building.

Unlike conventional structural engineering design, ASCE/SEI 7-16 Section E.6 requires the designer to consider the time and path dependence of fire effects on a structural system. While gravity loads on a structural system remain relatively constant during fire exposure (assuming most of the building contents are not burning), time-dependent temperature histories may result in time-varying member strength and thermally induced forces, depending on the temperatures reached by structural components. Hence, consideration of a specific static state may not be sufficient since preceding structural system behaviors may influence overall performance. For instance, the thermal expansion of secondary members may induce out-of-plane loads on primary members and column connections.

ASCE/SEI 7 Appendix E is referenced for structural fire engineering analyses in both the NFPA 5000 [48] and NFPA 101 [49] standards. Notably, NFPA 5000 is adopted as the governing building code in various Middle East regions. Also, NFPA 101 is adopted by some U.S. states. As a supplement to ASCE/SEI 7 Appendix E, ASCE/SEI Manual of Practice No. 138 [50] provides recommendations for analysis techniques, input parameters, and structural acceptance criteria. Also, the freely available ASCE/SEI Structural Fire Design Guide [51] explicitly demonstrates the proper application of ASCE/SEI 7 Appendix E for four anonymized steel-framed buildings. These resources in aggregate clearly demonstrate the proper interpretation and execution of ASCE/SEI 7 Appendix E provisions for structural fire engineering designs.



### ***2.2.3 Performance Expectations***

The majority of national codes default to prescriptive approaches where fire resistance is achieved by qualification against standard fire testing. Such approaches provide indeterminate performance, for they overlook key structural fire effects. Accordingly, a structural fire engineering approach is necessary to understand the level of anticipated performance.

Performance expectations relate to both occupant life safety and project-specific goals. In terms of life safety, occupants must have sufficient time and access to safely evacuate or move to an area of refuge within a given building. Accordingly, structural support of building egress routes must be maintained for a period of time necessary to ensure safe evacuation. Likewise, the building's refuge areas must remain safe for an indefinite period of time in order to maintain their design intent.

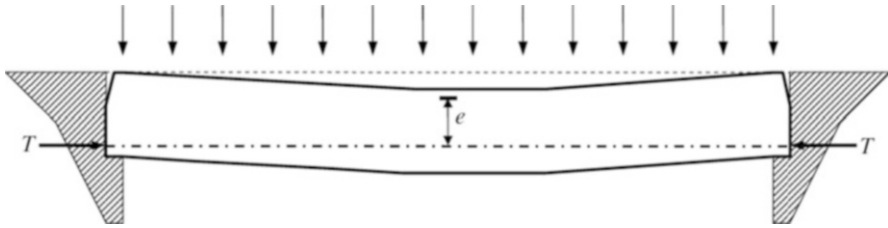
In addition to occupant life safety aspects, additional project-specific performance expectations may also be required. These are generally determined by the authority having jurisdiction and/or various stakeholders of the project. These may include concepts such as resilience: recovery of function, property protection, business continuity, environmental protection, adequate structural support of fire resistance-rated assemblies to limit fire and smoke spread, and structural support for first responders. In any case, project-specific (discretionary) performance objectives should be memorialized within a design brief (see Sect. 3.3.2).

### ***2.2.4 Restraint and Continuity***

In Sect. 2.1.4, the discussion on “restrained vs. unrestrained” focused on how structural elements are supported in standard fire testing. When the performance of a structural system is being assessed under the strength domain it is important to account for how restraint and continuity may contribute to the resistance of the structure. An explanation of how the building works in general is helpful to account for these effects.

Buildings are generally an assemblage of horizontal and vertical structural elements that are tied together. Although initial sizing of structural members may be performed considering them in isolation, the entire building works as a system, and taking advantage of this “continuity” allows redundancies to be introduced into the overall structure. The redundancy aids load sharing between members such that failure of an element may not result in failure of the entire building. In the event of a fire, structural continuity usually aids the overall performance of the building, but there are scenarios where restraint conditions may contribute to the collapse of the building.

The behavior of frames or structural systems is more complex than the behavior of individual elements, due to interactions between elements and fire-induced effects and coupling of the interactions and effects on the heated members as well as areas of



**Fig. 2.16** Effect of axial restraint force [52]

the building which may not be subject to direct heating. It is therefore important to examine the contributions of restraint and continuity in isolation. When structural elements are heated they expand in all directions. For isolated members, this expansion may occur freely and without inducing additional stresses on the particular member if the expansion is uniform across the depth of the cross section and there is no resistance to the free expansion of the member. On the other hand, for a structural member that is part of a system, the expansion of the member against cooler elements in its vicinity may increase its capacity or cause its failure.

Figure 2.16 shows a simply supported concrete beam carrying a uniformly distributed load between rigid supports. The supports allow rotation of the beam but prevent elongation. When the beam is exposed to fire at the bottom, there is differential thermal expansion through the depth of the beam, causing the bottom fibers to expand more rapidly than the top fibers. However, the presence of the rigid supports aids the development of axial thrust forces ( $T$ ) at the base of the beam, creating negative moments ( $Te$ ) that tend to resist the downward deflection induced by the differential heating through the beam's depth and the effect of the uniformly distributed load. In the figure "e" is the distance between the centroid of the beam's compressive stress region and the location of the resultant axial thrust. It is obvious from the figure that  $Te$  reduces vertical deflections as long as the thrust is below this centroid, and increases vertical displacements otherwise, as shown in Fig. 2.17(a).

The locations of several axial thrust forces are shown in Fig. 2.17. An axial thrust near the top of the beam in Fig. 2.17a would lead to failure of the beam in fire while Fig. 2.17b, c show systems that would increase the capacity of the beams. For built-in construction, where the line of action is not immediately known, as in Fig. 2.17d, the position of the axial thrust may vary. Mostly it is at the bottom, where most of the heating and thermal expansion occur.

The examples described above relate to reinforced concrete beams. In steel and composite construction, heated restrained beams develop compressive forces in their bottom flange as they expand against colder adjacent structure in the initial stages of a fire. This continues until a point at which local buckling of the bottom flange occurs, at about 300 °C as shown in Fig. 2.18. The loss of strength of the steel beam, coupled with the loss of axial thrust after buckling, induces large deflections, which eventually put the restrained beam into a catenary at temperatures above 800 °C. In Fig. 2.18, the axial forces show shortening of the beam in the cooling stage. This has

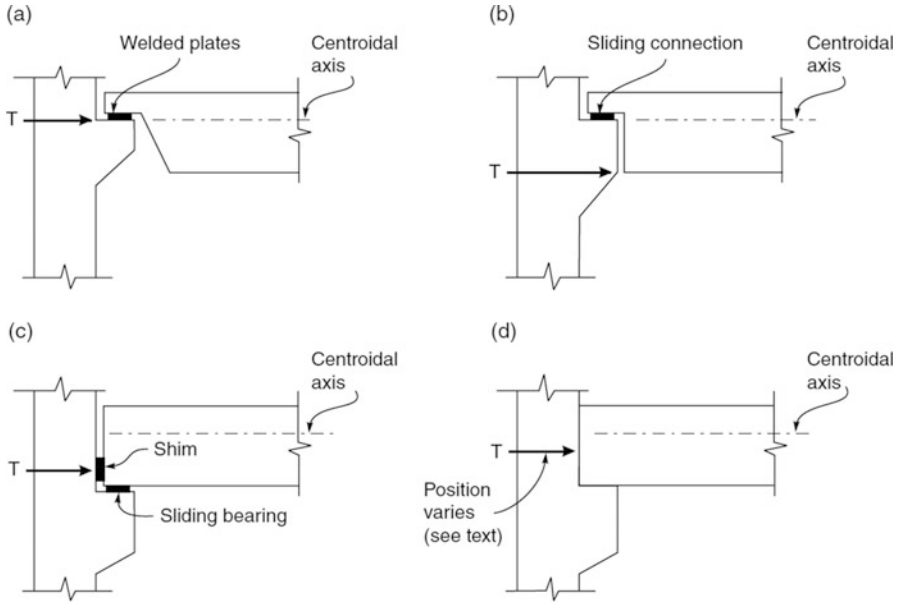


Fig. 2.17 Location of axial thrust for several support conditions [53]

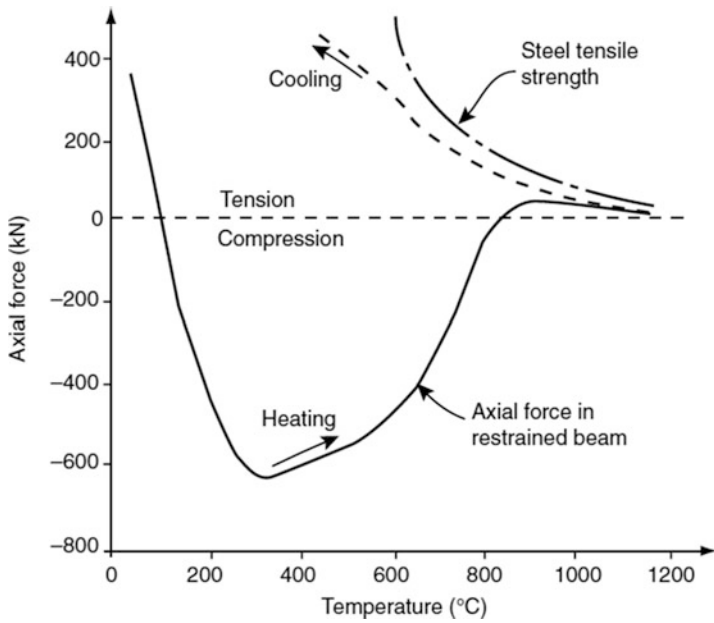


Fig. 2.18 Axial force in a restrained composite beam [54]

been known to cause failure of connections, as evidenced by the Cardington tests [55].

Restrained columns have many interactions with surrounding structure. Under fire conditions they are subject to significant changes in loading, which may affect their performance. Columns in buildings experience axial and rotational restraints. When a column is heated, it expands in all directions. When the elongation of the column is restrained, additional axial load is introduced into the column. A further increase in heating results in an increase of the induced load and reduces the column stiffness, which aids buckling. The buckling length of column is dictated by the amount of fixity at the ends of the column. As the relative fixity of the ends of the column changes throughout fire exposure, it is difficult to specify a unique design value for buckling length factor under fire conditions. Column-bending moments also change during the fire. This occurs as a result of the changing column-bending stiffness in relation to the surrounding structure. Bending moment is also affected by lateral loads induced in the column as a result of restrained thermal expansion of connected beams and p-delta effects due to the large eccentricity that occurs due to changes in initial straightness as the expansion of a connected beam is restrained.

Similar to restrained beams, restrained slabs expand against their supports. Rotational restraints along the slab boundary provide hogging (or negative) moments which help to limit vertical deflections. Axial thrusts that are at the base of the support due to the restrained thermal expansion tend to create a mechanism known as compressive membrane action. The mechanism, also known as arch action, increases the capacity of the restrained slab up to depths of the order of half the thickness of the slab. If the slab continues to experience restrained thermal expansion, then thermal buckling occurs which results in large deflections. The large deflections are only arrested if the slab can go into tensile membrane action—a mechanism that occurs in two-way bending slabs at deflections greater than the thickness of the slab. Compressive and tensile membrane action is covered in more detail in Chapters 6 and 7.

As discussed above, structural continuity has several advantages. However, in fires there are scenarios where this could contribute negatively to structural performance. The discussions above show that the negative moments at the ends of beams in particular allow them to carry more load. For a beam with doubly symmetric cross section (e.g., I-beam), positive and negative cross-section capacities are the same. In fire, as loads are maintained and structural capacities degrade, the supports yield first. The excess moments that were being carried at the supports before the loss of capacity are now redistributed to the beam midspan, which may eventually yield as the capacity of the beam reduces.

For situations where there are unequal capacities at the beam midspan and support or where the fire causes nonuniform heating along the beam, it is possible for a significant reduction in midspan beam capacity as a result of localized heating. Under this condition moments are redistributed to the supports. The behavior of the original fixed beam now becomes one representative of two cantilever beams.

### 2.2.5 Calculation Methods

Generally, the design of structures for fire effects requires the generation of fire and assessments of the thermal and mechanical responses of structures. Depending on the particular design scenario, the complexity involved in the selection of the fire and subsequent thermomechanical analysis varies. Historical models for fire exposure and corresponding structural response are presented by Purkiss and Li [56] and Buchanan and Abu [52]. Over time, there has been a shift towards large-scale, nonstandard fire testing. Generally, it is advised that when researchers carry out these tests, they should follow the accepted level of “consistent crudeness” [8]. Essentially, this principle recommends that researchers apply a similar level of crudeness to both the structural analysis in fire and the thermal insult to the structure.

Figure 2.19 shows how consistent crudeness may be applied to structural fire testing. This figure compares the complexity of the fire with the complexity of the structural analysis. The location of the intersect of the two levels of complexity indicates the credibility of the test. The intersect of the standard fire curve with a single structural element is representative of the standard fire test, used to determine

Structural Model \ Fire Model		Materials & Partial Elements	Single Elements	Sub-Frame Assemblies	Transiently Simulated Restrained Assemblies	Full-Scale Structures	
Elevated Temperature Exposures (Transient or Steady State)		Generate design/model input data	O/R	M/C	M/C	M/C	
Standard Fires		Generate design input data		O/R	M/C	M/C	
Equivalent Fire Severity to a Standard Fire		Validation of fire severity concept		O/R	O/R	M/C	
Parametrically Defined Fire Models		Generate design input data (highly dependant time-temperature phenomenon)		O/R	O/R	O/R	O/R
Numerical Fire Models		Generate design input data/ Research (highly dependant time-temperature phenomenon)		O/R	O/R	O/R	O/R
Real Fires		Research (highly dependant time-temperature phenomenon)		M/C	M/C	O/R	

**Fig. 2.19** Fire models and structural response models, where M/C indicates marginal credibility and O/R indicates occasional research [8]

structural fire resistance ratings. Comparatively, the intersect of a real fire exposure with a full-scale structure is representative of a real building fire. The diagonal connection of these two extremes represents the desired level of consistent crudeness.

Generally, the assessment of structural response to standard fire exposure is performed for single elements and subassemblies. Exposure to time-equivalent fires may be used for single elements, subassemblies, and full-frame structures while the complexity involved in modeling the effects of real fires may be applied to more complex, full-scale structural response models. Due to the growth of research in the structural fire engineering field on material behavior, the use of complex analysis is becoming more common in design. Thus a more structured design approach may be employed.

A general structural fire design typically proceeds in the following steps: First, the objectives for the design are set. Next, the required structural performance during the fire exposure must be defined, and the acceptance criteria will be determined. From this, an appropriate design fire can be selected. Member temperatures should be estimated, and the structural response of the test should be assessed. From this process, structural system characteristics can then be altered as needed, and the above process can be repeated until the design acceptance criteria are met.

This process, and in particular the steps of selecting a structural design fire, estimating the member temperatures, assessing structural response, and reassessing structural system characteristics, may require the use of a calculation method. Calculation methods may be “simple,” “advanced,” or a mixture of simple and advanced calculations. The choice of each depends on the complexity of the design problem. For example, the response of a simply supported steel beam in a small compartment may be determined by the use of the standard fire as the fire model, followed by an assessment of its thermal response using the simple lumped mass approach and then a verification of its strength loss in comparison with the applied loading.

On the other hand, the assessment of the failure of a structural connection in a composite structure under large deflections in fire conditions may require sophisticated use of an advanced fire model, an advanced thermal model, and an advanced structural model. These two examples demonstrate two extremes in the choice between simple and advanced calculation methods. However, an advanced structural analysis can also employ a simple fire model or a simple thermal model for the problem being considered, as appropriate.

After design requirements have been established, acceptance criteria are agreed upon by the stakeholders. The choice of acceptance criteria depends on the design requirements, level of conservatism to be achieved, structural design fires, familiarity of the designer with advanced calculation methods, and time allotted for analyses in the design process. In broad terms there are generally three categories of acceptance criteria: tabulated data, simple calculation methods, and advanced calculation methods.

The use of tabulated data (for most cases) does not require a consideration of the effects of applied loads at elevated temperature. Simple calculation models, on the

other hand, account for loads at the fire limit state. However, their use is limited to “simple” structural elements, as they do not account for structural continuity, load sharing, and effects of restrained thermal expansion. Advanced calculations are able to account for interactions between different structural elements, and thus provide more realistic structural behavior under fire conditions.

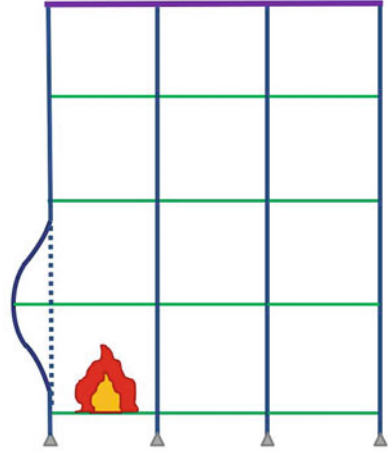
It is important to note that regardless of the selection of a calculation method the requirements of the design for fire conditions have to be satisfied. Basically, the effects of all actions at elevated temperatures must be less than the resistance that can be generated by the structure. This can simply be expressed by the inequality [57]:

$$\alpha E \leq \Phi R$$

In the equation above  $E$  is the cumulative effect of all actions on the structure. This includes permanent loads, variable loads, and effects of thermally induced actions.  $R$  is the resistance of the member.  $\alpha$  represents the resultant partial safety factor for loading at the fire limit state, which generally takes a value less than 1.0 as a result of the low likelihood of having significantly large fires and the full characteristic loads occurring at the same time, while  $\Phi$  is a partial safety factor for the given material, which typically takes a value of 1.0 for conservatism in the estimation of member response.

Single-member analyses are used to assess the response of structural elements isolated from the rest of the structure by the use of idealized boundary conditions (simple supports, pinned conditions, or fixed conditions). The analyses are usually performed by hand or by employing spreadsheets with very simple equations based on room-temperature structural analyses. Temperature distributions through the element of concern may be obtained by using tabulated data from standard fire experiments of similar structures or by simple heat transfer analyses such as the lumped temperature approaches, as outlined in Eurocode 3 for steel structures [58]. For exposure to other materials an advanced thermal analysis may be required. This typically involves the definition of the change of thermophysical properties (thermal conductivity, density, and specific heat capacity) with temperature and the use of finite differences or finite elements to solve for the member temperatures over the duration of the fire. It is important to note that single-member analyses may not sufficiently capture the effects of the thermal exposure (thermal expansion in all three directions and the effects of restrained thermal expansion or curvature), due to the simplicity of the problem setup. As such, it is recommended that these analyses are used for scenarios where the additional thermal induced effects are negligible.

Sub-frame analyses are typically two-dimensional in nature. An example of a sub-frame is shown in Fig. 2.20, which shows a two-dimensional frame of a building exposed to in-plane actions (p-delta effects). Due to the interactions between the elements a more realistic structural behavior may be captured with this structure than can be obtained from the single-element analyses. Element temperature distributions throughout the structure may be obtained similarly to what is described for single-member analysis. The two-dimensional setup allows the frame to account for the effects of restrained thermal expansion in the plane of the frame. Additional

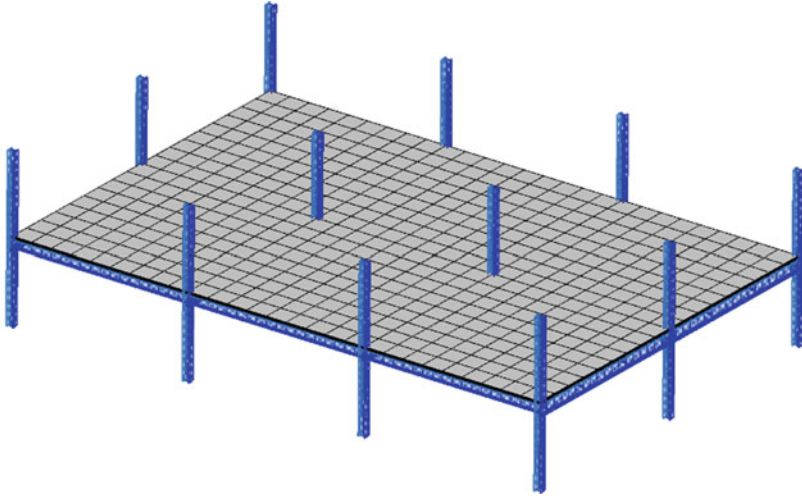
**Fig. 2.20** Sub-frame model

considerations include nonlinear material behavior and geometric nonlinear behavior. The frame can also be used to investigate the stability of the structure as well as explore alternative load paths as parts of the frame lose strength and stiffness. However, it is unable to capture the effects of thermal expansion or restraints in the direction perpendicular to the plane of the frame. It should be noted that fires burn in a three-dimensional space, and the transfer of heat throughout the structure is also three-dimensional. This implies that the use of 2D sub-frames as shown in Fig. 2.20 does not adequately account for loads or the behavior of the structure in the third dimension [59]. Thus, particular care should be taken when sub-frames are being used for analyses.

As observed from the previous section, sub-frame models are deficient in structural fire engineering analyses as thermal and mechanical effects in the third (perpendicular) direction cannot be accounted for. Thus full-frame analyses offer the solution to the problem. A typical full-frame model is shown in Fig. 2.21.

The effect of a fire that occurs underneath any of the structural bays shown in Fig. 2.21 can suitably be interpreted in terms of the thermal exposure of all elements in its vicinity (including slabs). For typical fully developed fire exposures it is assumed that the structural elements only experience temperature variations in their cross section and not along their axes. However, these may be modified when localized fires or fires that “travel” across a floor plate are encountered. The inclusion of the third dimension also allows slab effects to be considered in the analysis. This produces more representative behavior of a structure under fire conditions. The structural analyses are performed by the use of finite elements, as a number of thermophysical and mechanical properties need to be incorporated into the model.





**Fig. 2.21** Full-frame model

## References

1. ASTM. (2016). *E119-16a standard test methods for fire tests of building construction and materials*. ASTM International.
2. UL Fire Resistance Directory. (2015). Volume 1, Northbrook, IL: UL.
3. Reed, S. A. (1896) Work of the committee of fire-proofing tests. *Journal of the Franklin Institute*, 192(851), 322–335.
4. Andrews, Jaques and Rantoul. (1891). Tests of fireproof arches. *The American Architect and Building News*, 195–201.
5. Constable, S. (1897) Comparative standard fireproof floor tests of the new york building department. *The Engineering Record*, 337–340; 359–363; 382–387; 402–440.
6. Himmelwright, A. (1898). Fireproof Construction. *The Polytechnic*, 167-175.
7. Hutton, F. (1900). *Heat and heat engines*. Wiley, 611pp.
8. Gales, J., Bisby, L., & Maluk, C. (2012). Structural fire testing – Where are we, how did we get here, and where are we going? In *Proceedings of the 15th International Conference on Experimental Mechanics, Porto, Portugal*, 22 pp.
9. Woolson, I., & Miller, R. (1912). Fire tests of floors in the United States. In *International Association for Testing Materials 6th Congress*, New York.
10. Abraham, L. A. (1900). *Himmelwright's testimony, report of the special Committee of the Assembly, appointed to investigate the public offices and departments of the City of New York*. Albany.
11. Henning, G. (1905, May 2). To the editor of the New York Times.
12. Ingberg, S. (1921). *Fire tests of building columns, Technologic paper 184*. National Bureau of Standards, Washington
13. Ingberg, S. (1928). Tests of the severity of building fires. *NFPA Quarterly*, 22, 43–61.
14. Sachs, E. (1906). *Fire tests with floors: a floor of reinforced concrete on the coignet system*, 28pp.
15. Law, A., & Bisby, L. (2020). The rise and rise of fire resistance Fire Saf. J. <https://doi.org/10.1016/j.firesaf.2020.103188>

16. Jeanes, D. (1982, April 26–30). Predicting fire endurance of steel structures. In *American Society of Civil Engineers (ASCE) National Convention*, Las Vegas, Nevada. Preprint 82-033.
17. Ryan, J., & Robertson, A. (1959). Proposed criteria for defining load failure of beams, floors and roof constructions during fire tests. *Journal of Research of the National Bureau of Standards-C, Engineering and Instrumentation*, 63(2).
18. ASTM E 119. (1971). *Standard test methods for fire tests of building construction and materials*. ASTM International.
19. ASTM E 119. (2016). *Standard test methods for fire tests of building construction and materials*, ASTM International.
20. UL Fire Resistance Directory. (2015). Underwriters Laboratories, Northbrook, IL.
21. American Institute of Steel Construction (AISC). (2016). *AISC Standard 360-16, Appendix 4*, Chicago, IL.
22. Bailey, C., Lennon, T., & Moore, D. (1999). The behaviour of full-scale steel-framed buildings subjected to compartment fires. *The Structural Engineer*, 77(8).
23. LaMalva, K. J. (2017, August). Reexamination of restrained vs. unrestrained. *FPE Extra, Issue #20, Society of Fire Protection Engineers*
24. Carter, C. J., & Alfawakhiri, F. (2013, September). *Restrained or unrestrained?* Modern Steel Construction.
25. Gross, J., et al. (2005). *NIST NCSTAR 1-6B: Fire resistance tests of floor truss systems, federal building and fire safety investigation of the World Trade Center disaster*. National Institute of Standards and Technology.
26. ASCE/SEI 7-16. (2016). *Minimum design loads and associated criteria for buildings and other structures*. American Society of Civil Engineers: Structural Engineering Institute.
27. LaMalva, K. J. (2017). Chapter IV-9: Fire design. In *Architects guide to structures*. Routledge.
28. International Building Code 2015, International Code Council.
29. International Existing Building Code 2012, International Code Council.
30. ASCE/SEI/SFPE 29. (2005). *Standard calculation methods for structural fire protection*. Structural Engineering Institute, American Society of Civil Engineers.
31. Harmathy, T. (1965). Ten rules of fire endurance rating. *Fire Technology*, 1(2).
32. LaMalva, K. J. (2014). U.S. efforts toward standardization of structural fire engineering practice. In *Proceedings of the 10<sup>th</sup> International Conference on Performance-Based Codes and Fire Safety Design Methods*, Queensland.
33. Ellingwood, B., et al. (1982). Probability based load criteria: load factors and load combinations. *Journal of Structural Engineering, American Society of Civil Engineers: Structural Engineering Institute*, 108(5).
34. ISO 13824. (2009). *Basis of design of structures – General principles on risk assessment of systems involving structures*. International Organization for Standardization.
35. AISC 360. (2016). *Specification for structural Steel buildings*. American Institute of Steel Construction.
36. Ellingwood, B., & Bruce R. et al. (1980). *Development of a probability based load criterion for American National Standard A58: Building code requirement for minimum design loads in buildings and other structures*, NBS Special Publication 577, National Bureau of Standards.
37. LaMalva, K. J. (2017). Structural fire protection’s shifting paradigm. *Fire Protection Engineering, Issue #74*, Society of Fire Protection Engineers, Q2.
38. SFPE. (2007). *Engineering guide to performance-based fire protection* (2nd ed.), Society of Fire Protection Engineers.
39. SFPE. (2009). *Guidelines for peer review in the Fire protection design process*. Society of Fire Protection Engineers.
40. LaMalva, K. J. (2018, January). Developments in structural fire protection design - a U.S. perspective. *The Structural Engineer*, 96, Institution of Fire Engineers.
41. SFPE. (2003). *Engineering guide to human behavior in fire*. Society of Fire Protection Engineers.

42. NFPA. (2013). *557: Standard for determination of fire loads for use in structural fire protection design*. National Fire Protection Association.
43. SFPE S.01. (2011). *Engineering standard on calculating Fire exposures to structures*. Society of Fire Protection Engineers.
44. SFPE. (2014). *S.02: Engineering standard on the development and use of methodologies to predict the thermal performance of structural and fire resistive assemblies*. Society of Fire Protection Engineers.
45. Eurocode 1. (2001). *Basis of design and actions on structures, part 1.2: Actions on structures – Actions on structures exposed to fire, ENV 1991-1-2*. CEN.
46. SFPE G.06. (2011). *Engineering guidelines for substantiating a fire model for a given application*. Society of Fire Protection Engineers.
47. Ellingwood, B., & Corotis, R.. (1991). Load combinations for buildings exposed to fires. *Engineering Journal*. American Institute of Steel Construction.
48. NFPA. (2021). *5000: Building construction and safety code*. National Fire Protection Association. Quincy, MA.
49. NFPA. (2021). *101: Life safety code*. National Fire Protection Association, Quincy, MA.
50. ASCE/SEI. (2018). *Manual of practice no. 138: Structural fire engineering*. American Society of Civil Engineers: Structural Engineering Institute, Reston, VA.
51. ASCE/SEI. (2020). *Design guide (Performance-based structural fire design: Exemplar designs of four regionally diverse buildings using ASCE 7-16, Appendix E)*. American Society of Civil Engineers: Structural Engineering Institute and Charles Pankow Foundation. <https://ascelibrary.org/doi/book/10.1061/9780784482698>
52. Buchanan, A., & Abu, A. (2017). *Structural design for fire safety* (2nd ed.). Wiley.
53. Carlson, C., Selvaggio, S., & Gustaferro, A. (1965). A review of studies of the effects of restraint on the fire resistance of prestressed concrete. Portland Cement Association Research Department Bulletin 206, Portland Cement Association (USA)
54. Wang, Y., Burgess, I., Wald, F., & Gillie, M. (2012). *Performance-based fire engineering of structures*. CRC Press.
55. British Steel. (1999). *The behaviour of multi-storey steel framed buildings in fire*. Swinden Technology Centre.
56. Purkiss, J., & Li, L. (2014). *Fire safety engineering design of structures*. CRC Press.
57. Bisby, L. (2016). *Structural mechanics, SFPE handbook of fire protection engineering* (5th ed., pp. 255–276).
58. CEN. (2005b). *Eurocode 3: Design of steel structures - Part 1-2: General rules – Structural fire design. EN 1993-1-2*. European Committee for Standardization.
59. Wang, Y. C. (2002). *Steel and composite structures: Behaviour and design for fire safety*. Spoon Press.

# Chapter 3

## Keys to Successful Design



Martin Feeney, Kevin LaMalva, and Spencer Quiel

### 3.1 Project Conception

The adoption of a structural fire engineering approach for a given project usually hinges on the skill and care of the designer to properly introduce this alternative approach to project stakeholders. In many ways this is a marketing exercise to convince stakeholders of the merits and applicability of this nonconventional approach. Oftentimes, project stakeholders are not familiar and/or have no experience with the application of this approach, which can make this exercise evermore difficult. However, there are certain steps that the designer can take to increase the odds of successful adoption as described herein.

#### 3.1.1 Education of SFE Approach

In order to convince project stakeholders that adoption of a structural fire engineering approach for a given project is advantageous and appropriate, it is important for the designer to take a step back and educate these individuals on the general theory

---

M. Feeney  
Holmes Fire, Auckland, New Zealand  
e-mail: [Martin.Feeney@holmesfire.com](mailto:Martin.Feeney@holmesfire.com)

K. LaMalva (✉)  
Warringtonfire, Boston, MA, USA  
e-mail: [kevin.lamalva@warringtonfire.com](mailto:kevin.lamalva@warringtonfire.com)

S. Quiel  
Civil and Environmental Engineering Department, Lehigh University, Bethlehem, PA, USA  
e-mail: [seq213@lehigh.edu](mailto:seq213@lehigh.edu)

and basics of this alternative approach. Oftentimes, this requires devoted “lunch and learn” presentations to both the project architect and the relevant building authority. Each of these presentations is usually needed since both parties must first be amenable to the approach before it can be formally adopted as described in Sect. 3.3.2.

Overall, presentations to the stakeholders of a given project should describe the following aspects of structural fire engineering:

- Design Problem.
  - *What are we trying to solve?*
- Design Options.
  - *What is the difference between standard fire resistance design and structural fire engineering?*
- Industry Codes and Standards.
  - *What are the design constraints and requirements?*
- Limitations of the Default Approach.
  - *Why not simply follow the prescriptive requirements and be done with it?*
- Benefits of the Alternative Approach.
  - *What justifies the added engineering costs and time?*
- Exemplar Projects.
  - *Has this approach been used successfully in the past?*

For the project architect, it is advantageous for the designer to present the structural fire engineering approach primarily in terms of the value-added benefits (e.g., design freedom and cost optimization) that it can bring to the given project. For the building authority, these concepts may also be somewhat important, but the enhanced confirmation of intrinsic fire safety should be the focal point of the presentation. Obtaining endorsement of the alternative approach by the building authority early in the process can also alleviate any concerns from the project architect concerning heightened approval risks and liability.

Presenting structural fire engineering as a desirable alternative to simple prescriptive code compliance can be an art as much as it is a science. Using simple and straightforward imagery is a great tool to convey the basic concepts of the alternative approach to project stakeholders. Conversely, presenting the complex minutia of the technology may turn off the stakeholders, and decrease the chance that they will retain important concepts.

As an example of useful imagery for stakeholder presentations, Fig. 3.1 is a simple and convincing image that illustrates a major downside of using the code default standard fire resistance design approach. Specifically, this image highlights how this approach essentially decomposes a structural system into isolated parts

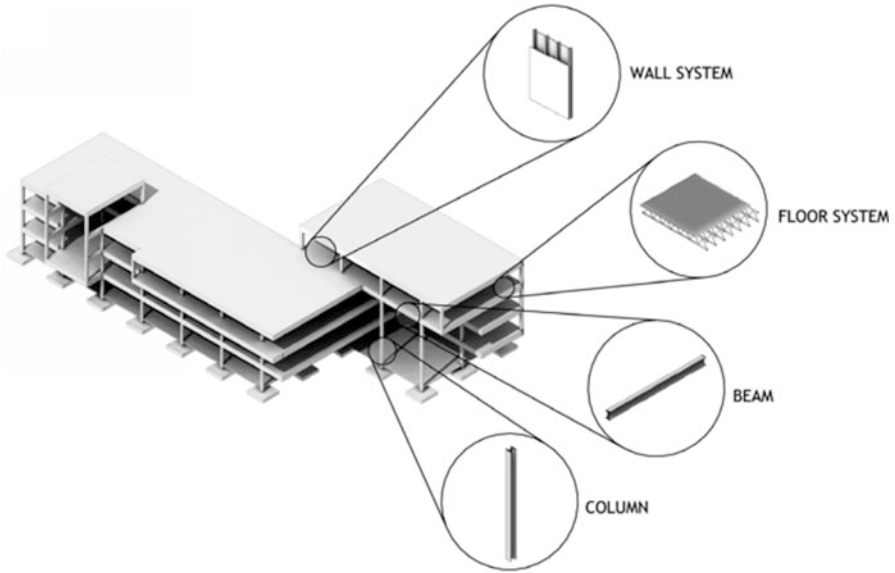
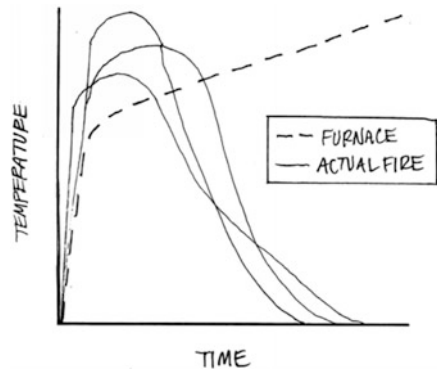


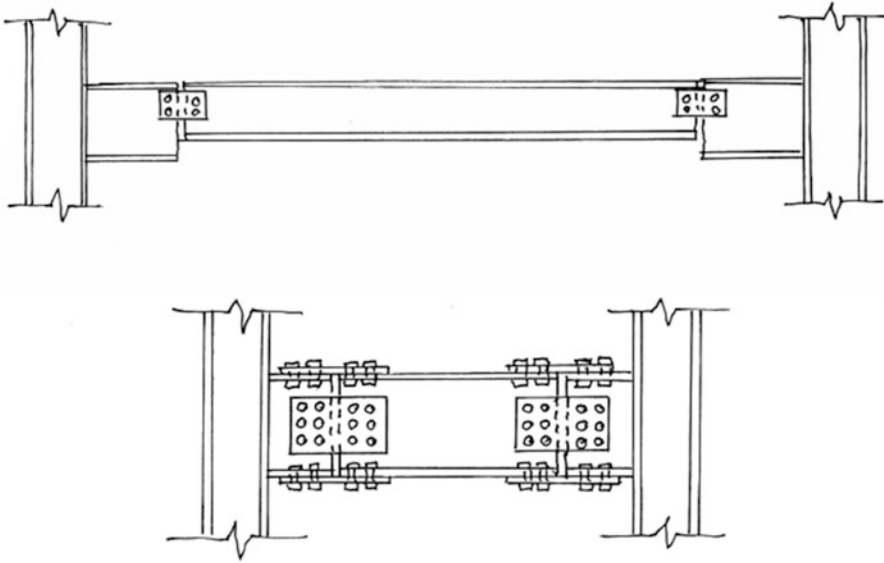
Fig. 3.1 Structural system decomposition for furnace testing [1]

Fig. 3.2 Comparison of furnace and actual fire exposures [1]



without interconnectivity for fire test qualification purposes. Moreover, this level of dissection effectively removes any appreciable contemplation of structural system performance from the design consciousness. Hence, project stakeholders would not be affirmatively informed about the risk of structural failure due to fire. This basic understanding is particularly important for building authorities, who must weigh the level of confirmation and safety actually provided by this approach as compared to a proposed structural fire engineering approach.

As it pertains to the treatment of the design hazard, Fig. 3.2 presents a simple comparison between standard fire resistance design and structural fire engineering that project stakeholders can appreciate. Whereas the standard fire resistance design

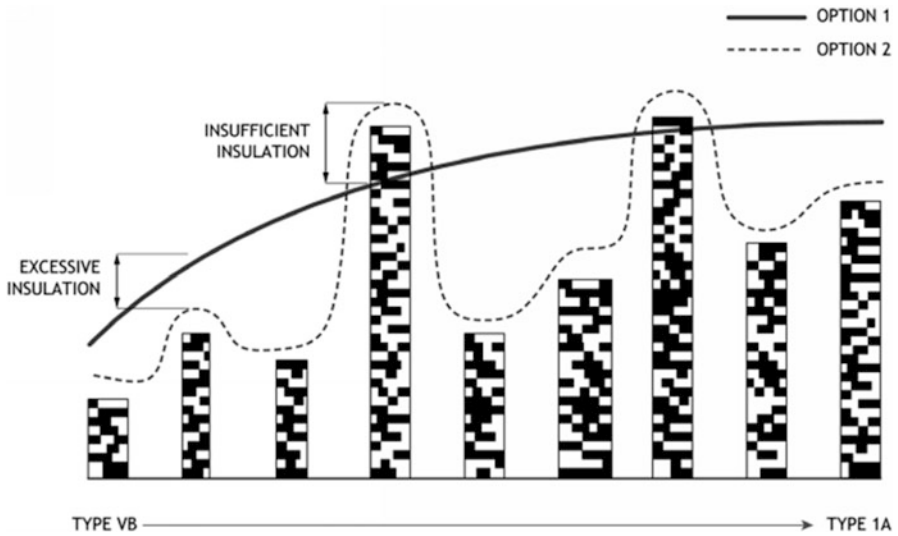


**Fig. 3.3** Comparison of hypothetical steel structures [1]

approach only considers an arbitrary furnace heating exposure, structural fire engineering contemplates credible and realistic fire exposures for the given project, accounting for special hazards (e.g., dense fuel load concentrations) as well as the cooling phase of a given fire exposure.

As it pertains to the prediction of structural behavior during fire conditions, Fig. 3.3 presents a useful example that demonstrates the structural performance indeterminacy of standard fire resistance design. Specifically, two hypothetical steel structures are shown, which have widely varying structural robustness to fire exposure. However, if both of these assemblies are protected with a conventionally-qualified insulation system (e.g., UL Design No. N706), they would both be deemed to provide 2 h of fire resistance. This illustration can be particularly striking for building authorities who may not appreciate the indeterminacy of the default approach, while also highlighting how structural fire engineering explicitly contemplates the true structural robustness to fire. Such understanding can help building authorities become comfortable with the alternative approach since it provides enhanced confirmation of intrinsic fire safety.

Of particular interest to architects, Fig. 3.4 is a useful illustration that compares the economy of structural fire engineering to standard fire resistance design as it pertains to applied insulation. Specifically, a hypothetical sampling of the building population is represented that ranges across the horizontal axis from the least restrictive to the most restrictive construction types. As shown, standard fire resistance design (Option 1) requirements for applied insulation are based exclusively on the construction-type classification, irrespective of the inherent structural system robustness to fire exposure. Alternatively, insulation is more rationally allocated



**Fig. 3.4** Comparison of the required level of insulation [1]

when employing structural fire engineering, for the inherent robustness of the structural system of each individual building is accounted for.

In addition to architects, Fig. 3.4 may be particularly striking to building authorities. Since standard fire resistance design prescribes the level of insulation protection based exclusively on the construction-type classification of buildings, the in situ performance expectation of a qualified protection scheme is highly dependent on non-contemplated aspects of the structural system design (e.g., seismic detailing). Consequently when standard fire resistance design is employed, this figure illustrates how the vulnerability of buildings to structural failure from fire is presumably variable across different jurisdictions, which have varying wind, seismic, and other structural design requirements. Conversely, structural fire engineering accounts for the variable robustness of host structural systems, and tailors protection schemes accordingly.

### 3.1.2 Stakeholder and Authority Goals

While presenting the merits of structural fire engineering to project stakeholders, the designer should be keen to derive the basic design goals for the given project, which usually differ somewhat among the various stakeholders. The key for the designer is to identify goals that are mutual among the stakeholders, and develop strategies to address certain goals that are exclusive to individual stakeholders, while still upholding the other goals. For instance, competing design goals between insulation economy and added building resilience to fire exposure should be rectified at a



conceptual level early in the design process, including discussion of specific strategies to help satisfy both. For instance, added insulation to steel columns may be specified as a perceived trade-off for removal of insulation from secondary floor beams. Notwithstanding, the overall structural system must perform adequately under fire exposure per the performance objectives.

Design goals of the building owner often include some of the following:

- Allowances for nonconforming existing building construction.
- Reduction and/or elimination of applied fire protection for economy.
- Expedition of critical path approval roadblocks.
- Mitigation of constructability issues.
- Building resilience to allow for efficient reconstruction following a fire.
- Building resilience to reduce business interruption.

Design goals of the project architect often include some of the following:

- Allowances for unprotected structural members (“expressed structure”).
- Allowances for specific building code variances (e.g., open atria).
- Allowances for nonconventional architecture (e.g., unlisted fire protection assemblies).

Design goals of building authorities often include some of the following:

- Confirmation of safe occupant evacuation to a public way.
- Enhanced protection of firefighting staging areas (e.g., stairwells).
- Prevention of disproportionate structural collapse.
- Understanding of structural failure states (i.e., the points of ultimate failure) to inform the overall fire risk mitigation strategy.

The stakeholder design goals in conjunction with minimal safety metrics provided by industry standards (e.g., ASCE/SEI 7 Appendix E) should define the structural fire engineering analysis scope. Formal definition of this scope is discussed in Sect. 3.2.

## 3.2 Project Definition

The project definition sets realistic expectations and ensures uniformity throughout the project. Performance objectives are a key area of negotiation, which may govern the level of engineering rigor/time required. Project definition does not provide definitive answers to the stakeholders regarding the structural fire protection solution, but the process may provide educated forecasts. Aspects of this design stage are examined in more detail below.

### 3.2.1 Performance Objectives

Explicit performance objectives for use in structural fire engineering are not provided in all building codes. However, Section E.4 of ASCE/SEI 7 [2] provides a US-based industry consensus on mandatory performance objectives. These performance objectives provide a minimum level of safety and are meant to apply in all cases, irrespective of project documentation and engineering judgment. Overall, these performance objectives are meant to uphold the intended functionality of occupant egress features during a fire event. Specifically, structural support of building egress routes must be maintained for a period of time necessary to ensure a safe and complete evacuation of building occupants to a public right of way. Also, structural support of building refuge areas must be maintained through full fire burnout and cooling.

Building codes limit egress travel distances to exits (e.g., stairways), but generally do not limit the total evacuation time. As the vertical remoteness of occupants from the point of discharge to a public way (e.g., a public street) is increased, the time required to evacuate the building will increase. Unlike standard fire resistance design, structural fire engineering explicitly contemplates the consequences of increased occupant evacuation times, and the reliance on building refuge areas to meet other code requirements [3].

In order to demonstrate the adequacy of occupant egress routes per the mandatory performance objectives of ACSE/SEI 7, the designer must employ an “ASET vs. RSET” analysis. The Available Safe Egress Time (ASET) should be determined by analyzing the endurance of the structural system to fire exposure. The Required Safe Egress Time (RSET) should be determined by analyzing the time it would take occupants to travel safely to refuge areas within the building or exit the building to a public way.

Aside from the mandatory performance objectives pertaining to occupant life safety, the provisions of ASCE/SEI 7 Appendix E deem all other performance objectives as discretionary. Accordingly, the need for and scope of such additional performance objectives must be agreed upon by the project stakeholders. For certain projects, the stakeholders may agree that fulfillment of the mandatory performance objectives alone is sufficient. In other cases, one or a number of the discretionary objectives may be enacted.

Discretionary performance objectives may include one or a number of the following for a given project:

- Prevention of any structural collapse.
- Prevention of collapse of the primary structural system only (i.e., columns, beams/girders that connect directly to columns, and other critical members).
- Protection of firefighting staging areas.
- Structural support of fire-resistive barriers.
- Containment of hazardous materials.
- Sustain business operations in unexposed building areas.
- Other project-specific objectives.

It should be noted that satisfaction of the mandatory performance objectives per ASCE/SEI 7 Appendix E may implicitly enhance performance pertaining to other objectives. For instance, added protection and robustness of structural elements supporting exit stairways in order to provide for safe occupant evacuation may implicitly provide a structurally safe staging area for firefighting. Similarly, designated areas of refuge that are designed to withstand fire burnout could also function as firefighter staging areas.

### ***3.2.2 Structural System Scope***

The extent of the given structural system that needs to be explicitly evaluated is usually governed by the anticipated behaviors that could result from heating due to fire exposure. Notable behaviors and their implications are examined herein.

The design of a building to resist fire will consider the following systems: (1) primary structural system, (2) secondary structural systems, and (3) nonstructural components and systems. The primary structural system (gravity and lateral) provides the last line of defense against fire-induced collapse and should be evaluated using appropriate levels of conservatism. Postfire damage to primary structural elements that withstand the fire event itself should be carefully considered, since this damage may adversely impact the structure's ability to subsequently resist other extreme loads (wind, seismic, snow, etc.). Structural fire design of secondary structural systems such as floors and non-gravity walls potentially offers more customizability. Collapse or severe damage to these systems during or following a fire may induce a more widespread progressive or disproportionate collapse of the primary structural elements. If they are able to survive the fire, secondary systems could be designed for acceptable damage tolerances based on the use of the building, the ease or difficulty associated with repair or replacement, or the owner's tolerance for loss of postfire functionality.

Structural fire design of the primary and secondary structural systems relies on the appropriate selection of the extent of the subassembly used for analysis as well as the boundary conditions placed at the extents. Realistic and/or conservative consideration of restraint of thermal expansion will depend on the degree of restraint provided by the boundary conditions. The designer should consider whether to model only the structural subassembly that will be exposed to the design fire scenario or to also include adjacent portions that are not directly heated by the fire. The use of boundary conditions that are closer to the heated elements rather than adjacent cool portions of the structure can provide either too much or too little restraint of thermal expansion and weakening-induced deflections. For example, the design of a single interior column for a fire surrounding it could in many cases appropriately consider the column by itself with boundary conditions applied to its ends. Conversely, a heated perimeter column can be pushed outward by the heated floor system and thus develop bending moment by providing thermal restraint to the floor. The design of the perimeter column as well as the heated floor system could

benefit from a modeling approach which includes both (or more) elements in a subassembly. The continuity conditions or lack thereof at the extents of the floor system model (including its framing connections, slab properties, etc.) should also be considered.

An evaluation of the structural system during the heating and cooling phase of a structural design fire should include thermally induced failure modes. When a structural member reaches its peak temperature, it may not be the failure point, due to the interaction of temperature-dependent material properties and thermally induced load effects. Failure modes may include (a) component failure, (b) assembly failure, (c) subsystem failure, (d) partial collapse, and (e) global collapse. More than one failure mode may occur. For example, a component or assembly failure, such as column buckling or connection failure, may lead to a partial or global collapse. Time-dependent evaluation of thermal effects should be performed using temperature-time histories of the structural members and assemblies from thermal analyses. For instance, axial tensile forces in floor beams can be developed during the cooling phase of a fire as the beam contracts. The connections may also experience an increase in tensile force, potentially leading to connection damage or failure. Heated structural members may also experience deflections that are an order of magnitude greater than deflection limits normally anticipated for structures under ambient conditions. Large deflections may induce forces in adjacent structural assemblies (e.g., connections) or adversely impact nonstructural components that inhibit fire spread (such as creating gaps in fire stops between floors or in fire-rated compartment partition).

Nonstructural systems are typically fire rated via standard testing, and calculations of their fire resistance are not included as part of the scope outlined here. However, nonstructural components can be compromised or damaged by fire-induced deflections of the primary and secondary structural elements. Performance-based design considerations for nonstructural elements could include the following objectives: (1) avoid damage to fire-rated compartmentation barriers or other firefighting systems and (2) avoid damage to other peripheral façade or architectural elements. If compartmentation partitions are compromised during the fire, the fire may spread and the design fire scenarios will need to be adjusted accordingly. These systems will usually need to be replaced after being exposed to fire, and the impact of postfire deflections would only be a consideration for elements that were not directly exposed. Damage to peripheral systems may lead to falling debris during the fire event and/or necessitate additional postfire repair or replacement.

### ***3.2.3 Fire Hazard Scope***

It is fundamentally important to understand how the fire hazard is accounted for in the structural fire engineering design. Historically, the fire hazard has not been quantified or even characterized in any way and prescriptive values of code-required

fire resistance ratings have been provided as the deemed-to-comply method for achieving compliance with building regulations. This historical oversimplification of the influence of fire hazard on structural performance is a predominant reason why the structural fire engineering design approach is not more readily embraced without an education process as outlined in Sect. 3.1.1.

To fully realize the opportunities from a structural fire engineering approach, a clear definition of the scope of the fire hazard is required. The description of the fire hazard should concentrate on factors which influence the characteristics of the fire itself and the fire environment it creates in an enclosure, without attempting to second guess the impact of the fire on the structure or the likelihood or consequences of adverse structural performance. While these other factors (structural response, likelihood, and consequence of failure) are obviously very important, it is helpful to consider these separately from the scope of defining the fire hazard. Through an iterative process, a review is needed of the input values and assumptions which define both the fire hazard and the structural response, in order to test for consistency and validity in an overall risk assessment sense.

At its most basic level, a nonscientific approach is to define an assumed level of fire hazard based on different occupancy types. For example, an expected level of structural fire performance may be associated with residential uses and accommodation uses, a different value for car parking areas, another for commercial uses such as workplace/office, another for retail/shops/hospitality uses, and so on. This approach is based on an assumed correlation between occupancy/building use and general magnitude of fuel load assumed to be present in the building in the areas associated with that occupancy type. While this approach recognizes at a very broad level one of the factors (fuel load) on the fire hazard and consequently on structural performance, it misses a number of other factors which are equally important in defining the fire environment for a structural fire engineering assessment.

Most practical structural fire engineering analyses are concerned with the impact of a fire which has reached a state (at least locally) of full development. In small enclosures, this fire state is often referred to as flashover—a fire condition characterized by a well-mixed fire environment where the fire temperature is more or less uniform in the enclosure, almost all of the fuel in the room is exposed to high levels of thermal radiation, most fuel surfaces are undergoing high levels of pyrolysis, and accordingly the enclosure is filled with more unburnt fuel than the available oxygen supply can react with. Accordingly, this condition is accompanied by large quantities of soot and unburnt fuel released through openings, to burn as external flames from windows or roof openings when the hot fire gases reach the outside air.

The concept of flashover as it applies to small enclosures is increasingly misleading as the size of the enclosure increases. Experimental tests and observations of natural fires in large enclosures show that fires do not create uniform fire conditions nor simultaneously consume all of the available fuel load in a space when either the floor area or the enclosure height and volume are a few times greater than those of the enclosure used for the standard fire test.

An appropriate definition of the scope of the fire hazard associated with fully developed fires takes into account a wide range of factors which together define:

- Where the fire is likely to occur (e.g., which room, which level in the building).
- Whether the fire size is likely to be controlled by some physical limit (such as the extent of a fire cell, or an inherent limit on fuel load or limit on available oxygen to sustain a certain rate of heat release).
- The amount of fuel load available in the enclosure of fire origin.
- The area, dimensions, location, and number of openings to the outside air which are present at the start of the fire or which might be created by the fire severity (e.g., fallout of glass windows).
- The thermal inertia and thermal insulation properties of the construction (ceiling, walls, and floor) bounding and forming the enclosure of fire origin.

Some structural fire engineering problems need to consider a fire environment prior to the fire reaching this fully developed burning state. These situations are less common and require an even more careful specification of the factors influencing fire growth as the particular definition of the fire hazard is more strongly influenced by time-dependent factors such as fire growth rate, and increasing variability of the factors influencing available oxygen supply prior to fire flashover.

For fully developed fires, the combination of these factors listed above can be used to define the fire hazard in a number of ways. Some building codes and simplified design methods take advantage of the fact that for most fire design problems the ranges of the variables for some of the factors listed above are relatively narrow. Depending on the complexity and precision intended by the design approach, “typical” values or assumed “upper limits” for design purposes are listed for common types of construction. These assumptions simplify the definition of the fire hazard in quantitative terms by reducing the number of input variables and equations needed to describe the fire hazard.

To test the influence and sensitivity of the structural fire engineering analyses in response to uncertainty in defining the scope of the fire hazard, the most important factors to concentrate on are those which influence the fire temperature within the enclosure as a function of time:

- The magnitude of fire rate of heat release.
- The ventilation available to the fire.
- The duration of the fire (at its associated peak heat release rate), hence the time at which the fire heat release rate diminishes.
- The rate of cooling of the fire enclosure.

The key influencers of these parameters are the total quantity and distribution of fuel load in the enclosure; the dimensions, total area, and position of openings from the fire enclosure to the outside; and the rate at which the fuel is assumed to be consumed (and whether this is strongly influenced only by the amount of enclosure fire ventilation, or by other factors such as fuel load spatial distribution and location of fire start).

For the other factors, assumptions are usually made which apply for a range of fire scenarios which are constant for a given fire scenario. For example, the thermal

properties of the enclosing surfaces are usually assumed not to vary over the fire duration.

In its most specific form, a closed-form definition of a “structural design fire” is obtained, where each of the factors described above is defined by a range of values, or by single input values. For practical design purposes, varying levels of this type of parameter definition are required to limit the scope of the fire hazard so that the structural fire engineering process is manageable, sufficiently accurate, and appropriately cautious while retaining enough control over the range of variables to be confident of acceptance for regulatory compliance.

Examples of this specification of the structural design fire include the parametric time-temperature design fire given in the Eurocode [4]. The parametric equations in Annex A of the Eurocode 1 characterize the growth, fully developed, and decay phase of fire exposure, with the following inputs:

- Total area of enclosure boundaries [ $\text{m}^2$ ]:
  - *Reasonable to consider the area of a single floor surrounded by exterior walls and/or fire resistance-rated construction, assuming no change from ambient (e.g., change in compartment geometry created by structural deformation).*
- Total area of ventilation openings [ $\text{m}^2$ ]:
  - *Reasonable to consider the maximum area considering all glazing to be broken, and assuming no change from ambient (e.g., new openings created by structural deformation). Although, a sensitivity study should be conducted assuming only a fraction of the glazing breaks.*
- Height of ventilation openings [m]:
  - *Reasonable to consider the weighted average of all ventilation openings, assuming no change from ambient (e.g., new openings created by structural deformation).*
- Density of enclosure boundaries [ $\text{kg}/\text{m}^3$ ]:
  - *Reasonable to consider the ambient value for gypsum board, concrete, and others.*
- Thermal conductivity of enclosure boundaries [ $\text{W}/\text{mK}$ ]:
  - *Reasonable to consider the ambient value for gypsum board, concrete, and others.*
- Specific heat of enclosure boundaries [ $\text{J}/\text{kgK}$ ]:
  - *Reasonable to consider the ambient value for gypsum board, concrete, and others.*
- Distributed fuel load [ $\text{MJ}/\text{m}^2$ ]:
  - *Reasonable to consider a value derived from the NFPA 557 standard, perhaps based upon on a particular consensus reliability fractile.*

- Correlation uncertainty factor [unitless]:
  - *May be prudent to include a factor which accounts for an imperfect model. However, there is currently no industry consensus on this aspect.*

### 3.3 Project Initiation

Once the designer has properly defined the structural fire engineering analysis scope (as discussed in Sect. 3.2), documentation of this scope and formal agreement between the stakeholders is an important next step. Speeding through this process without the necessary care can lead to confusion and unmet expectations later on in the project, which may result in significant project cost and schedule overruns. If project stakeholders are overly eager to “start the analysis,” it may be tempting for a designer to rush this process. Hence, it is important for the designer to properly educate the stakeholders on the basics of this alternative approach (as discussed in Sect. 3.1.1) prior to reaching this stage in the given project. Otherwise, project stakeholders may hold unrealistic expectations concerning the analysis time frame, unlike their routine acceptance of traditional structural engineering scopes.

#### 3.3.1 Design Metrics and Assumptions

Once the high-level goals of the project stakeholders are identified (as discussed in Sect. 3.1.2), the designer is then equipped to synthesize these goals into measurable design metrics and assumptions that will define the “ground rules” for evaluation of the prospective structural fire engineering design. The designer should enforce the necessary level of conservatism (commensurate on the level of understanding/knowledge/data) for key design metrics and assumptions.

Design metrics and assumptions may pertain to the following aspects of the structural fire engineering analysis:

- Allowable deflection of occupant egress routes.
- Allowable deflection/slope of accessible routes.
- Allowable deflection of occupant refuge areas.
- Floor deflection limit (indicative of runaway loss of stability).
- Stress/strain limit of connection components at elevated temperatures (indicative of material fracture or runaway strain).
- Assumed material yield point at elevated temperatures (e.g., percent strain offset method).
- Beam deflection limit for the mechanical integrity of spray-applied fire-resistive material (SFRM).
- Fire intensity limit for the mechanical integrity of SFRM.
- Beam deflection limit for mechanical integrity of fire barrier walls (for compartmentation).



- Composite construction shear stud behavior representation (stud yielding in combination with local concrete crushing).
- Strain limit of concrete floor reinforcement for stable tensile membrane action.
- Ultimate concrete slab deflection limit for stable tensile membrane action.
- Concrete temperature limit for the onset of spalling accounting for the mix design, moisture content, and presence of special additives.
- Nonlinear wood char rate for the anticipated fire exposures.
- Allowable axial thrust and rotation for mass timber connections.
- Timber temperature limit for stability of connections.
- Timber temperature limit for mechanical integrity of timber adhesive joints/connections (e.g., laminated veneer lumber).

Due to the esoteric and complex nature of many analysis metrics and assumptions in structural fire engineering, the building authority may require the involvement of an engineering third party to review these for accuracy and soundness to industry standards. If this is the case, it is advantageous for the designer to send the engineering third party periodic updates and deliverables to identify any areas of possible disagreement early in the process to help move the project along smoothly.

### ***3.3.2 Design Brief Documentation***

As discussed in Sect. 3.1.1, education about structural fire engineering can help to convince project stakeholders to adopt this alternative approach for projects. Once this adoption is achieved, it is important for the designer to develop a design brief document in accordance with the relevant SFPE standard [5]. This type of document establishes and memorializes the performance objectives for the given project, and confirms the metrics by which the proposed design will be evaluated. Once the design brief is composed, it should be reviewed by all stakeholders, revised if necessary, and then signed by all stakeholders. Henceforth, this document serves as a binding agreement between the stakeholders, which is critical given the performance-based nature of the approach and latitude provided to the design team to meet the performance objectives.

It is recommended that salient design metrics (e.g., allowable deflection of occupant egress routes) be agreed upon by the project stakeholders and documented in a design brief document, especially those that are not explicitly defined in industry standards. This is particularly important and should be conservative since the available literature is not robust enough to define generalized acceptance criteria for each of the various structural limit states for the full range of temperatures of interest in structural fire engineering.

The contents of a design brief document should include the following sections:

- Project Description.
- Document Review.
- Project Goals.

- Applicable Codes and Standards.
- Mandatory Performance Objectives (Industry Minimum).
- Discretionary Performance Objectives (Project Consensus).
- Structural Design Fire Scenarios.
- Key Assumptions.
- Acceptance Criteria.
- General Design Strategies.
- Analysis Tools.
- Deliverables and Schedule.

It is customary for the composition of the design brief document to be identified as a project scope item. However, the designer may choose to develop the design brief as part of the project proposal. The primary advantage to this approach is that it may decrease the risk of lost costs (consulting fees) for the owner/architect if the design brief is not eventually accepted by the building authority. As such, the designer would be required to perform such work at faith that the analysis moves forward, at which time the lost consulting costs could perhaps be recovered.

### ***3.3.3 Prevention of Scope Creep***

The most effective strategy to minimize scope creep is to communicate and clearly document the scope of the project in the design brief. In most cases, scope creep occurs because designers or the client (or both) have not clearly understood their scope limitations. If there is a need to redo design work, or investigate many more options or variations of an agreed design, the additional time or increased resources required to address these changes both alter the agreed design scope. Another common source of scope creep occurs when third parties assume that the structural fire engineering specialist will provide all of the answers to a wide range of information requirements, some of which might not be directly related to the scope of the original design assessment.

Common contributors to scope creep arise when:

- Structural fire engineers underestimate the number of input parameters for which there is a range of reasonable values and consequent outcomes, which all need to be evaluated. This is probably the most common source of scope creep, as the number of different analyses can increase exponentially for each realistic alternative that needs to be considered. Built-in conservatism early in the process and/or adoption of industry consensus judgments can help alleviate such risks.
- The structural fire engineer or the building authority or other regulatory review party does not have sufficient experience to know which design assumptions are suitably cautious (for design purposes) and which are merely alternatives, for which each alternative should be evaluated for potential adverse impact.
- Agreement cannot be reached when classifying evaluation methods for a range of design scenarios and structural fire analyses. In many cases, design scenario

variations can be evaluated semiquantitatively by comparing similar scenarios to a more challenging scenario which is evaluated quantitatively.

- In jurisdictions where structural fire engineering is relatively new, the building authority or other regulatory review party may not fully understand the aim and outcomes of a structural fire engineering analysis and require a much wider range of possible design scenarios to be documented even though these might have been previously agreed to be a subset of less challenging design cases. A common example of this is when the building authority or regulatory reviewer expects the analysis to consider a wider range of extreme design scenarios than is normally considered for similar buildings where structural fire engineering is not carried out (such as the simultaneous occurrence of a number of extremely low-probability loading conditions similar to an uncontrolled fire). Note that for some buildings and some design scenarios a more cautious range of design scenarios may be appropriate, depending on the outcome and consequences, and levels of tolerable risk in that regulatory environment.
- There is mismatch between client and designers about who is responsible for decisions around important fundamental inputs such as the range of occupancies to consider for the design, the agreed design loads, and/or the range of structural materials under consideration.
- There are different expectations concerning who is responsible for providing certain information (such as information about proprietary or design-build structural flooring types; design, documentation, detailing, and load capacity of connections; dimensioned plans).
- Expectations vary concerning the extent to which the design team will evaluate a range of design options in the early design phases.
- Contractors or clients expect that the structural fire engineer will fully specify all of the proprietary methods for fire protection coatings and systems that might be used in a project (when the structural fire engineer is expecting to provide a performance specification rather than a schedule of specific systems).

A further source of scope creep occurs when there is uncertainty about what the structural fire engineering designer is not doing. For example, other parties may not appreciate the clear distinction between assessing the performance of the structure to resist fire with or without various types of structural fire protection, and the consequent need—where structural fire protection is necessary—to specify the exact type of fire protection system. Although the structural fire engineer is involved with specifying the specific physical location and extent of structural fire protection, they may not be engaged or appropriately experienced to provide:

- A full specification for the range of fire protection systems selected.
- The detailed specification for their application.

The structural fire engineer may not be engaged as the party responsible for:

- Verifying correct application of the protection system to the structure (e.g., during the fabrication process, or on-site).
- Producing as-built documents of record.

- Providing the means for identifying structure in the completed building which is or is not provided with structural fire protection (and what type/specification/thickness).

On completion of a project the building owner or client may need to rely on plans to identify physically the fire-protected structure so that for any future works it is known what parts of the structure are fire protected and how. Producing these as-built documents at the end of the construction is another potential source of scope creep if the client has not engaged someone to provide these documents.

The common sources of scope creep in practice have been identified/summarized above, and should help proactive designers conduct preliminary stakeholder discussions and develop proposals that are more viable and preventative of unmet expectations. Such sources of scope creep are not necessarily unique to structural fire engineering, but may become amplified since this is a relatively new and emerging discipline within overall building design.

### **3.4 Design Implementation**

The optimum implementation of a structural fire engineering design depends on prior planning (per the sections above) and proactive engagement of design team members and stakeholders throughout the process. Accordingly, phased designs lend themselves well to such conditions. This section examines aspects of this design phase that require special attention and may govern the viability of a given design.

#### ***3.4.1 Design Team***

For a structural fire design, in addition to having members of the design team with the necessary skills and competence to carry out their particular engineering design roles, the members also need to understand the interrelationship between the fire engineering aspects and the structural engineering aspects of the inputs, problem specification, and sensitivity of outputs to various design assumptions. Fire engineering—and in particular the specification of the structural design fire conditions—is a relatively new engineering discipline compared to structural engineering. While the general physics of structurally challenging fires is reasonably well understood, there is no widespread agreement on exactly how to define input parameters for a suite of challenging design fires which capture a suitable range of potential fire conditions which might actually be experienced. There are a number of reasons for this, which all influence the skills needed for the members that make up the structural fire engineering design team:

1. Historically, fire engineers and structural engineers have evolved with different skill sets and via different education paths, which has resulted in most fire safety

engineers around the world not having a confident working knowledge of structural engineering concepts, load paths, structural redundancy, structural detailing, etc. Many fire safety engineers have a limited knowledge of structural material performance during fire. Similarly, many structural engineers have limited knowledge of the characteristics of a fire which might affect structural performance, and how different structure details and material types respond to fire attack. Some structural engineers also have limited knowledge of structural material performance during fire. Even in those few design and educational environments where engineers receive exposure to both the fire engineering and structural engineering aspects of structural fire engineering, the familiarity often extends only to the structural types, materials, and regulatory jurisdiction expectations that apply within a local region.

2. Another reason for this is the relatively small number of fires which prove challenging to structural performance and the even smaller number of these fires for which there is information available that describes those fire characteristics.

Accordingly, it is important to have design team members who:

- Are familiar with the structural design requirements that apply to a particular project and with structural engineering concepts in general.
- Understand the response of the structural material to fire.
- Appreciate the extent to which detailing may influence structural response and robustness when structures undergo inelastic deformations under fire exposure. In particular, it is valuable to have an understanding of how beam/column/floor systems interact through their connections.
- Understand the extent to which parts of structure may act compositely with other materials and elements and the effect this may have on structural response during fire (e.g., the extent that steel beams acting compositely with concrete floors; the participation of lateral force-resisting elements such as bracing to resist gravity loads or stabilize parts of the structural system weakened by fire exposure).
- Understand the fire safety regulatory requirements and the fire engineering strategy that applies for a particular project.
- Understand how any assumptions made by either the fire design strategy or the regulatory environment might influence assumptions made in the specification of the fire hazard or design fire scenarios.
- Understand how physical arrangements of enclosures such as size, height, volume, extent of ventilation openings, and interconnection of multiple floors can influence the assumptions made in the specification of a structural design fire.
- Are aware of various strategies available for protection of the various elements of a structure and the different material types. Depending on the way in which a structure is exposed to fire and the consequential effect, partial structural protection solutions may effectively mitigate the adverse effects of fire exposure.
- Appreciate the cost, constructability, and feasibility (in the local construction environment) of various methods of protecting the structure.

It is unlikely that all of these attributes will be fulfilled by only one or two members of the design team. Depending on the resources available for a particular project, the members who have input to the design team are likely to be structural engineers, fire safety engineers, architects and specifiers, construction engineers, cost consultants, and—where available—specialist structural fire engineers. Design team members who have a working knowledge of the other related design disciplines other than their own area of specialization (e.g., specialist structural fire engineers) will likely have the most valued input to the design team.

### ***3.4.2 Computational Resources***

Analysis techniques used to perform structural fire engineering design can range from simple closed-form calculations to complex finite element analyses (FEA). Simplified methods typically use lumped mass approaches to calculate heat transfer from the fire to the structural elements, and the mechanical response is modeled using single element or simplified subassembly calculations that rely on a broad set of assumptions (such as idealized boundary conditions and uniform temperature both along the length and across the section of the elements). Simplified methods of analysis may be sufficient when the scope of the structural fire engineering design is limited to single members and components rather than systems. The influence of the simplifying assumptions should be carefully considered, and the designer should provide adequate justification based on previous precedent or research. Simplified methods may also have value when used in the preliminary phases of a project to determine whether computationally demanding approaches are warranted.

Analytical methods applicable to structural fire engineering design are outlined in several existing standards and guidelines. For example, the Eurocode has several sections that are dedicated to the fire-resistant design of steel [6], concrete [7], and wood [8]. In the USA, AISC 360 Appendix 4 [9] provides equations for determining the strength of simply supported members in flexure, compression, and tension at elevated temperatures. However, AISC 360 Appendix 4 should not be relied upon exclusively for structural fire engineering designs since it lacks critical overarching and material-neutral requirements. Notably, structural analysis scope and other baseline requirements are left undefined/open-ended. In such cases, ASCE/SEI 7-16 Appendix E requirements would govern. Also, it is important to understand that many standards and guidelines are based on equivalence methods that are only applicable to standard fire resistance design and do not address structural performance under realistic fire exposure.

To evaluate subassemblies, FEA has been increasingly used for structural fire engineering applications. Typically, FEA approaches will first calculate the heat transfer to the elements and then the resulting mechanical response as decoupled steps (i.e., with no feedback from the structural analysis to the thermal analysis). Coupled analysis of the thermal and resulting mechanical effects may only be warranted in some cases (such as when passive protection may be damaged by

large fire-induced deflections) and has less precedent or supporting research to date. In current practice, full-scale structural fire testing of large assemblies is rare due to their significant cost. FEA is therefore useful in many cases to determine structural response to fire exposure by accounting for the framing layout, loading, and boundary conditions.

It should be noted that many of the structural analysis packages that are commonly used in current practice (which are preprogrammed to evaluate designs according to major codes and standards) are not outfitted to perform time-dependent structural fire analysis. These software packages are able to consider temperature loads but only as a static condition at relatively low temperature ranges corresponding to environmental conditions. Generalized FEA packages such as Abaqus [10], Ansys [11], or LS-Dyna [12] are equipped to perform structural fire analyses but may require more computational resources and additional licensing costs. Several FEA packages such as SAFIR [13], Vulcan [14], and the SiFBuilder interface for OpenSees [15] are specifically designed for structural fire applications and have been recently developed in Europe for this application.

Structural fire FEA simulations should account for reduced material properties as well as thermally induced interactions of heated and expanding structural assemblies with adjacent structural framing. FEA of system-level behavior of structures subjected to fire effects should adequately capture the local behavior of the individual structural members and provide reasonable predictions of large-scale structural interaction and load redistributions. FEA of component-level behavior should include appropriate levels of detail based on previous research and experience. Imperfections should be considered to enable the consideration of stability limit states. Nonlinear stress-strain relationships and plasticity are needed to allow permanent deformations. The temperature profile of the heated elements can be modeled as either uniform or nonuniform depending on their fire exposure. Well-executed FEA models will appropriately address the relevant aspects of structural response under fire exposure.

Significant reductions in computational time can be achieved with judicious selection of FEA element types and mesh discretization. It is the designer's responsibility to conduct appropriate convergence studies or provide references to justify the level of discretization used for each analysis, which may vary depending on the application. The key to any element selection is to reduce computational effort with negligible impact on computational accuracy. For example, beam elements may be a better choice for a system-level analysis depending on the limit states that are considered. For detailed analysis of structural components or connections, designers will typically choose between a shell and a solid element, and a common metric for this decision is the slenderness ratio of the structural member (i.e., the ratio of a structural member's length with respect to its thickness). The user should exercise caution when increasing the complexity of their models since the increase in sophistication is accompanied by an increase in input parameters and the amount of resulting data.

### ***3.4.3 Acceptance Criteria***

The acceptance criteria for a structural fire engineering design should be quantitative measures that fulfill the required performance objectives, ranging from collapse prevention to damage mitigation to preservation of postfire functionality. Relevant limit states should be identified, and modeling approaches should be selected accordingly. When undertaking a structural fire engineering design, the designer should exercise appropriate skill, care, and acquired competency in determining and using specific acceptance criteria for a given structural system. This may be facilitated by a third-party review at the discretion of the owner or building authority.

Different acceptance criteria should be selected to address (1) the primary structural system, (2) secondary structural systems, and (3) nonstructural components based on their materials, function, and their level of acceptable performance. Performance thresholds may vary from strict preservation of life safety (via egress and collapse avoidance) to reductions of postfire damage (to increase structural fire resilience and mitigate the loss of functionality as well as the duration and expense of potential repair). Similar to current seismic or blast design standards, acceptance criteria can be tailored to a project based on the building usage and occupancy as well as its vulnerability to fire hazards based on contents or location.

Since structural fire engineering is an emerging design discipline, it is incumbent on the structural designer to facilitate a conversation among the owner, architect, and authorities having jurisdiction to determine appropriate acceptance criteria. The level of acceptable performance and risk of damage for a structural fire engineering design approach should be consistent with that reflected in the building code for prescriptive fire-resistant design. Well-established standards such as the Eurocodes or other emerging standards such as Appendix E in ASCE 7-16 [2] can also be consulted for guidance regarding acceptance criteria. The designer should obtain, in writing, the approvals that will be needed for the resulting design configuration to be accepted. The designer should also encourage the owner to engage the building's insurer to determine any potential impact to pertinent rates during the building's operation.

### ***3.4.4 Periodic Stakeholder Briefings***

The optimum regularity of stakeholder briefings is influenced by the complexity and scale of the particular design project. For projects where the structural fire engineering design problem is familiar to the design team, and similar structural fire analyses have been carried out, approved, and successfully concluded, the briefings may be directed primarily towards those stakeholders who are less familiar with structural fire engineering design. Here the stakeholder briefings may concentrate mostly on educating those stakeholders who need this background information (refer Sect. 3.1.1).



For design problems which are complex and less routine and/or involve a range of stakeholders who are unfamiliar with the aims and design approaches used for structural fire engineering, the briefing process may be more involved. In particular, where building authorities need reassurance about the validity of outcomes from a structural fire engineering design, the stakeholder briefings may need to refer to supplementary background material to educate those parties who are new to the design approaches and their basis. This is particularly important in cases where independent third-party review is expected.

Depending on the project scale, complexity, time frames, size of the design team, and location of the various stakeholders, stakeholder briefing may be carried out through a series of in-person meetings, or by sharing status documents for information and comment. Often the briefing process will involve both of these methods.

The briefing process for complex, long-duration projects may also be phased, to accommodate the input on results from preliminary structural fire analyses. If the outcomes from preliminary design are different to what was expected, there may be a need to have iterative proposals and reviews with stakeholders to advise on design developments as the design progresses. These briefings may include review and discussion of interim design outcomes and solutions, to test ongoing stakeholder acceptance before advancing (e.g., with more sophisticated analyses or design optimization).

While there is no single optimal way of conducting the stakeholder briefings, the benefit and efficiency of capturing relevant input from stakeholders as the structural fire design progresses are important to realize.

### **3.5 Construction Administration and Due Diligence**

Once a structural fire engineering design is completed and accepted by the building authority, the designer may be further engaged during the construction project. Of paramount importance is for the designer to confirm that the construction does not violate key design assumptions and/or thresholds as derived from the analysis. Beyond the initial construction, the original designer (or perhaps a different designer) may be called upon to reevaluate the structural system if future modifications are sought. This section provides practical guidance on these possible endeavors as it relates to structural fire engineering design.

#### ***3.5.1 Confirmation of Design Assumptions***

Structural fire engineering analyses are often quite complex, relying on a series of assumptions relating to fire engineering design, structural design, construction, and building use over a building's design life. Some of these assumptions are general in scope, made routinely for many projects or design scenarios. Some assumptions are

specific to a particular building design, or even part of a building. Assumptions relating to the structural design are often specific to the particular structure.

It is important at the beginning of the design phase, and especially at the end of the design when the documentation is completed, to record the various assumptions that relate to the structural fire engineering design. This is necessary in order to be able to identify which later changes to the design, construction, and use of the building would alter the scope, assumptions, and outcomes from the structural fire engineering analyses and recommendations.

In particular, design assumptions which relate to the fire engineering design, or to the structural design, need to be coordinated with the parties that are carrying out those aspects of design for a project. It is helpful if the documentation separately and clearly lists the full range of fire engineering and structural engineering design assumptions, so these can be verified during construction as appropriate. The extent and formality of the process for verifying design assumptions will vary depending on the complexity of the project and the scopes of work for each participant in the design team. More formal verification of design assumptions is needed, for example, if the structural engineering, fire engineering, and structural fire engineering design are each carried out by a separate designer. When the same designer carries out structural design and structural fire engineering design, then more formal verification of design assumptions will occur at the interface between the fire engineering design assumptions and the impact of fire on structure. When the same designer carries out the fire engineering and the structural fire engineering, then more formal verification of design assumptions relating to the structure will occur, at the interface between the structural engineering designs for non-fire-related load conditions and fire conditions.

Design inputs which are often part of the general structural fire design assumptions relate to:

- Structural design loading standards.
- Structural design and construction standards.
- Structural material standards.
- Specifications for material strength, ductility, characteristic strength, fracture toughness, material grading, and species (wood structures).
- Specification of connection components and materials.
- Method and sequence of making connections, and fabricating splices and construction erection sequences.

The structural design loading standards often specify the types of loads that are expected to be resisted by the structure during a fire event. The load factors which apply to the various load components are (usually) specified in loading standards, to align general levels of exceedance probabilities with those which apply to other (non-fire) load combinations. The types of loads that apply vary depending on the loading standard, the geographic region and environment of the structure, and the loading standard's basis for tolerable risk. The types of loads that are assumed to apply to a structure in the event of fire, and the associated load factors that apply to the individual load components, vary nationally and internationally. For instance in

the USA, ASCE/SEI 7-16 specifies one load combination for extraordinary events, which is applied to structural fire engineering designs. Some loading standards require simultaneous consideration of the impact on the structure of fire together with other environmental time-variant load effects such as wind forces. Confirmation of the assumptions made about the applicability of the loading standard, the load combinations, and the associated loading factors should be sought and recorded as part of the design, and verified on completion so that the impact of future changes to loading standards can be readily understood.

Structural design and construction codes of practice and standards are usually specific to the type of structural materials (steel, concrete, masonry, timber, etc.). However, ASCE/SEI 7 is indeed material neutral. These material-specific design standards usually specify some constraints around material properties, structural detailing, and connection design. Granted, AISC 360 Appendix 4 does not contain affirmative guidance for the design of structural steel connections under fire conditions. A structural fire engineering design may take advantage of specific detailing or connection design requirements from such design standards, where the details improve the fire performance of the structure. It is important to verify any such design assumptions, particularly in cases where there are alternative applicable codes of practice or standards for structural design and construction.

A structural fire engineering design is required to either specify or make assumptions about the properties of structural materials, including strength, ductility, fracture toughness, moisture content, variation in strength and stiffness with temperature, and so forth. It is important to verify design assumptions about the specific material properties for the various structural elements that are analyzed for structural fire engineering purposes for the same reasons as verifying assumptions about structural design and construction codes of practice and standards. Even more important though is verifying any structural fire design assumptions made about the material properties of structural elements in specific locations, such as:

- Material specification for each specific beam, column, bracing member, floor slab, reinforcing steel, etc.
- Material specification for connection components (particularly ductility, strength, and fracture toughness), such as welds, bolts, splice plates, reinforcing couplers, and glues.

The structural fire engineering design may also make assumptions about the composition of composite members which may influence the performance in fire, such as the type of glue/adhesive in cross-laminated timber (CLT) or other laminated mass timber structure components, or the timber species used to make up various layers. Similarly, the extent and construction sequence of precast concrete components versus cast in situ concrete and location of the precast/cast in situ interfaces may be significant in the design assumptions made for structural fire engineering. Locations of site splices in members, and in particular the design of splices, might also be assumed as part of a structural fire engineering analysis. For example, this would be important if splices or connections are not as strong or ductile as the members they connect.

The impact of fire on structural response often results in the development of stresses or redistribution of load paths which are not anticipated when resisting other (non-fire) load combinations and these fire-induced stresses and deformations frequently concentrate forces of magnitude and direction which are quite different to those arising from non-fire load combinations. When the structural fire engineering design makes assumptions about the ability for splices and connections to resist forces of unusual magnitude or direction, these assumptions need to be coordinated with the structural design. For example, where it is assumed that connections are designed with a strength hierarchy in order to encourage favorable overstress behaviors (in fire conditions) over unfavorable behaviors, this assumption needs to be verified with the structural design.

The sequence of construction influences structural loads, which may or may not be accounted for formally in a structural fire engineering analysis. For example, the extent to which inclined or diagrid bracing structural members attract and support gravity loads depends not only on the structural form and load paths but also on the sequence of construction and extent of temporary support. This influences the magnitude of gravity loads present in such members at the time of a fire and also the extent to which these gravity loads can or need to be redistributed to other cooler parts of the structure. Another example is the sequence of placing concrete on or in composite steel-concrete or timber-concrete structural members. This sequence influences the stresses in the different structural components at the time of a fire, depending on the method of concrete placement and extent of any temporary support. Any design assumptions relating to the state of the structure at the time of a fire that influence a structural fire engineering analysis should also be coordinated and verified.

In most cases, a discussion (of the relevant points raised above) with the various designers during the stakeholder briefing process is the best way of identifying and subsequently verifying design assumptions so that the fire engineering design, structural design, and structural fire engineering analyses are well coordinated.

The coordination of design assumptions relating to connection design, fabrication, erection, and construction sequencing (as they affect structural fire engineering analyses) is particularly important when these design processes are transferred to a contractor and are carried out during the construction phase. The contractor and the specific parties involved in making decisions about connection design, fabrication, erection, and construction sequencing may not be involved during the stakeholder briefing process and therefore may not realize the need or significance for verification of design assumptions relating to the performance of the structure during fire.

### ***3.5.2 Change of Occupancy or Use***

During construction a building may undergo changes or clarification of occupancy or use. The range of changes of occupancy or use varies depending on the type of building and the degree of specialization needed for the building's function. For

some building types, variation in occupancy type and some limited variation in use are effectively a given, and the building design is expected to cater for these anticipated changes. Shopping centers, office buildings, and commercial buildings are building types which undergo frequent changes of tenancy, and therefore to some extent changes in occupancy.

For buildings in which a change in occupancy or use is routine, and may occur as occupancies are finalized during a construction phase, it is important to be aware of any impacts on the structural fire engineering design which might otherwise go unnoticed. This is especially true for occupancy decisions which are expected, and which may have been assumed to be covered by the design brief for the project. A clear list of the design assumptions as outlined in the previous section assists and should resolve any disconnects with post-design occupancy changes during the construction phase.

The key impacts on a change in occupancy or use from a structural fire engineering viewpoint usually relate to:

- A change to the structural design loading as a result of the change in occupancy or use.
- A change to the design fire load as a result of the change in occupancy or use.
- A change to the fire compartment containing the different occupancy or use, which changes the characteristics of fire exposure to the structure (for example: a change in compartment floor area, in addition to covering of or removal of external windows or similar changes which would affect the fire growth rate and fire energy release rate).

For some buildings, the structural design may have originally allowed for a full range of structural design loadings, so the change in occupancy may not appear to have an influence on structural fire engineering. However, if the structural fire engineering assessment has taken full account of the additional load capacity for the as-designed structure compared with the design loadings for the original (less challenging) occupancy loading, then the change in occupancy may erode some of the structure's available fire endurance/resiliency simply because of the change in occupancy loading. This highlights the benefit of providing the building owner with ongoing access to clear design documentation which outlines the design assumptions and design basis for a structural fire engineering analysis.

A change in occupancy or use which changes the design fuel load, or equally which changes the rate at which a fire grows and releases energy, influences the actual characteristics of a fire and its impact on the structure. The extent to which these changes affect the original structural fire engineering assessment will depend on the design assumptions made concerning the nature of and inputs to the design fire: its extent and characteristics and how these relate to the physical construction of the fire compartment.

Some of the most common effects arising from changes to occupancy and use which affect structural fire engineering analyses include:

- Finalizing tenancy spaces, which can result in merging or subdividing the floor area which can increase or decrease the size (floor area) of fire compartments.
- Finalizing tenancy spaces, which can result in changes to the position of compartment bounding walls; this in turn can affect assumptions made about the fire compartment and the ventilation through external windows that are provided to a fire.

### ***3.5.3 Modifications/Extensions of Existing Building***

As structural fire engineering design is applied to more buildings, it becomes increasingly likely in the future that modification or extension of an existing building cannot assume by default that the structure needs to meet only prescriptive fire resistance assessments for regulatory compliance. Over time it will become more likely that structural and fire engineers need to verify whether or not the structural performance during fire has been assessed using a structural fire engineering approach, and then—if it has—to be mindful of the implications of any modification of the structure on that previous analysis and outcomes. For example, if a structure resists the effects of fire by utilizing a secondary load path which is not the principal load path for non-fire structural loads, then this needs to be clearly identified in the structural design documents.

Similarly, where a certain type of applied fire protection solution, or protective coating, or reliance on an associated passive fire protection feature forms part of a specific structural fire engineering design, it is helpful if this is explicitly recorded in the documents of record. For example, if the structure is protected by a fire barrier which fulfils dual or multiple performance roles which include but are not limited to protecting parts of the structural system located on the non-fire side of that barrier, then these dual or multiple performance roles need to be clearly identified in the fire design documents so that all of the implications of modifying the building are fully understood.

Of course, this highlights the importance for documents of record for the structural design to be held by the building owner or the building authority to identify that the structure has been assessed quantitatively for performance in fire and that the solution for structural fire performance may differ from that normally used when adopting prescriptive “deemed-to-comply” solutions.

During its lifetime a building may undergo a number of changes in occupancy or use and may be subjected to modifications and extensions. The frequency and range of changes of occupancy or use vary depending on the type of building and the degree of specialization needed for the building’s original function. For some building types, variation in occupancy type and some limited variation in use are almost a given, and the original building design would be expected to cater for these anticipated changes.

For more specialized buildings, such as hospitals, transport facilities, auditoria, and similar public buildings, there is generally a lower likelihood of a major change

in occupancy or use. However, the impact of a change in use for a specialized building is likely to be much greater than for a building where the original design anticipates a certain amount of change. Fortunately, the significance of the impact of a change of use will likely be more constructively anticipated for a building whose original use is highly specialized.

Where a major change occurs to a building's original design occupancy or use, it is more likely that a structural assessment will take place. For buildings in which a structural fire engineering assessment has been carried out, a major change in occupancy or use should be accompanied by a thorough review of design assumptions, as discussed in Sect. 3.5.1. Where structural changes are planned as part of a change in occupancy or use, there are additional design implications on a structural fire engineering solution.

Examples of modifications to buildings which may influence a structural fire engineering assessment can include:

- Cutting large holes through existing floors, either for building service shafts, for access stairs, for view shafts, or for light penetration.
- Interconnection of floors in multilevel buildings creating a multilevel communicating volume of space.
- Changing building use or occupancy, even locally, in a way which increases the design gravity loads supported by the structure or otherwise influences the level of reserve strength that contributes to the available strength of the structure when exposed to fire temperatures.
- Altering penetrations through structural floor beams to accommodate changes to building services, which may affect the ultimate load capacity of the beam.
- Changing the external façade in a way that changes the ventilation available to the fire through external windows, or which otherwise changes the fire characteristics; the rates at which a fire grows and releases energy both influence the impact of a fire on the structure.

Cutting holes in floor slabs can change the way in which a floor slab responds to the deformations induced by fire temperatures and therefore to the way in which floor load paths are redistributed.

If a single floor region is openly interconnected to create a multilevel communicating volume of space, this can create a heating environment on the upper level which preheats the structure and also delays the timing and time frame for the cooling phase. Depending on the size of the opening relative to the floor areas at each interconnected level, for some fire scenarios the preheated structure is then subjected to the fire effects of combining fire load from multiple levels in one communicating volume. This creates a more challenging exposure than the more common arrangement of the structure being exposed to a more predictable single-region fire temperature-time characteristics.

Changes to the structural design loads, or the tributary-supported floor area, or to the structural load capacity of beams as a result of new service penetrations can each contribute to a reduction in the endurance/resiliency of the structure when the structural response to fire has been assessed on a performance design basis.

For design scenarios where the structural design fire is established from fire dynamics first principles (for example, the fire heat release rate and corresponding temperature-time relationship are based on ventilation-controlled burning), changes to the amount of ventilation available to the fire through external windows may have an effect on both the maximum fire temperature and the fire duration. Modifications to the building or extension to the size of a fire compartment may need to be reviewed for their impact on the structural fire design.

The building configuration/use sensitivities identified/summarized above should help proactive designers properly convey and document key assumptions, and promote reevaluations in warranted cases.

## References

1. LaMalva, K. (2017). *Chapter 9: Fire Design*, Architect's Guidebook to Structures: Special Structural Topics, Routledge.
2. ASCE/SEI 7-16. (2016). *Minimum design loads and associated criteria for buildings and other structures*. American Society of Civil Engineers/Structural Engineering Institute.
3. LaMalva, K. (2017). Structural fire protection's shifting paradigm. *Fire Protection Engineering, Q2(74)* Society of Fire Protection Engineers.
4. Eurocode 1. (2001). *Basis of design and actions on structures, Part 1.2: Actions on structures – Actions on structures exposed to fire, EN 1991-1-2*. Commission of European Communities.
5. SFPE. (2007). *Engineering guide to performance-based fire protection* (2nd ed.). Society of Fire Protection Engineers.
6. EN 1993-1-2 Eurocode 3. (2005). Design of steel structures. Part 1–2: General rules. In *Structural fire design*. Brussels: CEN.
7. EN 1992-1-2 Eurocode 2. (2004). Design of concrete structures – Part 1–2: General rules. In *Structural fire design*. Brussels: CEN.
8. EN 1995-1-2 Eurocode 5. (2004). Design of timber structures. Part 1–2: *Structural fire design*. Brussels: CEN.
9. AISC 360. (2016). *Specification for structural steel buildings*. Chicago: American Institute of Steel Construction.
10. Dassault Systèmes Simulia Corp. (n.d.). *Abaqus software*. Dessault Systèmes Simulia Corp.
11. Ansys, Inc. (n.d.). *ANSYS software*. Ansys, Inc..
12. LS-Dyna. Livermore Software Technology Corporation, an Ansys company, Livermore, CA, 2020
13. Franssen, J.-M., & Gernay, T. (2019). *SAFIR (Software Architecture For Information and Realtime systems)*. Univ. of Liège.
14. Vulcan. Version 12.1.6, *Vulcan solutions*. Sheffield, UK, 2020
15. OpenSees. Version 3.3.0, University of California, Berkeley, CA, 2021



# Chapter 4

## Design Fires and Actions



**Danny Hopkin, Ruben Van Coile, Charlie Hopkin, Kevin LaMalva, Michael Spearpoint, and Colleen Wade**

### 4.1 Introduction

This chapter addresses design fires in the context of structural fire safety. Figure 4.1 illustrates a typical structural fire engineering (SFE) design process. First, the design fuel load must be derived for the given space, which represents the potential energy that needs to be considered. Once the design fuel load is established, estimation of the fire exposure intensity on the structure is a key next step in the process. Specifically, thermal boundary conditions acting on structural and/or insulative exposed boundaries must be derived so that subsequent heat transfer analyses may be conducted to determine the temperature histories of the given structural system. Also, it is important to note that SFE typically only considers a subset of design fires, which are those that are uncontrolled (any cooling effects of active fire protection systems and/or manual intervention are neglected) and termed as structural design

---

D. Hopkin (✉) · M. Spearpoint  
OFR Consultants, Manchester, UK  
e-mail: [danny.hopkin@ofrconsultants.com](mailto:danny.hopkin@ofrconsultants.com); [michael.spearpoint@ofrconsultants.com](mailto:michael.spearpoint@ofrconsultants.com)

R. Van Coile  
Department of Structural Engineering, Ghent University, Ghent, Belgium  
e-mail: [ruben.vancoile@ugent.be](mailto:ruben.vancoile@ugent.be)

C. Hopkin  
Ashton Fire, Manchester, UK  
e-mail: [charlie.hopkin@ashtonfire.com](mailto:charlie.hopkin@ashtonfire.com)

K. LaMalva  
Warringtonfire, Boston, MA, USA  
e-mail: [kevin.lamalva@warringtonfire.com](mailto:kevin.lamalva@warringtonfire.com)

C. Wade  
Fire Research Group, Auckland, New Zealand  
e-mail: [colleen.wade@fireresearchgroup.com](mailto:colleen.wade@fireresearchgroup.com)

© Springer Nature Switzerland AG 2021

K. LaMalva, D. Hopkin (eds.), *International Handbook of Structural Fire Engineering*, The Society of Fire Protection Engineers Series,  
[https://doi.org/10.1007/978-3-030-77123-2\\_4](https://doi.org/10.1007/978-3-030-77123-2_4)

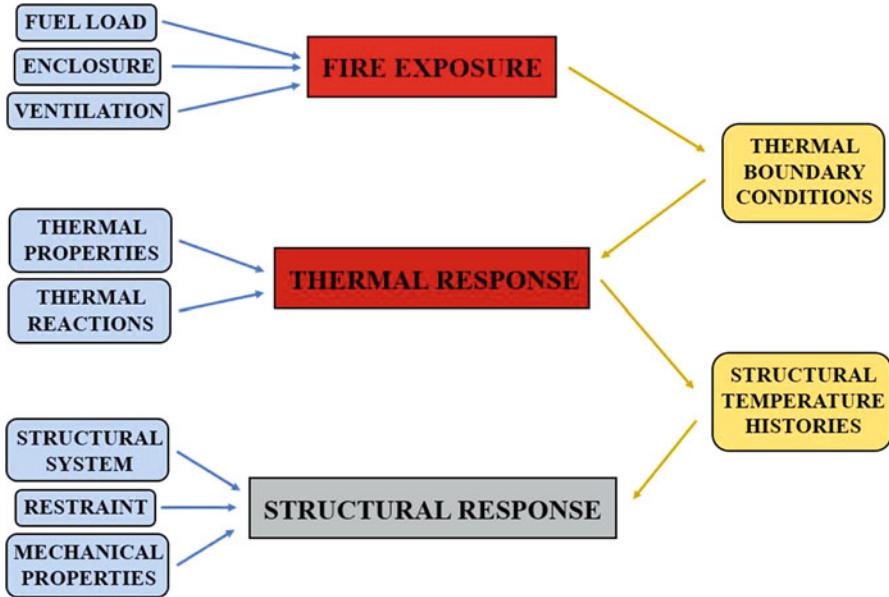


Fig. 4.1 SFE design process

fires. Other design fires (e.g. those used for determining the available safe escape time) would not commonly be used for SFE applications [1].

Structural design fires can usually be derived using hand calculations. This is unlike other fire engineering applications which focus on the transport of smoke and other products of combustion throughout a given building or space during the early and/or controlled phases of a fire (e.g. smoke control design). If necessary, zone models (Fig. 4.2) and/or computational fluid dynamics (CFD) simulation(s) (Fig. 4.3) may be conducted to determine more precise (but not necessarily more accurate/robust) time-temperature histories of structural design fire scenarios (e.g. to explicitly capture a travelling-type fire scenario).

The extent of heating from a structural design fire should be reasonable and conservative. Currently, an industry consensus on the selection of structural design fire scenarios does not exist and remains within the purview and judgment of the designer, in dialogue with the authority having jurisdiction (AHJ) and other stakeholders. In large open plan areas, it would be prudent to consider a fire spreading to consume all fuel within the fire compartment. Where a fire occurs in a cellularized space, e.g. apartments, it may be adequate to consider the fire as being constrained to the compartment of origin. Where it is expected that the structure may be particularly sensitive to multilevel fires, consideration may be given to vertically spreading fires. This may be most prudent for cases with open connections between floors, e.g. atria.

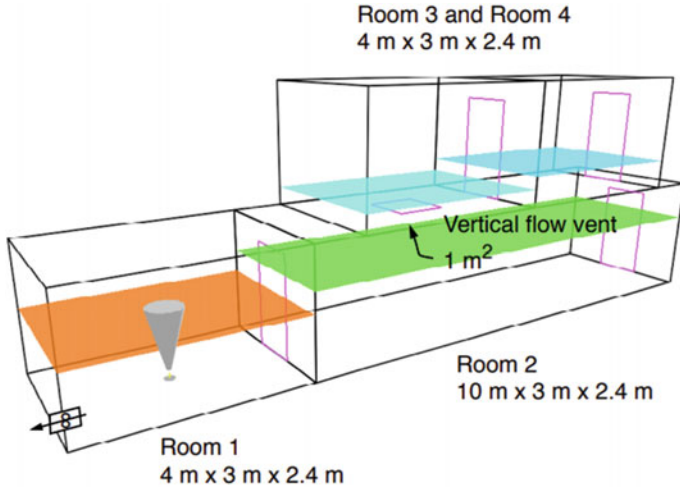


Fig. 4.2 Zone fire model [2]

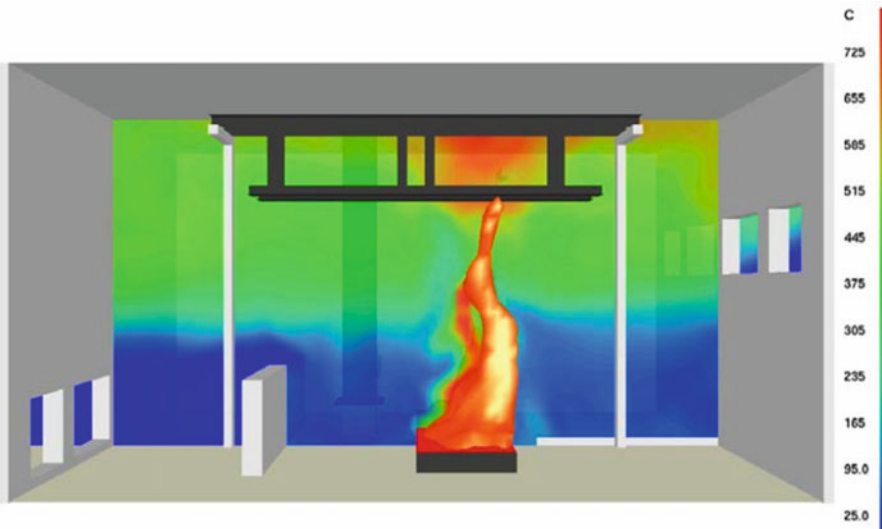


Fig. 4.3 CFD fire model [3]

## 4.2 Key Terminology

Fire exposure can be defined as the extent to which materials, products, or assemblies are subjected to the conditions created by fire. In the context of a structure, energy from the products of fire can be transferred by means of convection from the

hot gases adjacent to the structure and/or by thermal radiation from the flames or other hot surfaces, as well as any smoke. Heat transfer will also occur through the structure by means of conduction, and by radiation and convection within any cavities to structural elements, e.g. hollow sections.

Ignition is the process by which a fire within or in the locality of a structure starts. The process can lead to smouldering or flaming fires, but the emphasis in this book is on flaming fires because they generally have a greater impact on a structure (except in the specific cases of combustible structural elements, such as those formed of timber). The energy generated by a fire as a function of time is referred to as the heat (or energy) release rate (HRR). Typically, heat release rate values in the order of several megawatts or more are likely needed before the fire has any appreciable effect on the structure and can be considered a structurally significant fire.

Once ignition has occurred the fire enters the growth stage characterized by an increasing heat release rate as flame spreads over burning fuel items or ignites other fuel items located nearby. The rate at which a fire grows is a function of several variables, but the most important ones are the fuel type, the geometry and orientation of fuel surfaces, and the ignition properties of other fuel items.

Although fires that affect a structure can be developed in the open air, it is often fires within a structure that are of interest to designers. Fires within a structure are affected by its boundaries and also any internal partitions that form enclosures within the building envelope. Enclosures that have boundary elements that are designed to limit the transfer of heat and/or the transfer of hot gases to other parts of a building and/or to retain their structural adequacy are referred to as compartments. In such cases the boundary elements are referred to as a fire-resisting wall, door, etc.

Small fires relative to the size of the enclosure may remain localized because there are no other fuel items or those that are present are not sufficiently close for secondary ignition. These small fires produce two regions inside the enclosure: a region where the highest temperatures are located in the vicinity of the flames (the near field) and a region where lower temperatures are created by the hot gases (the far field). The far-field region is often much larger than the near field and may have little impact on the structure. Where the heat release rate is small, the near field is also not often of consequence to a structure. Conversely, fires that are able to spread to other items, or the initial fuel items are relatively large compared to the enclosure, have the potential to impact the structure.

The growth stage of a fire is accompanied by a corresponding increase in the gas-phase temperature and heat fluxes within an enclosure which in turn transfers heat to the structure. These increases in temperature may affect the thermo-mechanical properties of materials which can then lead to changes in the behaviour of a structure. In addition, the heated structure will reradiate thermal energy back into the enclosure affecting the development of the fire and heat transfer to other parts of the structure.

A fire is fully developed when it has reached its full potential within its enclosure. As such, the fire has reached its maximum achievable heat release rate, assuming that there are no external fire suppression influences. Where fuel items can burn freely, and the rate of heat release is limited by the amount, type and surface area of the

burning items, this is referred to as the fuel-controlled regime. A growing fire in an enclosure may transition to a point in which there is almost simultaneous involvement of all fuel items that have yet to ignite. This transition point is referred to as flashover.

A fire needs a sufficient supply of oxygen to maintain the burning of the fuel inside the enclosure. However, the supply of oxygen may be restricted by the available ventilation through openings in the enclosure or by mechanical air movement systems. In this case the available ventilation imposes an upper limit on the heat release rate inside the enclosure, and this is called the ventilation-controlled regime. The ventilation to a fire may not stay constant throughout its duration due to the breaking of windows, failure of other building elements such as partitions, fire service operations and/or changes in the air handling or smoke extract systems. These changes may affect the temperatures within an enclosure as a result of more fuel being able to burn, or because of heat losses to other parts of the structure or to the outside. Where the burning rate of the fuel inside the enclosure results in the production of volatiles beyond what can be combusted inside the enclosure, i.e. a ventilation-controlled regime, external flaming can occur, with the volatiles combusting outside of openings. This presents an external fire spread hazard that may influence the assumed extent of burning, e.g. multi-floor fires.

Once a fire reaches a stage in which there is less fuel to burn than during its fully developed phase then it will enter its decay phase. The rate of heat release and the temperatures within the enclosure typically undergo a decrease over time. Although the fire is decaying, temperatures within a structure may continue to increase due to heat transfer and thermal lag. If the fuel within an enclosure is completely consumed, then it is said that burnout has occurred. However, it is possible that a fire may self-extinguish during the growth, fully developed or decay stages due to a lack of oxygen or because the heat transfer from the fire and the enclosure is insufficient to support further burning of fuels.

In some situations, it is possible that a fire is only able to burn over a limited area of fuel but then moves through the enclosure as flames spread from one fuel item to another. This is known as a travelling fire and these occur inside enclosures which are typically large or are not ventilation constrained (see Sect. 4.5 below). The heat release rate is determined by the area of burning fuel between the leading edge of the spreading flames and the trailing edge where the fuel has been consumed or self-extinguishes. A travelling fire is essentially a moving localized fire and so produces near-field and far-field regions inside the enclosure.

The intervention of an automatic system, the fire service or occupants can affect a fire at any point. This intervention may reduce the rate of heat release to some lower value or initiate a period of decay that can also result in eventual extinction of the fire. Some intervention methods can directly reduce the temperature of the structure as well as affect the fire. These aspects are accounted for through risk reduction factor allowances for design fuel loads (e.g. Eurocode 1) [4], but may not be explicitly considered to affect the heat release rate nor the duration of a structural design fire.

### 4.3 Fundamentals of Fire Dynamics

Design fires for evaluating the response of structures to fully developed fires are commonly defined by a time-temperature curve and in the case of enclosure fires these can be derived from the application of mass and energy conservation equations for the enclosure. Many simplifying assumptions are typically made to limit the number of variables considered and for ease of calculation. Assumptions that are commonly made include:

- A uniform gas temperature throughout the enclosure (or the control volume).
- The burning rate of the fuel is controlled by the ventilation, i.e. the size of openings.
- The combustion energy is released entirely inside the enclosure.
- The duration of the fire is dependent upon the mass of the fuel available (i.e. fuel load).
- Radiative and convective heat transfer to the enclosure surfaces is uniformly distributed.
- The pressure in the enclosure is considered to be uniform but hydrostatic variations account for the pressure differences at free boundaries (and govern the vent flows).

A simple zone model may be used incorporating equations that represent the conservation laws describing mass and energy transport. Conservation of momentum is typically omitted from zone models and correlations are used instead to account for the momentum exchange in the vent jet flow equations.

As illustrated in Fig. 4.4, a simple energy balance for a control volume consisting of the entire enclosure and that ignores any storage of heat in the gas volume can be expressed as

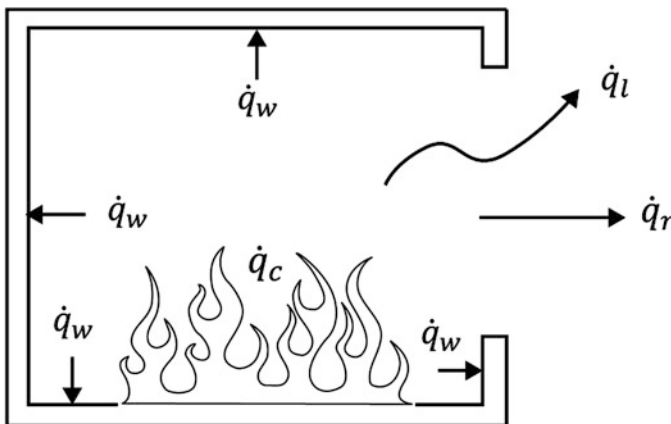


Fig. 4.4 Energy losses in a fully developed compartment fire, adapted from [5]

$$\dot{q}_c = \dot{q}_l + \dot{q}_w + \dot{q}_r \quad (4.1)$$

where  $\dot{q}_c$  is the energy release rate in the combustion reaction,  $\dot{q}_l$  is the heat loss rate in the enthalpy flow through the openings,  $\dot{q}_w$  is the heat loss rate to the compartment boundaries and  $\dot{q}_r$  is the rate of radiation loss through the openings.

### 4.3.1 Fire Growth

The fire growth phase is often characterized using a t-squared relationship, where the total heat release rate of the fire ( $\dot{Q}$ ) is expressed via a power law in function of time (t), as follows:

$$\dot{Q} = \alpha t^2 \quad (4.2)$$

Standardized growth rate parameters ( $\alpha$  in  $\text{kW}\cdot\text{s}^{-2}$ ) are found in codes globally, with common values given in Table 4.1.

For SFE purposes, it is often assumed that a fire will grow without intervention, until it becomes either ventilation- or fuel-controlled.

### 4.3.2 Ventilation-Controlled Fires

If the mass loss from the fuel during combustion is assumed to be very small compared to the mass flow entering or leaving the control volume, then under equilibrium conditions the mass flow entering and leaving the control volume will be the same. Applying the Bernoulli formula, it can be shown that the flow rate through the openings will be approximately proportional to the opening area and the square root of the opening height. This was confirmed in the 1950s by Kawagoe [7] based on burning wood cribs inside an enclosure with various opening sizes where he determined that

$$\dot{m}_b = 0.09A_o\sqrt{h_o} \text{ [kg/s]} \quad (4.3)$$

Where  $\dot{m}_b$  is the ventilation-controlled burning rate,  $A_o$  the opening area [ $\text{m}^2$ ] and  $h_o$  the opening height [m].

**Table 4.1** Standardized t-squared growth rates adapted from [6]

Growth rate	Time to reach 1055 kW[s]	$\alpha$ [ $\text{kW}/\text{s}^{-2}$ ]
Slow	600	0.0029
Medium	300	0.0117
Fast	150	0.0469
Ultra-fast	75	0.1876

This relationship only applies over a limited range of opening sizes where the fire can be described as ventilation-controlled as it is related to the rate at which air can enter the compartment. For a compartment with a single opening and assuming that the inflow and outflow are equal, and for stoichiometric burning where the combustion of wood requires approximately 5.7 kg of air per kg of wood burned, the mass flow of air through the opening ( $\dot{m}_{\text{out}}$  in kg/s) can be given as

$$\dot{m}_{\text{out}} \approx 0.5 A_o \sqrt{h_o} \text{ [kg/s]} \quad (4.4)$$

Since the energy released per kg of oxygen is 13,100 kJ/kg-O<sub>2</sub> or 3000 kJ/kg-air for a wide range of fuels, the ventilation-controlled heat release rate ( $\dot{Q}_v$ ) for a single opening can be estimated as

$$\dot{Q}_v \approx 1500 A_o \sqrt{h_o} \text{ [kW]} \quad (4.5)$$

This equation provides an estimate of the maximum possible heat release inside the enclosure assuming that all the oxygen in the enclosure is consumed and ignoring the fuel mass loss in the mass balance for the enclosure. However, this approach based on the ventilation factor can also underestimate fire severity in compartments with separate ventilation openings at floor and ceiling levels and it might not be appropriate for large compartments.

For more complicated arrangements (e.g. connected compartments) the ventilation-controlled heat release rate may instead be estimated from the available oxygen in the fire plume-entrained gases. This relationship is commonly adopted in multi-compartment computer zone models with a smoothing function added to account for the lower oxygen limit [2, 8]:

$$\dot{Q}_v \approx \tilde{m}_p Y_{O_2} \Delta H_{O_2} \quad (4.6)$$

where  $\tilde{m}_p$  is the mass flow of gases entrained into the fire plume,  $Y_{O_2}$  is the mass fraction of oxygen in the plume flow and  $\Delta H_{O_2}$  is the heat of combustion based on oxygen consumption (~13.1 MJ/kg for hydrocarbons).

### 4.3.3 Fuel-Controlled Fires

Fuel-controlled fires occur in specific situations, such as enclosures that are very well ventilated with a large amount of openings; very large compartments where fuel burns progressively through the compartment instead of uniformly across the floor area; or where the fuel arrangement is such that the surface area of the combustibles is small compared to the volume of the enclosure.

The burning rate of fuel-controlled fires is dependent upon the nature and surface area of the fuel. In many cases it is quite difficult to determine the burning rate



**Table 4.2** Identified heat release rate per unit area (HRRPUA) ranges available from literature, adapted from [10]

Occupancy	$\dot{Q}_f''$ HRRPUA (kW/m <sup>2</sup> )
Shops	270–1200 (maximum)
Offices	150–650 (maximum)
Hotel rooms	250 (average)
Residential	320–570 (maximum)
Industrial	90–620 (average)
Storage/stacked commodities	400–20,000 (maximum)

precisely due to the characteristics and geometry of the fuel packages. For simple, well-defined geometries such as timber cribs, equations exist that allow the fuel pyrolysis rate to be estimated based on the initial fuel mass per unit area and the remaining fuel mass per unit area at a given time [9].

The maximum heat release rate for a fuel-controlled fire is generally estimated from either (a) full-scale tests where the peak heat release rate can be directly measured with an oxygen calorimeter or (b) small-scale tests that measure the heat release rate per unit area (HRRPUA) for the material. In the latter case, the maximum heat release rate can be determined from

$$\dot{Q}_{\max} = \dot{Q}_f'' A_f \quad (4.7)$$

where  $\dot{Q}_{\max}$  is the maximum heat release rate,  $\dot{Q}_f''$  is the heat release rate per unit area (common values are given in Table 4.2) and  $A_f$  is the burning surface area of the fuel. Heat release rate per unit area (or mass loss rate per unit area) is typically measured with negligible radiation feedback from the surroundings. Sometimes, this effect on the burning rate may need to be considered.

In cases where multiple items are present, adding the respective maximum heat release rates per unit for all items and assuming that all items are burning at the same time provides a conservative estimate of the maximum rate of heat release. Alternatively, a time frame for the fire spread from item to item could also be included; however this is very dependent on the exact arrangement and spacing of the various items which could greatly vary from day to day.

#### 4.3.4 Decay

For a fully developed enclosure fire, the heat release rate as a function of time during the decay phase can be estimated assuming that a linear decay after 80% of the available fuel ( $q_f$ ) has been consumed.

The duration of the decay phase ( $t_{\text{decay}}$ ) can be estimated as [6]

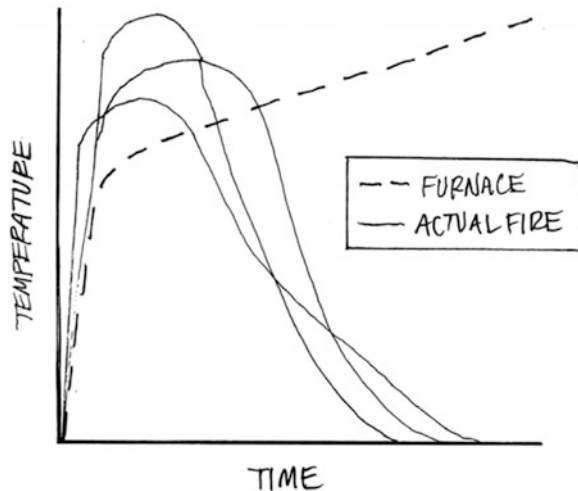
$$t_{\text{decay}} = \frac{0.4q_f}{\dot{Q}_{\text{max}}} \quad (4.8)$$

#### 4.4 Nominal/Standard Heating Exposures

Nominal or standard fire curves are the simplest and most commonly adopted means of representing a fire and are adopted within a standard fire resistance design (SFRD) framework. They have been developed to allow classification and assessment of construction products using commercial furnaces. Although they do not represent ‘real’ fire scenarios (see Fig. 4.5) they have been developed from the experience of real fires (albeit from knowledge/conditions dating back a century). Several different curves exist and the choice of curve for a situation will depend on the end use. Different curves are used for testing and assessment depending on whether the structural element or product is to be used in the construction of a normal building (office, dwelling, etc.), in the petrochemical or offshore industry, or for tunnels.

The time-gas-temperature ( $\theta_g$ ) history per ASTM E119 [12]/UL 263 [13] is used for the vast majority of fire resistance listings within SFRD and is meant to represent cellulosic type fires (even though modern building spaces have a mix of cellulosic and plastic fuel loads), albeit with continually increasing heating with no specific endpoint. The European/international equivalent to this heating exposure is found in ISO 834-1 (see Eq. (4.9), where  $t_m$  is time in minutes) [14], EN 1363-1 [15] and BS 476-20 [16]:

**Fig. 4.5** Furnace exposure vs. actual fire exposure (indicative) [11]



$$\theta_g = 20 + 345 \log_{10}(8t_m + 1) \quad (4.9)$$

Other than the E119/UL 263 standard heating exposure, the ‘rapid-rise’ or ‘hydrocarbon’ heat exposure may be prescriptively required for non-building structures such as tunnels. ASTM E1529 [17] and UL 1709 [18] provide the time-temperature history for such a test heating exposure. This heating exposure is significantly more intense than the cellulosic exposure but does share the commonality of continually increasing heating over time with no specific endpoint. A similar hydrocarbon fire curve is found in EN 1991-1-2 [4], per Eq. (4.10):

$$\theta_g = 1080(1 - 0.325e^{-0.167t_m} - 0.675e^{-2.5t_m}) + 20 \quad (4.10)$$

## 4.5 Localized and Travelling Fires (Pre-flashover)

### 4.5.1 Localized Fires

Localized fires represent cases where the fire only burns a small-sized fuel item relative to the overall size of the enclosure.

For the purposes of this handbook, a localized fire can be considered static, i.e. no other fuel items are nearby, or other fuel items are sufficiently far away to obviate subsequent ignitions. Localized fires would generally be expected to be fuel-controlled.

For structural assessment purposes, a localized fire can be characterized according to whether the flame impinges the ceiling or not. In the case of the latter, the heating from the plume is relevant with the mean centreline (or axial) excess gas temperature for an axisymmetric plume ( $\bar{\theta}_{cl}$  in K) that can be given by [19]

$$\bar{\theta}_{cl} = 25\dot{Q}_c^{2/3}(z - z_0)^{-5/3} \quad (4.11)$$

The above ceases to be valid near the mean flame height and below for fire sources without substantial in-depth combustion, i.e. where

$$(z - z_0)/\dot{Q}_c^{2/5} < 0.15 \quad \text{to} \quad 0.20 \text{ m kW}^{-2/5} \quad (4.12)$$

Below this limit, experiments indicate a convergence on a temperature rise deep in the flame of c. 900 K. Fires with very low flame heights can generally be expected to produce lower mean temperatures.

Note:

$$z_0 = -1.02D + 0.083\dot{Q}^{2/5} \quad (4.13)$$

$$\dot{Q}^* = \frac{\dot{Q}}{\rho_0 c_{p,0} T_0 g^{1/2} D^{5/2}} \quad (4.14)$$

With:

$\dot{Q}$	kW	Total heat release rate
$\dot{Q}_c$	kW	Convective heat release rate
$z$	m	Height above the fuel surface
$z_0$	m	Height of the virtual source above the fuel surface
$D$	m	Fire diameter or idealized equivalent
$g$	$\text{m} \cdot \text{s}^{-2}$	Acceleration due to gravity
$c_{p,0}$	$\text{kJ} \cdot \text{kg}^{-1} \cdot \text{K}^{-1}$	Specific heat capacity of ambient air
$\rho_0$	$\text{kg} \cdot \text{m}^{-3}$	Density of ambient air
$T_0$	K	Ambient air temperature

Once flames impinge on a ceiling, flame extension can occur in the near field, with a ceiling jet forming in the far field (Fig. 4.6).

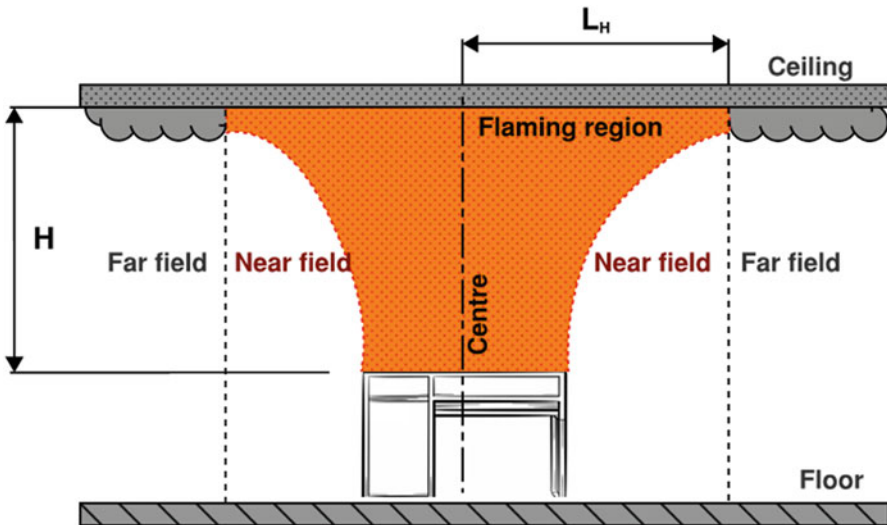


Fig. 4.6 Flame extension under a ceiling, adapted from [20]

Both the flame extension and the incident heat flux to the ceiling are described via non-dimensional parameters ( $Q_H^*$ ,  $Q_D^*$ ,  $z'$  and  $y$ ), [21] i.e.:

$$Q_H^* = \frac{\dot{Q}}{1.11 \times 10^6 H^{3/2}} \quad (4.15)$$

$$Q_D^* = \frac{\dot{Q}}{1.11 \times 10^6 \cdot D^3} \quad (4.16)$$

$$z' = 2.4D \left( Q_D^{*2/5} - Q_D^{*2/3} \right) \text{ for } Q_D^* < 1 \quad (4.17)$$

$$z' = 2.4D \left( 1 - Q_D^{*2/5} \right) \text{ for } \geq 1 \quad (4.18)$$

$$y = (r + H + z') / (L + H + z') \quad (4.19)$$

With  $D$  the fire diameter in [m],  $H$  the height from the fire to the ceiling [m],  $r$  the distance from the fire centreline to a lateral ceiling point and  $Q$  the fire total heat release rate [W].

Hasemi [22] notes the flame extension under the ceiling ( $L_H$ ) as

$$L_H = 2.9HQ_H^{*1/3} - H \quad (4.20)$$

Lattimer [21] proposes that the incident heat flux to the ceiling ( $q''_{\text{inc}}$  in  $\text{kW/m}^2$ ) is

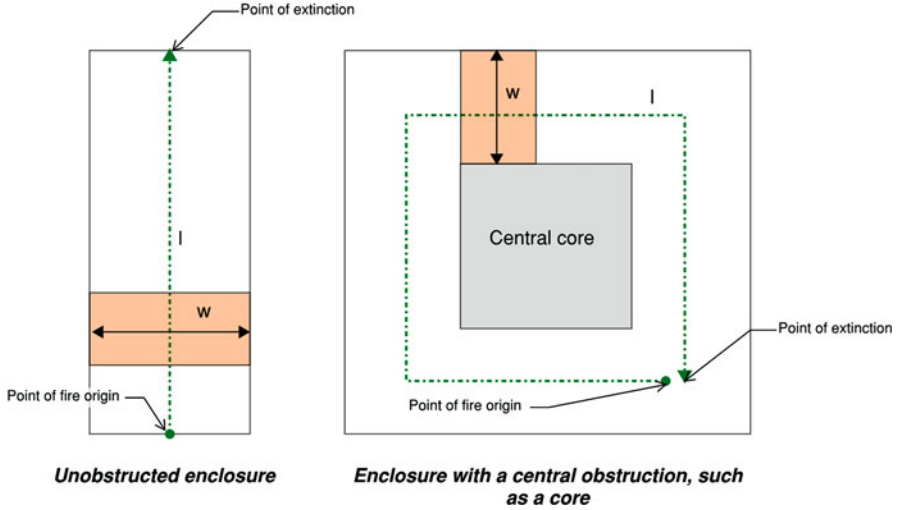
$$q''_{\text{inc}} = 120 \text{ kWm}^{-2} \text{ for } y \leq 0.5 \quad (4.21)$$

$$q''_{\text{inc}} = 682e^{-3.4y} \text{ for } y > 0.5 \quad (4.22)$$

At the tip of the flame, i.e.  $r = L_H$ ,  $q''_{\text{inc}}$  converges upon  $23 \text{ kW/m}^2$ . A more complete description of localized fires is presented by Heidari et al. [23].

### 4.5.2 Travelling Fires

A travelling fire shares similar characteristics to those of a localized fire. However, instead of remaining static, the fire travels towards unburnt fuel. Two idealized travelling fire arrangements are shown below (Fig. 4.7).



**Fig. 4.7** Two indicative travelling fire arrangements with fire travel path lengths and path widths, adapted from [6]

The travelling fire method [20, 24, 25] (TFM) produces a temporally and spatially non-uniform temperature distribution. To compute the thermal exposure to a ceiling structural element (i.e. beam), the travelling fire framework requires a computation of  $\dot{Q}$  and the time-varying relationship between the position of the fire relative to the structural element ( $r$ ).

The spread rates control the time required for the leading edge of the fire to travel towards a structural element. The trailing edge of the fire is governed by the time required for the fuel to burn out. Relevant correlations are given below:

Time to consume a unit area of fuel ( $t_{burn}$ ):

$$t_{burn} = \frac{q_f}{RHR_f} \tag{4.23}$$

Time to onset of decay phase ( $t_{decay}$ ):

$$t_{decay} = \max \left[ t_{burn}; \frac{l}{s} \right] \tag{4.24}$$

Time to peak fire size ( $t_{lim}$ ):

$$t_{lim} = \min \left[ t_{burn}; \frac{l}{s} \right] \tag{4.25}$$

Heat release rate during growth ( $\dot{Q}_{growth}$ ), i.e.  $t < t_{burn}$ :

$$\dot{Q}_{\text{growth}} = RHR_f \cdot w \cdot s \cdot t \tag{4.26}$$

Maximum (steady) heat release rate ( $Q_{\text{max}}$ ), i.e.  $t_{\text{lim}} < t < t_{\text{decay}}$ :

$$\dot{Q}_{\text{max}} = \min [RHR_f \cdot w \cdot s \cdot t_{\text{burn}} \text{ or } RHR_f \cdot w \cdot l] \tag{4.27}$$

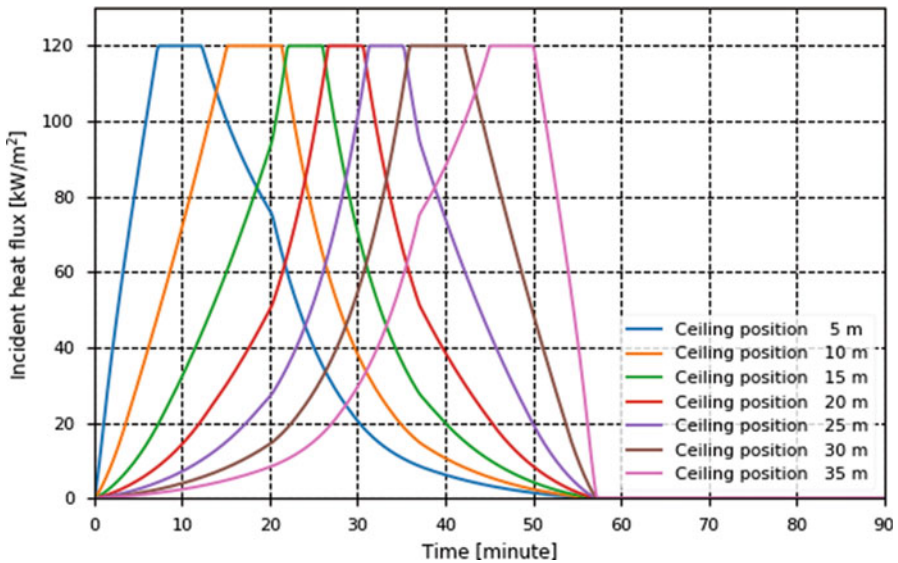
Heat release rate during decay ( $Q_{\text{decay}}$ ), i.e.  $t > t_{\text{burn}}$ :

$$\dot{Q}_{\text{decay}} = \text{Max}[\dot{Q}_{\text{max}} - ((t - t_{\text{decay}}) \cdot w \cdot s \cdot RHR_f) \text{ or } 0] \tag{4.28}$$

With:

$q_f$	[MJ/m <sup>2</sup> ]	is the fire load density
$RHR_f$	[MW/m <sup>2</sup> ]	is the heat release rate density or HRRPUA
$l$	[m]	is the length of the compartment (longest dimension)
$s$	[m/s]	is the fire spread rate (m/s)
$t$	[s]	is the time
$w$	[m]	is the width of the compartment

Once  $\dot{Q}$  is known, for a ceiling point at a distance  $r$  from the centre of the fire, the time-varying incident heat flux can be computed using correlations as presented in Sect. 4.5.1 (for example Fig. 4.8).



**Fig. 4.8** Illustrative ceiling incident heat flux in function of time for different distances from the point of ignition

Inputs for relevant parameters describing the fire are covered in more detail in Chap. 9.

## 4.6 Developed Fires (Post-flashover)

Post-flashover fire curves constitute a convenient approach for taking into account the compartment characteristics in SFE design. They represent parametrized (analytical) approximations to more elaborate, but still simplified, one-zone heat balance models or experiments. These curves are therefore also known as ‘parametric fire curves’. Considering their closer resemblance to physical fire behaviour, as opposed to the prescriptive heating exposures of Sect. 4.4, they are also referred to as ‘natural fire curves’. Importantly, parametric fire curves include not only a heating phase, but also a cooling behaviour, allowing the designer to assess structural performance up to and including burnout.

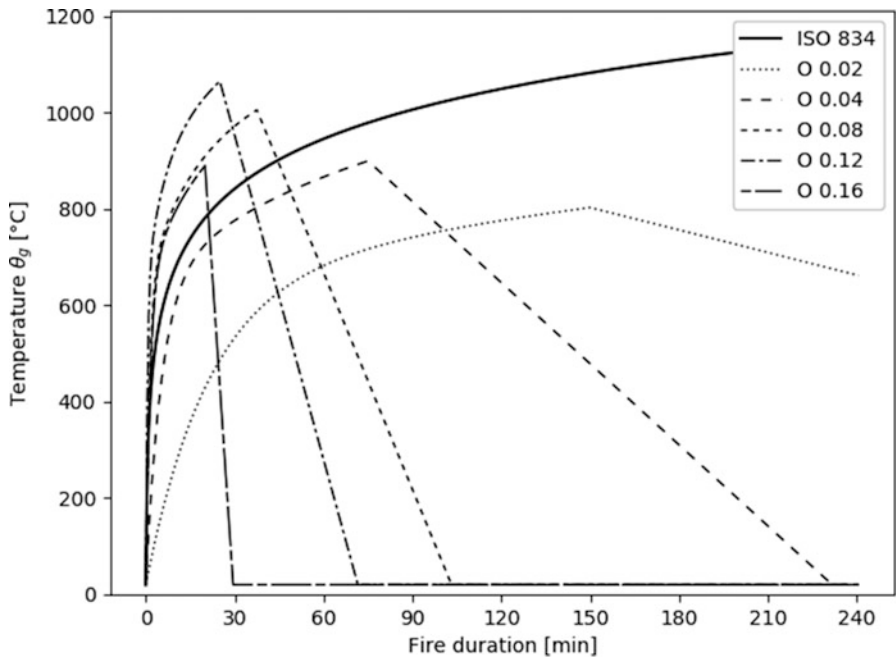
The most widely applied post-flashover fire curve is the Eurocode parametric fire curve, as specified in EN 1991-1-2:2002 [4]. In the following, this Eurocode parametric fire curve is introduced, followed by a discussion of its background and critiques raised. Finally, selected other parametric fire models are summarily discussed. The discussion on the background of the parametric fire curve highlights its limitations. This is particularly relevant considering the need for a ‘consistency of crudeness’ [26]; see Hopkin et al. [27] and other chapters within this handbook.

### 4.6.1 *The Eurocode Parametric Fire*

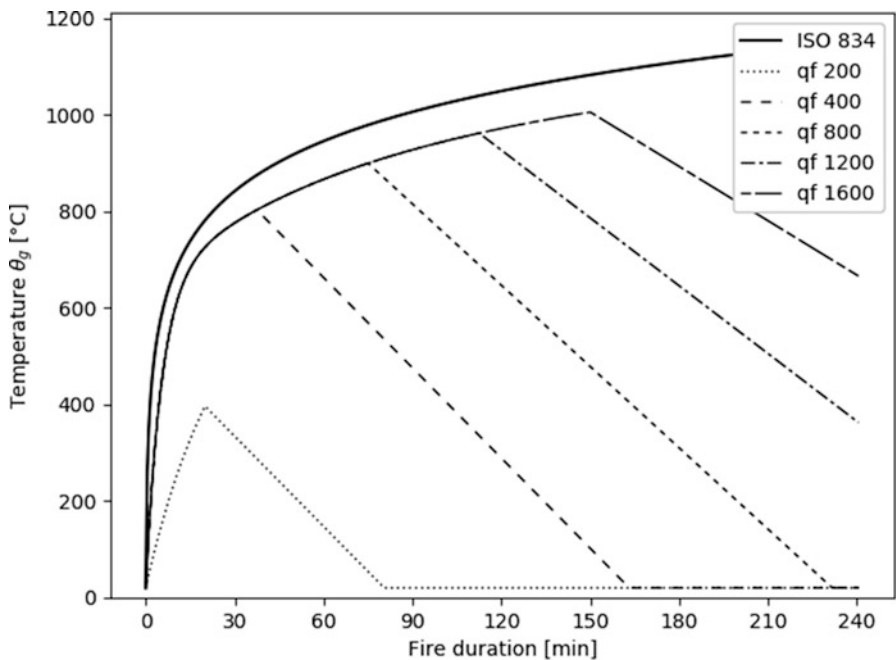
As indicated by its (colloquial) name, this fire curve has been specified as part of the Eurocodes, the European harmonised technical rules for the design of construction works. More specifically, the necessary equations are given in Annex A of EN 1991-1-2:2002. Figures 4.9 and 4.10 visualize the Eurocode parametric fire curves together with the ISO 834 standard fire curve, taken from [28]. The parametric fires start from a compartment with a floor area of  $10 \times 10 \text{ m}^2$ , a height of 3 m, thermal inertia of  $1500 \text{ J}/(\text{m}^2\text{s}^{0.5}\text{K})$ , opening factor of  $0.04 \text{ m}^{0.5}$  and fire load density of  $800 \text{ MJ}/\text{m}^2$ . Deviating parameters are as indicated in Figs. 4.9 and 4.10.

In accordance with the standard, the Eurocode parametric fire curve is valid for compartments up to  $500 \text{ m}^2$  floor area, with openings only in the walls (not roof), and up to a compartment height of 4 m. The model assumes complete burnout. The Eurocode parametric fire curve is presented in the following with reference to Franssen et al. [29], aiming to provide a clear view of the necessary inputs and calculation steps.





**Fig. 4.9** Eurocode parametric fire curves and ISO 834 standard fire curve. Parametric fire starting for a compartment with a floor area of  $10 \cdot 10 \text{ m}^2$ , a height of 3 m, thermal inertia of  $1500 \text{ J}/(\text{m}^2 \cdot \text{s}^{0.5} \cdot \text{K})$  and fire load density of  $800 \text{ MJ}/\text{m}^2$ , for different opening factor  $O [\text{m}^{0.5}]$



**Fig. 4.10** Eurocode parametric fire curves and ISO 834 standard fire curve. Parametric fire starting for a compartment with a floor area of  $10 \cdot 10 \text{ m}^2$ , a height of 3 m, thermal inertia of  $1500 \text{ J}/(\text{m}^2 \cdot \text{s}^{0.5} \cdot \text{K})$  and an opening factor of  $0.04 \text{ m}^{0.5}$ , for different fire load density  $q_f \text{ MJ}/\text{m}^2$

#### 4.6.1.1 Input Data

The necessary input data are:

*The geometry of the compartment.* The parameters needed are (1) the total floor area,  $A_f$ ; (2) the total enclosure area (including walls, ceilings and openings),  $A_e$ ; (3) the total area of all openings (windows and doors),  $A_v$ ; and (4) the weighted average height of the openings,  $h_{eq}$ . All these parameters should be specified, respectively, in  $m^2$  or  $m$ . For completeness, it should be noted that EN 1991-1-2:2002 does not specify how the weighted average should be taken. Commonly this is done through Eq. (4.29), as specified also by Franssen et al. [29], although Sleich [30], for example, applies Eq. (4.30), with the index  $j$  iterating across all vertical openings with height  $h_j$  and area  $A_{v,j}$ .

$$h_{eq} = \frac{\sum_j h_j A_{v,j}}{A_v} \quad (4.29)$$

$$h_{eq} = \left( \frac{\sum_j \sqrt{h_j A_{v,j}}}{A_v} \right)^2 \quad (4.30)$$

*The enclosure material build-up and thermal properties.* For the enclosure, the thermal conductivity  $\lambda$  [W/mK], specific heat  $c$  [J/kgK] and density  $\rho$  [kg/m<sup>3</sup>] are required. These parameters influence the fire development through the heat absorption by the enclosure, and are considered constant (irrespective of temperature) within the Eurocode parametric fire curve formulation. EN 1991-1-2:2002 specifies that ambient temperature values can be used, but equivalent values which take into account temperature dependency can be considered within the model as well. If a wall is made up of multiple layers, data on those materials is required (the two layers on the inside of the fire compartment).

*The expected fire growth rate* (slow, medium or fast). This defines a minimum duration of the fire,  $t_{lim}$ , of, respectively, 25, 20 or 15 min. Guidelines on the expected fire growth rate are listed in Annex E of the standard in function of the occupancy type. This recommendation is reprinted in Table 4.3.

*The fire load density,  $q_f$* , in MJ/m<sup>2</sup>. This parameter relates to the amount of combustibles in the compartment, relative to the floor area  $A_f$ . In function of the application, an expected value or a higher quantile of the fire load should be considered. Guidance on fire load densities is given in Annex E of the standard (see Table 4.3). These values relate to the movable fire loads in ordinary compartments for the specified occupancy types. Fire loads from construction elements, linings and finishing should be added to the listed values. Annex E of EN 1991-1-2:2002 furthermore gives a procedure for the specification of a design value  $q_{f,d}$ , commonly starting from the 80% quantile as characteristic value. This design value is based on reliability considerations and takes into account the fire risk and availability of active

**Table 4.3** Guidance of fire growth rate and fire load densities for different occupancies, as listed in Annex E of EN 1991-1-2:2002

Occupancy	Fire growth	Average fire load [MJ/m <sup>2</sup> ]	80% quantile fire load [MJ/m <sup>2</sup> ]
Dwelling	Medium	780	948
Hospital room	Medium	230	280
Hotel room	Medium	310	377
Library	Fast	1500	1824
Office	Medium	420	511
Classroom	Medium	285	347
Shopping Centre	Fast	600	730
Theatre (cinema)	Fast	300	365
Transport (public space)	Slow	100	122

fire protection measures for the given compartment. Annex E is less widely adopted than Annex A. Whether or not a design value is used does not affect the calculation steps.

#### 4.6.1.2 Calculation Steps

1. Evaluate the fire load density,  $q_t$  [MJ/m<sup>2</sup>], relative to the complete compartment enclosure area  $A_t$ :

$$q_t = q_f \frac{A_f}{A_t} \quad (4.31)$$

2. Evaluate the enclosure thermal inertia  $b$  [J/(m<sup>2</sup>s<sup>0.5</sup> K)].

The thermal inertia  $b$  of the compartment is the area-weighted average of the thermal inertia of the enclosure components, i.e. of the walls, floor and ceiling. Equation (4.32) applies, with the index  $i$  referring to the respective enclosure components exposed to the fire, and the area  $A_i$  calculated with exclusion of openings.

For a compartment boundary composed of a single material,  $b_i$  is given by Eq. (4.33). If a compartment boundary is made up of different layers of materials, then the first two layers are considered (index '1' for the material directly exposed, index '2' for the material behind it). If  $b_{i,1} < b_{i,2}$  (a 'lightweight' material insulating a 'heavy' material), then  $b_i = b_{i,1}$ . If the 'heavy' material is directly exposed, it has to be determined whether the heat penetrates the material sufficiently for the subsequent 'lightweight' material to influence the fire development. To this end a limiting thickness  $s_{i,\text{lim}}$  is calculated by Eq. (4.34). If  $s_{i,\text{lim}} < s_{i,1}$  (the thickness of the exposed layer), then  $b_i = b_{i,1}$ ; else  $b$  is given by Eq. (4.35).

Application of the Eurocode parametric fire curve requires that  $100 \leq b \leq 2200 \text{ J}/(\text{m}^2\text{s}^{0.5} \text{ K})$ , noting that  $t_{\max}$  [hr] is calculated in step 5:

$$b = \frac{\sum_i b_i A_i}{A_t - A_v} \quad (4.32)$$

$$b_i = \sqrt{c_i \rho_i \lambda_i} \quad (4.33)$$

$$s_{i, \text{lim}} = \sqrt{\frac{3600 t_{\max} \lambda_{i,1}}{c_{i,1} \rho_{i,1}}} \quad (4.34)$$

$$b_i = \frac{s_{i,1}}{s_{i, \text{lim}}} b_{i,1} + \left(1 - \frac{s_{i,1}}{s_{i, \text{lim}}}\right) b_{i,2} \quad (4.35)$$

3. Evaluate the opening factor  $O$  [ $\text{m}^{0.5}$ ], which relates to the supply of fresh air:

$$O = \frac{A_v \sqrt{h_{\text{eq}}}}{A_t} \quad (4.36)$$

4. Calculate the time-scaling factor  $\Gamma$  [-] through Eq. (4.37), with  $O_{\text{ref}} = 0.04 \text{ m}^{0.5}$  and  $b_{\text{ref}} = 1160 \text{ J}/(\text{m}^2\text{s}^{0.5} \text{ K})$ . A factor  $\Gamma = 1$  results in a heating phase close to the ISO 834 standard heating curve, while  $\Gamma > 1$  implies that higher temperatures are reached earlier, thus resulting in a fire which is colloquially ‘hotter’ than the standard heating curve. The opposite applies for  $\Gamma < 1$ :

$$\Gamma = \left(\frac{O/O_{\text{ref}}}{b/b_{\text{ref}}}\right)^2 \quad (4.37)$$

5. Evaluate the duration of the heating phase  $t_{\max}$  [h]:

$$t_{\max} = 0.2 \cdot 10^{-3} \frac{q_t}{O} \quad (4.38)$$

6. Compare  $t_{\max}$  with the minimum fire duration  $t_{\text{lim}}$  as listed in Table 4.4 in function of the assessed fire growth rate. If  $t_{\max} > t_{\text{lim}}$ , the fire is ventilation-controlled, otherwise fuel-controlled.

**Table 4.4** Minimum heating-phase duration  $t_{\text{lim}}$  in function of fire growth rate

Fire growth rate	$t_{\text{lim}}$ [min]	$t_{\text{lim}}$ [h]
Slow	25	5/12
Medium	20	1/3
Fast	15	1/4

If the fire is ventilation controlled, continue with Step 7a. For fuel-controlled fires, continue with Step 7b.

7a. *If the fire is ventilation-controlled, evaluate the fire curve as follows.* The heating-phase gas temperature is given by Eq. (4.39), in degree Celsius, and applies up to  $t = t_{\max}$ . This heating curve tends to an asymptotic temperature of 1345 °C as the heating-phase duration goes to infinity. Note that the time  $t$  is scaled by the time-scaling factor  $\Gamma$ , allowing a single equation to be applied both for a slowly rising fire and for a fire for which the temperature increases fast:

$$\theta_g = 20 + 1325(1 - 0.324e^{-0.2\Gamma t} - 0.204e^{-1.7\Gamma t} - 0.472e^{-19\Gamma t}) \quad (4.39)$$

The cooling phase is given by Eq. (4.40), with  $\theta_{\max}$  the maximum temperature reached in the heating phase, i.e. the temperature at  $t_{\max}$ :

$$\begin{aligned} \theta_g &= \theta_{\max} - 625(\Gamma t - \Gamma t_{\max}) \quad \text{for } \Gamma t_{\max} \leq 0.5 \text{ [h]} \\ \theta_g &= \theta_{\max} - 250(3 - \Gamma t_{\max})(\Gamma t - \Gamma t_{\max}) \quad \text{for } 0.5 \text{ [h]} \leq \Gamma t_{\max} \leq 2.0 \text{ [h]} \\ \theta_g &= \theta_{\max} - 250(\Gamma t - \Gamma t_{\max}) \quad \text{for } 2.0 \text{ [h]} \leq \Gamma t_{\max} \end{aligned} \quad (4.40)$$

The cooling-phase regime specifies a fast cooling rate of 625 °C per hour (scaled) time if  $\Gamma t_{\max} \leq 0.5$  h, and a slow cooling rate of 250 °C per hour scaled time if  $\Gamma t_{\max} \geq 2$  h. For intermediate values of  $\Gamma t_{\max}$  the cooling rate is a linear interpolation.

Since  $\Gamma t_{\max}$  relates directly to  $\theta_{\max}$ , the different cooling regimes can be directly specified with respect to  $\theta_{\max}$ . If  $\theta_{\max} \leq 841$  °C, the higher cooling rate applies, while the lower cooling rate applies for  $\theta_{\max} \geq 1048$  °C, and interpolated cooling rates are considered for intermediate maximum temperatures.

7b. *If the fire is fuel-controlled, evaluate the fire curve as follows.* A modified opening factor is considered in accordance with Eq. (4.41), where  $t_{\text{lim}}$  has the dimension [h]. Applying this modified opening factor, a modified time scaling factor  $\Gamma_{\text{lim}}$  is defined by Eq. (4.42), with  $O_{\text{ref}} = 0.04 \text{ m}^{0.5}$  and  $b_{\text{ref}} = 1160 \text{ J}/(\text{m}^2\text{s}^{0.5} \text{ K})$  as listed under Step 4:

$$O_{\text{lim}} = 0.1 \cdot 10^{-3} \frac{q_t}{t_{\text{lim}}} \quad (4.41)$$

$$\Gamma_{\text{lim}} = k \left( \frac{O_{\text{lim}}/O_{\text{ref}}}{b/b_{\text{ref}}} \right)^2 \quad (4.42)$$

The factor  $k$  equals unity, except for well-ventilated fuel-controlled fires ( $O > 0.04 \text{ m}^{0.5}$ ) where the fuel load and thermal inertia are small ( $q_t < 75 \text{ MJ}/\text{m}^2$ ;  $b < 1160 \text{ MJ}/\text{m}^2$ ). For those specific fires,  $k$  is given by

$$k = 1 + \left( \frac{O - 0.04}{0.04} \right) \left( \frac{q_t - 75}{75} \right) \left( \frac{1160 - b}{b} \right) \quad (4.43)$$

The heating-phase gas temperature is given by Eq. (4.44), which is the same general heating-phase formulation as for the ventilation-controlled fire, but with application of the limiting scaling factor  $\Gamma_{\text{lim}}$ . The obtained gas temperature is in degree Celsius and applies up to  $t = t_{\text{lim}}$ :

$$\theta_g = 20 + 1325(1 - 0.324e^{-0.2\Gamma_{\text{lim}}t} - 0.204e^{-1.7\Gamma_{\text{lim}}t} - 0.472e^{-19\Gamma_{\text{lim}}t}) \quad (4.44)$$

The cooling-phase temperature is specified through Eq. (4.45). This cooling-phase behaviour is the same as for ventilation-controlled fires, naturally starting from a different maximum temperature:

$$\begin{aligned} \theta_g &= \theta_{\text{max}} - 625(\Gamma t - \Gamma t_{\text{lim}}) \quad \text{for } \Gamma t_{\text{max}} \leq 0.5 \text{ [h]} \\ \theta_g &= \theta_{\text{max}} - 250(3 - \Gamma t_{\text{max}})(\Gamma t - \Gamma t_{\text{lim}}) \quad \text{for } 0.5 \text{ [h]} \leq \Gamma t_{\text{max}} \leq 2.0 \text{ [h]} \\ \theta_g &= \theta_{\text{max}} - 250(\Gamma t - \Gamma t_{\text{lim}}) \quad \text{for } 2.0 \text{ [h]} \leq \Gamma t_{\text{max}} \end{aligned} \quad (4.45)$$

#### 4.6.1.3 Equivalent Compartments Within the Eurocode Parametric Fire Curve

The specifications above seemingly indicate that the Eurocode parametric fire curve is the function of many parameters. Closer examination however indicates that the curve has only two degrees of freedom. This implies that any generic compartment (within the bounds of applicability of the parametric curve) can, for example, be translated into an equivalent reference compartment with an invariant geometry and thermal inertia by calculating appropriate equivalent values for the fire load density  $q_{t,\text{eq}}$  and opening factor  $O_{\text{eq}}$  for this equivalent compartment. These equivalent values need not be within the bounds of the Eurocode parametric fire curve's applicability, as the transformation is purely mathematical. The fire growth rate (i.e.  $t_{\text{lim}}$ ) is not affected by the transformation.

Application of an equivalent compartment allows to generalize results of structural performance beyond a single arbitrary compartment. Thienpont et al. [28] apply such a procedure to list generally applicable burnout resistance capacities for a concrete slab. They apply a square equivalent compartment of  $10 \times 10 \text{ m}^2$ , with a height of 3 m and thermal inertia of  $1450 \text{ J}/(\text{m}^2\text{s}^{0.5} \text{ K})$ .

The equivalency formulas are as follows (Thienpont et al., [28]), where the index ‘eq’ refers to the equivalent compartment with fixed geometry and thermal inertia:

$$O_{\text{eq}} = O \frac{b_{\text{eq}}}{b} \quad (4.46)$$

$$q_{f,\text{eq}} = q_f \frac{A_f}{A_{f,\text{eq}}} \frac{A_{t,\text{eq}}}{A_t} \frac{b_{\text{eq}}}{b} \quad (4.47)$$

If the fire in the generic compartment is fuel-controlled,  $\Gamma_{\text{lim}}$  is given by Eq. (4.48), indicating that  $\Gamma_{\text{lim}}$  can be evaluated either for the generic compartment or for the equivalent compartment. The factor  $k$  relates to the generic compartment, assuming that a convenient choice has been made to set  $b_{\text{eq}} \geq 1160 \text{ J}/(\text{m}^2 \text{ s}^{0.5} \text{ K})$ . More elaborate equations are required in case the equivalent reference compartment would be within the bounds where the  $k$ -factor applies ( $O_{\text{eq}} > 0.04$ ;  $q_{t,\text{eq}} < 75 \text{ MJ}/\text{m}^2$ ;  $b_{\text{eq}} < 1160 \text{ J}/(\text{m}^2 \text{ s}^{0.5} \text{ K})$ ):

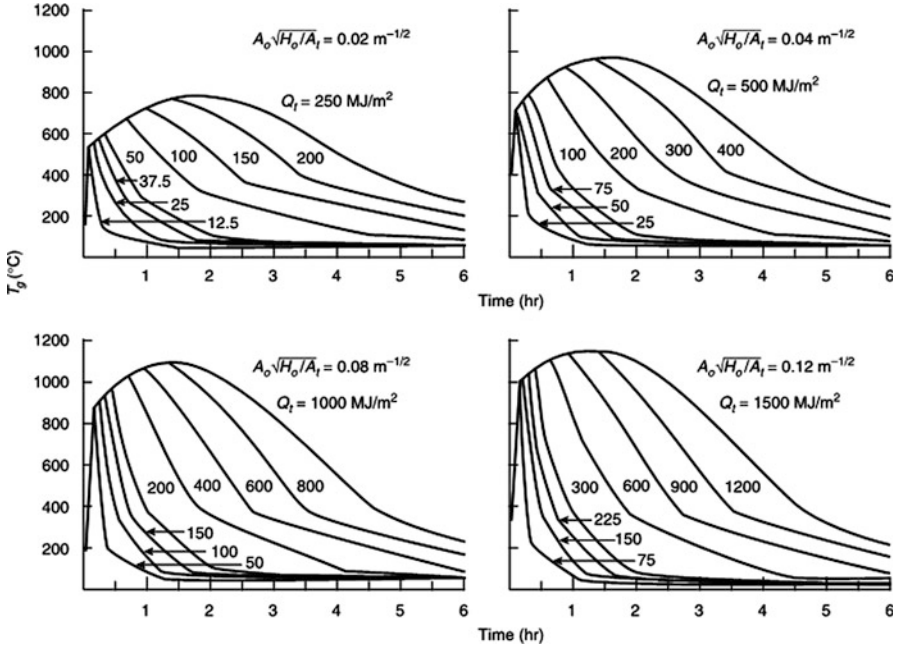
$$\Gamma_{\text{lim}} = k \left( \frac{O_{\text{lim}}/O_{\text{ref}}}{b/b_{\text{ref}}} \right)^2 = k \left( \frac{O_{\text{lim,eq}}/O_{\text{ref}}}{b_{\text{eq}}/b_{\text{ref}}} \right)^2 \quad (4.48)$$

## 4.6.2 Background to the Eurocode Parametric Fire Curve

Crucial steps in the development of a parametric description for a ‘general natural fire curve’ were made by Wickström in the early 1980s [31, 32]. Wickström’s formulation provided a basis for the provisional Eurocode parametric fire curve listed in ENV 1991-2-2:1996 [33]. Amongst others Franssen [34] proposed improvements to this provisional formulation, resulting in the Eurocode parametric fire curve as incorporated in EN 1991-1-2:2002. The Eurocodes are not static documents, and it can be reasonably foreseen that new formulations may be considered in future editions.

### 4.6.2.1 Wickström’s General Natural Fire Curve

In the 1970s, a series of studies were concluded in Sweden on the description of post-flashover fires and related structural fire engineering applications, e.g. Magnusson and Thelandersson [35] and Pettersson et al. [5]. Through heat balance considerations, temperature-time curves were numerically evaluated for compartment fires, considering a range of opening factors and fire loads, and different building types (i.e. different wall thermal responses). The obtained curves were published in graphical and tabular format for application in fire engineering design (see Magnusson and Thelandersson [35]) and have been commonly referred



**Fig. 4.11** Example gas time-temperature curves for post-flashover fires as a function of opening factor and fire load density with normal enclosure linings, adapted from [35]

to in the fire engineering community as the ‘Swedish curves’. An example set of these curves is shown in Fig. 4.11. Key assumptions underlying these curves are the following (Wickström [31]): (1) uniform temperature in the fire compartment; (2) all fuel burns inside the compartment; (3) the fire is ventilation-controlled; and (4) natural ventilation.

Wickström applied the same conceptual model in his derivation of a ‘general natural fire curve’. Crucially, a concept of scaled time was introduced, allowing post-flashover fires to be expressed in a single time-temperature curve for which time is scaled to account for the ventilation conditions and wall properties. While the method is a major improvement over the consideration of a standard heating regime (see Sect. 4.4), Wickström [32] highlights that the method is very approximate and should be used with care. To provide insight into the background of the Eurocode parametric fire curve, Wickström’s considerations are summarized in the following.

Considering the key assumptions above, the compartment acts as a well-stirred reactor. The heat balance for the compartment is given previously by Eq. (4.1).

The buoyancy-driven inflow of fresh air into the compartment is, considering for simplicity a single opening with area  $A_o$  and height  $h_o$ , proportional to  $A_o h_o^{0.5}$



(Drysedale, [36]) with flow constant  $\alpha_1$ . Considering all oxygen to be consumed by the fire, the combustion heat release rate is given by Eq. (4.49), with  $\alpha_2$  a coefficient for the heat released per unit of air. Similarly, the convective heat loss is given by Eq. (4.50), with  $c$  the specific heat of air and  $\theta_f$  the temperature rise inside the compartment relative to the outside air. The radiation losses are approximated by Eq. (4.51), with  $\sigma$  the Stefan-Boltzmann constant and  $T_f$  the absolute temperature within the compartment:

$$\dot{q}_c = \alpha_1 \alpha_2 A_0 \sqrt{h_0} \quad (4.49)$$

$$\dot{q}_l = c \theta_f \alpha_1 A_0 \sqrt{h_0} \quad (4.50)$$

$$\dot{q}_r = A_0 \sigma T_f^4 \quad (4.51)$$

Evaluation of the heat losses through the compartment boundaries is more elaborate as this term is time dependent considering the progressing temperature front within the walls and ceiling. Wickström tackles this in a three-pronged approach. First, Wickström notes that for typical fire durations the unexposed side of the wall does not influence the fire, and that the wall can be considered semi-infinite for all practical purposes. Secondly, the heat transfer resistance between the exposed wall surface and its surroundings is neglected, implying a surface temperature increase equal to the compartment temperature increase  $\theta_f$ . This assumption corresponds with an overestimation of heat losses and thus lower fire compartment temperatures, notably early in the fire. Thirdly, the wall thermal properties are represented through temperature-independent values, in effect through an equivalent thermal inertia  $b$ .

The temperature evolution within a semi-infinite slab with given (constant) surface temperature increase  $\theta_s$  has an analytical solution; see, e.g., Drysdale [36]. Specifically, the differential equation under consideration is given by Eq. (4.52), the Fourier equation, with boundary conditions as in Eq. (4.53). The solution is given by Eq. (4.54), with erf the error function. Note that  $\lambda/(\rho c)$  is often denoted as the thermal diffusivity  $\alpha$ :

$$\frac{\partial \theta}{\partial t} = \frac{\lambda}{\rho c} \frac{\partial^2 \theta}{\partial x^2} \quad (4.52)$$

$$\theta = 0 \text{ at } t = 0 \text{ for all } x \neq 0$$

$$\theta = \theta_f \text{ at } x = 0 \text{ for all } t$$

$$\theta = 0 \text{ as } x \rightarrow \infty \text{ for all } t \quad (4.53)$$

$$\theta = \theta_s \left( 1 - \operatorname{erf} \left( \frac{x}{2\sqrt{\frac{\lambda}{\rho c}}} \right) \right) \quad (4.54)$$

The conductive heat transfer at the surface is given by Eq. (4.55) and defines the heat loss into the compartment wall (for a constant surface temperature  $\theta_s$ ). Note the introduction of the thermal inertia  $b$ :

$$q = -\lambda \left( \frac{\partial \theta}{\partial x} \right)_{x=0} = \lambda \theta_s \sqrt{\frac{\rho c}{\lambda \pi t}} = \theta_s \sqrt{\frac{\lambda \rho c}{\pi t}} = \theta_s b \sqrt{\frac{1}{\pi t}} \quad (4.55)$$

The surface temperature, assumed equal to the compartment temperature, is however not constant. This can be taken into account by considering, as time progresses and the compartment temperature increases, further heat losses to be initiated through Eq. (4.55) for every further temperature increase. The total heat loss at the surface at time  $t$  is then the sum of the newly activated heat loss and the dissipating effects from earlier temperature increases. Mathematically, this is represented by the convolution integral equation (4.56), with  $\theta_{f,\tau}(t - \tau)$  the time derivative of the compartment temperature increase, evaluated at  $t - \tau$ , and  $\tau$  a dummy (time) variable for integration:

$$\dot{q}_w = A_t q(t) = A_t \int_0^t b \sqrt{\frac{1}{\pi \tau}} \theta_{f,\tau}(t - \tau) d\tau \quad (4.56)$$

Substituting the above derivations into gives Eq. (4.57). Dividing all terms by  $Ah^{0.5}$  and re-arranging give Eq. (4.58), where the constants  $C_1 = c\alpha_1$  and  $C_2 = \alpha_1\alpha_2$  have been introduced, and the opening factor  $O$  is given by  $Ah^{0.5}/A_i$ :

$$\alpha_1\alpha_2 A \sqrt{h} = c\theta_f \alpha_1 A \sqrt{h} + A_t \int_0^t b \sqrt{\frac{1}{\pi \tau}} \theta_{f,\tau}(t - \tau) d\tau + A\sigma T_f^4 \quad (4.57)$$

$$C_2 = C_1 \theta_f + \frac{b}{O} \frac{1}{\sqrt{\pi}} \int_0^t \frac{1}{\sqrt{\tau}} \theta_{f,\tau}(t - \tau) d\tau + \frac{\sigma T_f^4}{\sqrt{h}} \quad (4.58)$$

Wickström subsequently introduces the concept of scaled time, where  $t^* = \Gamma t$ . The dimensionless scaling factor  $\Gamma$  is specified by Eq. (4.59) and relates the enclosure characteristics to those of a reference compartment. This equation corresponds with the scaling factor in EN 1991-1-2:2002. Substituting the scaled time results in Eq. (4.60). This equation is in agreement with [32], but not with [31]. It is assumed that the discrepancy with the latter reference results from a printing error:

**Table 4.5** Coefficients for the generalized natural fire curve (heating regime), in accordance with different references

Parameter	Wickström [31]	Wickström [32]	EN 1991-1-2:2002 [4]
$B_0$	1110.0	1325	1325
$B_1$	-369.7	-430	-429.3
$\beta_1$	0.61	0.2	0.2
$B_2$	-200.4	-270	-270.3
$\beta_2$	4.94	1.7	1.7
$B_3$	-539.9	-625	-625.4
$\beta_3$	23.1	19	19

$$\Gamma = \left( \frac{O/O_{\text{ref}}}{b/b_{\text{ref}}} \right)^2 \quad (4.59)$$

$$C_2 = C_1 \theta_f + \frac{b_{\text{ref}}}{O_{\text{ref}}} \frac{1}{\sqrt{\pi}} \int_0^{t^*} \frac{1}{\sqrt{\tau^*}} \theta_{f,\tau^*}(t^* - \tau^*) d\tau^* + \frac{\sigma T_f^4}{\sqrt{h}} \quad (4.60)$$

In [31]  $O_{\text{ref}} = 0.04 \text{ m}^{0.5}$  and  $b_{\text{ref}} = 1165 \text{ J}/(\text{m}^2 \text{ s}^{0.5} \text{ K})$ . The latter value is updated to  $b_{\text{ref}} = 1160 \text{ J}/(\text{m}^2 \text{ s}^{0.5} \text{ K})$  in [32]. These values for  $O_{\text{ref}}$  and  $b_{\text{ref}}$  have been maintained within the Eurocode parametric fire format.

As the radiation contribution is considered small, Eq. (4.60) is dependent on the scaled time  $t^*$  only. Wickström confirmed this concept of scaled time by plotting the temperature-time curves of Magnusson and Thelandersson against the scaled time and confirming that the obtained curves largely coincide, except for small modified time values where the simplifying assumptions result in discrepancies (e.g. wall surface temperature equal to the compartment temperature). The obtained curve was named the ‘general natural fire curve’. If the radiation contribution is fully neglected, a closed-form solution is obtained [32]. In [31], an analytical formulation for this general natural fire curve was obtained by curve fitting. The curve is of the general format of Eq. (4.61), with coefficients as listed in Table 4.5. The obtained heating curve in [31] is close to the ISO 834 standard heating regime for reasonable fire durations, up to (for example)  $t^* = 3 \text{ h}$ . Arguably taking into account this small discrepancy between the curve fit and the ISO 834 heating regime, the coefficients applied in [32] are those listed in the then current Swedish building code as approximations for the ISO 834 standard heating regime. The general format of Table 4.5 applies to the Eurocode parametric curve as well (considering an ambient temperature of 20 °C). It is clear from Table 4.5 that the coefficients listed in [32] have been adopted in EN 1991-1-2:2002:

$$\theta_f(t^*) = B_0 + \sum_{i=1}^3 B_i \exp(-\beta_i t^*) \quad (4.61)$$

The above derivations apply for the heating phase only. The duration of the heating phase is governed by the assumptions of ventilation control and full combustion inside the compartment, resulting in a heating-phase duration proportional to the fire load density and inversely proportional to the ventilation factor, i.e. Eq. (4.62). Wickström does not provide values for the proportionality constant  $\alpha$ . These can however readily be assessed through simplifying assumptions on the heat release rate profile (for example: constant heat release linked to the steady-state inflow of oxygen); see, e.g., [37]:

$$t_{\max} = \alpha \frac{q_t}{O} \quad (4.62)$$

A key feature of a natural fire exposure is its finite duration, i.e. the presence of a cooling phase. Wickström adopted linear time-temperature relationships for the cooling phase listed in the then current ISO 834 standard [14], ‘for the sake of simplicity’. The constant cooling rate is defined by Eq. (4.63) [°C/h]. Comparing Eq. (4.63) with the cooling formulations in the Eurocode parametric fire curve indicates that Wickström’s simplifying assumption has been incorporated in EN 1991-1-2:2002. Examining the old standard ISO 834:1975 [38], the cooling rates were prescribed in case the structural element needs to perform functions also in the cooling phase. The standard specifies that the external load should remain constant during the cooling phase and prescribes the listed cooling rates up to the point where furnace temperature has reduced to 200 °C. No further specification is given on the further cooling to ambient temperatures:

$$\begin{aligned} \frac{d\theta_g}{dt^*} &= -625 \text{ for } \Gamma t_{\max} \leq 0.5 \text{ [h]} \\ \frac{d\theta_g}{dt^*} &= -250(3 - \Gamma t_{\max}) \text{ for } 0.5 \text{ [h]} \leq \Gamma t_{\max} \leq 2.0 \text{ [h]} \\ \frac{d\theta_g}{dt^*} &= -250 \text{ for } 2.0 \text{ [h]} \leq \Gamma t_{\max} \end{aligned} \quad (4.63)$$

#### 4.6.2.2 From Wickström [32] to the Eurocode Parametric Fire

In 1995 a provisional Eurocode ENV 1991-2-2:1995 was published, aimed at gathering experience/comments before publishing the final Eurocode. A parametric fire curve was included in Annex B, adopting the scaled time heating and cooling formulations as given by Wickström [32]. This formulation was later incorporated in EN 1991-1-2:2002. As a further specification, ENV 1991-2-2:1995 stated the

coefficient  $\alpha$  in Eq. (4.62) as being equal to  $0.13 \times 10^{-3} [\text{h m}^{2.5}/\text{MJ}]$ , i.e. Eq. (4.64). This equation can be related to an assumption that  $t_{\max}$  is achieved when 70% of the fuel is burned [34]:

$$t_{\max} = 0.13 \cdot 10^{-3} \frac{q_t}{O} \quad (4.64)$$

Furthermore, the validity range of the parametric fire curve was specified to  $50 \text{ MJ/m}^2 \leq q_t \leq 1000 \text{ MJ/m}^2$ ,  $A_f \leq 100 \text{ m}^2$ , compartment height  $\leq 4 \text{ m}$ ,  $1000 \text{ J}/(\text{m}^2\text{s}^{0.5}\text{K}) \leq b \leq 2000 \text{ J}/(\text{m}^2\text{s}^{0.5}\text{K})$  and  $0.02 \text{ m}^{0.5} \leq O \leq 0.20 \text{ m}^{0.5}$ . An equation for calculating the equivalent thermal inertia for a wall made up of layers of different materials was also introduced. The equivalent compartment thermal inertia was calculated without considering the presence of openings in the walls.

The validity of the ENV formulation was investigated amongst others as part of a large European research project ‘Competitive Steel Buildings Through Natural Fire Safety Concept’ [39]. To this end, a database of compartment fire tests was developed. Considering 48 experimental tests, Franssen [34] made a comparison between (1) observed and calculated maximum gas temperatures; (2) calculated maximum temperatures in an unprotected steel element considering on the one hand observed and on the other hand calculated gas temperatures; and (3) calculated maximum temperatures for a protected steel element, as in (2). For the respective comparisons, limited correlation was found between the calculated and observed maximum gas temperatures, but more consistent results were obtained for the calculated maximum temperature of the insulated steel member. The temperatures for the insulated steel section calculated considering the provisional Eurocode parametric fire curve were however generally lower than those calculated using the experimental gas temperature measurements. No direct comparison of the measured and calculated temperature-time curves was discussed.

To improve the parametric fire curve’s correlation with the experimentally based results, Franssen proposed a number of modifications. Firstly, a more precise procedure for evaluating the equivalent thermal inertia of a wall made up of different materials was presented. The original ENV formulation did not differentiate in the order of the materials, implying that a ‘lightweight’ material covered by a ‘heavy’ material would result in the same equivalent  $b$  as in case the order of materials would be reversed. Furthermore, no consideration was given to the depth of thermal penetration, implying that a very thick layer far from the exposed surface could govern the overall inertia. Franssen calibrated an alternative formulation through numerical thermal analyses using the SAFIR finite element model. Franssen’s proposal was incorporated in EN 1991-1-2:2002; the specifics of his proposal are listed as Step 2 above in Sect. 4.6.1.2. For a lightweight material covered by a heavier material, the formulation is very accurate. For a heavy material (large  $b$ ) covered by an insulating light material (low  $b$ ), the formulation underestimates the heat losses to the wall; this results in an overestimation of  $\Gamma$  and, equivalently, an overestimation of compartment temperatures. Considering the updated  $b$  values for the experimental tests used for validation, Franssen notes that the improved

equivalency rules increase the field of application of the parametric fire curve with respect to  $b$ .

Secondly, the assumption of a ventilation-controlled fire was questioned. When Eq. (4.64) is applied to compartments with a low fire load and high opening factor, the fire duration becomes unrealistically low. Franssen argues that the duration of free burning should be applied as a limiting case and proposes a limiting fire duration  $t_{lim}$ , equal to 20 min in accordance with the value set in Annex C of the ENV for thermal actions on external members. If the heating-phase duration  $t_{max}$  is smaller than  $t_{lim}$ , then a limiting opening factor  $O_{lim}$  is defined through Eq. (4.65). This limiting opening factor is smaller than the real opening factor  $O$  and is then applied to scale the time for the heating phase, through the scaling factor  $\Gamma_{lim}$  in Eq. (4.66), adopted in the EN 1991-1-2:2002. The limiting opening factor slows down the calculated fire development and is applied up to  $t_{lim}$ , after which the cooling phase starts. The cooling-phase formulation is not modified, and thus the cooling rates of Eq. (4.63), as assumed by Wickström, are applied with the regular scaling factor  $\Gamma$ . Franssen clarifies the use of the regular  $\Gamma$  in the cooling phase by stating that the cooling is not dependent on whether the fire development was ventilation- or fuel-controlled. Therefore, the cooling-phase behaviour should not be modified relative to the original proposal based on the differentiation between fuel-controlled and ventilation-controlled fires. The factor  $k$  is as specified by Eq. (4.43). This factor considers that  $O_{lim}$  underestimates the amount of heat lost through the openings and thus results in an overestimation of the compartment temperature. The formulation of the factor  $k$  is as specified in EN 1991-1-2:2002 and has been obtained through curve fitting [34]. Franssen reports that taking into account the suggested modifications significantly improves the correlation between the calculated and observed maximum gas temperatures, and also results in maximum temperatures for the insulated steel member which are no longer systematically underestimated:

$$O_{lim} = 0.13 \cdot 10^{-3} \frac{q_f}{t_{lim}} \quad (4.65)$$

$$\Gamma_{lim} = k \left( \frac{O_{lim}/O_{ref}}{b/b_{ref}} \right)^2 \quad (4.66)$$

Franssen's proposals were incorporated in the ProfilARBED background document [37]. As already indicated above, these formulations were adopted in EN 1991-1-2:2002, with two further modifications. First of all, the equivalent compartment inertia was updated to the formulation in Eq. (4.32), i.e. with explicit consideration for the presence of openings. Furthermore, Eq. (4.64) was updated into its final formulation in Eq. (4.38), and the coefficient in Eq. (4.65) was updated to the formulation in Eq. (4.41). These modifications in effect make a distinction for the coefficient  $\alpha$  when considering ventilation-controlled or fuel-controlled regimes. These adjustments were made following the addition of eight more experiments to the calibration database. The coefficient of Eq. (4.41) results from a calibration against tests [37]. The coefficient in Eq. (4.38) was derived considering full

consumption of the fuel at a constant (maximum) heat release rate. This coefficient can be well approximated by considering the inflow of air into the compartment to be given by Eq. (4.67) with the rate of air refreshing specified in [kg/s]; see Drysdale [36]. Taking a heat of combustion of 3 MJ/kg air, the rate of heat release (RHR) equals  $RHR \approx 3\dot{m}_{\text{air}}$  [MW], allowing to approximate  $t_{\text{max}}$  [h] by Eq. (4.68) where the factor 1/3600 accounts for the dimension change from seconds to hours. Crucially, the differentiation of coefficients for the ventilation-controlled and fuel-controlled fires results in a discontinuity in the fire curve at the point where  $t_{\text{max}}$  calculated by Eq. (4.38) equals  $t_{\text{lim}}$ :

$$\dot{m}_{\text{air}} \approx 0.52A_v\sqrt{h} \quad (4.67)$$

$$t_{\text{max}} \approx \frac{q_t A_t}{RHR} \cdot \frac{1}{3600} = \frac{1_t}{3600 \cdot 3 \cdot 0.52} \frac{q_t A}{A_v \sqrt{h}} = 0.185 \cdot 10^{-3} \frac{q_t}{O} \quad (4.68)$$

EN 1991-1-2:2002 adopted the proposals as listed in [37]. The only change is the consideration of different values for  $t_{\text{lim}}$  in function of the occupancy type; see Tables 4.3 and 4.4.

### 4.6.2.3 Criticism

The parametric fire formulation as applicable under EN 1991-1-2:2002 faces a number of criticisms. Most prominently, the adoption of distinct coefficients for  $\alpha$  when considering either a fuel-controlled or a ventilation-controlled fire has introduced a discontinuity in the model at the transition between both. Reitgrüber et al. [40] show how the maximum compartment temperature discretely jumps over a hundred degrees at the transition. This discontinuity is not based on physical considerations, and implies that a design which is seemingly acceptable may have been considered inadequate given a slight variation of input parameters.

Furthermore, Reitgrüber et al. came to the conclusion that the parametric fire curve calibration reported in [37] considers an effective heat of combustion of 18 MJ/kg of wood. This is at odds with the recommended value for the effective heat of combustion within Annex E of EN 1991-1-2:2002, where a value of 14 MJ/kg is recommended (considering a combustion factor of 0.8). Under the assumption that the Annex E heat of combustion is preferable, Reitgrüber et al. state that this implies an underestimation of compartment fire temperatures within the Eurocode parametric fire framework (also when the fire load is specified directly in MJ/m<sup>2</sup>).

Reitgrüber et al. recalibrated the parametric fire curve considering a heat of combustion of 14 MJ/kg, and recommend the use of a single coefficient  $\alpha$  with a value of  $0.14 \times 10^{-3}$  [h·m<sup>2.5</sup>/MJ] within the Eurocode parametric fire framework. They indicate that this suggested solution effectively addresses the two above points of criticism.

On a related note, Zehfuss and Hosser [41] note that the temperature-time curve of Annex A of EN 1991-1-2:2002 does not bear connection with the heat release rate

specifications of Annex E in the same standard. This also relates to the criticism that the Eurocode parametric time curve does not include a pre-flashover development stage. This latter point is not necessarily an important criticism by itself, as it can be argued that structural fire design is often considered for the post-flashover stage only, but it is an important consideration when comparing the parametric curve with other curves or with experiments.

Finally, and crucially, the cooling-phase formulation of the Eurocode parametric fire curve appears not to be based on thorough physical considerations. This is confirmed when considering the origins of the cooling-phase formulation as resulting from Wickström's [31] adoption of cooling curves prescribed by the then current ISO 834 standard. Also Barnett [42] questions the linear Eurocode cooling curve and indicates this as a motivation underlying his development of an alternative curve, the BFD curve discussed further below. Furthermore, the use of scaled time in the cooling phase can make the cooling rate unrealistically fast or slow [43]. Feasey and Buchanan [43] stress that the use of scaled time in the cooling phase has never been justified. They propose an alternative time scaling in the cooling phase. Their modification is however not commonly applied and is not discussed any further here.

In most of these parametric models, the physical phenomena that are taken into account are broadly the same [40]. In the following, the Institute of Building Materials, Concrete Structures and Fire Protection (iBMB) parametric curve and the BFD curve are summarily introduced. Alternative formulations have been presented, e.g., by Zhongcheng en Mäkeläinen [44].

### **4.6.3 Other Parametric Fire Curves**

#### **4.6.3.1 The iBMB Parametric Fire Curve**

The iBMB parametric fire curve for offices and residential buildings has been derived by Zehfuss and Hosser [41] from compartment heat balance simulations, similar to the concept underlying the Swedish curves of Magnusson and Thelandersson [35]. The simulation results are approximated analytically, resulting in 'empirical' equations for natural fire exposure. As the iBMB curve is directly linked to heat release rates, Zehfuss and Hosser argue that it provides a clearer relationship with the burning behaviour inside the compartment than the Eurocode parametric fire curve. Furthermore, the iBMB curve considers the modelled cooling behaviour, and also has a more gradual increase of temperature at the start of the fire.

#### **4.6.3.2 The BFD Curve**

The BFD curve has been proposed by Barnett [42] based on a curve-fitting procedure. The BFD curve consists of a single equation for the entire fire duration, and has three degrees of freedom: (1) the maximum temperature rise above ambient, (2) the



time since the start of the fire at which the maximum temperature rise occurs and (3) a shape factor. The shape factor is related to the heat release rate and opening factor through a regression analysis of experimental data. For assessing the maximum temperature rise, Barnett refers to other studies, such as those listed in the SFPE Handbook [45], while referring to design fire considerations (heat release rate) for evaluating the time of maximum temperature.

As demonstrated by Barnett [46], comparison between the BFD curve and the Eurocode parametric fire curve suggests that the BFD curve can approximate the Eurocode parametric curve when considering a built-in time shift in the Eurocode parametric curve (i.e. when taking into account that the fast temperature increase at the start of the Eurocode parametric fire presumes a prior fire development).

## 4.7 Computational Fire Modelling

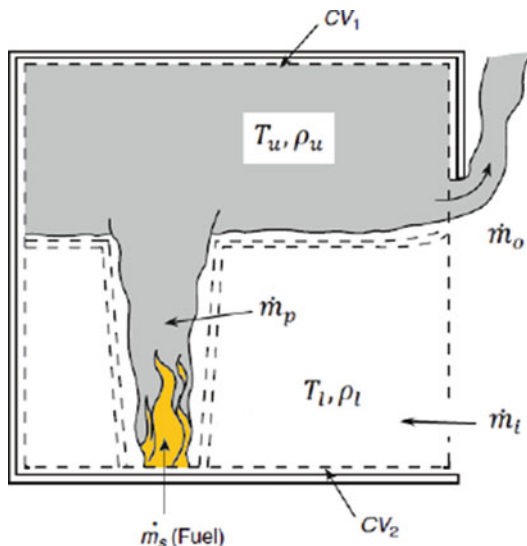
### 4.7.1 Zone Modelling

One common type of physically based fire model used in fire safety engineering is the *zone* model, which solves the conservation equations (i.e. conservation of mass and energy) for discrete control volumes. Although many zone models use two control volumes per room corresponding to an upper (hot) layer and a lower (cool) layer, other zone models may approach specific problems differently such as a single control volume for post-flashover fire modelling. Fire zone modelling can be traced to the mid-1970s when the effort to study the developing fire in an enclosure intensified. The first to publish a basis for the zone model approach was Fowkes [47] in relation to bedroom fire experiments at Factory Mutual. The more common zone models in use today include CFAST [2], OZONE [48] and B-RISK [8]. A more detailed description of the fundamental principles of enclosure fire zone models can be found elsewhere in the literature, e.g [49–51].

A simple two-zone model is illustrated in Fig. 4.12, where CV1 encloses the gases in the upper layer along with the plume, while CV2 encloses the remaining volume within the room representing the lower layer. The interface between the two layers is referred to as the layer height and this can move up or down in response to changes in the volume of each zone.

Burning fuel releases mass and energy which is transported by the buoyant plume and deposited in the upper part of the room. Air is entrained from the lower layer (CV2) into the plume as a result of buoyancy, causing the volume of the upper layer to increase and move the layer interface closer to the floor. As the layer descends below the top of an opening some of the gases (including mass and enthalpy) leave the room and are removed from control volume CV1. Hydrostatic pressure differences over the height of the opening create a flow of air from outside into the room at low level. The gas properties (including temperature, gas density and concentrations) of each control volume are assumed to be spatially uniform, but able to vary with

**Fig. 4.12** Two-zone enclosure model [51]



time. It is also assumed that the gases transported in the plume are instantaneously distributed across the ceiling.

The zone model approach typically uses a series of sub-models and source terms to quantify the various mass and energy flows. These can vary in complexity and usually include empirical relationships or correlations to describe phenomena such as the entrainment into the fire plume, shear mixing of flows near the openings as well as vent flows. Along with the heat enthalpy flows that accompany the transport of mass terms, additional heat transfer calculations to account for heat losses to the room-bounding surfaces are typically included. Some models also include additional sub-models designed to predict detector or sprinkler operation, visibility or tenability estimates and other parameters that may be useful for fire safety engineering.

Zone models allow for relatively inexpensive parametric studies by providing results very quickly on modern computers. This capability enables the uncertainty and sensitivity of the results to changes in input to be more easily evaluated, and by applying both engineering judgment and deterministic modelling, particular scenarios of interest can be isolated for which further in-depth field modelling (CFD) may be needed.

### 4.7.2 Computational Fluid Dynamics

The basis of computational fluid dynamics (CFD) modelling is governed by three fundamental principles: the conservative of mass, the conservation of momentum (Newton's second law) and the conservation of energy. These principles are expressed in general mathematical form usually as partial differential equations

[52], for example the Navier-Stokes equations. The Navier-Stokes equations can be examined as a means to estimate the behaviour of fluids, where these equations describe the dynamic motion of incompressible fluid, considering unknowns of velocity and pressure as functions of space and time [53].

In approximating the governing equations of CFD for non-laminar flow, consideration has to be given to irregular or ‘chaotic’ changes in pressure and velocity, referred to as turbulence. Different mathematical turbulence models can be adopted to describe and simplify the sub-grid-scale phenomena, including direct numerical simulation (DNS), Reynolds-averaged Navier-Stokes (RANS), detached eddy simulation (DES) and large eddy simulation (LES), discussed in greater detail elsewhere [54].

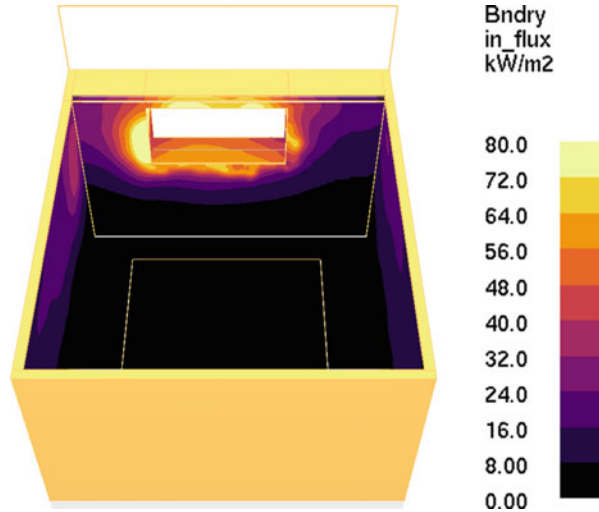
Unlike with the development of zone modelling, it can be seen that CFD techniques were originally established by practitioners outside of the fire engineering community and were later incorporated into it [55]. It was identified by fire engineers that CFD could be used as a tool to estimate the flow of smoke and hot gases in a fire-affected environment, assessing factors such as tenability conditions (with respect to temperature and visibility), radiative heat transfer and exchanges of heat/energy at solid or open boundaries.

There are several CFD-based fire and smoke modelling tools which have developed over the course of fire engineering history, such as SMARTFIRE [56] from the University of Greenwich and FireFOAM [57] from FM Global. Perhaps the most commonly adopted CFD tool in modern fire engineering application is Fire Dynamics Simulator (FDS) [58, 59], developed by the National Institute of Standards and Technology (NIST) in the USA. FDS was created with an intention of focusing specifically on smoke and heat transport from fires, solving a form of the Navier-Stokes equations considered appropriate for low-speed and thermally driven fluid flow. By default, FDS adopts a very large eddy simulation (VLES) turbulence model [58], allowing for a compromise between computational efficiency and precision of the model.

In structural fire engineering, CFD-based fire and smoke modelling can be used to help inform and define the thermal boundary conditions for structural elements, where this information can subsequently be fed into or coupled with structural models. That is, by undertaking CFD, thermal conditions to which elements may be exposed can be estimated and then applied as a boundary condition to a solid-phase model. Typically, specialist finite element models are used for estimating the transfer of heat within a structure, although CFD tools may incorporate solid-phase sub-models to partially represent these factors.

The benefit CFD models have over zone models is the option to assess a given problem with a greater degree of detail and precision, observing the possible variations and fluctuations in estimated thermal conditions across surfaces, rather than collating this output as a uniform value across a control volume, e.g. upper layer temperature. An example visualization of a more ‘detailed’ boundary condition is shown in Fig. 4.13. This visualization shows the estimation of the incident heat flux on surfaces around a window opening, for a simple room fire simulated in FDS.

**Fig. 4.13** Example visualization of incident heat flux in a simple room fire



Despite CFD allowing for the evaluation of problems with greater precision when compared to other approaches, its application comes with several pitfalls. Given the relative complexity of CFD as a tool for assessing fire phenomena, it may be reasoned that there is a greater stress and reliance on the practitioner's competence in adequately applying the tool. CFD modelling also comes at a much greater computational cost than zone modelling, with each individual simulation requiring a much longer length of time to run. This cost means that the practitioner will need to restrict the number of scenarios they intend to assess, providing less opportunity to examine the potential variability of input parameters and to undertake intensive sensitive studies. For this reason, a 'reasonable worst case' is typically defined, where this case sits on a spectrum of possibilities which are not typically evaluated [60]. Conversely, zone modelling tools like B-RISK [8] can assess the impact of fire and smoke stochastically, considering distributions for many input parameters.

When adopting CFD modelling tools to assess a problem, the representation of fire and smoke parameters can sometimes appear relatively simplified in comparison to the detailed assessment of outputs, depending on the decisions made by the practitioner. Hence, simpler modelling methods, such as zone models, may be selected to maintain a 'consistent level of crudeness', where it has been argued historically that the level of detail in a process should be governed by the crudest part of that process [61]. A high level of care therefore needs to be taken when defining fire scenarios and selecting input parameters for CFD simulation, also ensuring that the tool is appropriate for the situations being evaluated.

## 4.8 Actions on Structures in Fire

The mechanical loading acting on a structure in the event of fire is stochastic, with a more thorough discussion provided in Chap. 9, Van Coile et al. [62] and Ellingwood [63]. Compared to ambient temperature design, most design codes around the world permit consideration of a reduced action acting on the structure at the time of a fire event. This is expressed through (reduced) partial safety factors applied to the permanent ( $G_k$ ) and imposed ( $Q_k$ ) loads. In the case of the Eurocodes, detailed guidance is given in EN 1990 [64] and associated national application documents, e.g. PD 6688-1-2 [65] in the case of the UK.

The design effects of actions for the fire situation in the Eurocode framework can be calculated from the general form of the accidental load combinations given by Eqs. (4.69) and (4.70):

$$\sum_{j \geq 1} G_{k,j} + P + A_d + \Psi_{1,1} Q_{k,1} + \sum_{i \geq 2} \Psi_{2,i} Q_{k,i} \quad (4.69)$$

$$\sum_{j \geq 1} G_{k,j} + P + A_d + \sum_{i \geq 1} \Psi_{2,i} Q_{k,i} \quad (4.70)$$

where the terms  $P$  and  $A_d$  refer to prestressing load and indirect fire actions, respectively.

The differentiation is made between Eqs. (4.69) and (4.70) depending upon whether the partial safety factor ( $\Psi$ ) is taken as the frequent value ( $\Psi_1$ ) or the quasi-permanent value ( $\Psi_2$ ). The choice is left to each member state [66]. In the special case of roofs, both  $\Psi_1$  and  $\Psi_2$  take the value of zero. Otherwise,  $\Psi_1$  ranges from 0.5 to 0.9 for imposed loads associated with offices to storage.  $\Psi_2$  takes the range of 0.3 to 0.8 for imposed loads associated with offices to storage.

For other jurisdictions, Buchannan and Abu [67] note combinations for the USA and Australia/New Zealand per Eqs. (4.71) and (4.72), respectively:

$$1.2G_k + 0.5Q_k \quad (4.71)$$

$$G_k + 0.4 \text{ to } 0.6Q_k \quad (4.72)$$

The 0.6 in Eq. (4.72) relates to imposed loads for storage facilities. Regarding Eq. (4.71), it is noted that the factor of 1.2 should be reduced to 0.9 where the permanent load provides a stabilizing effect.

In general, given the many nuances and differences in load combinations and factors between nations, it is strongly recommended that there be recourse to national design codes for the purpose of determining the relevant actions on structures in the event of fire.

## References

1. American Society of Civil Engineers. (2018). *Structural fire engineering*. Reston, VA: American Society of Civil Engineers/Structural Engineering Institute, Manual of Practice No. 138.
2. Peacock, R. D., McGrattan, K. B., Forney, G. P., & Reneke, P. A. (2017). *CFAST – Consolidated fire and smoke transport (version 7) volume 1: Technical reference guide*. National Institute of Standards and Technology, NIST Technical Note 1889v1.
3. Hamins, A. P., et al. (2005, September 1–5). *Experiments and modeling of structural steel elements exposed to fire*. National Institute of Standards and Technology.
4. BSI. (2002). *BS EN 1991-1-2:2002 Eurocode 1. Actions on structures. General actions. Actions on structures exposed to fire*. British Standards Institution.
5. Pettersson, O., Magnusson, O., & Thor, J. (1976). *Fire engineering design of steel structures, Bulletin 52, Publication 50*. Swedish Institute of Steel Construction.
6. BSI. (2019). *PD 7974-1: 2019 application of fire safety engineering principles to the design of buildings. Initiation and development of fire within the enclosure of origin (Sub-system 1)*. BSI.
7. Kawagoe, K. (1958). *Fire behaviour in rooms*. Building Research Institute, Report 27.
8. Wade, C., Baker, G., Frank, K., Harrison, R., & Spearpoint, M. (2016). *B-RISK 2016 user guide and technical manual*, BRANZ, SR364.
9. Babrauskas, V. (2016). Heat release rates. In *SFPE handbook of fire protection engineering* (5th ed.). Springer.
10. Hopkin, C., Spearpoint, M., & Hopkin, D. (2019). A review of design values adopted for heat release rate per unit area. *Fire Technology*, 55(5), 1599–1618. <https://doi.org/10.1007/s10694-019-00834-8>.
11. LaMalva, K., 'Chapter IV-9: Fire Design,' Architects Guide to Structures, Routledge, 2017
12. ASTM. (2019). *ASTM E119 - 19 standard test methods for fire tests of building construction and materials*. ASTM.
13. ANSI/UL. (2001). *Standard for fire tests of building construction and materials*. Underwriters Laboratories, ANSI/UL 263.
14. ISO. (1999). *ISO 834-1:1999 Fire-resistance tests — Elements of building construction — Part 1: General requirements*. International Organization for Standardization.
15. BSI. (2012). *BS EN 1363-1:2012 Fire resistance tests. General requirements*. BSI.
16. BSI. (1987). *BS 476-20:1987 Fire tests on building materials and structures. Method for determination of the fire resistance of elements of construction (general principles)*. BSI.
17. ASTM. (2016). *ASTM E1529 - 16e1 standard test methods for determining effects of large hydrocarbon pool fires on structural members and assemblies*. ASTM.
18. UL 1709. (2011). *Standard for rapid rise fire tests of protection materials for structural steel*. Underwriters Laboratories.
19. Heskestad, G. (1984, January). Engineering relations for fire plumes. *Fire Safety Journal*, 7(1), 25–32. [https://doi.org/10.1016/0379-7112\(84\)90005-5](https://doi.org/10.1016/0379-7112(84)90005-5).
20. Rackauskaite, E., Hamel, C., Law, A., & Rein, G. (2015, August). Improved formulation of travelling fires and application to concrete and steel structures. *Structure*, 3, 250–260. <https://doi.org/10.1016/j.istruc.2015.06.001>.
21. Lattimer, B. Y. (2016). Heat transfer from fires to surfaces. In *SFPE handbook of fire protection engineering* (5th ed., pp. 745–798). Springer.
22. Hasemi, Y., Yokobayashi, S., Wakamatsu, T., & Ptchelintsev, A. (1995). Fire safety of building components exposed to a localized fire: Scope and experiments on ceiling/beam system exposed to a localized fire. In *AsiaFlam '95*.
23. Heidari, M., Kotsovinos, P., & Rein, G. (2020). Flame extension and the near field under the ceiling for travelling fires inside large compartments. *Fire and Materials*. <https://doi.org/10.1002/fam.2773>.
24. Stern-Gottfried, J., & Rein, G. (2012, November). Travelling fires for structural design—Part I: Literature review. *Fire Safety Journal*, 54, 74–85. <https://doi.org/10.1016/j.firesaf.2012.06.003>.

25. Stern-Gottfried, J., & Rein, G. (2012, November). Travelling fires for structural design-part II: Design methodology. *Fire Safety Journal*, 54, 96–112. <https://doi.org/10.1016/j.firesaf.2012.06.011>.
26. Buchanan, A. (2008). The challenges of predicting structural performance in fires. *Fire Safety Science*, 9, 79–90. <https://doi.org/10.3801/IAFSS.FSS.9-79>.
27. Hopkin, D. J., Van Coile, R., & Lange, D. (2017). Certain uncertainty - Demonstrating safety in fire engineering design and the need for safety targets. *SFPE Europe*, Q3(7), 1–5.
28. Thienpont, T., Van Coile, R., Caspeele, R., & De Corte, W. (2019). Comparison of fire resistance and burnout resistance of simply supported reinforced concrete slabs exposed to parametric fires. In *3rd International Conference on Structural Safety under Fire and Blast*. Brunel University.
29. Franssen, J.-M., Zaharia, R., & Kodur, V. (2009). *Designing steel structures for fire safety*. CRC Press/Balkema.
30. Schleich, J. (2005). Fire actions in buildings. In *Implementation of the Eurocodes: Handbook 5: Design of buildings for the fire situation*. Leonardo Da Vinci Pilot Project CZ/02/B/F/PP-134007.
31. Wickström, U. (1981). Temperature calculation of insulated steel columns exposed to natural fire. *Fire Safety Journal*, 4(4), 219–225. [https://doi.org/10.1016/0379-7112\(81\)90024-2](https://doi.org/10.1016/0379-7112(81)90024-2).
32. Wickström, U. (1985). Application of the standard fire curve for expressing natural fires for design purposes. In T. Harmathy (Ed.), *Fire safety: Science and engineering* (p. 145–159). ASTM International.
33. CEN. (1996) Eurocode 1. Basis of design and actions on structures. Actions on structures exposed to fire. ENV 1991-2-2:1996. European Committee for Standardization.
34. Franssen, J. M. (2000). Improvement of the parametric fire of Eurocode 1 based on experimental test results. *Fire Safety Science*, 6, 927–938.
35. S. Magnusson and S. Thelamderson, 'Temperature - Time curves of complete process of fire development', Lund Institute of Technology, Bulletin of division of structural mechanics and concrete construction, Bulletin 16, 1970.
36. Drysdale, D. (2011). *An introduction to fire dynamics* (3rd ed.). Wiley.
37. ProfilARBED. (2001). *Background document on Parametric temperature-time curves according to Annex A of prEN1991-1-2*. Document No. EC1-1-2/72, CEN/TC250/SC1/N298A.
38. ISO. (1975). *ISO 834:1975 Fire-resistance tests — Elements of building construction*. International Organization for Standardization.
39. Schleich, J., & Cajot, L.-G. (2001). *Valorisation project - natural fire safety concept*. Profil Arbed.
40. Reitgrüber, S., Pérez-Jimenez, C., Di Blasi, C., & Franssen, J.-M.. (2006) Some comments on the Parametric Fire Model of Eurocode 1. In *Conference on Fire in Enclosures, Jordanstown* [Online]. Retrieved from <http://hdl.handle.net/2268/70848>.
41. Zehfuss, J., & Hosser, D. (2007, March). A parametric natural fire model for the structural fire design of multi-storey buildings. *Fire Safety Journal*, 42(2), 115–126. <https://doi.org/10.1016/j.firesaf.2006.08.004>.
42. Barnett, C. R. (2002, July). BFD curve: A new empirical model for fire compartment temperatures. *Fire Safety Journal*, 37(5), 437–463. [https://doi.org/10.1016/S0379-7112\(02\)00006-1](https://doi.org/10.1016/S0379-7112(02)00006-1).
43. Feasey, R., & Buchanan, A. (2002, February). Post-flashover fires for structural design. *Fire Safety Journal*, 37(1), 83–105. [https://doi.org/10.1016/S0379-7112\(01\)00026-1](https://doi.org/10.1016/S0379-7112(01)00026-1).
44. Zhongcheng, M., Mäkeläinen, P. (2000). *Parametric temperature-time curves of medium compartment fires for structural design*. *Fire Safety Journal*, 34(4), 361–375, ISSN 0379-7112
45. Hurley, M., et al. (2016). *SFPE handbook of fire protection engineering* (5th ed.). Springer.
46. Barnett, C. R. (2007, June). Replacing international temperature-time curves with BFD curve. *Fire Safety Journal*, 42(4), 321–327. <https://doi.org/10.1016/j.firesaf.2006.11.001>.
47. Fowkes, N. D. (1975). A mechanistic model of the 1973 and 1974 bed-room test fires. FMRC Technical Report No. 21011.4.

48. Cadorin, J.-F., & Franssen, J.-M. (2003, September). A tool to design steel elements submitted to compartment fires—OZone V2. Part 1: Pre- and post-flashover compartment fire model. *Fire Safety Journal*, 38(5), 395–427. [https://doi.org/10.1016/S0379-7112\(03\)00014-6](https://doi.org/10.1016/S0379-7112(03)00014-6).
49. Quintiere, J. G. (1989, August). Fundamentals of enclosure fire “zone” models. *Journal of Fire Protection Engineering*, 1(3), 99–119. <https://doi.org/10.1177/104239158900100302>.
50. Janssens, M. (1992). Room fire models. In V. Babrauskas & S. J. Grayson (Eds.), *Heat release in fires*. Essex.
51. Quintiere, J. G., & Wade, C. A. (2016). Compartment fire modeling. In *SFPE handbook of fire protection engineering* (5th ed., pp. 981–995). Springer.
52. Anderson, J., Jr. (2009). Basic philosophy of CFD. In *Computational fluid dynamics, an introduction* (3rd ed., pp. 3–14). Springer.
53. Łukaszewicz, G., & Kalita, P. (2016). *Navier-stokes equations, an introduction with applications* (Vol. 34). Springer.
54. Wilcox, D. (1994). *Turbulence modeling for CFD*. DWX Industries.
55. McGrattan, K., & Miles, S. (2016). Modelling fires using computational fluid dynamics (CFD). In *SFPE handbook of fire protection engineering* (5th ed., pp. 1034–1065). Springer.
56. SMARTFIRE. (2020). *Fire Safety Engineering Group*. Retrieved February 13, 2020, from <https://fseg.gre.ac.uk/smartfire/>
57. Open Source Fire Modeling (FireFOAM). (2020). *FM Global*. Retrieved February 13, 2020, from <https://www.fmglobal.com/research-and-resources/research-and-testing/theoretical-computational-and-experimental-research/open-source-fire-modeling>
58. McGrattan, K., Hostikka, S., McDermott, R., Floyd, J., & Vanella, M. (2019). *Fire dynamics simulator user's guide*. National Institute of Standards and Technology, NIST SP 1019. <https://doi.org/10.6028/NIST.SP.1019>
59. McGrattan, K., Hostikka, S., McDermott, R., Floyd, J., & Vanella, M. (2019). *Fire dynamics simulator technical reference guide volume 1: Mathematical model*. National Institute of Standards and Technology, NIST SP 1018-1. <https://doi.org/10.6028/NIST.SP.1018>
60. Hopkin, D., Hopkin, C., Spearpoint, M., Ralph, B., & Van Coile, R. (2019). ‘Scoping study on the significance of mesh resolution vs. scenario uncertainty in CFD modelling of residential smoke control systems’, in *Interflam 2019*, Royal Holloway.
61. Elms, D. G. (1992). Consistent crudeness in system construction. In B. H. V. Topping (Ed.), *Optimization and artificial intelligence in civil and structural engineering: Volume I: Optimization in civil and structural engineering* (pp. 71–85). Springer.
62. Van Coile, R., Hopkin, D., Elhami Khorasani, N., Lange, D., & Gernay, T. (2019). Permanent and live load model for probabilistic structural fire analysis: A review. In *3rd International Conference on Structural Safety under Fire and Blast*.
63. Ellingwood, B. R. (2005, February). Load combination requirements for fire-resistant structural design. *Journal of Fire Protection Engineering*, 15(1), 43–61. <https://doi.org/10.1177/1042391505045582>
64. BSI. (2005). *BS EN 1990:2002+A1:2005 Eurocode. Basis of structural design*. BSI Standards Publication.
65. BSI. (2007). *PD 6688-1-2:2007 Background paper to the UK National Annex to BS EN 1991-1-2*. BSI.
66. Franssen, J.-M., & Real, P. V. (2010). *Fire design of steel structures: Eurocode 1: actions on structures, part 1–2: General actions - Actions on structures exposed to fire - Eurocode 3: design of steel structures, part 1–2: General rules - Structural fire design, 1*. ECCS: Ernst & Sohn.
67. Buchanan, A. H., & Abu, A. (2017). *Structural design for fire safety* (2nd ed.). Wiley.



# Chapter 5

## Heat Transfer to Structural Elements



Kevin LaMalva, Cristian Maluk, Ann Jeffers, and Allan Jowsey

This chapter covers the following topics:

- Fundamentals of heat transfer and description of basic engineering concepts for describing the thermal boundary conditions for solid elements (e.g., structural elements) during fire.
- Formulation of heat transfer from the fire to structural elements in terms of heat fluxes.
- The thermal properties of materials used in a heat transfer analysis.
- Special design considerations associated with nontypical heating conditions and nonstandard materials.

---

K. LaMalva (✉)  
Warringtonfire, Boston, MA, USA  
e-mail: [kevin.lamalva@warringtonfire.com](mailto:kevin.lamalva@warringtonfire.com)

C. Maluk  
School of Civil Engineering, University of Queensland, Brisbane, QLD, Australia  
e-mail: [c.maluk@uq.edu.au](mailto:c.maluk@uq.edu.au)

A. Jeffers  
Civil and Environmental Engineering Department, University of Michigan, Ann Arbor, MI,  
USA  
e-mail: [jffrs@umich.edu](mailto:jffrs@umich.edu)

A. Jowsey  
PFP Specialists, Sudbury, UK  
e-mail: [allan.jowsey@pfp-specialists.co.uk](mailto:allan.jowsey@pfp-specialists.co.uk)

## 5.1 Fundamentals of Heat Transfer

This section covers the fundamentals of heat transfer and describes basic engineering concepts for describing the thermal boundary conditions for solid elements (e.g., structural elements) during fire.

### 5.1.1 Summary of Heat Transfer

When analyzing the heat transfer from the fire to a structural element the problem needs to be formulated in terms of heat fluxes. While temperature of the solid phase results from solving the energy conservation equations, all quantities to be balanced are energies. The correlation between temperature and heat flux can be linear, but this is only under the assumption that an overall constant heat transfer coefficient can be established in space and time. An important aspect, many times overlooked, is the need to make sure that the thermal boundary conditions are properly represented.

The thermal boundary conditions at the surface of the solid are defined by means of the equation below:

$$\dot{q}''_{Tot} = -k \frac{\partial T}{\partial x} \Big|_{x=0}$$

where  $k$  is the thermal conductivity of the solid material.

In this section some basic heat transfer concepts are reviewed simply to extract the relevant parameters that will be used in later sections for discussion. These concepts are not novel and can be found in any heat transfer book. Heat is transferred from gases to solid surfaces via radiation and convection resulting in a total heat flux,  $\dot{q}''_{Tot}$ , where

$$\dot{q}''_{Tot} = \dot{q}''_{rad} + \dot{q}''_{con}$$

where  $\dot{q}''_{rad}$  is the heat transfer via radiation and  $\dot{q}''_{con}$  is the heat transferred via convection. For simplicity, within the scope of this chapter, the problem will only be examined in the direction of the principal heat flux, hence considered to be a one-dimensional problem and with the thermal boundary condition of the solid element (i.e., structural element) defined as

$$\dot{q}''_{Tot} = -k_i \frac{\partial T}{\partial x} \Big|_{x=0}$$

which is a generic version of the former equation, and where the thermal conductivity ( $k_i$ ) is a property of the solid and the gradient of temperature is taken at the surface. In other words, all the heat arriving at the surface of the solid is conducted

into the solid. If there are multiple layers then at each interface the following boundary condition should apply:

$$-k_i \frac{\partial T}{\partial x} = -k_s \frac{\partial T}{\partial x}$$

where the gradients correspond to each side of the interface and the subindex “s” is a generic way to represent the next layer of solid. Once the thermal boundary conditions are defined, the energy equation can be solved for each material involved. In the case where two layers of solid are involved (“i” and “s”), then the energy equations take the following form:

$$\rho_i C p_i \frac{\partial T}{\partial t} = \frac{\partial}{\partial x} \left( k_i \frac{\partial T}{\partial x} \right)$$

and

$$\rho_s C p_s \frac{\partial T}{\partial t} = \frac{\partial}{\partial x} \left( k_s \frac{\partial T}{\partial x} \right)$$

The solution of the energy conservation equations yields the temperature evolution of the material in space and time. The equations above could be repeated for as many layers as necessary. If the geometry or the fire exposure is complex, then the problem needs to be resolved in two or even three dimensions. If the properties vary with temperature then, as the temperature increases, these properties need to evolve with the local temperature. Variable properties thus require a numerical solution. If a simple analytical solution is to be obtained, then adequate global properties need to be defined. It is important to note that whatever the solution methodology adopted, the temperature of the structure is the result of the resolution of the two equations above using thermal boundary conditions such as those formerly shown. To obtain the numerical solution it is necessary to input material properties for the different layers (“i” and “s”). The material properties required are all a function of temperature and are as follows:

$$\rho_i, C p_i, k_i \text{ and } \rho_s, C p_s, k_s$$

where  $(\rho_i, \rho_s)$ ,  $(C p_i, C p_s)$ , and  $(k_i, k_s)$  are the densities, specific heat capacity, and thermal conductivity for each layer, respectively.

An assessment of the role of detailed boundary conditions is shown above. Structural performance is an unavoidable result of the real evolution of the in-depth temperature of a structural element in space and time. To define the performance of a structural system in fire it is necessary to establish the correct thermal boundary condition. The evolution of this boundary condition will determine internal temperature distributions and thus structural behavior.

### 5.1.2 Thermal Boundary Conditions

Fire exposures to structures produce thermal boundary conditions that are most commonly expressed as combined convection and radiation at the surface, as given in the equation above. Specifically, for a solid that is immersed in an optically thick gas with uniform temperature  $T_g$  (e.g., as would be the case of a structural element in a furnace), the net heat flux is given as

$$\dot{q}''_{\text{Tot}} = \varepsilon\sigma\left(\overline{T}_g^4 - \overline{T}_s^4\right) + h(T_g - T_s)$$

where  $\varepsilon$  = emissivity,  $\sigma$  = Stefan-Boltzmann constant ( $5.67 \times 10^{-8} \text{ W m}^{-2} \text{ K}^{-4}$ ),  $h$  = convection heat transfer coefficient, and  $T_s$  = surface temperature of the solid. Note that the temperatures needed for the radiative heat flux (i.e.,  $\overline{T}_g$  and  $\overline{T}_s$ ) must be expressed in units of Kelvin, whereas the temperatures for the convective heat flux (i.e.,  $T_g$  and  $T_s$ ) may be given in Celsius.

The equation below is often used to represent heat transfer under standard fire exposure, where the gas temperature  $T_g$  follows the ISO 834 [1] standard time-temperature relationship:

$$T_g(t) = 20 + 345 \log\left(\frac{8t}{60} + 1\right)$$

Note that time  $t$  is in seconds and temperature  $T_g$  is in  $^{\circ}\text{C}$ .

In structural fire engineering, the post-flashover fire exposure in a building is often treated the same as the furnace exposure. In other words, the former equation is used to represent the net heat flux at the structure's surface. The gas temperature can be determined from references such as Eurocode 1 [2] or SFPE S.01 [3]. These references provide parametric time-temperature relationships for the fire based on factors such as the fuel load density, thermal properties of the compartment linings, and ventilation conditions in the room. One salient feature of the Eurocode and SFPE fire models is that they include a cooling phase, whereas the standard fire exposure does not.

Another type of heating scenario that is common in structural fire engineering is the heating of materials by radiant panels or heaters, as would be the case, for example, in a cone calorimeter test. In this case, the engineer would likely know the radiant heat flux  $\dot{q}''_{\text{inc}}$  produced by the panel. The boundary condition at the solid's surface is then expressed as

$$\dot{q}''_{\text{Tot}} = \varepsilon\left(\dot{q}''_{\text{inc}} - \sigma\overline{T}_s^4\right) + h(T_g - T_s)$$

Note that the equation above separates the radiant heat flux from the gas temperature, whereas the former equation presumes that the radiation temperature and convection temperature are equal to one another. It follows that  $\dot{q}''_{\text{inc}} = \sigma\overline{T}_r^4$ ,

where  $\bar{T}_r$  is the blackbody radiation temperature (in Kelvin). Thus, the equation above can be expressed as

$$\dot{q}''_{\text{Tot}} = \varepsilon\sigma(\bar{T}_r^4 - \bar{T}_s^4) + h(T_g - T_s)$$

An important point to mention is that equations above are nonlinear in temperature, whereas most software for heat transfer analysis use linear equation solvers that solve for temperature in the governing differential equation. As a result, the radiation term is linearized as follows:

$$\dot{q}''_{\text{rad}} = h_r(\bar{T}_r - \bar{T}_s)$$

where

$$h_r = \varepsilon\sigma(\bar{T}_r^2 + \bar{T}_s^2)(\bar{T}_r + \bar{T}_s)$$

The assumed form of the thermal boundary conditions drives the selection of instrumentation in structural fire experiments. In furnace tests, for example, it is common to have a measurement of the gas temperature  $T_g$ , which is determined using thermocouples. However, it is generally accepted that gas temperature is inadequate for measuring the amount of heat that the structure absorbs by radiation, and so some researchers have advocated for the introduction of plate thermometers in structural fire experiments to measure a property called *adiabatic surface temperature*. Adiabatic surface temperature  $T_{\text{AST}}$  is defined as the temperature of a perfectly insulated surface. Wickström [4] shows that  $T_{\text{AST}}$  is a single parameter that will allow the analyst to uniquely account for radiation and gas temperatures (i.e.,  $T_r$  and  $T_g$ , respectively) that are not the same. In particular

$$T_{\text{AST}} = \frac{h_r\bar{T}_r + hT_g}{h_r + h}$$

One important thing to note is that, in this case,  $h_r$  is dependent on  $T_{\text{AST}}$ , so the equation above is not explicit. Nevertheless, the thermal boundary condition may be expressed in the following manner:

$$\dot{q}''_{\text{Tot}} = \varepsilon\sigma(\bar{T}_{\text{AST}}^4 - \bar{T}_s^4) + h(T_{\text{AST}} - T_s)$$

Other methods exist for measuring the heat flux to a fire-exposed surface, although the methods have some limitations. One approach, for example, uses a water-cooled heat flux gauge to measure the heat flux incident on a surface. For a heat flux  $\dot{q}''_f$  measured by the heat flux gauge, the net heat flux at the surface is as follows [5]:

$$\dot{q}''_{\text{Tot}} = \dot{q}''_f - \varepsilon\sigma(\bar{T}_s^4 - \bar{T}_g^4) - h(T_s - T_g)$$

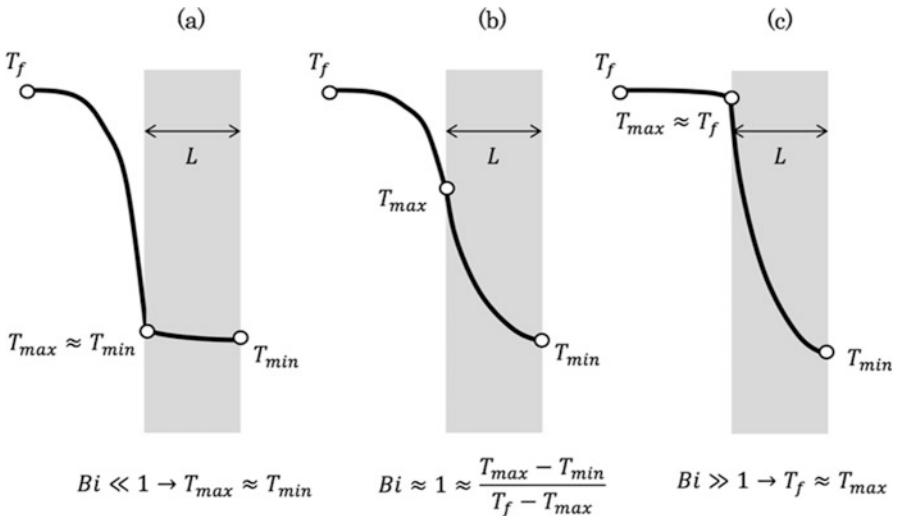
### 5.1.3 Biot Number

The nature of temperature gradients can be defined by the Biot number,  $Bi$ . The Biot number provides a simple representation of the relationship between the temperature gradients in the gas phase and the temperature gradients in the solid phase:

$$Bi = \frac{h\tau d}{k}$$

For extreme values of the Biot number, very large or very small, the temperature gradients in the solid phase are very insensitive to gradients in the gas phase. Therefore, for extreme values of the Biot number, the gas phase and temperature of the solid phase at the exposed surface can be treated with a very simple approximation. Intermediate-range values of the Biot numbers will require precise treatment and most simplifying assumptions will lead to major errors.

Figure 5.1 provides a simple schematic showing the influence of the Biot number in a one-dimensional heat transfer—evidencing the scope for potential simplifications of the heat transfer problem. If the Biot number is close to one (case (b) in Fig. 5.1) temperature gradients in the gas and solid phases are large and therefore equations used to define the thermal boundary conditions will need to be fully resolved, and hence no simplifications are possible. If the Biot number is much greater than one (case (c) in Fig. 5.1) the temperature differences in the gas phase are much smaller than those in the solid phase and it can be assumed that surface and gas temperatures are almost the same. This simplification is very important when modeling furnace tests because it enables the designer to ignore the complex



**Fig. 5.1** Schematic of the typical temperature distributions for values of the Biot number [(a) Biot number much smaller than one (b) Biot number close to one (c) Biot number much greater than one] [6]

boundary condition imposed by the furnace and simply impose the monitored gas temperature at the surface of the solid. Finally, if the Biot number is much smaller than 1 (case (a) in Fig. 5.1) then the temperature differences in the solid phase are much smaller than those in the gas phase; therefore, temperature gradients in the solid phase can be ignored and a single temperature can be assumed for the solid. Heat conduction within the solid can be approximated by the boundary conditions and the equations used to define the thermal boundary conditions lead to a single temperature solution.

The representation of the thermal response of a structural element by means of a single temperature is therefore only valid if  $Bi \ll 1$ . This simplification is called a “lumped capacitance formulation” and while it does not resolve spatial temperature distributions it still requires an adequate definition of the heat transfer between the source of heat (e.g., furnace or “real” fire) and the solid. An important observation is that for materials with Biot numbers much smaller than 1, the thermal energy is rapidly diffused through the integrity of the material, so if the density was to be high, then the lumped solid will lag significantly when compared to the gas-phase temperature. Heat transfer is therefore dominated by the temperature difference between the solid and the gas phase, and errors in the definition of the heat transfer coefficient become less relevant.

It is common for studies attempting to understand the behavior of structures in fire to make use of constant heat transfer coefficients; this will be appropriate for materials with a  $Bi \ll 1$ . Nevertheless, there is also significant inconsistencies in the numbers quoted and furnace heat transfer coefficients are many times extrapolated to natural fire coefficients. These values are not necessarily the same, in particular if radiation and convection are to be amalgamated into a single heat transfer coefficient.

Given the importance of the Biot number in the characteristics of the temperature gradients, it is important to estimate the thickness of a material that leads to a  $Bi = 1$ . Samples that are much thicker will allow approximating the surface temperature to that of the gas phase. Samples that are much thinner will allow to “lump” the solid phase into a single temperature.

Table 5.1 shows typical thermal properties for different construction materials and the characteristic thickness ( $L$ ) that will result in a Biot number of unity. As can be seen for high-thermal-conductivity materials like aluminum or steel, sections a few millimeters thick can be lumped without any major error. In a similar manner very-low-thermal-conductivity materials like plasterboard or expanded polystyrene (EPS) would allow for the assumption that the surface temperature of the solid is that of the gas phase. In contrast, concrete has a Biot of unity for a thickness of 50 mm that is in between typical concrete cover thicknesses and the overall thickness of the sample. The boundary condition cannot be simplified because the thermal gradients are fully defined by  $\dot{q}''_{\text{Tot}}$ .

The Biot number can be used to establish if it is necessary to conduct a transient thermomechanical analysis as well as to determine the level of precision necessary when treating the thermal boundary conditions. The following conclusions can be drawn:

**Table 5.1** Typical thermal properties for different construction materials

Material	Density ( $\rho$ , kg/m <sup>3</sup> )	Thermal conductivity ( $k$ , W/mK)	Specific heat ( $Cp$ , J/kg K)	Thermal diffusivity ( $\alpha$ , m <sup>2</sup> /s)	" $L$ " for $Bi = 1$ (mm)
Aluminum	2400	237	900	1.10E-04	5300
Steel	7800	40	466	1.10E-05	900
Concrete	2000	2.5	880	1.42E-06	50
Plasterboard	800	0.17	1100	1.93E-07	4
Expanded polystyrene (EPS)	20	0.003	1300	1.15E-07	0.1

- The Biot number is a simple nondimensional parameter that combines material characteristics and thermal boundary condition allowing to establish the sensitivity of structural behavior to the precision of the boundary conditions as well as to the transient behavior.
- The Biot number is an effective method to classify different forms of thermally induced structural behavior. The higher the Biot number the lesser transient effects and the more effective the steady-state modeling of a structure to define the worst-case conditions. The lower the Biot number the more important to model transient behavior.
- For the particular case studied, the greater the Biot number the less significant the effect of a fire on structural deformations.

## 5.2 Heat Transfer Analysis

The heat transfer analysis from the fire to structural elements is formulated in terms of heat fluxes. While temperature of the solid phase results from solving the energy conservation equations, all quantities to be balanced are heat fluxes. For simplicity, commonly the heat transfer analysis is only examined in the direction of the principal heat flux, hence considered to be a one-dimensional problem. This section describes a range of engineering methods and tools for the practical analysis of heat transfer in structural elements.

### 5.2.1 Lumped Mass Method

As discussed in Sect. 5.1.3, a lumped capacitance (or lumped mass) method is appropriate if  $Bi \ll 1$ . The lumped mass method is a step-by-step (i.e., quasi-steady) energy-balance calculation technique that simulates "0-D" heat transfer (i.e., heat transfer with no directionality). Essentially, this method assumes a uniform temperature of a given cross section at any point. Due to its high thermal



conductivity, this method lends itself well to unprotected steel. However, this method would not capture possible longitudinal heat sink effects [7].

Considering an unprotected steel member, the equation below solves for the change in temperature of the steel due to fire exposure over a given time step [8]:

$$\Delta T_s = \left(\frac{F}{V}\right) \left(\frac{1}{\rho_s c_s}\right) \left\{ h_c (T_f - T_s) + \sigma \varepsilon (T_f^4 - T_s^4) \right\} \Delta t$$

$\Delta T_s$  is the change in steel temperature over the time step (K),  $\Delta t$  is the time step (s),  $F$  is the surface area of unit length of the member ( $\text{m}^2$ ),  $V$  is the volume of steel in unit length of the member ( $\text{m}^3$ ),  $\rho_s$  is the density of steel ( $\text{kg}/\text{m}^3$ ),  $c_s$  is the specific heat of steel ( $\text{J}/\text{kg K}$ ),  $h_c$  is the convective heat transfer coefficient ( $\text{W}/\text{m}^2 \text{K}$ ),  $\sigma$  is the Stefan-Boltzmann constant ( $56.7 \times 10^{-12} \text{kW}/\text{m}^2 \text{K}^4$ ),  $\varepsilon$  is the resultant emissivity,  $T_f$  (K) is the temperature of the fire environment, and  $T_s$  is the steel temperature (K). The convective heat transfer coefficient is recommended to be taken as  $25 \text{ W}/\text{m}^2 \text{K}$ . Emissivity of the radiating fire gases is recommended to be taken as 1.0 [9]. Thus, the incident radiation is calculated as the blackbody radiation temperature equal to the gas temperature.

The equation above accounts for the geometry of the member (e.g., W-shape beam). Importantly, the  $F/V$  ratio represents the influence of the heated perimeter compared to the area of the section. Members with a high  $F/V$  ratio would heat up more quickly than comparable members with lower ratios. This effect is evident in many fire-resistant listings, which allow for less protective insulation for more massive members (with a lower  $F/V$  ratio). It is recommended that the time step be 30 s or less, and the  $F/V$  ratio be at least  $10 \text{ m}^{-1}$  [10]. Otherwise, the equation may not be valid for the application.

When analyzing structural members with a high thermal capacitance (e.g., concrete members) or steel members with applied protective insulation, the lumped mass method is less suitable. In these cases, the use of a finite element or finite difference model would be significantly more accurate. Nonetheless, if the designer deems this method as conservative, the equation above could be applied directly (e.g., concrete member), or adapted as follows for a steel member with protective insulation [8].

$$\Delta T_s = \left(\frac{F}{V}\right) \left(\frac{k_i}{d_i \rho_s c_s}\right) \left\{ \frac{\rho_s c_s}{\rho_s c_s + \frac{(F/V) d_i \rho_i c_i}{2}} \right\} (T_f - T_s) \Delta t$$

The equation above does not include heat transfer coefficients, for it is assumed that the external surface of the protective insulation is at the same temperature as the fire environment. It is also assumed that the internal temperature of the protective insulation equals the steel temperature.  $c_i$  is the specific heat of the protective insulation ( $\text{J}/\text{kgK}$ ),  $\rho_i$  is the density of the protective insulation ( $\text{kg}/\text{m}^3$ ),  $k_i$  is the thermal conductivity of the protective insulation ( $\text{W}/\text{mK}$ ), and  $d_i$  is the thickness of

the protective insulation ( $m$ ). For the equation above, it is assumed that the temperature gradient in the insulation is linear. For a steel member with protective insulation, this approximation improves with decreasing insulation thickness.

When using the equation above, the temperature dependence of the protective insulation's thermal properties may be represented by updating the parameter values with each increment of time. However, this exercise would require significant judgment/approximation since this method does not solve for the temperature history of the protective insulation itself. Accordingly, for protective insulation materials that exhibit a strong dependence of its thermal properties on temperature (e.g., gypsum-based material that undergoes an endothermic calcination process during heating), the use of a finite element or finite difference model would be significantly more accurate.

As mentioned above, the lumped mass method does not capture possible longitudinal heat sink effects (e.g., steel girder connection to a heavy column as illustrated in Fig. 5.2). Hence, this method would only provide output on the heating of the section at a significant distance away from heat sinks (e.g., at the girder mid-span). Also, the vertical heat sink effect of a concrete slab and its convective/radiative cooling from its top surface would not be accounted for using this method (as illustrated in Fig. 5.3). These limitations of the method may lead to significant overestimation of the section's temperature history.

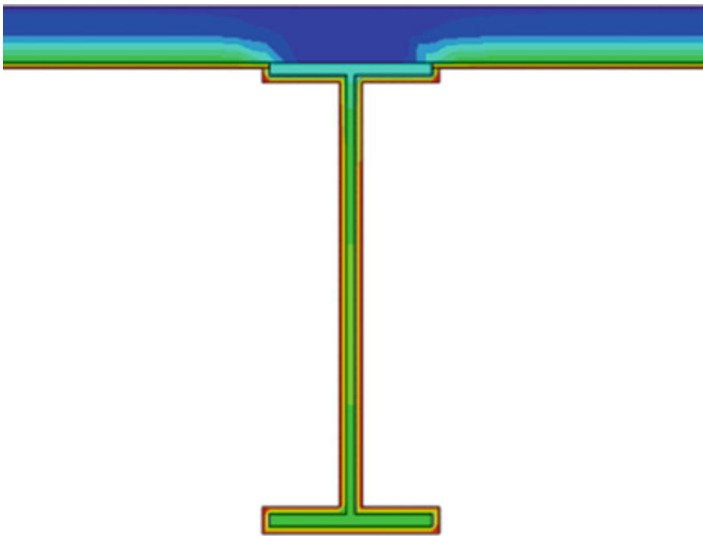
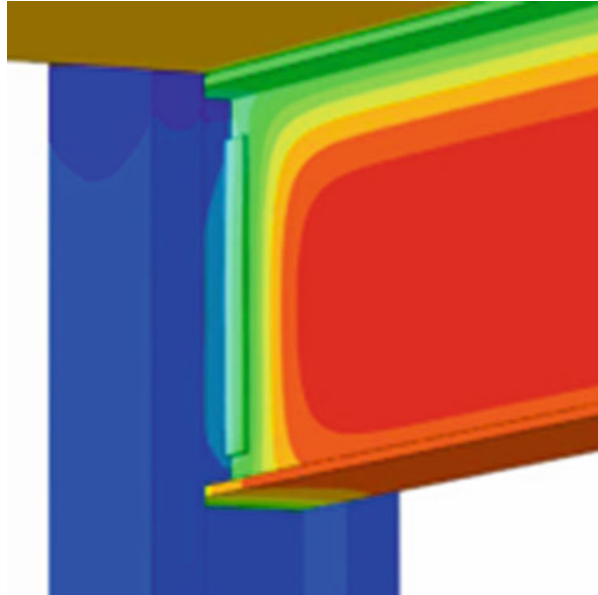
### 5.2.2 *Finite Difference Method*

A frequent problem in conduction heat transfer involves ascertaining a solution to a transient heat transfer assessment associated with a complex geometry. This is often coupled with the desire to incorporate temperature-dependent material properties which make the application of simplified analytical techniques such as lumped mass not the most appropriate option. Instead, a numerical solution is likely to be a more efficient design tool.

The finite difference method is a numerical technique to solve differential equations by approximating them with difference equations in which finite differences approximate the derivatives. It involves discretization of the geometry of interest into small segments using a series of nodes which are connected by lines to form a grid or mesh. This approach will therefore approximate the geometry with the result being a more refined mesh (smaller grids) that will provide increased accuracy but potentially more computational time. In contrast to an analytical solution which allows for temperature determination at any point within a medium, finite difference will only allow determination of temperature at discrete locations aligned with the nodal positions comprising the mesh.

More than one method exists for obtaining numerical approximations to the solutions of the time-dependent ordinary and partial differential equations. Both explicit and implicit methods are approaches used in numerical analysis of such applications. Explicit methods calculate the state of a system at a later time from the

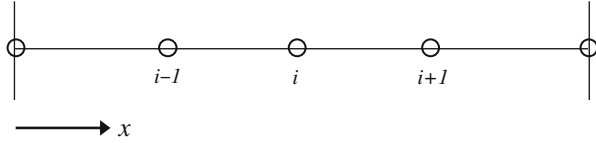
**Fig. 5.2** Steel girder connected to heavy column (thermal response)



**Fig. 5.3** Protected steel girder below a concrete slab (thermal response)

state of the system at the current time, while implicit methods find a solution by solving an equation involving both the current state of the system and the later one. Explicit methods often require impractically small time steps to keep the error associated with the calculation within a reasonable limit (numerical stability). Implicit methods typically take less computational time as they can take advantage

**Fig. 5.4** Schematic of a simplified finite difference grid



of larger time steps. Depending on the type of problem to be solved it may be that either an explicit or an implicit approach may be the best.

The finite difference method typically uses a Taylor series expansion to reformulate the partial differential equation, resulting in a set of algebraic equations. Consider the basic equation describing heat conduction within a solid:

$$\rho c \frac{\partial T}{\partial t} = \frac{\partial}{\partial x} \left( k_1 \frac{\partial T}{\partial x} \right) + \frac{\partial}{\partial y} \left( k_2 \frac{\partial T}{\partial y} \right) + \frac{\partial}{\partial z} \left( k_3 \frac{\partial T}{\partial z} \right) + q_i'''$$

where  $q_i'''$  is the rate of change of thermal energy stored per unit volume.

In relation to Fig. 5.4, the explicit finite difference form of this for transient heat conduction with no internal heat generation is given as

$$C_i \frac{(T'_i - T_i)}{\Delta t} = \frac{\frac{k_m(T_{i+1} - T_i)}{\Delta x} - \frac{k_n(T_i - T_{i-1})}{\Delta x}}{\Delta x}$$

where

$$T_i$$

the temperature at node  $i$  at time  $t$ .

$$T'_i$$

the temperature at node  $i$  after time step,  $\Delta t$ .

$$k_m = \frac{1}{2}(k_{i+1} + k_i)$$

$$k_n = \frac{1}{2}(k_i + k_{i-1})$$

$$C_i = \rho c_p \Delta x$$

Alternatively, an implicit formulation can be applied in the form of

$$C_i \frac{(T'_i - T_i)}{\Delta t} = \frac{\frac{k_m(T'_{i+1} - T'_i)}{\Delta x} - \frac{k_n(T'_i - T'_{i+1})}{\Delta x}}{\Delta x}$$

The advantage of this approach is that it is numerically stable for any time step or grid size. The disadvantage is that all of the equations are coupled as the right-hand side of the equation including nodal temperatures at the end of the time step. Therefore all the equations must be solved simultaneously.

For more complex geometry including 2D or 3D problems, the finite difference equation for a node may also be obtained by applying conservation of energy to a

control volume about the nodal region. This method is often referred to as a heat balance or energy balance approach.

Commercially available software exists to perform finite difference heat transfer calculations.

### 5.2.3 *Finite Element Method*

Finite element methods (FEM) are efficient numerical methods for solving problems of engineering. Typical applications include structural analysis, heat transfer, fluid flow, mass transport, etc. Similar to the finite difference method, the finite element method can be applied to problems in transient conduction heat transfer associated with a complex geometry.

The finite element method consists of discretizing a geometry into a mesh consisting of nodes and “finite” elements as shown in Fig. 5.5. It is typically possible to generate results either at nodal points or from within elements.

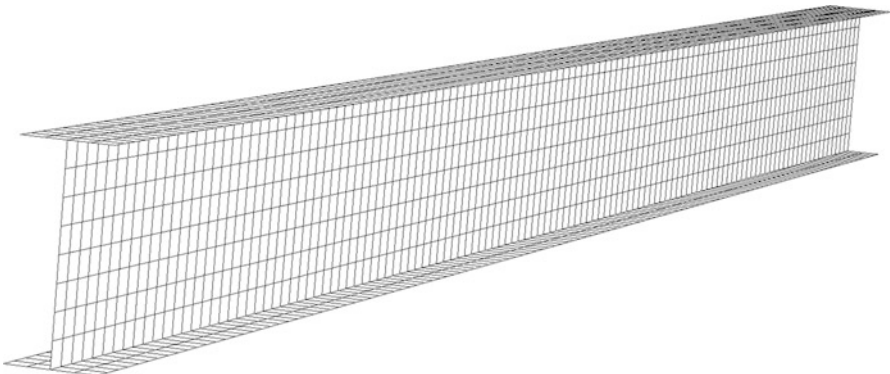
The primary difference in comparison to finite difference methods is that it uses an exact governing equation. Finite element formulations typically use a polynomial fit of the temperature profile within an element to solve the equation. This approach will generally be more accurate for a coarser grid than a finite difference method.

The fundamental equations are outside the scope of this book, but other industry references are available that can explain in further detail. From a high-level perspective, a resulting set of equations are assembled into a matrix in the form of:

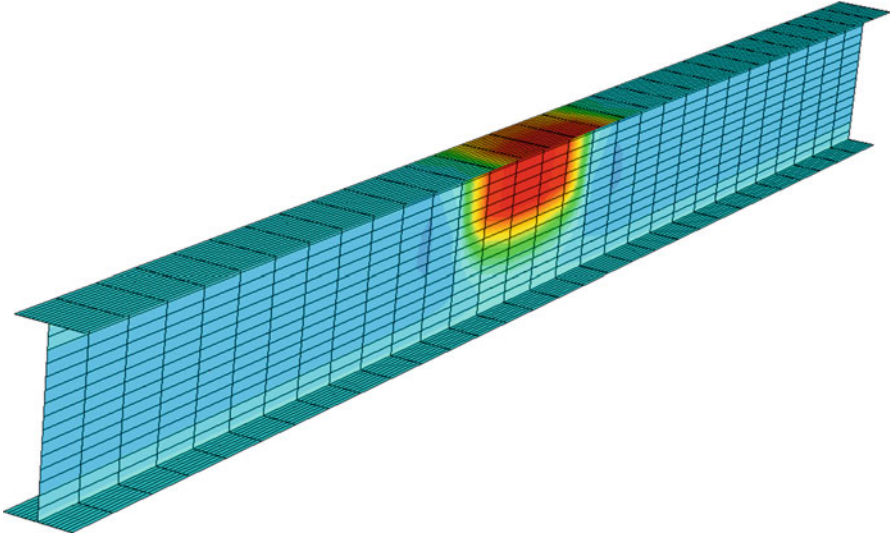
$$[C]\{\dot{T}\} + [K]\{T\} = \{Q\}$$

Where

$C$   
is the capacitance matrix, accounting for pc product associated with each element.



**Fig. 5.5** Schematic of a finite element mesh for a beam modeled using shell elements



**Fig. 5.6** Typical example of a FEM heat transfer assessment

$K$

is the conductivity matrix, accounting for conductivity of the element.

$T$

is a vector (column matrix), which represents temperature at each node.

$Q$

is a vector (column matrix), which represents heat generation at each node.

Determination of the temperature profile within an object requires solving the matrix-based solutions. Commercially available software exists for this purpose. An example of a finite element method heat transfer application associated with temperature contours of a structural arrangement is shown in Fig. 5.6.

### 5.2.4 Example Problems

Example problems for heat transfer analyses can be found throughout various heat transfer textbooks (e.g., Introduction to Heat Transfer [11]). More specific to structural fire engineering, the SFPE S.02 standard [12] provides the following 16 example problems in its Annex A:

- Lumped Mass Subjected to Standard Fire.
  - *Simplified (0-D) furnace test thermal prediction.*
- Lumped Mass Subjected to Incident Flux.
  - *Simplified (0-D) general-purpose thermal prediction.*

- 1-D Heat Transfer with Cooling by Convection
  - *Unexposed surface thermal prediction.*
- 1-D Axisymmetric Heat Transfer by Convection
  - *Circular cross-section thermal prediction (convection only).*
- Axisymmetric Heat Transfer by Convection and Radiation.
  - *Circular cross-section thermal prediction (convection and radiation).*
- 2-D Heat Transfer with Cooling by Convection
  - *Spatial-varying cross-section thermal prediction (convection only).*
- 2-D Heat Transfer by Convection and Radiation
  - *Spatial-varying cross-section thermal prediction (convection and radiation).*
- 2-D Heat Transfer with Temperature-Dependent Conductivity
  - *Spatial-varying cross-section thermal prediction (convection, radiation, and temperature-dependent conductivity).*
- 2-D Heat Transfer in a Composite Section with Temperature-Dependent Conductivity
  - *Spatial-varying composite cross-section thermal prediction (convection, radiation, and temperature-dependent conductivity).*
- 2-D Axisymmetric Heat Transfer with Nonuniform Heat Flux
  - *Spatial-varying cross-section thermal prediction (convection, radiation, and nonuniform heat flux).*
- Lumped Mass with Moisture Evaporation.
  - *Simplified (0-D) general-purpose thermal prediction including latent heat effect.*
- 1-D Heat Transfer with Moisture Evaporation
  - *General-purpose thermal prediction including latent heat effect.*
- 2-D Heat Transfer with Moisture Evaporation
  - *Spatial-varying cross-section thermal prediction including latent heat effect.*
- 2-D Heat Transfer in a Composite Section with Moisture Evaporation and Temperature-Dependent Conductivity
  - *Spatial-varying composite cross-section thermal prediction (latent heat effect and temperature-dependent conductivity).*
- 2-D Heat Transfer in a Composite Section with Cavity Radiation

- *Spatial-varying composite cross section including cavity radiation.*
- 3-D Heat Transfer with Nonuniform Heat Flux
  - *General-purpose spatial-varying thermal prediction including nonuniform heat flux.*

Each example problem from the SFPE S.02 standard is material generic (*see Sect. 5.3 for thermal properties of specific construction and protective materials*) and has solved temperature history results. Hence, these example problems can be used to verify model/software predictions as well as adapt to specific materials and fire conditions. Also, these example problems have escalating levels of precision/complexity, the need for which will depend upon the specific structural fire engineering application.

## 5.3 Thermal Properties of Materials

The thermal properties of materials used in a heat transfer analysis govern the temperature gradients within the structural element. Therefore, it is key to assess thermal conditions as a function of the thermal properties of the material. The key thermal properties used for heat transfer analysis in structural fire engineering design include density, thermal conductivity, specific heat, and emissivity/absorptivity. In heat transfer analysis, it is usually assumed that absorptivity of materials is equal to their emissivity; hence, the term emissivity is used herein to reference both material properties.

### 5.3.1 Steel

Compared to other construction materials, steel has thermal properties that are very well established and relatively consistent among various sources. The key thermal properties of steel for use in structural fire engineering design include density, emissivity, thermal conductivity, and specific heat. Steel does not experience any appreciable latent heat effects at elevated temperatures.

The density of steel has a value of  $7850 \text{ kg/m}^3$ . This value does not appreciably change at elevated temperatures, and may be taken as constant.

The emissivity of steel varies depending upon aspects of its surface finish, including surface roughness, presence of oxidation, presence of galvanic coating, polishing, and/or presence of paint. Eurocode 3 specifies design values of 0.7 and 0.4 for carbon steel and stainless steel, respectively [10]. However, it should be noted that the emissivity of steel at ambient can range from 0.2 to 0.9 [13].

It is typical to assume that the emissivity of steel is constant with temperature. However, temperature-dependent expressions have been proposed, including the following [14]:



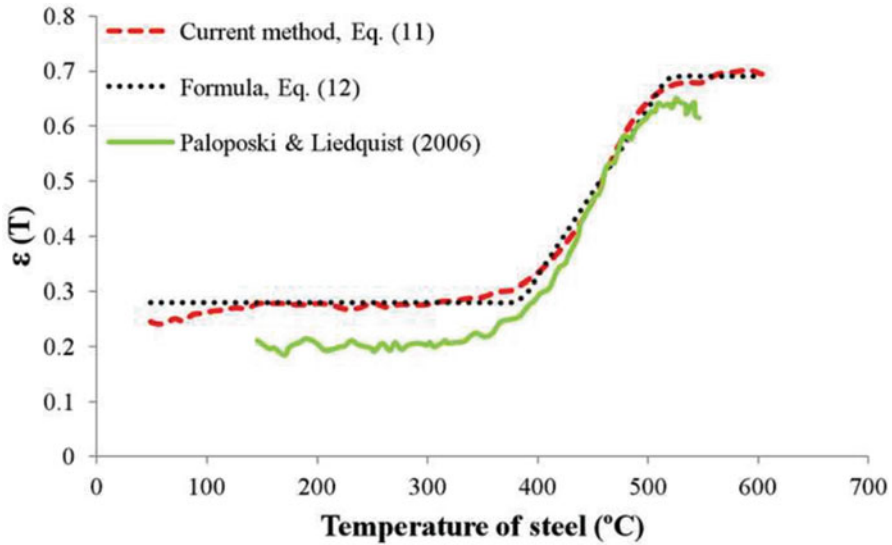


Fig. 5.7 Steel emissivity expression and test results [14]

For  $T < 380^{\circ}\text{C}$ ,  $\varepsilon = 0.28$

For  $380^{\circ}\text{C} \leq T < 520^{\circ}\text{C}$ ,  $\varepsilon = 0.00304T - 0.888$

For  $520^{\circ}\text{C} \leq T$ ,  $\varepsilon = 0.69$

Figure 5.7 plots the expression above along with test results obtained by Paloposki and Liedquist [15].

In addition to temperature dependence, the emissivity of steel may also vary depending upon the level of adhesion of soot to the surface during a fire. Except for extremely thin films, adhered soot has an emissivity of approximately 0.95 [16], which may be considered as constant. Hence, it may be prudent to consider a steel emissivity value toward the higher end of reported ranges if soot adherence is anticipated.

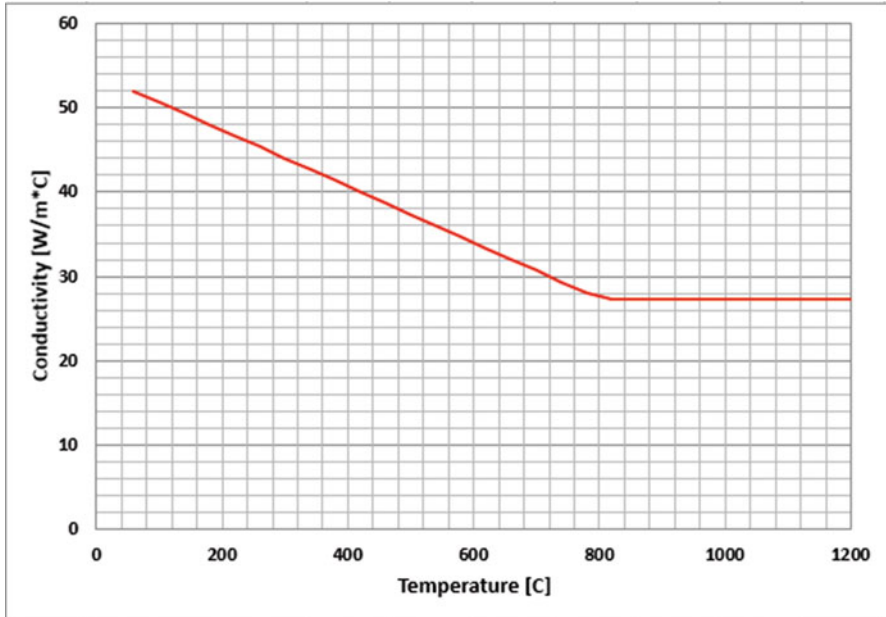
It is well known that steel is a very high conductor of heat. Eurocode 3 provides the following expression for the thermal conductivity of steel as a function of temperature [10]:

For  $20^{\circ}\text{C} \leq T \leq 800^{\circ}\text{C}$ ,  $k = 54 - 0.0333T$

For  $800^{\circ}\text{C} < T \leq 1200^{\circ}\text{C}$ ,  $k = 27.3$

Figure 5.8 plots the expression above.

The specific heat of steel remains relatively constant with temperature, except within a small-temperature bandwidth (between  $700^{\circ}\text{C}$  and  $800^{\circ}\text{C}$ ) in which a pronounced metallurgical change occurs. Accounting for this metallurgical change, Eurocode 3 provides the following expression for the specific of steel as a function of temperature [10]:



**Fig. 5.8** Steel thermal conductivity

For  $20^{\circ}\text{C} \leq T \leq 600^{\circ}\text{C}$ ,  $c_p = 425 + 0.773T - 0.00169T^2 + 0.00000222T^3$

For  $600^{\circ}\text{C} < T \leq 735^{\circ}\text{C}$ ,  $c_p = 666 + 13002/(738 - T)$

For  $735^{\circ}\text{C} < T \leq 900^{\circ}\text{C}$ ,  $c_p = 545 + 17820/(T - 731)$

For  $900^{\circ}\text{C} < T \leq 1200^{\circ}\text{C}$ ,  $c_p = 650$

Figure 5.9 plots the expression above.

### 5.3.2 Concrete

The thermal properties of concrete depend upon the following inherent characteristics:

- Moisture content.
- Porosity.
- Density.
- Aggregate type.

Although moisture in concrete will evaporate to a certain extent under heating, it generally does not change considerably with temperature, and therefore can be treated as constant. Otherwise, the reduction in density due to free water loss and

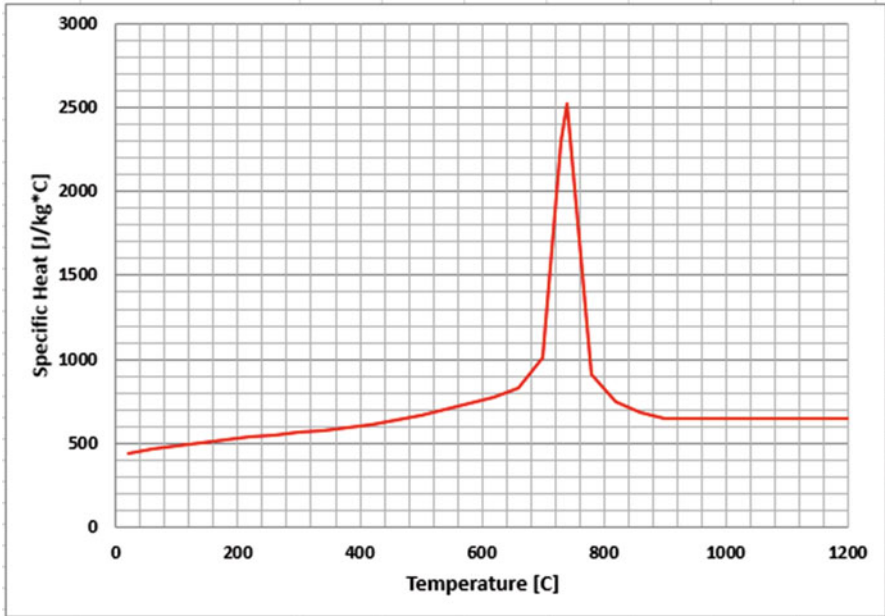


Fig. 5.9 Steel-specific heat

the density  $\rho_c$  (in  $\text{kg/m}^3$ ) at temperature  $T$  (in Celsius) may be determined by the following equation [17]:

$$\rho_c = \begin{cases} \rho_{c,20} & \text{for } 20\text{ C} \leq T \leq 115\text{ C} \\ \rho_{c,20}[1 - 0.02(T - 115)/85] & \text{for } 115\text{ C} < T \leq 200\text{ C} \\ \rho_{c,20}[0.98 - 0.03(T - 200)/200] & \text{for } 200\text{ C} < T \leq 400\text{ C} \\ \rho_{c,20}[0.95 - 0.07(T - 400)/800] & \text{for } 400\text{ C} < T \leq 1200\text{ C} \end{cases}$$

where  $\rho_{c,20}$  is the density of concrete at ambient temperature (in  $\text{kg/m}^3$ ).

Also from Eurocode 2, the thermal conductivity  $k_c$  (in  $\text{W/m-K}$ ) of normal-weight concrete at temperature  $T$  (in Celsius) can be determined between the upper and lower limits given in the following equations:

$$k_c = \begin{cases} 2 - 0.2451(T/100) + 0.0107(T/100)^2 & \text{upper limit} \\ 1.36 - 0.136(T/100) + 0.0057(T/100)^2 & \text{lower limit} \end{cases}$$

For most applications, the consideration of the upper limit thermal conductivity would yield conservative results.

For lightweight concrete with density between  $1600\text{ kg/m}^3$  and  $2000\text{ kg/m}^3$ , the conductivity  $k_c$  (in  $\text{W/m-K}$ ) is given as [17]

$$k_c = \begin{cases} 1 - (T/1600) & \text{for } 20 \text{ C} \leq T \leq 800 \text{ C} \\ 0.5 & \text{for } 800 \text{ C} < T \leq 1200 \text{ C} \end{cases}$$

Per Eurocode 2, for normal-weight concrete, the specific heat of dry concrete  $C_c$  (in J/kg-K) at temperature  $T$  (in Celsius) is given as

$$c_c = \begin{cases} 900 & \text{for } 20 \text{ C} \leq T \leq 100 \text{ C} \\ 900 + (T - 100) & \text{for } 100 \text{ C} < T \leq 200 \text{ C} \\ 1000 + \frac{T - 200}{2} & \text{for } 200 \text{ C} < T \leq 400 \text{ C} \\ 1100 & \text{for } 400 \text{ C} < T \leq 1200 \text{ C} \end{cases}$$

When moisture content is not modeled explicitly, the specific heat of concrete  $c_c^*$  (in J/kg-K) can be considered for the following moisture content values ( $u$ ) at 115 °C:

$$c_c^* = \begin{cases} 1470 & \text{for } u = 1.5\% \\ 2020 & \text{for } u = 3.0\% \\ 5600 & \text{for } u = 10.0\% \end{cases}$$

The parameter  $u$  is the moisture content. For lightweight concrete with density between 1600 kg/m<sup>3</sup> and 2000 kg/m<sup>3</sup>, the specific heat is assumed to be independent of temperature and of magnitude 840 J/kg-K.

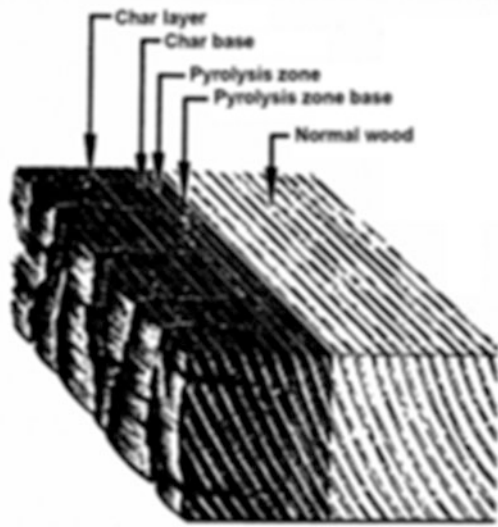
For normal-weight and lightweight concrete, the emissivity of concrete generally ranges between 0.85 and 0.95 [13].

### 5.3.3 Timber

Unlike steel and concrete, timber is a combustible material. As such, it undergoes thermal decomposition when exposed to fire, as illustrated in Fig. 5.10. The thermal decomposition of wood is governed by physical and chemical processes that transform the wood to char, a process that is known as *pyrolysis*. Some key features of the pyrolysis of wood include mass loss, discoloration, and emission of gaseous by-products [19]. Pyrolysis of wood is incredibly complex and depends on several factors including oxygen concentration, moisture content, and orientation of the specimen to the heat source [20]. In practice, the charring of timber usually occurs between 280 and 320 °C, with a temperature of 288 °C used to locate the pyrolysis front in wood specimens using embedded thermocouples [21].

The thermal analysis of wood must take into account the fact that the thermal decomposition of wood changes the physical properties of the material. Thus, heat

**Fig. 5.10** Char layer and pyrolysis zone in wood [18]



transfer analysis of fire-exposed structures inevitably includes some level of modeling of the pyrolysis front, which is the transition zone between the virgin wood and the char layer (Fig. 5.10). A variety of simple and advanced calculation methods can be found in the literature.

It is important to note that, while pyrolysis is inherently a complex and nonlinear process, simplified models, such as the linear model in Eurocode 5 [22] or the nonlinear model in the National Design Specification [23], are based on a single parameter: the nominal char rate. The nominal char rate  $\beta_0$  is defined as the char rate at 1 h of standard fire exposure. The nominal char rate depends on the species of wood (i.e., softwood versus hardwood), whether the member is solid-sawn wood or is a built-up member (e.g., glue-laminated timber), the moisture content of the wood, and the direction of heating (i.e., parallel to the grain versus perpendicular to the grain). Nominal char rates for various wood products can be found in the literature (e.g., FPL [24] and Eurocode 5).

Knowing the nominal char rate, the depth of the char layer can then be determined as a function of time. According to the linear model in Eurocode 5, for example, the depth of the char layer is given as

$$d_{char} = \beta_0 t$$

where  $t$  = time [min] and  $\beta_0$  is the nominal char rate [mm/min]. Note that the equation above is a one-dimensional model. Additional factors (e.g., corner rounding) must be taken into account when a member is heated on more than one side.

In regard to the thermal properties (i.e., density, conductivity, and specific heat), it is recommended that temperature-dependent properties be obtained from

experimental tests, especially given the sensitivity of these properties to the wood species, the moisture content, etc. However, Annex B of Eurocode 5 provides design values that may be useful for some design applications.

### 5.3.4 *Applied Passive Fire Protection*

Where a structural or heat transfer assessment determines that a member requires the application of an applied passive fire protection material, there are a number of options available to a designer. A non-exhaustive list of insulating materials includes:

- Spray fire-resistive materials (SFRM).
- Intumescent coatings (or reactive coatings).
- Fire-rated board.
- Fire-rated blankets.
- Concrete encasement.
- Concrete filling.
- Timber.
- Water filling.

For each material, the principal remains the same. They work to restrict the transmission of heat to the underlying or associated substrate to ensure that it keeps sufficiently cool with the intent of maintaining stability in the event of a fire.

The choice of protective material is often dictated by architectural or constructional design considerations (e.g., durability or ease/speed of application). For example, for aesthetical reasons an intumescent coating (Fig. 5.11) may be preferential, while for cost reasons a SFRM material may be more appealing. Nonetheless,

**Fig. 5.11** Shop application of an intumescent coating [Image courtesy of International Paint Ltd.]



the choice of material warrants careful consideration at the design and specification stages of a project.

All passive fire protection materials are subject to rigorous fire testing to and certification against a recognized standard. The choice of the appropriate testing, assessment, and certification requirement for the product will depend on the region or project location. For example, a project in Australia requires testing to AS 1530–4 and assessment to AS 4100. However, New Zealand typically accepts the BS 476–21 standard. Similarly there are different test standards that are required for mainland Europe, North America and Canada, Russia, China, etc. to which products need to be tested and assessed.

The following standards are typically referenced and requested for passive fire protection materials:

- BS 476 Parts 20–22 (historically common due to the influence of British Standards).
- EN 13381 Part 4 (passive materials) and Part 8 (reactive materials).
- ASTM E-119/UL 263 (North America-based codes).
- GB 14907 (Chinese fire test standard).
- GOST (Russia and Commonwealth of Independent States (CIS) region).

Manufacturers of proprietary passive fire protection materials are generally able to supply data relating to thickness for specific structural designs in relation to certified testing. Datasets like these are typically acceptable by authorities having jurisdiction.

For cases where a nonstandard design warrants further attention via an engineering study it may be beneficial to undertake either a heat transfer assessment or bespoke testing. The former is a common method but not all manufacturers will be able to provide a set of temperature-dependent material properties. Product data sheets may state values relating to density, specific heat capacity, and thermal conductivity but the designer should satisfy themselves that any such values are valid over the temperature range of interest and not just measured ambient values. Ideally, any such engineering assessment should reference back to available supporting test data where it is available to ensure a robust study.

## 5.4 Special Design Considerations

Although typically heat transfer analysis of structural elements is simplified under a range of possible assumptions, there are particular applications in which a more complex analysis is required in order to account for special design considerations.

### 5.4.1 Phase Change

In structural fire engineering, a phase change occurs when the temperature is high enough to cause a solid to transition into a liquid (i.e., melting) or a liquid to transition into a gas (i.e., evaporation). Temperatures associated with fires in buildings are generally not hot enough to cause melting of structural materials (e.g., steel, concrete, and timber). Some materials, like concrete and timber, however, do contain moisture, and it is important to note that the evaporation of moisture can directly affect the temperature in the structure.

From principals of thermodynamics, the amount of heat  $Q$  that is needed to cause a mass  $m$  to undergo a phase change from solid to liquid is given as

$$Q = mL_f$$

Similarly, the amount of heat  $Q$  that is needed to cause a mass  $m$  to undergo a phase change from liquid to gas is

$$Q = mL_v$$

Here,  $L_f$  = latent heat of fusion, and  $L_v$  = latent heat of vaporization. The latent heat of fusion and the latent heat of vaporization are properties that are unique to the specific material. Water, for example, has a latent heat of fusion  $L_f$  of 334 kJ/kg and a latent heat of vaporization of  $L_v$  is 2260 kJ/kg.

In conduction heat transfer, latent heat effects are added to the sensitive heat effects in the energy storage term of the heat conservation equation. Wickström [4] explains how to model latent heat effects associated with moisture evaporation in a solid using *specific volumetric enthalpy*. Wickström also derives an *effective* specific heat capacity that accounts for the latent heat effect. The effective specific heat results in a spike in the specific heat when temperature reaches the boiling point for water. The spike implicitly represents the energy storage associated with the phase change. It is important to note that the methods of using specific volumetric enthalpy and effective specific heat are equivalent, and both are suitable for structural fire engineering applications.

### 5.4.2 Insulation Mechanical Integrity

In the context of structural fire protection, mechanical integrity is defined as the ability of protective insulation to maintain its function under fire exposure. Changes in thermal properties at elevated temperatures are considered separately, for mechanical integrity primarily relates to the integrity of protective insulation. Accordingly, the following phenomena would represent mechanical integrity failures:



- Loss of adhesion (e.g., of SFRM) (Fig. 5.12).
- Loss of cohesion (e.g., of SFRM) (Fig. 5.13).
- Local damage (e.g., due to impact) (Fig. 5.14).
- Delamination (e.g., of gypsum wallboard layers) (Fig. 5.15).
- Loss of attachment (e.g., of gypsum wallboard layers).
- Spalling (e.g., of high-strength concrete) (Fig. 5.16).
- Other failures (e.g., degradation/disintegration of material).



Fig. 5.12 SFRM adhesion failure (localized) [25]



Fig. 5.13 SFRM cohesion failure (during a pull test) [25]



**Fig. 5.14** SFRM local damage due to impact [25]

**Fig. 5.15** Gypsum wallboard delamination due to fire exposure [26]



The mechanical integrity of protective insulation under fire exposure cannot be reliably predicted using analytical tools. Heat transfer calculations inherently assume that protective insulation will remain in place during fire exposure. Accordingly, the designer should be confident that protective insulation will stay in place long enough to fulfill the required performance objectives.

**Fig. 5.16** Reinforced concrete wall that experienced spalling [27]



The mechanical integrity of protective insulation under fire exposure remains a major knowledge gap/research frontier within structural fire engineering. Consequently, there is significant onus on the designer to derive appropriate empirical data and employ careful judgment based on this data and its applicability to the application.

The determination of adequate mechanical integrity of protective insulation is typically evaluated using standard fire testing within standard fire resistance design. However, standard fire testing does not adequately capture the effect of structural deformations on the mechanical integrity of protective insulation, which can be significant. For instance, large deflection of long-span beams under fire exposure may cause protective insulation to undergo adhesion failure, or gypsum board encasement systems to become unstable [25]. Standard fire testing does not inform the designer about these effects since realistic fire exposure and structural deformations are not simulated, and the supporting boundaries of the furnace apparatus do not undergo any deformation. Hence, addressing this concern requires the designer to develop specific performance criteria per the discretion of the building authority.

Fire resistance listings define appropriate extrapolations from test conditions, such as application to heavier steel sections than tested. However, dimensional scaling is usually not appropriate to qualify the mechanical integrity of protective insulation as part of a structural fire engineering design. For instance, the

endothermic calcination process that SFRM undergoes upon heating (which enhances its insulating capability) cannot be scaled based upon its thickness. Other examples include a very thin material that may not maintain its mechanical integrity, or an intumescent material that will yield little or no additional benefit if a thicker layer is applied. Hence, the use of protective insulation thicknesses that are outside the range included in specific fire resistance listings should not be done without validation testing or specific information from the manufacturer, as materials are often not as useful at thicknesses outside the range included in the testing.

Information derived from standard fire testing could be used to assist designers evaluating the anticipated level of mechanical integrity of protective insulation under fire exposure. At a minimum, the applicability of the standard furnace exposure to the structural design fires under consideration should be evaluated. Accordingly, the designer should exercise caution if a structural design fire is significantly more severe (e.g., sharper growth) as compared to the standard furnace test exposure. This may require the specification of applied insulation that has been qualified for challenging exposures (e.g., the UL 1709 exposure [28]).

In addition comparing structural design fires to test exposures, the designer may consult the relevant manufacturer for specific information, or refer to publicly available test data. At a minimum, the designer should adhere to the manufacturer's installation requirements (e.g., restrictions on the use of steel primers prior to the application of SFRM).

The industry has yet to develop a test method to qualify the mechanical integrity performance of protective insulation for nonstandard fire exposure and generalized application in structural fire engineering. Hence, it is currently within the purview of the designer to provide sufficient evidence, analysis, and judgement in this respect. This may require specific information from the relevant manufacturer. In this respect, the availability of information from relevant manufacturers is paramount, and perhaps indicative of their competitive advantage for inclusion in structural fire engineering applications.

## References

1. ISO 834-11: Fire Resistance Tests—Elements of Building Construction, 2014.
2. EN 1991-1-2: Eurocode 1: Actions on structures—Part 1–2: General actions—Actions on structures exposed to fire, 2002.
3. SFPE S.01, Engineering Standard on Calculating Fire Exposures to Structures, Society of Fire Protection Engineers, Bethesda, MD, 2011.
4. Wickström, U. (2016). *Temperature calculation in fire safety engineering*. Springer.
5. Lattimer, B. Y. (2008). Heat fluxes from fires to surfaces. In Dinunno et al. (Eds.), *The SFPE Handbook of Fire Protection Engineering* (4th ed.). National Fire Protection Association.
6. Torero, J. L., Law, A., & Maluk, C. (2017). Defining the thermal boundary condition for protective structures in fire. *Structures*, 149, 104–112.
7. LaMalva, K. (2011). Thermal response of steel structures to fire: Test versus field conditions. *Journal of Fire Protection Engineering*, 21, 4.
8. Buchanan, A., & Abu, A. (2017). *Structural design for fire safety* (2nd ed.). John Wiley & Sons.

9. Eurocode 1: Actions on structures, Part 1–2: General actions—Actions on structures exposed to fire, Brussels, Belgium, European Committee on Standardization, 2002.
10. Eurocode 3: Design of steel structures: General rules—Structural fire design, Belgium, European Committee on Standardization, 1995.
11. Incropera, F., DeWitt, D., Bergman, T., & Lavine, A. (2009). *Introduction to heat transfer*. Wiley.
12. SFPE S.02: Standard on calculation methods to predict the thermal performance of structural and fire resistive assemblies, Society of Fire Protection Engineers, 2015.
13. FABIG, Fire Resistant Design of Offshore Topside Structures, Fire and Blast Information Group, Technical Note No. 1, The Steel Construction Institute, Berkshire, UK, 1993.
14. Sadiq, H., Wong, M., Tashan, J., Al-Mahaidi, R., Zhao, X.. Determination of steel emissivity for the temperature prediction of structural steel members in fire, 2013.
15. Paloposki, T., Liedquist, L. (2005). Steel emissivity at high temperatures, Report VTT-TIED-2299, VTT Technical Research Centre of Finland
16. Libert, C., Hibbard, R. (1970). Spectral emittance of soot, NASA Technical Note D-5647, National Aeronautics and Space Administration, Washington, D.C.
17. Eurocode 2: Design of concrete structures—Part 1–2: General rules—Structural fire design, EN 1992-1-2: 2004.
18. Schaffer, E.L. (1967). Charring Rate of Selected Woods—Transverse to Grain. Res. Pap. FPL 69. Madison, WI: USDA Forest Service, Forest Products Laboratory.
19. Buchanan, A. (2002). *Structural design for fire safety*. John Wiley & Sons, Ltd..
20. Moghtaderi, B. (2006). The state-of-the-art in pyrolysis modelling of lignocellulosic solid fuels, fire and materials, No. 30.
21. Schaffer, E. (1984). *Structural fire design: Wood, Forest Products Laboratory Research Paper FPL 450*. USDA Forest Service.
22. EN 1995-1-2: Eurocode 5: Design of timber structures—Part 1–2: General—Structural fire design, 2004.
23. AWC. (2012). *National design specification (NDS) for wood construction*. American Wood Council.
24. FPL, Wood Handbook: Wood as an Engineering Material, Forest Products Laboratory General Technical Report FPL-GTR-190, USDA Forest Service, Madison, WI, 2010.
25. Carino, N., et al. (2005). *NIST NCSTAR 1-6A passive fire protection, federal building and fire safety investigation of the world trade center disaster*. National Institute of Standards and Technology.
26. TFRI Fire Test of Wood Frame Assembly, European Wood, Brussels, Belgium, <http://jp.europeanwood.org>, 2017.
27. Jansson, R. (2013). *Fire spalling of concrete: Theoretical and experimental studies, doctoral thesis in concrete structures*. KTH Royal Institute of Technology.
28. UL 1709: Standard for rapid rise fire tests of protection materials for structural steel, Underwriters Laboratories, Northbrook, IL, 2011.

# Chapter 6

## Concrete Structures



**Thomas Gernay, Venkatesh Kodur, Mohannad Z. Naser, Reza Imani, and Luke Bisby**

### 6.1 Overview

Concrete is the most widely used man-made material in the world, with an average global yearly consumption exceeding  $1 \text{ m}^3$  per person. It is used in a large variety of applications ranging from building structures to infrastructure such as tunnels to mass concrete structures such as dams. Concrete, as a construction material, has a series of competitive advantages that support this extensive use. These advantages include the material durability, its workability and formability into various structural components, the high stiffness of the structural concrete elements compared to steel structural elements, as well as the relatively short duration of works on-site made possible by the development of precast concrete, to name a few.

Another important advantage of concrete is related to its fire behavior. Indeed, concrete is generally regarded as providing a superior fire resistance, inherently,

---

T. Gernay (✉)

Johns Hopkins University, Baltimore, MD, USA  
e-mail: [tgernay@jhu.edu](mailto:tgernay@jhu.edu)

V. Kodur

Michigan State University, East Lansing, MI, USA  
e-mail: [kodur@egr.msu.edu](mailto:kodur@egr.msu.edu)

M. Z. Naser

Clemson University, Clemson, SC, USA  
e-mail: [mznaser@clemson.edu](mailto:mznaser@clemson.edu)

R. Imani

ImageCat, Los Angeles, CA, USA

L. Bisby

Civil and Environmental Engineering Department, University of Edinburgh,  
Edinburgh, Scotland, UK  
e-mail: [luke.bisby@ed.ac.uk](mailto:luke.bisby@ed.ac.uk)

© Springer Nature Switzerland AG 2021

K. LaMalva, D. Hopkin (eds.), *International Handbook of Structural Fire Engineering*, The Society of Fire Protection Engineers Series,  
[https://doi.org/10.1007/978-3-030-77123-2\\_6](https://doi.org/10.1007/978-3-030-77123-2_6)

**Fig. 6.1** Fire-induced collapse of a concrete apartment building in Russia, 2002 (from [1])



when compared with steel and timber construction materials. This reputation relies mainly on the fact that concrete is a noncombustible material that has a lower conductivity than steel and, combined with the higher massivity of concrete sections, this typically results in a relatively long fire resistance of concrete structures without the need for protection material. Therefore, concrete is also found in applications where the fire resistance is an issue or in other applications where elevated temperature can arise such as in nuclear vessels.

However, this favorable thermal behavior of the material does not mean that concrete structures are immune to the effects of fire. Catastrophic failure of concrete structures in fire, although rare, has been observed in a few instances. For instance, these include the collapse of a department store in Katrantzos in Greece in 1980 and of an apartment block building in Saint Petersburg in Russia in 2002. The latter was a nine-story concrete apartment block that totally collapsed after about a 1-h fire (Fig. 6.1, [1]). In some cases, fire-induced collapse of concrete structures occurs during the cooling phase of the fire. This was the case of the fire-initiated collapse of a six-story reinforced concrete factory in Alexandria, Egypt, in 2000. The building suddenly collapsed approximately 9 h after the start of the fire, while the firefighters were seemingly in control of the blaze, resulting in the death of 27 people [1]. Fire can also lead to significant structural damages which, even if a full collapse does not occur, can lead to the need for a complete refurbishment. This was the case in the Mont Blanc Tunnel, which was under repair during 3 years following the fire event in 1999. As a result, the designer of a concrete structure should ensure that the fire-loading case is adequately considered and that the concrete structure provides sufficient safety with respect to this accidental scenario.

Analyzing the effects of fire on concrete material and concrete structures is a complex task. Concrete is, by itself, a complex composite material, composed of aggregates and a cementitious matrix that hardens over time. There exists a large variety of concrete compositions, which differ by the types of aggregates and cementitious matrix, as well as the presence of fibers and other adjuvants. These different compositions result in a variety of concretes that are generally grouped under categories based on weight, strength, presence of fibers, and performance

level. Furthermore, as the type of aggregate influences the fire behavior of concrete, normal-weight concretes are commonly subdivided into silicate (siliceous) and carbonate (limestone) aggregate concrete, according to the composition of the principal aggregate. Indeed, some aggregates break up at 350 °C whereas others (e.g., granite) remain thermally stable up to 600 °C [2]. When subjected to fire, a concrete structure is exposed to heat flow into the exposed surfaces. This heat flow generates temperature, moisture, and pore pressure gradients across the sections. At the material scale, these gradients lead to thermal strains, stresses, cracking, and potentially explosive spalling. Besides, the heating generates physicochemical changes in the cement paste and in the aggregates, as well as thermal incompatibilities between the two. This results in a loss of mechanical properties (strength and stiffness) of concrete with temperature. The reinforcing steel, and the bond between the steel rebars and the concrete, also experiences a reduction of mechanical properties upon heating. Finally, at the structural level, thermal strains may generate additional forces in a structure due to restraints. Designing for fire requires ensuring that all these effects combined do not prejudice the safety of the structure.

This chapter aims at describing the behavior of concrete and concrete structures in the fire situation, as well as the methods employed to design concrete structures in fire. The chapter is structured as follows. Section 6.2 presents briefly the different types of concrete which are the most common and relevant to the field of structural fire engineering. These include normal-strength concrete, high-strength concrete, lightweight concrete, steel fiber-reinforced concrete, and polymer fiber-reinforced concrete. Section 6.3 discusses the behavior of reinforced and prestressed concrete structures in fire, including the general design principles, temperature profiles, effects of restraints, possibility of spalling, and important failure modes. Section 6.4 presents the main properties affecting fire resistance. Sections 6.5 and 6.6 examine the material properties of concrete (5) and reinforcing and prestressing steel (6) at elevated temperatures. These sections cover the thermal, mechanical, and deformation properties of the materials. Section 6.7 examines the design methods for concrete members subjected to fire. Finally, Sect. 6.8 discusses special considerations about shear and punching shear, torsion and anchorage, effects of thermal restraint and thermal expansion, buckling length, reinforced concrete frames, and tensile and compressive membrane behavior.

## 6.2 Specific Types of Concrete

### 6.2.1 *Normal-Strength Concrete*

The most commonly used concretes, classified as normal-strength concrete (NSC), have a compressive strength ranging from 20 to 50 MPa. The aggregates consist of coarse gravel and finer materials such as sand. Coarse aggregates are either calcareous (e.g., limestone) or siliceous (e.g., quartz) in nature. The binder is most typically a Portland cement, i.e., a hydraulic cement consisting mainly of calcium



silicates originating from limestone. Production of concrete results from the mixing of the cement (presented as dry powder) and aggregates with water. The chemical reaction between cement and water bonds the different elements together. Concrete can be cast in place, or precast in a plant using reusable molds, and transported to the construction site after curing. The density of a normal concrete is about 2300–2400 kg/m<sup>3</sup>.

The water-to-cement ratio, defined as the ratio of the weight of water to the weight of cement used in the mix, is an important parameter affecting the strength, durability, and workability. This ratio also plays a particular role in fire due to the vaporization and transport mechanisms of heated water. For the hydration reaction to be fully complete, a ratio of 0.35 is required. However, workability demands more water than is strictly required from a chemical reaction point of view. As a result, water-to-cement ratio between 0.45 and 0.60 is typically used in normal-strength concrete. Yet, water that is not chemically bonded in concrete eventually leaves the material resulting in microscopic pores that lead to increased porosity and reduced strength of the hardened concrete. Excessive use of water also generates increased shrinkage as excess water leaves, resulting in additional internal cracking. The water-to-cement ratio in the mix can be reduced by using additives such as superplasticizers to overcome the workability issue. Lowering the water-to-cement ratio allows obtaining concretes with higher strength and lower permeability. In fire, the water-to-cement ratio notably influences the propensity to explosive spalling. Lower ratios (such as in high-strength concrete), by leaving few micropores in the concrete mass, promote explosive spalling due to the buildup of internal pressure. In contrast, higher ratios that are associated with increased permeability allow dissipating the internal pressures from vaporization of free water, therefore leading less frequently to explosive spalling. The moisture content in a concrete also influences the thermal behavior. Since free water will absorb a certain quantity of heat, most notably during vaporization, the temperature increase of a concrete member is slightly slower for higher moisture contents.

Concrete is weak in tension, and therefore is usually used in conjunction with steel reinforcement. Concrete and steel work jointly with the concrete withstanding the compressive forces and providing stiffness whereas the steel withstands the tensile forces. In reinforced concrete, steel reinforcement bars are embedded passively in the concrete before the concrete sets. In prestressed concrete, steel tendons are stressed in tension prior to the application of any external loading, in order to create an initial state of compression in the concrete which improves the behavior of the structure under working loads. In the fire situation, the heating of the steel bars or tendons plays a crucial role in the behavior of the heated concrete structure.

### ***6.2.2 High-Strength Concrete***

High-strength concrete (HSC) generally refers to concretes with a compressive strength in the range of 50–120 MPa. Over the last decades, they have become commonly used in a number of applications, such as in tall buildings where the use

of HSC allows to increase the net marketable area. High-strength concrete is obtained by lowering the water-to-cement ratio and using additives such as silica fume and superplasticizers.

High-strength concrete members tend to be proportionally more affected by fire than normal-strength concrete members, due to a number of factors. First, HSC experiences higher rates of strength loss with temperature, compared with NSC [3]. The difference is particularly significant at temperatures between 50 and 250 °C. Second, HSC members are more prone to spalling, due to reduced permeability. Experimental research has shown that this spalling can impair the fire resistance of HSC members [4, 5]. Risk of spalling in HSC members is usually mitigated through the addition of polypropylene fibers in the mix. Third, HSC is often used to reduce the size of structural members, taking advantage of the fact that the material carries the load more effectively than NSC. This size reduction leads to faster temperature increase in the section core of the members and to increased slenderness, both of which may be detrimental to the fire performance. In total, these combined factors may partly neutralize the advantages of high-strength concrete over normal-strength concrete when taking into account the fire loading, although this may not be practically significant for relatively stocky members [6].

Recently, developments of new concrete types have led to compressive strengths in the range of 150–200 MPa. Such concretes are referred to as ultrahigh-performance concrete (UHPC). They contain a significant amount of steel fibers. UHPC also contains high-strength cements, silica fume, and fine-grained sand, but they do not include coarse aggregates.

### 6.2.3 *Lightweight Concrete*

Structural lightweight concrete generally refers to concretes with a density ranging from 1000 to 2200 kg/m<sup>3</sup>. Lightweight concrete (LWC) provides several advantages when compared with normal-strength concrete, including reduction in dead loads and improved thermal properties. In particular, LWC has a lower thermal conductivity leading to improved fire resistance of LWC members compared with NSC members [7, 8]. The compressive strengths of LWC can range between 1 and 100 MPa [9].

Structural lightweight concrete is most commonly obtained from replacing the coarse or fine aggregates found in normal concrete with lightweight aggregates. Lightweight aggregates may be from natural materials such as volcanic pumice, or from thermally treated (expanded) raw materials such as clay, slate, or shale. Industrial by-products such as fly ash can also be manufactured into lightweight aggregates. Since many types of lightweight aggregates have experienced a high-temperature manufacture treatment, they remain very stable under fire exposure. Namely, compared with NSC, LWC has a lower thermal conductivity and lower thermal expansion coefficient, because the high-temperature treatment of lightweight aggregates results in a more porous structure of the aggregates [10].

Tabulated data for prescriptive fire design of concrete members generally include specific provisions for lightweight concrete that account for the superior fire behavior of this type of concrete. For instance, Eurocode tabulated data specify that the minimum dimension of the cross section in beams or slabs may be reduced by 10% if lightweight aggregates are used, compared with normal-weight siliceous aggregates [11].

### **6.2.4 Steel Fiber-Reinforced Concrete**

Steel fiber-reinforced concrete (SFRC) refers to concretes containing 0.1–2.5% of steel fibers by volume of concrete. The fibers, which are generally 25–40 mm long, are uniformly distributed and randomly oriented. Round fibers are the most common type with a diameter ranging from 0.25 to 0.75 mm. Rectangular steel fibers are also used with a typical thickness of 0.25 mm. The fibers may have crimped or hooked end to improve the bond with concrete.

The primary function of the steel fibers is to mitigate the plastic and drying shrinkage of concrete. As they lessen the permeability of concrete, the fibers improve the concrete durability. In addition, steel fibers increase the concrete toughness, strength, and energy absorption capacity [12]. The most common applications are tunnel linings, slabs, and airport pavements, as well as specific application where impact resistance is required.

The thermal and mechanical properties of steel fiber-reinforced concrete have been studied in the literature. Results indicate that the fibers have a limited effect on the thermal properties, notably through minor influence on specific heat of concrete. Compared with NSC, steel fiber-reinforced concrete displays a higher specific heat in 400–800 °C temperature range. The presence of steel fibers has a more notable effect on the mechanical behavior. Notably, the presence of steel fibers in concrete leads to reduced strength loss rate at elevated temperatures and increased ductility and ultimate strain [13, 14].

### **6.2.5 Polymer Fiber-Reinforced Concrete**

Polymer fiber-reinforced concrete (PFRC) encompasses a wide variety of compositions and applications. However, PFRC has a particular interest with respect to fire resistance. Namely, the addition of polypropylene fibers within a concrete mix (at least 0.1% by weight) has shown to be probably the most efficient method to mitigate explosive spalling under fire exposure [15, 16]. The beneficial effect of polypropylene fibers is primarily linked to the increased permeability resulting from the melting (~170 °C) and subsequent vaporization (~340 °C) of the fibers, and to the introduction of additional interfacial transition zones between the fibers and the cement paste [17].

Polypropylene fibers do not significantly influence the mechanical properties of concrete. Regarding the thermal behavior, since the burning of polypropylene fibers produces microchannels for release of vapor, the amount of heat absorbed is less for dehydration of chemically bound water resulting in a slightly lower specific heat in the temperature range of 600–800 °C.

### 6.3 Behavior of Concrete Structures in Fire

Concrete presents a certain number of characteristics that make it an inherently well-armed material to withstand the effects of fire. It is a noncombustible material. It combines a low thermal conductivity with relatively massive sections, which delays the heat transfer throughout the section. This leads to very important temperature gradients between the outer part of the section and the inner core. As a result, the cooler inner core, which maintains most of its strength, continues carrying the load for a significant duration of fire exposure. As the reinforcing steel is protected by a concrete cover, the temperature increase in the steel is also limited. These characteristics lead to the situation that, under certain circumstances, limited specific provisions, if any, are sufficient for providing a concrete structure with a good fire behavior. As a result, fire resistance can often be achieved in building structures made of concrete at economic costs. The use of structural concrete is thus common in applications where the fire resistance is an issue or in other applications where elevated temperature can arise such as in nuclear vessels.

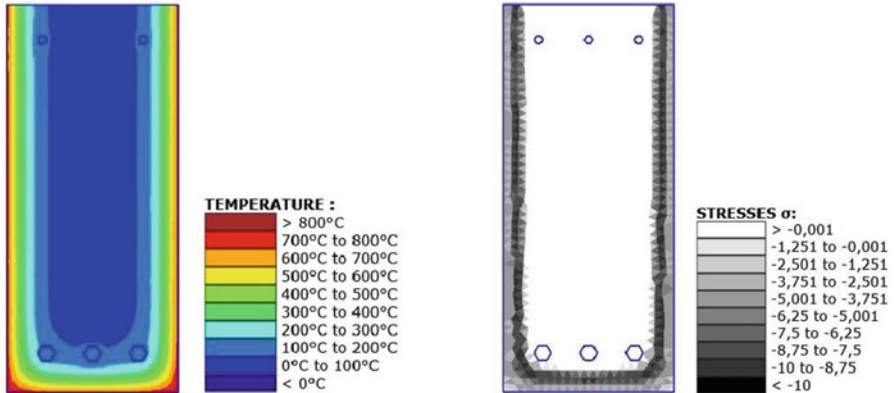
However, concrete structures are far from immune to the effects of fire. The mechanical properties of concrete and reinforcing steel are affected by temperature. If the fire exposure lasts for a significant time, the temperature increase in the section becomes notable and leads to a reduction of strength and stiffness of the materials. This can lead to increased deformations and possible failure. Meanwhile, concrete heated under compressive stress develops transient creep strains, a specific strain component that influences the structural behavior [18]. Furthermore, temperature increase induces thermal expansion. In building structures, thermal deformations are generally restrained. Therefore, thermally induced forces are generated and can lead to failure of the heated members or of adjacent parts of the structure. Finally, spalling may occur. Spalling is the separation, possibly in an explosive manner, of pieces of concrete from the cross section, when exposed to fire. It can result in the reinforcing steel being directly exposed to the fire. These phenomena impair the capacity of a concrete structure to withstand the applied loads during a fire, possibly resulting in failure. Hence, fire represents a significant threat to the stability of concrete structures and, despite the favorable characteristics of the material listed above, the behavior under fire exposure needs to be carefully assessed.

### 6.3.1 Reinforced Concrete

Reinforced concrete members are designed to resist by compression in concrete and tension in reinforcing steel. Steel reinforcement also provides supplemental shear resistance. In the fire situation, major factors influencing the behavior are the temperatures reached in the reinforcing steel and in the concrete compression zone. The temperature of the reinforcing steel depends on the concrete cover. Therefore, specific design prescriptions relative to cover apply in the fire situation. The temperature of the concrete compression zone depends on the section dimensions and fire exposure. In the case of a simply supported slab exposed on its lower face, the compressive zone is not affected by temperature. The load-carrying capacity in the fire situation is then solely a function of the temperature of the bottom reinforcing steel. Simple hand calculations can be used for design, accounting for the reduction of steel yield strength due to elevated temperatures. In contrast, in the case of a column heated on three or four sides, the strength of the compressive zone is reduced. Hence design prescriptions specify minimum section dimensions to ensure a satisfying fire behavior. In the latter case, design calculations must consider the effects of elevated temperature on the compression strength of concrete and on the yield strength of steel. Besides, the behavior may be affected by deformations caused by thermal gradients as well as possible instability failures. Therefore, design calculation methods are more complex.

Significant thermal gradients develop in concrete sections under fire conditions. These thermal gradients are highly nonlinear. They result in a combination of thermal deformations and/or restraint axial forces, thermal curvature and/or restraint bending moment, and auto-equilibrated stresses. It is worth noting that an unloaded concrete section exposed to fire will crack due to the effects of thermal stresses. Indeed, differential thermal elongations between the hotter outer part and the cooler inner core will generate tensile forces in the inner core (Fig. 6.2).

In fire-exposed concrete structures, the effects of member restraint by other parts of the structure are of particular importance. These effects arise when a heated member or assembly is restrained from thermal expansion by the surrounding structure. These effects may be beneficial. For instance, axial restraint may have a positive effect on the fire performance of reinforced concrete slabs or beams. This requires that the surrounding structure be sufficiently stiff and that the line of thermally induced thrust be below the compressive stress block. The axial thrust then plays the role of an external prestressing, creating a bending moment that opposes the externally applied moment. However, thermally induced restraint forces may also have detrimental effects on the fire performance of concrete structures. Excessive axial restraints may lead to buckling of the heated member. The moment generated by the axial restraint may add to the applied moment if beam mid-span deflections become excessive or if, depending on the support conditions, the line of thrust develops above the compressive stress block. Finally, thermally induced forces may damage the surrounding structure. Observations from real fire events have shown that failure of concrete structures in fire often results from shear or



**Fig. 6.2** Unloaded reinforced concrete beam section exposed to ISO fire on three sides. Temperature distribution (left) and stress distribution (right), after 30 min. Large thermal gradients develop in the section, resulting in thermal stresses with the cooler inner core cracked in tension

buckling failures of stiff vertical members (columns, walls) due to their inability to absorb the large thermal deformations imposed by the heated members.

### 6.3.2 *Prestressed Concrete*

In prestressed concrete, the structural members are stressed prior to the application of any external loads. The objective is to apply an initial state of compression to the concrete material to enhance its behavior under external loading. The prestressing force is introduced through steel tendons which are stressed in tension. The distinction is made between pretensioned concrete and posttensioned concrete to refer to situations where the tensile force in the steel tendons is applied before or after the concrete has cured, respectively. In pretensioned concrete, the concrete is cast around the stressed tendons. After the concrete has cured, the tendons are cut, releasing the prestressing force which is resisted by bond stresses between the concrete and the tendons. In posttensioned concrete, the concrete is cast with ducts for the steel tendons, unstressed at that time. After the concrete has cured, the tendons are put in tension with hydraulic jacks, and anchored at the extremities of the member. The introduction of the prestressing force in the member is thus realized at anchorage points.

Generally speaking, the same design principles apply to prestressed concrete as to reinforced concrete. However, prestressed concrete structures are often more vulnerable to the effects of fire. This is due to three reasons. First, mechanical properties of prestressing steel tendons reduce faster with temperature compared with the properties of reinforcing bars. Prestressing steels need to have a high strength at ambient temperature for the prestressing effect to be efficient. The tendons are made

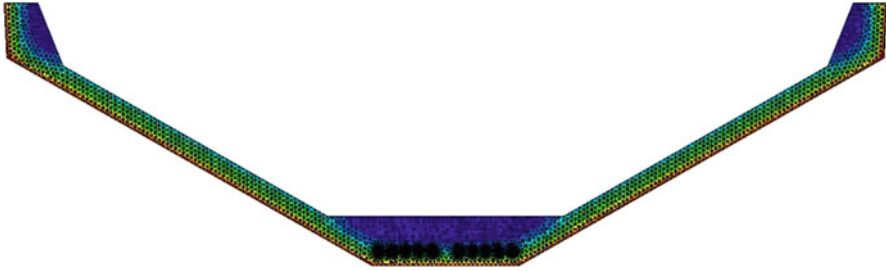
of cold-worked wires and strands or quenched and tempered bars. Due to the manufacturing process, these steels are more sensitive to elevated temperature than mild steel-reinforcing bars. The second reason comes from the fact that some failure modes are particularly critical in prestressed concrete subject to fire. For instance, bond failure in pretensioned concrete members can lead to premature failure. In pretensioned hollow core slabs, debonding near the ends of the members may lead to reduction of compressive stresses and subsequent shear failure in the webs [19, 20]. Spalling is also more prone to happen in prestressed members due to the existence of large prestressing compressive stresses in the concrete, which combines with thermal stresses and pore pressures. The third reason that explains the particular vulnerability of prestressed members to fire relates to their typical design at ambient temperature. Usually, prestressed members are more slender than reinforced concrete members. They also use thin concrete covers, resulting in less thermal protection for the steel than in reinforced concrete design. Finally, prestressed members often have little or no shear reinforcement, with the shear resistance being provided by the pre-compressed concrete. This absence of shear reinforcement may lead to premature failure in case of loss of prestressing during fire, as observed in some hollow core slabs.

### ***6.3.3 Temperature Profiles in Concrete Members***

The temperature profile in the members is a major factor influencing the fire behavior of concrete structures. Therefore, establishing the temperatures in the concrete sections is an essential part of any fire design of a concrete structure.

As previously stated, the temperature distribution in concrete members is highly nonlinear. Indeed, important thermal gradients develop due to the low conductivity and the high massivity of the sections. Unlike steel members, in which the simple lumped mass approach is a valid approximation in some cases, it cannot be assumed that a unique temperature exists in a concrete section at any given time. As a result, no simple calculation approach is available for the determination of the transient temperature profiles in concrete sections.

Tables and design charts have been derived to give temperature profiles in concrete sections exposed to standard fire. Temperature profiles are available for beams, columns, as well as slabs and walls exposed on one side. These profiles result from numerical calculations. They can be found in the literature as well as in the Eurocode (EN1992-1-2) [11]. However, such tables and charts are only valid for the specific fire exposure that was considered in the calculation, namely the standard fire. They cannot be applied for any other fire exposure. For evaluating the temperature distribution under realistic fires, it is recommended to use advanced finite element analysis. Numerical calculations can indeed be used to perform the thermal analysis of concrete members under any fire exposure. Advanced analysis is also the only solution for the thermal analysis of complex shapes, sections including cavities,



**Fig. 6.3** Temperature profile in a prestressed concrete V-beam, obtained from thermal analysis by the finite element method [21]

or any specific configuration for which no empirical calculation method is available (Fig. 6.3).

The thermal analysis of a concrete member should account for the temperature-dependent thermal properties of concrete. Thermal conductivity decreases with temperature. The effect of moisture content should also be accounted for, possibly through a modification of the specific heat to include the energy required for evaporation. In case of realistic fire exposure including a cooling phase, it is reasonable to assume that the properties are not reversible. In thermal calculations of reinforced or prestressed concrete members, a common assumption consists of neglecting the effect of the steel reinforcement on the heat transfer. This assumption is valid because the effect is very local, with most reinforcing steel being parallel to the fire-exposed surface.

### 6.3.4 Spalling

Spalling may be observed in fire-exposed concrete as a result of the combined effect of stresses (mechanical and thermal) and pore pressure. It is often explosive, occurring as a single explosion or a series of explosions and characterized by typically loud explosive noises. Concrete layers of 100–300 mm in length and 15–20 mm in depth may be removed by each explosion, which is dangerous for the integrity of the structure and may cause physical damage on impact.

High-strength concrete is more prone to spalling than normal-strength concrete. This can be explained by the fact that higher strength is achieved by reducing the water/cement ratio, which induces lower permeability and therefore enhances pore pressure spalling. High heating rates increase the probability of explosive spalling because they generate excessive temperature gradients in the concrete, thus inducing significant compressive stresses close to the heated surface and tensile stresses in the interior regions. Combination of external applied loads resulting in compressive stresses with thermal stresses due to the temperature gradients increases the susceptibility of concrete members to spalling. Other factors influence the occurrence of



spalling such as the section shape (acute-angled corners are critical), moisture content and permeability (through their effects on pore pressure), or type of aggregate (probability of thermal stress spalling is less for concrete with a low-thermal-expansion aggregate) [22].

Recent research has proved that explosive spalling could be eliminated by adding polypropylene fibers (at least 0.1% by weight) in a concrete mix; the result was very effective even in high-strength concrete (60–110 MPa).

### ***6.3.5 Case Studies, Failure Modes, and Full Structure Response***

Lessons from real fire accidents allow highlighting potential failure modes in fire-exposed concrete structures. For instance, shear punching failure has been observed in flat slab-column structures. In 2004, a fire took place in an underground car park in Gretzenbach, Switzerland. The fire was localized and not very severe. After approximately 90 min of fire, the concrete roof slab of the car park collapsed due to shear punching. This resulted in the death of seven firefighters. The structure was made of flat slabs supported by concrete columns. Such structures are known to be sensitive to punching failure at ambient temperatures. During fire, due to restrained sagging of the slabs towards the fire, thermally induced increase of the load is introduced at the supports. Thermal expansion of columns may also lead to additional increase of axial load. These result in increase of the punching load at the column-slab connection, possibly leading to premature collapse [23, 24].

Collapse of precast pretensioned hollow core slabs has been observed in fire events. For instance, in 2007, a fire occurred in the open car park of the Harbour Edge apartment building in the Netherlands. The building structure was made of prestressed hollow core slabs with a cast-in situ concrete topping as compression layer. The compression layer was between 70 mm and 90 mm thick, with additional reinforcement as a tension ring to increase the slab thickness. The design fire resistance was 120 min. At the time of the accident, seven cars were parked at the level where the fire took place. The structure partially collapsed during the fire. Several hollow core slabs developed horizontal cracks through the webs, separating the slabs into an upper and lower half, due to the restraint to thermal expansion exerted by the compression layer. These horizontal cracks led to failure of the bottom of the hollow core slabs. Further collapse of slabs occurred during the cooling phase and in the hours after the fire [25]. Hollow core slabs may also be subject to shear failure in fire after loss of prestress due to anchorage failure near the ends of the slabs.

Shear failure may be a problem in parts of a structure that are not directly heated by the fire, due to the inability to accommodate the thermal deformations of adjacent elements. Consideration of full structure response, rather than isolated members' behavior, is thus essential for accounting for these indirect effects of actions. In

**Fig. 6.4** Shear failure of concrete columns due to thermal elongation of the ceiling [26]



2010, a fire occurred in the “Tour d’Ivoire” building in the city of Montreux in Switzerland. Thermal elongation of concrete slabs subjected to the action of two burning cars led to the collapse in shear of a column that was several meters away from the fire source (Fig. 6.4) [26].

In prescriptive design approaches, the fire action is typically idealized by a monotonously increasing temperature-time relationship. Yet, real fires comprise a heating phase followed by a cooling-down phase. Cooling phases generate different phenomena in concrete structures that may result in additional damage or even collapse [27]. First, it is clear that, during a fire, the maximum temperatures inside concrete members are reached after the time of maximum gas temperature, due to thermal inertia. This means that highest temperatures in the section occur during the cooling phase. Furthermore, concrete material experiences an additional loss of strength while cooling, compared to the strength loss at the maximum reached temperature [28]. Other properties are irrecoverable. Notably, transient creep strain must be explicitly treated as a permanent strain which has significant influence on the stiffness in cooling [29]. Finally, when considering the full structure response, the recovery of thermal strains that occur during the cooling phase may lead to indirect effects of actions that endanger the structural stability. For these reasons, it is important to take into account the effects of the cooling phase of fires on concrete structures [30], especially because of the potential threat that delayed collapses pose to fire brigades.

## 6.4 Properties Influencing Fire Resistance

The fire response of reinforced concrete (RC) members is influenced by the characteristics of constituent materials, namely concrete and reinforcing steel and/or prestressing steel. These include (a) thermal properties, (b) mechanical properties, (c) deformation properties, and (d) material-specific characteristics such as spalling. These properties vary significantly with temperature and are also dependent on the composition and characteristics of concrete batch mix as well as heating rate and other environmental conditions.

The thermal properties determine the extent of heat transfer to the structural member, whereas the mechanical properties of constituent materials determine the extent of strength loss and stiffness deterioration of the member. The deformation properties, in conjunction with mechanical properties, determine the extent of deformations and strains in the structural member. In addition, fire-induced spalling of concrete can play a significant role in the fire performance of RC members [4]. All these properties vary as a function of temperature and depend on the composition and characteristics of concrete as well as those of the reinforcing steel [31]. The primary focus of this chapter is on the effect of temperature on properties of concrete and the temperature-induced variation on properties of steel reinforcement can be found elsewhere [31, 32].

Concrete is available in various forms and it is often grouped under different categories based on weight (as normal-weight and lightweight concrete), strength (as normal-strength, high-strength, and ultrahigh-strength concrete), presence of fibers (as plain and fiber-reinforced concrete), and performance (as conventional and high-performance concrete). Fire safety practitioners further subdivide normal-weight concretes into silicate (siliceous) and carbonate (limestone) aggregate concrete, according to the composition of the principal aggregate. Also, when a small amount of discontinuous fibers (steel or polypropylene) is added to concrete batch mix to improve performance, this concrete is referred to as fiber-reinforced concrete (FRC). In this section, the various properties of concrete are mainly discussed for conventional concrete. The effect of strength, weight, and fibers on the properties of concrete at elevated temperatures is highlighted.

Traditionally, the compressive strength of concrete used is around 20–50 MPa, which is classified as normal-strength concrete (NSC). In recent years, concrete with a compressive strength in the range of 50–120 MPa has become widely available and is referred to as high-strength concrete (HSC). When compressive strength exceeds 120 MPa, it is often referred to as ultrahigh-performance concrete (UHP). The strength of concrete degrades with temperature and the rate of strength degradation is highly influenced by the compressive strength of concrete.

The thermal properties that influence temperature rise and distribution in a concrete structural member are thermal conductivity, specific heat, thermal diffusivity, and mass loss. Thermal conductivity is the property of a material to conduct heat. Thermal conductivity is usually measured by means of “steady state” or “transient” test methods [33]. Transient methods are preferred to measure thermal conductivity

of moist concrete over steady-state methods [34–36], as physiochemical changes of concrete at higher temperatures cause intermittent direction of heat flow. On average, the thermal conductivity of conventional normal-strength concrete, at room temperature, ranges between 1.4 and 3.6 W/m·°C (0.81–2 BTU/h ft·°F) [37].

Specific heat is the amount of heat per unit mass, required to change the temperature of a material by one degree, and is often expressed in terms of thermal (heat) capacity which is the product of specific heat and density. Specific heat is highly influenced by moisture content, aggregate type, and density of concrete [38–40]. The specific heat of concrete varies between 400 and 750 J/kg °C. The variation of specific heat with temperature used to be determined through adiabatic calorimetry until 1980s. Since the 1980s, differential scanning calorimetry (DSC) has been the most commonly used technique for mapping the curve in a single temperature sweep at a desired rate of heating [41]. Unfortunately, the accuracy of the DSC technique in determining the sensible heat contribution to the apparent specific heat may not be particularly good (sometimes it may be as low as  $\pm 20\%$ ). The rate of temperature rise in DSC tests is usually 5 °C min<sup>-1</sup>. At higher heating rates, the peaks in the DSC curves tend to shift to higher temperatures and become sharper. For temperatures above 600 °C, a high-temperature differential thermal analyzer (DTA) is also used to evaluate specific heat.

The density, in an oven-dry condition, is the mass of a unit volume of the material, comprising the solid itself and the air-filled pores. With increasing temperature, materials that have high amount of moisture, such as concrete, will experience mass loss resulting from evaporation of moisture due to chemical reactions. Assuming that the material is isotropic with respect to its dilatometric behavior, its density (or mass) at any temperature can be calculated from thermogravimetric and dilatometric curves [42].

The mechanical properties that determine the fire performance of RC members are compressive and tensile strength, modulus of elasticity, and stress-strain response of constituent materials at elevated temperatures.

Compressive strength of concrete at elevated temperature is of primary interest in fire resistance design. Compressive strength of concrete at ambient temperature depends on water-cement ratio, aggregate-paste interface transition zone, curing conditions, aggregated type and size, admixture types, and type of stress [43]. At high temperature, compressive strength is highly influenced by room-temperature strength, rate of heating, and binders in batch mix (such as silica fume, fly ash, and slag). Unlike thermal properties at high temperature, the mechanical properties of concrete are well researched. The strength degradation in HSC is not consistent and there are significant variations in strength loss, as reported by various authors.

Concrete is weak in tension; thus tensile strength of concrete is often neglected in strength calculations at room and elevated temperatures. For example, tensile strength in NSC is only 10% of its compressive strength and for HSC tensile strength ratio further reduces. However it is an important property, because cracking in concrete is generally due to tensile stresses and the structural damage of the member in tension is often generated by progression in microcracking [44]. Under fire conditions tensile strength of concrete can be even more crucial in cases where

fire-induced spalling occurs in a concrete structural member [45]. Tensile strength of concrete is dependent on almost the same factors as compressive strength of concrete [46, 47].

Another property that influences fire resistance is the modulus of elasticity of concrete which decreases with temperature. At high temperature disintegration of hydrated cement products and breakage of bonds in the microstructure of cement paste reduce elastic modulus and the extent of reduction depends on moisture loss, high-temperature creep, and type of aggregate.

The deformation properties that determine the fire performance of reinforced concrete members are thermal expansion and creep. In addition, transient strain that occurs at elevated temperatures in concrete can enhance deformations in fire-exposed concrete structural members.

The thermal expansion characterizes the expansion (or shrinkage) of a material caused by heating and is defined as the expansion (shrinkage) of unit length of a material when the temperature of concrete is raised by one degree. The coefficient of thermal expansion is defined as the percentage change in the length of a specimen per degree temperature rise. The expansion is considered to be positive when the material elongates and is considered negative (shrinkage) when it shortens. In general, the thermal expansion of a material is dependent on the temperature and is evaluated through dilatometric curve, which is a record of the fractional change of a linear dimension of a solid at a steadily increasing or decreasing temperature [42]. Thermal expansion is an important property to predict thermal stresses that get introduced in a structural member under fire conditions. Thermal expansion of concrete is generally influenced by cement type, water content, aggregate type, temperature, and age [36, 48].

Creep, often referred to as creep strain, is defined as the time-dependent plastic deformation of the material. At normal stresses and ambient temperatures, deformations due to creep are not significant. However, at higher stress levels and/or at elevated temperatures, the rate of deformation caused by creep can be substantial. Hence, the main factors that influence creep are the temperature, the stress level, and their duration [49].

Transient strain occurs during the first-time heating of concrete and is independent of time. It is essentially caused by thermal incompatibilities between the aggregate and the cement paste [50]. Transient strain of concrete, similar to that of high-temperature creep, is a complex phenomenon and is influenced by factors such as temperature, strength, moisture content, loading, and mix proportions. It is irreversible and may considerably influence the behavior of concrete structures in fire [29].

Since concrete structures are often reinforced with reinforcing and/or prestressing steel, the properties of steel reinforcement are also required to evaluate fire performance of concrete structures. A brief review on the properties of steel reinforcement is provided in Sect. 6.6.

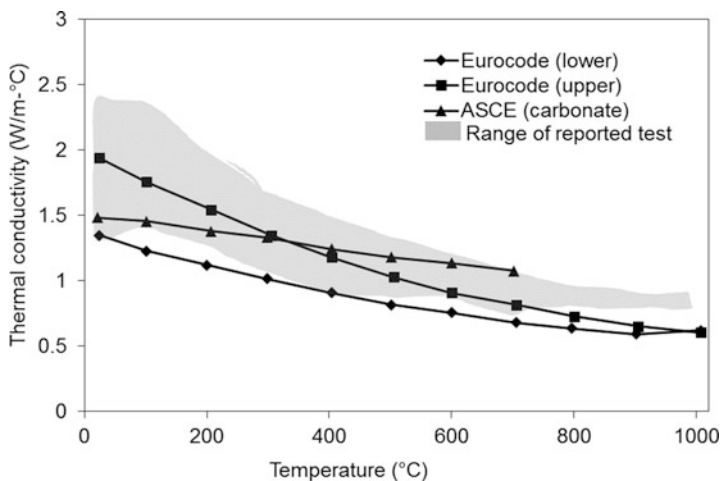
## 6.5 Material Properties of Concrete at Elevated Temperatures

### 6.5.1 Thermal Properties of Concrete at Elevated Temperatures

The thermal properties that govern temperature-dependent properties in concrete structures are thermal conductivity, specific heat (or heat capacity), and mass loss. These properties are significantly influenced by the aggregate type, moisture content, and composition of concrete mix. A detailed review on the effect of temperature on thermal properties of different concrete types is given by Khaliq [51], Kodur et al. [52], and Flynn [53].

#### 6.5.1.1 Thermal Conductivity

Thermal conductivity of concrete at room temperature is in the range of 1.4 and 3.6 W/m<sup>2</sup>K and varies with temperature [37]. Figure 6.5 illustrates the variation of thermal conductivity of NSC as a function of temperature based on published test data and empirical relations. Overall thermal conductivity decreases gradually with temperature and this decrease is dependent on the concrete mix properties, specifically moisture content and permeability. This decreasing trend in thermal conductivity can be attributed to variation of moisture content with increase in temperature [37]. It should be noted that there are very few standardized methods available for measuring thermal properties. Also plotted in Fig. 6.5 is both upper and lower bound



**Fig. 6.5** Variation in thermal conductivity of normal-strength concrete as a function of temperature [54]

values of thermal conductivity as per EC2 provisions and this range is for all aggregate types. However, thermal conductivity shown in Fig. 6.5, as per ASCE relations, is applicable for carbonate aggregate concrete.

Thermal conductivity of HSC is higher than that of NSC due to low w/c ratio and use of different binders in HSC [55]. Generally thermal conductivity of HSC is in the range between 2.4 and 3.6 W/m<sup>2</sup>K at room temperature. Thermal conductivity for fiber-reinforced concretes (with both steel and polypropylene fibers) almost follows a similar trend as that of plain concrete and lies closer to that of HSC. Therefore it is deduced that there is not much of a significant effect of fibers on the thermal conductivity of concrete in 20–800 °C temperature range [45].

### 6.5.1.2 Specific Heat

Specific heat of concrete at room temperature varies in the range of 840 and 1800 J/kg K for different aggregate types. Often specific heat is expressed in terms of thermal capacity which is the product of specific heat and density of concrete. The specific heat property is sensitive to various physical and chemical transformations that take place in concrete at elevated temperatures. This includes the vaporization of free water at about 100 °C, the dissociation of Ca(OH)<sub>2</sub> into CaO and H<sub>2</sub>O between 400 and 500 °C, and the quartz transformation of some aggregates above 600 °C [42]. Specific heat is therefore highly dependent on the moisture content and considerably increases with higher water-to-cement ratio.

Figure 6.6 illustrates the variation of specific heat for NSC with temperature as reported in various studies based on test data and different standards. The specific heat of this concrete type remains almost constant up to 400 °C, followed by

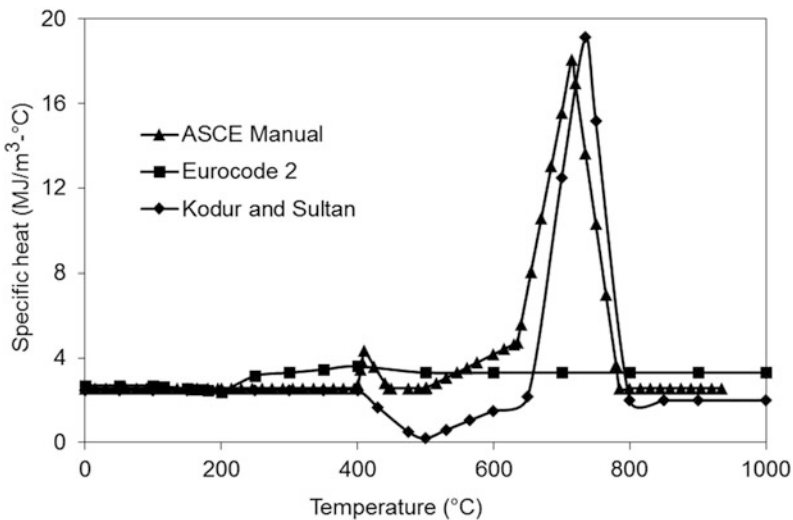


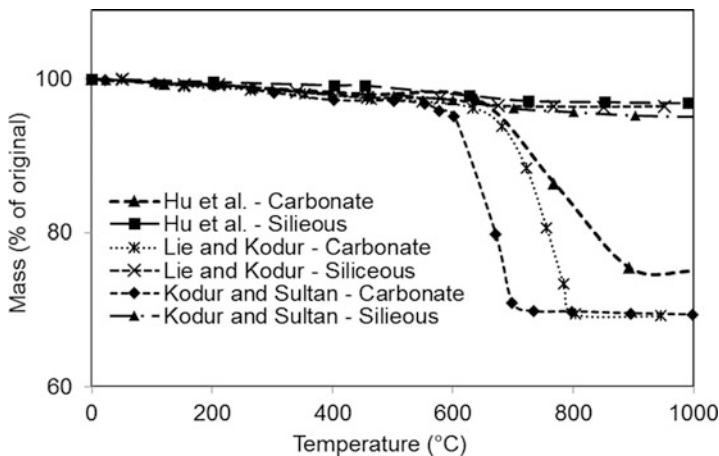
Fig. 6.6 Variation in specific heat of normal-strength concrete as a function of temperature [54]

increases up to about 700 °C, and then remains constant between the 700 and 800 °C range. Of the various factors, aggregate type has a significant influence on the specific heat (thermal capacity) of concrete. This effect is captured in ASCE-specified relations for specific heat of concrete [36]. Carbonate aggregate concrete has higher specific heat (heat capacity) in the 600–800 °C temperature range and this is caused by an endothermic reaction, which results from the decomposition of dolomite and absorbs a large amount of energy [31].

As compared to NSC, HSC exhibits slightly lower specific heat throughout the 20–800 °C temperature range. The presence of fibers also has minor influence on specific heat of concrete. For concrete with polypropylene fibers, the burning of polypropylene fibers produces microchannels for release of vapor, and hence the amount of heat absorbed is less for dehydration of chemically bound water; thus its specific heat reduces in the temperature range of 600–800 °C. However, concrete with steel fibers displays a higher specific heat in the 400–800 °C temperature range, which can be attributed to additional heat absorbed for dehydration of chemically bound water.

### 6.5.1.3 Mass Loss

Depending on the density, concretes are usually subdivided into two major groups: (1) normal-weight concretes with densities in the 2150–2450 kg m<sup>-3</sup> range and (2) lightweight concretes with densities between 1350 and 1850 kg m<sup>-3</sup>. The density or mass of concrete decreases with increasing temperature due to loss of moisture. The retention in the mass of concrete at elevated temperatures is highly influenced by the type of aggregate [14, 39]. Figure 6.7 illustrates the variation in the mass of



**Fig. 6.7** Variation in the mass of concrete with different aggregates as a function of temperature [54]



concrete as a function of temperature for concretes made with carbonate and siliceous aggregates. The mass loss is minimal for both carbonate and siliceous aggregate concretes up to about 600 °C. However, the type of aggregate has significant influence on mass loss in concretes beyond 600 °C. In the case of siliceous aggregate concrete, mass loss is insignificant even above 600 °C. However, beyond 600 °C, carbonate aggregate concrete experiences larger percentage of mass loss as compared to siliceous aggregate concrete. This higher percentage of mass loss in carbonate aggregate concrete is attributed to dissociation of dolomite in carbonate aggregate at around 600 °C [31].

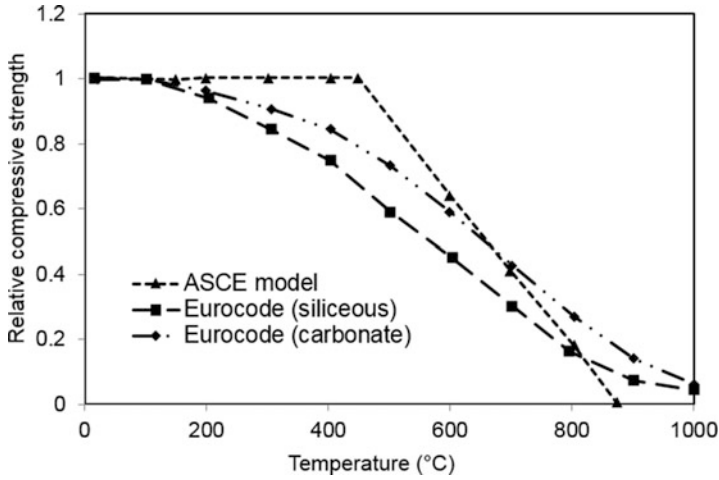
### ***6.5.2 Mechanical Properties of Concrete at Elevated Temperatures***

The mechanical properties that are of primary interest in fire resistance design are compressive strength, tensile strength, elastic modulus, and stress-strain response in compression. High-temperature mechanical property tests are generally carried out on concrete specimens that are typically cylinders or cubes of different sizes. Unlike room-temperature property measurements, where there are specified specimen sizes as per standards, the high-temperature mechanical properties are usually carried out on a wide range of specimen sizes due to lack of standardized test specifications for undertaking high-temperature mechanical property tests [56, 57].

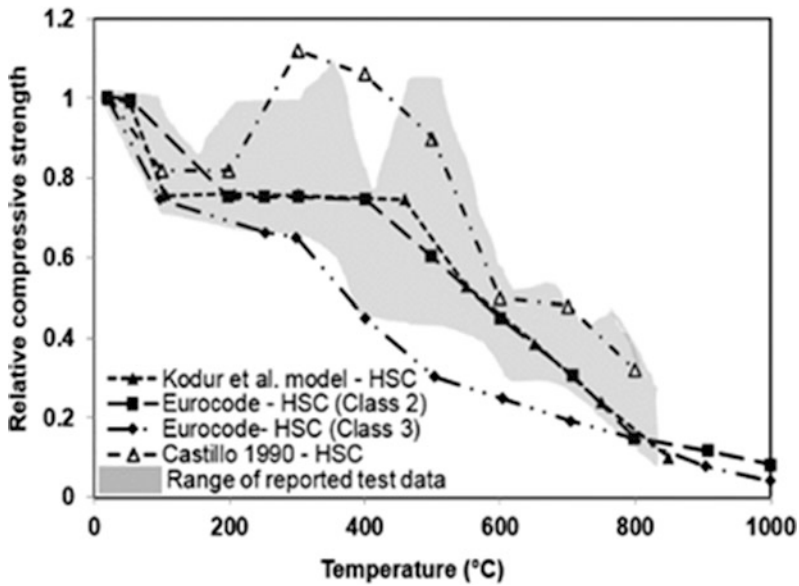
#### **6.5.2.1 Compressive Strength**

Figures 6.8 and 6.9 illustrate the variation of compressive strength ratio for NSC and HSC at elevated temperatures, respectively, with upper and lower bounds (of shaded area) showing a range of variation in reported test data. Also plotted in these figures is the variation of compressive strength as obtained using Eurocode [11], ASCE [36], and Kodur et al. [52] relations. Figures 6.8 and 6.9 show a large but uniform variation of the compiled test data for NSC and HSC. Overall, the variations from different tests can be attributed to using different heating or loading rates, specimen size and curing, condition at testing (moisture content and age of specimen), and use of admixtures.

In the case of NSC, the compressive strength of concrete is marginally affected by temperature up to 400 °C. NSC is usually highly permeable and allows easy diffusion of pore pressure as a result of water vapor. On the other hand, use of different binders in HSC produces a superior and dense microstructure with less amount of calcium hydroxide which ensures a beneficial effect on the compressive strength at room temperature [58]. Binders such as slag and silica fume give best results to improve compressive strength at room temperature which is attributed to



**Fig. 6.8** Variation of relative compressive strength of normal-strength concrete as a function of temperature [54]



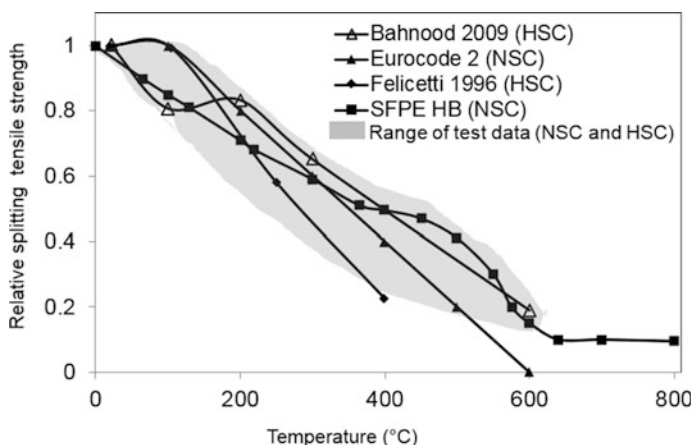
**Fig. 6.9** Variation in relative compressive strength of high-strength concrete as a function of temperature [54]

dense microstructure. The presence of steel fibers in concrete helps to slow down strength loss at elevated temperatures [13, 14].

### 6.5.2.2 Tensile Strength

The tensile strength of concrete is much lower than that of compressive strength and hence tensile strength of concrete is often neglected in strength calculations at room and elevated temperature. However from a fire resistance point of view, it is an important property, because cracking in concrete is generally due to tensile stresses and the structural damage of the member in tension is often generated by progression in microcracking [44]. Figure 6.10 illustrates the variation of splitting tensile strength ratio of NSC and HSC as a function of temperature as reported in previous studies and Eurocode provisions [32, 59–61]. The shaded portion in this plot shows a range of variation in splitting tensile strength as obtained by various researchers for NSC with conventional aggregates. The decrease in tensile strength of NSC with temperature can be attributed to weak microstructure of NSC allowing initiation of microcracks. At 300 °C concrete loses about 20% of its initial tensile strength. Above 300 °C, the tensile strength of NSC decreases at a rapid rate due to more pronounced thermal damage in the form of microcracks and reaches to about 20% of its initial strength at 600 °C.

HSC experiences rapid loss of tensile strength at higher temperatures due to development of pore pressure in dense microstructured HSC [58]. The addition of steel fibers to concrete enhances its tensile strength and the increase can be up to 50% higher at room temperature [62, 63]. Further, the tensile strength of steel fiber-reinforced concrete decreases at a lower rate than that of plain concrete throughout



**Fig. 6.10** Variation in relative splitting tensile strength of concrete as a function of temperature [54]

the temperature range of 20–800 °C [64]. This increased tensile strength can delay the propagation of cracks in steel fiber-reinforced concrete structural members.

### 6.5.2.3 Elastic Modulus

The modulus of elasticity of various concretes at room temperature varies over a wide range,  $5.0 \times 10^3$  to  $35.0 \times 10^3$  MPa, and is dependent mainly on the water-cement ratio in the mixture, the age of concrete, the method of conditioning, and the amount and nature of the aggregates. The modulus of elasticity decreases rapidly with the rise of temperature, and the fractional decline does not depend significantly on the type of aggregate [65]. It appears, however, that the modulus of elasticity of normal-weight concretes decreases at a higher pace with the rise of temperature than that of lightweight concretes. Figure 6.11 illustrates variation of ratio of elastic modulus at target temperature to that at room temperature for NSC and HSC [32, 40, 66]. The degradation modulus in both NSC and HSC can be attributed to excessive thermal stresses and physical and chemical changes in concrete microstructure.

### 6.5.2.4 Stress-Strain Response

The mechanical response of concrete is usually expressed in the form of stress-strain relations, which are often used as input data in mathematical models for evaluating fire resistance of concrete structural members. Generally, because of the decrease in compressive strength and increase in ductility of concrete, the slope of stress-strain

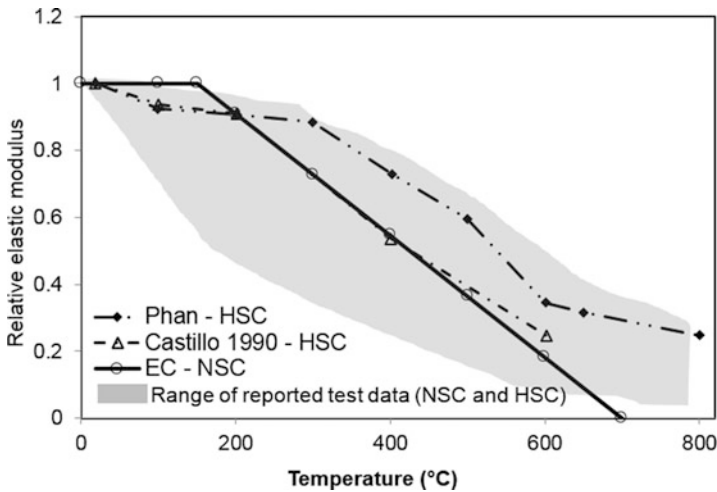
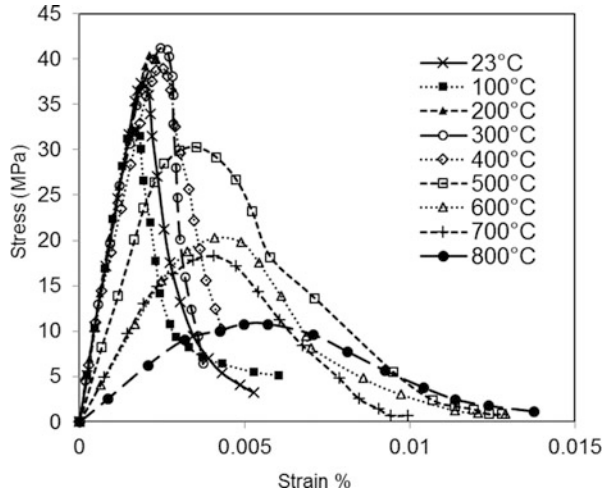
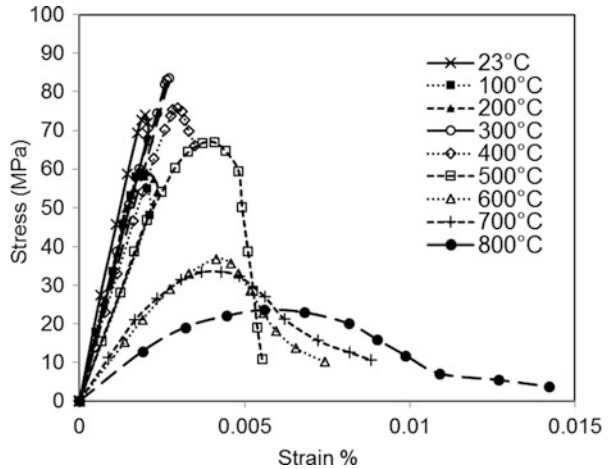


Fig. 6.11 Variation in elastic modulus of concrete as a function of temperature [54]

**Fig. 6.12** Stress-strain response of normal-strength concrete at elevated temperatures [54]



**Fig. 6.13** Stress-strain response of high-strength concrete at elevated temperatures [54]



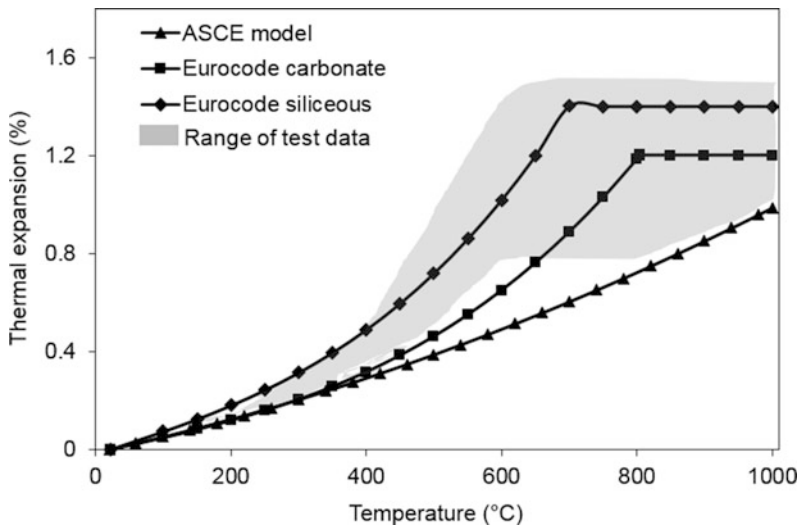
curve decreases with increasing temperature. The strength of concrete has a significant influence on stress-strain response both at room and elevated temperatures. Figures 6.12 and 6.13 illustrate stress-strain response of NSC and HSC, respectively, at various temperatures [66, 67]. At all temperatures both NSC and HSC exhibit a linear response followed by parabolic response until peak stress, and then a quick descending portion prior to failure. In general, it is established that HSC has steeper and more linear stress-strain curves in comparison to NSC at 20–800 °C. The strain corresponding to peak stress starts to increase, especially above 500 °C. HSC specimens exhibit brittle response as indicated by post-peak behavior of stress-strain curves shown in Fig. 6.13 [68]. In the case of fiber-reinforced concrete, especially with steel fibers, the stress-strain response is more ductile.

### 6.5.3 Deformation Properties of Concrete at Elevated Temperatures

Deformation properties that include thermal expansion, creep strain, and transient strain are highly dependent on the chemical composition, the type of aggregate, and the chemical and physical reactions that occur in concrete during heating [69].

#### 6.5.3.1 Thermal Expansion

Figure 6.14 illustrates the variation of thermal expansion in NSC with temperature [32, 36], where shaded portion indicates the range of test data reported by different researchers [52, 70]. In general, concrete generally undergoes expansion when subjected to elevated temperatures. The thermal expansion of concrete increases from zero at room temperature to about 1.3% at 700 °C and then generally remains constant through 1000 °C. This increase is substantial in the 20–700 °C temperature range, and is mainly due to high thermal expansion resulting from constituent aggregates and cement paste in concrete. Thermal expansion of concrete is complicated by other contributing factors such as additional volume changes caused by variation in moisture content, by chemical reactions (dehydration, change of composition), and by creep and micro-cracking resulting from nonuniform thermal stresses [37]. In some cases thermal shrinkage can also result from loss of water



**Fig. 6.14** Variation in linear thermal expansion of normal-strength concrete as a function of temperature [54]

due to heating, along with thermal expansion, and this might lead to overall volume change to be negative, i.e., shrinkage rather than expansion.

Eurocode [32] accounts for the effect of type of aggregate on the variation of thermal expansion of concrete with temperature. Concrete made with siliceous aggregate has higher thermal expansion than carbonate aggregate concrete. However ASCE provisions [36] provide only one variation for both siliceous and carbonate aggregate concrete.

### 6.5.3.2 Creep and Transient Strain

Time-dependent deformations in concrete such as creep and transient strains get highly enhanced at elevated temperatures under compressive stresses [37]. Creep in concrete under high temperatures increases due to moisture movement out of concrete matrix. This phenomenon is further intensified by moisture dispersion and loss of bond in cement gel (C-S-H). Therefore the process of creep is caused and accelerated mainly by two processes: (1) moisture movement and dehydration of concrete due to high temperatures and (2) acceleration in the process of breakage of bond.

Transient strain occurs during the first-time heating of concrete, but it does not occur upon repeated heating [71]. Exposure of concrete to high temperature induces complex changes in the moisture content and chemical composition of the cement paste. Moreover there exists a mismatch in thermal expansion between the cement paste and the aggregate. Therefore factors such as changes in chemical composition of concrete and mismatches in thermal expansion lead to internal stresses and micro-cracking in the concrete constituents (aggregate and cement paste) and result in transient strain in the concrete [69]. It is recognized that transient strain considerably influences the response of concrete structures in fire. Several models have been proposed to incorporate explicitly the transient strain into the concrete constitutive model [29, 69, 72, 73].

## 6.6 Material Properties of Reinforcing and Prestressing Steel at Elevated Temperatures

Due to the poor tensile behavior of concrete, concrete structures are always embedded with steel reinforcement. This reinforcement can be comprised of reinforcing or prestressing steel. Typical steel reinforcement includes those made of carbon steel bars (plain/deformed), deformed steel wire, and prestressing wires, strands, or bars. In some specific applications, stainless steel and galvanized carbon steel are used to provide enhanced corrosion resistance. Steel reinforcement can be produced through hot-rolling and cold-working methods. Some of the commonly used steel

reinforcement types include ASTM A615 Grade 40 and 60, ASTM A706 Grade 60, British BS 4449 and BS 4461, quenched and self-tempered steel, and AISI 316 (stainless steel).

While conventional steel reinforcement is made through hot-rolling process, prestressing steel, on the other hand, is made by cold-working high carbon steel strand, which is then thermomechanically treated and slowly cooled through a solid-state transformation called “eutectoid reaction” to improve relaxation properties required for prestressing application. This forming process impacts its mechanical properties at elevated temperatures, as well as its residual properties after cooling following a fire exposure.

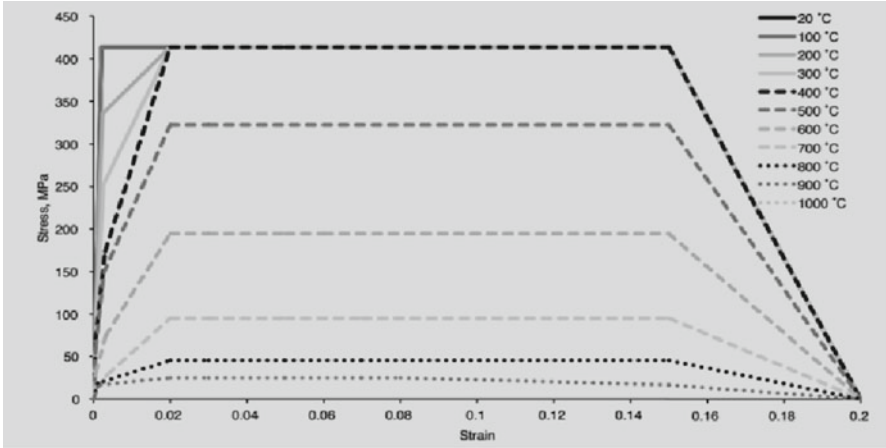
For structural fire engineering applications, the thermal properties of steel reinforcement are often neglected as the thermal mass of reinforcement is very small compared to that of the surrounding concrete. In fact, temperature in steel reinforcement bars or strands is assumed to be same as that of concrete along the same depth and width. The thermal properties of steel reinforcement are specified in Eurocode 2 [11].

Unlike thermal properties of reinforcing and prestressing steel, the mechanical properties of steel reinforcement are needed to enable accurate evaluation of the behavior of concrete structures under fire conditions. These properties comprise stress-strain relations, yield strength, modulus of elasticity, creep, as well as prestress loss in prestressing steel.

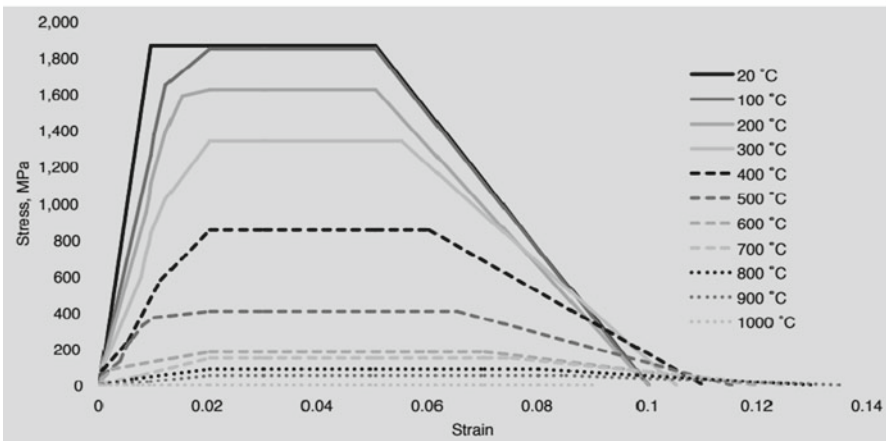
### **6.6.1 Stress-Strain Properties**

Eurocode 2 [11] provides the variation of mechanical properties of carbon steel reinforcement with elevated temperatures. The Eurocode treats hot-rolled reinforcement as hot-rolled structural (carbon) steel, and applies different models for reinforcement made through cold-working process. The temperature-dependent stress-strain relations for reinforcing and prestressing steel in Eurocode 2 idealize the mechanical behavior into a trilinear form, by truncating response at a stress level, typically taken as the yield stress and ignoring any strain-hardening phase. In addition, Eurocode 2 also assumes a continuous increase in ductility with temperature, as reflected by progressing rupture strain in the 20–1200 °C temperature range. Figure 6.15 shows variation in stress-strain of conventional steel reinforcement plotted using the model adopted by Eurocode for establishing the stress-strain relationship of reinforcement steel. It is worth noting that this model was based on the work of Anderberg [75]. In a recent study, Shakya and Kodur proposed relations for developing temperature-dependent stress-strain curves for low-relaxation seven-wire prestressing strand [76].





(a)

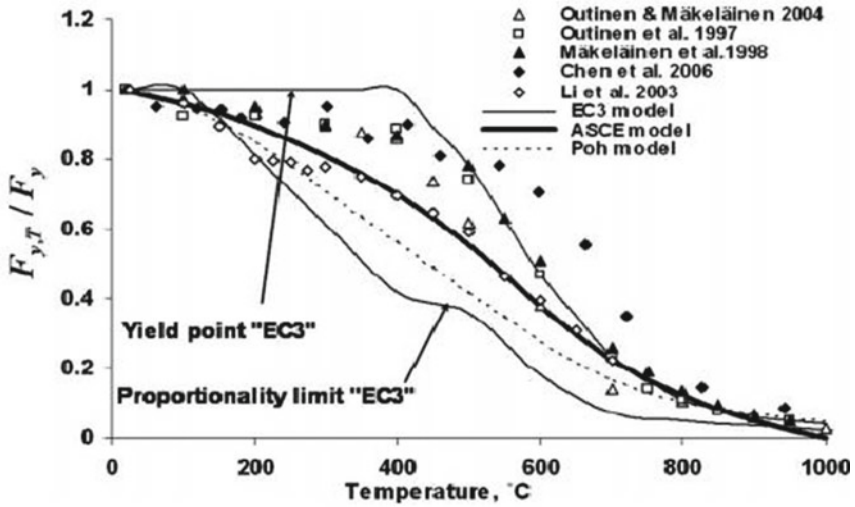


(b)

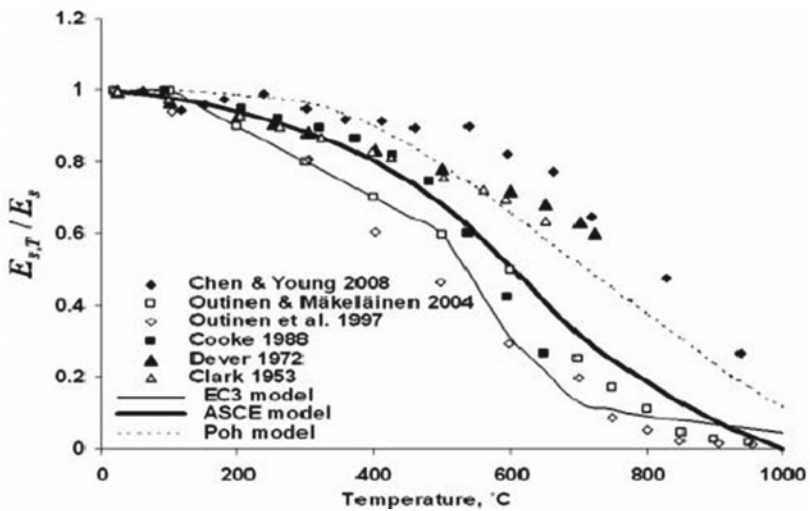
**Fig. 6.15** Stress-strain of reinforcement steel at elevated temperatures adopted by Eurocode 2 [74]. (a) Reinforcing steel with yield strength = 425 MPa. (b) Prestressing steel with yield strength = 1850 MPa

### 6.6.2 Yield Strength and Elastic Modulus

The yield strength and elastic modulus constitutive relationships from the ASCE manual, Eurocode, and those proposed by Poh [77] are also shown in Fig. 6.10. The high-temperature reduction factors for the yield strength and elastic modulus of steel are also presented in the “Mechanical Properties” section of the Appendix for ASCE, EC3, and Poh. Figure 6.16 shows the yield strength and modulus of elasticity of steel



(a)



(b)

**Fig. 6.16** Mechanical properties of steel at various elevated temperatures [78]. (a) Yield strength of steel as predicted by different models and as measured in different tests. (b) Elastic modulus of steel as predicted by different models and as measured in different tests

as a function of temperature, respectively. The test data plotted in this figure are compiled from various high-temperature property tests. Both the yield strength and elastic modulus decrease as temperature increases. This decrease can be attributed to the nucleus of the iron atoms in steel moving farther apart due to rising temperature in steel, leading to decreased bond strength, which in turn reduces the yield strength and elastic modulus.

### 6.6.3 Creep and Prestress Loss

At room temperature and under service load levels, creep deformations of steel are insignificant; however, at elevated temperatures, creep deformations accelerate as a result of thermal energy supplied by fire effects. Generally, creep deformations in steel become noticeable at temperatures above 400 °C. However, it was found experimentally that when the stress level is high, the effect of creep becomes significant in steel members even at temperatures of 300 °C [79]. Few creep tests were carried out in the past years and conducted for steel and metal alloys with variable chemical compositions [80–82], and very little information is available on the effect of high-temperature creep on the structural response.

In prestressing steel, there is a gradual loss of prestress that occurs up to approximately 315 °C, followed by a more drastic decrease above this temperature. Sources in the literature provide models to predict the transient creep relaxation of prestressing tendons at elevated temperature [83–85]. Wei [86] and Gales [87] modified these models to include the tertiary creep stage characterized by increasing strain rate until rupture, resulting in an overall improved prediction of prestress loss due to high-temperature exposure. These models should be carefully evaluated by the designer for appropriate application prior to implementation.

## 6.7 Design of Concrete Members Exposed to Fire

### 6.7.1 Simply Supported Flexural Members

An analytical method for the design of flexural members exposed to fire is presented in the ACI 216.1–14 [88] “Code Requirements for Determining Fire Resistance of Concrete and Masonry Construction Assemblies.” For simply supported members, assuming that the unfactored service-level moment,  $M$ , is constant during the fire-resisting period, the design check is defined as

$$M_{n\theta} \geq M$$

in which  $M_{n\theta}$  is the flexural capacity of simply supported beam or one-way slab under fire conditions. ACI 216.1-14 provides multiple graphs to calculate fire rating

based on aggregate type, steel reinforcing type, concrete cover, and service moment demand-to-capacity ratio in room-temperature condition. Different guidelines are provided for the determination of effective concrete cover for beams and one-way slabs.

## 6.7.2 *Continuous Flexural Members*

Flexural members (beams or slabs) that run continuously over one or multiple supports will allow for moment redistribution during the fire-resisting period. Per ACI 216.1-14, during fire the moment capacity of the slab/beam has to be larger than the maximum redistributed moment values at failure conditions for the continuous member. Figures are provided in ACI 216.1-14, for example to demonstrate the redistributed moment diagrams for uniformly loaded flexural members continuous over one or two supports. Steps for moment capacity calculation are summarized below.

### 6.7.2.1 *Continuous Slabs*

For this case, the positive moment capacity is calculated similar to the capacity of any concrete beam/one-way slab with the exception that reduced concrete compressive strength and steel yield strength values should be used for high-temperature conditions. The standard provides a number of graphs to aid the designer to determine the temperature at critical moment locations for slabs, based on ASTM E119 [89] test results with various durations on slabs with different thicknesses and aggregate types. Once the critical temperature is known, reduced steel and concrete strength values can be determined from available curves. The positive moment capacity can be alternatively calculated as a fraction of room-temperature capacity similar to the procedure discussed for simply supported members.

Negative moment capacity is calculated similar to the positive moment capacity with an additional requirement to keep the negative reinforcement index,  $w_\theta$ , below the limit of 0.3 to avoid compression failing in the negative moment region. The reinforcement index is defined as

$$w_\theta = A_s f_y / f'_c b d$$

where  $A_s$  and  $f_y$  are area and yield stress of steel and  $f'_c$  refers to the maximum compressive strength of the concrete material. Note that  $f_{y\theta}$  and  $f'_{c\theta}$  should be used for fire conditions. Parts of the concrete section with temperatures above 1400 °F shall be neglected.

### 6.7.2.2 Continuous Beams

The procedure explained above for slabs can be used for the design of beams except that a different set of graphs presented in ACI 216.1-14 shall be used for the determination of member's critical temperature. The standard also provides a different definition of effective concrete cover for beams.

### 6.7.3 Two-Way Members (Slabs)

ACI 216.1 does not have any specific prescriptive requirements for the design of two-way slabs against fire, as the tabulated minimum thickness values for different fire resistance rating levels are only dependent on the aggregate type and do not differentiate between one-way and two-way slabs. Further, the standard's section on analytical design methods is only limited to one-way flexural members. However, research has demonstrated that under relatively large deformations, fire resistance of two-way concrete slabs can increase significantly due to tensile membrane action [90, 91]. Tensile membrane effects in slabs can vary based on the duration of fire exposure, edge restraints, and arrangement of slab reinforcement.

The Slab Panel Method (SPM) was introduced by Clifton et al. [92] as a general-purpose design approach to determine if a composite steel-concrete slab is able to withstand the applied mechanical loads in flexure and shear under a specified duration of fire exposure while accounting for two-way action. The details of the method can be found in Hera Report R4-131 (2010). The application of the model involves multiple steps as summarized below:

- Determination of design fire load (severity and exposure time).
- Determination of temperatures of all slab members due to the specified fire loading and the corresponding material mechanical properties at elevated temperatures.
- Calculation of the yield line load-carrying capacity of slab at elevated temperatures while accounting for membrane action.
- Determination of the maximum allowed vertical deflection for the slab.
- Checking of moment/tension membrane and shear capacity adequacy.
- Determination of reinforcement required for preventing passage of fire through cracks.

### 6.7.4 Hollow Core Slabs

Prescriptive requirements of ACI 216.1 for design of hollow core concrete slabs include minimum values for cover protection of reinforcement and slab thickness to achieve fire resistance rating of 1–4 hours. The only difference with the procedure

applied to the solid slabs occurs in the definition of the equivalent thickness for hollow slabs to account for the voids in the system. The equivalent thickness is simply defined as the net cross-sectional area divided by the panel width. The standard notes that the fire resistance of a hollow slab will be the same as that of a solid slab if all the voids are filled with grout or a loose fill material such as perlite, vermiculite, sand or expanded clay, shale, slag, or slate.

### **6.7.5 Reinforced Concrete Columns**

ACI 216.1 divides reinforced concrete columns into two different categories based on their respective design concrete compressive strength,  $f'_c$ , at room temperature:

#### **6.7.5.1 Reinforced Concrete Columns with $f'_c \leq 12,000$ psi**

Least dimension of concrete columns in this category shall conform to the tabulated requirements of ACI 216.1 based on the desired fire resistance rating ranging between 1 and 4 hours. The aforementioned tables are arranged to account for different aggregate types and number of column sides exposed to fire. An additional requirement applies to rectangular columns with fire exposure on 3 or 4 sides to be at least 36 inches long in two parallel sides.

#### **6.7.5.2 Reinforced Concrete Columns with $f'_c > 12,000$ psi**

For this category, the standard requires a minimum dimension of 24 inches for the fire resistance range of 1–4 h. In addition, ties are required to be formed with hooks attached to longitudinal bars and extended for a minimum length of 6 times longitudinal bar diameter into the loop. Hooks for rectangular and circular hoops need to be built with minimum 135° and 90° bends, respectively.

Regardless of concrete aggregate type and compressive strength, minimum cover to main longitudinal bars shall be the lesser of 2 and 1 inch times the number of required hours specified for fire resistance rating.

### **6.7.6 Reinforced Concrete Walls (Incl. Cantilever Walls)**

The requirements in ACI 216.1 for fire design of reinforced concrete walls are based on providing a minimum thickness that will reach a certain temperature insulation level to satisfy the desired fire resistance rating ranging between 1 and 4 h. The standard provides a table in which minimum “equivalent thickness” values are

presented for concrete walls based on the aggregate type and fire rating time. For solid flat walls, the equivalent thickness is defined as the actual wall thickness. Different procedures are presented for hollow core, tapered, and multilayer walls. In addition to thickness requirements, ACI 216.1 contains general provisions for protection of steel reinforcement with concrete cover.

Aside from minimum thickness requirements to satisfy temperature insulation, no analytical methods are directly suggested in ACI 216.1 for the design of reinforced concrete walls subjected to fire. Although sufficient temperature insulation prevents the materials located on the unexposed side of walls from igniting, it does not provide detailed information on the load-bearing capacity of the wall itself at different points of time during fire.

The ACI procedure for fire design of concrete walls follows the conventional prescriptive method and does not provide much guidance to practicing engineers to adopt a performance-based design approach, as recently recognized by ASCE 7-16 [93]. In general, little information is provided in building codes for rational design of reinforced concrete walls for fire conditions, leaving the burden on engineers to utilize advanced analysis techniques to study the complicated behavior of these members during fire. The Eurocode refers to these procedures as “advanced calculation methods” and provides some guidance on the selection of appropriate thermal and structural material models for analysis [11].

### **6.7.7 Prestressed Concrete Members**

ACI 216.1 provides separate tables for prescriptive concrete cover requirements for prestressed members. The analytical methods explained in Sects. 6.7.1 and 6.7.2 for design of simply supported and continuous flexural members for fire conditions per ACI 216.1 are applicable to prestressed concrete members with small changes in the equations as presented in the standard.

### **6.7.8 Joints**

#### **6.7.8.1 Joints between Precast Concrete Wall Panels**

Joints between precast concrete wall panels need to be insulated if the design does not allow openings or requires protected openings. In some cases, a certain percentage of openings is allowed to be unprotected, thereby imposing a limit on the number of uninsulated joints. ACI 216.1 provides graphs to determine the required thickness of ceramic fiber insulation for joints of 3/8" and 1" in width for fire rating ranging between 1 and 4 h. The standard allows for interpolation for any width between 3/8" and 1".

### 6.7.8.2 Joints between Precast Concrete Slabs

ACI 216.1 allows the designer to ignore the joints between precast concrete slabs for calculation of slab equivalent thickness provided that a minimum 1" thick concrete topping layer is used. In the absence of topping layer, the joints are required to be filled with grout to a minimum depth of one-third of slab thickness. For hollow core slabs, the grout depth need not exceed the sum of thicknesses for top and bottom shells. It is also acceptable to use ceramic fiber insulation as explained for precast concrete wall panel joints.

## 6.8 Special Considerations

### 6.8.1 *Tensile and Compressive Membrane Action in Concrete Slabs*

Membrane forces can play a significant role in the behavior of concrete slabs, leading to an improved performance compared to provisions based on bending theory. Two mechanisms are typically distinguished, respectively, tensile and compressive membrane action. Tensile membrane action occurs at large displacements and, in two-way bending members, it does not require any horizontal restraint to develop. Compressive membrane action occurs at small displacements and requires horizontal restraint at the boundaries. Although these mechanisms have long been recognized at ambient temperature, the effects of high temperatures (particularly thermal expansion) make them particularly relevant in structural fire design. These two types of behavior are discussed hereafter in the context of structures in fire.

Tensile membrane action (TMA) refers to a load-bearing mechanism in reinforced concrete or composite steel-concrete slabs where, due to large deflection, radial tension develops in the central part of the slab and is equilibrated by a compressive ring developing in the periphery of the slab. It can develop in thin slabs (i.e., with a low depth/span ratio). This mechanism requires large vertical displacements to develop. For this reason, it is most commonly used for structural fire design or robustness design, but not at ambient temperature where serviceability requirements make it impractical. To develop TMA, a slab needs vertical edge support along all of its four edges, but no horizontal restraint is required owing to the self-equilibrating nature of the mechanism. The absence of necessity of a horizontal restraint is a major advantage that makes tensile membrane action in two-way bending members easier to implement in practice than catenary action in one-way bending members (as the latter requires the ability of the surrounding structure to equilibrate the tensile forces).

The development of tensile membrane action has been extensively studied in the literature, starting with the Cardington tests in the UK and the analyses that ensued (e.g., [94, 95]), followed by a number of additional experimental tests (e.g., [96–99])



and the formulation of design methodologies (e.g., [99], [100], [101]). This mechanism has been utilized in the structural fire design of real buildings such as The Shard in the UK and the JTI building in Switzerland [102]. Although it is most commonly used with steel-concrete composite slabs, TMA works also with conventional reinforced flat slabs.

In terms of structural fire design, consideration of tensile membrane action enables a designer to leave some of the supporting beams unprotected. Indeed, some of the beams required for ambient temperature design can be “lost” in the fire situation where large deflections are acceptable as long as the stability is ensured through the development of TMA in the floor. The designer can therefore divide the floor into rectangular zones (so-called slab panels). Each zone is delimited by peripheral protected beams providing sustained vertical support during the fire. The beams in the interior of each panel can be left unprotected. In case of fire, these interior beams quickly lose strength and stiffness, the deflections increase, and the slab transitions to tensile membrane action to carry the load. The steel reinforcement in the slab must be designed to sustain the tensile forces that build up in the central part. Notably, the amount of steel reinforcement in the direction perpendicular to the spanning direction at ambient temperature might need to be increased since TMA involves two-way bending. The cover must be sufficient to limit the temperature increase in the steel reinforcement. The concrete slab thickness must be designed to sustain the compressive force in the peripheral part. Failure by concrete crushing in the corners has been observed in some tests. Finally, the bending capacity of the boundary beams also needs a specific verification as the loss of the interior beams leads to an additional load on these members. Providing that these provisions are implemented, tensile membrane action has proven to be an efficient, safe, and economic mechanism for structural fire resistance.

Compressive membrane action (CMA) refers to a mechanism in which an arching effect develops within a concrete horizontal member resisting a vertical applied load. It occurs, at small displacement, in members that have (partly) restrained boundary conditions at least at two opposite support lines. As these boundary conditions restrain the member tendency to expand, in-plane compression builds up in the member. This leads to a load-carrying capacity that is enhanced compared to estimates obtained from considering only flexural theory. At ambient temperature, the tendency of a reinforced concrete member to expand results from bending under applied load. In the fire situation, this tendency to expand is significantly amplified by the thermal expansion. The term arching action is normally used to describe the arching phenomenon in one-way spanning slabs and compressive membrane action is normally used to describe the arching phenomenon in two-way spanning slabs. The compressive membrane action has been found to be sensitive to the duration of fire exposure, the location of the restraint on the edges of the slab, the arrangement of reinforcing bars in the slab, and the span-to-thickness ratio of the slab [90, 91].

### **6.8.2 Shear, Punching Shear, and Torsion**

Shear failures due to fire are uncommon in reinforced concrete members. The Eurocode states that, when the design of a heated concrete member is based on minimum dimensions from tabulated data, no further check for shear, torsion, or anchorage is required. But when a shear or torsion verification is required, the usual approach consists of extending the ambient temperature methods using reduced material properties for each part of the section (EN 1992-1-2; [103]). When the simplified reduced cross-section method is applied to determine the ultimate load-bearing capacity of a heated cross section, the Eurocode allows applying the design method for ultimate limit state in shear at ambient temperature directly to the reduced cross section. However, special considerations should be given when no shear reinforcement is provided or the shear capacity relies mainly on the tensile strength of concrete.

Shear may be more critical in prestressed concrete. For instance, in precast pretensioned hollow core and double-tee slabs, a loss of prestress may occur due to bond failure near the ends of slabs, leading to shear failures. Some incidences of shear-related failure of hollow core slabs during tests and building fires have been reported, although further research indicated that hollow core floor systems that are properly designed and detailed (notably, tying together and grouting the hollow core slabs) behave well when subjected to fire [104–106].

Shear punching is a potential failure mode in concrete flat slabs at ambient temperature as well as in the fire situation, which is particularly dangerous because it is brittle and occurs suddenly. In fire, the problem may be amplified by thermal forces, as restrained thermal deflections can increase support reactions. Shear punching was identified as the failure mode in the 2004 car park collapse in Gretzenbach, Switzerland. As a consequence, recent experimental studies have investigated this failure mode in heated slabs, e.g., Annerel et al. [23, 24] and Smith [107]. Currently, design code provisions for shear punching elevated temperature design are simplistic and based on extension of the ambient temperature approach, with a temperature degradation of the parameters. In Eurocode, support conditions are not considered, although in-plane thermal expansion generally brings some degree of restraint in real structure fires. Future modeling efforts based on recent test data should improve the high-temperature design methods by, notably, considering the reinforcement and concrete contributions as well as whole structural behavior.

### **6.8.3 Effect of Cooling Phase**

Failure of concrete structures has been observed after the time of peak gas temperature. This was the case, for instance, in the 2004 Gretzenbach fire that led to the collapse of an underground car park in Switzerland [108]; the cast-in-place concrete

flat slab structure collapsed in punching shear during the cooling phase after a fire of limited severity. Another example is the 2008 full-scale fire test on a composite steel-concrete floor conducted in the Czech Republic [109]. Yet, the effects of natural fires (i.e., fires including a heating phase followed by a cooling phase) on concrete structures have been little investigated. Due to the traditional adoption of prescriptive fire resistance concept, based on standard fires that are indefinitely increasing in temperature, the emphasis during decades has been on the effects of heating alone. Recent research works have aimed at filling this gap of knowledge [30]. In particular, one can mention the experimental research by Gales et al. [87] on the response of continuous and restrained posttensioned concrete slabs exposed to natural fires; the computational studies by Bamonte et al. [103] on prestressed concrete beams; the works by Kodur and Agrawal [110] to identify the critical factors governing the residual response of reinforced concrete beams after fire exposure; and the numerical analyses by Gernay and Franssen [111] to highlight the possibility of structural collapse during and after the cooling phase and propose a new performance indicator for structures under natural fires. All these studies point to the possibility of delayed failures for reinforced or prestressed concrete members under fires with heating and cooling phases. Therefore, limiting the attention to the effects of the heating phase is not sufficient.

Causes for delayed failure include the fact that maximum temperatures in the section (and in the steel reinforcement) can be reached long after the onset of cooling, the fact that concrete experiences additional compressive strength loss during cooling compared with the strength at maximum reached temperature (EN 1994-1-2) [28], and the fact that significant load redistributions may occur due to the interaction between structural members under restrained thermal strains. In relation to the latter, it must be stressed that transient creep strain is physically not recovered during cooling and/or unloading of concrete. Transient creep strain plays a considerable role in the response of concrete members under heating-cooling and assuming it wrongly as recoverable (for instance, through an implicit model) can lead to erroneous estimations of the structural behavior particularly in cooling [29, 112, 113]. Factors influencing the structural behavior under natural fire include, notably, the fire duration, cooling rate, and load level. Construction details such as proper anchorage and grouting of hollow core slabs or other precast concrete elements are also of importance to ensure a robust response during cooling [104]. Depending on these factors, the structural behavior after the time of peak gas temperature can vary from an almost complete recovery of the initial configuration to runaway failure [27, 103].

#### **6.8.4 Residual Load-Bearing Capacity and Resilience**

For most fires occurring in buildings with a concrete structural system, the structural elements do not collapse during fire exposure, and further use of the building after fire may be possible. However, the fire event will generally have resulted in some

damage and, possibly, a permanent loss of strength of the structure. A postfire evaluation is required for assessing the residual load-bearing capacity to inform decisions on continued use and need for structural repairs. Enabling an accurate and fast postfire evaluation is a critical aspect to improve the *resilience* of the built environment to fire hazard, as the objective is to maintain functionality and ensure fast recovery for buildings and other infrastructure in the wake of a disaster, notably through efficient decision-making. Such postfire evaluation is a complex task due to, amongst other factors, the complex thermal-mechanical behavior of concrete structures and the many uncertainties associated with the fire exposure, the characteristics of the structural elements, and the material and structural response to high temperatures. Reliability-based methodologies have recently been proposed that account for the effects of heating and cooling and quantify the residual safety of the concrete elements after a fire [114, 115].

## References

1. Beitel, J., Iwankiw, N. (2008). Analysis of needs and existing capabilities for full-scale fire resistance testing. US Department of Commerce, National Institute of Standards and Technology.
2. Khoury, G. A. (2000). Effect of fire on concrete and concrete structures. *Progress in Structural Engineering and Materials*, 2(4), 429–447.
3. Phan, L., & Carino, N. (1998). Review of mechanical properties of HSC at elevated temperature. *Journal of Materials in Civil Engineering (ASCE)*, 10:1(58), 58–65.
4. Dwaikat, M. B., & Kodur, V. K. R. (2010). Fire induced spalling in high strength concrete beams. *Fire Technology*, 46(1), 251–274.
5. Kodur, V. K. R. (2000). Spalling in high strength concrete exposed to fire: Concerns, causes, critical parameters and cures. *Advanced Technology in Structural Engineering*, 1–9.
6. Gernay, T. (2016). Fire performance of columns made of Normal and high strength concrete: A comparative analysis. *Key Engineering Materials*, 711, 564–571. Trans Tech Publications.
7. Go, C. G., Tang, J. R., Chi, J. H., Chen, C. T., & Huang, Y. L. (2012). Fire-resistance property of reinforced lightweight aggregate concrete wall. *Construction and Building Materials*, 30, 725–733.
8. Chandra, S., & Berntsson, L. (2002). *Lightweight aggregate concrete*. Elsevier.
9. Topçu, İ. B., & Uygunoğlu, T. (2007). Properties of autoclaved lightweight aggregate concrete. *Building and Environment*, 42(12), 4108–4116.
10. Mun, K. J. (2007). Development and tests of lightweight aggregate using sewage sludge for nonstructural concrete. *Construction and Building Materials*, 21, 1583–1588.
11. Eurocode (2004). “EN, 1992-1-2: design of concrete structures. Part 1–2: general rules—structural fire design,” Eurocode 2, European Committee for Standardization, Brussels, Belgium.
12. Altun, F., Haktanir, T., & Ari, K. (2007). Effects of steel fiber addition on mechanical properties of concrete and RC beams. *Construction and Building Materials*, 21(3), 654–661.
13. Lau, & Anson, M. (2006). Effect of high temperatures on high performance steel fibre reinforced concrete. *Cement and Concrete Research*, 36(9), 1698–1707.
14. Lie, T. T. and Kodur, V. R. (1995). “Thermal properties of fibre-reinforced concrete at elevated temperatures,” IR 683, IRC, National Research Council of Canada, Ottawa, Canada.

15. Kalifa, P., Chene, G., & Galle, C. (2001). High-temperature behaviour of HPC with polypropylene fibres: From spalling to microstructure. *Cement and Concrete Research*, *31*(10), 1487–1499.
16. Bangi, M. R., & Horiguchi, T. (2012). Effect of fibre type and geometry on maximum pore pressures in fibre-reinforced high strength concrete at elevated temperatures. *Cement and Concrete Research*, *42*(2), 459–466.
17. Zeiml, M., Leithner, D., Lackner, R., & Mang, H. A. (2006). How do polypropylene fibers improve the spalling behavior of in-situ concrete? *Cement and Concrete Research*, *36*(5), 929–942.
18. Anderberg, Y., & Thelandersson, S. (1976). *Stress and Deformation Characteristics of Concrete at High Temperatures. 2. Experimental Investigation and Material Behaviour Model. (Bulletin of Division of Structural Mechanics and Concrete Construction, Bulletin 54; Vol. Bulletin 54)*. Lund Institute of Technology.
19. Andersen, N. E., & Lauridsen, D. H. (1999). *Hollow core concrete slabs*. Danish Institute of Fire Technology.
20. Andersen, N.E., Lauridsen, D.H. (1999). TT-roof slabs. Hollow core concrete slabs. Technical report X52650, parts 1 and 2. Danish institute of fire technology, Hvidovre.
21. Pedron, A., & Tondini, N. (2021). Fire behaviour of a prestressed thin-walled concrete V-beam. *Fire Technology*. <https://doi.org/10.1007/s10694-021-01149-3>
22. Majorana, C. E., Salomoni, V. A., Mazzucco, G., & Khoury, G. A. (2010). An approach for modelling concrete spalling in finite strains. *Mathematics and Computers in Simulation*, *80*, 1694–1712.
23. Annerel, E., Taerwe, L., Merci, B., Jansen, D., Bamonte, P., & Felicetti, R. (2013a). Thermo-mechanical analysis of an underground car park structure exposed to fire. *Fire Safety Journal*, *57*, 96–106.
24. Annerel, E., Lu, L., & Taerwe, L. (2013b). Punching shear tests on flat concrete slabs exposed to fire. *Fire Safety Journal*, *57*, 83–95.
25. Overbeek, A., Gijsbers, F. (2008). Study of the structural behavior during fire of hollow core slabs as used in the Lloyd Street in Rotterdam, TNO-Report no. 2007-D-R1236/C, (in Dutch).
26. Burnier, O. (2011). Reconstitution de l'incendie de deux voitures dans le parking de la Tour d'Ivoire à Montreux, le 9 décembre 2010, Travail de diplôme, heig-vd ed., Yverdon-les-Bains.
27. Gernay, T., & Dimia, M. S. (2013). Structural behaviour of concrete columns under natural fires. *Engineering Computations*, *30*(6), 854–872.
28. Yi-Hai, L., & Franssen, J. M. (2011). Test results and model for the residual compressive strength of concrete after a fire. *Journal of Structural Fire Engineering*, *2*(1), 29–44.
29. Gernay, T., & Franssen, J. M. (2012). A formulation of the Eurocode 2 concrete model at elevated temperature that includes an explicit term for transient creep. *Fire Safety Journal*, *51*, 1–9.
30. Gernay, T. (2019). Fire resistance and burnout resistance of reinforced concrete columns. *Fire Safety Journal*, *104*, 67–78.
31. Kodur, V. R., & Harmathy, T. Z. (2008). Properties of building materials. In P. J. DiNenno (Ed.), *SFPE handbook of fire protection engineering*. National Fire Protection Association.
32. Eurocode 2 (2004) “EN, 1992-1-2: design of concrete structures. Part 1–2: general rules—structural fire design,” Eurocode 2, European Committee for Standardization, Brussels, Belgium.
33. ASTM E1530 (2011) “Standard test method for evaluating the resistance to thermal transmission of materials by the guarded heat flow meter technique,” ASTM E1530, ASTM International, West Conshohocken, PA, USA.
34. Adl-Zarrabi, B., Bostrom, L., & Wickstrom, U. (2006). Using the TPS method for determining the thermal properties of concrete and wood at elevated temperature. *Fire and Materials*, *30*(5), 359–369.

35. Shin, K.-Y., Kim, S.-B., Kim, J.-H., Chung, M., & Jung, P.-S. (2002). Thermo-physical properties and transient heat transfer of concrete at elevated temperatures. *Nuclear Engineering and Design*, 212(1–3), 233–241.
36. ASCE (1992). Structural Fire Protection, ASCE Committee on Fire Protection, Structural Division, American Society of Civil Engineers, New York, NY, USA.
37. Bažant, Z. P., & Kaplan, M. F. (1996). *Concrete at high temperatures: Material properties and mathematical models*. Longman Group Limited.
38. Harmathy, T. Z., & Allen, L. W. (1973). Thermal properties of selected masonry unit concretes. *Journal American Concrete Institution*, 70(2), 132–142.
39. Kodur, V. R., & Sultan, M. A. (1998). Thermal properties of high strength concrete at elevated temperatures. *American Concrete Institute, Special Publication, SP-179*, 467–480.
40. Phan, L. T. (1996). “Fire performance of high-strength concrete: a report of the state-of-the-art,” Tech. Rep., National Institute of Standards and Technology, Gaithersburg, MD, USA.
41. ASTM C1269 (2011) “Standard test method for determining specific heat capacity by differential scanning calorimetry,” ASTM C1269, ASTM International, West Conshohocken, PA, USA.
42. Harmathy, T. Z. (1970). Thermal properties of concrete at elevated temperatures. *ASTM Journal of Materials*, 5(1), 47–74.
43. Mehta, P. K., & Monteiro, P. J. M. (2006). *Concrete: Microstructure, properties, and materials*. McGraw-Hill.
44. Mindess, S., Young, J. F., & Darwin, D. (2003). *Concrete*. Pearson Education.
45. Khaliq, W., & Kodur, V. (2012). *An approach to model the effect of tie configuration on fire performance of concrete columns*. ACI Spring Convention.
46. Neville, M. (2004). *Properties of concrete*. Pearson Education.
47. Shah, S. P. (1991). Do fibers increase the tensile strength of cement based matrixes? *ACI Materials Journal*, 88(6), 595–602.
48. Bazant, Z. P., & Chern, J.-C. (1987). Stress-induced thermal and shrinkage strains in concrete. *Journal of Engineering Mechanics*, 113(10), 1493–1511.
49. Harmathy, T. Z. (1967). A comprehensive creep model. *Journal of Basic Engineering*, 89(3), 496–502.
50. Purkiss, J. A. (2007). *Fire safety engineering design of structures*. Butterworth-Heinemann.
51. Khaliq, W. (2012). Performance characterization of high performance concretes under fire conditions [Ph.D. thesis], Michigan State University.
52. Kodur, V. K. R., Dwaikat, M. M. S., & Dwaikat, M. B. (2008). High temperature properties of concrete for fire resistance modeling of structures. *ACI Materials Journal*, 105(5), 517–527.
53. Flynn, D. R. (1999). “Response of high performance concrete to fire conditions: review of thermal property data and measurement techniques,” Tech. Rep., National Institute of Standards and Technology, Millwood, VA, USA.
54. Kodur, V. (2014). Properties of concrete at elevated temperatures. *ISRN Civil Engineering*, 2014, 1–15.
55. Kodur, V., & Khaliq, W. (2011). Effect of temperature on thermal properties of different types of high-strength concrete. *Journal of Materials in Civil Engineering, ASCE*, 23(6), 793–801.
56. RILEM TC 129-MHT. (1995). Test methods for mechanical properties of concrete at high temperatures—Compressive strength for service and accident conditions. *Materials and Structures*, 28(3), 410–414.
57. RILEM Technical Committee 200-HTC Ulrich. (2007). Recommendation of RILEM TC 200-HTC: mechanical concrete properties at high temperatures—modelling and applications: Part 2: Stress–strain relation. *Materials and Structures*, 40, 855–864.
58. Peng, G., & Anson, M. (1999). Fire behavior of high-performance concrete made with silica fume at various moisture contents. *Materials Journal*, 96(3), 405–409.
59. Behnood, A., & Ghandehari, M. (2009). Comparison of compressive and splitting tensile strength of high-strength concrete with and without polypropylene fibers heated to high temperatures. *Fire Safety Journal*, 44(8), 1015–1022.

60. Carette, G. G., Painter, K. E., & Malhotra, V. M. (1982). Sustained high temperature effect on concretes made with normal Portland cement, normal Portland cement and slag, or normal Portland cement and fly ash. *Concrete International*, 4(7), 41–51.
61. Felicetti, R., Gambarova, P. G., Rosati, G. P., Corsi, F., and Giannuzzi, G. (1996). “Residual mechanical properties of high strength concretes subjected to high-temperature cycles,” in Proceedings of the International Symposium of Utilization of High-Strength/High-Performance Concrete, pp. 579–588, Paris, France.
62. Purkiss, J. A. (1984). Steel fibre reinforced concrete at elevated temperatures. *International Journal of Cement Composites and Lightweight Concrete*, 6(3), 179–184.
63. Rossi, P. (1994). Steel fiber reinforced concretes (SFRC): An example of French research. *ACI Materials Journal*, 91(3), 273–279.
64. Kodur, V. R. (1999). Fibre-reinforced concrete for enhancing structural fire resistance of columns. *Fibre-Structural Applications of Fibre-Reinforced Concrete*, ACI, SP-182, 215–234.
65. Cruz, C. R. (1966). Elastic properties of concrete at high temperatures. *Journal of the PCA Research and Development Laboratories*, 8, 37–45.
66. Castillo, C., & Durrani, A. J. (1990). Effect of transient high temperature on high-strength concrete. *ACI Materials Journal*, 87(1), 47–53.
67. Kodur, V. K. R., Wang, T. C., & Cheng, F. P. (2004). Predicting the fire resistance behaviour of high strength concrete columns. *Cement and Concrete Composites*, 26(2), 141–153.
68. Chen, B., & Liu, J. (2004). Residual strength of hybrid-fiber-reinforced high-strength concrete after exposure to high temperatures. *Cement and Concrete Research*, 34(6), 1065–1069.
69. Schneider, U. (1988). Concrete at high temperatures—A general review. *Fire Safety Journal*, 13(1), 55–68.
70. Raut, N. (2011). Response of high strength concrete columns under fire induced biaxial bending [Ph.D. thesis], Michigan State University, East Lansing, Mich, USA.
71. Khoury, G. A., Grainger, B. N., & Sullivan, P. J. E. (1985). Strain of concrete during fire heating to 600°C. *Magazine of Concrete Research*, 37(133), 195–215.
72. Torelli, G., Gillie, M., Mandal, P., & Tran, V. X. (2017). A multiaxial load-induced thermal strain constitutive model for concrete. *International Journal of Solids and Structures*, 108, 115–125.
73. Terro, M. (1998). Numerical modeling of the behavior of concrete structures in fire. *ACI Structural Journal*, 95(2), 183–193.
74. Shakya, A. M. (2016). Flexural and shear response of precast prestressed concrete hollowcore slabs under fire conditions. PhD dissertation. Michigan State University
75. Anderberg, Y. (1988). Modelling steel behaviour. *Fire Safety Journal*, 13.
76. Shakya, A. M., & Kodur, V. K. R. (2016). Effect of temperature on the mechanical properties of low relaxation seven-wire prestressing strand. *Construction and Building Materials*, 124, 74–84.
77. Poh, K. W. (2001). Stress-strain-temperature relationship for structural steel. *Journal of Materials in Civil Engineering*, 135, 371–379.
78. Dwaikat, M. B. (2009). Flexural response of reinforced concrete beams ex-posed to fire. PhD dissertation. Michigan State University
79. Huang, Z.-F., Tan, K.-H., & Ting, S.-K. (2006). Heating rate and boundary restraint effects on fire resistance of steel columns with creep. *Engineering Structures*, 28, 805–817.
80. Kirby, B., & Preston, R. (1988). High temperature properties of hot-rolled, structural steels for use in fire engineering design studies. *Fire Safety Journal*, 13, 1.
81. Harmathy, T., Stanzak, W. (1970). Elevated-Temperature Tensile and Creep Properties of Some Structural and Prestressing Steels, In Fire Test Performance, ASTM STP 464, American Society for Testing and Materials.
82. Kodur, V. K., & Aziz, E. M. (2015). Effect of temperature on creep in ASTM A572 high-strength low-alloy steels. *Materials and Structures*, 48(6), 1669–1677.

83. MacLean, K. (2007). Post-fire assessment of unbonded post-tensioned concrete slabs: Strand Deterioration and Prestress Loss, Master's Thesis, Queen's University, Kingston, Ontario, Canada.
84. MacLean, K., Bisby L., MacDougall, C. (2008). Post-fire assessment of unbonded post-tensioned slabs: Strand deterioration and prestress loss, ACI-SP 255: Designing Concrete Structures for Fire Safety, American Concrete Institute.
85. Abrams, M. S., and Cruz, C. R.. (1961). The Behavior at High Temperature of Steel Strand for Prestressed Concrete. No. 134.
86. Wei, Y., Zhang, L., Au, F., Li, J., & Tsang, N. (2016). Thermal creep and relaxation of prestressing steel. *Construction and Building Materials*, 128.
87. Gales, J., Robertson, L., & Bisby, L. (2016). Creep of prestressing steels in fire. *Fire and Materials*, 40.
88. ACI (2014). "Code Requirements for Determining Fire Resistance of Concrete and Masonry Construction Assemblies" ACI 216.1–14, American Concrete Institute, Detroit, MI, USA.
89. ASTM. (2018). "Standard test methods for fire tests of building construction and materials" *ASTM E119-18a*. ASTM International.
90. Moss, P. J., Dhakal, R. P., Wang, G., & Buchanan, A. H. (2008a). The fire behaviour of multi-bay, two-way reinforced concrete slabs. *Engineering Structures*, 30(12), 3566–3573.
91. Moss, P. J., Dhakal, R. P., Wang, G., & Buchanan, A. H. (2008b). The fire behaviour of multi-bay, two-way reinforced concrete slabs. *Journal of Engineering Structures*, 30, 12.
92. Clifton, G. C., Gillies, A., Mago, N. (2010). "The slab panel method: Design of composite floor systems for dependable inelastic response to severe fires" Proceedings of the 6<sup>th</sup> International Conference of Structures in Fire (SiF), East Lansing, MI, USA.
93. ASCE. (2016). *ASCE/SEI 7 minimum design loads for buildings and other structures*. American Society of Civil Engineers.
94. Bailey, C. G. (2004). Membrane action of slab/beam composite floor systems in fire. *Engineering Structures*, 26, 1691–1703.
95. Wang, Y. C. (2000). An analysis of the global structural behaviour of the Cardington steel-framed building during the two BRE fire tests. *Engineering Structures*, 22(5), 401–412.
96. Lim, L., Buchanan, A., Moss, P., & Franssen, J. M. (2004). Numerical modelling of two-way reinforced concrete slabs in fire. *Engineering Structures*, 26(8), 1081–1091.
97. Vassart, O., Bailey, C. G., Hawes, M., Nadjai, A., Sims, W. I., Zhao, B., Gernay, T., & Franssen, J. M. (2012). Large-scale fire test of unprotected cellular beam acting in membrane action. *Proceedings of the Institution of Civil Engineers: Structures and Buildings*, 165(7), 327–334.
98. Zhao, B., & Rosefid, M. (2011). Experimental and numerical investigations of steel and concrete composite floors subjected to ISO fire condition. *Journal of Structural Fire Engineering*, 2(4), 301–310.
99. Bailey, C. G., & Toh, W. S. (2007). Behaviour of concrete floor slabs at ambient and elevated temperatures. *Fire Safety Journal*, 42(6–7), 425–436.
100. Vassart, O., Zhao, B. (2012). MACS+ for membrane action of composite structures in case of fire. Design guide.
101. Clifton, G. C. (2006). "Design of composite steel floor systems for severe fires", HERA Report R4-131, New Zealand HERA: Manukau City, Auckland, New Zealand.
102. Lelli, L., & Loutan, J. (2018). Advanced analyses of the membrane action of composite slabs under natural fire scenarios: A case study of the JTI headquarters. *Journal of Structural Fire Engineering*, 9(1), 77–90.
103. Bamonte, P., Gambarova, P. G., Kalaba, N., & Tattoni, S. (2018). Some considerations on shear and torsion in R/C structural members in fire. *Journal of Structural Fire Engineering*, 9(2), 94–107.
104. Bisby, L., Mostafaei, H., Pimienta, P. (2014). *White Paper on Fire Resistance of Concrete Structures*. US Department of Commerce, National Institute of Standards and Technology.



105. de Feijter, M. P., & Breunese, M. P. (2007). *2007-Efectis-R0894(E)—Investigation of fire in the Lloydstraat Car Park, Rotterdam*. Efectis.
106. Bailey, C. G., & Lennon, T. (2008). Full scale fire tests on hollow core slabs. *The Structural Engineer*, *86*(6), 33–39.
107. Smith, H. (2016). Punching shear of flat reinforced-concrete slabs under fire conditions. The University of Edinburgh, PhD thesis.
108. Muttoni, A., Furst, A. A., Hunkeler, F. (2005). Deckeneinsturz der Tiefgarage am Staldenacker in Gretzenbach, Solothurn, Switzerland, November, Medieninformation vom 15.11.2005.
109. Kallerova, P., & Wald, F. (2009). *Fire test on experimental building in Mokrsko*. CTU.
110. Kodur, V. K. R., & Agrawal, A. (2016). An approach for evaluating residual capacity of reinforced concrete beams exposed to fire. *Engineering Structures*, *110*, 293–306.
111. Gernay, T., & Franssen, J. M. (2015). A performance indicator for structures under natural fire. *Engineering Structures*, *100*, 94–103.
112. Gernay, T. (2012). Effect of transient creep strain model on the behavior of concrete columns subjected to heating and cooling. *Fire Technology*, *48*(2), 313–329.
113. Law, A. Gillie, M. (2008) Load induced thermal strain: implications for structural behavior, in: Proceedings of the Fifth International Conference—Structures in Fire, SIF, Singapore, pp. 488–496.
114. Molkens, T., Van Coile, R., & Gernay, T. (2017). Assessment of damage and residual load bearing capacity of a concrete slab after fire: Applied reliability-based methodology. *Engineering Structures*, *150*, 969–985.
115. Van Coile, R., Caspeele, R., & Taerwe, L. (2014). Towards a reliability-based post-fire assessment method for concrete slabs incorporating data from inspection. *Structural Concrete*, *15*(3), 395–407.

# Chapter 7

## Steel and Composite Structures



Anthony Abu, Ruoxi Shi, Mostafa Jafarian, Kevin LaMalva,  
and Danny Hopkin

### 7.1 Mechanical Properties

The heating of steel products (structural steel, steel bolts, steel reinforcement, steel shear studs and steel welds) under fire exposure changes their mechanical properties which is not contemplated in conventional structural engineering design. Although the Poisson's ratio of steel may be considered temperature independent, other mechanical properties such as yield strength and elastic modulus are highly temperature dependent as described herein.

#### 7.1.1 Structural Steel

For structural limit state design (see Sect. 7.5.1 below), Eurocode 3 [1] and similarly AISC 360 Appendix 4 [2] provide temperature-dependent nominal strength

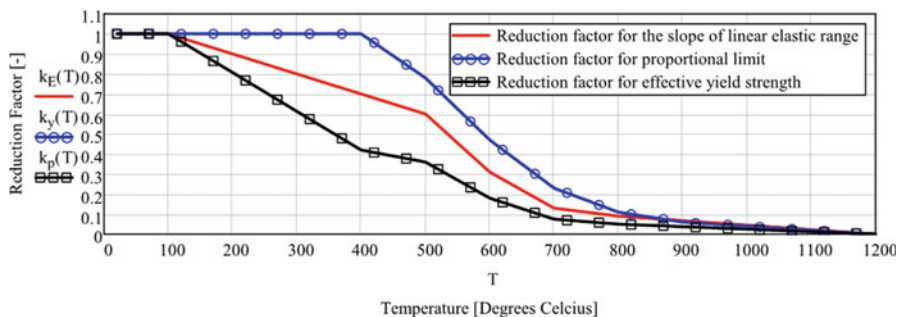
---

A. Abu  
Civil & Natural Resources Engineering Department, University of Canterbury, Christchurch,  
New Zealand  
e-mail: [anthony.abu@canterbury.ac.nz](mailto:anthony.abu@canterbury.ac.nz)

R. Shi · D. Hopkin (✉)  
OFR Consultants, Manchester, UK  
e-mail: [ruoxi.shi@ofrconsultants.com](mailto:ruoxi.shi@ofrconsultants.com); [danny.hopkin@ofrconsultants.com](mailto:danny.hopkin@ofrconsultants.com)

M. Jafarian  
Warringtonfire, Warrington, UK  
e-mail: [Mostafa.Jafarian@warringtonfire.com](mailto:Mostafa.Jafarian@warringtonfire.com)

K. LaMalva  
Warringtonfire, Boston, MA, USA  
e-mail: [kevin.lamalva@warringtonfire.com](mailto:kevin.lamalva@warringtonfire.com)



**Fig. 7.1** Strength parameters for hot-rolled structural steel vs. temperature

parameters for structural steel, which are compatible with conventional strength reduction factors contained in these references. Granted, AISC 360 Appendix 4 should not be relied upon exclusively for structural fire engineering designs since it lacks critical overarching and material-neutral requirements. Notably, structural analysis scope and other baseline requirements are left undefined/open-ended. In such cases, ASCE/SEI 7-16 Appendix E requirements would govern as described in Chap. 2 [3].

Figure 7.1 plots the reduction of yield strength, proportional limit and elastic modulus as a function of temperature for structural steel based on the above-identified references.

For simulation of structural system response (see Sect. 7.5.2 below), Eurocode 3 equations may be used to represent the temperature-dependent uniaxial stress-strain curves of structural steel as shown in Table 7.1 and plotted in Fig. 7.2 for a representative grade of steel.

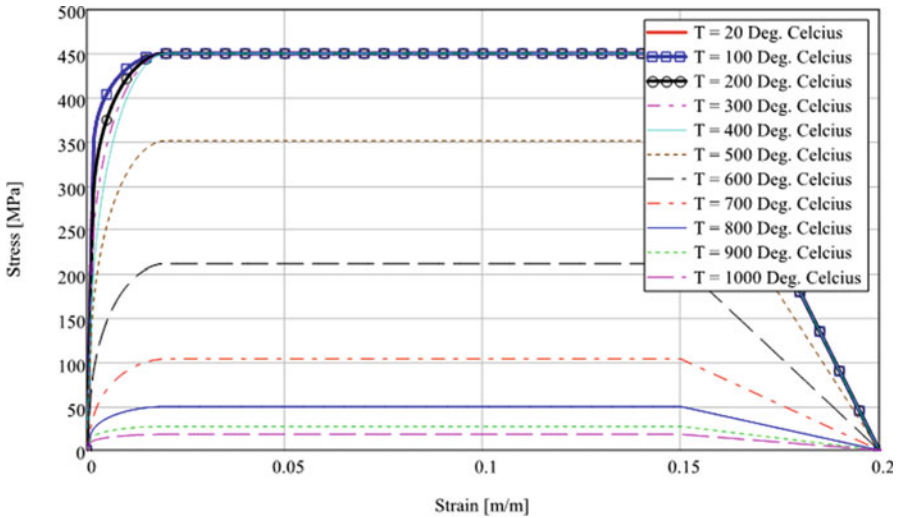
It should be noted that the Eurocode 3 model implicitly accounts for thermal creep and is permitted for steel heating rates of 2 °C/min and faster. Slower heating rates are not usually anticipated for structural fire engineering applications. However, there may be cases in which the explicit representation of structural steel thermal creep is necessary.

Thermal creep of structural steel is highly affected by the type of steel, applied stress, temperature and duration of loading. There are two types of creep models: explicit and implicit. As mentioned, Table 7.1 is an implicit representation, which consists of creep strains being incorporated within the stress-strain definition of the material. Implicit inclusion of creep into stress-strain curves results in a change in the stress-strain curve for structural steel at temperatures greater than 400 °C.

Explicit creep models of structural steel are calculation intensive and consist of the inclusion of creep strains into the strain profile of the member section. Typically, this is implemented by calculating a strain profile at the instance when the internal forces in the cross section are at equilibrium with the applied forces. The time-hardening power law, which modifies the nominal Eurocode 3 stress-strain model (Table 7.1) as a function of uniaxial equivalent deviatoric stress, time and temperature, may be used to explicitly represent the thermal creep of structural steel. Eq. 1 specifies the power law function and temperature-dependent inputs:

**Table 7.1** Structural steel temperature-dependent stress-strain model

Strain range	Stress $\sigma$	Tangent modulus
$\epsilon \leq \epsilon_{p,T}$	$\epsilon E_T$	$E_T$
$\epsilon_{p,T} < \epsilon < \epsilon_{y,T}$	$F_{p,T} - c + (b/a)\sqrt{a^2 - (\epsilon_{y,T} - \epsilon)^2}$	$\frac{b(\epsilon_{y,T} - \epsilon)}{a\sqrt{a^2 - (\epsilon_{y,T} - \epsilon)^2}}$
$\epsilon_{y,T} \leq \epsilon \leq \epsilon_{i,T}$	$F_{y,T}$	0
$\epsilon_{i,T} < \epsilon < \epsilon_{u,T}$	$F_{y,T} \left[ 1 - \frac{(\epsilon - \epsilon_{i,T})}{(\epsilon_{u,T} - \epsilon_{i,T})} \right]$	-
$\epsilon = \epsilon_{u,T}$	0	-
Parameters	$\epsilon_{p,T} = \frac{F_{p,T}}{E_T}; \epsilon_{y,T} = 0.02; \epsilon_{i,T} = 0.15; \epsilon_{u,T} = 0.02$	
Functions	$a^2 = (\epsilon_{y,T} - \epsilon_{p,T})(\epsilon_{y,T} - \epsilon_{p,T} + c/E_T)$ $b^2 = c(\epsilon_{y,T} - \epsilon_{p,T})E_T + c^2$ $c = \frac{(F_{y,T} - F_{p,T})^2}{(\epsilon_{y,T} - \epsilon_{p,T})E_T - 2(F_{y,T} - F_{p,T})}$	
Definitions of terms	$E_T$ : elastic modulus at temperature $T$ $F_{y,T}$ : effective yield strength at temperature $T$ $F_{p,T}$ : proportional limit at temperature $T$ $\epsilon_{y,T}$ : strain at yield at temperature $T$ $\epsilon_{p,T}$ : strain at proportional limit at temperature $T$ $\epsilon_{i,T}$ : limit strain for yield strength at temperature $T$ $\epsilon_{u,T}$ : ultimate strain at temperature $T$	



**Fig. 7.2** Stress vs. strain vs. temperature for ASTM A992 Steel

$$\epsilon_{cr} = At^B \sigma^C \quad (1)$$

$$A = \frac{1}{100} \begin{cases} 10^{-(6.10+0.00573T)} & \text{for } T < 500^\circ \text{C} \\ 10^{-(13.25-0.00851T)} & \text{for } T > 500^\circ \text{C} \end{cases}$$

$$B = -1.1 + 0.0035T$$

$$C = 2.1 + 0.0064T$$

$t$ : time

$q$ : uniaxial equivalent deviatoric stress

$A$ ,  $B$  and  $C$ : temperature-dependent constants

### 7.1.2 Steel Reinforcement

For structural limit state design (see Sect. 7.5.1 below), temperature-dependent retention factors for composite floors in flexure in conjunction with equations in AISC 360 Chap. I account for steel reinforcement. Otherwise, AISC 360 Appendix 4 (and similarly Eurocode 3) temperature-dependent nominal strength parameters for structural steel may be used for the analysis of steel reinforcement. However, AISC 360 Appendix 4 should not be relied upon exclusively as described in Sect. 7.1.1 above.

For simulation of structural system response (see Sect. 7.5.2 below), Eurocode 2 equations for Class N carbon steel reinforcement (Class N broadly covers Class A, B, C steel reinforcement types) should be used to represent the temperature-dependent uniaxial stress-strain behaviour of steel reinforcement as shown in Table 7.2.

Explicit representation of thermal creep of steel reinforcement is usually not required for structural fire engineering applications. Previous research has shown that thermal creep is not very critical in reinforcing bars, since the bars typically would not reach a temperature at which creep is significant and because constant long-term loading conditions are not a typical loading scenario for reinforcing bars [4]. However, the Harmathy creep model may be used to explicitly represent the thermal creep of steel reinforcement if necessary [5].

### 7.1.3 Steel Shear Studs

For structural limit state design (see Sect. 7.5.1 below), temperature-dependent retention factors for composite floors in flexure in conjunction with equations in AISC 360 Chap. I account for steel shear studs. Granted, AISC 360 Appendix 4 should not be relied upon exclusively as described in Sect. 7.1.1 above.

**Table 7.2** Steel reinforcement temperature-dependent stress-strain model

Range	Stress $\sigma(\theta)$		Tangent modulus			
$\epsilon_{0p, \theta}$	$\epsilon E_{s, \theta}$		$E_{s, \theta}$			
$\epsilon_{sp, \theta} \leq \epsilon \leq \epsilon_{sy, \theta}$	$f_{sp, \theta} - c + (b/a)[a^2 - (\epsilon_{sy, \theta} - \epsilon)^2]^{0.5}$		$\frac{b(\epsilon_{sy, \theta} - \epsilon)}{a[a^2 - (\epsilon - \epsilon_{sp, \theta})^2]^{0.5}}$			
$\epsilon_{0y, \theta} \leq \epsilon \leq \epsilon_{st, \theta}$	$f_{sy, \theta}$		0			
$\epsilon_{st, \theta} \leq \epsilon \leq \epsilon_{su, \theta}$	$f_{sy, \theta} [1 - (\epsilon - \epsilon_{st, \theta}) / (\epsilon_{su, \theta} - \epsilon_{st, \theta})]$		-			
$\epsilon = \epsilon_{su, \theta}$	0.00		-			
Parameters*	$\epsilon_{sp, \theta} = f_{sp, \theta} / E_{s, \theta} \epsilon_{sy, \theta} = 0.02 \epsilon_{st, \theta} = 0.15 \epsilon_{su, \theta} = 0.20$ Class A reinforcement : $\epsilon_{st, \theta} = 0.05 \epsilon_{su, \theta} = 0.10$					
Functions	$a^2 = (\epsilon_{sy, \theta} - \epsilon_{sp, \theta})(\epsilon_{sy, \theta} - \epsilon_{sp, \theta} + c/E_{s, \theta})$ $b^2 = c(\epsilon_{sy, \theta} - \epsilon_{sp, \theta})E_{s, \theta} + c^2$ $c = \frac{(f_{sy, \theta} - f_{sp, \theta})^2}{(\epsilon_{sy, \theta} - \epsilon_{sp, \theta})E_{s, \theta} - 2(f_{sy, \theta} - f_{sp, \theta})}$					
Steel Temperature $\theta$ [°C]	$f_{sy, \theta} / f_{yk}$		$f_{sp, \theta} / f_{yk}$		$E_{s, \theta} / E_s$	
	Hot rolled	Cold worked	Hot rolled	Cold worked	Hot rolled	Cold worked
1	2	3	4	5	6	7
20	1.00	1.00	1.00	1.00	1.00	1.00
100	1.00	1.00	1.00	0.96	1.00	1.00
200	1.00	1.00	0.81	0.92	0.90	0.87
300	1.00	1.00	0.61	0.81	0.80	0.72
400	1.00	0.94	0.42	0.63	0.70	0.56
500	0.78	0.67	0.36	0.44	0.60	0.40
600	0.47	0.40	0.18	0.26	0.31	0.24
700	0.23	0.12	0.07	0.08	0.13	0.08
800	0.11	0.11	0.05	0.06	0.09	0.06
900	0.06	0.08	0.04	0.05	0.07	0.05
1000	0.04	0.05	0.02	0.03	0.04	0.03
1100	0.02	0.03	0.01	0.02	0.02	0.02
1200	0.00	0.00	0.00	0.00	0.00	0.00

\* for prestressing steel and definition of Class A reinforcement, see Eurocode 2 provisions for details

For simulation of structural system response (see Sect. 7.5.2 below), the shear force-slip characteristics of each individual steel shear stud should be characterised within a given model. The force-slip relationship is generally obtained using push-out tests. A set of push-out tests at ambient and high temperatures has been conducted to determine the force-slip relationship for shear stud behaviour [6]. Based on the data derived from this testing, the temperature-dependent force-slip behaviour of individual steel shear studs may be represented as shown in Fig. 7.3. The stiffness of shear studs in all other directions may be assumed as ideally rigid.

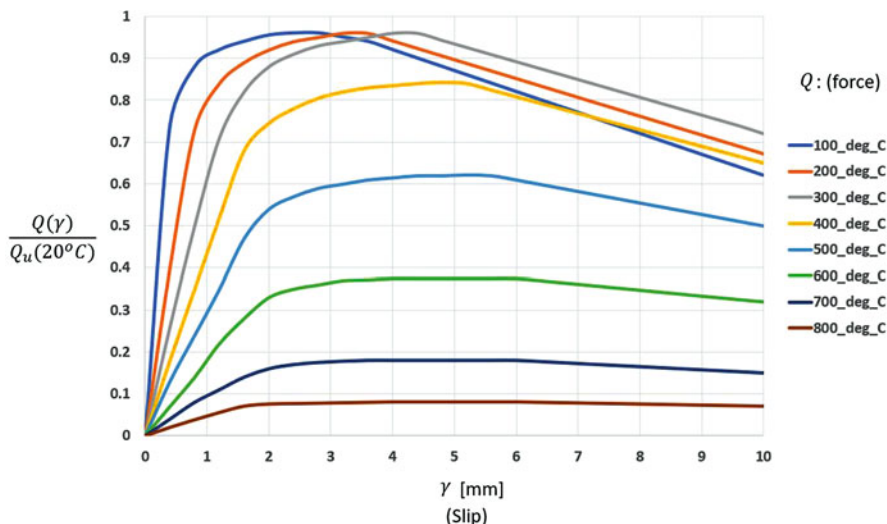


Fig. 7.3 Steel shear stud force-slip relationship

## 7.2 Performance of Individual Steel Elements

Designing structural elements under fire conditions can be undertaken in different domains (time, temperature, resistance) and under different paradigms (performance based or prescriptive). Nearly all methods require cognisance of the temperature history of the structural member, the action on the structural element and the mechanical properties as a function of temperature. In some cases, the latter two points can be reduced to a utilisation. However, Sect. 7.5 below should be consulted for specific restrictions contained in North American standards.

Designing structures in accordance with Eurocode allows two main approaches of prescriptive or performance-based models, including member analysis, analysis of a part of the structure or analysis of the whole system.

Analysis of a member in isolation can provide a good first approximation of the member performance under fire. However, since the member analysis neglects the effect of fire on representative boundary conditions, it does not capture temperature distribution along the elements of the structures, frame effects (such as restrained thermal expansion) and load redistribution between the elements during the course of fire. Therefore, member analysis in fire is more typically undertaken within a fire resistance/prescriptive framework (e.g. under ISO 834 heating), where the fire resistance rating of a member is sought. Analyses of structural subframes or full frames typically require advance calculation methods and are most valuable in elucidating the expected fire performance of structures under realistic heating conditions.

Currently, EN1993-1-2 [1, 8] provides guidance to use a simple calculation method for designing steel structural members under compression, bending, tension

and combined axial and bending. Henceforth, this section will present the design procedure for each of these cases.

### 7.2.1 Columns

Similar to design at ambient temperature, the ultimate aim is to make sure that the structural elements will have sufficient resistance capacity to withstand the loadings applied at elevated temperature. In the Eurocode, fire has been categorised as an accidental loading which means that the sections should be checked at ultimate limit state.

In line with the current EN1993-1-2 [1], the design procedure at elevated temperature for simple calculations is similar to that employed at ambient temperature with some modifications to take into account the variation in material properties at elevated temperature. For a member which is partially or fully under compression, the slenderness of the part which would be under compression should be classified.

EN1993-1-2 [8] defines four classes of cross sections, where Class 1 is a stocky cross section which can reach its plastic capacity, Class 2 is a member that can reach plastic capacity with limited rotation capacity before local buckling, Class 3 is a member which can reach its elastic moment resistance but where local buckling prevents it from reaching its plastic capacity and finally Class 4 is a member in which its resistance is governed by elastic buckling and cannot reach its yield moment (more detail in this regard can be found in Gardner and Nethercot [9]). For fire conditions, the same procedure can be used for the classification of the cross section with the yield and the elastic modulus of the steel affected by fire; EN1993-1-2 suggests to use a modified  $\varepsilon$  value as  $0.85\sqrt{\frac{235}{f_y}}$ .

If the cross section is classified as Class 1, 2 or 3, with a uniform temperature of  $\theta_a$ , EN1993-1-2 [1] allows to design a column as follows:

$$N_{b,fi,t,Rd} = \frac{\chi_{fi} A k_{y,\theta} f_y}{\gamma_{M,fi}} \quad (2)$$

Where

$A$  is the gross cross-section area.

$f_y$  is the yield strength.

$k_{y,\theta}$  is the reduction factor for the yield strength of steel at temperature  $\theta_a$ .

$\gamma_{M,fi}$  is the partial factor for relevant material property, for the fire situation.

$\chi_{fi}$  is the reduction factor for flexural buckling in the fire design situation.

The parameter  $\chi_{fi}$  which should be taken as the lowest of the values about y-y and z-z axes is a function of the slenderness of the column and can be calculated as follows:



$$\chi_{fi} = \frac{1}{\varphi_{\theta} + \sqrt{\varphi_{\theta}^2 - \bar{\lambda}_{\theta}^2}} \quad (3)$$

where

$$\varphi_{\theta} = \frac{1}{2} \left[ 1 + \alpha \bar{\lambda}_{\theta} + \bar{\lambda}_{\theta}^2 \right] \quad (4)$$

$$\alpha = 0.65 \sqrt{\frac{235}{f_y}}$$

And the non-dimensional slenderness  $\bar{\lambda}_{\theta}$  for temperature  $\theta_a$  is given by

$$\bar{\lambda}_{\theta} = \bar{\lambda} \sqrt{\frac{k_{y,\theta}}{k_{E,\theta}}} \quad (5)$$

$k_{y,\theta}$  is the reduction factor for yield strength of steel at the steel temperature  $\theta_a$  reached at time  $t$ .

$k_{E,\theta}$  is the reduction factor for the slope of the linear elastic range at the steel temperature  $\theta_a$  reached at time  $t$ :

$$\bar{\lambda} = \sqrt{\frac{Af_y}{N_{cr}}} = \frac{L_{cr}}{i} \frac{1}{\lambda_1}$$

Where

$N_{cr}$  is the elastic critical buckling.

$L_{cr}$  is the buckling length in the buckling plane under consideration.

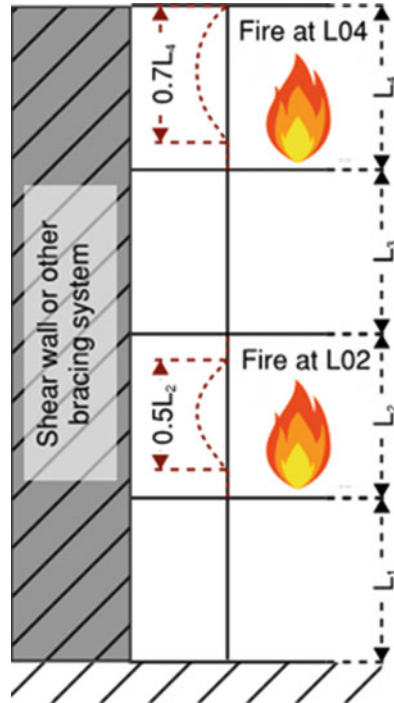
And

$$\lambda_1 = \pi \sqrt{\frac{E}{f_y}} = 93.9\varepsilon$$

$$\varepsilon = \sqrt{\frac{235}{f_y}}$$

Per the above, accurate evaluation of the critical length of the column is key because it may vary from ambient temperature design. Current EN1993-1-2 [1] suggests that if the column member is a part of braced frame, the buckling length can be improved depending on its location (Fig. 7.4). However, if that is not the case, the buckling length of the column for the fire design situation should be determined as for normal temperature design.

**Fig. 7.4** EN1993-1-2 recommendation for buckling length of a column as a part of a braced frame



Similar to the other cases, members classified with a Class 4 cross section can be used as a part of a design provided that the temperature of those elements is below the critical temperature. EN1993-1-2 offers two methods to evaluate such critical temperatures. Either take the critical temperature as a default value of  $350\text{ }^\circ\text{C}$  or the section should be designed according to recommendations given in Annex E of that document.

For the cases where the temperature of a column is nonuniform, the standard suggests that for Class 1 through 3 cross sections, the design may be based on the assumption of uniform temperature. However, this recommendation depends on the slenderness of the column. Hence, such cases should be considered in detail with additional imposed affect induced due to the non-uniformity of the temperature as part of the overall evaluation of the section’s resistance.

### 7.2.2 Beams

Similar to the design of columns under fire condition, the design of beams at elevated temperatures is comparable to that at ambient temperature. Notably, beams should generally be checked for bending resistance, shear resistance, and lateral torsional buckling.

### 7.2.2.1 Moment Resistance

When a flexural member is exposed to fire conditions, the temperature of the element may be either uniform or non-uniform. If the temperature distribution is uniform and provided that the section is classified as Class 1 or 2, the bending resistance of the element may be calculated with respect to plastic moment resistance of the section by applying the reduction factor to yield strength as follows:

$$M_{fi,\theta,Rd} = k_{y,\theta} \left[ \frac{\gamma_{M0}}{\gamma_{M,fi}} \right] M_{Rd} \quad (6)$$

Where

$M_{Rd}$  is the plastic moment resistance of the gross cross section.

$M_{pl, Rd}$  is for normal temperature design, according to EN 1993-1-1, or the reduced moment resistance for normal temperature design, allowing for the effects of shear if necessary, according to EN1993-1-1.

$k_{y, \theta}$  is the reduction factor for the yield strength of steel at temperature  $\theta_a$ .

For Class 3 cross sections, the method of calculation would be the same as above except that the elastic moment resistance  $M_{el, Rd}$  should be used in the calculation.

For non-uniform beam temperature distributions, the standard offers two methods to take this affect into account. The first method (for Classes 1 and 2) is to divide the cross section into a number of 'blocks', in which each block has an assigned temperature and it is assumed that all blocks reach their yield capacity. Also, the neutral axis should be calculated to differentiate those blocks in either compression or tension. Thereafter, the moment resistance of the cross section may be calculated as suggested by EN1993-1-2 [1] as follows:

$$M_{fi,t,Rd} = \sum_i^n \frac{A_i z_i k_{y,\theta,i} f_{y,i}}{\gamma_{M,fi}} \quad (7)$$

Where

$z_i$  is the distance from the plastic neutral axis to the centroid of the elemental area  $A_i$ .

$f_{y, i}$  is the nominal yield strength  $f_y$  for the elemental area  $A_i$  taken as positive on the compression side of the plastic neutral axis and negative on the tension side.

$A_i$  is an elemental area of the cross section with a temperature  $\theta_i$ .

$k_{y, \theta, i}$  is the reduction factor for the yield strength of steel at temperature  $\theta_i$ .

The method described above is suitable for cases where the temperature distribution along the cross section is known. If such information is not available, EN1993-1-2 [1] offers a second method in which the moment resistance of the section can be calculated in a similar fashion as that for uniform temperature distributions. Accordingly, two modification factors  $\kappa_1$  and  $\kappa_2$  are used to address the non-uniformity of temperature distribution as follows:

$$M_{\bar{f}_i, t, Rd} = \frac{M_{\bar{f}_i, \theta, Rd}}{\kappa_1 \kappa_2} \quad (8)$$

Where

$M_{\bar{f}_i, \theta, Rd}$  is the design moment resistance of the cross section for a uniform temperature  $\theta_a$  which is equal to the uniform temperature  $\theta_a$  at time  $t$  in a cross section which is not thermally influenced by the support.

$\kappa_1$  is an adaptation factor for non-uniform temperature across the cross section. It is equal to 1.0 for a beam exposed on all four sides; equal to 0.7 for an unprotected beam exposed on three sides, with a composite or concrete slab on side four; and equal to 0.85 for a protected beam exposed on three sides, with a composite or concrete slab on side four.

$\kappa_2$  is an adaptation factor for non-uniform temperature along the beam. It is equal to 0.85 for the supports of a statically indeterminate beam and is equal to 1.0 in all other cases.

For Class 3 cross sections, the second method described above may be used when the temperature distribution is non-uniform, except that the moment used to calculate  $M_{\bar{f}_i, \theta, Rd}$  should be equal to  $M_{el, Rd}$ .

### 7.2.2.2 Shear Resistance

Similar to the calculation described above for moment resistance at elevated temperatures, the shear resistance of a section is determined at ambient temperature and then multiplied by a modification factor to take into account the strength reduction factor at a corresponding temperature as follows:

$$V_{\bar{f}_i, t, Rd} = k_{y, \theta, web} V_{Rd} \left[ \frac{\gamma_{M0}}{\gamma_{M, \bar{f}_i}} \right] \quad (9)$$

Where

$k_{y, \theta, web}$  is the reduction factor for the yield strength corresponding to average temperature of the web  $\theta_{web}$ .

$V_{Rd}$  is the shear resistance of the gross cross section for normal temperature design, according to EN1993-1-1.

### 7.2.2.3 Lateral Torsional Buckling

Similar to beams at ambient temperature, if the compression flange does not have continuous restraint, it should be checked for lateral torsional buckling. Similar to previous parts, the method of calculation for the fire condition would follow the methods of calculation at ambient temperature, except that the slenderness, yield strength and elastic modulus should be modified for the fire condition. On this basis, the lateral torsional buckling resistance moment at time  $t$  of a laterally unrestrained member with a Class 1 or Class 2 cross section can be evaluated as follows:

$$M_{b,fi,t,Rd} = \frac{\chi_{LT,fi} W_{pl,y} k_{y,\theta,com} f_y}{\gamma_{M,fi}} \quad (10)$$

Where

$\chi_{LT, fi}$  is the reduction factor for lateral-torsional buckling in the fire design situation.

$k_{y, \theta, com}$  is the reduction factor for the yield strength of steel at the maximum temperature in the compression flange  $\theta_{a, com}$  reached at time  $t$ .

The lateral torsional buckling reduction factor  $\chi_{LT, fi}$  in the above formulation for elevated temperature can be calculated as

$$\chi_{LT,fi} = \frac{1}{\varphi_{LT,\theta,com} + \sqrt{\varphi_{LT,\theta,com}^2 - \bar{\lambda}_{LT,\theta,com}^2}} \quad (11)$$

Where

$$\varphi_{LT,\theta,com} = \frac{1}{2} \left[ 1 + \alpha \bar{\lambda}_{LT,\theta,com} + \bar{\lambda}_{LT,\theta,com}^2 \right] \quad (12)$$

$$\alpha = 0.65 \sqrt{\frac{235}{f_y}}$$

$$\bar{\lambda}_{LT,\theta,com} = \bar{\lambda}_{LT} \sqrt{\frac{k_{y,\theta,com}}{k_{E,\theta,com}}} \quad (13)$$

For sections classified as Class 3, the procedure of the calculation would be same as above, except that  $W_{pl, y}$  should be replaced by  $W_{el, y}$  in the above expressions.

### 7.2.3 Tension Members

As a part of a structure, there are cases where a member should be checked for tension including bracings, suspended structures, a member forming part of a truss system, cables, etc. Similar to the design of columns and beams, the design of these types of elements for fire conditions involves an adaptation of their designs for ambient temperature.

For a uniform temperature distribution, the resistance of the element can be evaluated by using reduction factor  $k_{y, \theta}$  on yield strength at a known temperature of  $\theta_a$ . On this basis the design resistance of a tension member in EN1993-1-2 is expressed as

$$N_{f_i, \theta, Rd} = k_{y, \theta} N_{Rd} \frac{\gamma_{M,0}}{\gamma_{M, f_i}} \quad (14)$$

Where

$N_{Rd}$  is the design resistance of the cross section for normal temperature design, according to EN1993-1-1.

$k_{y, \theta}$  is the reduction factor for the yield strength of steel at temperature  $\theta_a$  reached at time  $t$ .

For a non-uniform temperature distribution, EN1993-1-2 allows the evaluation of resistance by dividing the section to discrete the number of areas with specific temperature so that an appropriate reduction factor can be applied to each of them. Accordingly, EN1993-1-2 suggests using the following equation for this case:

$$N_{f_i, t, Rd} = \sum_i^n \frac{A_i k_{y, \theta, i} f_{y, i}}{\gamma_{M, f_i}} \quad (15)$$

Where

$f_{y, i}$  is the nominal yield strength at 20 °C.

$A_i$  is an elemental area of the cross section with a temperature  $\theta_i$ .

$k_{y, \theta, i}$  is the reduction factor for the yield strength of steel at temperature  $\theta_i$ .

$\theta_i$  is the temperature in the elemental area  $A_i$ .

Conservatively, a tension member with a non-uniform temperature distribution can still be assumed to have a uniform temperature distribution provided that the highest temperature throughout the section is used in the calculation.

## 7.2.4 Trusses

One of the most effective ways of covering large spans is the use of trusses which are made of slender struts and ties. Such elements can be particularly vulnerable when exposed to fire. Notably, compression members of trusses can fail at the early stages of a fire. This is why in some documents such as the work by Phan et al. [10] a recommendation is made to properly protect the compression members of trusses with the smallest section sizes.

Similar to other structural elements discussed, the design of truss members for fire conditions includes the evaluation of member forces followed up by calculation of the critical temperature with usage of relevant reduction factors to the resistance of the section at ambient temperature. However, the works by researchers such as Ozyurt and Wang [11] indicate that such an approach may not be conservative. This is due to the fact that a truss member may undergo a high level of deformation under fire exposure since trusses usually cover large spans. Also, the temperature along a given truss may not be uniform. Non-uniform temperature distributions not only along the depth but also along the length of a truss can lead to the inducement of

additional forces which can have a detrimental impact on the overall performance of the system (additional information about this subject can be found in Ozyurt and Wang [12], Chen and Zhang [13], Lin et al. [14]).

## **7.3 Performance of Composite Systems**

Observations of structural behaviour under fire conditions have shown that the design of members on the assumption of isolated behaviour in fire can be over-conservative. The interactions between various parts of a three-dimensional structure often show the existence of high inherent fire performance. In the 1990s, a number of accidental fires and specially designed large-scale fire tests on steel-framed buildings with composite floors demonstrated the over-conservativeness of the associated prescriptive designs, and provided an incentive for the development of performance-based design methods.

### ***7.3.1 Relevant Testing and Real Fire Events***

#### **7.3.1.1 Broadgate Fire**

In 1990, fire broke out on the first floor of an uncompleted 14-storey steel-framed office block at the Broadgate development in London. At the time of the fire, the sprinkler system and other active measures had not been installed. Also, passive fire protection of the exposed steel beams was not complete. Gas temperatures were estimated to have reached over 1000 °C, with unprotected steelwork temperatures at about 600 °C. However, the integrity of the composite slab was maintained, although a separation of the steel deck from the concrete slab was observed. Deflections of composite beams were between 82 and 270 mm with a 600 mm maximum deflection of the slab. There was no observed structural failure of the building, except for large distortions in the form of local buckling of the bottom flanges of beams near their supports and the shortening of smaller columns. These were all due to restraint of thermal expansion of these members by other parts of the structure, which were at considerably lower temperatures [15].

#### **7.3.1.2 Cardington Tests**

The Broadgate fire had shown that, although some structural elements lost their load-bearing capacity in fire, the composite slab, with its supporting steelwork and other cooler parts of the building, positively influenced the stability of the structure by acting as a membrane to distribute loads away from the weakened members. Churchill Plaza—a 90-min-rated 12-storey steel-framed building with composite floors, which had a large fire in 1991 [16]—provided confirmation of the over-

conservative nature of the traditional design of protecting all exposed steelwork. A load test on the most degraded part of the composite slab had shown that an excess capacity existed even after the fire, but this could not be quantified. Several large-scale tests were also carried out in Australia to demonstrate real building behaviour during fires. The key observations were that unprotected beams in composite flooring systems had significant reserve capacity, even when they were shielded by non-fire-rated suspended ceilings. However, any reliance on these suspended ceilings does not allow for an easy assessment of the advantages of applying this procedure in practice.

The inadequate representation of structural elements by the standard fire test and the observations of real building fires led to the development of several fire tests at the Building Research Establishment (BRE)'s Large Building Test Facility at Cardington between 1995 and 2003. In all, seven tests were performed on a specially designed 8-storey steel-framed building. Six tests were performed between January 1995 and July 1996, while the seventh was in January 2003. The tests demonstrated the behaviour of real structures under fire conditions and provided test data for the development and calibration of computer programs. The building was braced to resist lateral loads and had a floor footprint of 21 m x 45 m and an overall height of 33 m, with a 9 m x 2.5 m central lift core and two stairwells. It was designed as per BS5950 [17, 18], and checked against Eurocodes 3 and 4 (CEN, 1992; [19]) for compliance, using S275 (255 MPa) and S355 (355 MPa) hot-rolled steel sections and a 130 mm deep composite slab on a 0.9 mm thick PMF CF70 steel deck. The slab was made of lightweight Grade 35 concrete, reinforced with a standard A142 mesh (142 mm<sup>2</sup>/m in both directions). Two views of the structure are presented in Fig. 7.5. Live loading at the fire limit state was simulated with sandbags, each weighing 11 kN, giving an overall loading of 5.48 kN/m<sup>2</sup>.

The first six tests were on: a restrained beam, a plane frame, two corner compartments, a large compartment and an office fire demonstration. The seventh test was



Fig. 7.5 Cardington test building [20]



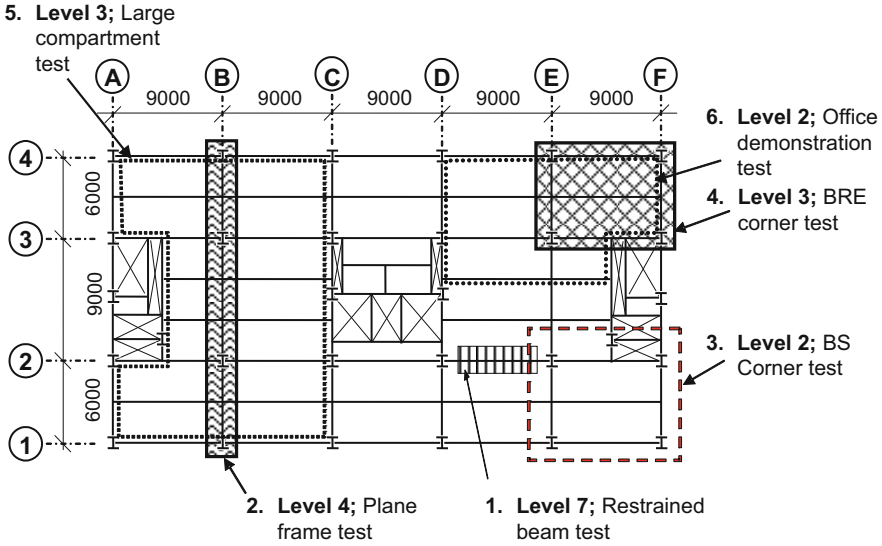


Fig. 7.6 Location of the first 6 Cardington tests [20]

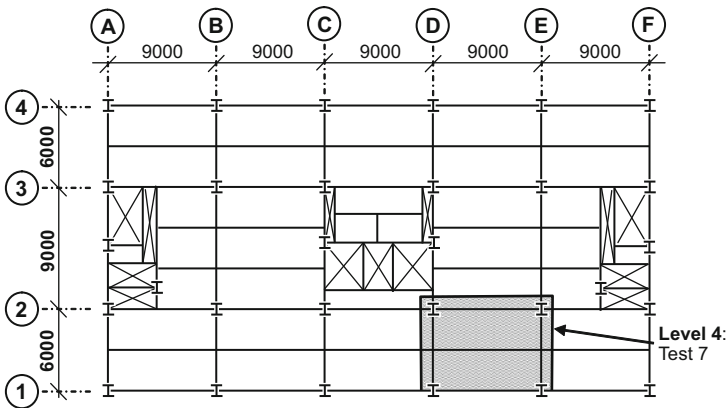


Fig. 7.7 Location of the 7th Cardington test [20]

conducted to collect more data on the behaviour of beam-to-beam and beam-to-column connections, especially in the wake of the collapse of the World Trade Center towers. The test also provided the opportunity to check the suitability of specialised numerical modelling software [20]. The locations of the tests are shown in Figs. 7.6 and 7.7.

The tests established that, for the stability of a structure, structural damage should be limited to the fire compartments of origin, and therefore recommended the protection of the entire lengths of columns in any fire compartment, although steel

beams could be left unprotected. Composite beam temperatures reached between 800 and 1150 °C (well above their limiting design temperature of about 680 °C, according to BS5950-8 [21]), with maximum slab displacements between 232 and 641 mm. It was concluded that, although most floor beams lost strength and stiffness, flexural bridging at relatively small deflections and membrane action of the composite slabs at large deflections introduced structural stability and alternative load paths. Catenary action of beams and slabs bending in single curvature contributed to their enhanced capacity at large deflections. The ability of the composite slabs to bear considerably higher loads at large deflections and in biaxial bending was attributed to tensile membrane action [20, 22, 23].

### 7.3.2 Tensile Membrane Action Theory

Tensile membrane action is a mechanism which provides thin slabs with large load-bearing capacity, resulting from large vertical displacements, where induced radial tension in the centre of the slab (due to the large deflection) is resisted by a peripheral compression ring. A diagrammatic representation of this mechanism is shown in Fig. 7.8. A vertical deflection of at least the thickness of the slab marks the beginning of the mechanism. The conditions necessary for effective tensile membrane action are two-way bending and vertical support along all the slab's four edges. The self-sustaining nature implies that the process occurs with or without horizontal restraint once the basic requirements of biaxial bending and vertical edge support are satisfied. Tensile membrane action works for all thin two-way concrete slabs, whether they are conventionally reinforced flat slabs or composite steel-concrete slabs. This mechanism works best for square slabs, or where the aspect ratio is no more than 2:1. Tensile membrane action applies to ambient temperature conditions

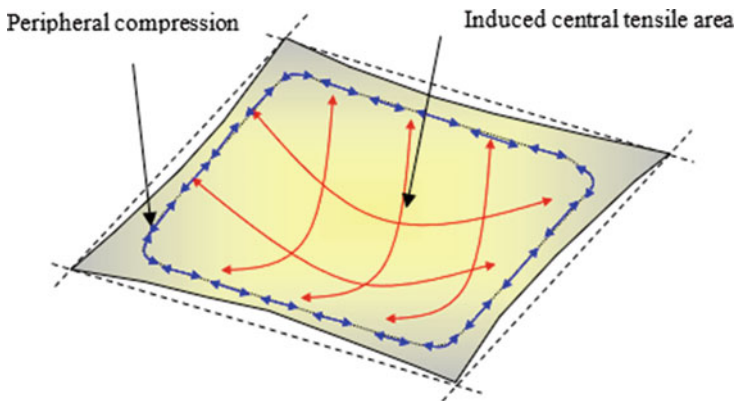
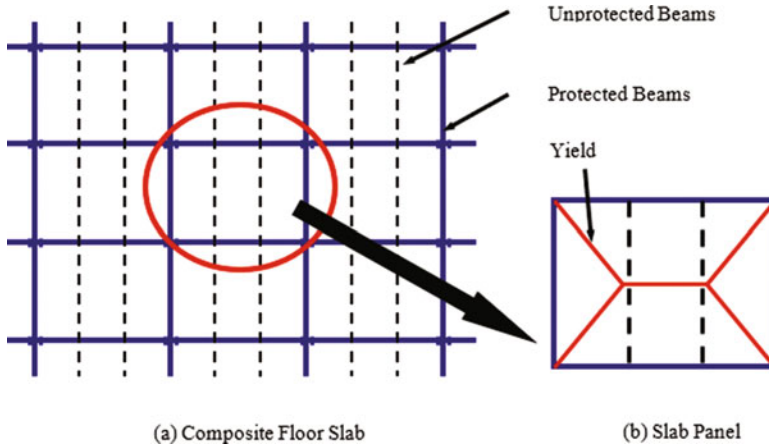


Fig. 7.8 Tensile membrane action [26]



**Fig. 7.9** Application of tensile membrane action to real building design [26]

[24], but it is particularly useful for structural fire design, where large deflections more often occur [25].

For the fire design of a composite floor to take advantage of this mechanism, the floor is divided into rectangular zones known as ‘slab panels’. The slab panels are made up of unprotected composite beams in the interior of each panel and protected composite beams along their edges on the column grid, to provide the necessary vertical support (Fig. 7.9). The slab panels do not need any horizontal restraint at their edges. When fire is exposed to the underside of the composite slab, the unprotected beams lose strength and stiffness rapidly, and their loads are then carried by the composite slab in tensile membrane action. The effective utilisation of tensile membrane action in structural fire engineering of steel-concrete composite structures is able to provide sufficient safety with economy in fire protection, by allowing a significant number of steel floor beams to be left unprotected.

### 7.3.3 Tensile Membrane Action Design Methods

#### 7.3.3.1 The Membrane Action Calculation Method

This calculation method is sometimes also referred to as the Bailey-BRE method. The approach devised by Bailey and Moore [27, 28] was the first simplified design approach for composite slabs at high temperatures that incorporated the benefits of tensile membrane action. It assesses the structural capacity of a composite slab in fire by calculating the tensile membrane enhancement to the traditional flexural capacity of the slab.

The method proceeds by dividing a composite floor into several slab panels, as described above, shown in Fig. 7.9. With increasing exposure to elevated temperatures, the formation of plastic hinges in the unprotected beams redistributes the applied loads to the two-way bending slab, undergoing large vertical deflections. Based on the rigid-plastic theory with large changes of geometry, and following a similar procedure to the one derived by Hayes [29] for room-temperature tensile membrane action, the additional slab capacity provided by the induced in-plane stresses is calculated as an enhancement to the traditional small-deflection yield-line capacity [27, 28]. Figure 7.10 shows the distribution of tensile and compressive stresses along the yield lines when a slab panel such as that in Fig. 7.9 approaches failure. See Bailey and Toh [30] for derivation and explanation of the terms in Fig. 7.10.

Failure of the slab panel is defined as the tensile fracture of reinforcement across the shorter span of the slab or the compressive crushing of concrete at its corners [30]. The method conservatively ignores any contribution of the tensile strength of concrete to the capacity of the slab. It assumes that fire protection applied to steel beams on the gridlines will provide the necessary vertical support along the slab

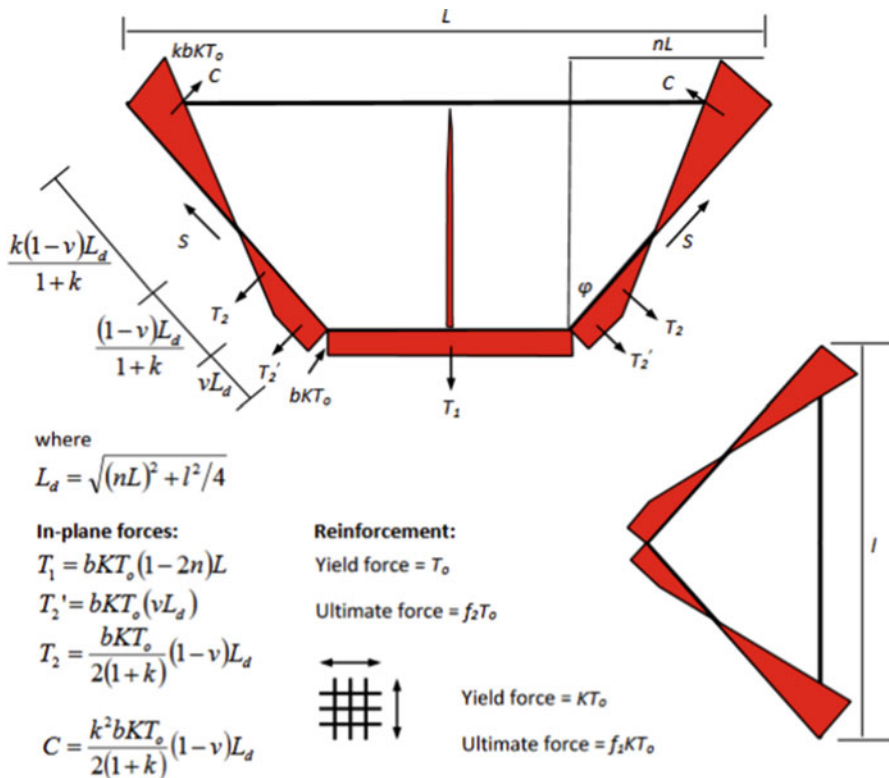


Fig. 7.10 In-plane stress distribution for the Bailey-BRE Method [30]

panel boundaries. As part of the design, the capacity of protected secondary beams must be checked for the increased load and load capacity at elevated temperatures.

To predict failure at the fire limit state, a vertical displacement limit (derived from a combination of thermal bowing of the slab and mechanical strain in the reinforcement) is defined as shown in Eq. 16, which has been calibrated against the Cardington fire tests. The deflection due to mechanical strain of the reinforcement is limited to  $l/30$ , where  $l$  is the length of the shorter span of the slab panel. A full derivation of the method, and its recent modifications, for both isotropic and orthotropic reinforcements can be found in the references [30, 32–35].

$$v = \frac{\alpha(T_2 - T_1)l^2}{19.2h} + \sqrt{\left(\frac{0.5f_{y,\theta}}{E_\theta}\right) \times \frac{3L^2}{8}} \quad (16)$$

where

$\alpha$  coefficient of thermal expansion of the concrete slab

$T_2$  bottom-surface temperature of the slab

$T_1$  top-surface temperatures of the slab

$h$  effective thickness of the slab

$f_{y,\theta}$  reinforcement strength at a given time

$E_\theta$  Young's modulus at a given time

The composite slab capacity at any given time in fire is calculated as:

$$w_{p\theta} = e \left( \frac{\text{Internal work done by the composite slab in bending}}{\text{External work done by the applied load per unit load}} \right) + \frac{\text{Internal work done by the beams in bending}}{\text{External work done by the applied load per unit load}} \quad (17)$$

where

$w_{p\theta}$  slab panel capacity at a given time

$e$  enhancement of the slab capacity [30]

A primary advantage of the membrane action method is its simplicity, as it is suitable for implementation in spreadsheet software. The Steel Construction Institute (SCI) in collaboration with CTICM of France has further developed the method, and has implemented it in software MACS+ (a previous version existed known as TSLab), which is available from the ArcelorMittal website. This software extends the basic Bailey-BRE membrane action method by performing thermal analyses on the unprotected intermediate beams and the composite slab. Then, using the temperatures of the individual components and its allowable vertical deflection criterion, it calculates the total capacity of the simply supported slab panel model (by summation of the residual unprotected beam capacity and the enhanced slab capacity). This capacity is then checked against the applied load in the fire limit state. If the capacity of the panel is found to be below the applied load at the fire limit state, then either the resistance of the internal beams or the reinforcement mesh size must be increased.

Since the initial development of the Bailey-BRE method, attempts have been made by various researchers to enhance design methodologies employing tensile membrane action through experimental, analytical and numerical approaches.

### 7.3.3.2 Slab Panel Method (SPM)

Clifton [36] expanded the initial Bailey-BRE method to include the effects of continuity and additional reinforcement that may be present in the ribs of slabs. The method, generally known as the slab panel method (SPM), has some considerable differences from the Bailey-BRE method. In addition to the consideration of slab continuity, the SPM includes the contribution of the unprotected secondary beams in its yield-line load-carrying capacity. It performs a shear check of the panel and allows for some deflection of the protected secondary beams.

The method proceeds with the calculation of the fire limit state loading on the slab, following the loading standard of the particular jurisdiction. The yield-line capacity of the slab is calculated by aggregating the contributions of the reinforcing mesh, any reinforcing bars that may be present in the ribs of the composite slab and the residual capacity of the unprotected beams at the design time of the fire. The negative moments along continuous edges are also calculated. Two slab yield-line capacities are determined:

- One is calculated to include all pinned and fixed boundaries, as suggested by Park [24].
- The other is calculated as the yield-line load capacity of a simply supported slab. It is to this capacity that the membrane enhancement is applied.

A deflection limit is calculated based on the desired fire design time, and this is used to determine the potential enhancement, like the process in the Bailey-BRE method. Once the enhancement has been calculated the capacity of the slab panel is determined as

$$W_u = (w_{yl\theta} - w_{yl\theta,ss}) + w_{yl\theta,ss}e. \quad (18)$$

where

- $w_u$  slab panel load-carrying capacity
- $w_{yl\theta}$  yield-line load-carrying capacity in fire
- $w_{yl\theta,ss}$  simply supported yield-line load-carrying capacity in fire
- $e$  tensile membrane enhancement factor

Structural safety is confirmed if  $W_u$  is greater than the fire limit state loading. The shear capacity of the slab is checked near the supporting beams. The slab thickness is the minimum slab thickness (using just the thickness of concrete above the ribs), with further reductions in thickness due to the loss of strength of concrete at elevated temperatures. The SPM recognises that protected secondary beams can deflect under load and heat, and so it includes an edge beam deflection of span/100 in the

calculation of its slab panel deflection limit. Details of the method can be found in the references [37, 38].

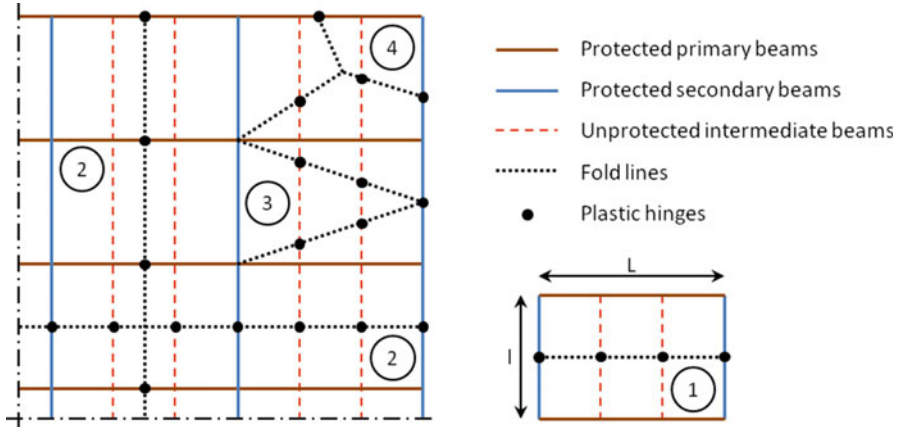
### 7.3.4 *Key Failure Modes*

The Bailey-BRE method and the slab panel method both assume that full vertical support is available at all the slab panel boundaries. In practice, this is achieved by protecting the slab panel's edge beams, which must lie on the column grid of the building. When the unprotected secondary beams lose most of their strength at very high temperatures there is a redistribution of the loads carried by these protected edge beams; the primary beams lose load because of the loss of load capacity of the unprotected beams whose ends they support, whereas the protected secondary beams gain load by tending to support the floor area with which they would be associated in a non-composite two-way-spanning slab.

The Bailey-BRE method therefore requires that the protected secondary beams are designed for increased load ratios at the fire limit state. As the protected beams lose strength with time, and the load redistribution at the fire limit state causes increased deflections at the panel boundaries, the assumption of continuous vertical support along the panel edges becomes progressively less valid. The use of yield-line theory as the baseline for the strength enhancement also dictates that a slab panel's capacity increases with increased reinforcement area unless the increase is arrested by a compressive failure criterion, as identified by Bailey and Toh [30]. However, since the primary requirements for tensile membrane action to be mobilised are double-curvature bending, large deflections and vertical edge support, excessive deflections of the protected edge beams can result in the double-curvature bending being converted into single-curvature bending. In consequence the panel may fail structurally, so that the reinforcement's tensile strength is not usefully employed.

Slab panels are usually continuous over at least two supports. Continuity provides higher slab panel resistance in fire. However, depending upon the extent of the fire in a building and the lightness of the reinforcement used in composite floor construction, the continuity may be lost, or significantly higher loads may be imposed on the protected perimeter beam between two adjacent slab panels. Coupled with thermal degradations, these beams can experience large deflections and may collapse. Therefore, Duchow and Abu [31] have proposed alternative collapse mechanisms for these slab panels, to ensure that designs following the simple approaches can dependably generate full tensile membrane capacity and not fail by the loss of support from the protected beams. An examination of all possible scenarios offers the possibility of selecting the mechanism which requires the least plastic energy.

The collapse mechanism which occurs in a fire will depend on the aspect ratio of the slab, relative beam sizes, location of the slab panel within the building and extent of the fire. With reference to Fig. 7.11, the simplified design approaches are based on the failure of an isolated slab panel. Collapse Mechanism 1 examines the failure of isolated slab panels. Collapse Mechanism 2 addresses large compartments, such as



**Fig. 7.11** Collapse mechanisms of composite slab panels, including failure of protected beams [31]

open-plan offices where many slab panels could be involved in the fire. Collapse Mechanism 3 is for slab panels located at the edge of a building, with Collapse Mechanism 4 developed for slab panels located at the corner of a building.

However, in real fires the maximum tensile stresses may not necessarily occur at the slab centre, but could be located in the concrete slab above the protected edge beams. Also, irrespective of the presence of interior beams, it is found that tensile membrane action can be mobilised at a deflection equal to approximately 0.9–1.0 of the slab thickness. This may cause different failure modes for floor assemblies, compared with isolated slab panels [40]. Further research has also revealed different ‘composite’ failure modes of the floor assemblies. These include:

- Fracture of reinforcement in the vicinity of protected edge beams.
- Crushing of the compression ring or folding in single curvature by formation of plastic hinges in the secondary edge beams. However, no fracture of reinforcement was observed at the mid-span of these slabs.

### 7.3.5 Hand Calculations Vs. Finite Element Analyses

When considering a whole structure, it must be recognised that the performance of any structural member depends on its interactions with the surrounding structure. The loss of strength and stiffness of one member results in the redistribution of loads to other members, which may in turn have either degraded or enhanced performance due to their thermal exposure and the deformations they experience. For a thorough understanding of the behaviour of any structural member exposed to fire conditions, it is prudent to examine the fire behaviour of the whole structure. Numerical analysis



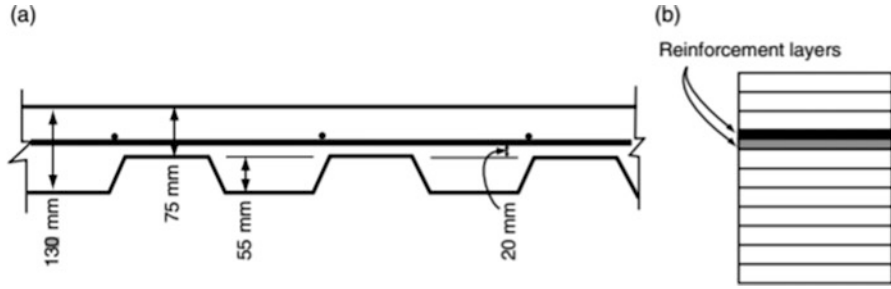
of the whole structure allows an investigation of local degradation of any heated structural member including its interaction with adjacent members and the surrounding structure.

Finite element analysis is a valuable tool which can account for varying capacities of the entire structure, as individual members lose strength or are subjected to increased loading. The finite element method allows the definition of thermal and mechanical actions on structural members or frames while accounting for the change in material properties with temperature. The finite elements are specified over small segments of the structural member and may have varying properties through the cross section. As different structural and material properties can be assigned to different parts of different members, finite element analysis aids the simulation of progressive deformations of complex structures when exposed to fire. It also helps to track realistic behaviour of structures under different fire exposure scenarios and is very useful in optimising fire-resistant design as well as predicting collapse mechanisms of structures. It helps to promote the idea of performance-based engineering as it uses rational engineering approaches to provide the requisite fire safety, by taking the real behaviour of the three-dimensional structure into account [41]. This rational approach should involve realistic estimates of thermal properties of materials at elevated temperatures, interaction of structural elements in load-sharing mechanisms and geometrically non-linear behaviour of structural elements at elevated temperatures. Tracking the complete behaviour of full-frame structures gives an understanding of the different load paths that can occur. Unlike single-element analysis where a reduction of material strengths may be accompanied by increasing temperature to estimate reduced capacities in comparison to the applied loads, finite elements allow for the inclusion of thermally induced effects such as thermal bowing and restrained thermal expansion.

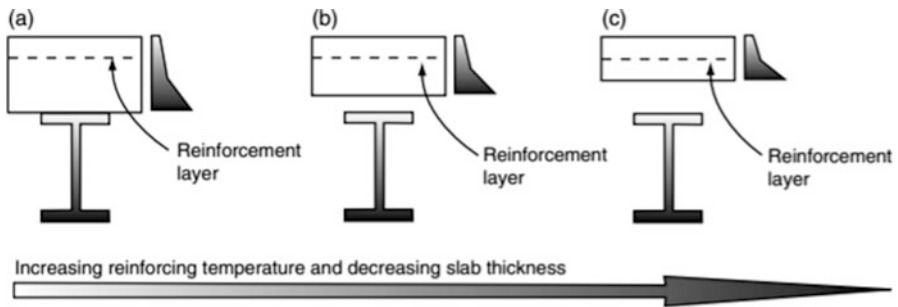
Slabs are structural members with two dimensions much larger than the third dimension. They are normally modelled with shell or plate finite elements, as these model 2D planar behaviour. However, slabs can be modelled with brick elements as well. The general cross section of a steel-concrete composite slab is shown in Fig. 7.12. Shell elements treat slabs as being flat. With fire exposure only at the bottom, slabs are normally discretised as horizontal layers of thin strips of concrete and reinforcing, as shown in Fig. 7.12(b). Reinforcing bars are typically modelled as thin steel layers (a smeared mesh). These layers can also be modified to act only in one direction. Different stress-strain relationships can be specified for each layer, based on their unique temperatures. Cracking of concrete is typically distributed over the surface of the element rather than being concentrated at specific points—this approach is known as the smeared cracking approach.

There are three different ways to transform the original slab cross section in Fig. 7.12(a) into the discretised flat form in Fig. 7.12(b). This can be achieved by:

1. Modelling the full depth of the slab
2. Modelling the average (or effective) depth of the slab
3. Modelling the thin continuous depth of the slab (above the trough)



**Fig. 7.12** Modelling composite slabs with shell elements. (a) Profile of a Hibond composite slab. (b) Layered shell element



**Fig. 7.13** Options for modelling composite slabs in fire conditions: (a) full depth; (b) average depth; and (c) thin continuous depth

The three approaches are schematically explained in Fig. 7.13. A full-depth flat slab is stiffer in bending than the profiled slab in Fig. 7.12(a). Hence modelling with option 1 requires a reduction of bending stiffness in the direction parallel to the ribs. This is achieved by using what is known as an effective stiffness approach [42] which assigns relative stiffnesses to both directions to effectively mimic the different bending stiffnesses. Option 2 generates an equivalent flat slab that has the same overall bending stiffness as the full composite cross section, the same in both directions. Annex D of Eurocode 4 Part 1.2 [43] provides a calculation method to determine the effective depth, based on the original slab profile (either trapezoidal or re-entrant). Option 3 is the most conservative. It requires that only the top continuous concrete (above the trough) is discretised as a flat slab. This option has the highest reinforcing temperatures and the lowest bending stiffness, ensuring that the design would be appropriate since the real stiffness will be greater and the actual reinforcing temperatures (in the parts above the ribs) will be lower.

### 7.3.6 *Influence of Key Design Parameters*

A numerical study was conducted to investigate the effects of reinforcement ratios on slab panel capacities in fire [26]. The study examined the recent improvements in the Bailey method in comparison to Vulcan, the University of Sheffield's specialist fire engineering software. The comparison shows that, for smaller reinforcement mesh sizes, the Bailey method is conservative, but that it gives very optimistic slab panel capacities with high reinforcement ratios. Vulcan, on the other hand, shows modest increases in capacity with increasing reinforcement size, even when the supporting edge beams are assumed to remain intact throughout fire exposure.

Further investigations carried out with a larger variation of mesh sizes have confirmed the disproportionate increase in slab panel capacity predicted with larger reinforcement meshes by the Bailey-BRE method, especially for small panels. Vulcan investigations have further revealed that higher reinforcement mesh sizes are required for large panels, and when higher fire resistance times are needed on small-sized panels. An investigation into the relationship between reinforcement mesh sizes and slab dimensions has also shown that higher tensile tractions increase with increasing reinforcement and larger slab spans.

The study has therefore found that, even with the recent advances of the Bailey-BRE method, it loses conservatism where higher reinforcement ratios are concerned. It has also been found that larger panels require higher reinforcement areas to generate sufficient tensile capacity, while higher reinforcement mesh sizes are only required by small panels when higher fire resistances are required.

Another numerical study using the finite element software LS-DYNA also proved that the increased concrete cover and reinforcement ratio significantly delayed the failure of slabs exposed to fire [44]. However, the use of the increased reinforcement ratio is recommended, since it can not only reduce the deflection but even prevent the runaway collapse of slabs. The idea was supported by other research which showed that both reinforcement continuity over the supporting edge beams and the presence of interior beams can reduce deflections and greatly enhance the load-bearing capacity of these slab-beam systems. The observed enhancement factors were 1.96, 2.55, and 1.54 above the yield-line capacity in three different model scenarios [40].

In addition, an opposite opinion was suggested in relation to slab thickness which is based on the related experimental results [45]. It was observed that thinner slabs actually led to less compressive membrane action and higher loading capacities once the tensile membrane range was reached.

Finally, the recent research also found that the reinforcement along the short span played a key role in the load-bearing capacity of slabs at elevated temperature. So, it suggested to place more reinforcement along the short span to enhance the tensile membrane action and thus prevent the failure of slabs [44].

## 7.4 Performance of Structural Connections

Steel connections act as links between key structural elements in steel and composite structures. The common connection types include beam-to-beam and beam-to-column connections. Traditionally, connections are considered as less vulnerable structural members in fire since (a) the same level of structural fire protection is applied to connections as other structural members and (b) there is lower rate of temperature increase due to connections' relatively high mass and low-exposed surface area. However, connections could become the weakest spots at elevated temperature, as unveiled by large-scale fire tests and tragic events such as the collapse of World Trade Center Building 7 [46].

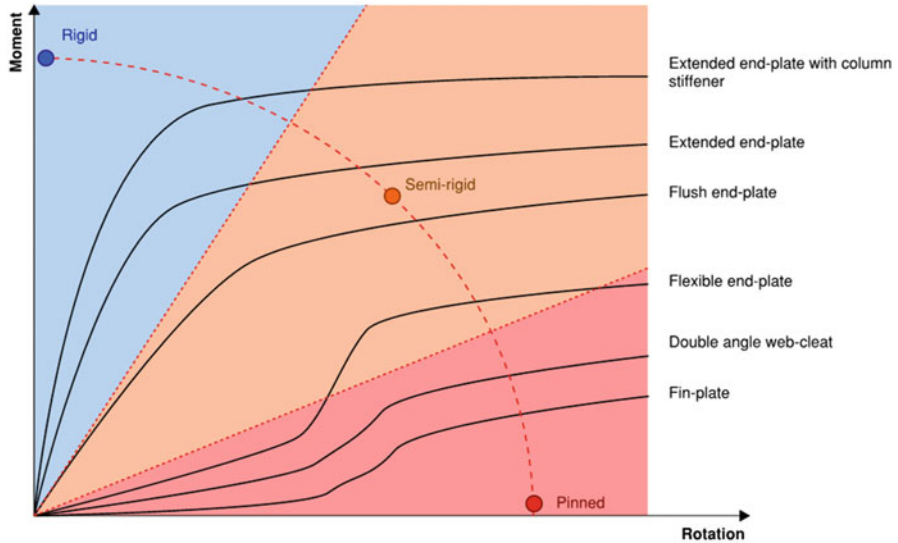
Conventionally, connections are solely designed and studied under ambient temperature in terms of their moment-rotation behaviour and are often regarded as less important than other structural members. With the improved understating of a connections' role and behaviour through investigations, more focus was paid to connections, leading to the publication of BS EN 1993-1-8 [1], which is dedicated to steel connection-related topics. Recent studies have established the significance of connection ductility on frame response at elevated temperature, which is distinctly important in keeping structural integrity in the event of a fire. BS EN 1993-1-2 [8] Annex D provides a simple calculation method to estimate the resistance of connections at high temperature. This Eurocode approach employs temperature-dependent strength reduction factors for bolts and welds with a simple method of estimating component temperatures.

This section aims to provide introductory information on connections in fire. For ambient temperature properties, behaviours and designs, thorough explanations can be found in Steel Designers' Manual [47].

### 7.4.1 Classifications of Connections

Steel connections can be classified based on various criteria, e.g. strength, rigidity/ductility/flexibility. In terms of structural fire behaviour, the ductility of the connections is the main criterion to consider. Theoretically, connections are often classified into three main categories based on their moment-rotation behaviour (rotational stiffness, rotational ductility and moment capacity) as shown in Fig. 7.14:

- Simple (pinned) connections—connections that only transmit end shear, and their resistance to moments is negligible. Thus, this type of connection can rotate freely but cannot move axially. Common types are fin plate, flexible end plate and web cleat.
- Ductile (semi-rigid) connections—connections that can partially transmit both end shear and moment. This type of connection can provide both rotational and axial ductility. Common types are flush end plate, and top and seat angle with double web angle.



**Fig. 7.14** Conventional connections with stiffness classification adapted from [39]

- Rigid connections—connections that transmit both moment and end shear wholly. This type of connection does not have any axial or rotational ductility. Common types are welded, extended end plate and extended end plate with column stiffener.

To simplify the analysis and the design process, connections are often considered as either extremely rigid or extremely flexible. However, all connections have certain degrees of axial and rotational ductility, which may have various levels of impact on global frame behaviour in fire. Therefore, it is essential for structural fire engineers to take the ductility provided by the connections into consideration when trying to understand frame response at elevated temperature.

### 7.4.2 Fire Effects on Connections

In the event of a fire, the global frame response is closely linked to the behaviour of connections. When excessive axial and rotational deformations occur at high temperature, the connections need to be robust enough to provide structural integrity.

Typically, connections are designed for the ultimate limit state at ambient temperature. When the connections are under fire attack, the force scenario changes significantly and becomes much more complicated than at ambient temperature. The forces that the connections experience undergo several phases in fire, for example:

- At the early stage of a fire, the connections experience compressive forces generated by beam thermal expansion, since the heated beam is usually restrained by the adjacent colder structures surrounding it.
- While the temperature increases, a gradual reduction in compression on the connections is often observed. This is the result of material strength and stiffness degradation causing the beam to sag to a large deflection.
- As the temperature continues to increase to very high temperatures, the connections are subject to tensile forces as beams pull inwards. This is caused by the beam losing almost all its bending stiffness, which makes it hang in catenary action between the connections.
- If the fire decays and the frame enters into a cooling stage from a high temperature before the connection fails, the connections may be pulled inwards further than at high temperatures and are subject to an even higher tensile force. This large tensile force is normally induced very quickly, generated by thermal contraction, which itself is caused as rapid material cooling and stiffening occur. Therefore, even if the connections survive the heating phase of a fire, they may fail during the cooling phase. This can lead to progressive collapse, which may put the lives of firefighters and rescue workers at significant risk.

There are three categories of connection failures in fire, similar to at ambient temperature, which are connector failure, connected component failure and a combination of both. Connectors, often structural steel bolts, may fail under a range of scenarios including shear, bearing, tension and bending, or could fail because of thread stripping. Connected parts may fail due to shear, bearing and tension.

The temperature distribution of the connection with respect to time in a fire is complex. Steel has high thermal conductivity, but with the significant thermal mass present at the connections and the complicated geometry, some components heat up slower than the others. In BS EN 1993-1-2 [8], the temperature of the connection is dependent on the local massivity factors,  $A/V$ , of the connection's components. To estimate the temperature, the expressions below which are based on the depth of the beam can be used:

Depth of the beam  $\leq 400$  mm

$$\theta_h = 0.88\theta_o[1 - 0.3(h/D)] \quad (19)$$

Depth of the beam  $> 400$  mm

and  $h \leq \frac{D}{2}$

$$\theta_h = 0.88\theta_o \quad (20)$$

and  $h > \frac{D}{2}$

$$\theta_h = 0.88\theta_o[1 + 0.2(1 - 2h/D)] \quad (21)$$

where

$\theta_h$ —Temperature at height  $h$  (mm) of the steel beam

$\theta_o$ —Bottom flange temperature of the steel beam remote from the joint

$h$ —Height of the component being considered above the bottom of the beam in mm

$D$ —Depth of the beam

Connections usually are made up of connectors, often structural steel bolt assemblies (often made up of bolts, nuts and washers) and connected parts. Depending upon the type of connections, connected parts can be plates, including end plates, fin plates or stiffeners, or angles. Usually, connected parts are made of structural steel, whose material behaviour under high temperature has been discussed in Sect. 7.1.1. Similarly, structural steel bolt assemblies and welds soften, losing their stiffness and strength gradually with the increasing temperature. A set of strength reduction factors,  $k_{b, \theta}$  for bolts and  $k_{w, \theta}$  for welds, are provided in Annex D of BS EN 1993-1-2 [8] to describe this degradation and are reproduced in Fig. 7.15 with a comparison to the structural steel reduction factor. Like structural steel, the strength of bolts and welds suffers from significant losses at around 300 and 700 °C, which is reflected on the sudden change of the gradients of the reduction factors.

For structural bolts, the reduction factor  $k_{b, \theta}$  is used for predicting the shear, bearing and tensile resistances of the bolts under elevated temperature. These resistances can be determined from the following equations:

$$\text{Shear resistance } F_{v, t, Rd} = F_{v,Rd} k_{b,\theta} \frac{\gamma_{m2}}{\gamma_{m,fi}} \quad (22)$$

$$\text{Bearing resistance } F_{b, t, Rd} = F_{b,Rd} k_{b,\theta} \frac{\gamma_{m2}}{\gamma_{m,fi}} \quad (23)$$

$$\text{Tensile resistance } F_{ten, t, Rd} = F_{t,Rd} k_{b,\theta} \frac{\gamma_{m2}}{\gamma_{m,fi}} \quad (24)$$

where

$F_{v, t, Rd}$ —Fire design resistance of bolts loaded in shear

$F_{b, t, Rd}$ —Fire design resistance of bolts loaded in bearing

$F_{ten, t, Rd}$ —Fire design resistance of bolts loaded in tension

$F_{v, Rd}$ —Design shear resistance of the bolt

$F_{b, Rd}$ —Design bearing resistance of the bolt

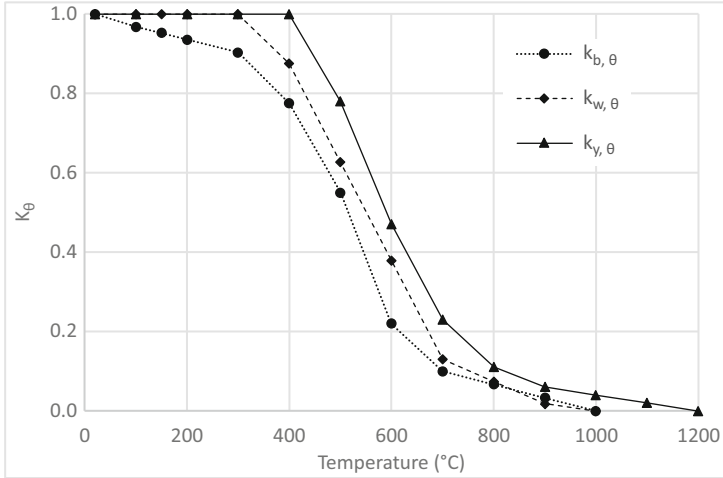
$F_{t, Rd}$ —Design tensile resistance of the bolt

$k_{b, \theta}$ —Bolt strength reduction factor dependent on temperature

$\gamma_{m2}$ —Partial safety factor at ambient temperature

$\gamma_{m, fi}$ —Partial safety factor at high temperature

For welds, their strength is calculated in the same fashion as for the bolts. There are two common types of welds that are used in steel connections, which are fillet welds and butt welds. Fillet welds, which is the more common type of weld used in steel connections, are to join two perpendicular pieces together, for example, the beam and the end plate. Butt welds are often used to connect two pieces in-line, for



**Fig. 7.15** Reduction factors of steel and connection components at elevated temperature [3]—subscript: b = bolts, w = weld and y = steel yield strength

example joining two pieces of rolled steel sections to form a longer beam. The weld reduction factors can be used directly for fillet welds. For butt welds, the reduction factors of structural steel should be used for up to 700 °C, and the weld reduction factors can be used for butt welds subject to temperatures higher than 700 °C.

$$\text{Weld resistance } F_{w, t, Rd} = F_{w,Rd} k_{w,\theta} \frac{\gamma_{m2}}{\gamma_{m,fi}} \tag{25}$$

where

- $F_{w, t, Rd}$  Fire design resistance of welds in fire
- $F_{w, Rd}$  Design tensile resistance of welds
- $k_{w, \theta}$  Weld strength reduction factor dependent on temperature
- $\gamma_{m2}$  Partial safety factor at ambient temperature
- $\gamma_{m, fi}$  Partial safety factor at high temperature

### 7.4.3 Simulation of Connection Performance

Connection behaviours at elevated temperature are traditionally studied through experiments. However, it is not always feasible to carry out many tests due to significant costs in finance, time, labour, and resource. To aid the comprehension of connection behaviours in fire, a wide range of modelling approaches have been adopted, which can be classified into three main categories:



- Curve-fitting method.
- Finite element simulation.
- Component-based method.

Curving-fitting method is often referred to as the empirical approach, which typically involves generating mathematical models to fit experimental results. The proposed mathematical models, usually made up of physical dimension-related parameters, are then used to carry out further studies on the connections. Some research studies [48–50] were conducted using this method at the early stage of high-temperature connection modelling. Compared with the other methods, curve fitting is relatively simple, but the major flaw is that experimental data is required as a starting point. This means that only connections with similar physical geometry, heating and loading conditions, and material properties as those in the experiments can be modelled. Any changes are very likely to have a major impact on the reliability of the modelling results. Due to the high cost of running experiments, the number of investigations feasible is limited with this approach.

Finite element simulation was developed in parallel with the curve-fitting method. Commercial packages, e.g. *ABAQUS* and *ANSYS*, were adopted and widely used among researchers to build connection models without the assistance of experimental data. Connections are modelled as assemblies of three-dimensional components, whose non-linear material and geometrical properties at elevated temperature can be customised. The interactions between components can also be captured, making the simulation results much more realistic. An example comparison between finite element modelling visualisation and experimental results is shown in Fig. 7.16. A wide range of connection types and properties were able to be investigated to aid the understanding of steel connections in fire [51, 53–61]. Undoubtedly, a finite element modelling approach can provide accurate predictions of high-temperature connection behaviours without the need to conduct experiments beforehand. However, it needs to be highlighted that this approach is often limited to localised or small-scaled models because of the length of computational time and sensitivity of input parameters.

The component-based method approach treats the connections as an assembly of several axial springs. These springs represent their respective active component of the connections in tension, compression or shear. An example of a flush end plate connection in component-based model is illustrated in Fig. 7.17. For each active component, its physical configurations, ambient and high-temperature behaviours and loading-unloading responses are captured to generate the non-linear spring properties. This approach is included in BS EN 1993-1-8 [1]. After it was first proposed in the 1980s [62], the component-based method was developed, refined and adapted for a wide range of connection types, which enabled investigations of connection behaviour in fire to be carried out at relatively low cost [39, 48, 50, 61, 63–74]. The extensive studies enhanced the understanding of connections' important role in global frame response in fire. The component-based method, compared with the other approaches, can provide more accurate representations of connections and global frame in fire without prolonged computational time.

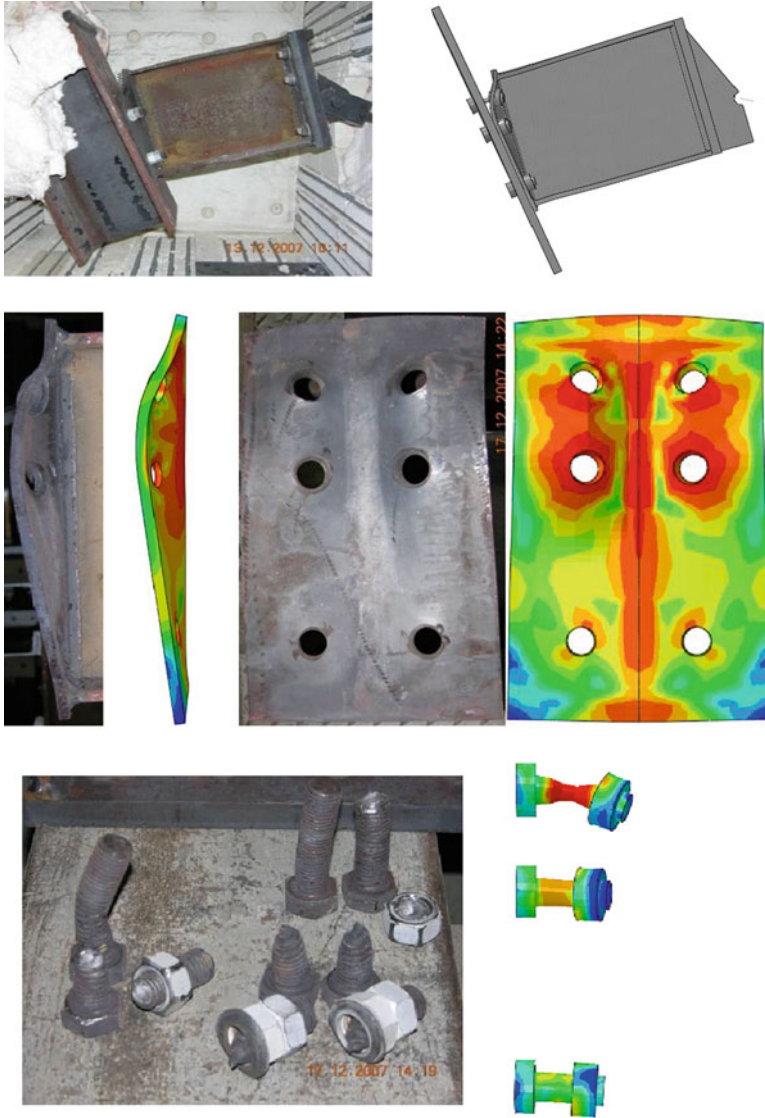
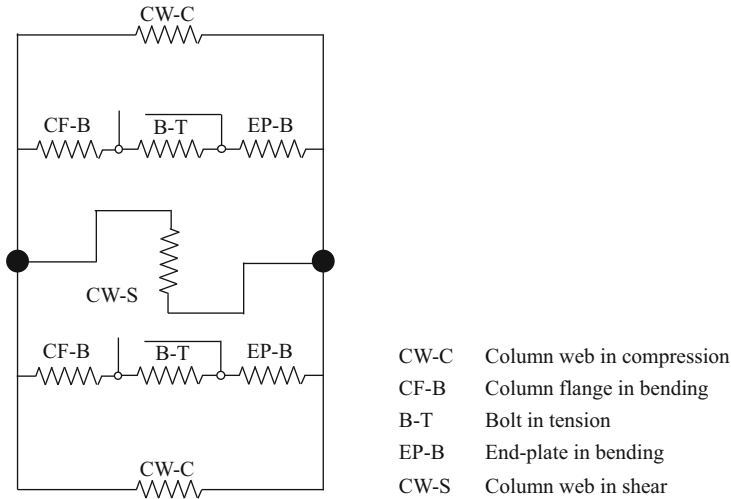


Fig. 7.16 Deformation comparisons between finite element modelling and experimental results [51, 52]

These modelling methods theoretically aim to provide realistic and reliable representations of high-temperature connection behaviours. However, it should be highlighted that the reliability of the results is highly dependent on the development of the method, the accuracy of the input parameters, the interpreting of the results and a wide range of other criteria. Therefore, any simulation methods and results



**Fig. 7.17** Flush end plate connection in component-based method

should be considered carefully and should be analyzed in conjunction with the input parameters and assumptions to fully enable correct interpretation of the results.

## 7.5 Design Philosophies

Three design philosophies are discussed in this section to provide the designer a level of latitude to design structures for fire. The limit state design method is often referred to as ‘DCR’ calculations (demand-to-capacity) and is similar to conventional structural engineering design for other hazards. The structural system response simulation method permits the structural fire engineer to demonstrate system-level strength and stability by capturing indeterminacy and load redistribution using computational resources (notably finite element software). The member utilisation method hypothesises critical failure temperatures of structural system elements based upon the ratio of their mechanical loading under fire conditions divided by their design mechanical loading.

It should be noted that North American standards and related guidance documents (e.g. ASCE Manual of Practice No. 138 [75]) do not permit the member utilisation method. Notably, ASCE 7 Section E.3 requires either a limit state design approach or the simulation of structural system response [3]. In all cases, ASCE 7 requires for the structural fire engineer (with verification by the structural engineer of record, if the two are not the same) to assess and judge the structural system response by tracing all structural loads to ground while accounting for all structural limit states, potential modes of instability and any second-order phenomena.

### 7.5.1 *Limit State Design*

Limit state hand calculations may be conducted in accordance with Eurocode 3 or AISC 360 Appendix 4, which is assumed to provide enough conservatism for complex behaviours to be neglected (e.g. non-uniform column heating in conjunction with lateral loading from connecting girder expansion). Accordingly, ambient strength reduction factors in conjunction with temperature-dependent material strength reduction retention factors should be used to determine DCR ratios for all applicable limit states. Granted, AISC 360 Appendix 4 should not be relied upon exclusively as described in Sect. 7.1.1 above. Notably, AISC 360 Appendix 4 does not contain affirmative guidance for the limit states design of structural steel connections under fire conditions.

When conducting a limit state design, the structural fire engineer must perform the following in accordance with applicable industry standards and guidance based on the derived temperature histories (see Chap. 5 for more information):

- Recognise structural boundary conditions and idealise end conditions as pinned or fixed, or with appropriate spring stiffness using conservative judgment.
- Recognise the relevant loads acting on the structural system.
- Assess the design loading level based on the required load combinations of the applied structural regulations.
- Consider the reduction of structural material mechanical properties using appropriate reduction factors.
- Trace all structural loads to ground while accounting for all structural limit states.
- Assess and judge global and local structural system capacities and employ the appropriate margins of safety for various potential failure modes.
- Justify and defend the structural calculations to a controlling body of structural engineers with a similar level of rigor and liability as for other structural loads (e.g. blast, wind and seismic).

### 7.5.2 *Structural System Response Simulation*

Simulation of structural response should include geometric non-linearity (large deflection theory) and non-linear temperature-dependent material behaviour, which would adequately capture any global buckling modes. Explicit or implicit finite element analysis techniques may be employed for simulations. If an explicit solver is used, artificial dynamic effects should be minimised to a negligible level by limiting the mechanical loading rate. If an implicit solver is used, parasitic strain energy should be minimised to a negligible level in the case that viscous damping is introduced to assist with model convergence.

When conducting a structural system response simulation, framing members may be represented by beam-type elements with a torsional/warping degree of freedom and specified beam camber may be neglected. The concrete slab may be represented

by shell-type elements with multiple integration points through its represented thickness. The associated steel reinforcement may be represented as part of these shell elements using a layered rebar technique.

When connections are considered in an ideal sense (pinned or fixed) within a structural system response simulation, a separate evaluation of the connections should be conducted using the limit state design method discussed in Sect. 7.5.1 above. This evaluation may be conducted using material strength retention factors from Eurocode 3 or AISC 360. Also, the forces acting on connections may be extracted from a simulation model and/or conservatively derived from first principles. Where slab reinforcement is discontinuous, inadequately lapped at the connection region, or absent, or its capacity is exceeded, the contribution of the slab to moment resistance at a connection should be neglected during the heating phase. During the cooling phase, resistance to thermal contraction may be evaluated based on the ambient temperature capacity of steel connections and slab reinforcement.

As an alternative to the approach described above, steel connections may be explicitly evaluated by representing each as an array of non-linear springs in series/parallel as previously described in this chapter. In this case, the connections would be qualified based upon their ability to support the forces developed in a model. Specifically, springs acting in the plane of the connecting beam should have non-linear behaviour assigned, and a gap element should represent any contact between the beam lower flange and the connecting girder/column during the heating phase. The stiffness of springs in other degrees of freedom should be considered as ideally rigid.

Due to the metal decking geometry (flutes/troughs), the concrete thickness is often variable in a periodic fashion. For simulation of structural response, only the top concrete (constant) thickness (i.e. above the deck flutes) should be considered. Otherwise, the anisotropic geometric properties of the slab may be accounted for explicitly. The thermal and structural performance of the metal decking itself may be neglected, since it would likely delaminate from the concrete in the early stages of a fire. However, the metal decking may be relied upon to provide lateral restraint to floor beams.

Generally, reinforcement continuity across a given floor is beneficial to its performance under fire exposure. If reinforcement continuity is not provided over primary member framing (and if the tension strength of the concrete is exceeded), the degree of freedom for bending moment should be released within the concrete slab shell elements, along the lines of girder framing. This can be accomplished by specifying discontinuous (coincident) nodes within the shell element mesh if applicable. When reinforcement continuity is provided, the strength of this reinforcement should be analysed in conjunction with steel connections for their ability to resist the bending moment demand. If the reinforcement (and concrete) is expected to fail, the degree of freedom for bending moment should be released within the given model.

When conducting a structural system response simulation, the structural fire engineer must perform the following in accordance with applicable industry standards and guidance based on the derived temperature histories (see Chap. 5 for more information):

- Recognise structural boundary conditions and define the scope of the structural analyses.
- Recognise the relevant loads acting on the structural system.
- Assess the design loading level based on the required load combinations of the applied structural regulations.
- Formulate temperature-dependent mechanical properties of structural materials (see Sect. 7.1 above).
- Evaluate appropriate structural performance criteria for the analysis and appropriate engineering methods for structural calculations.
- Appraise appropriate structural models that can account for the relevant structural responses.
- Trace all structural loads to ground while accounting for all structural limit states, potential modes of instability and any second-order phenomena.
- Compare the results of structural analyses with performance criteria and evaluate the margins of safety.
- Justify and defend the structural analyses to a controlling body of structural engineers with a similar level of rigor and liability as for other structural loads (e.g. blast, wind and seismic).

### 7.5.3 Member Utilisation Method

Where permitted and in cases that structural elements are expected to have a uniform temperature distribution, verifications can be undertaken in the temperature domain, applying the concept of critical (also known as limiting) temperature.

In the temperature domain, the relevant limit state is

$$\theta_{a,cr} \geq \theta_d \quad (26)$$

with  $\theta_{a, cr}$  being the critical temperature and  $\theta_d$  the design temperature. The critical temperature is a function of the member utilisation ( $\mu_0$ ) and the failure mode of the member, e.g. pure bending, tension, compression, flexural buckling and lateral torsional buckling.

The utilisation is generally defined relatively to the ambient (20 °C) member resistance. As given by Franssen and Vila Real [76], the utilisation can be expressed as

$$\mu_0 = \frac{E_{fi,d}}{R_{fi,d,0}} \quad (27)$$

with  $E_{fi, d}$  being the design effect of actions in the case of fire and  $R_{fi, d, 0}$  the design resistance at time zero, i.e. 20 °C.

### 7.5.3.1 Beams Not Undergoing Buckling and Tension Members

Where the load-bearing capacity in a fire situation is directly proportional to the effective yield strength, i.e. tension members and beams failing under pure bending, the utilisation can be directly related to the proportion of yield strength that must be retained upon heating ( $k_{y, \theta}$ ):

$$k_{y, \theta} = \mu_0 = \frac{E_{f_i, d}}{R_{f_i, d, 0}} \quad (28)$$

It follows that if a relationship between member temperature and retained proportion of yield strength is known, a critical temperature can be defined for this specific case. The reduction in effective yield strength given in EN 1993-1-2 can be approximated by

$$k_{y, \theta} = \left[ 0.9674 \left( e^{\frac{\theta - 482}{39.19}} + 1 \right) \right]^{-1/3.833} \quad (29)$$

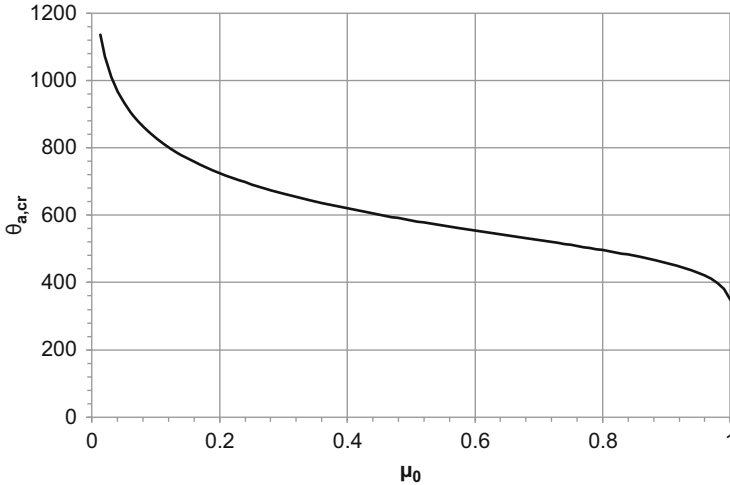
which when rearranged in terms of  $k_{y, \theta}$  gives the critical temperature relationship in EN 1993-1-2:

$$\theta_{a, cr} = 39.19 \ln \left[ \frac{1}{0.9674 \mu_0^{3.833}} - 1 \right] + 482 \quad (30)$$

It should be noted that  $\mu_0$  must not be taken to be less than 0.013. Figure 7.18 plots the relationship between utilisation and critical temperature for cases where load-bearing capacity is directly proportional to effective yield strength.

### 7.5.3.2 Other Members and Default Critical Temperatures

The relationship for critical temperatures applicable to beams not undergoing buckling or tension members does not hold for buckling cases as there is further dependence upon the degradation of elastic modulus. This necessitates a specific evaluation of the resistance at each temperature step. In lieu, it is common to adopt 'default' limiting temperatures, e.g. as adopted in the UK NA to EN 1993-1-2 and the French and Belgian ENV versions of Eurocode 3 Part 1.2 (as given in Franssen & Vila Real [76]). Examples are given in Table 7.3.



**Fig. 7.18** Utilisation vs. critical temperature for cases where load-bearing capacity in fire is proportional to effective yield strength, as adopted in EN 1993-1-2

### 7.5.3.3 Application of Critical Temperature in Evaluating Passive Fire Protection Requirements

In combination with the design fire resistance period, critical temperatures are adopted to determine if passive fire protection is necessary and, if so, what thickness of protection is appropriate to ensure that the critical temperature is not exceeded after a defined period of furnace exposure.

By way of an example, a beam of profile HEB 140 B is required to achieve 60-min structural fire resistance, as defined by the project's structural engineer/fire safety engineer. The beam has a section factor ( $H_p/A$ ) of  $88 \text{ m}^{-1}$ , when calculated according to the EN 1993-1-2 and incorporating the shadow effect. This assumes three-sided exposure, as the beam supports a concrete slab. The beam has a utilisation in the fire condition  $\mu_0$  of 0.6. With reference to Table 7.3, the UK NA to EN 1993-1-2 would define the critical temperature to be either 587 or 621 °C, depending upon whether the beam is to remain unprotected or protection is to be applied.

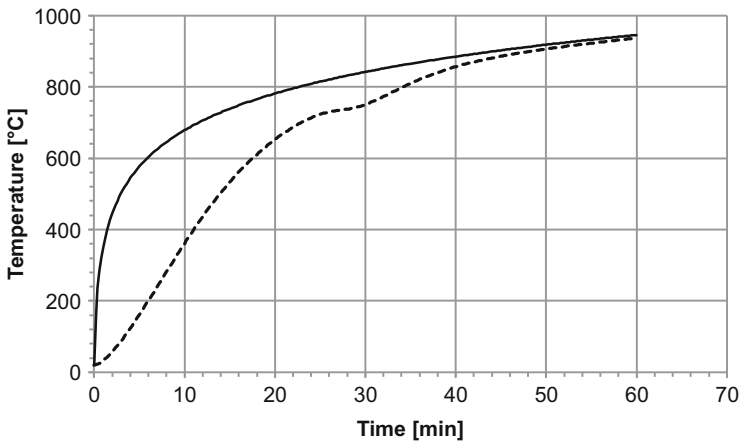
Figure 7.19 shows the relationship between time and temperature for the unprotected section, when exposed to 60 min of standard fire exposure. This is calculated using the lumped capacitance method of EN 1993-1-2, as discussed in Chap. 5.

From Fig. 7.19, it is seen that the unprotected section temperature after 60 min is c. 937 °C. This is relative to a critical temperature of 621 °C in the unprotected case, i.e. the section cannot achieve 60-min fire resistance inherently. For completeness,



**Table 7.3** ‘Default’ limiting temperatures for different members (various sources)

Source	Member	$\mu_0$ [-]						
		0.7	0.6	0.5	0.4	0.3	0.2	
UK NA to EN 1993-1-2	Compression members in function of ambient non-dimensional slenderness	$\bar{\lambda} = 0.4$	485	526	562	598	646	694
		$\bar{\lambda} = 0.8$	451	510	546	583	627	678
		$\bar{\lambda} = 1.2$	422	502	538	573	614	668
		$\bar{\lambda} = 1.6$	411	500	535	571	610	665
	Protected beams supporting concrete slabs		558	587	619	654	690	750
	Unprotected beam supporting concrete slabs		594	621	650	670	717	775
	Tension members		526	558	590	629	671	725
French & Belgian ENV 1993-1-2	Non-buckling beams (isostatic)		540 (independent of utilisation)					
	Columns and beams undergoing lateral torsional buckling		500 (independent of utilisation)					
	Tension members		540 (independent of utilisation)					



**Fig. 7.19** Time-temperature relationship for a HEB 140 B beam, exposed on three sides and subject to 60-min standard fire exposure

Fig. 7.19 indicates that the unprotected section exceeds 621 °C after 18.5 min, implying a corresponding inherent period of fire resistance.

Table 7.4 gives an illustrative/mock multi-temperature analysis (MTA) for a fire protection coating, where the applied protection thickness (microns) varies in function of the section factor ( $H_p/A$ ) and critical temperature. Typically, an MTA would be produced for each fire resistance period increment (30, 60, 90 min, etc.), and exposure condition (three sided vs. four sided), with this case intended to be illustrative of 60-min and three-sided exposure.

**Table 7.4** Demonstration of multi-temperature analysis for intumescent giving protection thickness (microns) at 60 min

Hp/A [m <sup>-1</sup> ]	Critical temperature [°C]							
	450	500	550	600	620	650	700	750
30	600	500	359	300	300	300	300	300
....								
50	1250	1050	725	600	550	475	300	300
55	1325	1150	825	700	625	550	350	300
60	1400	1225	950	825	700	600	425	400
....								
90	1850	1750	1200	1175	1100	875	720	700
....								
120	2300	2200	1450	1350	1300	1125	975	950

The unprotected element evaluation confirms that the critical temperature is exceeded well before (18.5 min) the target fire resistance time of 60 min. Therefore, passive fire protection is to be applied. With reference to Table 7.4, a Hp/A of c. 90 m<sup>-1</sup> and critical temperature of 587 °C (for the protected beam case in Table 7.3) result in an applied protection thickness of between 1175 and 1200 microns.

The assessment process for the production of MTAs is outside the scope of this handbook and is discussed further in, for example, EN 13381-8 [77].

## References

1. CEN. (2005b). *BS EN 1993-1-2 Eurocode 3: Design of steel structures - part 1-8: Design of joints*. British Standards Institution.
2. American Institute of Steel Construction (AISC). (2016). AISC Standard 360-16, Appendix 4, Chicago, IL.
3. ASCE/SEI 7-16: Minimum Design Loads and Associated Criteria for Buildings and Other Structures, American Society of Civil Engineers: Structural Engineering Institute, 2016.
4. Elghazouli, A., Cashell, K., & Izzuddin, B. (2009). Experimental evaluation of the mechanical properties of steel reinforcement at elevated temperature. *Fire Safety Journal*, 44(6), 909–919.
5. Harmathy, T. (1967). A comprehensive creep model. *Journal of Basic Engineering*, 89(3), 496–502.
6. Zhao, B., & Kruppa, J. (1997). Fire resistance of composite slabs with profiled steel sheet and of composite steel concrete beams Part 2: Composite beams. Final report EUR 16822. ISSN 10185593.
7. Eurocode 1: Basis of Design and Actions on Structures, Part 1.2: Actions on Structures – Actions on Structures Exposed to Fire, ENV 1991-1-2, CEN, Brussels, Belgium, 2001.
8. CEN. (2005a). *BS EN 1993-1-2 Eurocode 3: Design of steel structures - part 1-2: Actions on structures exposed to fire*. British Standards Institution.

9. Gardner, L., & Nethercot, D. A. (2011). *Designers' Guide to Eurocode 3*, Thomas Telford, ISBN: 9780727741721
10. Phan, L. T., McAllister, T. P., Gross, J. L. and Hurley, M. J. (2010). Best Practice Guidelines for Structural Fire Resistance Design of Concrete and Steel Buildings NIST Technical note 1681. *National Institute of Standards and Technology, Technology Administration, US Department of Commerce, Gaithersburg, MD*
11. Ozyurt, E., & Wang, Y. C. (2015). Effects of truss behaviour on critical temperatures of welded steel tubular truss members exposed to uniform fire. *Engineering Structures*, 88, 225–240.
12. Ozyurt, E., & Wang, Y. C. (2016). Effects of non-uniform temperature distribution on critical member temperature of steel tubular truss. *Engineering Structures*, 116, 95–106.
13. Chen, C. K., & Zhang, W. (2012). Comparative experimental investigation on steel staggered-truss constructed with different joints in fire. *Journal of Constructional Steel Research*, 77, 43–53.
14. Lin, S. M., Du, Y. and Fu, J. X. (2014). Design strategies of fire safety for steel roof trusses exposed to localised fire. In *8th International conference on structures in fire, Shanghai, China* (pp. 163–170)
15. Newman, G. N., Robinson, J. T., & Bailey, C. G. (2006). *Fire safe design: A new approach to multi-storey steel-framed buildings* (2nd edn.), Steel Construction Institute Publication 288.
16. Newman, G., Robinson, J., and Bailey, C. G. (2000). 'SCI P288 A new approach to multi-storey steel framed buildings', Steel Construction Institute, Ascot, SCI P288.
17. BSI. (1990a). *Structural use of steelwork in building – Part 1: Code of practice for design in simple and continuous construction: hot rolled sections*. British Standards Institute.
18. BSI. (1990b). *Structural use of steelwork in building – Part 3: Design in composite construction*. British Standards Institute.
19. CEN (1994). *Eurocode 4: Design of Composite Steel and Concrete Structures – Part 1.2: General Rules – Structural Fire Design (Draft)*, European Committee for Standardization.
20. Foster, S., Chladna, M., Hsieh, C. B., & I and Plank, R. (2007). Thermal and structural behaviour of a full-scale composite building subject to a severe compartment fire. *Fire Safety Journal*, 42, 183–199.
21. BSI. (2003). *Structural use of steelwork in building—Part 8: Code of practice for fire resistant design*. British Standards Institute.
22. Huang, Z., Burgess, I. W., & Plank, R. J. (2002). Modelling of six full-scale fire tests on a composite building. *The Structural Engineer*, 80(19), 30–37.
23. Martin, D. and Moore, D. (1999). *The behaviour of multi-storey steel framed buildings in fire: A European Joint Research Programme*. Cardington Test Report, prepared by British Steel Plc.
24. Park, M. E., (1964). Tensile membrane behaviour of uniformly loaded rectangular reinforced concrete slabs with fully restrained edges, Magazine of Concrete Research, ICE Publishing. <https://doi.org/10.1680/macr.1964.16.46.39>
25. Lim, L. (2003). *Membrane action in fire exposed concrete floor systems*, PhD Thesis, University of Canterbury, New Zealand
26. Abu, A. (2009). *Behaviour of composite floor systems in fire*. PhD thesis, University of Sheffield, UK
27. Bailey, C. G., & Moore, D. B. (2000). The structural behaviour of steel frames with composite floor slabs subject to fire – Part 1 Theory. *The Structural Engineer*, 78(11), 19–27.
28. Bailey, C. G., & Moore, D. B. (2000). The structural behaviour of steel frames with composite floor slabs subject to fire – Part 2: Design. *The Structural Engineer*, 78(11), 28–33.
29. Hayes, B. (1968). Allowing for membrane action in the plastic analysis of rectangular reinforced concrete slabs. *Magazine of Concrete Research*, 20(65), 205–212.
30. Bailey, C. G., & Toh, W. S. (2007). Behaviour of concrete floor slabs at ambient and elevated temperatures. *Fire Safety Journal*, 42, 425–436.
31. Duchow, M. and Abu, A. K. (2014). *Collapse mechanisms of edge and corner slab panels in fire conditions*. Proceedings of the 8th International Conference on Structures in Fire, 11–13 June 2014, Shanghai, China, pp. 335–342.

32. Bailey, C. G. (2000). *Design of steel structures with composite slabs at the fire limit state*, Final Report No. 81415, prepared for DETR and SCI, The Building Research Establishment, Garston, UK
33. Bailey, C. G. (2001). Membrane action of unrestrained lightly reinforced concrete slabs at large displacements. *Engineering Structures*, 23, 470–483.
34. Bailey, C. G. (2003). Efficient arrangement of reinforcement for membrane behaviour of composite floors in fire conditions. *Journal of Constructional Steel Research*, 59, 931–949.
35. Bailey, C. G. (2004). Membrane action of slab/beam composite floor systems in fire. *Engineering Structures*, 26, 1691–1703.
36. Clifton, C. (2001). “Design of multi-storey steel framed buildings with unprotected secondary beams or joists for dependable inelastic response in severe fires.” Steel Design and Construction Bulletin 60, New Zealand Heavy Engineering Research Association (HERA), 1–58
37. Clifton, G. C. (2006). *Design of composite steel floor systems for severe fires*. HERA Report R4–131, Manukau City, Auckland.
38. Clifton, G. C., Gillies, A. G. and Mago N. (2010). *The slab panel method: design of composite floor systems for dependable inelastic response to severe fires*. Proceedings of the 6th International Conference on Structures in Fire (SiF’10), 2–4 June 2010, East Lansing, MI, USA, pp. 492–499
39. Taib, M., (2012). *The performance of steel framed structures with fin-plate connections in fire*, PhD Thesis: The University of Sheffield.
40. Nguyen, T., Tan, H., & Burgess, I. (2015). Behaviour of composite slab-beam systems at elevated temperatures: Experimental and numerical investigation. *Engineering Structures*, 82, 199–213.
41. Buchanan, A. H., & Abu, A. (2017). *Structural design for fire safety* (2nd ed.). John Wiley & Sons.
42. Huang, Z., Burgess, I. W., & Plank, R. J. (2000). Effective stiffness modelling of composite concrete slabs in fire. *Engineering Structures*, 22, 1133–1144.
43. CEN (2005c). *Eurocode 4: Design of composite steel and concrete structures—Part 1–2: General rules - Structural fire design*. EN 1994–1-2. European Committee for Standardization, Brussels.
44. Jiang, J., & Li, G. (2018). Parameters affecting tensile membrane action of reinforced concrete floors subjected to elevated temperatures. *Fire Safety Journal*, 96, 59–73. <https://doi.org/10.1016/j.firesaf.2017.12.006>
45. Botte, W., Gouverneur, D., Caspeepe, R., & Taerwe, L. (2015). Influence of design parameters on tensile membrane action in reinforced concrete slabs. *Structural Engineering International*, 25(1), 50–60. <https://doi.org/10.2749/101686614X14043795570174>
46. McAllister, T., Gann, R., Averill, J., Gross, J., Grosshandler, W., Lawson, J., McGrattan, K., Nelson, H., Pitts, W., Prasad, K., Sadek, F. (2008). Federal building and fire safety investigation of the world trade center disaster: Structural fire response and probable collapse sequence of world trade center building 7. NIST NCSTAR 1–9. National Institute of Standards and Technology, Gaithersburg, MD.
47. Davison, B., & Owens, G. (2012). *Steel designers' manual* (7th ed.). John Wiley & Sons.
48. Al-Jarbri, K. (1999). *The behaviour of steel and composite beam-to-column connections in fire*, PhD thesis: The University of Sheffield.
49. El-Rimawi, J., Burgess, I., & Plank, R. (1997). The influence of connection stiffness on the behaviour of steel beams in fire. *Journal of Constructional*, 43, 1–15.
50. Leston-Jones, L. (1997). *The influence of semi-rigid connections on the performance of steel framed structures in fire*, PhD thesis: The University of Sheffield.
51. Shi, R. (2017). *A simplified steel beam-to-column connection modelling approach and influence of connection ductility on frame behaviour in fire*, PhD thesis: The University of Sheffield.
52. Yu, H.-X., Burgess, I., Davison, J. & Plank, R. (2008). *Experimental investigation of the behaviour of flush end-plate connections in fire*. Singapore, Proceedings of Structures in Fire Conference, pp. 150–157.

53. Al-Jarbri, K., Seibi, A., & Karrech, A. (2006). Modelling of unstiffened flush endplate bolted connections in fire. *Journal of Constructional Steel Research*, 62, 151–159.
54. Augusto, H., Simoes da Silva, L., Rebelo, C., & Castro, J. (2016). Characterization of web panel components in double-extended bolted end-plate steel joints. *Journal of Constructional Steel Research*, 116, 271–293.
55. Dai, X., Wang, Y., & Bailey, C. (2010). Numerical modelling of structural fire behaviour of restrained steel beam-column assemblies using typical joint types. *Engineering Structures*, 32, 2337–2351.
56. Haremza, C., et al. (2016). Composite joints under MN at elevated temperatures. *Journal of Constructional Steel Research*, 124, 173–186.
57. Liu, T. (1996). Finite element modelling of behaviours of steel beams and connections in fire. *Journal of Constructional Steel Research*, 36(3), 181–199.
58. Liu, T. C. (1999). Moment-rotation-temperature characteristics of steel/composite connections. *Journal of Structural Engineering*, 125(10), 1188–1197.
59. Sarraj, M., Burgess, I., Davison, J., & Plank, R. (2007). Finite element modelling of steel fin plate connections in fire. *Fire Safety Journal*, 42, 408–415.
60. Selamet, S., & Garlock, M. (2014). Fire resistance of steel shear connections. *Fire Safety Journal*, 68, 52–60.
61. Spyrou, S. (2002). *Development of a component-based model of steel beam-to-column joints at elevated temperatures*, PhD thesis: The University of Sheffield.
62. Tschemmermegg, F., & Humer, C. (1988). The Design of Structural-Steel Frames under consideration of the nonlinear behavior of joints. *Journal of Constructional Steel Research*, 11(2), 73–103.
63. Block, F., Burgess, I., Davison, J. & Plank, R. (2004). *A component approach to modelling steelwork connections in fire: behaviour of column webs in compression*. Nashville, Tennessee, Proceedings of ASCE Structures Congress.
64. Block, F., Burgess, I., Davison, J., & Plank, R. (2007). The development of a component-based connection element for end-plate connections in fire. *Fire Safety Journal*, 42, 498–506.
65. Dong, G., Burgess, I. & Davison, J. (2011). *Component-Based Element for Endplate Connections in Fire*. Prague, Proceedings of Application of Structural Fire Engineering, pp. 195–200.
66. Dong, G., Burgess, I. & Davison, J. (2012). *Application of a general component-based connection element in structural fire analysis*. Qingdao, Proceedings of 11th Int. Conference on Steel, Space and Composite Structures.
67. Dong, G., Burgess, I., Davison, J., & Sun, R.-R. (2015). Development of a general component-based connection element for structural fire engineering analysis. *Journal of Structural Fire Engineering*, 6(4), 247–253.
68. Gentili, F., Costa, R. & Simoes da Silva, L. (2014). *Development of a simplified model for joints in steel structures*. Aveiro, Proceedings of 9<sup>o</sup> Congresso Nacional de Mecânica Experimental.
69. Hu, Y., Davison, J., Burgess, I., & Plank, R. (2009). Component modelling of flexible end-plate connections in fire. *International Journal of Steel Structures*, 9, 29–38.
70. Ramli-Sulong, N., Elghazouli, A., Izzuddin, B., & Ajit, N. (2010). Modelling of beam-to-column connections at elevated temperature using the component method. *Steel and Composite Structures*, 10(1), 23–43.
71. Shi, R., S-S, H., & JB, D. (2018). A simplified steel beam-to-column connection modelling approach and influence of connection ductility on frame behaviour in fire. *International Journal of High-Rise Buildings*, 7(4), 343–362.
72. Simoes da Silva, L., Santiago, A., & Real, P. (2001). A component model for the behaviour of steel joints at elevated temperatures. *Journal of Constructional*, 57, 1169–1195.
73. Sun, R., Burgess, I., Huang, Z., & Dong, G. (2015). Progressive failure modelling and ductility demand of steel beam-to-column connections in fire. *Engineering Structures*, 89, 66–78.

74. Yu, H.-X., Burgess, I., Davison, J., & Plank, R. (2009). Tying capacity of web cleat connections in fire, part 2: Development of component-based model. *Engineering Structures*, 31, 697–708.
75. ASCE/SEI (2018). Manual of Practice No. 138: Structural Fire Engineering, American Society of Civil Engineers: Structural Engineering Institute, Reston, VA.
76. Franssen, J., & VilaReal, P. (2010). Fire design of steel structures, ECCS – European Convention for Steelwork, ISBN 978-9147-099-0
77. EN 13381-8, Test methods or determining the contribution to the fire resistance of structural members: applied reactive protection to steel members, European Committee for Standardization, CEN, 2010.

# Chapter 8

## Timber Structures



Daniel Brandon, Danny Hopkin, Richard Emberley, and Colleen Wade

### 8.1 Introduction

Timber is an inherently sustainable material which is important for future global construction. In recent years many developments have been made in relation to timber technology and construction products. As the construction industry continues to look to construct more efficient, cost-effective, and sustainable buildings, a number of new engineered timber products have emerged which are principally manufactured off-site. These engineered wood products, such as cross-laminated timber (CLT), have permitted increasingly large, tall, and complex wooden structures to be conceived and delivered.

The renaissance of timber as a construction material, allied to its application in less common building forms, has led researchers to map many challenges that should be considered and addressed when seeking to demonstrate that an adequate level of structural fire safety has been achieved when adopting timber (e.g., [1–3]). In parallel, new research studies have emerged which fundamentally seek to understand

---

D. Brandon  
Research Institutes of Sweden (RISE), Borås, Sweden  
e-mail: [daniel.brandon@ri.se](mailto:daniel.brandon@ri.se)

D. Hopkin (✉)  
OFR Consultants, Manchester, UK  
e-mail: [danny.hopkin@ofrconsultants.com](mailto:danny.hopkin@ofrconsultants.com)

R. Emberley  
California Polytechnic State University, San Luis Obispo, CA, USA  
e-mail: [remberle@calpoly.edu](mailto:remberle@calpoly.edu)

C. Wade  
Fire Research Group, Hawkes Bay, New Zealand  
e-mail: [colleen.wade@fireresearchgroup.com](mailto:colleen.wade@fireresearchgroup.com)

the timber pyrolysis process and its translation to the enclosure fire context (e.g., [4, 5]). These challenges and the recent prevalence of timber-associated fire research shape the content of this chapter.

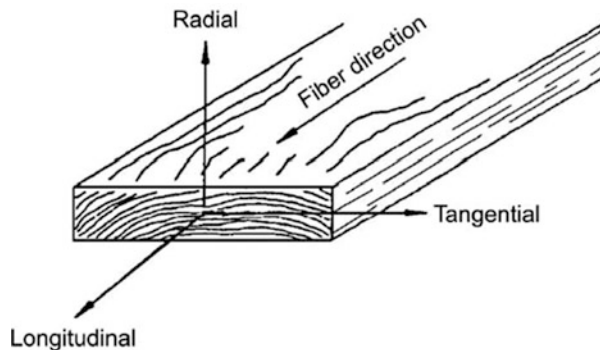
### 8.1.1 *Composition of Timber*

Timber is made up of lignin, cellulose, and hemicellulose and depending on the species, the proportion of each of the organic materials varies. In general, the cellulose forms bundles of cells and the lignin acts as an adhesive holding the bundles together. This alignment of the cells gives timber its traditional grain orientation structure. Three grain orientations exist: longitudinal, radial, and tangential (Fig. 8.1) [6]. Due to the grain orientation, the mechanical and thermal properties of timber vary depending on the grain direction. These are typically described as parallel (longitudinal) or perpendicular (radial and tangential) to the grain. As an example of the variations in timber properties, the modulus of elasticity of timber can be 30 times more parallel to the grain than perpendicular [7].

As an organic and porous material, timber naturally has a moisture content from cell-bound water. Depending on the moisture content, timber can be classified as seasoned ( $MC < 15\%$ ) and unseasoned ( $MC \geq 15\%$ ) [8]. Timber used for structural purposes is seasoned timber cut to length to remove impurities such as knots, graded to determine the strength of the timber, and then dried. This process ensures that the timber used in construction has known strength values and has completed a rigorous quality control process.

The ability for timber to hold moisture is also a disadvantage to using traditional sawn lumber. The moisture content of timber is subject to changes depending on atmospheric and structural conditions. As the moisture content in timber increases and decreases, the timber member will experience expansion and shrinkage. These volumetric changes to structural members can create unwanted strains in the members and the connections. As such, expansion and contraction need to be accounted for in sawn lumber. Advances in engineered timber—such as cross-laminated timber—have created building products that are not as susceptible to expansion and shrinkage.

**Fig. 8.1** Timber grain orientation [6]





## 8.2 Fundamentals of Timber Combustion

Unlike the other main structural materials—steel and concrete—timber is a combustible material and when exposed to a sufficient amount of heat it will pyrolyze and ignite. To assess the structural and fire performance of timber and apply correct design methods to higher consequence buildings, the fundamentals of timber combustion must be detailed and properly accounted for.

### 8.2.1 Heat and Mass Transfer

Two main physical processes govern the ignition process of timber: pyrolysis and combustion. Pyrolysis is thermal decomposition of a substance from a solid to gas. Combustion is the chemical reaction of a gas (i.e., between an oxidizing agent and gas, leading to heat).

When a solid is exposed to an external heat source, energy is transferred from the source to the target (in this case timber). Energy transferred to the solid will increase the temperature of the surface. As the temperature is increased above ambient conditions, energy transfer from the surface will be determined by the three forms of heat transfer: conduction, convection, and radiation. Convection (heat transfer through a fluid) and radiation (heat transfer through electromagnetic waves) will contribute to the heat transfer from the fire to the solid surfaces. Conduction (heat transfer through a solid) will transfer the energy into the material away from the surface and increase the temperature of the solid [9]. Figure 8.2 from Torero [9] details the heat and mass transfer from a solid exposed to an external heat source.

As the temperature of the solid increases, thermal, mechanical, and chemical changes occur to the solid. Thermal and mechanical changes are covered in Sect. 8.4. Chemical changes will occur when the temperature of the solid increases to levels where the increase of energy will initiate decomposition of the solid. The decomposition breaks the solid into gases and char, depending on the solid burned. In the case of non-charring materials, the solid will just be decomposed into a gas. Timber is considered a charring material (Sect. 8.2.2.2) and the charring rates are dependent on the rate of the decomposition of the timber into combustible gases. The rate at which the decomposition occurs is based on the temperature, thermal penetration depth, and type of reaction (Eq. 8.4). As such, charring rates are an average of the decomposition rate.

Browne [10] detailed four temperature zones within a sample exposed to an external heat flux (Fig. 8.3). Zone A indicates temperature between 100 and 200 °C. In this zone, the water begins to evaporate from the wood and cells and the molecules of the wood. In Zone B, the temperatures are between 200 and 280 °C and the wood begins to slowly pyrolyze. In Zone C, the temperatures between 280 and 500 °C cause rapidly increasing pyrolysis and charring. The char layer acts as an insulator and begins to crack. Finally, in Zone D, the temperatures are

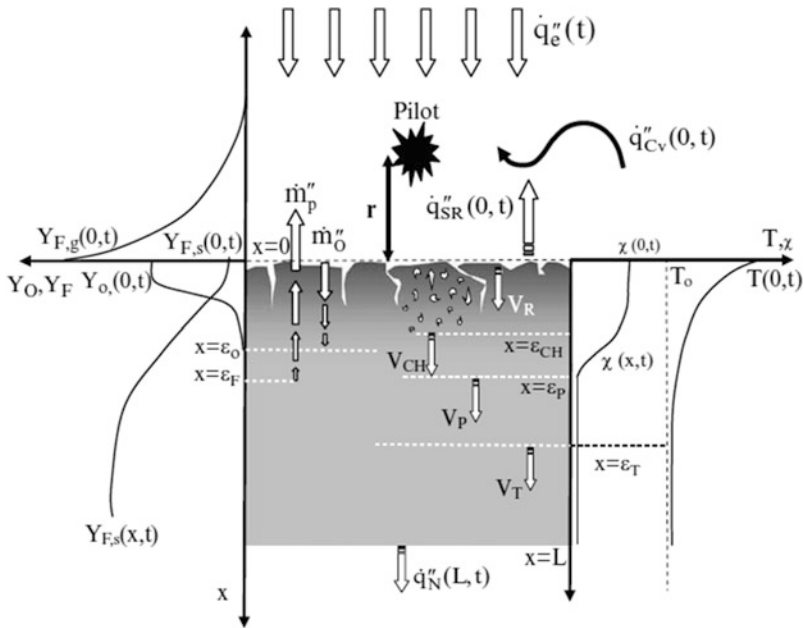


Fig. 8.2 Heat and mass transfer from a solid [9]

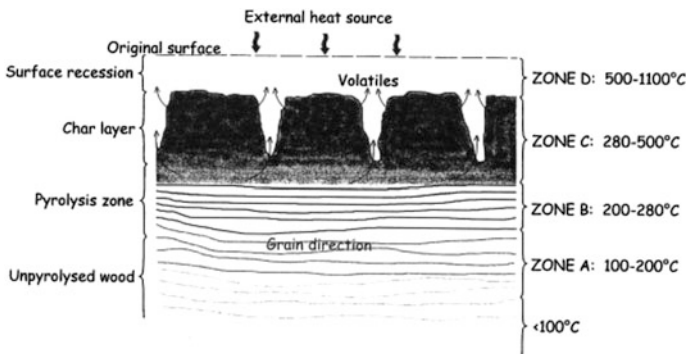


Fig. 8.3 Temperature zones in charring wood [11]

between 500 and 1100 °C, and the char continues to oxidize on the surface resulting in surface recession, if sufficient oxygen is available.

As the solid is decomposed, the combustible gases (i.e., mass) will be transferred from the surface into the boundary layer and then transported away from the surface due to natural convection (buoyancy) of the hot combustible gases. The combustible gases enter the boundary layer, and mix with any available oxygen from the surrounding air. The mixture of combustible gases and oxygen will not be ignitable unless the mixture is within the flammability limits of the mixture itself. Since the

mixture is governed by a boundary layer of natural convection, an increase in the mass loss rate is necessary to increase the combustible gas concentration in the boundary layer above the lower flammable limit of the mixture. As such, there exists a critical mass loss rate for ignition [12]. Once the critical mass loss rate has been achieved, ignition is possible.

## 8.2.2 *Flaming Combustion*

Both the processes of pyrolysis and combustion (reaction) are necessary to produce flaming combustion. Pyrolysis produces the combustible vapors; mass transport mixes the combustible gases in the boundary layer; and then if enough energy is added to the flammable mixture, ignition and sustained flaming combustion can occur.

### 8.2.2.1 Ignition

Two forms of ignition exist: piloted and autoignition. Both forms of ignition add energy to the combustible gas mixture; however, piloted ignition comes from an added energy source and autoignition comes from increasing the temperature of the mixture to start a self-sustaining reaction [12].

Piloted ignition is used to measure the lower bound of ignition for solids. Due to the localized energy of a pilot (typically a spark), a reaction can start locally and then propagate outwards once ignition has occurred. Two levels of piloted ignition exist: flash point and fire point. Depending on the boundary-layer conditions, geometry of the sample, and other factors, a localized area of combustible gases could be present in the area of a pilot that are above the lower flammable limit. If the reaction occurs, however, the mass loss rate from the solid will not be sufficient to sustain the reaction and thus ignition flashes but a self-sustaining flame is not possible since the amount of heat given off from the flames is not enough to increase the mass loss rate to the critical value. For the fire point, enough combustible gases are being produced and transported to the reaction zone such that once ignition occurs, the flame is able to sustain and in most cases increase the mass loss rate. Autoignition is an upper bound of ignition as this represents a scenario where the temperature of the gases has to increase in order to maintain combustion.

Several ways to describe ignition limits are used in literature and engineering: heat flux, surface temperature, and mass loss rate. Surface temperature is the most common way to describe ignition limits of solids; however, measuring the surface temperature is dependent upon the geometry, measuring equipment, and boundary-layer velocity, among other properties. The wide range in limits was documented by Babrauskas [13] for timber where the author compiled literature on piloted ignition temperatures ranging between 210 and 497 °C. The range in temperatures for autoignition was between 200 and 510 °C. The wide range in results was attributed

to ignition definition, conditions of the test, test apparatus, timber specimen conditions, and timber species. Drysdale [12] provides a narrower range for piloted and autoignition and separates the values for variations in heat flux. For solely radiant heating, the temperature for piloted ignition was 300–410 °C and for convective heating 450 °C. The temperature for autoignition with radiant heating was 600 °C and with convection heating was 490 °C.

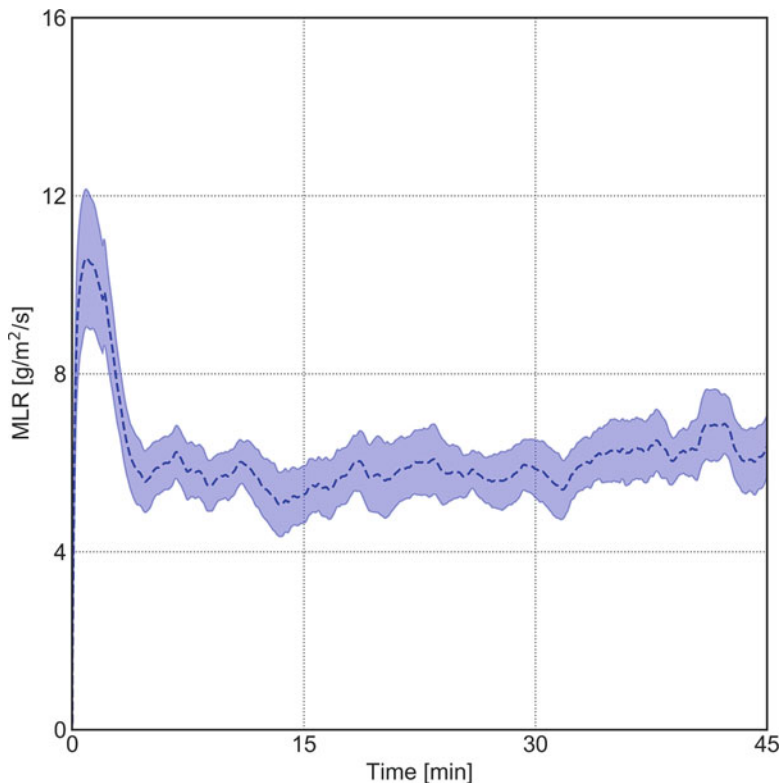
Heat flux is another common indicator of ignition. The critical heat flux for ignition is the amount of energy necessary for ignition, whether piloted or autoignition. The critical heat flux is less dependent upon the external conditions of the test. Typically values for critical heat flux for timber are 12.5 kW/m<sup>2</sup> (piloted) and 28 kW/m<sup>2</sup> [12, 13].

Finally, as in the discussion in Sect. 8.2, mass loss rate is the final indicator of ignition. Since mass loss rate is the driver of the combustion reaction for delivering combustible gases to the boundary layer, a critical mass loss rate for both piloted ignition and autoignition exists. Values between 1.8 and 4.0 g/m<sup>2</sup>s have been reported [12].

### 8.2.2.2 Charring

After wood pyrolyzes, a char layer remains which is composed of excess carbon. The char which is less dense than the timber acts as an insulator to the remainder of the cross section and thus regulates the amount of energy that reaches the pyrolysis zone. The insulating nature of the char can be seen on a typical mass loss rate curve for a burning timber sample [4]. After ignition, the mass loss rate of the timber reaches a peak due to the fact that all the energy is going into increasing the temperature of the wood and the rate of pyrolysis (Fig. 8.4). However, after a period of decreasing mass loss rate, it reaches steady state. The decreasing mass loss rate is due to the fact that the char-layer thickness is increasing and absorbing the energy that is being transferred from an external source to the sample (Fig. 8.5). As the char layer increases, more energy is absorbed before it reaches the pyrolysis region. This regulation slows the mass loss rate. However, due to further thermal oxidation (subject to sufficient oxygen being available) of the char layer on the surface of the char, a constant char-layer thickness is eventually achieved and the mass loss rate reaches a steady-state value. While the charring rate is traditionally reported as a single value, the charring rate varies with the thickness of the char layer and thus is time dependent.

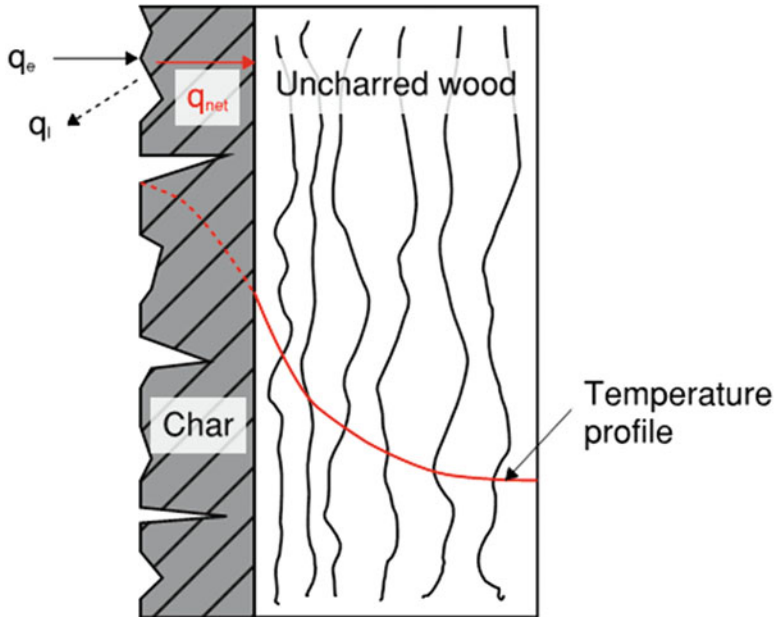
The charring rates of wood have been studied extensively for a variety of species and wood products and under a variety of dependent variables such as density, moisture content, heat transfer direction, char contraction, char oxidation, scaling effect, heat flux, and oxygen concentration [11, 15, 16]. Increases in density and moisture generally yield lower average charring rates. Timber chars faster when the grain is in the longitudinal direction. Charring occurs faster with higher heat fluxes [17].



**Fig. 8.4** Transient (c. 0 to 5 min) and steady-state (> 5 min) mass loss rate of CLT from [14]

### 8.2.2.3 Self-Extinction

Due to the insulating properties of the char layer and the regulation of the heat flux into the pyrolysis zone, timber can achieve self-extinction. Self-extinction is a phenomenon where the heat flux provided by a material's flaming combustion is not sufficient to sustain the combustion process. As a result, an external heat flux is necessary to maintain the mass loss rate at a level where the combustion can continue. The phenomenon of self-extinction of materials was studied fundamentally by Petrella [18] and Tewarson and Pion [19]. The authors studied a wide variety of materials and measured and calculated the surface heat losses as well as the heat flux from the flames. Based on the results and physical observations, they showed that the heat flux from the flames ( $\dot{Q}_F$ ) needs to be less than the heat losses from the surface ( $\dot{Q}_L$ ) in order for self-extinction to occur. Babrauskas [13] summarizing an unpublished work by J. Hall showed that timber reaches self-extinction after heat flux removal. In J. Hall's study, a flame was impinged on the surface for between 1 and 5 min and then removed. Drysdale [12] distinguished between thermally thin



**Fig. 8.5** Heat transfer in wood exposed to an external heat flux, adapted from [15]

and thermally thick timber samples, in that thermally thin timber samples would not self-extinguish when ignited.

Emberley et al. [4] conducted self-extinction tests on solid and engineered timber where instead of completely removing the heat flux, the heat flux was decreased until self-extinction was achieved in order to measure the critical external heat flux and critical mass loss rate for self-extinction. The studies measured a wide variety of timber species but as an example, for European spruce (*Picea abies*), the critical external heat flux for flaming combustion was  $43.6 \pm 4.7 \text{ kW/m}^2$  and the critical mass loss rate was  $3.93 \pm 0.4 \text{ g/m}^2\text{s}$ . The studies highlighted the importance of maintaining the integrity of the bond line for engineered timber. Debonding of the timber plies due to adhesive degradation prevented the engineered timber from reaching self-extinction.

Bartlett et al. [1] conducted similar tests on softwood-engineered timber and measured the critical mass loss rate of the timber to be  $3.48 \text{ g/m}^2\text{s}$  and the critical heat flux to be  $31 \text{ kW/m}^2$ . Subsequently, Bartlett et al. [20] present a review of factors affecting the burning behavior of wood, which notes: “extinction conditions are less well defined and understood, with critical mass loss rates for extinction varying from 2.5 to  $5 \text{ g/m}^2\text{s}$ .”

### 8.2.3 Smoldering Combustion

Smoldering combustion is the continued charring process after flaming combustion has ceased or before flaming combustion has commenced. The critical heat flux to maintain smoldering has been studied by a few researchers. Ohlemiller and Shaub [21], Ohlemiller [22], Beyler et al. [23], and Swann et al. [24] found the critical heat flux for smoldering combustion to be 10 and 8 kW/m<sup>2</sup>, respectively. Crielaard et al. [25] measured the smoldering critical heat flux at 5–6 kW/m<sup>2</sup>. These values indicated that between the flaming self-extinction limit (approximately 31–43.6 kW/m<sup>2</sup>) and the smoldering limit (approximately 5–6 kW/m<sup>2</sup>) smoldering and continued charring (e.g., loss of cross section) will continue. The limiting heat flux for smoldering was premised upon an airflow speed of less than 0.5 m/s.

## 8.3 Timber Construction

Timber structures broadly fall into two categories: heavy timber construction and light timber frame [26]. Within both types of construction, there is often another subdivision which distinguishes between structures that are formed from solid-section timber and those made of “engineered” timber. Heavy timber construction typically refers to structures formed from large-section (generally in excess of 300 mm) sawn wood or glulam beams, columns, trusses, and slabs. Due to the large cross section of such members, passive fire protection is generally not applied and any fire resistance is “inherent.” Light timber frame structures differ as they are formed from smaller timber elements in the shape of stud walls and joist floors. Such small sections would be engulfed in a fire in very little time. As a result, they are typically protected with timber product boards, fire-retardant treatments, gypsum plasterboards, or a combination of these methods.

Timber is a nonhomogeneous material as it is organic. The formation of knots and the direction of the grain are among a number of important factors that heavily influence the strength of a timber structural element. Members formed from large continuous pieces of timber contain many defects. As a result, the timber strengths quoted in the grading process can be extremely conservative as they are based on observed defects rather than on the true strength of the wood. In recognition of this, many engineered wood products are now available which reduce waste through more efficient use of material, while allowing for the “true” strength of timber to be utilized. As a result, in terms of light timber frames, products like engineered floor joists incorporating systems such as timber I-joists, steel truss web joists, and timber truss girders are beginning to replace traditional solid-section studs and solid flexural elements. Similarly, off-site components like structural insulated panels (SIPs) are used to form building envelopes and vertical structural members such as walls. In the

case of large-section “heavy” timber construction, glue-laminated (glulam) or laminated veneer lumber (LVL) is often adopted in favor of solid members. Similarly, cross-laminated timber (CLT) is often used as a direct substitute for solid-section timber slabs and panels [27].

### **8.3.1 Heavy Timber Construction**

Heavy timber construction is a traditional technique originally used in ancient churches, temples, housing, and industrial buildings, and descended from post-and-beam construction [28, 29]. At its core, the designation of “heavy timber” originates from US fire service practices, in seeking to differentiate the more “fire-resistant” performance characteristics of large timber sections, versus the litany of other US construction typologies [28].

In the USA, heavy timber construction has a very specific meaning, as is defined in the International Building Code (IBC) [30] for Type IV structures: “type of construction in which the exterior walls are of non-combustible materials and the interior building elements are of solid or laminated wood without concealed spaces,” and “minimum solid sawn nominal dimensions are required.”

For the purpose of this chapter, heavy timber construction is simply intended to cover solid timber elements which achieve fire performance inherently by virtue of having minimum dimensions. This can be augmented with further applied fire-protective linings.

### **8.3.2 Engineered Mass Timber**

Dickson and Parker [31] note that there are numerous products originating from timber whose properties are optimized from the original material.

Engineered timber includes factory products such as glue-laminated timber (glulam), laminated veneer lumber (LVL), oriented strand lumber, parallel strand lumber, oriented strand board (OSB), cross-laminated timber (CLT), and plywood. A more exhaustive discussion of engineered timber and the manufacturing process can be found in Lam [32], with the following subsections providing the context for the scope of technologies covered within this chapter.

#### **8.3.2.1 LVL and Glulam**

Glulam and LVL are potentially interchangeable terms, and are used to describe structural components formed from thin laminations of timber which are compressed together and fixed using an adhesive. The two may be differentiated from each other



by the thickness of the laminations adopted, with the former typically being significantly thicker.

Typically, in traditional laminated products, such as LVL or glulam, the grain orientation of each veneer is aligned [33, 34]. The laminated cross section forms a stronger structural unit when compared to solid-section timber as defects, such as knots and other natural weaknesses, are eliminated from the cross section. Laminated products may also be used for much larger spans and loads when compared to solid-section timber. This is because cross sections of any size (or shape within reasonable limits) can be manufactured from multiple laminations.

### 8.3.2.2 Cross-Laminated Timber (CLT)

When the grain orientation of the laminations (commonly termed “layup”) varies with depth CLT is formed. Layers of veneers are gradually built up with perpendicular grain orientations to form a product which has better orthogonal properties than glulam or LVL. Due to the cross lamination of the timber plies, CLT exhibits much better dimensional stability than glulam or LVL sections as thermal expansion is more even in all directions [35]. The number of layers is typically between three and seven with layer thickness in the range of 16–51 mm, and board widths in the range of 60–240 mm [36].

Sutton et al. [37] note that CLT normally forms the structural floor and wall element of buildings and has been used successfully to build up to nine stories in the UK. It is typically used in off-site-manufactured panels delivered to site for erection. Since 2011, CLT structures have been pushed to more significant heights, such as “the Treet” in Bergen, Mjøstårnet in Brumunddal, and HoHo in Vienna, at 14, 18, and 24 stories high, respectively.

### 8.3.3 Light Timber Frame

Light timber frame conventionally refers to stud-and-joist construction, with each provided at regular centers, but of smaller dimension. Due to the size of the section, the phrase “stick-build” is not uncommonly used to describe the form of construction. Also due to section size, the timber elements do not typically achieve their fire resistance inherently. Instead, protective lining materials are provided that delay the onset of timber degradation with increasing temperature.

Light timber frame construction is typically characterized as either closed or open panel:

1. Closed panel—Made from studs, rails, and insulation, with sheathings and/or linings on the faces of the panel. A vapor barrier is also provided on the warm side of the insulation and a breather membrane on the outer face of the panel.

2. Open panel—Structurally engineered panels that form the inside load-bearing leaf of the external wall, comprising studs, rails, sheathing on one face, and a breather membrane. The open-panel system is made from treated softwood timber framing, over which a structural sheet material of either ply or OSB board is fixed.

Increasingly, engineered floor joists are used as a direct substitute for traditional solid timber joists. This is largely because they are more lightweight and structurally efficient, requiring less material to achieve the same or similar stiffness to that of a solid timber joist. The three most common types of engineered floor joists are “timber I-joists,” “steel truss web joists,” and “timber truss girders.”

Timber I-joists refer to narrow I-sections formed from two solid or LVL timber “flanges” joined via glue to a slender oriented strand board (OSB) or a similar board product web. The adopted glues are typically phenol-formaldehyde (PF)- or phenol-resorcinol-formaldehyde (PRF)-based adhesives [38]. Typically, the flanges are made of 45 mm square sections; however, variations exist depending upon the loads and spans required. The timber board web will typically measure 8–10 mm in thickness but variations also exist depending upon the requirements of a given project.

In principle, steel truss web joists are formed in a similar manner to timber I-joists. However, the slim timber board web is replaced by discrete pressed steel truss sections which are mechanically fixed to the top and bottom flanges via nailing plates. The top and bottom flanges in this instance may be a little wider than those of a timber I-joist and would typically measure 45 × 100 mm. Again, variations exist depending upon specific requirements.

Timber truss girders are similar in shape to traditional steel truss girders. They are formed from two timber or LVL flanges separated by a network of timber bracing. The various components are joined via mechanical methods, such as nailing plates.

### **8.3.4 Timber Board Products**

Many timber board products have emerged in the last few decades which make use of the waste products associated with timber cutting and preparation. Most common of these are chipboard, oriented strand board (OSB), and medium-density fiber board (MDF). Chipboard (or particle board as it is often referred to) combines wood chips and resin in a random orientation [39]. MDF is a very similar product to that of chipboard. However, in this instance wood fibers, extracted using a defibrator, are mixed with resin and wax to form a smooth, flake-free board [39]. OSB is also similar to chipboard and can essentially be considered as a resin-bonded particle board that incorporates 30–50 mm length timber flakes that are oriented in three distinct layers. OSB has evolved from wafer board which is characterized by a “random array of chips or flakes up to 50 mm in both length and width” [40], into a thinner sheet material. In essence, a three-layer board is manufactured whereby the core flakes are approximately aligned at right angles to the orientation of the surface layers [40].

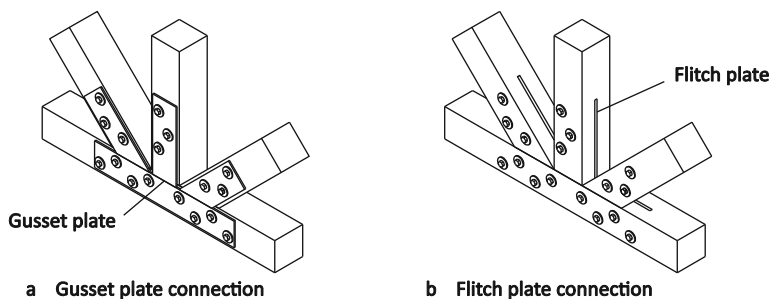
### 8.3.5 Connections

Connections between structural members or timber frame assemblies can have a structural and/or a fire compartment-separating function and generally comprise mechanical fasteners, such as nails, screws, bolts, and dowels. Alternatively, glued connections of members can be used, but due to requirements of ambient conditions for gluing and curing, glued connections are rarely realized on building sites.

The types of timber connections that are applicable differ significantly for varying types of structures. In light timber frame structures, a large number of fasteners, commonly nails, screws, and brackets of various types, are used to connect components of timber frame assemblies, such as studs, joists, and boards. Prefabricated assemblies such as wall and floor slabs are typically connected to each other using screws or brackets that ensure that axial and/or shear loads are transmitted from slab to slab. Connections between CLT members in heavy timber structures often consist of (self-tapping) screws directly connecting two adjacent slabs or brackets. However, due to the application of CLT in tall buildings, which generally have significant requirements regarding the load-bearing capacity, stiffness, earthquake resistance, fire resistance, etc., a number of innovative connection systems have been introduced recently, such as posttensioned structural systems [41].

In post-and-beam and braced frame timber structures, heavy timber columns, beams, and braces are connected to transfer axial forces, shear forces, and sometimes bending moments. A large variety of connections are applied in practice, but the most commonly used timber connections are those comprising dowel-type fasteners [33]. Common dowel-type fasteners are nails, screws, bolts, dowels, and threaded rods which are made of steel and mainly loaded in shear. In combination with dowel-type fasteners, gusset plates or flitch plates can be used to connect timber members that are in a common plane. Large span roof trusses often have timber members in a common plane (e.g., Fig. 8.6).

Connections in multi-storey post-and-beam structures generally have significant requirements regarding stiffness [42], fire resistance, and earthquake resistance. Some innovative connections were proposed in order to improve one or more of these aspects [43–45].



**Fig. 8.6** Connections of timber members in a common plane: (a) gusset plate; and (b) flitch plate

## 8.4 Timber Properties at High Temperature

The structural performance of timber elements in fire is dependent upon the mechanical properties of the member, which in turn are temperature dependent. Due to the generally high temperature gradients in timber members exposed to fires, mechanical properties of timber vary significantly throughout the member. It is possible to predict the capacity of timber members exposed to fire using temperature-dependent mechanical properties. However firstly, temperature calculations are needed in order to perform these predictions.

### 8.4.1 Timber Thermophysical Properties

The conductive heat flux through a solid is dependent on the temperature gradient within the solid and its thermophysical properties (thermal conductivity, specific heat, and density). The heat flux through timber is, however, dependent not only on conduction, but also on mass transfer. Additional complicated phenomena, such as cracking and oxidation of char, complicate predictive calculations of the temperatures throughout the structure. Approaches taken to predict the temperatures of timber in fire conditions involve (1) the use of effective values instead of “true” values for the thermal conductivity, density, and specific heat or (2) reaction schemes in which different components of wood decompose at different rates, resulting in reaction-dependent changes of thermal properties.

#### 8.4.1.1 Observations on Timber Conductivity

Many researchers have studied the conductivity of timber at elevated temperature including Fredlund [46], Janssens [47], Knudson and Schniewind [48], and White and Schaffer [49], all of which are shown in Fig. 8.7. In addition, further conductivity values are shown which include properties by Thomas [50], which are based on those proposed by Fredlund [46] and Harmathy [51] and are similar to those of Gammon [52] and König and Walleij [53]. The latter were numerically calibrated and now form the basis of the values contained in EN 1995-1-2 [54].

All of the properties are generally agreeable up to 300 °C ([50], noted a spike over the temperature range of 80–120 °C). The difference beyond this temperature for the various properties presented depends largely upon whether they represent the true conductivity of timber or the apparent conductivity which implicitly includes the effects of mass transfer, cracking, etc. These behaviors are particularly pronounced and critical for the char layer. In the case of Thomas [50] and König and Walleij [53] the conductivity properties were numerically calibrated against experiments exposed to standard fire exposure. As a result, König and Walleij’s [53] properties as now contained in EN 1995-1-2 Annex B are limited to standard fire exposure and have

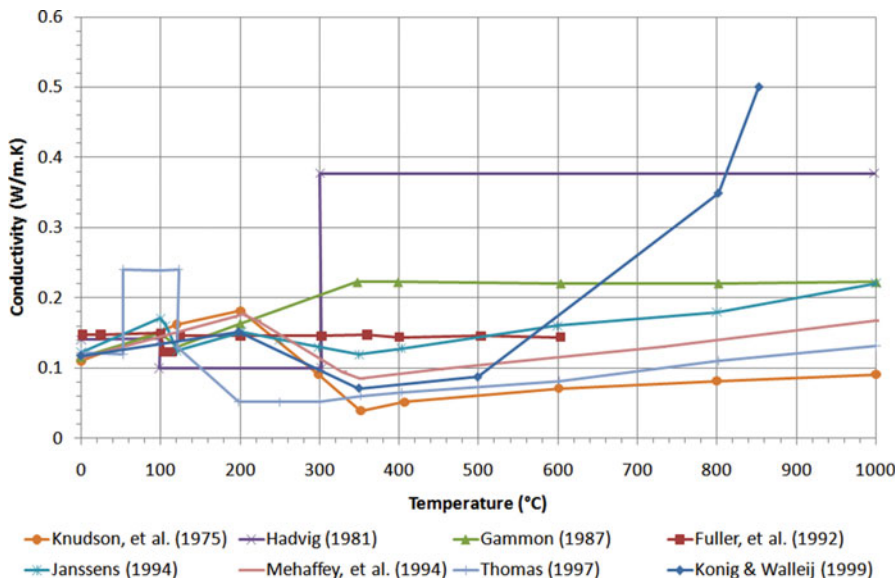


Fig. 8.7 Conductivity of timber versus temperature from various sources

been shown to give poor correlation with natural fire or representations of natural fire exposure [55].

### 8.4.1.2 Observations on Timber-Specific Heat

Similar studies have been conducted on the specific heat properties of solid timber. The specific heat properties of timber have been subject to studies dating back as far as the 1900s. Dunlap [56] developed an empirical expression for the specific heat ( $c$  in J/kg K) of timber as a function of temperature ( $T$  in °C) which is shown below (Eq. 8.1):

$$c = 1110 + 4.84T \tag{8.1}$$

The early work of Dunlap [56] was later built upon by Knudson and Schniewind [48] who analytically added a specific heat spike (13,000 J/kg K) at 100 °C to account for the latent heat of vaporization of the water contained in timber. Similar further refinements were made by Janssens [47], who accounted for the additional moisture bound in the cell walls of timber (see Eq. 8.2), and Fuller et al. [57] who also accounted for bound water but with much higher specific heat values at around 100 °C:

$$c = \frac{c_0 + 4187u}{1 + u} + \Delta c \tag{8.2}$$

Where

$$c_0 = 1159 + 3.86T$$

$$\Delta c = (23.55T - 1326u + 2417)u$$

$u$  = moisture mass fraction of timber (-).

In addition to these studies, further numerically calibrated specific heat properties were proposed by Fredlund [46], who quoted a specific heat spike of 13,500 J/kg K at 100 °C, and König and Walleij [53], which again represent those used in EN 1995-1-2 [54]. Similar analytical specific heat values are proposed by Mehaffey et al. [58] which include a char-specific heat proposed by Lie [59] of 690 J/kg K. All of these properties are compared in Fig. 8.8. It should be noted that not all authors included the latent heat of vaporization in the specific heat. For example, Janssens [47] accounted for latent heat separately in the heat equation so it is not shown in this figure. Further to this, Cachim and Franssen [60] recognized the limitations of the Eurocode thermal properties for timber (by [53]) and numerically derived changes to make the specific heat properties of softwood dependent upon moisture content. Through their study, it was noted that the properties contained in Annex B of EN

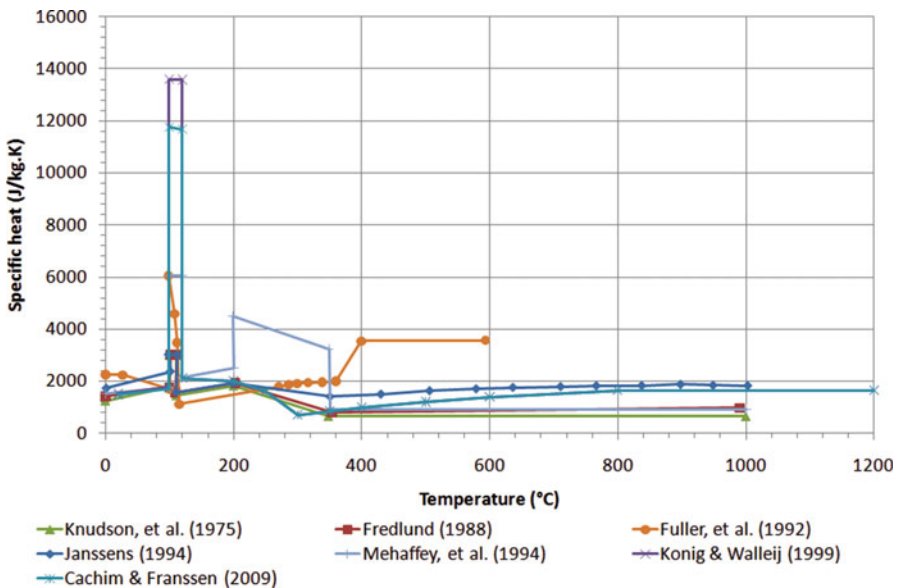


Fig. 8.8 Effective specific heat of timber as a function of temperature—various sources

1995-1-2 were only valid for timber moisture contents ( $\omega$ ) of 0.12 (mass fraction) and densities of  $450 \text{ kg/m}^3$ . In a correction to this Cachim and Franssen [60] proposed the modifications shown in Table 8.1.

### 8.4.1.3 Observations on Timber Density

The density of timber as a function of temperature has also been the subject of much research. The density of timber varies depending upon timber species (e.g., hardwoods and softwoods) and moisture content. Table 8.2 gives ambient temperature density for different structural wood species.

The density of timber, particularly softwood, reduces significantly at temperatures corresponding to the vaporization of free water ( $100 \text{ }^\circ\text{C}$ ). Typically, at around  $100 \text{ }^\circ\text{C}$  timber loses roughly 10% of its density (corresponding to the typical free moisture of timber), while at approximately  $300 \text{ }^\circ\text{C}$  where char forms, the density may be as low as 20% of that at ambient temperature [62]. Many of the researchers mentioned previously, i.e., Knudson and Schniewind [48], Fredlund [46], Fuller et al. [57], Janssens [47], and König and Walleij [63], have produced density properties as a function of temperature (Fig. 8.4). These datasets are a mixture of experimentally and numerically derived relationships. All the datasets are generally in good agreement and show that timber undergoes density changes as a result of free water vaporization, pyrolysis (mass loss), and char formation (Fig. 8.9).

**Table 8.1** Specific heat of timber modified for moisture content (after [60])

Temperature ( $^\circ\text{C}$ )	Density ratio, G	Specific heat capacity of wood (EN 1995-1-2) (J/kg K)	Moisture modified specific heat (J/kg K)
20	$1 + \omega$	1530	$(1210 + 4190\omega)/G$
99	$1 + \omega$	1770	$(1480 + 4190\omega)/G$
99	$1 + \omega$	13,600	$(1480 + 114600\omega)/G$
120	1	13,580	$(2120 + 95,500 \omega)/G$
120	1	2120	2120/G
200	1	2000	2000/G

**Table 8.2** Ambient temperature density of wood by species [61]

Species	Wood type	Mean density ( $\text{kg/m}^3$ )
Douglas fir	Softwood	530
European larch	Softwood	550
American red oak	Hardwood	790
Radiata pine	Softwood	480
Sitka spruce	Softwood	450
Purpleheart	Hardwood	880

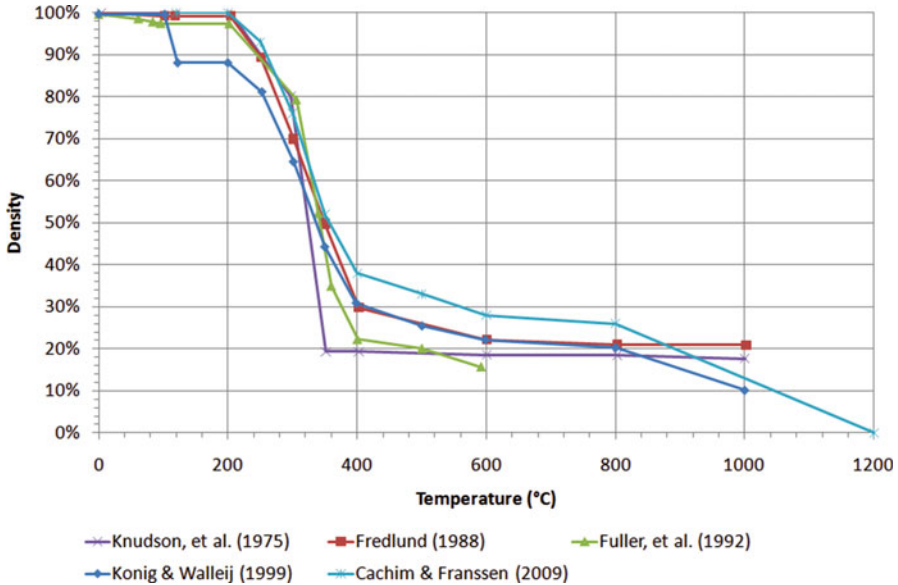


Fig. 8.9 Density reduction of timber versus temperature from various sources

### 8.4.2 Timber Kinetic Properties

Sections 8.4.1.1–8.4.1.3 all speak to the challenges of interpreting and applying experimentally observed timber thermophysical properties to a range of heating regimes. This is because, as is noted, the properties gathered from experiments are effective, and implicitly capture occurring physical processes that arise from reactions, the rate of which differs depending upon heating conditions.

Increasingly, reaction schemes are adopted to better describe the degradation of timber upon heating and the associated impact on apparent thermophysical properties. Studies in the literature include those by Matala et al. [64], Hopkin [67], Wang et al. [68], Mindeguia et al. [69], and Richter et al.[70].

Mindeguia et al. [69] proposed that the effective thermophysical properties can be estimated from the mass fractions of three key phases: (s) dry wood—dictated by the decomposition of lignin (l), (w) water, and (char) char layer:

$$\begin{aligned}
 \lambda_{\text{sol}} &= (1 - \chi_l) \cdot \lambda_s + \frac{\rho_s}{\rho_{\text{char}}} \cdot \gamma \cdot \chi_l \cdot \lambda_{\text{char}} + \frac{\rho_s}{\rho_w} \cdot \beta \cdot (1 - \chi_w) \cdot \lambda_w \\
 \rho_{\text{sol}} &= \rho_s \cdot [1 + \chi_l \cdot (\gamma - 1) + \beta \cdot (1 - \chi_w)] \\
 C_{p_{\text{sol}}} &= \frac{(1 - \chi_l) \cdot C_{p_s} + \gamma \cdot \chi_l \cdot C_{p_{\text{char}}} + \beta \cdot (1 - \chi_w) \cdot C_{p_w}}{[1 + \chi_l \cdot (\gamma - 1) + \beta \cdot (1 - \chi_w)]}
 \end{aligned}
 \tag{8.3}$$

With  
 $\beta$  the water content (%).



$\rho$  the density of differing phases ( $\text{kg/m}^3$ ).

$\lambda$  the conductivity of the differing phases ( $\text{W/m K}$ ).

$\gamma$  the char yield (as a mass fraction of initial dry wood).

$C_p$  the specific heat of the differing phases ( $\text{J/kg K}$ ).

$\chi$  the relative reaction progress of each phase, i.e., unity would imply a complete reaction.

The reaction rate for a given phase ( $d\chi_i/dt$ ) can be calculated from the common Arrhenius function, requiring the inputs of the so-named kinetic triplet comprising a pre-exponential factor ( $A$ ), activation energy ( $E$ ), and reaction model  $f(\chi)$ :

$$\frac{\partial \chi_i}{\partial t} = (1 - \chi_i) A_i \exp(-E_i/RT) \quad (8.4)$$

With

$i$  indicating the  $i$ th reaction.

$T$  the temperature ( $\text{K}$ ).

Matala et al. [64] estimated the kinetic properties for the wood constituents given in Table 8.3 using thermogravimetric experiments and a genetic algorithm.

Wade et al. [71] coupled a kinetic pyrolysis model to the fire zone model B-RISK to simulate timber-lined enclosures exposed to fire. This adopted a multiple-component scheme assuming that wood is composed of cellulose, hemicellulose, lignin, and water. Heat transfer to the enclosure surface was calculated using a one-dimensional finite difference scheme with the reaction rate determined for each element in the scheme based on the calculated temperature of that element. Solving the governing equations of the zone model provided the thermal boundary conditions for the heat transfer calculations.

The reaction rate for each component is described with a first-order differential equation where  $Y_{i,j}$  is the mass fraction ( $m_i/m_{i,o}$ ) of component  $i$  at time  $j$ ,  $m_i$  is the mass of component  $i$ , and  $m_{i,o}$  is the initial mass of component  $i$ .

For each component, the initial mass fraction is  $Y_{i,o} = 1$  at the start of the simulation and 0 when fully converted to char.  $c_i$  is the initial fraction of the overall unheated composite solid represented by component  $i$ , i.e.,  $(m_{i,o}/m_o)$ , and  $T_j$  is the temperature of the solid. Eq. 8.5 was solved using a Runge-Kutta numerical method to give the residual mass fraction value for each component ( $Y_i$ ) at each time step for each element comprising the enclosure wall or ceiling surface:

**Table 8.3** Kinetic parameters for wood from Matala et al. [64]

Component	$E_i$ (J/mol)	$A_i$ ( $\text{s}^{-1}$ )	$n_i$	Residue
Hemicellulose	$1.64 \times 10^5$	$5.78 \times 10^{13}$	4.166	0.268
Cellulose	$1.95 \times 10^5$	$2.68 \times 10^{14}$	0.85	0.1
Lignin	$1.38 \times 10^5$	$2.18 \times 10^{10}$	7.0	0.567
Water	$1.62 \times 10^5$	$1.0 \times 10^{20}$	1.0	0

$$\frac{Y_{i,j}}{dt} = c_i A_i \exp\left(-\frac{E_i}{RT_j}\right) (Y_{i,j})^{n_i} \quad (8.5)$$

For the cellulose, hemicellulose, and lignin, a char residue yield  $v_i$  was specified. The mass fraction of char  $X_{i,j}$  at time  $j$  is then given by

$$X_{i,j} = (1 - Y_{i,j}) v_i \quad (8.6)$$

The mass fraction of char residue at time  $j$  for a given layer and for the three components is

$$X_j = \sum_{i=1}^3 (X_{i,j} c_i) = \sum_{i=1}^3 ((1 - Y_{i,j}) v_i c_i) \quad (8.7)$$

At a given time  $j$  the mass of solid wood that remains per unit volume is given per the below, where  $\rho_o$  is the initial mass of wood per unit volume:

$$m_{s,j} = \sum_{i=1}^3 (Y_{i,j} c_i \rho_o) \quad (8.8)$$

The total volumetric mass loss rate (in  $\text{kg m}^{-3} \text{s}^{-1}$ ) is then estimated by

$$\frac{dm}{dt} = -\frac{(m_j - m_{j-1})}{\Delta t} \quad (8.9)$$

At each time step the total mass loss rate (in  $\text{kg/s}$ ) contributed by the solid wood surface can be summed over all the layers ( $L = 1$  to  $n$ ) in the finite difference scheme using Eq. 8.10 where  $A_s$  is the exposed surface area and  $\Delta x$  is the thickness of each layer, and assuming that the gases are instantly transported to the fire-exposed surface of the material where they may burn:

$$\dot{m}_j = \sum_{L=1}^n \left( \sum_{i=1}^3 A_s (Y_{i,j} - Y_{i,j-1}) c_i \rho_o \Delta x \right) \quad (8.10)$$

The mass loss from the exposed wood surfaces can be combined with the mass loss from the movable fire load and the total rate of heat release (which includes burning both within and external to the enclosure) is taken as the product of the total mass loss rate and the effective heat of combustion.

### 8.4.3 Timber Mechanical Properties

Timber is a complex structural material that not only is orthotropic but also has strength characteristics that depend upon species, density, moisture content, stress state, and loading duration. Natural unmodified timber has mechanical properties that depend upon its grain orientation. The parallel to the grain orientation is the strongest and stiffest from a structural perspective. Pure timber, i.e., clear from defects and with perfectly aligned grain orientation, is the strongest in tension with strengths ranging from 70 to 140 MPa for 12% moisture content. Similarly, the compressive strength will typically be in the range of 30–60 MPa [72]. However, timber in reality is not free from defects and thus these values would not typically form the basis of designs. For design purposes timber is graded according to its bending strength using samples of representative size with inherent defects. Tensile strength, due to lack of confinement, is influenced to a larger extent by defects, such as knots, than compressive strength. As a result, in the grading process tensile strength will nearly always be lower than compressive strength. An extract for the strength classes of softwood taken from EN 338: 2003 is shown in Table 8.4 [65]. For ambient design purposes 90th percentile properties are typically adopted, with further modification for loading duration and exposure conditions.

In the determination of bending strengths, timber is loaded in flexure until failure. From this failure load, assuming a linear elastic stress distribution, bending strengths are determined. However, further inspection of the constitutive behavior of timber shows that the bending and tensile strengths shown above are significantly idealized and may be inappropriate for adoption in more complex calculation methods. At ambient temperature the constitutive behavior of timber is widely accepted as being elastoplastic in compression and linear-elastic brittle in tension (Fig. 8.10).

**Table 8.4** Grading properties of timber from EN 338:2003 [65]

Class		C14	C16	C18	C20	C22
<i>Strength properties (N/mm<sup>2</sup>)</i>						
Bending	$f_{M,k}$	14	16	18	20	22
Tension parallel	$f_{t,0,k}$	8	10	11	12	13
Tension perpendicular	$f_{t,90,k}$	0.4	0.5	0.5	0.5	0.5
Compression parallel	$f_{c,0,k}$	16	17	18	19	20
Compression perpendicular	$f_{c,90,k}$	2	2.2	2.2	2.3	2.4
Shear	$f_{v,k}$	1.7	1.8	2	2.2	2.4
<i>Stiffness properties (N/mm<sup>2</sup>)</i>						
Mean MOE parallel	$E_{0,mean}$	7	8	9	9.5	10
5% MOE parallel	$E_{0,05}$	4.7	5.4	6	6.4	6.7
Mean MOE perpendicular	$E_{90,mean}$	0.23	0.27	0.3	0.32	0.33
Mean shear modulus	$G_{mean}$	0.44	0.5	0.56	0.59	0.63
<i>Density (kg/m<sup>3</sup>)</i>						
Density	$\rho_k$	290	310	320	330	340
Mean density	$\rho_{mean}$	350	370	380	390	410

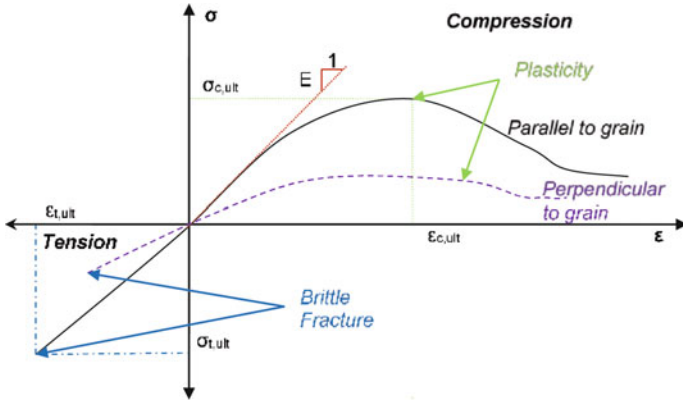


Fig. 8.10 Typical stress-strain behavior of wood (adapted from [26])

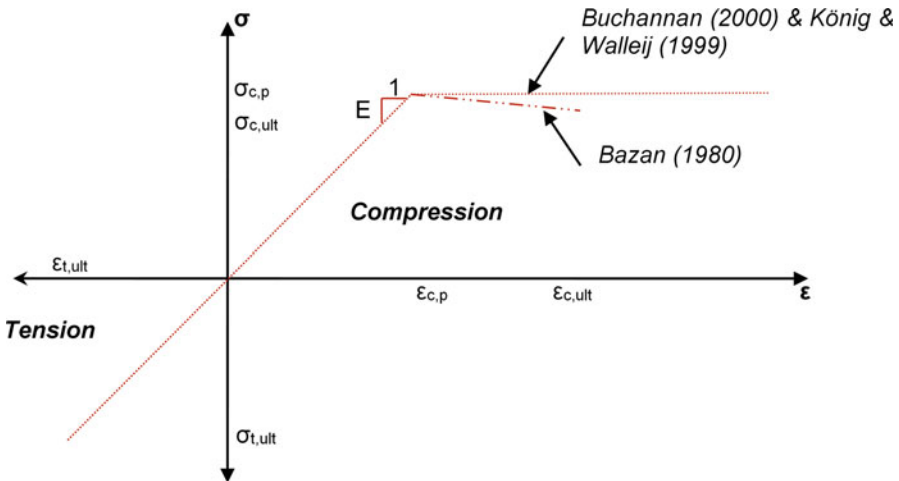
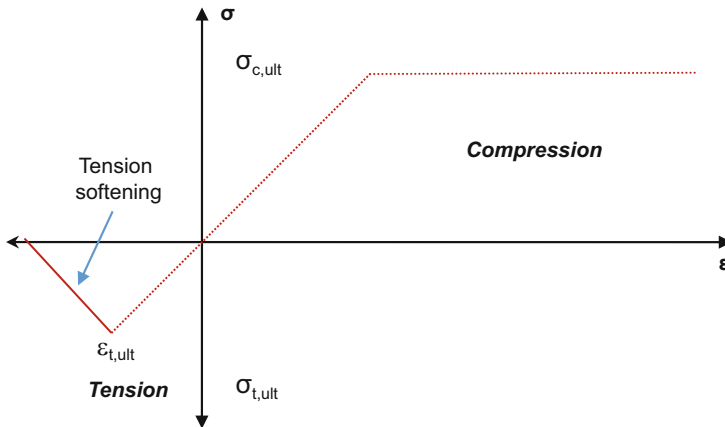


Fig. 8.11 Idealized stress-strain behavior of wood according to Bazan [66], Buchanan [62], and König and Walleij [63]

Observations of this behavior stem back to the 1940s [73] and over the years various simplified elastoplastic stress-strain curves have been proposed (see Fig. 8.11).

Following brittle fracture, the strain energy is not instantaneously released. Instead, there is a tension softening, whereby the achievable tensile stress reduces with increasing crack strain. The integral of the tension-softening stress-strain curve is often referred to as the fracture energy, and has been subject to limited research at elevated temperature for wooden structures.

Studies by Hopkin et al. [74] investigated the influence of fracture energy and tension-softening regime on the failure time of simply supported flexural timber



**Fig. 8.12** Idealized stress-strain behavior of wood according to Hopkin et al. [74], incorporating tension softening

members subject to ISO 834 heating. The parametric study compared numerical simulations against calculations undertaken using the Eurocode 5 Part 1.2 reduced cross-section method, with simulation deviation from the Eurocode approach noted in the function of fracture energy. Based upon this, and associated work [75], an alternative constitutive regime for wood was proposed, incorporating tension-softening postfracture. This is as shown in Fig. 8.12.

A constant fracture energy of c.  $600 \text{ Nm/m}^2$  was shown to give results best aligned with Eurocode 5 part 1.2. However, Hopkin et al. [74] further discuss that increasing fracture energy with increasing temperature may be a pragmatic way of overcoming numerical instability in finite element analyses, without artificially increasing the mechanical resistance of the timber sections.

#### 8.4.3.1 Degradation at High Temperature

Timber, like most structural materials, undergoes some degradation in strength and stiffness at elevated temperature. However, unlike materials like steel and concrete, this degradation for timber occurs over a much narrower temperature range. Typically, timber (both soft- and hardwoods) loses all of its strength and stiffness (regardless of grain orientation) over the temperature range of c.  $20\text{--}300 \text{ }^\circ\text{C}$ , i.e., after undergoing pyrolysis, ignition, and subsequent charring.

Many textbooks and reference documents for timber in fire, such as Buchanan [26] and König and Walleij [53], have collated various strength and stiffness retention factors for timber in fire from classical experimental studies like those of Kollman [76], Schaffer [77, 78], Knudson and Schniewind [48], Gerhards [79], and Östman [80]. These have been summarized in Figs. 8.13–8.15 for tensile strength, compressive strength, and elastic modulus, respectively. In all instances the study

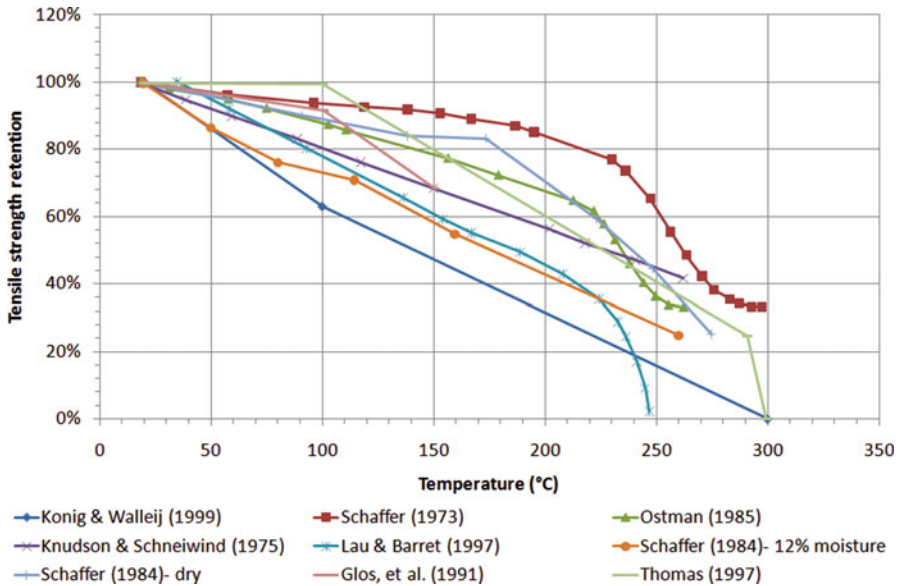


Fig. 8.13 Tensile strength reduction with temperature—various sources

of König and Walleij [53] is also shown as these properties are codified in EN 1995-1-2.

The tensile strength of timber is shown to degrade at a steady rate by all authors included in Fig. 8.13. The properties proposed by Knudson and Schneiwind [48] were derived from small-scale experiments on samples of Douglas fir with a typical moisture content of 12% by weight. Östman [80] tested the tensile strength of small samples of spruce measuring 1 by 10 mm in cross section and derived a constitutive model for timber at elevated temperature. Lau and Barrett [81] conducted experiments on a significant number of  $90 \times 30$  mm boards which were heated to various temperatures before being load tested some 20–25 min later. Schaffer [77, 78] conducted more small-scale experiments on samples that were both kiln-dried and natural (12% moisture content) timber. The tension properties proposed by Thomas [50] were developed on the basis of numerical calibrations using results from experiments by König & Noren [82] and Collier [83]. These properties were later further refined by König and Walleij [53] through further experiments conducted by SP Trätec in 1997 [84].

The compressive strength of timber is shown, in a similar manner to the tension case, to decrease at a steady rate as a function of temperature. However, many of the studies highlighted in Fig. 8.14 were conducted on dry timber, with only nominal moisture content. Gerhards [79] gives upper and lower bounds for the compressive strength variation of softwood with increasing temperature. Separate boundaries are given for dry timber and timber with moisture content in excess of 12% by weight. Schaffer [78] conducted compression tests on small samples of wood with 10% and

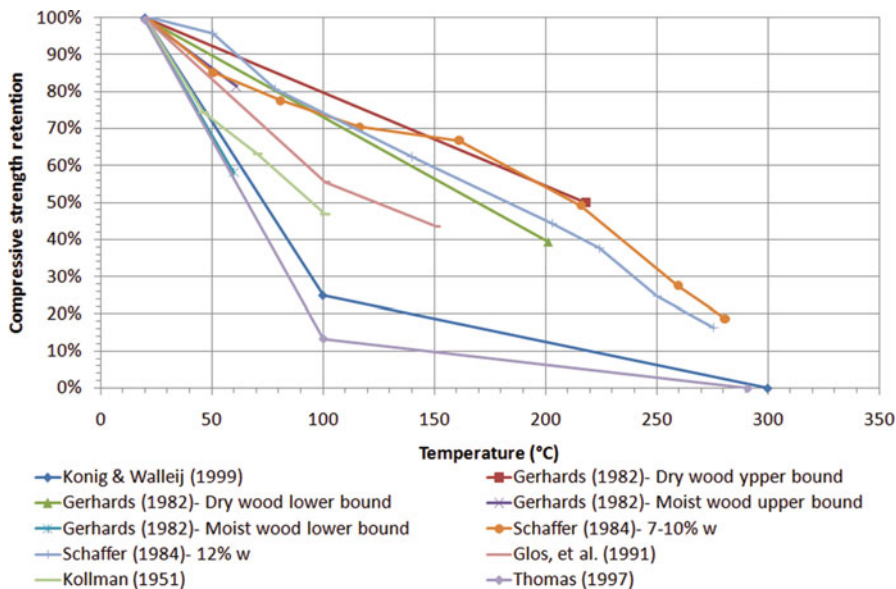


Fig. 8.14 Compressive strength reduction with temperature—various sources

12% moisture content by weight and noted only a marginal difference in strength reduction for the two cases. Many authors [26, 85] note that moisture has a significant influence on both the ambient and elevated compressive strength of timber due to fiber softening. As seen in Fig. 8.14, dry timber undergoes an almost linear decrease in strength with temperature which differs significantly from the degradation noted in wet or moist timber. However, studies indicate that once the moisture content of wet timber is driven away by high temperatures, the timber compressive strength reverts back to that of dry timber.

It can be seen in Fig. 8.15 that there is a clear grouping of the modulus of elasticity (MOE) properties. Experimental studies by Nyman [86], Preusser [87], Schaffer [78], and Östman [80] are generally agreeable. In addition the numerically derived relationship by Thomas [50] is also consistent. All, with the exception of Preusser [87], indicate a linear decrease in MOE with increasing temperature. Although it is not clearly defined in all cases it appears that these properties correspond with the MOE of wood parallel to the grain measured from tensile experiments and this has been confirmed for studies by Östman [80], Preusser [87], and Thomas [50].

The experimental study presented by Kollman [76] was conducted on bending members heated to a constant temperature of 40, 60, 80, and 100 °C, respectively, which were loaded and unloaded in time increments of 1.5 min for an overall

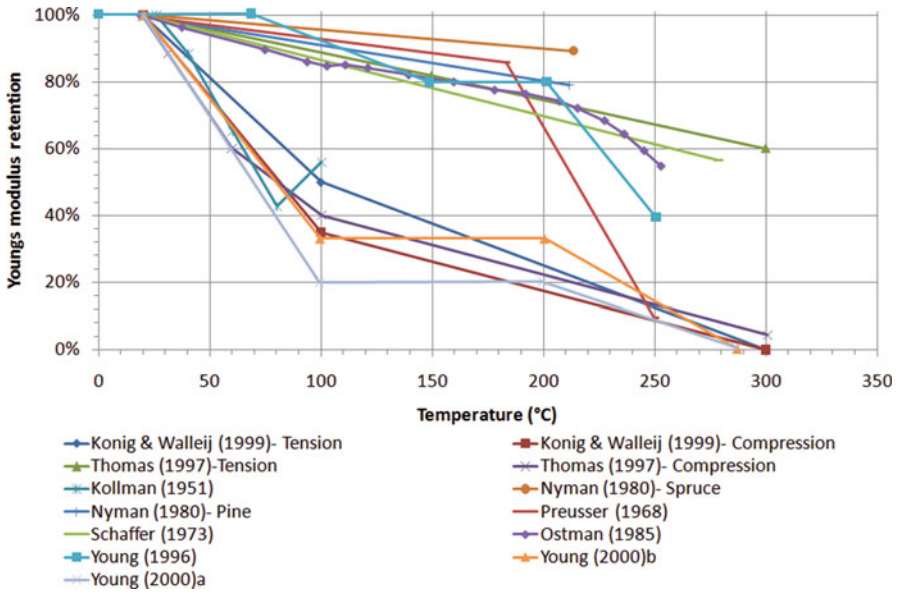


Fig. 8.15 Elastic modulus reduction with temperature—various sources

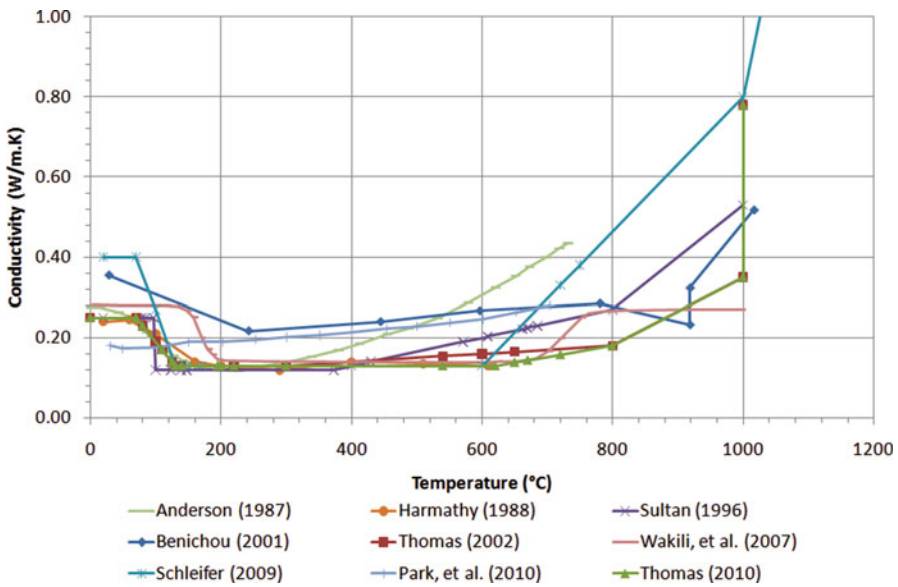


Fig. 8.16 Conductivity of gypsum plasterboard as a function of temperature (various)



experiment duration of 60 min. The lowest parallel to grain MOE was measured in the second or third cycle when the temperature was almost uniform.

In addition to these studies separate more pessimistic MOE correlations are shown by König and Walleij [53] for softwood in both tension and compression.

## 8.5 Protection Methods and Insulation for Timber Structures

Timber frame assemblies, particularly light timber frame construction, derive their fire performance from protective linings and, in some cases, inclusion of insulation within the construction depth.

By far the most common protection choice is gypsum plasterboard. However, this may also be used with timber-based sheathing board products, for example oriented strand board (OSB) or plywood. Where insulation is adopted between, for example, joists and studs, this is most commonly fiber based, using materials like glass or mineral wool. This section summarizes properties of common protection materials, and failure times of protective linings.

### 8.5.1 *Thermophysical Characteristics of Protection Materials and Insulations*

Per Sect. 8.4.1 properties for lining and insulation are given in terms of apparent conductivity, specific heat, and percent of density retained, all as a function of increasing temperature.

#### 8.5.1.1 Gypsum Plasterboard

Plasterboard is perhaps the most widely used passive fire protection (PFP) for timber structures, especially in the case of light timber frame construction. Studs and joists are typically protected with gypsum plasterboard of nominal sheet size of 1.2 by 2.4 m (other variations do exist). Plasterboard is formed by pressing gypsum between two paper facing sheets. In Europe plasterboard is graded. Wallboard, or type A plasterboard [88], refers to standard gypsum core board. Similarly fire-resistant board (American) type X [89] or type C or (European) type F plasterboard (EN 520, [88]) refers to board with enhanced core adhesion at elevated temperature. The improved performance is typically achieved through the introduction of glass fibers or minerals like bentonite or vermiculite, which expand and prevent cracking at high temperature. Similar grading systems exist in the USA and Japan for standard wallboard and fire-resistant plasterboard.

The basis of the desirable fire resistance characteristics of gypsum plasterboard stems from the fact that it is a hygroscopic material. Upon heating gypsum (calcium sulfate dihydrate) undergoes chemical decomposition reactions. The first reaction results in the breakdown of gypsum to calcium sulfate hemihydrate. The second reaction breaks down the calcium sulfate hemihydrate to calcium sulfate anhydrite [90]. Through both these reactions water of crystallization is released (approximately 21% of plasterboard by weight) which requires vast amounts of energy to be evaporated before the gypsum can rapidly increase in temperature in fire situations. The temperature and energy required to mobilize such reactions have been studied widely. However, no definitive answers have been agreed in the literature. As a result, the properties of gypsum are still an area of research interest today. In the aforementioned reactions, the energy assumed to be required to evaporate the resulting released water and the temperatures at which the reactions occur impact heavily the thermal properties of gypsum, specifically the conductivity, specific heat, and mass loss rate.

The heat transfer characteristics of plasterboard have been subject to a number of studies over the last 20 years. A number of widely used temperature-dependent conductivity and specific heat properties exist which have been accurately implemented in the simulation of timber and steel stud walls [58, 90–92]. The most common gypsum properties adopted in such models are shown in the figures that follow, namely the experimental studies of Harmathy [51], Mehaffey et al. [58], and Sultan [92]. In addition to these more cited studies further properties have been derived by Benichou et al. [93], Thomas [90] based on the work of Mehaffey et al. [58], Ang and Wang [94] based on the work of Thomas [90], Park et al. [95], Wakili et al. [96], and a further investigation by Thomas [97]. These are also included in Figs. 8.17–8.19. The studies of Thomas [90, 97] and Ang and Wang [94] adopt gypsum properties derived on the basis of mathematical formulations and are not empirical.

In all cases, the presented properties are effective or apparent—that is, they implicitly include phenomena and degradation that are sensitive to the thermal boundary conditions. Hopkin et al. [74] adapted thermal properties for gypsum plasterboard from the works of Ang and Wang [94], Thomas [90], and Schleifer [98] and applied them in the simulation of temperature development within structural insulated panels (SIPs) subject to furnace conditions. Further, as part of this work, the properties were adopted in the simulation of gypsum-protected engineered floor joist assemblies subject to real fire conditions, with benchmarking against the experimental data of Lennon et al. [99]. These properties were shown to give good agreement with standard fire tests and real fire experiments. Heat capacitance was expressed in terms of enthalpy, with properties as indicated in Fig. 8.19.

### 8.5.1.2 Fiber-Based Insulation Products

Fiber-based insulation is still the most commonly used in timber frame construction, in particular light timber frame. Materials like rock, mineral, and glass fiber have

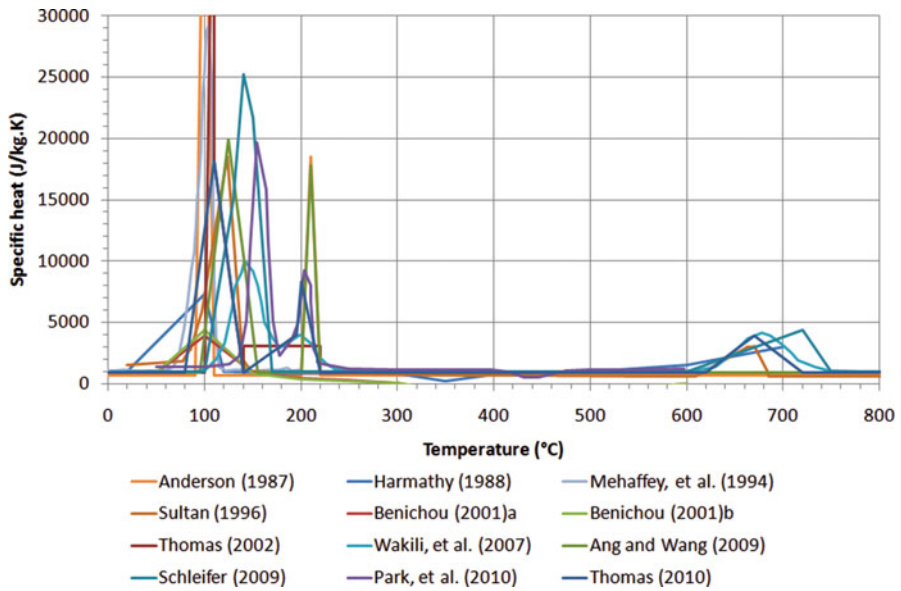


Fig. 8.17 Specific heat of gypsum plasterboard as a function of temperature (various)

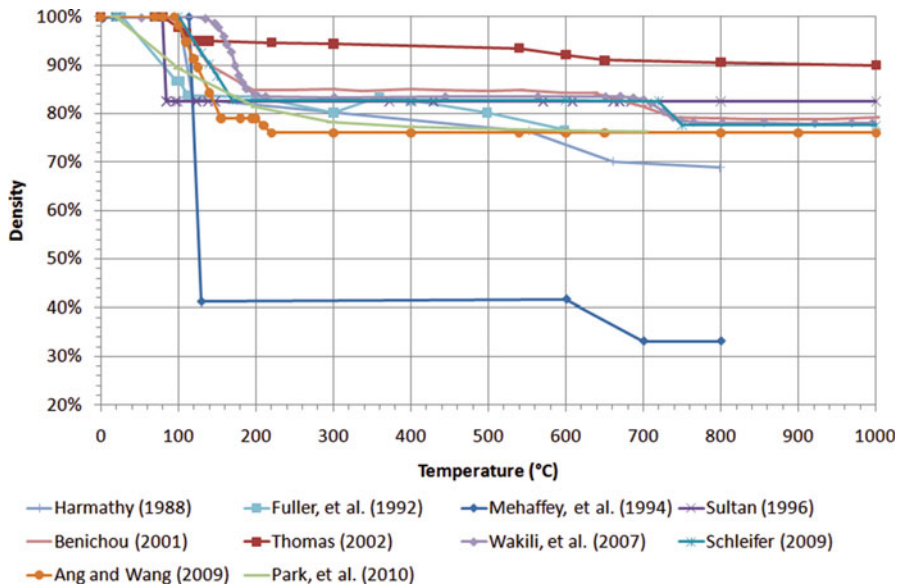
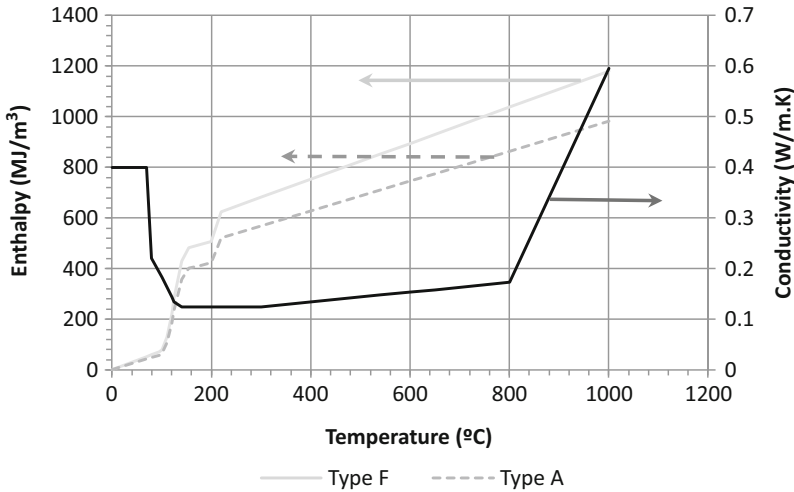


Fig. 8.18 Density retention of gypsum plasterboard as a function of temperature (various)



**Fig. 8.19** Gypsum properties for type F/X and type A/C according to Hopkin et al. [74]

been the subject of investigation by authors like Benichou et al. [93], Jansson [100], and Schleifer [98] at elevated temperature. Twilt and Van Oerle [101] give properties for ceramic blanket, derived as part of the natural fire safety concept research program, which can loosely be considered as an insulant for timber frame, although it is more commonly adopted in fire testing. In addition, Feng et al. [102] in a study of light gauge steel walls also assumed properties for rock fiber insulation which were shown to result in agreeable temperatures with those measured in experiments. In all studies it is apparent that mineral-based wools exhibit more desirable properties than glass fiber-based wools as the former are less likely to melt at high temperatures. Plots of conductivity, specific heat, and density ratio are shown in Figs. 8.20–8.22 summarizing the properties collected by these authors.

### 8.5.2 Failure Conditions/Criteria for Protection Materials

The many thermophysical properties presented for plasterboard previously are only useful and valid while plasterboard remains attached to the element of structure that it is protecting. Plasterboard, depending upon the specification and level of fixing, will not remain fixed in place indefinitely in a fire and will ultimately become detached and fall away. Failure to recognize and predict this in any simulation of a timber frame assembly protected by gypsum board will result in grossly inaccurate predictions of fire performance.

This aspect of gypsum fire performance is recognized in EN 1995-1-2 [54] which gives failure time equations for plasterboard of limited specification exposed to standard fires only. In an extension of this, Just et al. [103–105] and Sultan [106]

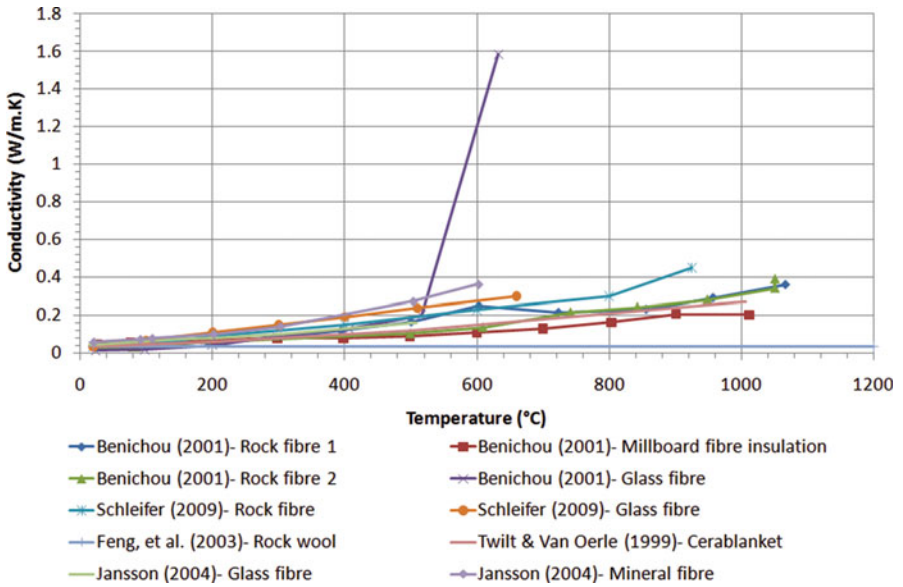


Fig. 8.20 Conductivity versus temperature for various fiber insulation studies

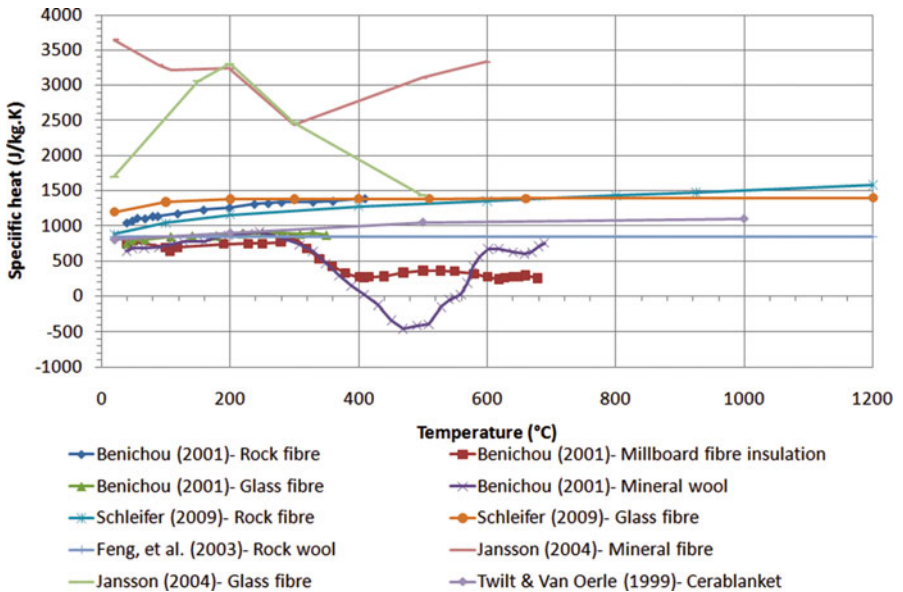


Fig. 8.21 Specific heat versus temperature for various fiber insulation studies

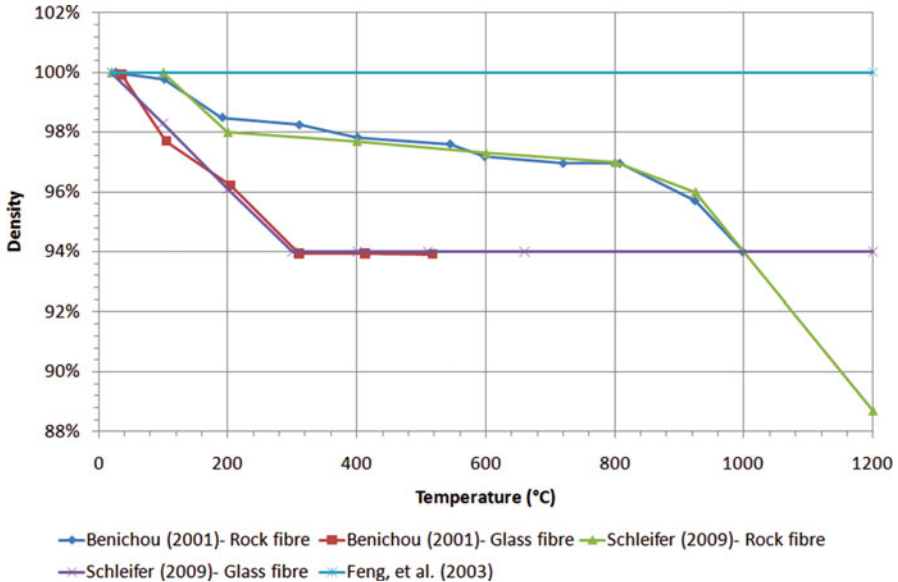


Fig. 8.22 Density retention (%) versus temperature for various fiber insulation studies

have proposed criteria for the prediction of plasterboard failure in standard fires, but for wider specifications of plasterboard than are currently covered by EN 1995-1-2.

Just et al., through access to an extensive database of standard fire tests performed both as research and by manufacturers as part of product certification, propose equations for the determination of plasterboard failure time, in standard fires, for different applications. Proposed correlations between failure time and board thickness are given by Just et al. [103] for multilayered plasterboard specification and distinction is made between plasterboard fixed to ceilings and walls. Unlike EN 1995-1-2, Just and colleagues acknowledged that plasterboard fixed to ceilings is likely to become detached in fires sooner than that fixed to walls in a vertical orientation. The correlations proposed by Just et al. were derived through the determination of pessimistic linear regression lines of best fit, based upon the most onerous plasterboard falloff time, in any given category. The correlations proposed by Just et al. are given dependent on the thickness of a single gypsum board layer,  $h_p$ , and the total thickness of multiple layers,  $h_{p,tot}$ , in Table 8.5.

Sultan [106], also for standard fire exposure, approached the fall-off prediction of plasterboard in a different way to Just et al., by using the concept of critical fall-off temperatures. Sultan [106], through studies of various standard fire tests conducted at NRC, correlated the time at which plasterboard broke away with the rear of the board temperature. Sultan [106] found that this temperature was relatively consistent for a given plasterboard specification, i.e., single layer, double layer, and with or without insulation. Critical fall-off temperatures, complete with standard deviations

**Table 8.5** Estimation of plasterboard failure time in fire resistance test conditions according to Just et al. [103–105]

Specification	Walls		Ceilings	
Type F single layer	$4.5h_p - 24$	$9 \leq h_p \leq 18$ mm	$h_p + 10$	$12.5 \leq h_p \leq 16$ mm
	57	$h_p > 18$ mm	26	$h_p > 16$ mm
Type F double layer	$4.5h_p - 40$	$25 \leq h_p \leq 31$ mm	$2h_p - 3$	$25 \leq h_p \leq 32$ mm
	100	$h_p > 31$ mm	61	$h_p > 32$ mm
Type F + type A <sup>a</sup>	81	$h_p \geq 15$ mm <sup>b</sup>	59	$h_p \geq 15$ mm <sup>b</sup>
Type A single layer	$1.9h_p - 7$	$9 \leq h_p \leq 15$ mm	$1.8h_p - 7$	$12.5 \leq h_p \leq 15$ mm
	21.5	$h_p > 15$ mm	20	$h_p > 15$ mm
Type A double layer	$2.1h_p - 14$	$25 \leq h_p \leq 30$ mm		
	49	$h_p > 30$ mm		

<sup>a</sup>Outer layer type F, inner layer type A<sup>b</sup>Thickness of first (type F) layer**Table 8.6** Critical rear-face falloff temperatures under standard fire exposure as proposed by Sultan [106]—wall assemblies

Wall assembly characteristics		Falloff temperature and standard deviation (°C)		
Insulation	Screw spacing (mm)	Single layer	Double layer	
			Face layer	Base layer
No insulation in cavity	406	***	$780 \pm 45$	***
	610	$775 \pm 20$	***	***
Insulation in cavity against gypsum boards	406	$755 \pm 30$	$790 \pm 20$	$640 \pm 20$
	610	$785 \pm 35$	***	***
Spray-on insulation	406	***	$830 \pm 25$	$625 \pm 20$
	610	***	***	***

\*\*\* not investigated

derived by Sultan [106] for wall and floor linings, are shown in Tables 8.6 and 8.7, respectively.

Just et al. [103–105] gives further temperatures behind plasterboard at the time of failure for type F and type X boards in wall and ceiling configurations, as a function of furnace exposure time. These are shown in Fig. 8.23.

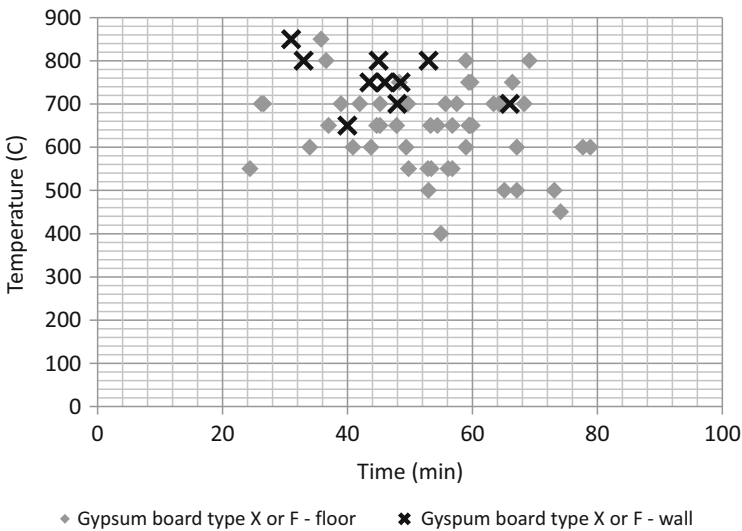
## 8.6 Observations from Contemporary Research

Designing ambitious and uncommon structures with timber requires a full understanding of the fire dynamics of a compartment with timber linings (both encapsulated and exposed), the combustion of timber (ignition and self-extinction), as well

**Table 8.7** Critical rear-face falloff temperatures under standard fire exposure as proposed by Sultan [106]—floor assemblies

Floor assembly characteristics		Falloff temperature and standard deviation (°C)		
Insulation	Screw spacing (mm)	Single layer	Double layer	
			Face layer	Base layer
No insulation in cavity	406	460 ± 20	620 ± 50	430 ± 90
	610	***	510 ± 50	330 ± 40
Insulation in cavity against gypsum board	406	680 ± 50	680 ± 40	620 ± 40
	610	***	640 ± 40	480 ± 40
Spray-on insulation	406	670 ± 40	***	***
	610	***	600 ± 40	380 ± 30

\*\*\* not investigated



**Fig. 8.23** Temperatures behind gypsum plasterboard at the moment of failure, for type F and type X gypsum boards [103–105]

as the structural behavior of timber (solid and engineered). This section highlights scientific observations in the research method in the previous sections as well as documents recent compartment tests of encapsulated and exposed timber. Areas of further research and study to close the research gap for timber are detailed.



### 8.6.1 Extinction

Self-extinction of flaming combustion of timber is essential to utilize timber in structures with prolonged evacuation and/or fire brigade intervention times. Without self-extinction, burnout of a compartment and maintaining of structural integrity are not achievable. Section 8.2.2.3 speaks to the conditions necessary to realize self-extinction, whereby in the absence of an external heat flux, self-extinction can occur where the mass loss rate drops below anything from 2.5 to 5 g/m<sup>2</sup>.s. Demonstrating that self-extinction is achievable requires full consideration of the energy balance in a compartment, i.e., convective and radiative losses via openings, losses to the enclosure boundaries, energy stored in the gas, and consideration of reradiation between exposed flaming and hot surfaces.

Bartlett et al. [20] give a thorough review of correlations relating to flame extinction. Therein, the authors cite Quintiere and Rangwala [107] who proposed a critical mass flux for extinction as a function of the oxygen concentration, external heat flux, and heat losses, as given in Eq. 8.11:

$$\dot{m}''_{cr,ex} = \frac{1}{L_v} \left[ \frac{h_c}{C_p} \left[ \frac{Y_{ox,\infty} \Delta H_c}{\nu} - C_p (T_p - T_\infty) \right] + \dot{q}''_{e,r} - \sigma (T_p^4 - T_\infty^4) \right] \quad (8.11)$$

where  $L_v$  is the heat of vaporization,  $Y_{ox,\infty}$  is the ambient oxygen concentration,  $\nu$  is the stoichiometric oxygen-fuel ratio,  $T_p$  is the pyrolysis temperature,  $\Delta H_c$  is the heat of combustion, and  $\dot{q}''_{e,r}$  is the external radiant heat flux.

For an estimation of the mass loss rate per unit area within an enclosure, Bartlett et al. [20] give

$$\dot{m}'' = \frac{\dot{q}''_e + \dot{q}''_f - \dot{q}''_l}{L_v} \quad (8.12)$$

where  $q''$  is the heat flux, with subscripts e, f, and l representing net heat external heat flux, heat flux from the flames, and heat losses, respectively. Bartlett et al. [20] note: “it is the net heat flux at the char-timber interface that is of interest.” Thus,  $L_v = \Delta H_v$ , with  $\Delta H_v$  the heat of vaporization.

### 8.6.2 Structural Response

The structural response of timber in fire is dependent on the thermal exposure and other parameters, such as oxygen concentration of surrounding gases [108, 109] and air velocity ([110]). Different testing methods control the thermal exposures in different ways under different conditions. However, most current knowledge of the structural behavior of timber in fire conditions was obtained from fire resistance tests, in which standard thermocouples are used to follow a nominal fire exposure

(further discussed in Chapter 2). Nonstandard fire tests have also been performed to obtain knowledge of the behavior of structural timber in fire, including furnace tests following parametric time-temperature curves and tests in which a mobile radiant panel induces a controlled heat flux to a specimen.

Most of the recent research of the structural behavior of timber in fire was performed for the development and evaluation of methods to calculate the resistance of light timber frame assemblies [111, 112], sawn and glue-laminated timber [113, 114], CLT [115, 116], and connections between glue-laminated beams (e.g., [117, 118]) subjected to nominal fire exposure. Barber [119], Ronstad and Ek [120], and Brandon et al. [121] identified that the most common types of connections tested are not relevant for tall timber structures and published test results of a number of shear-loaded column beam connections with a fire resistance of 90 or 120 min, which are relevant for tall timber buildings.

A number of studies focused on the structural behavior of timber in other fire conditions ([122, 123]; Brandon et al. [124]. Lange et al. [122] and Brandon et al. [124] studied the behavior of timber subjected to parametric fire exposure. Traditionally, the charring rate is used to calculate the reduction of the load-bearing capacity of timber members. However, recent studies have shown that this is not straightforward during a decay phase of a fire as the load-bearing capacity of a structure continues to decrease even after charring stops [124–126]. These studies also indicated that structural failure can occur after extinguishment of a fire.

### 8.6.3 *Compartment Fire Experiments*

Due to the combustible nature of timber, the presence of exposed and sometimes initially protected timber can influence the development and duration of a compartment fire. Numerous full-scale compartment fire experiments have been performed in order to study the response of structural timber to a compartment fire and to study the influence of the timber on compartment fire dynamics. Table 8.8 gives an overview of studies for which compartment fire experiments were conducted. In the table, the main structural materials are indicated as LTF (light timber frame), HLT (heavy parallel-laminated timber slabs), CLT (cross-laminated timber), NLT (nail-laminated timber), or GLT (glue-laminated timber). The table indicates the number of experiments that are performed with each category of structural system. For heavy timber structures, the table indicates whether surfaces are protected (P), partially protected (PP), or unprotected (UP). The opening factor was calculated using  $O = A_o\sqrt{H_o}/A_t$ , where  $A_o$  and  $H_o$  are the area and height of the opening in meters and  $A_t$  is the total area of the boundary surfaces. If multiple experiments were performed within the same test series, the main varied parameters are indicated in the table.

**Table 8.8** Overview of fire experiments of compartments with timber structure. Dimensions and fire load density are given for the ignited compartment

Ref.	No. of tests	Floor area (m <sup>2</sup> )	Vent area (m <sup>2</sup> )	Opening factor	Main struct. Members	Varied parameters in different tests	Movable fire load density (MJ/m <sup>2</sup> )
Lennon et al. [127]	1	N.F.	N.F.	N.F.	LTF	N.A.	N.F.
Hakkarainen [128]	4	15.8	2.76	0.042	2 × HLT (P) 1 × HLT (UP) 1 × LTF	– Presence of protection – Type and number of protective gypsum layer – Structural system	Wood cribs: 900 <sup>a</sup>
Frangi and Fontana [129]	6	18.0	2.55	0.041	LTF	– Combustibility of cladding materials – Presence of sprinklers – Number and thickness of gypsum board layers	Cribs and bed: 211–237
Frangi et al. [130–132]	1	11.1	2.00	0.032	CLT (P)	N.A.	Cribs and bed: 790
Lennon et al. [99]	3	12.0	1.40	0.024	LTF	– Type of light timber frame floor assembly	Wood cribs: 450
McGregor [133] Li et al. [134] Medina Hevia [135]	11	15.8	2.14	0.042	3 × CLT (P) 2 × CLT (UP) 3 × CLT (PP) 2 × LTF 1 × LSF	– Structural system – Area of exposed surface – fuel type and density	2 × propane: 182 or 486 9 × furniture: 532–615
Su and Loughheed [136]	4	52.5	4.50	0.031	2 × LTF 1 × CLT (P) 1 × LSF	– Structural system	Furniture: 550
Su and Muradori [137]	1	23.7	4.70	0.064	CLT (P)	N.A.	Furniture and wood cribs: 790
Kolaitis et al. [138]	1	4.9	0.42	0.015	CLT (P) and LTF	N.A.	Wood cribs: 420
Janssens [139]	2	14.8	3.9	0.084		– Structural system	Furniture: 575–600 <sup>b</sup>

(continued)

Table 8.8 (continued)

Ref.	No. of tests	Floor area (m <sup>2</sup> )	Vent area (m <sup>2</sup> )	Opening factor	Main struct. Members	Varied parameters in different tests	Movable fire load density (MJ/m <sup>2</sup> )
Hox [140]	2	13.3	3.27	0.070 <sup>c</sup>	1 × CLT (P) 1 × CLT and NLT (P) 2 × CLT (PP)	– Presence of sprinklers	Desk, mattress, cribs: 653
Hadden et al. [5]	5	7.4	1.4	0.042	5 × CLT (PP)	– Area of exposed surface	Wood cribs: 132
Janssens [141]	3	15.9	1.8	0.033	3 × CLT (UP)	– type of adhesive of CLT	Propane: 456
Brandon et al. [108, 109]	1	15.8	4.50	0.077	CLT (PP)	N.A.	Furniture: 550
Su et al. [142]	6	41.9	3.6	4 × 0.032 6 × 0.065	2 × CLT (P) 4 × CLT (PP)	– Opening dimensions – Area of exposed surface	Furniture: 550
Zelinka et al. [143]	5	82.8	17.8	0.105	1 × CLT (P) 2 × CLT (PP) 2 × CLT (UP)	– Area of exposed surface – Presence of sprinklers	Furniture: 550
Su et al. [144]	5	10.8	1.6	0.03	1 × CLT (P) 1 × CLT (P) and GLT (UP) 2 × CLT (PP) 1 × CLT (PP) and GLT (UP)	– Area of exposed surface – Presence of exposed glue-laminated beam and column	Wood cribs: 550

<sup>a</sup>The reported effective fuel load density was 720 MJ/m<sup>2</sup> (80% of 900 MJ/m<sup>2</sup>), which was determined with a combustion efficiency of 0.8. For consistency with other rows in this table, the given fuel load density does not account for the combustion efficiency

<sup>b</sup>Value determined from a graph in the resource

<sup>c</sup>Window was initially closed

This section separately discusses studies involving compartment experiments of (1) light timber frame structures, (2) heavy timber structures with solely encapsulated timber, and (3) heavy timber structures with at least a part of timber surfaces exposed.

### 8.6.3.1 Compartment Fire Experiments of Light Timber Frame Structures

Fire experiments of compartments made of light timber frame (LTF) structures were reported by Lennon et al. [127], Hakkarainen [128], Frangi and Fontana [129], Li et al. [134], and Su and Loughheed [136]. Additionally, Lennon et al. [99] reported fire tests of three compartments with masonry walls and different light timber frame floor assemblies and Kolaitis et al. [138] performed a compartment fire experiment made of a variety of mass timber and light timber frame assemblies. Parameters of these tests can be found in Table 8.8.

The fire performance of light timber frame structures is to a large extent dependent upon the performance of the cladding of assemblies. Su and Loughheed [136] reported two full-scale fire experiments of compartments which had light timber frame structures lined with two layers of 12.7 mm type X gypsum boards. Their tests indicated that falloff of gypsum boards increases the heat release rate if the timber frame becomes involved in the fire. In both experiments, the timber structure became involved in the fire and both experiments were manually extinguished. The authors reported a similar experiment of a compartment made of CLT with similar gypsum board protection. In contrast with the experiments of the light timber frame structure, the gypsum board remained in place during the experiments of the CLT structure. Also Li et al. [134] observed that falloff times of gypsum boards are dependent upon the structure of the ceiling or wall members, as they observed significantly quicker gypsum board falloff in an experiment with encapsulated light steel frames than in tests with light timber frames. Comparisons of temperatures measured in the walls suggested that the protection effect of gypsum boards was better in CLT walls than in light timber frame walls. Li et al. [134] performed two compartment experiments made of light timber frame structures encapsulated with two layers of 12.7 mm thick type C gypsum boards, as a part of a large study with 11 compartment tests (as indicated in Table 8.8). In both experiments, two layers of type C gypsum boards were sufficient to avoid involvement of the timber structure in the fire. The fire decayed in a similar fashion as other experiments with sufficient protection and no signs of heat release rate or temperature increase were observed before the end of the experiment.

Frangi and Fontana [129] presented three pre-flashover and three post-flashover fire experiments of light timber frame compartments. The three pre-flashover experiments aimed to study the effect of sprinklers on fires in compartments with combustible linings. The three post-flashover experiments were each conducted on a two-story setup and the linings of the compartments were either combustible or noncombustible. The window of the ignited lower floor compartment was open and

the window of the second floor was closed. The fire in the compartment with solely combustible linings had a significantly higher fire plume out of the ventilation opening, which resulted in failure of the double-glazed upper window after just 7.5 min. In the two experiments with solely noncombustible (gypsum board) linings the upper window failed after more than 40 min, which was significantly later.

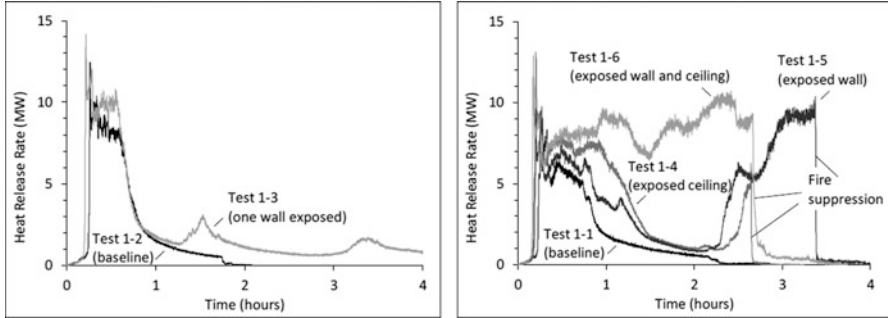
### 8.6.3.2 Compartment Fire Experiments of Heavy Timber Structures with Exposed CLT

Two studies in the early 2000s compared fire tests of compartments with noncombustible linings (baseline test) and fire tests of similar compartments with solely timber linings [128, 129]. In both studies the baseline compartment fire test involved a ventilation-controlled phase and in both studies the contribution of exposed timber was evidenced by a significantly larger fire plume out of the ventilation opening of a compartment.

Studies involving full-scale fire tests of compartments with exposed CLT have been performed by McGregor [133], Medina Hevia [135], Hox [140], Emberley et al. [4], Hadden et al. [5], Brandon et al. [108, 109], Su et al. [142], Zelinka et al. [143], Janssens [141], and Su et al. [144]. Multiple tests of these studies indicated that debonding of exposed CLT can lead to fire regrowth and continuous fires. Figure 8.24 shows a photo of a compartment fire test reported by Su et al. [142]. The photo shows fires at 1 h after ignition in two similar compartments with similar contents. The left-hand compartment comprises solely encapsulated CLT and the right-hand compartment has an exposed CLT ceiling and one exposed CLT wall. At 1 h after ignition the compartment on the left-hand side (test 1–1 by Su et al.) decayed and was approaching self-extinguishment. The compartment on the right-hand side (test 1–6 by Su et al.), however, had an increase of intensity around



**Fig. 8.24** Fully encapsulated compartment (left) and compartment with an exposed CLT wall and ceiling (right) 1 h after ignition (frame of a video by NIST, USA)



**Fig. 8.25** Heat release rates of compartments with a large opening (left) and compartment with a small opening (right), from Su et al. [142]

1 h after ignition, which was caused by debonding. This test was continued until the ceiling collapsed. Figure 8.25 shows heat release rates of fires in fully encapsulated compartments (test 1-1 and 1-2) and similar compartments with some exposed CLT surfaces. A significant cause of the differences between the curves is due to the occurrence of debonding in compartments with exposed CLT.

Although the majority of reviewed compartment tests with exposed regular CLT resulted in continuous fires, studies by Medina Hevia [135], Emberley et al. [4], Hadden et al. [5], and Zelinka et al. [143] included fire compartment tests without the occurrence of debonding that self-extinguished, even though a (limited) area of CLT surface was exposed.

Emberley et al. [4] conducted a large-scale compartment test in order to compare self-extinction observations and data from small-scale tests to the results seen in the large-scale tests. The compartment internal dimensions were  $3.5 \times 3.5 \times 2.7$  m with a single opening ( $0.8 \times 2.1$  m). One wall and ceiling were left as exposed timber and the remaining walls were encapsulated with Knauf FireShield. 80 kg of fuel was placed within the compartment and the amount of fuel was designed to yield a fire duration that allowed the flames to self-extinguish. Heat flux gauges were placed near the surface of the walls and ceiling to compare the external heat flux on the exposed surfaces during the duration of the test. The results (Fig. 8.26) show good agreement with the self-extinction critical heat flux measured by thin skin calorimeters (TSC) in the small-scale tests. The study confirmed the phenomena of self-extinction in compartment fires where debonding does not occur.

A test by Brandon et al. [108, 109] and one out of six tests by Su et al. [142] indicated that debonding of CLT does not always lead to a fully developed fire. Compartments of those two tests had a relatively high opening factor and followed, despite the occurrence of debonding, a decaying trend.

Debonding is caused by weakening of the adhesive bond due to increased temperatures. Therefore, the occurrence of debonding is dependent on the type of adhesive used in CLT. Studies by Janssens [141] and Brandon and Dagenais [145] proposed methods to identify adhesives that do not lead to debonding. Su et al. [144] performed similar, but smaller scale, tests as were presented earlier in the same year

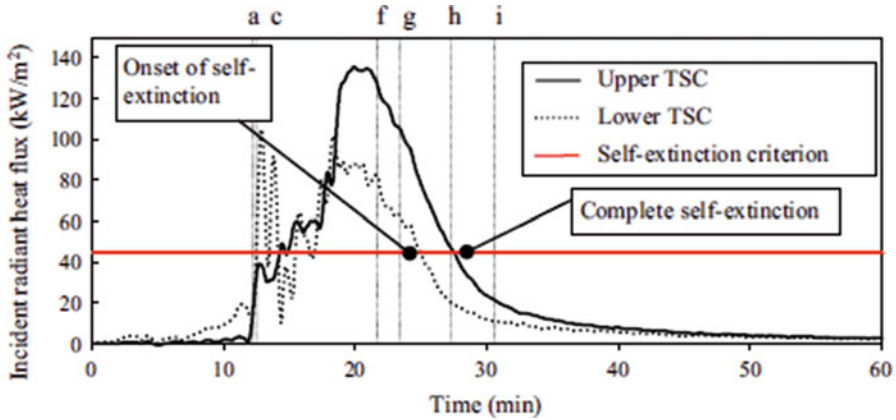


Fig. 8.26 Wall external heat flux at the top and bottom of the wall [4]

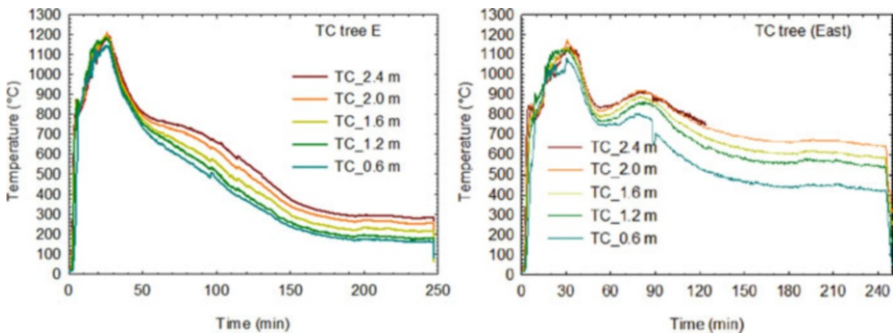


Fig. 8.27 Temperatures of a compartment fire test with left, one wall and 10% of the ceiling exposed (test 2), and right, relatively large (in comparison with the room size) columns and beam exposed (test 3) [144]

by a group with the same main author [142]. However, in the new series compartments were made of CLT with a polyurethane adhesive that was identified as a non-delaminating adhesive in both studies by Janssens [141] and Brandon and Dagenais [145]. Figure 8.27 shows results of two of the five tests by Su et al. [144]. Although the base layer of two ½ inch type X gypsum board layers remained in place to protect the CLT, the CLT started charring and contributing to the fire in the room. This prevented full decay of the compartment fire. Exposing more surface area of CLT led to an increased contribution of the protected CLT. Debonding of CLT was successfully avoided by using CLT that did not delaminate in the standard compartment fire test required by ANSI/APA PRG320 [146].



### 8.6.4 Engineered Timber and Debonding

Reducing debonding of engineered timber is of utmost importance for ensuring self-extinction of any form of timber. Charring rates have been shown to double when char and timber ply debonding occurs and consequences such as increased heat release rates, sustained post-flashover thermal loads, and even secondary flashover can occur if debonding occurs.

Very little research has been conducted on factors influencing debonding; however, conceptual research points towards a combination of thermal degradation, thermal stresses, and interfacial stresses playing significant roles in the propensity for engineered timber to debond [4].

The bond of a composite (which engineered timber is) is designed to transfer shear and normal forces from one lamella (ply) to adjacent lamella. This composite action comprises the benefit and strength of a composite. For a composite material to remain intact and continue to carry the loads applied to it, the adhesive must be able to transfer the loads between the lamella. However, at elevated temperatures, adhesive bond strength begins to decrease. Several researchers have studied the bond strength of engineered timber adhesives at elevated temperatures. Frangi et al. [147] conducted adhesive shear tests with bonded lengths of 40 mm. The results (Table 8.9) show how susceptible certain adhesives are to temperature. Clauß et al. [148] also studied debonding but used a 10 mm bond length. Seven different adhesives were studied and the results yield similar results to Frangi et al. [147].

Studying the adhesive performance under elevated temperature alone is not enough to determine the overall performance of a composite material such as engineered timber. Several studies [4, 149, 150] showed the importance of bond length and the resulting interfacial stresses in the overall performance of a bond. Nicolaidis et al. [150] showed that bond length coupled with temperature effects on the adhesive is important for ultimate strength. Figure 8.28 shows three single-lap shear tests (600 mm bond length) at three different temperatures. The ambient tests reached an ultimate load and failed by brittle timber failure. The 80 °C test exhibited a much larger displacement indicating that debonding of the joint occurred but that the transfer of the loads through the interface resulted in debonding and large displacements. The 150 °C test yielded complete adhesive failure and no large displacements. This is indicative of a bond that has debonded but the bond length was not sufficient to achieve full ultimate load.

**Table 8.9** Failure temperatures of adhesive bonds (40 mm) under shearing loads [147]

Adhesive	Failure temperature
Kauresin 460 (resorcinol-formaldehyde)	>170 °C
Kauranat 970 (1 component—Polyurethane)	180–190 °C
Balcotan 107 TR (1 component—Polyurethane)	50–60 °C
Balcotan 60,190 (1 component—Polyurethane)	190–200 °C
Purbond HB 110 (1 component—Polyurethane)	60–70 °C
Purbond VN 1033 (1 component—polyurethane)	150–160 °C

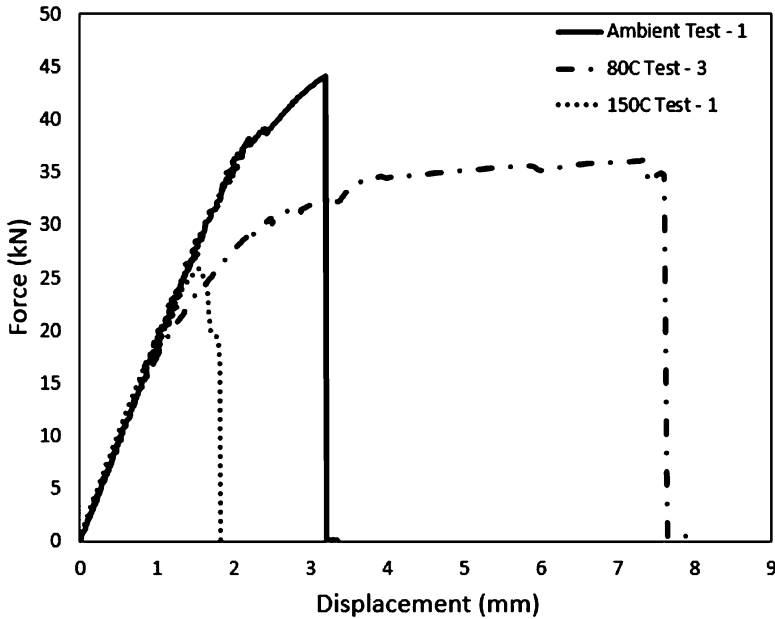


Fig. 8.28 Force displacement of single-lap shear tests at elevated temperatures [150]

Emberley [4] also documented the importance of interfacial stresses on the debonding potential of engineered timber. Local discontinuities result in increased levels of normal forces. These increased forces contribute to debonding failure. The results of Emberley [4] showed that debonding is a complex interaction between applied load, interfacial stresses, adhesive degradation, temperature elevation, and composite type, among others. Understanding the full thermomechanical behavior of a bonded joint is necessary to ensure that debonding does not occur and compromise not only the fire performance but also the structural integrity of the engineered timber.

## 8.7 Design Fires and Wooden Structures

Chapter 4 provides a broad discussion on design fires in the context of structural fire safety. This section serves to discuss the implications of timber's inherent combustibility on the design fire conditions, and how this has been addressed by different researchers and practitioners. In practice effective cross-section methods are commonly used to predict the structural capacity of timber members in a fire. These methods account for a complete loss of strength and stiffness in the char layer and a reduction of properties in a heated zone of the remaining material, to estimate the capacity of a timber member. The char layer, which is dependent on the charring rate

and the duration of the exposure, is, therefore, an important parameter for the implementation of effective cross-section methods.

### 8.7.1 Constant Heat Flux

For steady-state design fire conditions, expressed in terms of an exposure (constant) heat flux, the rate of char formation has been subject to much research.

Butler [151] compared Baltic redwood at heat fluxes between 5 and 60 kW/m<sup>2</sup> and Guatemala cedar tested in a carbon arc for short durations at heat fluxes of 300–3300 kW/m<sup>2</sup>. From this, a relationship between incident heat flux [kW/m<sup>2</sup>] and charring rate [mm/min] is given in Eq. 8.13:

$$\beta = 0.022\dot{q}'' \quad (8.13)$$

where  $\beta$  is the charring rate in mm/min.

Through a collection of references for timber of different species and subject to differing incident heat flux, Bartlett et al. [20] note a revised linear dependence on incident heat flux [kW/m<sup>2</sup>] and charring rate [mm/min], as given in Eq. 8.14:

$$\beta = 0.020\dot{q}'' \quad (8.14)$$

### 8.7.2 Nominal Time-Temperature Curves

Nominal time-temperature curves refer to those adopted for compliance and classification purposes, e.g., as is subject to further discussion in Chaps. 2 and 4, the standard ISO834 heating regime.

Many researchers have focused upon charring rates under standard fire conditions. Lie [59] after Schaffer [152] indicated a linear relationship between charring rate and density for standard fire exposure. This was further complicated by the introduction of moisture content. Buchanan [26] notes that the Australian fire code [153] gives similar charring rate values to those proposed by Lie [59] for standard fire exposure, with charring rates for moisture contents of 10–15% given by Eq. 8.15. In this instance the equation expresses charring rate ( $\beta$  in mm.min<sup>-1</sup>) as a function of density ( $\rho$  in kg/m<sup>3</sup>):

$$\beta = 0.4 + \left(\frac{280}{\rho}\right)^2 \quad (8.15)$$

In expansion of this concept White [154] proposed that the assumption of a constant charring rate for standard fire exposure was an oversimplification. He

gives the following relationship (Eq. 8.15) for the charring rate of softwood (again in mm/min):

$$\beta = 2.58 \left( \frac{\beta_n}{t} \right)^{0.187} \quad (8.16)$$

where  $\beta_n$  is the nominal charring rate obtained from the depth of char measured after 1 h of ISO834 [155] fire exposure ( $\beta_n = 0.635$  mm/min) and  $t$  is time in minutes.

### 8.7.3 Simplified Post-Flashover Fire Models

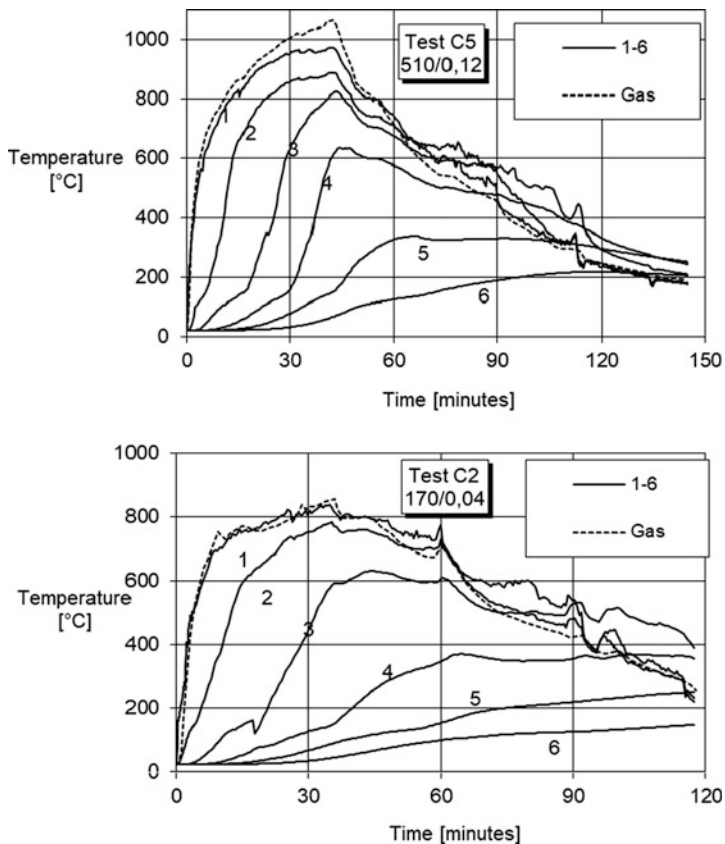
A number of studies have sought to establish and provide a means of designing/evaluating timber structures when subject to simplified idealizations of realistic fire conditions. These, in the main, have focused on post-flashover fire models, such as the Eurocode parametric fire.

Initial research into timber performance in natural fires was conducted in Scandinavia ([156, 157], and [63]) which would later form the parametric charring method in EN 1995-1-2. König and Walleij [63] investigated charring depth and temperature profiles in solid timber slabs ( $325 \times 225 \times 95$  mm) subject to parametric fires. The parametric fires corresponded with opening factors and fire load density (relative to the enclosure surface area) of  $0.12 \text{ m}^{0.5}/510$  and  $0.04 \text{ m}^{0.5}/170 \text{ MJ/m}^2$ . Temperatures through the depth of the timber element were measured at (1) 0 mm, (2) 6 mm, (3) 18 mm, (4) 30 mm, (5) 42 mm, and (6) 54 mm, relative to the exposed surface. Sample temperature profiles for two of the six experiments are shown in Fig. 8.29.

The main motivation for the König and Walleij [63] experimental study was to determine char depth as a function of time for heating exposures that were not the ISO 834 time-temperature regime, and to adopt these in the verification of an empirical charring depth model for parametric fires proposed by Hadvig [156]. For completeness, the correlations are summarized below, and the char development process is split into three stages: (a) the constant charring rate phase—from time zero to  $t_0$ ; (b) the decaying charring rate phase—from  $t_0$  to  $3t_0$ ; and (c) the charring termination phase, i.e., no further char development—for times  $>3t_0$ :

$$\beta_{\text{par}} = 1.5\beta_0 \frac{0.2\sqrt{\Gamma} - 0.04}{0.16\sqrt{\Gamma} + 0.08} \quad (8.17)$$

$$t_0 = 0.009 \frac{q_{t,d}}{O} \quad (8.18)$$



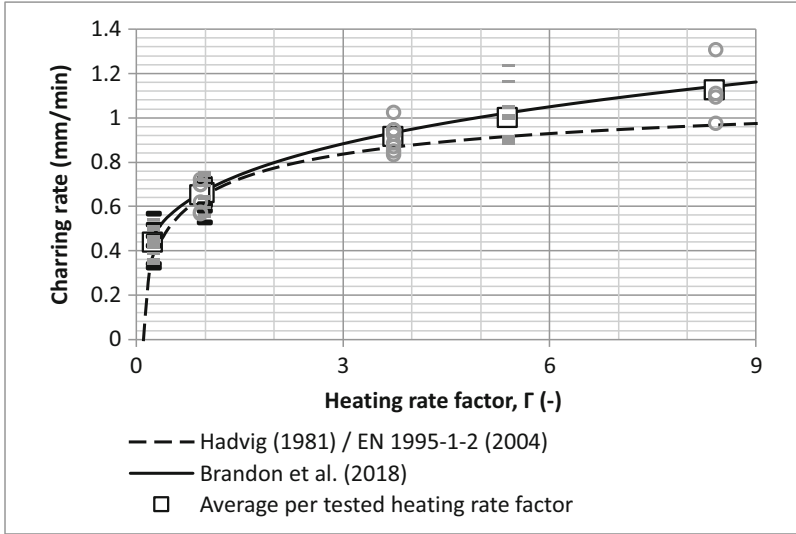
**Fig. 8.29** Temperature profile through wood, adapted from König and Walleij [63]: top— $0.12 \text{ m}^{0.5}/510 \text{ MJ/m}^2$ , and bottom— $0.04 \text{ m}^{0.5}/170 \text{ MJ/m}^2$

$$d_{\text{char}} = \beta_{\text{par}} t \quad \text{for } t \leq t_0 \tag{8.19}$$

$$d_{\text{char}} = \beta_{\text{par}} \left( 1.5t - \frac{t^2}{4t_0} - \frac{t_0}{4} \right) \quad \text{for } t_0 < t < 3t_0 \tag{8.20}$$

$$d_{\text{char;end}} = 2\beta_{\text{par}} t_0 \quad \text{for } t \geq 3t_0 \tag{8.21}$$

with  $\beta_0$  the ISO834 exposure charring rate (mm/min),  $\Gamma$  the parametric time modifier (–) as defined in EN 1991-1-2,  $t$  the time (min),  $O$  the opening factor ( $\text{m}^{0.5}$ ), and  $q_{td}$  the fire load density per unit area of fire enclosure surfaces ( $\text{MJ/m}^2$ ).



**Fig. 8.30** Charring rates during the fully developed stage of parametric fires [108, 109]

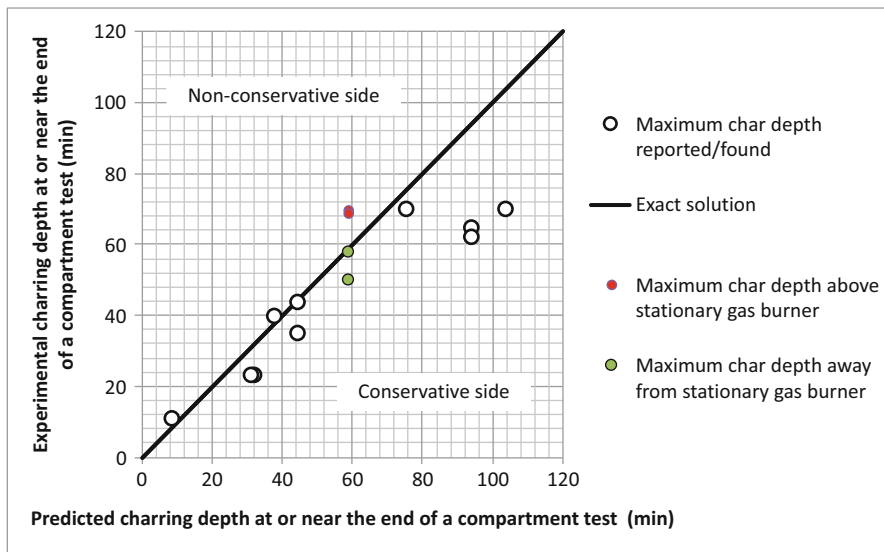
Brandon et al. [108, 109] re-evaluated Hadvig’s method with results of fire tests in modern furnaces (Fig. 8.30), in which the exposure is controlled using plate thermometers, and suggested an alternative equation of Eq. 8.17:

$$\beta_{\text{par}} = \beta_0 \Gamma^{0.25} \quad (8.22)$$

The parametric fire exposure charring rates presented by Hadvig [156] and further studied by König and Walleij [63] and Brandon et al. [108, 109] were developed predominantly with glulam or other forms of heavy timber construction, i.e., where the additional contribution of the timber to the fuel is very small, such that the fire severity does not change much compared to a noncombustible enclosure.

Recent trends, as discussed by Hopkin et al. [3] and Bartlett et al. [1, 2], highlight a movement towards CLT construction in increasingly tall applications, partial encapsulation, and/or architectural expression of the timber structural elements. In such cases, it has been robustly argued, e.g., see further Hadden et al. [5] and Hopkin et al. [158], that there needs to be an explicit consideration of the exposed structure’s impact on fire development and the ability of the structural system to withstand burnout. This is of particular importance in cases where evacuation times are prolonged and fire brigade interventions more challenging, e.g., high-rise, residential buildings adopting “stay put” policies, and healthcare facilities—where evacuation might be progressive.

A simple and potentially pragmatic approach of addressing the impact of the structure’s combustion on fire development is proposed in NFPA report FPRF-2018-04 [159] for parametric fire exposure, and involves the iterative computing of



**Fig. 8.31** Maximum charring depths reported/found in compartment tests versus predicted charring rates

charring depth using either Hadvig’s [156] or Brandon et al.’s [124] parametric charring rate model, assuming that the fire load represented by the char can be added to the enclosure variable fire load (furniture, etc.). This method requires assurance that debonding does not occur (in the case of CLT), and where (partial) protection/lining is provided to a timber substrate, it survives burnout without falling off. To validate the model, the maximum char depths measured at or near the end of full-scale flashover fire experiments of compartments were set against two model predictions (Fig. 8.31).

A similar approach is presented by Barber et al. [160]. However, the approach includes a second check for smoldering extinction of CLT. This involves a calculation of the incident radiant heat flux on the timber surface, with verification that this is below a critical value proposed by Crielaard [161] allowing smoldering extinction of the timber to be assumed.

### 8.7.4 Modified Effective Thermal Properties for Natural Fire Exposure

König and Walleij [63], in support of developing the Annex B properties of EN 1995-1-2, identified that the “effective” relationships between temperature and conductivity, specific heat, and density were not readily applicable outside of ISO

834 (standard fire) conditions. The Annex B properties (as have been presented in Sect. 8.4), which are numerically derived from experimental results, implicitly capture complex behaviors such as moisture movement, combustion, cracking, and char falloff. The manifestation of the char layer, the particulars of moisture movement, and other physical considerations, such as how cracks and fissures develop, were all noted to vary depending upon heating rate. Therefore, inaccuracies were found to occur when these properties were applied outside of the original calibration heating profile (i.e., the standard fire exposure). In addition, during the cooling phases of realistic fire exposures, char depth development was found to be under-predicted as combustion of the timber elements became a significant contributor to temperature development.

König [55] later proposed a means of addressing the influence of combustion during the cooling phase of realistic fire exposures, via a modified gas temperature concept. The study proposes that the thermal exposure condition be increased in severity, resulting in an effective gas temperature, which results in a continuation of charring into the cooling phase of a decaying fire. However, the proposal did not fully quantify how the effective gas temperature manifests for different fire curves.

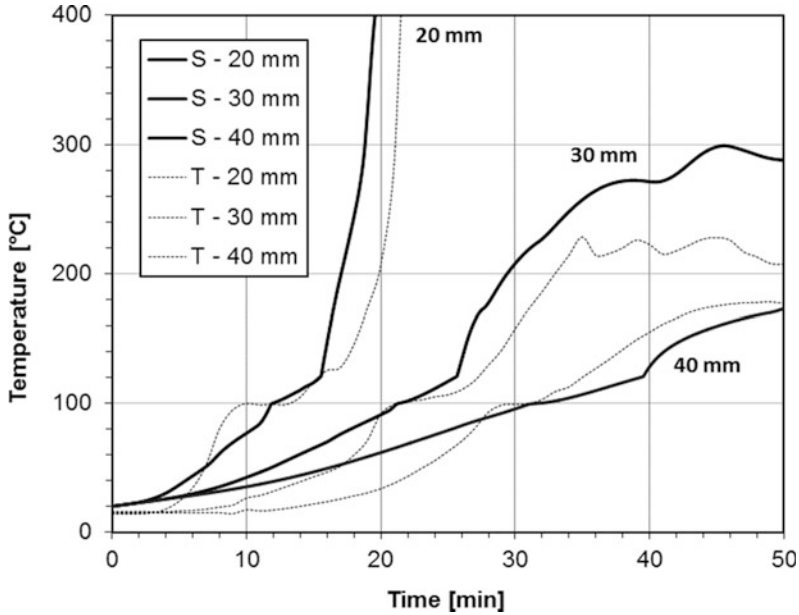
Hopkin sought to incorporate two important characteristics of timber behavior in fire identified by König [55]: namely that (a) the char layer forms differently depending on the rate of heating and (b) that combustion has a significant influence on char evolution during the cooling phase of natural fires [67]. To address issue (a) the conductivity of the char layer was modified by a constant (Table 8.10), which was described as both a function of the parametric time modifier as defined in EN 1991-1-2 [158] ( $\Gamma$ ) and fire load density ( $q_{td}$ ). The means of deriving both values is as described in EN 1991-1-2. In the case of (b), Arrhenius functions (as discussed in Sect. 8.4.2) were adopted to simulate decomposition and associated energy production. The resulting “combustion energy” was introduced as a source term within the heat transfer model. Figure 8.32 compares the temperature development of the “uncharred” portion of a CLT slab subject to parametric fire exposure, as observed experimentally (T) by Friquin [162], versus simulated (S) by Hopkin et al. [3].

Further development in this area has been followed by Brandon et al. [108, 109] using experimental data from Lange et al. [122] and Brandon et al. [124]. In order to allow performing calculations with most commercial finite element software, a solution was sought that only requires a set of effective thermal properties. The effective thermal properties were numerically derived from results of unloaded parametric fire tests [124], implicitly capturing complex behaviors such as moisture

**Table 8.10** Modified conductivity model from Hopkin [67] for the heating phase of parametric fires

Temperature (°C)	$\lambda$ (W/m K)	Correlations
20	0.12	$k_{\lambda,mod} = k_{\Gamma,mod} \cdot k_{qtd,mod}$ $k_{\Gamma,mod} = 1.5\Gamma^{-0.48}$ $k_{qtd,mod} = (q_{td}/210)^{0.5}$
200	0.15	
350	0.07	
500	0.09 $k_{\lambda,mod}$	
800	0.35 $k_{\lambda,mod}$	
1200	1.50 $k_{\lambda,mod}$	



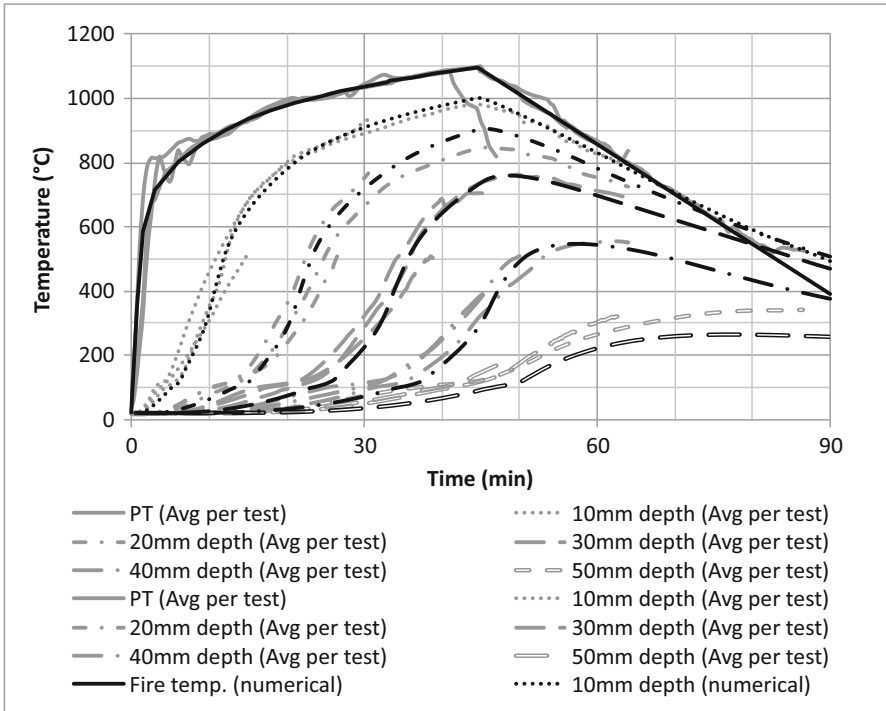


**Fig. 8.32** Time vs. temperature development in “uncharred” zone of a 120 mm CLT slab subject to a parametric fire ( $O$  of  $0.04 \text{ m}^{0.5}$  and  $q_{td}$  of  $83 \text{ MJ/m}^2$ )—comparison of experiment (T) and simulation (S), from [3]

movement, combustion, cracking, and char falloff. As the decay phase also involves these complex behaviors including char oxidation at increasing oxygen concentrations, reversible properties were assumed allowing this approach to be used to determine properties that are effective to predict temperatures for the entire fire duration including the decay phase (Fig. 8.33). Similar to the model by Hopkin [67], the conductivity of the char layer is multiplied by a constant at certain temperatures. However, in this model, this constant was only described as a function of the parametric time modifier ( $\Gamma$ ) (Table 8.11). Comparisons between temperature predictions and test series by Lange et al. [122] and Brandon et al. [108, 109] were used to validate the predictions.

### 8.7.5 Zone Fire and CFD Models

Given the acknowledgement of an increasing need to explicitly consider the impact of combustible structures on fire development, recent research efforts have focused on developing numerical models capable of approximating the fire characteristics within combustible enclosures. These research efforts can be split into two categories, zone models and computational fluid dynamics (CFD) models.

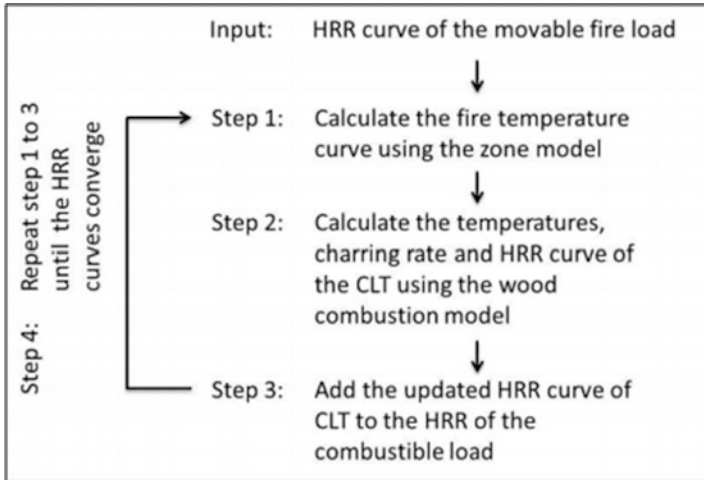


**Fig. 8.33** Time vs. temperature development of a glue-laminated beam slab subject to a parametric fire. Comparison of average temperatures at specific depths and numerical simulation

**Table 8.11** Modified conductivity model per Brandon [159] for the heating phase of parametric fires

Temperature (°C)	Thermal conductivity (W/mK)		Specific heat (J/kg K)		Density (kg/m <sup>3</sup> )
	Proposed	EN1995-1-2	Proposed	EN1995-1-2	
20	0.12	0.120	1530	1530	495
98	0.133	0.133	1770	1770	495
99	0.265	0.265	13,600	13,600	495
120	0.272	0.272	13,500	13,500	495
121	0.137	0.137	2120	2120	495
200	0.150	0.150	2000	2000	495
250	0.136 $k_{\lambda,mod}$	0.123	3337	1620	460
300	0.106 $k_{\lambda,mod}$	0.097	1463	710	257
350	0.077 $k_{\lambda,mod}$	0.070	1751	850	188
400	0.084 $k_{\lambda,mod}$	0.077	2060	1000	163
500	0.099 $k_{\lambda,mod}$	0.090	2472	1200	155
600	0.194 $k_{\lambda,mod}$	0.177	2884	1400	139
800	0.385 $k_{\lambda,mod}$	0.350	3399	1650	129
1200	1.65 $k_{\lambda,mod}$	1.500	3399	1650	0

$$k_{\lambda,mod} = 1.541\Gamma^{-0.24}$$



**Fig. 8.34** Stepwise process for calculating the contribution of CLT structure to a fire's HRR, according to Brandon [163]

### 8.7.5.1 Application of Zone Models to Timber Enclosures

Brandon [163] developed a one-zone (post-flashover) model incorporating a wood combustion sub-model. The process of applying the model required iteration, involving the steps outlined in Fig. 8.34.

In iteration one, the HRR of the variable (movable) fire load (i.e., excluding the contribution of the exposed structure) is adopted within a typical one-zone model to compute the enclosure time-temperature relationship (i.e., step one). This enclosure time-temperature relationship is employed within the finite element software SAFIR [164] to compute the temperature profile through a CLT boundary element, assuming one-dimensional heat transfer and adopting the thermophysical properties in Annex B of EN 1995-1-2. From the heat transfer model, the depth of char with respect to time is computed, assuming that the char interface coincides with the 300 °C isotherm. The time derivative of the charring depth gives the charring rate as a function of time.

The wood combustion model determines the contribution of the timber to the fire's HRR using a constant heat release rate per millimeter of charring of 5.39 MJ/m<sup>2</sup>.mm for a char layer thicker than 10 mm. This was based on a series of cone calorimeter tests by Crielaard [161]. For charring depths of less than 10 mm, the heat release rate per millimeter of charring increases linearly from 2.70 MJ/m<sup>2</sup>.mm at 0 mm to 5.39 MJ/m<sup>2</sup>.mm at 10 mm. These heat release rates in the function of charring depth are combined with the charring rates deduced from the tracking of the 300 °C isotherm to yield a time-dependent HRR contribution per unit area of exposed CLT. Once integrated over the surface area of exposed CLT within the enclosure, a HRR relationship with respect to time is produced, which is summed

with that attributed to variable fire load. Where the HRR exceeds that of the ventilation-controlled limit for the enclosure, external flaming is assumed instead of a prolonging of the fire's duration. This process must be completed via multiple iterations until the HRR with respect to time converges on a consistent relationship. When benchmarked against the experiments of McGregor [133] and Medina Hevia [135], the approach of Brandon [113] showed good agreement up until the point debonding of the CLT was observed.

Building upon the work of Brandon [163], Hopkin et al. [165] sought to resolve the need to iterate through multiple fire model realizations, and instead directly coupled a wood combustion sub-model with a single-zone model. The single-zone model followed the theory presented by Zhang & Li [166], with the wood combustion sub-model per that adopted in Brandon [163], albeit with a constant heat release rate per millimeter of charring of  $5.39 \text{ MJ/m}^2 \cdot \text{mm}$  irrespective of char depth.

At each time step within the zone model, the heat losses to the CLT enclosure were evaluated through a nonlinear one-dimensional heat transfer model, as presented by Maluk [167]. The char layer conductivity was adjusted per Hopkin [67], via an a priori estimation of the parametric time modified ( $\Gamma$ ) and the fire load density ( $q_{td}$ ), considering solely the variable fire load. With each time step, the  $300^\circ\text{C}$  isotherm position was recorded, with the change relative to the previous time step computed to derive the instantaneous charring rate. From this charring rate, the increase in enclosure HRR due to the CLT contribution was estimated adopting a heat release rate per millimeter of charring of  $5.39 \text{ MJ/m}^2 \cdot \text{mm}$ . This led to an instant updating of the enclosure HRR, directly affecting the enclosure temperature.

Like Brandon, the zone model was found to give good agreement with the experiments by McGregor [133] and Medina Hevia [135], prior to debonding, and in particular for cases where the proportion of exposed CLT was relatively small, i.e., one or two walls exposed.

Wade et al. [168] separately added functionality to the established zone modeling software B-RISK to allow the contribution of exposed timber surfaces to the fire development to be included. Differing from the approaches of Brandon and Hopkin et al., the B-RISK implementation does not directly couple the charring depth to the heat release rate. Instead, the  $300^\circ\text{C}$  isotherm position is tracked via nonlinear one-dimensional wall/ceiling heat transfer models, with the resulting mass from the char layer added to the moveable fire load at each time step during the simulation. The initial design fire is specified by the user, e.g.,  $t^2$  up until flashover (when either the upper layer reaches  $500^\circ\text{C}$  or the heat flux at the floor exceeds  $20 \text{ kW/m}^2$ ). After flashover, the moveable fire load is represented as wood cribs considering both ventilation and fuel surface control burning regimes and the total fire load is updated to include the additional fuel from the wood surfaces. Global equivalence ratio can also be controlled by the user to assume external burning or not.

Wade et al. [71] then improved the B-RISK model further by including an alternative three-component kinetic pyrolysis model where the decomposition of the exposed wood surfaces is described by an Arrhenius equation that gives a relationship between the reaction rate and temperature of the solid as described in Sect. 8.4.2. The model was benchmarked against 19 full-scale experiments in fully

and partly exposed CLT enclosures [169] with generally good predictions of the peak gas temperature and time to reach the peak temperature but final char depth predictions were not always conservative.

### 8.7.6 Models for Self-Extinction

As described in Sect. 8.2.2.3, values for the critical heat flux and critical mass loss rate for self-extinction have been measured. To date, one design methodology using self-extinction values has been detailed [1, 2]. Table 8.12 describes the self-extinction methodology which as stated by the authors needs to be performed as time-dependent analyses. The design methodology for self-extinction is applicable only if debonding of engineered timber and falloff of encapsulation do not occur. Debonding of CLT (Sect. 8.6.3) has been shown to prevent self-extinction from occurring and could lead to continuous burning and in some cases secondary flashover of a compartment. Encapsulation falloff, if not designed for, can increase the amount of exposed timber and thus increase the burning duration and maintain post-flashover thermal loads onto the timber for longer than anticipated.

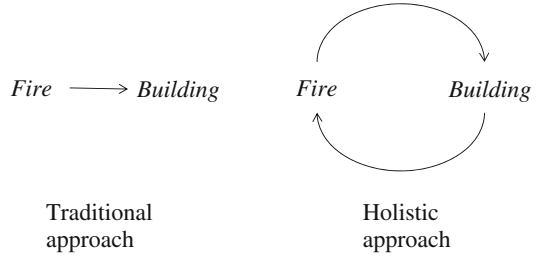
## 8.8 Calculation Methods

Regulations in most countries require a demonstration of sufficient load-bearing capacity of structures and sufficient performance of fire compartment-separating elements, when exposed to prescribed fire conditions or temperatures. In most cases it is required that the structural and the separating performance is either tested in a standard fire resistance test or calculated for the same conditions. Therefore, calculation methods provided in standards correspond mostly to the nominal exposure applied in standard fire resistance tests.

**Table 8.12** Self-extinction design methodology [1, 2]

Step	Method
1.	Determine time to burnout of compartment fuel load
2.	Based on the amount of exposed timber after burnout, calculate view factors and incident heat flux
3.	Make an estimate of surface temperature based on heat transfer analysis/experimental data
4.	Estimate heat losses based on compartment geometry and surface temperatures
5.	Determine if mass loss rate is less than the critical value
6.	Repeat for next time step until: <ol style="list-style-type: none"> <li>a. Auto-extinction occurs</li> <li>b. Predefined failure criteria are met</li> <li>c. A steady state is achieved</li> </ol>

**Fig. 8.35** Schematic representation of a traditional approach and holistic approach



However, the use of standard fire exposure for assessment is not always sufficient to demonstrate compliance with fire safety requirements. Some performance-based requirements require a more holistic approach which does not only account for the response of a building to a fire, but also for the influence of the building properties (geometry, materials, etc.) on the fire dynamics (Fig. 8.35). An example of such a performance-based requirement is the requirement *for certain (usually tall) buildings to withstand a complete natural fire without collapse, assuming absence of effective extinguishment by the rescue service* (which is required in a number of European countries). As seen in Sect. 8.7.3 the fire development and the duration of natural fires are significantly dependent on the design of the fire compartment. Therefore, for an assessment of compliance with such requirements, a suitable calculation method needs to involve realistic fire scenarios based on the design of the building. Where appropriate, this should include demonstrating that extinction is possible.

This section gives an overview of calculation methods for the assessment of heavy timber and light timber frame structures under nominal fire exposure and calculation methods using a natural or parametric fire exposure that is dependent on the design and fuel load of the building to assess timber structures.

Most calculation methods from design standards are simplified methods that are possible to perform without computer simulations. This section summarizes such calculation methods, but at the end also discusses principles of numerical methods.

### 8.8.1 Heavy Timber Construction in Nominal Fire Exposure

Heavy timber construction consists of elements that achieve fire performance inherently by virtue of having minimum dimensions. These elements generally have a structural purpose. Mass panel materials such as cross-laminated timber can also function as separations between compartments. Most knowledge of the fire performance of heavy timber structural elements is based on standard fire resistance tests.

Calculations for fire resistance ratings are generally performed to check or demonstrate compliance with regulatory requirements. The fire resistance rating indicates the number of minutes that a building element is able to withstand

conditions of a fire resistance test, while satisfying a (1) structural criterion and/or (2) insulation and (3) integrity criteria. Calculation methods exist, which demonstrate whether a building element satisfies the structural criterion, i.e., withstands the conditions of a fire resistance test for a required period of time under relevant mechanical loads without exceeding specific deflection conditions. Additionally, there are methods available to demonstrate satisfaction of the insulation criterion, i.e., the temperature increase on the unexposed side of the building element is limited according to the regulations. It should, however, be noted that there are no reliable calculation methods to show compliance with the integrity criterion. In practice the integrity of a separating building element is the responsibility of the contractor using detailing and assembly methods that have been shown to be effective in fire resistance tests.

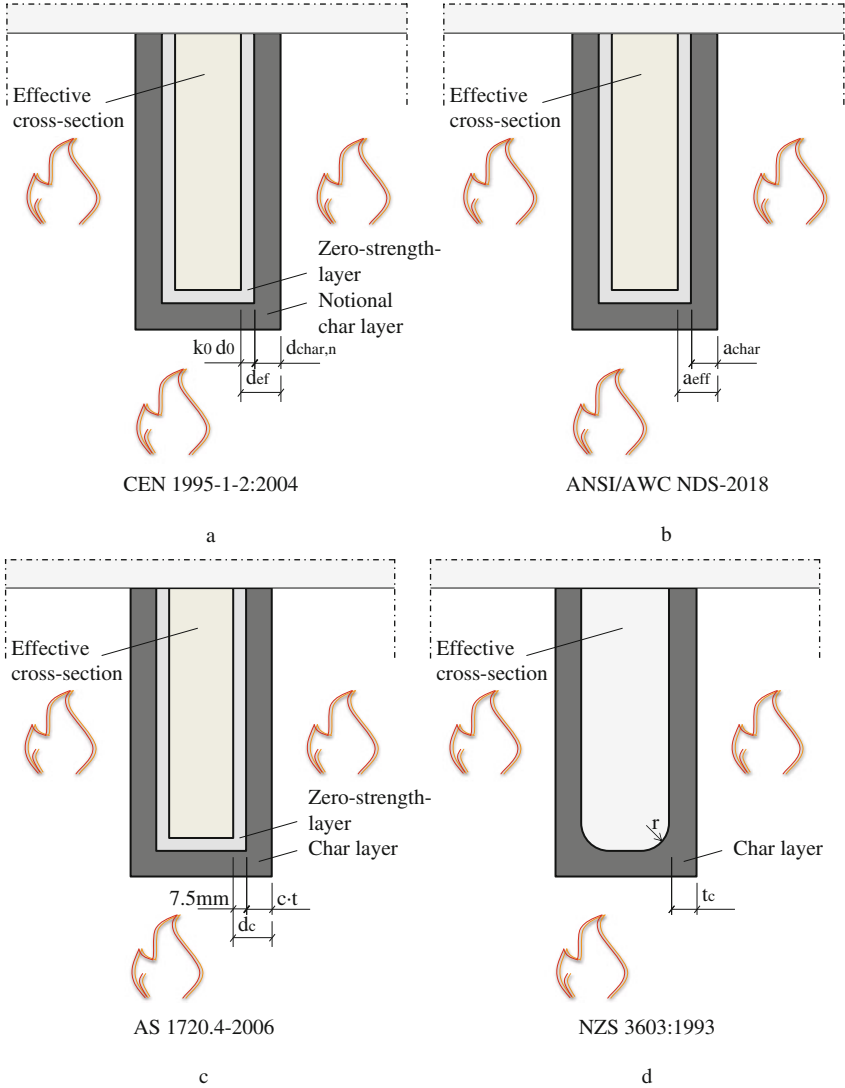
### **8.8.1.1 Effective Cross-Section Method for Sawn Timber and Parallel Laminated Timber Materials**

Timber chars at a predictable rate when exposed to nominal fire exposure. Mechanical properties of timber reduce at elevated temperature (Sect. 8.4.3.1) and become negligible after charring. However, due to the relatively slow heat conduction through char and timber in fire, a significant part of a timber member can remain undamaged if the dimensions of the timber member are sufficient.

Effective cross-section methods are used to determine the load-bearing capacity of structural elements exposed to fire by only considering a reduced cross section of the element. Effective cross-section methods are being used in multiple design standards for timber structures around the world with only slight variations. However, all methods involve the subtraction of a notional char layer from the initial cross section for calculation of the load-bearing capacity during nominal or parametric fire exposures. The uncharred timber near the char line also has reduced strength, which is generally taken into account by subtracting a so-named zero-strength layer, which makes some allowance for the heat-affected zone below the char layer. Variations of the effective cross-section method in Europe, the USA, Canada, Australia, and New Zealand are discussed in the following subsections. Due to different notations, names, and approaches in different standards caution is advised. Figure 8.36 indicates the layers that need to be subtracted from the initial cross section to obtain the effective cross section that can be used for structural fire design in different countries/continents. The Canadian method is somewhat similar to the European method and is not included in the figure.

#### **European Effective Cross-Section Method**

The effective cross-section method of EN 1995-1-2 [54] can be used to approximate the capacity of timber members in nominal fire exposure (ISO 834). In this clause, an updated method is discussed including adaptations resulting from recent research.



**Fig. 8.36** Effective cross section of a beam with three-sided fire exposure according to methods from (a) Europe, (b) the USA, (c) Australia, and (d) New Zealand

Differences between the method discussed here and the method of Eurocode 5 are indicated.

The effective cross-section method involves a subtraction of a char layer from all exposed sides of the original cross section to exclude the material of negligible strength from the structural calculation. Additionally, a *zero-strength layer* is



subtracted from the uncharred cross section to compensate for timber that is weakened, but not charred. After subtraction of both layers an effective cross section remains which can be used to determine the capacity of the member under standard fire exposure (see Fig. 8.36a). The total thickness of the layers that must be subtracted from the exposed side of the member can be calculated using

$$d_{\text{ef}} = d_{\text{char}} + k_0 d_0 \quad (8.23)$$

where  $d_{\text{ef}}$  is the total thickness of the ineffective layer,  $d_{\text{char}}$  is the char depth,  $k_0 d_0$  is the zero-strength layer with  $k_0 = \min(1; t/20)$ , and  $t$  is the time in minutes. For sawn timber and engineered timber elements comprised of parallel lamellas or plies,  $d_0$  equals 7 mm for exposures exceeding 20 min according to [54]. For materials with nonhomogeneous cross sections, such as CLT or certain LVL materials, another approach is needed. Implementation of the effective cross-section method for CLT is discussed in Sect. “European Effective Cross-Section Method for CLT”.

The char depth should be determined using a notional char rate:

$$d_{\text{char}} = \beta_n t \quad (8.24)$$

where  $\beta_n$  is the notional charring rate.

The notional charring rate is dependent on a one-dimensional charring rate and a number of coefficients [115] as seen in Eq. 8.25. The number of coefficients can increase based upon future research:

$$\beta_n = \beta_0 \cdot k_s \cdot k_{pr} \cdot k_n \cdot k_g \quad (8.25)$$

*Note: In the above equation the notional charring rate  $\beta_n$  is in accordance with Klippel et al. [115] and does not correspond to equations given in Eurocode 5. The use of this alternative notation is more practical and allows implementation of recent findings in the effective cross-section method. The use of this notation instead of the notation used in Eurocode 5 does not influence the outcome of calculations that were covered by Eurocode 5, where  $\beta_0$  is one-dimensional, which is provided by Eurocode 5 as shown in Table 8.13, and the k-coefficients account for the following effects:*

- $k_s$  is a section coefficient, which accounts for an increased charring rate for slender beams and columns exposed on three or four sides of the cross section. The increase of charring rate should only be accounted for from the narrow-exposed side(s) of the cross section. The following values of  $k_s$  can be assumed,

where  $b$  is the smallest dimension of the member’s cross section [170]:  $k_s =$

$$\begin{cases} 1.2 & \text{for } 40 \text{ mm} \leq b \leq 60 \text{ mm} \\ 1.3 - 0.00167 \cdot b & \text{for } 60 \text{ mm} \leq b \leq 180 \text{ mm}, \\ 1.0 & \text{for } b \geq 180 \text{ mm} \end{cases}$$

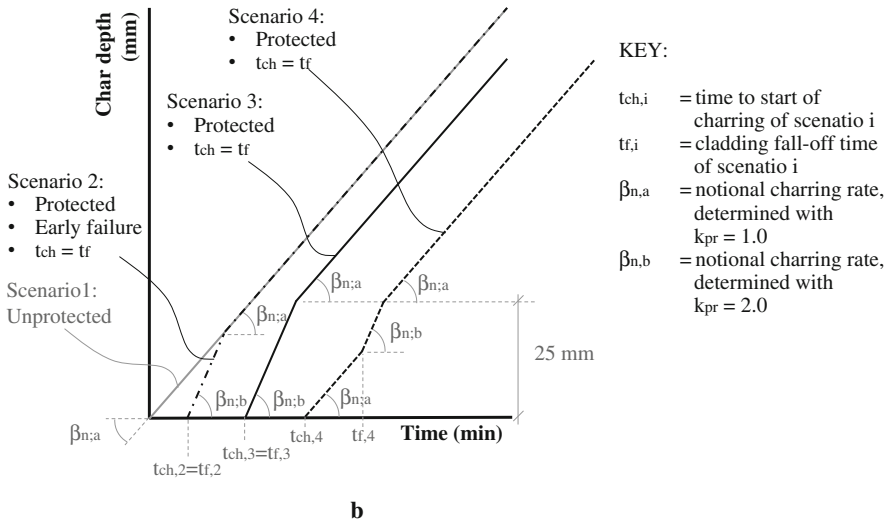
**Table 8.13** One-dimensional and notional charring rates in directions perpendicular to the grain corresponding to EN1995-1-2

Material	$\beta_0$ (mm/min)	$k_n$
<b>Softwood and beech</b>		
Glue-laminated timber or LVL with a characteristic density of $\geq 290 \text{ kg/m}^3$	0.65	1.1
Solid timber with a characteristic density of $\geq 290 \text{ kg/m}^3$	0.65	1.25
<b>Hardwood</b>		
Solid or glue-laminated hardwood with a characteristic density of $\geq 450 \text{ kg/m}^3$	0.50	1.1

- $k_{pr}$  is a protection coefficient which accounts for the potential presence or removal of protective materials. Values of  $k_{pr}$  can change during the fire as is discussed later in this section and Sect. “European Effective Cross-Section Method for CLT”.
- $k_n$  is a corner coefficient that compensates for an increased char depth at exposed corners of the cross section for cross sections with two or more adjacent sides exposed. If exposed sides of the cross section are not adjoining  $k_n = 1.0$  can be assumed. Otherwise, values from Table 8.13 which correspond to EN 1995-1-2 can be assumed.
- $k_g$  is a gap coefficient which accounts for potential presence of gaps in glued members, which is particularly relevant for CLT members as gaps can be present between parallel lamellae of one ply. For plies with a maximum gap width ranging from 2 mm to 6 mm,  $k_g = 1.2$  can be assumed. If there is no gap present in a ply,  $k_g = 1.0$  can be assumed [115]. One CLT member can have different gap coefficients for different plies.

In accordance with the effective cross-section method, the material properties of timber at ambient temperature (20 °C) and cross-sectional dimensions of the effective cross section can be assumed to calculate the load-bearing capacity in standard fire resistance tests. EN 1995-1-2 allows the use of a 20th percentile strength value of timber for fire situations instead of the, lower, usual fifth percentile strength value, to account for a change of distribution of strength properties. However, comparisons between fire resistance tests and calculations have indicated that this should not be done and leads to nonconservative predictions [43]. Therefore, it is recommended to calculate the structural capacity of the effective cross section with the same characteristic strength value as is used for structural calculations in ambient temperature (i.e., fifth percentile).

Passive fire protection by cladding and/or insulation materials can delay charring of the structural timber. The time at which the timber member starts to char is dependent upon the insulation properties and the integrity of the cladding material. The model of Eurocode 5 includes charring models for five possible scenarios related to fire protection. The applicability of the scenarios is dependent upon the start time of charring behind the cladding  $t_{ch}$  and the falloff time of the cladding  $t_f$ . The char models for the different scenarios are visualized in Fig. 8.37 and explained as follows:



**Fig. 8.37** Charring models for different protection scenarios for standard fire resistance tests

- Scenario 1: The timber surface is unprotected and the notional charring rate can be assumed similar to as shown in Table 8.13. The protection coefficient to calculate the charring rate is  $k_{pr} = 1.0$ .
- Scenario 2: The timber surface is protected, but the cladding falls off early. After the falloff time is reached charring starts, assuming a notional rate calculated using protection coefficient  $k_{pr} = 2.0$ . In scenario 2, charring starts later but increases more rapidly than in scenario 1. According to the model, the char depth of scenario 2, however, cannot surpass the char depth of scenario 1, which is in accordance with a rule of fire resistance rating by Harmathy [171], stating that the fire resistance cannot be reduced by adding a layer of material. If the char line of scenario 1 does not reach a depth of 25 mm at the time the char line of scenario 2 reaches a depth of 25 mm, scenario 3 can be assumed.
- Scenario 3: The timber surface is protected and the cladding falls before the timber starts to char. After the falloff time is reached, charring starts assuming a notional rate calculated using protection coefficient  $k_{pr} = 2.0$ . After a char depth of 25 mm is reached, a lower notional charring rate with  $k_{pr} = 1.0$  is assumed.
- Scenario 4: The timber surface is protected and the timber starts charring before the falloff time is reached. According to the model, timber starts charring with a similar rate as unprotected timber. After the falloff time is reached, the notional charring rate is doubled assuming a protection coefficient  $k_{pr} = 2.0$ . After a char depth of 25 mm is reached, a lower notional charring rate with  $k_{pr} = 1.0$  is assumed.
- Scenario 5 (not shown in Fig. 8.37): The timber surface is protected and the cladding does not fall before the char line reaches a depth of 25 mm. According to

the model, timber starts charring with a similar rate as unprotected timber at the start time of charring. Charring is assumed constant for the entire duration of the fire.

Values of the start time of charring and falloff time of protective cladding can be determined from standard fire resistance tests using temperature measurements at the interface between protective layers. Values for the start time of charring and falloff time and falloff time of European graded type F and type A gypsum boards were provided by Östman et al. [172], and are shown in Tables 8.5 and 8.14.

### USA Effective Cross-Section Method

The national design specification of the USA (ANSI/AWC NDS-2018) has an approach that is somewhat different to that in most other countries as it requires the use of nonlinear charring rates. The char depth according to US code-compliant methods can be calculated using

$$a_{\text{char}} = \beta_t \cdot t^{0.813} \quad (8.26)$$

where  $t$  is the exposure time ( $h$ ).

$\beta_t$  of  $1.5 \text{ in./hr}^{0.813}$  is commonly assumed for sawn lumber, glue-laminated softwood timber, laminated veneer lumber, parallel strand lumber, laminated strand lumber, and cross-laminated timber [173].

According to ANSI/AWC NDS-2018 the total ineffective layer thickness should then be calculated using

$$a_{\text{eff}} = 1.2 \cdot a_{\text{char}} \quad (8.27)$$

Caution is advised, as solely a layer with thickness  $a_{\text{eff}}$  is subtracted from the initial cross section, as shown in Fig. 8.36b. This layer includes both char and heat-affected timber.

The strength of the timber material used for capacity calculations of performance of timber sections at ambient is the fifth percentile strength of the wood and tabulated design values for different species and grades of wood are given by the various timber agencies across North America (e.g., the Northern Softwood Lumber Bureau or the Western Wood Products Association). For fire design, however, ultimate strength-based design is used (rather than the allowable stress design basis recommended for ambient design) and therefore these design values must be multiplied via the factors shown in Table 8.15 prior to use for fire design at the ultimate limit state.

When considering the effect of applied fire protection to timber structures, the US standards use a “component additive method,” based on the empirical principle by Harmathy [171] that the fire resistance of two or more parallel layers is higher than that of the fire resistance of these layers separately. AWC-TR10–1810 [174] states

**Table 8.14** Start of charring behind gypsum plasterboards  $t_{ch}$  in minutes with outer board thickness  $h_p$  and total board thickness  $h_{p,tot}$  [172]

Cladding	Walls	Floors
Type A and F, one layer	$1.8 h_p^{-7}$ $25.5$	$1.8 h_p^{-7}$ $25.5$
Type F, two layers Type F (exposed) + type A, two layers	$\min \begin{cases} 2.1h_{p,tot} - 7 \\ 3.5h_p + 7 \end{cases}$	$\min \begin{cases} 2.1h_{p,tot} - 7 \\ 4h_p - 14 \end{cases}$
Type A, two layers	$\min \begin{cases} 2.1h_{p,tot} - 7 \\ 1.6h_p + 13 \end{cases}$	$\min \begin{cases} 2.1h_{p,tot} - 7 \\ 1.6h_p + 11 \end{cases}$

$9 \text{ mm} \leq h_p \leq 18 \text{ mm}$   
 $h_p > 18 \text{ mm}$   
 $25 \text{ mm} \leq h_{p,tot} \leq 31 \text{ mm}$   
 $9 \text{ mm} \leq h_p \leq 18 \text{ mm}$   
 $18 \text{ mm} \leq h_{p,tot} \leq 31 \text{ mm}$   
 $9 \text{ mm} \leq h_p \leq 18 \text{ mm}$

**Table 8.15** Design value adjustment factors required for use with timber sections under fire state conditions according to ANSI/AWC NDS-2018

	Allowable stress design (ASD) only					
	Design stress to member strength factor	Size factor <sup>a</sup>	Volume factor <sup>a</sup>	Flat use factor <sup>a</sup>	Beam stability factor <sup>a</sup>	Column stability factor <sup>a</sup>
Bending strength	2.85	•	•	•	•	
Beam buckling strength	2.03					
Tensile strength	2.85	•				
Compressive strength	2.58	•				•
Column buckling strength	2.03					

<sup>a</sup>For values of adjustment factors see ANSI/AWC NDS-2018

**Table 8.16** Additional fire resistance time for type X gypsum boards [174]

Protection description	Maximum fastener spacing (inches)	Added fire resistance time per layer (min)
1/2-inch type X gypsum board	12" o.c.	30
5/8-inch type X gypsum board	12" o.c.	40

that it is permitted to use type X gypsum boards to increase the calculated fire resistance of wood members and assemblies. The additional fire resistance periods that can be added can be found in Table 8.16, provided that requirements regarding the gypsum boards and fasteners of AWC-TR10, 4.4.2 [174], are met.

### Canadian Effective Cross-Section Method

The Canadian method is primarily a simplified version of the European method. Each timber construction type has two char rates, a one-dimensional char rate  $\beta_0$  and a notional char rate  $\beta_n$ . For situations such as solid walls and floors where the heating is one-dimensional across the whole element, or for large rectangular cross sections where the heating is one-dimensional apart from at the corners, then  $\beta_0$  should be used. In the latter case, explicit consideration must be given to corner rounding and the radius of the corner should be taken as the charred layer depth due to one-dimensional charring.

For all other cases, the notional char rate  $\beta_n$  should be used. The depth of the charring is then calculated using Eq. 8.28:

**Table 8.17** Canadian design charring rates [mm/min]

	$\beta_0$	$\beta_n$
Solid sawn timber	0.65	0.8
Glue-laminated timber	0.65	0.7
Structural composite lumber	0.65	0.7

*Note: Values only applicable to wood-based structural composite lumber products*

**Table 8.18** Canadian design fire state strength factors

	$K_{fi}$
Solid sawn timber	1.5
Glue-laminated timber	1.35
Structural composite lumber	1.25

$$x_c = \beta \cdot t \quad (8.28)$$

where  $x_c$  is the char depth and  $t$  the fire exposure duration. Subscripts of 0 and  $n$  should be used on  $x$  and  $\beta$  to represent one-dimensional and notional charring, respectively.

The charring rates for different timber product types can be seen in Table 8.17.

Like the European model, in addition to the char layer, a zero-strength layer must be added to account for the unburnt, but heated, wood beyond the char front. The size of this zero-strength layer,  $x_t$ , shall be taken as 7 mm after 20 min of exposure, while for shorter time periods it shall be calculated as follows:

$$x_t = \frac{t}{20} \cdot 7 \quad (8.29)$$

where  $t$  is the time in minutes (up to 20 min).

The strength of timber to be used in calculations under the Canadian method is modified from the fifth percentile strengths specified at ambient temperature to mean strengths via a strength adjustment factor  $K_{fi}$ . The factors for the different timber types can be seen in Table 8.18, while it should be noted that, as with the European method, mean strength values have been found to give unconservative results by recent research [43].

Unlike the European method where the timber is protected by gypsum boards, an additional fire resistance time period is added to the calculated fire resistance, rather than a reduced charring rate. The additional time periods specified are 15, 30, and 60 min for type X gypsum boards of 12.7, 15.9, and  $2 \times 15.9$  mm, respectively. The standard also specifies requirements for gypsum board fastener provision and joint finishes for the protection periods to be utilized.

### Australian Effective Cross-Section Method

Rather than specified charring rates for types of timber, the Australian method, as described in AS 1720.4–2006, varies the charring rate in relation to the timber density (at 12%) using the formulae below:

$$c = 0.4 + \left(\frac{280}{\delta}\right)^2 \quad (8.30)$$

where  $c$  is the notional charring rate (in mm per minute) and  $\delta$  is the timber density in  $\text{kg/m}^3$ .

This is then used to calculate an “effective char depth” which is the depth of charring from the notional rate, plus a 7.5 mm layer equivalent to the zero-strength layer used in other methods:

$$d_C = c \cdot t + 7.5 \quad (8.31)$$

where  $d_C$  is the effective char depth and  $t$  the duration of the fire in minutes.

The strength used for fire limit state design is the fifth percentile strength as specified in accordance with AS 1720.1. This should be combined with a load duration factor corresponding to 5 h also from AS-1720.1.

A combination method is used for evaluating the structural performance of sections with additional external protection (such as gypsum boarding). The final fire resistance period is then governed by

$$T_p = t_i + t_M \quad (8.32)$$

where  $T_p$  is the final combined fire-resistant period,  $t_i$  is the period from the protective system, while  $t_M$  that of the structural member.

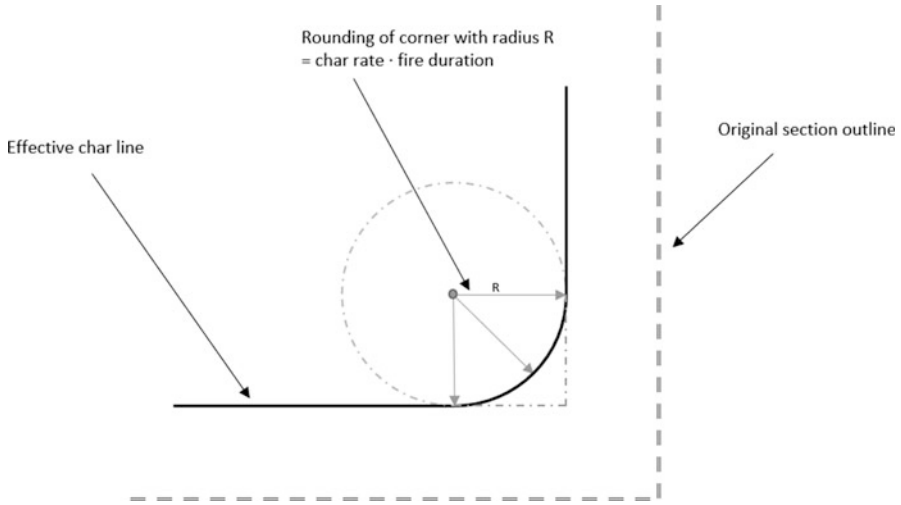
The performance of the structure is calculated as described above, but with the charring rate multiplied by a factor of 1.1, while the protective system’s provision is provided by the manufacturer from testing in accordance with AS 1530.4.

### New Zealand Effective Cross-Section Method

The New Zealand effective cross section is detailed in NZS 3603:1993 [175]. This standard specifies a charring rate of 0.65 mm/min for radiata pine and other similar softwoods, while other woods of significantly different densities require individual testing to establish their charring rate.

The New Zealand design standard requires the designer to explicitly account for the increased charring at the corners and to round these with a radius equal to the charring rate multiplied by the fire duration (Fig. 8.38).





**Fig. 8.38** Corner rounding under the New Zealand methodology

In accordance with NZS3603\_1993, the section modulus,  $Z_r$ , of a charred beam with initial breadth,  $b$ , and initial depth,  $d$ , for four-sided exposure can be calculated as follows:

$$Z_r = \frac{1}{6} \left[ (b - 2t_c)(d - 2t_c)^2 - 2.58t_c^2(d - 2t_c) \right] \quad (8.33)$$

For three-sided fire exposure:

$$Z_r = \frac{1}{6} \left[ (b - 2t_c)(d - t_c)^2 - 1.29t_c^2(d - t_c) \right] \quad (8.34)$$

The strength used for fire limit state design is the specified (fifth percentile) strength matching that required for ambient design. No method is given with the New Zealand standard as to how to establish the impact of additional protection to the timber structure. However, the standard is planned to be replaced with the updated, soon-to-be-published, AS/NZS 1720.4 standard.

### 8.8.1.2 Effective Cross-Section Method for CLT

The effective cross-section method discussed in Sect. 8.8.1.1 cannot be used for cross-laminated timber (CLT) for the following reasons:

- CLT debonding caused by fire exposure is currently allowed in most countries, with the exception of the USA and Canada. When exposed to fire, debonding causes an increase of “average” charring rates.
- The zero-strength layer which is used in Sect. 8.8.1.1 is based on the assumption that the material properties of the structural timber element are homogeneous (consistent throughout the cross section). Due to the cross-layered composition of CLT these properties are, however, not homogeneous.

Not all design specifications include methods for the calculation of the fire resistance of CLT. In the USA such a method is provided in the national design specification (NDS). In Europe such a method is not regulated yet, but in practice calculation methods are often provided by the CLT producer. Additionally, a method developed by Klippel et al. [115] is being adopted.

### European Effective Cross-Section Method for CLT

Based on the results of 123 standard fire resistance tests of CLT, Klippel et al. [115] proposed charring models for CLT wall and floor panels which account for debonding.

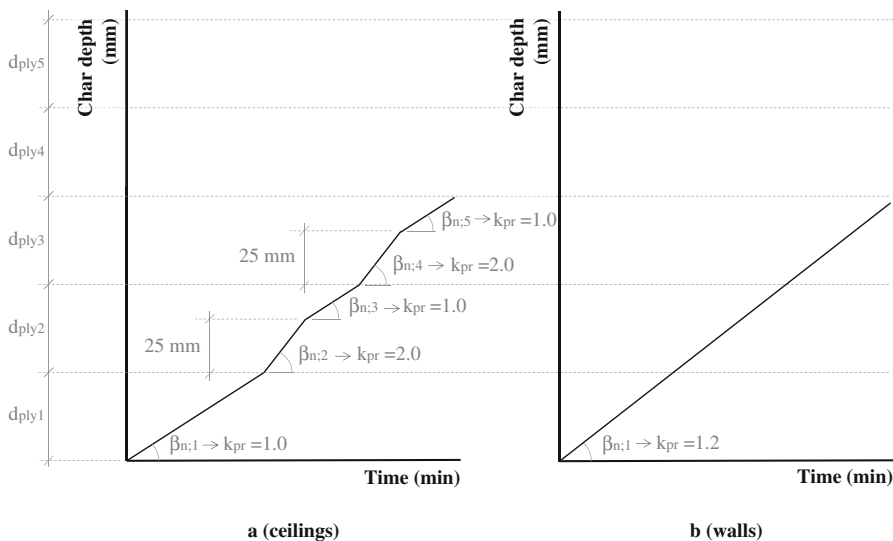
The charring model for the ceiling involves phases with alternating notional charring rates. Based upon experimental evidence, the model assumes that debonding occurs when the char line reaches a bond line. For CLT ceilings that are initially unprotected the notional charring rate can be determined using a protection coefficient of  $k_{pr} = 1.0$ . For the duration of the fire (i.e., the required fire resistance time) the protection coefficient, used to calculate the nominal charring rate, is doubled each time the char line reaches a bond line, until the char layer in the subsequent ply is 25 mm. Unless the ply thickness is 25 mm or thinner,  $k_{pr} = 1.0$  is assumed for charring of the remaining thickness of the ply, as is shown in Fig. 8.39.

The wall tests that were analyzed for the development of a charring model for walls showed less pronounced debonding than the ceiling tests. The proposed model, therefore, did not include stepwise changes of the notional charring rate. For walls  $k_{pr} = 1.2$  is assumed for the entire fire duration. For both ceiling and wall members, the calculation method should not be used to demonstrate fire resistance ratings exceeding 120 min. For charring of exposed CLT made of non-delaminating adhesives a protection coefficient of  $k_{pr} = 1.0$  can be assumed for the duration of standard fire exposure.

Based upon numerical simulations and experimental verification Schmid et al. [176] proposed a conservative approach to calculate the ineffective layer thickness on the exposed sides of a cross section:

$$d_{ef} = d_{char} + k_0 s_0 \quad (8.35)$$

where  $s_0$  is the thickness of a compensating layer for cross-laminated timber exposed on one side according to Table 8.19.



**Fig. 8.39** Char depth and protection coefficient during a standard fire of an exposed CLT ceiling (a) and an exposed CLT wall (b)

Equation 8.35 is based on CLT that does not exhibit debonding but is conservative for CLT that is prone to debonding. Therefore, the use of equation is recommended independent of the adhesive performance.

The effective cross section is determined by subtracting a layer with a thickness of  $d_{ef}$  from the exposed side(s) and by subtracting lamellas of which the effective depth is 3 mm or less. The bending and compression capacity of the CLT member can be determined using the characteristic parallel to the grain strength, for lamellae that are stressed in the parallel-to-grain direction. The bending, compression, and tensile strength of the other lamellae should be neglected. The classical beam theory may be assumed for the calculation of the moment capacity and buckling.

### USA Effective Cross-Section Method for CLT

The US National Design Specification (NDS) offers a method to calculate the fire resistance of CLT members exposed to a nominal fire. According to this method, the charring rate of CLT can be calculated as

$$a_{char} = n_{lam}h_{lam} + \beta_t(t - (n_{lam}t_{gi}))^{0.813} \tag{8.36}$$

where

**Table 8.19** Compensating layer thickness  $s_0$  in mm for CLT slabs with layers of equal thickness where  $h$  is the total thickness of the CLT member in mm [172]

No. of plies	Floors		Walls	
	Exposed side	Unprotected	Protected	Unprotected
<b>3</b>	<b>Tension side</b>	$\frac{h}{30} + 3.7$	10	
	<b>Compression side</b>	$\frac{h}{25} + 4.5$	$\min \left\{ \begin{array}{l} 13.5 \\ \frac{h}{12.5} + 7 \end{array} \right.$	$\frac{h}{12.5} + 3.95$ $\min \left\{ \begin{array}{l} 14.5 \\ \frac{h}{12.5} + 7 \end{array} \right.$
<b>5</b>	<b>Tension side</b>	$\frac{h}{100} + 10$	For $75 \leq h \leq 100$ : $-\frac{h}{4} + 34$ For $h > 100$ : $\frac{h}{35} + 6$	
	<b>Compression side</b>	$\frac{h}{20} + 11$	18	$\frac{h}{15} + 10.5$ 20
<b>7</b>	<b>Tension side</b>	For $105 \leq h \leq 175$ : $\frac{h}{6} + 2.5$ For $h > 175$ : 10	For $105 \leq h \leq 175$ : $\frac{h}{6} + 2.5$ For $h > 175$ mm: 10	
	<b>Compression side</b>	For $105 \leq h \leq 175$ : $\frac{h}{6} + 2.5$ For $h > 175$ : 13	For $105 \leq h \leq 175$ : $\frac{h}{6} + 2.5$ For $h > 175$ : 13	For $105 \leq h \leq 175$ : $\frac{h}{6} + 4$ For $h > 175$ : 16

$$t_{gi} = \left( \frac{h_{lam}}{\beta_t} t_{gi} \right)^{1.23} \quad (8.37)$$

$$n_{lam} = \frac{t}{t_{gi}} \quad (8.38)$$

$t_{gi}$  is the time for the char front to reach the glued interface in hours.

$h_{lam}$  is the lamination thickness in inches.

$n_{lam}$  is the number of laminations charred (rounded to the lowest integer).

The thickness of the total ineffective layer that needs to be subtracted from exposed sides of the original cross section can be calculated according to Eq. 8.27 in Sect. “USA Effective Cross-Section Method”.

### 8.8.1.3 Connections

Due to the large variety of configurations of connections, calculation methods for the fire resistance of exposed connections subject to nominal fire exposure do not exist for all types of connections. However, as dowel-type connections are the most common type of connections used in heavy timber structures, most available calculation methods aim to predict the capacity of dowel-type timber connections only (and under furnace conditions).

#### European Method 1: Tabulated Data

Eurocode 5 (EN 1995-1-2) offers two methods for estimating the fire resistance of timber connections. The simplest method involves tabulated data. Table 8.20 shows the fire resistance of connections comprising different fasteners according to Eurocode 5, provided that the dimension requirements of the fastener diameter  $d$  and the side member thickness  $t_l$  are met. Increasing the minimum edge and end distances of the dowel-type fasteners, the minimum thickness of the side member by a distance of  $a_{fi}$  allows the use of an increased fire resistance  $t_{req}$ , which is not allowed to exceed 30 min:

$$a_{fi} = \beta_n \cdot k_{flux}(t_{req} - t_{d,fi}) \quad (8.39)$$

where

**Table 8.20** Fire resistance ratings  $t_{d,fi}$  of timber connections with timber side members (EN 1995-1-2)

	Time of fire resistance $t_{d,fi}$ (min)	Provisions
Nails	15	$d \geq 2.8$ mm
Screws	15	$d \geq 3.5$ mm
Bolts	15	$t_l \geq 45$ mm
Dowels	20	$t_l \geq 45$ mm

$\beta_n$  is the notional charring rate according to Eq. 8.25.

$k_{\text{flux}}$  is a coefficient accounting for increased heat flux through the fastener ( $k_{\text{flux}} = 1.5$ ).

$t_{\text{req}}$  is the required standard fire resistance period ( $t_{\text{req}} \leq 30$  min).

$t_{d,fi}$  is the base fire resistance rating according to Table 8.19.

Protection of fire-rated gypsum board of type F can be taken into account by using the start time of charring given in Table 8.14 and the following expression:

$$t_{\text{ch}} \geq t_{\text{req}} - 1.2t_{d,fi} \quad (8.40)$$

In order to take gypsum board protection into account, it is important to make sure that applied fixing methods do not lead to premature falloff of gypsum boards. Eurocode 5 also includes additional rules for the dimensions of potential steel flitch plates within a timber connection.

#### European Method 2: Reduced Load-Bearing Capacity

A second method that is offered by Eurocode 5 gives the reduction of load-bearing capacity in a fire in the form of

$$F_{v,Rk,fi} = \eta \cdot F_{v,Rk} \quad (8.41)$$

with

$$\eta = e^{-k \cdot t_{\text{req}}} \quad (8.42)$$

where

$F_{v,Rk}$  is the characteristic load-bearing capacity calculated in accordance with EN1995-1-1;  $k$  is a factor given in Table 8.21 for different fasteners; and  $t_{\text{req}}$  is the required fire resistance rating.

Eurocode 5 gives values of  $k$  that are only valid for design fire resistance of 20–40 min as indicated in Table 8.21. In accordance with Eurocode 5 the method should only be used for connections with timber side members with a thickness equal to or greater than  $t_1$  (mm):

$$t_1 = \max \begin{cases} 50 \\ 50 + 1,25(d - 12) \end{cases} \quad (8.43)$$

The protection of fire-rated gypsum boards of type F can be accounted for using Eq. 8.40. However, in this case the value of  $t_{d,fi}$  is not obtained from Table 8.20, but using.

**Table 8.21** Fastener parameter  $k$  (EN 1995-1-2)

Connection with	$k$	Maximum period of validity for parameter $k$ in an unprotected connection min
Nails and screws	0,08	20
Bolts wood-to-wood with $d \geq 12$ mm	0,065	30
Bolts steel-to-wood with $d \geq 12$ mm	0,085	30
Dowels wood-to-wood <sup>a</sup> with $d \geq 12$ mm	0,04	40
Dowels steel-to-wood <sup>a</sup> with $d \geq 12$ mm	0,085	30
Connectors in accordance with EN 912	0,065	30

<sup>a</sup>The values for dowels are dependent on the presence of one bolt for every four dowels

$$t_{d,fi} = -\frac{1}{k} \ln \frac{\eta_{fi} \gamma_{M,fi}}{\gamma_M k_{fi}}$$

where  $k$  is the fastener parameter according to Table 8.21 and  $\eta_{fi}$  is the reduction factor for the design load in the fire situation.  $\gamma_M$  is the partial safety factor corresponding to the connection (which is given in EN 1995-1-1:2004) and  $\gamma_{M,fi}$  is the partial safety factor for timber in fire conditions, which is generally 1.0, but possibly different in certain European countries.  $k_{fi}$  is a factor accounting for the variability of material properties, which is 1.25 for sawn timber and 1.15 for glue-laminated timber and wood-based panels.

### 8.8.2 Heavy Timber Construction in Parametric Fire Exposure

In the field of fire safety engineering, performance-based design methods are increasingly used to demonstrate the fire safety of building designs. However, performance-based design is not commonly used for the design of timber structures, as there are not many relevant assessment methods available [172]. For assessment whether the design of a building meets certain criteria, a design fire scenario is needed. Design fires often describe the temperature throughout a compartment fire and are often based on dimensions, ventilation conditions, and fuel load of the compartment. Parametric fires are such design fires, used for structural calculations corresponding to ventilation-controlled post-flashover fires in compartments, based on the compartment's dimensions, ventilation openings, lining materials, and fuel load. Eurocode 1 (EN1991-1-2) [177] includes parametric fires. These parametric design fires are also used in several non-European countries. It should be noted that parametric design fires only correspond to underventilated fires in compartments of

limited dimensions. Eurocode 1 limits the use of parametric design fire exposure to compartments with floor areas up to 500m<sup>2</sup>. The Swedish fire curves from which the parametric fires originated were originally only used for compartments with floor areas up to 100 m<sup>2</sup> [178].

As timber is combustible it contributes to the fuel load of a fire. If large surfaces of wood are exposed, its contribution should be included in the fuel load used to determine the parametric fire. Methods to do this were proposed by Brandon [159] and Barber et al. [160] as was discussed in Sect. 8.7.3.

Once the parametric fire curve is determined the structural analysis can be performed. Three methods have been proposed previously [108, 109, 122, 124]. Two of these three methods account for the reduction of the load-bearing capacity during a fire by reducing the load-bearing cross section of structural elements [122, 124]. The other method accounts for the reduction of load-bearing capacity by reducing the mechanical properties throughout the structural element based on temperature calculations [108, 109]. Only the last mentioned is suitable for structural members with an inhomogeneous built-up, such as CLT members. All three methods are discussed here.

#### **8.8.2.1 Lange et al. [122] Effective Cross-Section Method 1**

A method developed by Lange et al. [122] to predict the structural behavior of timber elements exposed to the parametric fires of EN 1991-1-2 involves reducing the cross section of the load-bearing member from exposed sides. According to this method, a char layer and a zero-strength layer should be subtracted from the initial cross section of the timber member. The load-bearing capacity of the element throughout the fire can then be calculated as the load-bearing capacity of the effective cross section with unchanged mechanical properties.

Lange et al. proposed to calculate the char depths in accordance with Hadvig [156], which can be calculated using Eqs. 8.17–8.20, as previously discussed. Based on a series of fire tests, Lange et al. determined that the zero-strength layer was 15 mm thick for long cool fires of the test series and 8 mm thick for the short hot fires of the test series. To be conservative it was, therefore, chosen to implement a zero-strength layer of 15 mm for the calculations.

The application of the zero-strength layer is based on an assumption that the mechanical properties within the cross section are homogeneous. Therefore, the reduced cross-section method as it is presented here cannot be implemented to determine the fire resistance and the structural capacity of CLT in fires.

#### **8.8.2.2 Brandon et al. Effective Cross-Section Method 2**

Brandon et al. [124] developed a calculation model based on multiple test series. A numerical model was developed to calculate temperatures within exposed timber members in a wide range of parametric fires. Using the numerical model, it was



shown that the zero-strength layer is not constant during the fire and increases in size during the cooling phase, because of heat dissipation. Therefore, Brandon et al. proposed a new effective cross-section method.

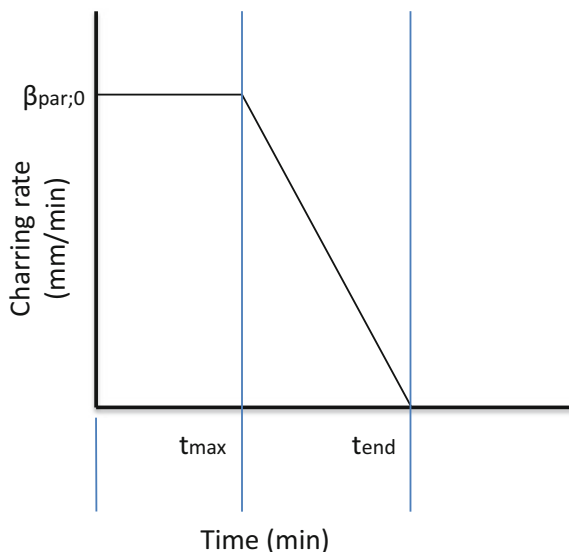
Predictions of the char layer have traditionally been used for calculations of the capacity of timber members exposed to nominal fire conditions following ISO 834. The nominal fire exposure involves solely a heating phase until the test is stopped. This heating phase corresponds to an approximately constant zero-strength layer. Therefore, the charring depth has a straightforward correlation with the capacity of the structural elements. In the cooling phase of parametric fires, the relationship between the charring rates and the reduction of the load-bearing capacity is, however, not straight forward. Therefore, Brandon et al. [124] proposed to use an effective char depth that allowed the implementation of a constant zero-strength layer after the first 20 min of the fire. The effective char depth exceeds the real char depth in the decay phase, but is the same as the real char depth in the fully developed (heating) phase.

In the calculation the zero-strength layer is constant, but dependent on the parametric time modifier as defined in EN 1991-1-2 and can be calculated using the following expression:

$$d_0 = 8.0 + 0.02\Gamma - 0.05\Gamma^2 \quad (8.44)$$

According to the proposed model by Brandon et al., the effective charring rate is the same as the charring rate according to Eq. 8.22 until the start of the decay phase,  $t_{\max}$ . During the decay phase the charring rate reduces linearly until the time at which the temperature of the parametric fire curve returns back to 20 °C,  $t_{\text{end}}$  (as shown in Fig. 8.40):

**Fig. 8.40** Proposed effective charring model



$$t_{\text{end}} = \frac{625t_{\text{max}}x \times \Gamma + \Theta_{\text{max}} - 20}{625 \times \Gamma} \text{ if } t_{\text{max}} \times \Gamma \leq 0.5 \quad (8.45)$$

$$t_{\text{end}} = \frac{-250t_{\text{max}}^2x \times \Gamma^2 + 750t_{\text{max}}x \times \Gamma + \Theta_{\text{max}} - 20}{250 \times \Gamma(t_{\text{max}} \times \Gamma - 3)} \text{ if } 0.5 < t_{\text{max}} \times \Gamma < 2 \quad (8.46)$$

$$t_{\text{end}} = \frac{250t_{\text{max}}x \times \Gamma + \Theta_{\text{max}} - 20}{250 \times \Gamma} \text{ if } t_{\text{max}} \times \Gamma \geq 2 \quad (8.47)$$

An effective charring model is proposed with significant differences from the current charring model in EN1995-1-2. In the proposed model the charring rate is constant for the entire heating phase. It should be noted that  $t_0$  of the Eurocode 5 model is not equal to the duration of the heating phase,  $t_{\text{max}}$ . As mentioned before,  $t_{\text{end}}$  is the time at which the temperature of the parametric fire curve returns back to 20 °C:

$$t_{\text{end}} = \frac{625t_{\text{max}}x \times \Gamma + \Theta_{\text{max}} - 20}{625 \times \Gamma} \text{ if } t_{\text{max}} \times \Gamma \leq 0.5 \quad (8.48)$$

$$t_{\text{end}} = \frac{-250t_{\text{max}}^2x \times \Gamma^2 + 750t_{\text{max}}x \times \Gamma + \Theta_{\text{max}} - 20}{250 \times \Gamma(t_{\text{max}} \times \Gamma - 3)} \text{ if } 0.5 < t_{\text{max}} \times \Gamma < 2 \quad (8.49)$$

$$t_{\text{end}} = \frac{250t_{\text{max}}x \times \Gamma + \Theta_{\text{max}} - 20}{250 \times \Gamma} \text{ if } t_{\text{max}} \times \Gamma \geq 2 \quad (8.50)$$

The maximum fire temperature  $\Theta_{\text{max}}$  can be obtained by substituting  $t_{\text{max}}$  for  $t$  in the temperature function. The effective charring depth,  $d_{\text{char;ef}}$ , at any time can be calculated using

$$d_{\text{char;ef}} = \beta_{\text{par}}t \text{ for } t \leq t_{\text{max}} \quad (8.51)$$

$$d_{\text{char;ef}} = \beta_{\text{par}}t_{\text{max}} + 0.5 * \left( \frac{-\beta_{\text{par}}}{t_{\text{end}} - t_{\text{max}}} \right) \times (t - t_{\text{max}})^2 + \beta_{\text{par}}(t_{\text{end}} - t_{\text{max}}) \text{ for } t_{\text{max}} < t \leq t_{\text{end}} \quad (8.52)$$

### 8.8.2.3 Brandon et al. Numerical Method (Method 3)

Brandon et al. [108, 109] proposed a change of the so-named *Advanced Calculation Method* described in Annex B of EN 1995-1-2, so that it is suitable for structural predictions of timber members exposed to parametric fires, as previously discussed in Sect. 8.7.4. In contrast with previously discussed structural calculations for timber in parametric fire exposure, the method is suitable for members with inhomogeneous cross sections, such as CLT members. Chapter 10 discusses principles of such numerical methods.

## 8.8.3 Light Timber Frame Structures in Nominal Fires

Dependent on the function of light timber frame assemblies, it can be needed to assess the load-bearing capacity and/or the ability to separate fire compartments in nominal fire exposure. The fire resistance of timber frame assemblies is in practice, determined using either fire resistance tests or calculations. Used calculation methods for light timber frame assemblies differ globally. Methods used in North America and Europe are discussed in this section.

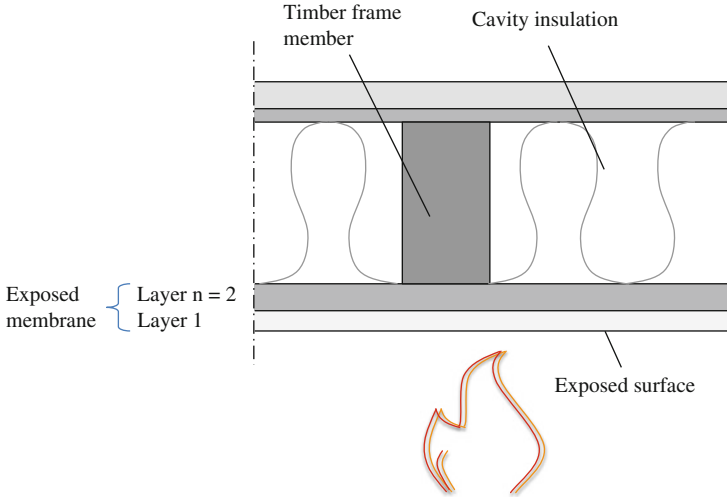
### 8.8.3.1 Load-Bearing Light Timber Frame Structures in Nominal Fires

Calculations discussed in this clause aim to predict the structural fire resistance of light timber frame members. In North America, a so-named component additive method is used for the assessment of loaded and unloaded timber frame assemblies.

#### North American Component Additive Method for Loaded and Unloaded Assemblies

The 2012 International Building Code published by the International Code Council provides a method to calculate the fire resistance rating of loaded and unloaded timber frame assemblies. The approach is based on some of the ten rules of fire resistance rating by Harmathy [171], which were obtained from the analysis of 208 fire resistance tests of loaded and unloaded timber frame floor and wall assemblies, resulting in fire resistance ratings from 20 to 90 min. The two rules that were most relevant for the development of the North American component additive method are the following [171]:

- *The thermal fire endurance of a construction consisting of a number of parallel layers is greater than the sum of the “thermal” fire resistance characteristics of the individual layers when exposed separately to fire.*



**Fig. 8.41** Numbering of membrane layers

- *The fire resistance of an assembly cannot be increased by increasing the thickness of an air layer.*

Based on the first rule the contribution of the membrane to the fire resistance is calculated by addition of assigned times of protection of the membrane components (or layers), which are based on the ability of the layers to remain in position during a fire resistance test. In this component additive method, the total fire resistance rating of timber frame assemblies is calculated from the assigned protection time of the exposed membrane and the time to destruction of the framing members. The fire resistance can be increased if the cavity of the assembly is filled with rock wool or glass wool insulation. The fire resistance is calculated as follows:

$$t_{res} = \sum_{i=1}^{i=n} t_{m,i} + t_{f,timber} + t_{add} \quad [\text{min}] \quad (8.53)$$

where  $t_{m,i}$ ,  $t_{f,timber}$ , and  $t_{add}$  are the fire resistance contribution of the membrane in minutes.  $i$  denotes the layer number as indicated in Fig. 8.41.

### European Method

The most studied and developed method available to calculate the structural fire resistance of timber frame assemblies is the effective cross-section method presented in Eurocode 5. Similar to the method discussed in Sect. “European Effective Cross-Section Method”, a char layer and a compensating zero-strength layer are subtracted from the load-bearing timber cross section. Extensions of the method are

presented by Just et al. [103–105] and Tiso et al. [112]. Incorporated charring rates for the effective cross-section method are dependent on the performance of the encapsulation board materials and the presence and performance of insulation material.

Due to a large variety of insulation materials and significant differences of performance of these insulation materials, Tiso et al. proposed the implementation of three protection levels for insulation materials, to account for different performances of different materials. To determine the protection level a furnace test of a specific timber frame assembly exposed to nominal fire temperatures should be performed. For each protection level, different charring rates and thicknesses of zero-strength layers are assumed.

### ***8.8.4 Light Timber Frame Structures in Parametric Fire Exposure***

As appeared from recent research (Sect. 8.6.3.1) the performance of light timber frame structures is significantly dependent on the performance of encapsulation. The use of parametric fires can be justified if the contribution of the timber frame to the fire load is insignificant. However, no analytical methods to determine gypsum board falloff in parametric fires exist. Therefore, the use of numerical methods is recommended. It should, however, be noted that no comparative studies were found, in which numerical predictions of gypsum board falloff in compartments with light timber frame assemblies were set against parametric or compartment fire test results, and that research indicated that encapsulation failure occurs earlier if applied on light timber frames than if applied directly on heavy timber surfaces. Therefore, benchmark tests comparing predictions with results of timber frame assemblies in compartment or parametric fire tests are highly recommended when performing such calculations.

## **References**

1. Bartlett, A., Hadden, R., Bisby, L. and Lane, B. (2016). “Auto-extinction of engineered timber in relation to fire point theory,” in Proceedings of the 2016 Interflam Conference, Royal Holloway, 2016.
2. Bartlett, A., Wiesner, F., Hadden, R., Bisby, L., Lane, B., Lawrence, A., Palma, P. & Frangi, A. (2016), Needs for total fire engineering of mass timber buildings. In 2016 World Conference on Timber Engineering (WCTE 2016). Vienna.
3. Hopkin, D., et al. (2016). Timber structures subject to non-standard fire exposure—advances & challenges. Proceedings of the World Conference on Timber Engineering 2016 (WCTE 2016), TU Wien, Aug 22–25.
4. Emberley, R., Gorska, P. C., Bolanos, A., Lucherini, A., Solarte, A., Soriguer, D., Gutierrez, G. M., Humphreys, K., Hidalgo, J. P., Maluk, C., Law, A., & Torero, J. L. (2017). Description

- of small and large-scale CLT fire tests. *Fire Safety Journal*. <https://doi.org/10.1016/j.firesaf.2017.03.024>
5. Hadden, R. M., Bartlett, A. I., Hidalgo, J. P., Santamaria, S., Wiesner, F., Bisby, L. A., Deeny, S., & Lane, B. (2017). Effects of exposed cross laminated timber on compartment fire dynamics. *Fire Safety Journal*, *91*, 480–489.
  6. Green, D. W., Winandy, J. E., & Kretschmann, D. E. (1999). 'Chapter 4 – Mechanical properties of wood' *wood handbook—Wood as an engineering material*. Gen. Tech. Rep. FPL–GTR–113 (p. 45). U.S. Department of Agriculture, Forest Service, Forest Products Laboratory.
  7. Peng, L. (2010). *Performance of heavy timber connections in fire*. Thesis. Department of Civil and Environmental Engineering Carleton University.
  8. American Institute of Timber Construction. (2012). *Timber construction manual*. J Wiley & Sons.
  9. Torero, J. (2016). Flaming ignition of solid fuels. In M. J. Hurley et al. (Eds.), *SFPE handbook of fire protection engineering*. Springer.
  10. Browne, F.L. (1958). Theories of the combustion of wood and its control. A survey of the literature. Report 2136. Madison, Wisconsin: Forest Products Laboratory, US Department of Agriculture.
  11. Friguin, K. L. (2011). Material properties and external factors influencing the charring rate of solid wood and glue-laminated timber. *Fire and Materials*, *35*, 303–327. <https://doi.org/10.1002/fam.1055>
  12. Drysdale, D. (2011). *An introduction to fire dynamics* (3rd ed.). Wiley.
  13. Babrauskas, V. (2002). Ignition of wood: A review of the state of the art. *Journal of Fire Protection Engineering*, *12*(3), 163–189.
  14. Hopkin, D., Gorska, C., Spearpoint, M. J., Fu, I., Krenn, H., Sleik, T., & Stapf, G. (2021). Experimental characterisation of the fire behaviour of CLT ceiling elements from different leading suppliers, in: Applications of Structural Fire Engineering. Presented at the Applications of Structural Fire Engineering, Ljubljana, Slovenia.
  15. Mikkola, E. (1990). *Charring of wood*. VTT research report 689. Technical Research Centre of Finland.
  16. White, R. H., & Nordheim, E. V. (1992). *Fire Technology*, *28*, 5. <https://doi.org/10.1007/BF01858049>
  17. Tran, H. C., & White, R. H. (1992). Burning rate of solid wood measured in a heat release rate calorimeter. *Fire and Materials*, *16*(4), 197–206.
  18. Petrella, R. V. (1979). The mass burning rate and mass transfer number of selected polymers, wood, and organic liquids. *Polymer-Plastic Technology and Engineering*, *13*(1), 83–103.
  19. Tewarson, A., & Pion, R. F. (1976). Flammability of plastics—I. burning intensity. *Combustion and Flame*, *26*, 85–103.
  20. Bartlett, A. I., Hadden, R. M., & Bisby, L. A. (2019). *Fire Technology*, *55*, 1. <https://doi.org/10.1007/s10694-018-0787-y>
  21. Ohlemiller, T., & Shaub, W. (1988). Products of wood smolder and their relation to wood-burning stoves (No. NBSIR-88-3767). National Bureau of Standards, Washington, DC (USA). Center for Fire Research.
  22. Ohlemiller, T. J. (2002). Smoldering combustion. *SFPE handbook of fire protection engineering*, 3.
  23. Beyler, C. L., Gratkowski, M. T., Sikorski, J. (2006). Radiant smoldering ignition of virgin plywood and plywood subjected to prolonged smoldering. International Symposium on Fire Investigation and Technology.
  24. Swann, J. H., Hartman, J. R., Beyler, C. L. (2008). Study of radiant smoldering ignition of plywood subjected to prolonged heating using the cone calorimeter, TGA, and DSC. Proceedings of the 9th IAFSS Symposium, 9, 155–166.

25. Crielaard, R., van de Kuilen, J.-W., Terwel, K., Ravenshorst, G., Steenbakkers, P., (2019). Self-extinguishment of cross-laminated timber. *Fire Safety Journal* 105, 244–260. <https://doi.org/10.1016/j.firesaf.2019.01.008>
26. Buchanan, A. H. (2001). *Structural design for fire safety* (1st ed.). John Wiley and Sons Ltd.
27. Hopkin, D. (2011). *Fire performance of engineered timber products and systems*. Thesis. Loughborough University, UK.
28. Heitz, J. (2016). Fire resistance in american heavy timber construction. [https://doi.org/10.1007/978-3-319-32128-8\\_2](https://doi.org/10.1007/978-3-319-32128-8_2)
29. Kurokawa, T. (1990). Heavy timber construction. *Habitat Intl.*, 14(2/3), 255–261.
30. ICC. (2015). *2015 international building code*. International Code Council.
31. Dickson, M., & Parker, D. (2015). Engineered timber and structural form in sustainable design. *Proceedings of the Institution of Civil Engineers - Construction Materials*, 168(4), 161–172.
32. Lam, F. (2010). Timber products and manufacturing processes. ICE Manual of Construction Materials. Institution of Civil Engineers
33. Thelandersson, S., & Larsen, H. (2003). *Timber engineering*. John Wiley & Sons. ISBN9780470844694.
34. Aghayere, A., & Vigil, J. (2007). *Structural wood design—A practice oriented approach using the ASD method* (1st ed.). Wiley.
35. Kolb, J. (2008). *Systems in timber engineering* (1st ed.). Birkhauser Lignum DGfH.
36. Karacebeyli, E., & Douglas, B. (2013). CLT handbook-US edition. FPInnovations and Binational Softwood Lumber Council, Point-Claire, Quebec.
37. Sutton, Black, & Walker. (2011). *Cross-laminated timber. An introduction to low-impact building materials*. IP 17/11. BRE-IHS Press.
38. Richardson, L. R. (2004). Failure of floor assemblies constructed with timber joists, wood trusses or I joists during fire resistance tests. In V. Babrauskas (Ed.), *Interflam 2004- proceedings of the tenth international conference, 5th–7th July 2004* (pp. 603–608). Interscience.
39. Dinwoodie, J. M. (2000). *Timber- nature and behavior* (1st ed.). Taylor and Francis.
40. Illston, J. M. (1994). *Construction materials—Their nature and behavior* (2nd ed.). E & FN Spon.
41. Ho, T. X., Dao, T. N., Aaleti, S., van de Lindt, J. W., & Rammer, D. R. (2017). Hybrid system of Unbonded post-tensioned CLT panels and light-frame wood shear walls. *Journal of Structural Engineering*, 143, 2.
42. Leijten, A. J. M. (2011). Requirements for moment connections in statically indeterminate timber structures. *Engineering Structures*, 33(2011), 3027–3032. <https://doi.org/10.1016/j.engstruct.2011.03.014>
43. Brandon, D., Maluk, C., Ansell, M. P., Harris, R., Walker, P., Bisby, L., & Bregulla, J. (2015). Fire performance of metallic-free timber connections. *Proceedings of the Institute of Civil Engineers*, 168(4), 173–186.
44. Buchanan, A., Deam, B., Fragiacomio, M., Pampanin, S., & Palermo, A. (2008). Multi-storey prestressed timber buildings in New Zealand. *Structural Engineering International*, 18(2), 166–173.
45. Leijten, A. J. M. (1998). Densified veneer wood reinforced timber joints with expanded tube fasteners. PhD thesis, Delft University Press. ISBN 90–407–1757-5.
46. Fredlund, B. (1988). *A model for heat & mass transfer in timber structures during fire: A theoretical, numerical and experimental study*. LUTVDG/(TVBB-1003). Lund University.
47. Janssens, M. (1994). Thermo-physical properties for wood pyrolysis models, Proceedings of the Pacific timber engineering conference, July 11th–15th 1994, Gold Cost, Australia.
48. Knudson, R. M., & Schniewind, A. P. (1975). Performance of structural wood members exposed to fire. *Forest Products Journal*, 25(2), 23–32.
49. White, R. H., & Schaffer, E. (1978). Application of CMA programme to wood charring. *Fire Technology*, 15, 279–290.

50. Thomas, G. (1997). *Fire resistance of light timber framed walls and floors*. Thesis. University of Canterbury Press.
51. Harmathy, T. Z. (1988). Properties of building materials—Section 1 chapter 26. In P. J. Dinunno, C. L. Beyler, R. L. Custer, W. D. Walton, & J. M. Watts (Eds.), *The SFPE handbook of fire protection engineering* (pp. 388–391). NFPA.
52. Gammon, B. W. (1987). *Reliability analysis of wood frame wall assemblies exposed to fire*. PhD thesis edn. University of California.
53. König, J., & Walleij, L. (2000). *Timber frame assemblies exposed to standard and parametric fires part 2: A design model for standard fire exposure*. I0001001. SP Trätekt.
54. European Committee for Standardization. (2004). *Eurocode 5: Design of timber structures—Part 1–2: General – Structural fire design*. EN 1995-1-2. CEN.
55. König, J. (2006). Effective thermal actions and thermal properties of timber members in natural fires. *Fire and Materials*, 30(2), 51–63.
56. Dunlap, F. (1912). *The specific heat of wood*. Bulletin 110. US forest service.
57. Fuller, J. J., Leichti, R. J., & White, R. H. (1992). Temperature distribution in a nailed gypsum stud joint exposed to fire. *Fire and Materials*, 16(2), 95–99.
58. Mehaffey, J. R., Cuerrier, P., & Carisse, G. (1994). A model for predicting heat transfer through gypsum board wood-stud walls exposed to fire. *Fire and Materials*, 18(5), 297–305.
59. Lie, T. T. (1992). *Structural fire protection*. ASCE manuals and reports of engineering practice. ASCE.
60. Cachim, P. B., & Franssen, J. M. (2009). Comparison between the charring rate model and the conductive model of Eurocode 5. *Fire and Materials*, 33(3), 129–143.
61. Trada (2019). Wood species database | TRADA. [online] [Trada.co.uk](https://www.trada.co.uk/wood-species/). from <https://www.trada.co.uk/wood-species/>. Retrieved July 29, 2019
62. Buchanan, A. H. (2000). Fire performance of timber construction. *Progress in Structural Engineering and Materials*, 2(3), 278–289.
63. König, J., & Walleij, L. (1999). *One-dimensional charring of timber exposed to standard and parametric fires in initially unprotected and post protection situations I9908029*. SP Trätekt.
64. Matala, A., Hostikka, S., & Mangs, J. (2008). Estimation of pyrolysis model parameters for solid materials using thermogravimetric data. In *Fire safety science—Proceedings of the 8<sup>th</sup> international symposium* (pp. 1213–1224). International Association of Fire Safety Science.
65. European Committee for Standardization. (2003). *Structural timber—Strength classes*. EN 338:2003. CEN.
66. Bazan, I. M. M. (1980). *Ultimate bending strength of timber beams*. Thesis edn. Nova Scotia Technical College.
67. Hopkin, D. (2012). Predicting the thermal response of timber structures in natural fires using computational 'heat of hydration' principles. *Fire and Materials*. <https://doi.org/10.1002/fam.2133>
68. Wang, X., Fleischmann, C., & Spearpoint, M. (2016). Parameterising study of tunnel experiment materials for application to the fire dynamics simulator pyrolysis model. *Journal of Fire Sciences*, 1–25. <https://doi.org/10.1177/0734904116667738>
69. Mindeguia, J.-C., Cuff, G., Dréan, V., & Auguin, G. (2018). Simulation of charring depth of timber structures when exposed to non-standard fire curves. *Journal of Structural Fire Engineering*, 9(1), 63–76. <https://doi.org/10.1108/JSFE-01-2017-0011>
70. Richter, F., Atreya, A., Kotsovinos, P., & Rein, G. (2019). The effect of chemical composition on the charring of wood across scales. *Proceedings of the Combustion Institute*, 37(3), 4053–4061.
71. Wade, C., Hopkin, D., Su, J., Spearpoint, M., & Fleischmann, C. (2019). *Enclosure fire model for mass timber construction—Benchmarking with a kinetic wood pyrolysis sub model*. Interflam.
72. Harte, A. (2009). Timber engineering: An introduction. In M. Forde (Ed.), *ICE manual of construction materials* (Vol. 2, 1st ed., pp. 707–715). Thomas Telford.



73. Thunnel, B. (1941). *Hallfastetsegenskaper hos svenskt furuvirke utan kvistar och defekter. Handlingar Nr. 161*. Ingenjorsvetenskapsakademien.
74. Hopkin, D., El-Rimawi, J., Silberschmidt, V., & Lennon, T. (2011). The impact of assumed fracture energy on the fire performance of timber beams. In F. Wald (Ed.), *Proceedings of the 2nd international conference on applications in structural fire engineering, 29th April 2011* (pp. 349–354). Czech Technical University.
75. Hopkin, D., Lennon, T., El-Rimawi, J., & Silberschmidt, V. (2012). Advanced fire Design of Timber Structures Using Computational Techniques—Simple Indeterminate Structures. *Journal of Structural Fire Engineering*, 3(2), 215–233.
76. Kollman, F. (1951). *Über das mechanische verhalten von kiefernholz bei biegun und temperaturen zwischen 20 und 100. Meddelande 22*. Svenska Traforskningsintitutet.
77. Schaffer, E. L. (1973). Effect of pyrolytic temperatures on the longitudinal strength of dry Douglas fir. *ASTM Journal for Testing and Evaluation*, 1(4), 319–329.
78. Schaffer, E. L. (1984). *Structural fire design: Wood. FFL 450*. Forest products lab.
79. Gerhards, C. C. (1982). Effect of moisture content and temperature on mechanical properties of wood: An analysis of immediate effects. *Wood and Fiber Science*, 14(1), 4–36.
80. Östman, B. (1985). Wood tensile strength at temperatures and moisture contents simulating fire conditions. *Wood and Science Technology*, 19, 103–106.
81. Lau, P. W. C. and Barrett, J. D. (1997). Modelling tension strength behavior of structural lumber exposed to elevated temperatures. Proceedings of the fourth international symposium on fire safety science. Australia: Melbourne
82. König, J., & Noren, J., (1991). Fire exposed load bearing wood frame members. 9112080. Stockholm: SP Träteck.
83. Collier, P. (1993). *A method to predict the fire resistance performance of load bearing light timber framed walls*. Building research association of New Zealand.
84. König, J., Noren, J., Olesen, F. B., & Hansen, F. T. (1997). *Timber frame assemblies exposed to standard and parametric fires part 1: Fire tests. I9702015*. SP Träteck.
85. Young, S. A. (1996). *Elevated temperature mechanical properties of radiata pine in compression. Internal report for CESARE*. Victoria University.
86. Nyman, C. (1980). *The effect of temperature and moisture on the strength of wood and glue joists. VTT forest products no. 6*. Technical Research Centre of Finland.
87. Preusser, R. (1968). Plastic and elastic behavior of wood affected by heat in open systems. *Holztechnologie*, 9(4), 229–231.
88. British Standards Institution. (2004). *Gypsum plasterboards- definitions, requirements and test methods. BS EN 520:2004*. BSI.
89. ASTM C1396 / C1396M – 17 (2017) Standard specification for gypsum board. ASTM International, .
90. Thomas, G. (2002). Thermal properties of gypsum plasterboard at high temperatures. *Fire and Materials*, 26(1), 37–45.
91. Clancy, P. (2001). Advances in modelling heat transfer through wood framed walls in fire. *Fire and Materials*, 25(6), 241–254.
92. Sultan, M. A. (1996). A model for predicting heat transfer through non-insulated unloaded steel-stud gypsum board wall assemblies exposed to fire. *Fire Technology*, 32(3), 239–259.
93. Benichou, N., Sultan, M. A., Maccallum, C., & Hum, J. (2001). *Thermal properties of wood, gypsum and insulation at elevated temperatures. IR-710*. NRC.
94. Ang, C. N., & Wang, Y. C. (2009). Effect of moisture transfer on the specific heat of gypsum plasterboard at high temperatures. *Construction and Building Materials*, 23(2), 675–686.
95. Park, S. H., Manzello, S. L., Bentz, D. P., & Mizukami, T. (2009). Determining thermal properties of gypsum board at elevated temperatures. *Fire and Materials*, 34(5), 237–250.
96. Wakili, K. G., Hugli, E., Wullschleger, L., & Frank, T. H. (2007). Gypsum board in fire— modeling and experimental validation. *Journal of Fire Sciences*, 25(3), 267–282.
97. Thomas, G. (2010). Modelling thermal performance of gypsum plasterboard-lined light timber frame walls using SAFIR and TASEF. *Fire and Materials*, 34(8), 385–406.

98. Schleifer, V. (2009). *Zum Verhalten von raumabschliessenden mehrschichtigen Holzbauteilen im Brandfall. PhD Thesis ETH No. 18156*. ETH.
99. Lennon, T., Hopkin, D., El-Rimawi, J., & Silberschmidt, V. (2010). Large scale natural fire tests on protected engineered timber floor systems. *Fire Safety Journal*, 45(2010), 168–182.
100. Jansson, R. (2004). *Measurement of thermal properties at elevated temperatures- Brandforsk project 328–031. SP REPORT 2004:46*. SNTRI.
101. Twilt, L., & Van Oerle, J. (1999). *Fire characteristics for use in a natural fire design of building structures. CEC agreement 7210-SA/125–937*. Profil Arbed.
102. Feng, M., Wang, Y. C., & Davies, J. M. (2003). Thermal performance of cold-formed thin-walled steel panel systems in fire. *Fire Safety Journal*, 38(4), 365–394.
103. Just, A., Schmid, J., & König, J. (2010). Failure times of gypsum boards. In V. R. Kodur & J. M. Franssen (Eds.), *Proceedings of the sixth international conference on structures in fire, 2nd-4th June 2010* (pp. 593–601). DESTech.
104. Just, A. (2010). *Structural fire design of timber frame assemblies insulated by glass wool and covered by gypsum plasterboard*. Tallinn University of Technology.
105. Just, A. (2010). Post protection behavior of wooden wall and floor structures completely filled with glass wool. In V. R. Kodur & J. M. Franssen (Eds.), *Proceedings of the sixth international conference on structures in fire, 2nd-4th June 2010* (pp. 584–592). DESTech.
106. Sultan, M. A. (2010). Comparison of gypsum board fall-off in wall and floor assemblies exposed to furnace heat. In S. Grayson (Ed.), *12th international fire science and engineering conference (Interflam), 5th–7th July 2010* (pp. 1677–1682). Interscience.
107. Quintiere, J. G., & Rangwala, A. S. (2004). A theory for flame extinction based on flame temperature. *Fire Materials*, 28, 387–402. <https://doi.org/10.1002/fam.835>
108. Brandon, D., Just, A., Andersson, P., & Östman, B. (2018). Mitigation of fire spread in multi-storey timber buildings – Statistical analysis and guidelines for design. *RISE Report, 2018*, 43.
109. Brandon, D., Schmid, J., Su, J., Hoehler, M., Östman, B. & Kimball, A. (2018). Experimental Fire-Simulator for Post-Flashover Compartment Fires. In: SiF 2018—The 10th International Conference on Structures in Fire, Belfast, UK: Paper presented at SiF 2018 - The 10th International Conference on Structures in Fire, Belfast, UK. New University of Ulster.
110. Schmid, J., Santomaso, A., Brandon, D., Wickström, U., & Frangi, A. (2018). Timber under real fire conditions – The influence of oxygen content and gas velocity on the charring behavior. *Journal of Structural Fire Engineering*, 9(3), 222–236. <https://doi.org/10.1108/JSFE-01-2017-0013>
111. Mäger, K. N., Just, A., Schmid, J., Werther, N., Klippel, M., Brandon, D., & Frangi, A. (2017). Procedure for implementing new materials to the component additive method. *Fire Safety Journal*. In press. <https://doi.org/10.1016/j.firesaf.2017.09.006>
112. Tiso, M., Just, A., Schmid, J., & Klippel, M. (2018). Effective cross-section method for timber frame assemblies—Definition of coefficients and zero-strength layers. *Fire and Materials*, 2018, 1–17. <https://doi.org/10.1002/fam.2645>
113. Brandon, D., Schmid, J., & Just, A. (2016). Eurocode 5 design in comparison with fire resistance tests of unprotected timber beams. In Proceedings of 11th Conference on Performance-Based Codes And Fire Safety Design—SFPE
114. Schmid, J., Klippel, M., Just, A., & Frangi, A. (2014). Review and analysis of fire resistance tests of timber members in bending, tension and compression with respect to the reduced cross-section method. *Fire Safety Journal*, 68, 81–99, ISSN 0379-7112. <https://doi.org/10.1016/j.firesaf.2014.05.006>
115. Klippel, M., Schmid, J., Frangi, A. (2016). Fire design of CLT, Proceedings of the Joint Conference of COST Actions FP1402 and FP1404, March 10–11, Stockholm, Sweden
116. Schmid, J., Just, A., Klippel, M., & Fragiaco, M. (2015). The reduced cross-section method for evaluation of the fire resistance of timber members: Discussion and determination of the zero-strength layer. *Fire Tech.*, 51(6), 1285–1309.

117. Dhima, D., Audebert, M., & Bouchaïr, A. (2014). Analysis of the Thermo-mechanical behavior of steel-to-timber connections in bending. *Journal of Structural Fire Engineering*, 5(2), 97–112. <https://doi.org/10.1260/2040-2317.5.2.97>
118. Palma, P. (2016). Fire behavior of timber connections. PhD Thesis, ETH Zürich: Dept. of Civil, Environmental and Geomatic Engineering (D-BAUG)
119. Barber, D. (2017). *Glulam connection fire test summary report*. Arup USA.
120. Ronstad, D., Ek, N. (2018). Study of glued-laminated timber connections with high fire resistance using expanded steel tubes. Master Thesis, Department of Civil, Environmental and Natural Resources Engineering, Luleå University of Technology, Sweden.
121. Brandon, D., Landel, P., Ziethen, R., Albrektsson, J., Just, A. (2019) High-fire-resistance glulam connections for tall timber buildings. RISE Report, 2019:26. Research Institutes of Sweden. ISBN 978–91–88907-52-3.
122. Lange, D., Boström, L., Schmid, J., & Albrektsson, J. (2015). The reduced cross section method applied to glulam timber exposed to non-standard fire curves. *Fire Technology*. <https://doi.org/10.1007/s10694-015-0485-y>
123. Lineham, S., Thomson, D., Bartlett, A., Bisby, L., & Hadden, R. (2016). Structural response of fire-exposed cross-laminated timber beams under sustained loads. *Fire Safety Journal*, 85, 23–34.
124. Brandon, D., Just, A., Lange, D., & Tiso, M. (2017). Parametric fire design—Zero-strength-layers and charring rates. In R. Görlacher (Ed.), *INTER proceedings meeting fifty (Kyoto)*. *INTER / 50–16 – 2*. Timber Scientific Publishing, KIT Holzbau und Baukonstruktionen. ISSN 2199-9740. <http://holz.vaka.kit.edu/public/inter2017.pdf>
125. Wiesner, F., Bisby, L. A., Bartlett, A. I., Hidalgo, J. P., Santamaria, S., Deeny, S., & Hadden, R. M. (2019). Structural capacity in fire of laminated timber elements in compartments with exposed timber surfaces. *Engineering Structures*, 179, 284–295. <https://doi.org/10.1016/j.engstruct.2018.10.084>
126. Wiesner, F., & Bisby, L. (2019). The structural capacity of laminated timber compression elements in fire: A meta-analysis. *Fire Safety Journal*, 107, 114–125. <https://doi.org/10.1016/j.firesaf.2018.04.009>
127. Lennon, T., Bullock, M. J., Enjily, V. (2000). The fire resistance of medium-rise timber frame buildings. BRE Report No 79485–1, BRE, Watford, UK.
128. Hakkarainen, T. (2002). Post-flashover fire in light and heavy timber construction compartments. *Journal of Fire Sciences*, 20(2002), 133–175.
129. Frangi, A., & Fontana, M. (2005). *Fire performance of timber structures under natural fire conditions*. *Fire safety science symposium 8: 279–290*. IAFSS.
130. Frangi, A., Bochicchio, G., Ceccotti, A., & Lauriola, M. P. (2008). *Natural full-scale fire test on a 3 storey XLam timber building, proceedings of the 10th world conference on timber engineering (WCTE), 2nd-5th June 2008*. Curran Associates, Inc.
131. Frangi, A., Bochicchio, G., Ceccotti, A., & Lauriola, M. (2008). *Natural full-scale fire test on a 3 storey XLam timber building*. Engineered Wood Products Association.
132. Frangi, A., Erchinger, C., & Fontana, M. (2008). Charring model for timber frame floor assemblies with void cavities. *Fire Safety Journal*, 43(8), 551–564.
133. McGregor, C. J. (2013). Contribution of cross-laminated timber panels to room fires. Master thesis. Department of Civil and Environmental Engineering Carleton University. Ottawa-Carleton Institute of Civil and Environmental Engineering, Ottawa, Ontario, Canada.
134. Li, X., Zhang, X., Hadjisophocleus, G., & McGregor, C. (2014). Experimental study of combustible and non-combustible construction in a natural fire. *Fire Technology*, 2014.
135. Medina Hevia, A. R. (2014). Fire resistance of partially protected cross-laminated timber rooms. Master thesis. Department of Civil and Environmental Engineering Carleton University. Ottawa-Carleton Institute of Civil and Environmental Engineering, Ottawa, Ontario, Canada.

136. Su, J. Z. and Lougheed, G. D. (2014). Report to research consortium for wood and wood hybrid mid-rise buildings—Fire safety summary—Fire research conducted for the project on mid-rise wood construction. National Research Council Canada, Client report: A1–004377.1, Ottawa, Ontario, Canada.
137. Su, J. Z. and Muradori, S. (2015). Fire demonstration—Cross-laminated timber stair/elevator shaft. National Research Council Canada, Client report: A1–004377.1, Ottawa, Ontario, Canada
138. Kolaitis, D. I., Asimakopoulou, E. K., & Founti, M. A. (2014). Fire protection of light and massive timber elements using gypsum plasterboards and wood based panels: A large-scale compartment fire test. *Construction and Building Materials*, 73(2014), 163–170.
139. Janssens, M. (2015). CLT compartment fire test results. Video presentation. from <http://www.awc.org/Code-Officials/2015-IBC-Code-Changes>. Retrieved October 26, 2015
140. Hox, K. (2015). Branntest av massivtre. SPFR-rapport SPFR A15101. SP Fire Research, Trondheim, Norway (unpublished) (in Norwegian)
141. Janssens. (2017). *Development of a fire performance assessment methodology for qualifying cross-laminated timber adhesives*. South West Research Institute.
142. Su, J., Lafrance, P.-S., Hoehler, M., Bundy, M. (2018). Cross Laminated Timber Compartment Fire Tests for Research on Fire Safety Challenges of Tall Wood Buildings—Phase 2.
143. Zelinka, S. L., Hasburgh, L. E., Bourne, K. L., Tucholski, D. R., & Oullette, J. P. (2018). *Compartment fire testing of a two-story mass timber building. General technical report FPL-GTR-247*. U.S. Department of Agriculture, Forest Service, Forest Products Laboratory.
144. Su, J., Leroux, P., Lafrance, P.-S., Berzins, R., Gibbs, E., Weinfurter, M. (2018). Fire testing of rooms with exposed wood surfaces in encapsulated mass timber construction. NRC CNRC Report A1–012710.1
145. Brandon, D. (2018) Fire Safety Challenges of Tall Wood Buildings—Phase 2: Task 4 -Engineering methods. National Fire Protection Association. NFPA report: FPRF-2018-4.
146. APA – The Engineered Wood Association. (2018). ANSI/APA PRG 320-2018 Standard for performance-rated cross-laminated timber. APA – The Engineered Wood Association, Tacoma, WA.
147. Frangi, A., Fontana, M., & Mischler, A. (2004). Shear behavior of bond lines in glued laminated timber beams at high temperatures. *Wood Science and Technology*, 38(2), 119–126. <https://doi.org/10.1007/s00226-004-0223-y>
148. Clauß, S., Gabriel, J., Karbach, A., Matner, M., & Niemi, P. (2011). Influence of the adhesive formulation on the mechanical properties and bonding performance of polyurethane prepolymers. *Holzforschung*, 65, 835–844.
149. Emberley, R., Nicolaidis, A., Fernando, D., & Torero, J. L. (2016). Changing failure modes of cross-laminated timber. *Structures in Fire*, 643–649.
150. Nicolaidis, A., Emberley, R., Fernando, D., Torero, J. L. (2016). Thermally driven failure mode changes in bonded timber joints. In: Proceedings of the World Conference on Timber Engineering, Vienna, Austria
151. Butler, C. P. (1971). *Notes on charring rates in wood. Fire research note 896*. FRS.
152. Schaffer, E. L. (1967). *Charring rate of selected woods- transverse to the grain. US forest service research paper FPL69*. Forest products laboratory.
153. Standards Association of Australia. (1990). *Timber structures, part 4: Fire resistance of structural timber members. ASI720.4-1990*. SAA.
154. White, R. H. (1988). *Charring rates of different wood species. PhD thesis edn*. University of Wisconsin.
155. International Organization for Standardization. (1999). *Fire-resistance tests - elements of building construction—Part 1: General requirements. ISO 834-1:1999*. ISO.
156. Hadvig, S. (1981). *Charring of wood in building fires. Research. Report edn*. Technical University of Denmark.

157. Hansen, F. T., & Olesen, F. B. (1992). *Full-scale tests on loaded glulam beams exposed to natural fires. Researchreport edn.* Aalborg University.
158. Hopkin, D., Spearpoint, M., Gorksa, C., Krenn, H., Sleik, T., & Milner, M. (2020). Compliance road-map for the structural fire safety design of mass timber buildings in England. SFPE Europe Q4.
159. Brandon, D., & Dagenais, C. (2018). *Fire safety challenges of tall wood buildings – Phase 2: Task 5 – Experimental study of delamination of cross laminated timber (CLT) in fire.* Fire Protection Research Foundation, Quincy, MA.
160. Barber, D., Crielaard, R., Li, X. (2016). Towards fire safe design of exposed timber in tall timber buildings. In Proc. World Conference of Timber Engineering, August 22–25, 2016, Vienna, Austria
161. Crielaard, R. (2015). Self-extinguishment of cross-laminated timber. Master’s Thesis report, Faculty of Civil Engineering and Geosciences, Delft University of Technology
162. Friquin, K. L. (2010). “Charring rates of heavy timber structures for fire safety design—A study of the charring rates under various fire exposures and the influencing factors.” PhD Thesis. Trondheim: Norwegian University of Science and Technology.
163. Brandon, D. (2016). Practical method to determine the contribution of structural timber to the heat release rate and fire temperature of post-flashover compartment fires. Technical Research Institute of Sweden SP, SP Rapport 2016:68, Borås, Sweden.
164. Franssen, J., & Gernay, T. (2017). Modeling structures in fire with SAFIR®: Theoretical background and capabilities. *Journal of Structural Fire Engineering*, 8(3), 300–323. <https://doi.org/10.1108/JSFE-07-2016-0010>
165. Hopkin, D., Anastasov, S., & Brandon, D. (2017). Reviewing the veracity of a zone-model-based-approach for the assessment of enclosures formed of exposed CLT, in M Gillie, Y Wang Applications of Fire Engineering-proceedings of the International Conference of Applications of Structural Fire Engineering, Manchester, UK, pp. 151–160.
166. Zhang, C., & Li, G., (2013). Modified one zone model for fire resistance design of steel structures. *Advanced Steel Construction* 9, 282–297. <https://doi.org/10.18057/IJASC.2013.9.4.2>
167. Maluk, C. (2014). Development and application of a novel test method for studying the fire behaviour of cfrp prestressed concrete structural elements. Thesis, University of Edinburgh Press, UK.
168. Wade, C., Spearpoint, M., Fleischmann, C., Baker, G. and Abu, A. 2018. “Predicting the fire dynamics of exposed timber surfaces in compartments using a two-zone model.” *Fire Technology* 54, no. 4. p893–920. doi:<https://doi.org/10.1007/s10694-018-0714-2>.
169. Wade, C (2019). A theoretical model of fully developed fire in mass timber enclosures. PhD Thesis, University of Canterbury, Department of Civil and Natural Resources Engineering
170. Frangi, A., & König, J. (2011). Effect of increased charring on the narrow side of rectangular timber cross-sections exposed to fire on three or four sides. *Fire and Materials*, 35(8), 593–605.
171. Harmathy, T. Z. (1965). Ten rules of fire endurance rating. *Fire Technology*, 1(2), 93–102.
172. Östman, B., Mikkola, E., Stein, R., Frangi, A., König, J., Dhima, D., Hakkarainen, T., & Bregulla, J. (2010). *Fire safety in timber buildings- technical guideline for Europe. SPReport 2010:19.* SP Trätek.
173. American Wood Council. (2018). National design specification (NDS) for wood construction with commentary.
174. AWC (2018). Calculating the fire resistance of wood members and assemblies. Technical Report No.10. American Wood Council, Leesburg, VA, USA
175. Standards New Zealand. (1993). *Code of practice for timber design. NZS 3603:1993.* SNZ.
176. Schmid, J., König, J., & Kohler, J. (2010). Design model for fire exposed cross-laminated timber. In V. R. Kodur & J. M. Franssen (Eds.), *Proceedings of the sixth international conference on structures in fire, 2nd-4th June 2010* (pp. 511–519). DEStech.

177. British Standards Institution. (2002). *Eurocode 1: Actions on structures – Part 1–2: General actions – Actions on structures exposed to fire. BS EN 1991-1-2*. BSI.
178. Magnusson, S. E., & Thelandersson, S. (1970). *Temperature—Time curves of complete process of fire development. Bulletin of division of structural mechanics and concrete construction* (Vol. 16). Lund University of Technology.
179. Buchanan, A. H. (1990). Bending strength of lumber. *Journal of Structural Engineering*, 116(5), 1213–1229.
180. European Committee for Standardization. (2004). *Eurocode 5: Design of timber structures—Part 1-1: General – Common rules and rules for buildings. EN 1995-1-1*. CEN.
181. Tiso, M., Just, A., Schmid, J., & Klippel, M. (2018). Effective cross-sectional method for timber frame assemblies—definition of coefficients and zero-strength layers. *Fire and Materials*, 42(8), 897–913.

# Chapter 9

## Uncertainty in Structural Fire Design



Ruben Van Coile, Negar Elhami Khorasani, David Lange,  
and Danny Hopkin

### 9.1 Introduction

#### 9.1.1 Structural Design and Uncertainty

Probabilistic methods form the basis of verification of structural design under ambient conditions in most structural engineering standards around the world. Safety factors are specified based on statistical variations in load and resistance of a structure, applying reliability goals as a benchmark for verification that a structure provides an acceptable level of safety. Despite this fundamental principle, current structural fire engineering approaches are intrinsically deterministic and incorporate neither of the above two concepts of safety factors or reliability goals.

Instead, structural fire engineering analysis typically relies on the evaluation of the response of a structure to a single or very few deterministic scenarios which although often conservative do not normally account for uncertainties in the input,

---

R. Van Coile  
Department of Structural Engineering and Building Materials, Ghent University, Ghent,  
Belgium  
e-mail: [Ruben.VanCoile@UGent.be](mailto:Ruben.VanCoile@UGent.be)

N. Elhami Khorasani  
Department of Civil, Structural and Environmental Engineering, University at Buffalo, Buffalo,  
NY, USA  
e-mail: [negarkho@buffalo.edu](mailto:negarkho@buffalo.edu)

D. Lange  
University of Queensland, St Lucia, QLD, Australia  
e-mail: [d.lange@uq.edu.au](mailto:d.lange@uq.edu.au)

D. Hopkin (✉)  
OFR Consultants, Manchester, UK  
e-mail: [Danny.Hopkin@ofrconsultants.com](mailto:Danny.Hopkin@ofrconsultants.com)

the modelling approach, or the output. This approach does not address in any meaningful way the amount of conservativeness inherent in a design, or provide any meaningful information about the actual level of safety. The evaluation is carried out in one of a number of ways, with verification done in either the time, the temperature, or the strength domain with the intent being simply to demonstrate that for a given scenario the fire resistance of an element or a structure is greater than or equal to the fire intensity. When verification is done in the temperature or the strength domain, this is almost always done based on the analysis of the response of the structure to one or a few design fires which represent a range of possible fires that could occur inside of that building. However, while these fires may be identified and elaborated using some risk-based technique, the analyses remain purely deterministic and the actual level of safety, margin of safety, probability of failure, or reliability is almost never calculated.

This deterministic demand/capacity evaluation in the strength or temperature domain is often termed performance-based design since the performance criteria may be set based on the unique features of the building in question and taking into account input from the various stakeholders in the project. The basic elements of performance-based design are defined in such a way as to allow the user freedom to compose any solution to a given engineering problem, allowing also the freedom to employ new techniques and technologies as they become available. The objectives must be clearly stated at the outset of the project, and any design solution which fulfils these objectives while still adhering to the performance targets of the design framework should be permitted. The effect of this on the spectrum of possible solutions available for any problem and the impact of this on verification requirements are shown in Fig. 9.1. As the design process tends towards a performance-based approach, the spectrum of possible solutions opens up, allowing more bespoke solutions to a problem.

Performance-based design is a necessity where buildings fall outside of either the classification afforded by prescriptive building codes around the world or where the materials or methods of construction are such that they introduce new risks or challenge the fire strategy of buildings in ways which were unforeseen in the development of the current regulations. In such cases, the building design falls outside of the bounds by which the fire engineering community can confidently rely on the collective experience of the profession (see Sect. 9.2). It is therefore not

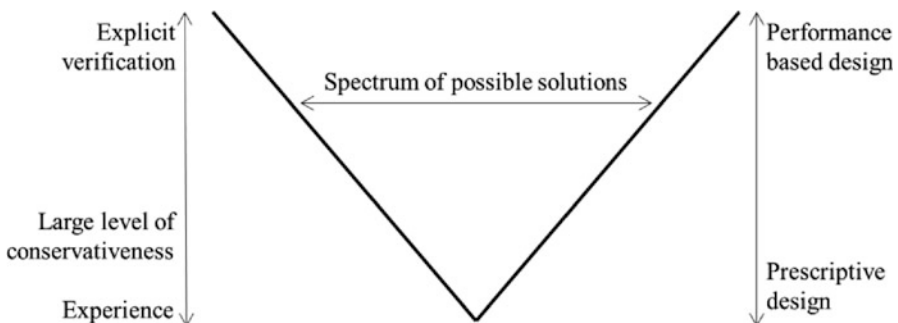


Fig. 9.1 Expanding spectrum of solutions and verification in performance-based design



possible to ensure safety through the application of prescriptive codes based on the nearest existent classification. Therefore, two lines of action are open to the engineer: either the building design should be modified such that it falls within the scope of the classifications available or engineering analysis has to be undertaken to demonstrate that the level of safety provided by the building is consistent with the performance that may be expected by the society.

This may result in the situation whereby although the targets in terms of life, property, and business protection may remain similar to those in prescriptive design codes, these targets should typically remain independent of the prescriptive building code performance goals. Most legislative objectives are related to preventing loss of life—either of the building occupants or of the first responders working inside of a burning building [1]—and damage to neighbouring property. However, performance-based design also opens the possibility for alternative objectives to be considered such as limiting direct or indirect financial losses to a building's owner, limiting environmental impact, or preservation of historic structures [2].

Also, when applying performance-based design, the collective experience of the profession in applying these techniques to the specific type of structure may be insufficient to guarantee a sufficient level of safety. In those situations, an explicit verification or quantification of the resulting safety level needs to be undertaken. This is discussed in some detail elsewhere [3]. In summary, and as discussed further in Sect. 9.2, this explicit verification of the safety level aims to ensure that the uncertainties associated with the demand/capacity evaluation do not result in a too high (unknown) likelihood of the structure not fulfilling the design objectives.

### 9.1.2 Importance of Considering Uncertainty

The basis of demand/capacity-based design in structural engineering is that the resistance of a structure is greater than the load applied on the structure. Consider, to illustrate the concept, an axially loaded element under ambient conditions (Fig. 9.2). The linear elastic response of the system may be defined according to several very simple relationships (see Table 9.1 for definitions):

$$\sigma = \frac{P}{A} \quad (9.1)$$

$$\varepsilon = \frac{\sigma}{E} = \frac{P}{AE} \quad (9.2)$$

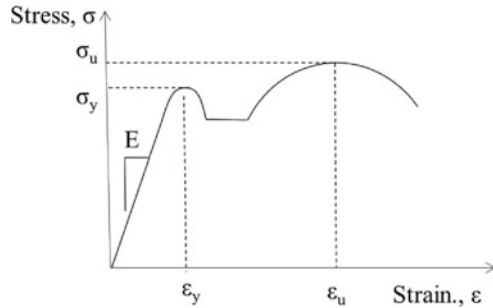
**Fig. 9.2** Simple system under axial load



**Table 9.1** Sources and summary of uncertainties in the simple model described

Input	P
System properties	$E, A, L, \sigma_y, \epsilon_y, \sigma_u, \epsilon_u$
Model	Linearity, dimensionality, material model adopted, boundary conditions

**Fig. 9.3** Example relationship between stress and strain at ambient



$$\Delta L = \epsilon L = \frac{PL}{AE} \tag{9.3}$$

Here,  $\sigma$  is the stress;  $P$  is an applied axial load;  $A$  is the cross-sectional area of the element;  $\epsilon$  is the strain;  $E$  is the modulus of elasticity of the material; and  $L$  is the length of the element being analysed. Each of these relationships is related to the material properties, an external condition or input to the system, or a feature of the system.

Assuming some relationship between stress and strain which defines the modulus of elasticity, as well as the yield and ultimate stresses and strains as per Fig. 9.3, the failure of this system can be defined according to various different criteria, in function of the performance objective: for example, an evaluation based on a deformation criterion, i.e.  $\Delta L > \Delta L^*$ , with  $\Delta L^*$  being a limiting deformation, or according to criteria based on the material response, e.g.  $\sigma > \sigma_y$ ;  $\sigma > \sigma_u$ ;  $\epsilon > \epsilon_y$ ; or  $\epsilon > \epsilon_u$ .

Even for this simple system, the evaluation of such criteria incorporates, to some degree or another, uncertainties. In the case of the input to the system, there are uncertainties regarding the load which is applied. In the case of the system properties, there are uncertainties with regard to the material response as well as the geometry of the system. When considering the model chosen to analyse this system, there arise model uncertainties associated with the formulation of the material in the model or any discretization or simplifications to the model made by the user. Referring to the uncertainties inherent in the system, these may largely be attributed to aleatoric uncertainties, or aleatory variability, arising from the natural randomness in a process or in the input variables. This randomness can usually be measured and quantified. For discrete variables the randomness can generally be parametrized by different probability mass functions. Uncertainties related to the modelling of the system are referred to as epistemic uncertainties. Different models inherently contain

a different degree of epistemic uncertainty. With regard to these epistemic uncertainties, the impact of this on structural design under ambient conditions is well illustrated in the work by Fröderberg and Thelandersson [4]; the impact on structural fire engineering is illustrated in the work by Lange and Boström [5].

At this point, it should be clear that the simple problem presented above contains a multitude of uncertainties: aleatory uncertainty arising from the input to the model in the form of the applied force or the different properties of the system and epistemic uncertainty arising from the modelling approach adopted and any simplifications or assumptions made. As a result of the combined effect of these uncertainties, we cannot always be sure that the condition of capacity being greater than demand, under any of the failure criteria identified above, is satisfied for a given design. The implication is that some degree of risk is being adopted in the acceptance of any model of this problem.

If temperature is introduced to this problem, the nature of the uncertainties remains largely the same; however the complexity of the problem multiplies. The stress-strain relationship of the material becomes a function of temperature, and thermal expansion means that both the cross-sectional area and the length of the element change. Each of the very simple relationships presented above now becomes also a function of temperature:

$$\sigma(T) = \frac{P}{A(T)} \quad (9.4)$$

$$\epsilon(T) = \frac{P}{A(T)E(T)} \quad (9.5)$$

$$\Delta L(T) = \frac{P}{A(T)E(T)} + \alpha \Delta T L \quad (9.6)$$

where  $\alpha$  denotes the coefficient of thermal expansion, and  $\Delta T$  denotes a change in temperature.

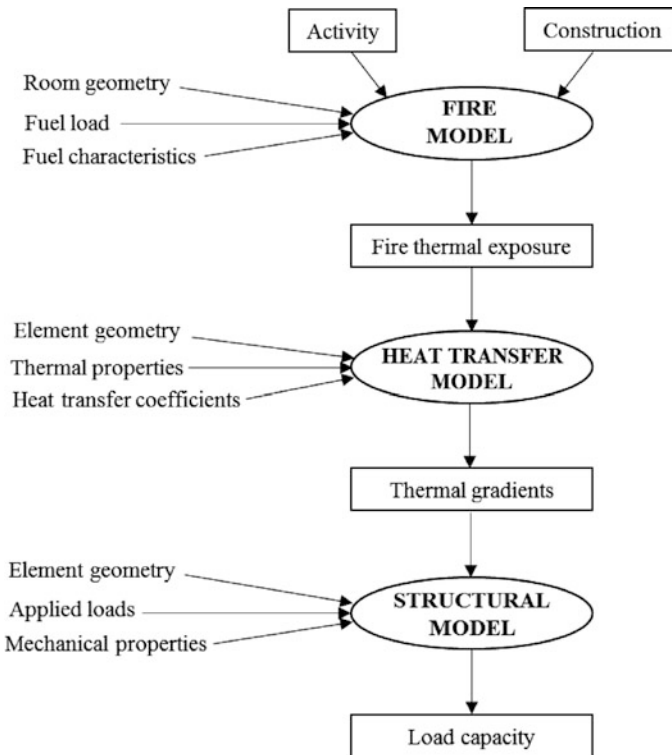
Having introduced temperature to the problem, it becomes also necessary to calculate temperature. As discussed in Chap. 5, the heat transfer inside the solid is governed by Fourier's law, while convective and radiative heat transfers are to be taken into account at the surface. Each of these processes of heat transfer, conduction, convection, and radiation, now introduces additional variable uncertainties into our system, including conductivity, convective heat transfer coefficient, and emissivity required for calculation of heat transfer by radiation. The complexity of and thus the overall uncertainty associated with this simple problem have now increased dramatically, simply by the introduction of temperature. The certainty that the capacity is always greater than the demand, for any of the criteria listed, is now diminished.

As indicated in Sect. 9.1.1, the traditional means of addressing this uncertainty in structural fire engineering has always been to overestimate the load and to underestimate the capacity, thus accounting for uncertainties by increasing the nominal margin of safety. However, this indirect approach fails to acknowledge that engineering failures occur where the distributions of demand and capacity overlap,

i.e. where demand > capacity within the tails of the distributions of the demand and capacity (see Fig. 9.6). Therefore, increasing the margin of safety by increasing the distance between the average demand and the average capacity in an arbitrary way cannot ensure that failure has a probability which is acceptably low to society. Thus, when an explicit verification of the safety level is required, the uncertainties associated with the design need to be explicitly considered.

### 9.1.3 Sources of Uncertainty

In structural fire engineering, uncertainties arise from many sources. Referring to the process of structural fire engineering described by Buchanan and Abu [6], Fig. 9.4, sources of aleatoric uncertainty can be seen to be introduced at every stage, and epistemic uncertainty arises depending on the models used at each stage. The nature of the sources of uncertainties means that uncertainties propagate through any analysis. The uncertain input variables are propagated through uncertain models which results in uncertain outputs from models.



**Fig. 9.4** Flow chart for calculating the strength of a structure exposed to fire, adopted from Buchanan and Abu [6]

When developing the fire model, uncertainties in the geometry of the fire compartment, fuel load, and fire characteristics arise. Arguably uncertainties associated with room geometry are significantly smaller than uncertainties associated with the fuel or the characteristics of the fire and can therefore be ignored. However, the fuel load and the fire characteristics are arguably very significant uncertainties in the entire process and generally cannot be ignored. In the Eurocode, uncertainties associated with the fuel load are treated by adopting some high-percentile fuel load from a distribution which varies with occupancy—increasing the demand for the design, as described above. Other uncertainties related to the fire characteristics however are not treated in any way satisfactorily; for example, the opening factor upon which the burning behaviour is largely dependent is usually treated entirely deterministically. Further uncertainty arises from the choice of fire model; as will be discussed later, different representations of fire (standard fire, parametric fire, travelling fire, zone models, field models) account for different factors related to the overall fire behaviour. The uncertainty associated with the use of these different models will be discussed later in this chapter.

Any uncertainties in the input variables to the fire model as well as uncertainties inherent in the fire model itself are propagated into an uncertainty for the thermal exposure which is an input to the heat transfer model, along with details of the geometry, the thermal properties, and the heat transfer coefficients. Element geometry is arguably similar to the room geometry in that the effects of uncertainties are likely to be relatively inconsequential compared with the uncertainties of thermal exposure, heat transfer coefficients, and material thermal properties. In this chapter, there is a discussion of the variability in thermal properties as well as heat transfer coefficients as input to the heat transfer model. Heat transfer is discussed in Chap. 5. It should be noted that any uncertainties in inputs or resulting from the modelling approach with respect to the fire model propagate through the analysis.

Uncertainties in the inputs to the heat transfer model are propagated, as well as any uncertainties in the model itself, to the structural model where the geometry, the applied loads, and the mechanical properties of the material all are subject to uncertainty. The overall effect of this propagation of uncertainty is a multiplicity of possible outcomes at every stage in the analysis process including in the final determination of the load capacity.

The above gives an overview of the many uncertainties associated with each of the steps in structural fire engineering analysis. These uncertainties can generally be parametrized by different probability distributions. The ability to do this depends to a large extent on the quality of information which is available about the specific variables. This is often cited as one of the most significant obstacles to the use of probabilistic methods in structural fire engineering that the rate of occurrence of events is typically so low that the informativeness of any resulting distributions is low. However, as will be shown in this chapter, many of the variables can be satisfactorily parametrized for a number of different applications. Where variables cannot be parametrized, or where epistemic uncertainties exist, then the sensitivity of solutions can be probed and engineering judgement can be exercised to ensure that design objectives are met.

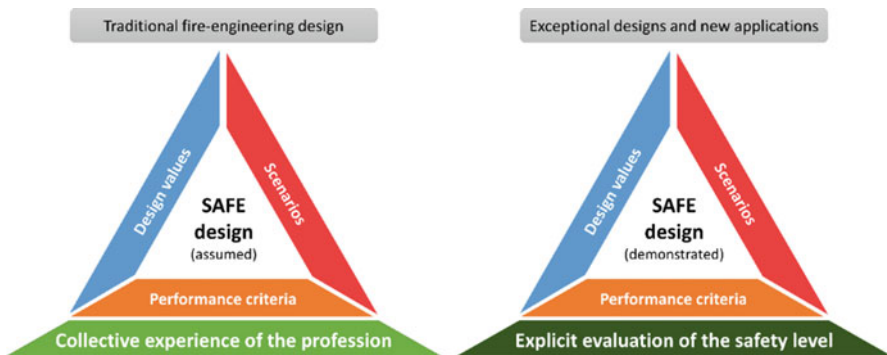
## 9.2 Reliability and Risk Acceptance

### 9.2.1 Risk Acceptance in Structural Fire Design

As indicated in Sect. 9.1, traditional performance-based (structural) fire safety design is deterministic in nature, requiring the selection of design inputs, scenarios, and performance criteria that are deemed appropriately conservative by the engineer. In such a process, the safety level (or residual risk) associated with a given design is not evaluated, and the full spectrum of consequences and their associated probabilities are not interrogated. Instead, it is assumed that an adequate, but unquantified, level of safety is attained based upon engineering judgement and considerations: (a) that real fire events have occurred, with performance observed, and (b) that society has not expressed dissatisfaction with the levels of performance witnessed. In other words, the basis for acceptance of traditional performance-based design (or the safety foundation) is the experience of the fire safety profession (see left-hand side of Fig. 9.5) proposed in Hopkin et al. [7]. This safety foundation can only be justified where there are sufficient real fire events to observe, guide design processes, and offer society opportunities to express views on their dissatisfaction (or otherwise) of the consequences witnessed.

Traditional (structural) fire safety design and its associated safety foundation cannot, however, be extrapolated to exceptional structures, i.e. those with atypical consequences of failure or adopting innovative materials, as it is likely that insufficient instances exist where fires have occurred and performance is witnessed. For such complex cases, there is a need to explicitly evaluate the residual risk (see right-hand side of Fig. 9.5).

Within the framework presented by Van Coile et al. [3], there is an expectation that probabilistic risk assessment (PRA) methods be employed to demonstrate adequate safety for cases where the collective experience of the profession cannot be called upon to guide design approaches. In doing so, any design must be



**Fig. 9.5** (Left) assumed basis of safe design, (right) demonstrated basis of safe design where experience is not an adequate basis, Hopkin et al. [7]

demonstrated to be tolerable to the society, and the residual risk as low as is reasonably practicable (ALARP). In structural safety, the full cost-benefit analysis implied by the ALARP evaluation is typically substituted by a reliability analysis, allowing to determine design acceptance based on structural failure probabilities only [3].

### 9.2.2 What Is Reliability?

ISO 2394:2015 [8] defines reliability as the ‘ability of a structure or structural member to fulfill the specified requirements, during the working life, for which it has been designed’. Reliability is expressed in terms of probability and can cover safety, serviceability, and durability of a structure. In the Eurocodes, no in-depth definition of reliability is given. However, in the fundamental requirements it is currently stated: ‘a structure shall be designed and executed in such a way that it will, during its intended life with appropriate degrees of reliability and in an economic way:

- Remain fit for the use for which it is required; and.
- Sustain all actions and influences likely to occur during execution and use’.

In the latter bullet point, a fire condition falls within the definition of ‘all actions’. To satisfy the above considerations in relation to reliability, Holicky [9] notes that there should be four important elements requiring consideration:

- The definition of a failure, i.e. the *limit state*.
- The time (reference) period under consideration.
- The reliability level, i.e. an assessment of the failure probability.
- The conditions of use (and the associated impact on the input uncertainties).

Importantly, the concept of absolute reliability does not generally exist (apart from in exceptional cases), i.e. few structures have a zero-failure probability and there must be an acceptance that there is a certain, small probability that a failure may occur within the intended lifespan of a structure [9]. This principle extends to structural design for fire safety, where structural elements or systems must have an acceptable failure probability that varies in function of the failure consequences. In the absence of such an acceptable failure probability, the drive towards absolute reliability would (sooner or later) result in grossly disproportionate costs to society, as more and more resources need to be spent to further reduce the failure probability.

In the context of structural design for fire, many fire safety objectives may exist (see Sect. 9.1.1), which are translated into functional requirements and performance criteria; see ISO 24679-1:2019 [10]. For each of the performance criteria, a reliability target can be specified, for example, a business continuity-driven performance requirement of a high certainty (reliability) of limited permanent deflection post-fire.

In most common structural fire design situations, maintaining structural stability during fire is the primary functional requirement (relating, e.g., to a primary objective of life safety, possibly in conjunction with property protection). For this functional requirement, reliability in consideration of fire can be defined as *the probability that the structure or structural member will maintain its load-bearing function in the event of fire*, i.e. reliability is the complement of the failure probability. This definition of reliability in structural (fire) engineering will be applied herein.

Applying the above, the performance criterion can for example be specified as (i) a maximum deflection  $v_{\max}$  being smaller than a limiting value  $v_{\lim}$  or (ii) the load-bearing capacity of the structure  $R$  being larger than the load on the structure  $E$  (including self-weight). In the first illustrative case failure is defined by the exceedance of a (possibly deterministic) limiting deflection, while in the second case failure is defined as the exceedance of the resistance effect by the load effect. For the latter example, the failure probability definition is thus specified by Eq. (9.7). Thus, the limit defining the boundary between the failure domain and boundary of the safe domain is given by  $Z = R - E = 0$ . This is commonly referred to as the *limit state* corresponding with the performance criterion.

A limit state is a condition of a structure or component beyond which the structure no longer fulfils certain criteria for design. Examples of limit states in structural engineering include ultimate limit states beyond which it is expected that a structure will no longer carry the applied load and serviceability limit states beyond which it is expected that the level of comfort or confidence of the users of the building as a result of, e.g., deflections or vibrations, is no longer adequate. Ultimate limit states are of relevance for accidental actions such as fire whereas serviceability limit states have little arguable application for accidental actions.

In structural fire design situations, performance (and thus failure) is commonly evaluated given the occurrence of a fire. Consequently, the load reference period is recommended to be taken as the instantaneous load situation, i.e. an arbitrary-point-in-time load. Taking into account the specifics of the structure (i.e. the *conditions of use* referenced by Holicky [9]), the load and resistance effects are thus defined. A conceptual visualization of these is given in Fig. 9.6, showing the variation of the resistance effect  $R$  and the load effect  $E$ , as well as the ‘safety margin’ defined here by the difference in expected values  $\mu_R$  and  $\mu_E$ . As illustrated in Fig. 9.6, despite the nominal safety margin, situations of  $E$  exceeding  $R$  occur in the tails of the distribution. The acceptability of this observed failure probability now depends on the (availability of) maximum allowable failure probabilities, or in other words: target reliability levels.

$$P_f = P[R - E < 0] \quad (9.7)$$



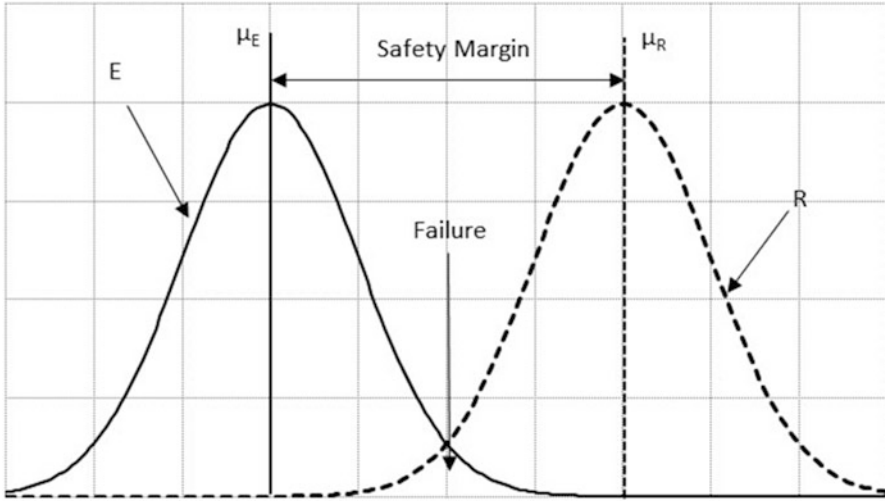


Fig. 9.6 Concept visualization of load and resistance effects, including situations with failure ( $R < E$ ) given a nominal ‘safety margin’

### 9.2.3 Target Reliability Indices for Structural Design

Defining maximum allowable (target) failure probabilities is central to the application of reliability methods. Relative to the full ALARP evaluation highlighted in Sect. 9.2.1, specified target failure probabilities allow to omit cost evaluations from the design, thus restricting the design problem to engineering considerations (and not, e.g., discount rate assessments).

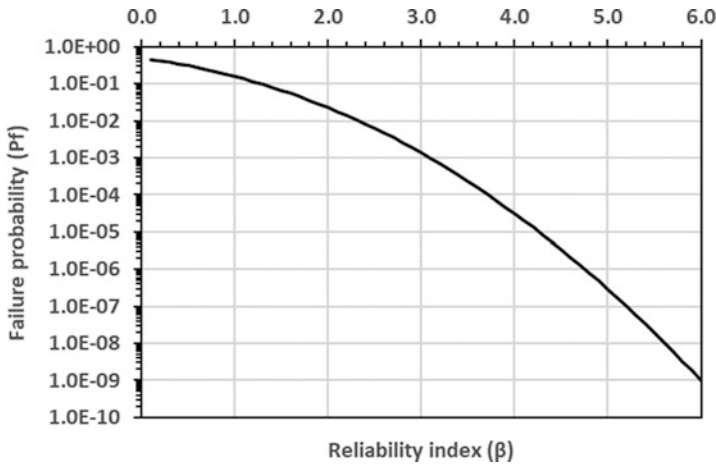
Commonly, a (target) failure probability is expressed in an alternative form as a reliability index ( $\beta$ ), with

$$\beta = -\Phi^{-1}(P_f) = \Phi^{-1}(1 - P_f) \tag{9.8}$$

$\Phi^{-1}$  is the inverse standard normal cumulative distribution function, as applied amongst others in EN 1990. For completeness, the relationship between ( $P_f$ ) and ( $\beta$ ) is as shown in Fig. 9.7. In the following subsections, target reliability indices for structural design are summararily presented both for ambient conditions and for fire.

#### 9.2.3.1 Reliability Indices at Ambient Temperature

As noted in Sect. 9.1.1, reliability-based design has found wide application in structural engineering. For example, as the basis of the partial safety factors applied in the Structural Eurocodes, the target reliability index,  $\beta$ , governs everyday



**Fig. 9.7** Relationship between reliability index and failure probability

**Table 9.2** Target  $\beta$ -values for elements (lifetime), ISO 2394:1998

Relative costs of safety measures	Consequences of failure			
	Small	Some	Moderate	Great
High	0	1.5	2.3	3.1
Moderate	1.3	2.3	3.1	3.8
Low	2.3	3.1	3.8	4.3

structural engineering practice. Different (recent) target values are, however, available from several sources [11].

Target failure probabilities ( $P_{f,t}$ ) for ambient design have received much attention in the literature, e.g. see Rackwitz [12] and Fischer et al. [13]. Target values have even been included in international standards, which can be linked to the Eurocode target reliability indices. ISO 2394:1998 [14] lists ‘example’ lifetime target reliabilities as a function of the failure consequence and the relative costs of safety measures (Table 9.2). Based on the formulation in ISO 2394:1998, these values have been informed by cost optimization and calibrated against existing practice. The standard further recommends the values 3.1, 3.8, and 4.3 to be used in ultimate limit state design based on both consequence of failure and cost of safety measures. Considering the general content of the standard, these values are considered applicable at an element level.

Target reliability indices specified in EN 1990 [15] as a function of the ‘reliability class’ are given in Table 9.3. The reliability classes can be associated with the consequence classes (i.e. high, medium, low). As also noted in ISO 2394:1998, considerations such as brittle or ductile failure may influence the chosen target.

**Table 9.3** Target reliability index for structural elements in accordance with EN 1990:2002

Reliability class	Consequences	Target reliability index $\beta_{t,ref}$		Examples of buildings
		$t_{ref} = 1 \text{ year}$	$t_{ref} = 50 \text{ years}$	
3: High	High	5.2	4.3	Bridges, public buildings
2: Normal	Medium	4.7	3.8	Residential, office
1: Low	Low	4.2	3.3	Agricultural

**Table 9.4** Target  $\beta$ -values for structural systems (1 year), JCSS, and adopted in ISO 2394:2015

Relative costs of safety measures	Consequences of failure		
	Minor ( $\xi < 2$ )	Moderate ( $2 < \xi < 5$ )	Large ( $5 < \xi < 10$ )
High	3.1	3.3	3.7
Moderate	3.7	4.2	4.4
Low	4.2	4.4	4.7

The Eurocode target reliability indices are specified both for a 1-year reference period and a 50-year reference period (where 50 years equals the indicative design working life for common structures). Both sets, however, correspond with the same target reliability level, considering independence of yearly failure probabilities; that is, irrespective of how long a structure has been standing, it is assumed that the per annum failure likelihood is constant. There is thus close agreement between  $\beta_{t,50}$  in Table 9.3 and lifetime targets in ISO 2394:1998.

The material-specific Eurocodes apply the 50-year reliability index of 3.8 on an element basis for the definition of partial safety factors. In case of additional redundancy in the system (e.g. due to robustness considerations), this will result in a higher system reliability index.

Target values for a 1-year reference period are given in the Probabilistic Model Code developed by the Joint Committee on Structural Safety [16]; see Table 9.4. These recommended values were derived from a calibration process with respect to the existing practice and are considered compatible with cost-benefit analyses, with explicit reference to the analysis by Rackwitz [12], and can be considered to relate to an updated recommendation relative to ISO2394:1998.

Table 9.4 is applicable to structural systems. In case of a single-element failure mode dominating system failure, these targets are directly applicable to the structural element. The target values are given as a function of the ratio  $\xi$  of the failure plus reconstruction cost to the construction cost and an obsolescence rate on the order of 3% is considered. For very large consequences ( $\xi > 10$ ) an explicit cost-benefit analysis is recommended. The target reliabilities in Table 9.4 have been incorporated into ISO 2394:2015.

It is noteworthy that the reliability targets presented previously are in some manner linked to cost optimization, where the direct and indirect consequences resulting from ‘loss of the structure’ are taken into account. Mindful of the need for potential fatalities being tolerable, as is discussed by Van Coile et al. [3], this may

be considered beyond the ambit of a direct life safety evaluation, which is generally concerned only with averting fatalities. Fischer et al. [17] proposed an alternative perspective, where (societal) life safety cost optimization is concerned solely with the preservation of life through incorporation of the life quality index (LQI); that is, safety investments are balanced directly against the reduction in risk to life. The obtained acceptable failure probability is then considered an absolute lower bound safety requirement for further reliability assessments and more general cost optimization considerations. This acceptable failure probability is given in Eq. (9.9) for coefficients of variation in the resistance and action effects of 0.1–0.3:

$$P_{f,acc} = \frac{1}{5} \frac{C_1(\gamma_s + \omega)}{N_f SCCR} \quad (9.9)$$

where  $C_1$  is the marginal safety cost,  $\gamma_s$  the discount rate,  $\omega$  the obsolescence rate,  $N_f$  the number of fatalities in case of failure, and SCCR the societal capacity to commit resource metric.

By way of an example, taking a consequence class 3 structure from ISO 2394:2015, the expected number of fatalities in the event of structural failure is less than 50 persons. If the building were in the UK, the SCCR for a 3% discount rate is \$3,665,000 ppp (purchasing power parity) according to ISO 2394:2015. For a construction cost ( $C_0$ ) of \$40,000,000 ppp and a normal marginal safety cost ( $C_1/C_0$ ) of 1%, the marginal safety cost is \$400,000 ppp. Adopting an obsolescence rate of 2% and societal discount rate of 3%, the acceptable failure probability is  $2 \times 10^{-5}$  for a 1-year reference period. This would coincide with  $\beta = 4.1$ , i.e. a significantly less onerous reliability target when compared to the figures in EN 1990. This value should however be considered as an absolute lower bound, as it is (implicitly) assumed that there are no further benefits to society from the safety investment apart from averting fatalities [18]. For example, the benefit of reducing the risk of city conflagration or network resilience is not taken into account.

### 9.2.3.2 Reliability Targets and Fire

The application of the ambient reliability targets to structural fire design has received considerable research attention. In the Natural Fire Safety Concept (NFSC) [19], the Eurocode target reliability index of 3.8 (50-year reference), i.e. 4.7 for 1-year reference, was adopted as a starting point. By further assuming that the yearly probability of a fire-induced structural failure should be as unlikely as the yearly probability of a ‘normal-design’ structural failure, and considering fire-induced structural failures to be conditional on the occurrence of a ‘significant’ fire, the NFSC derives a target reliability index,  $\beta_{t,fi}$ , for structural fire design through Eq. (9.10), with  $\lambda_{fi}$  being the annual occurrence rate of a structurally significant fire:

$$\begin{aligned}\Phi(-\beta_{t,fi}) &= P_{f,t,fi} = \frac{P_{f,t,EN1990}}{\lambda_{fi}} = \frac{\Phi(-\beta_{t,EN1990})}{\lambda_{fi}} \Rightarrow \lambda_{fi} P_{f,t,fi} \\ &= P_{f,t,EN1990}\end{aligned}\quad (9.10)$$

Nevertheless, the NFSC goes on to consider that an acceptable target failure probability should be differentiated from that at ambient temperature in function of the building evacuation mode, in consideration that at the time of fire occurrence, in many buildings, occupants are actively encouraged to evacuate (reducing the potential number of fatalities), i.e.:

- Normal evacuation:  $1.3 \times 10^{-4} [y^{-1}]$ .
- Difficult evacuation:  $1.3 \times 10^{-5} [y^{-1}]$ .
- No evacuation:  $1.3 \times 10^{-6} [y^{-1}]$ .

This concept is explored by Hopkin et al. [20] where the time-dependent failure probability of a steel structure is coupled with a stochastic evacuation timeline for a series of reference office buildings in determining so-named risk indicators.

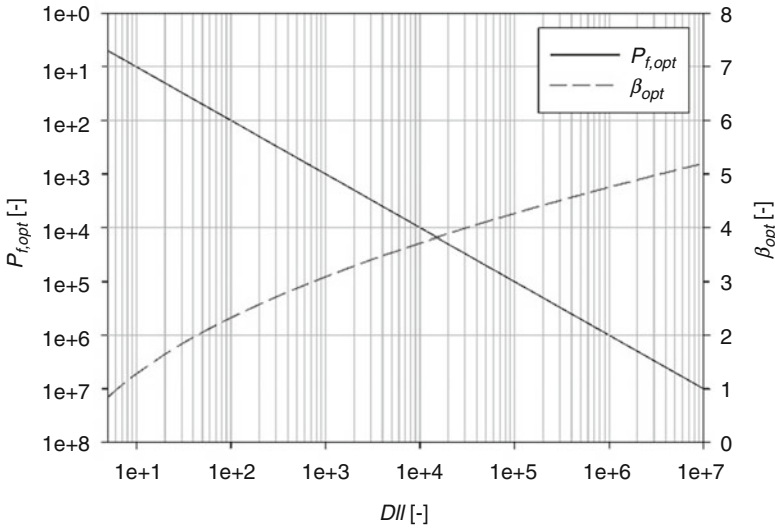
One difficulty noted with the NFSC approach is discussed by Van Coile et al. [11] and Van Coile et al. [21]. There, it is highlighted that the Eurocode target reliability levels for ambient design which form the basis of the NFSC can be considered compatible with cost optimization considerations, as discussed above. The basic assumptions underlying the cost optimizations for ambient design conditions are however not necessarily applicable to structural fire design. Within Van Coile et al. [21] target failure probabilities are expressed in an alternative general form, in function of a damage to investment indicator (DII), expressed as

$$DII = \frac{\xi\lambda}{b(\gamma + \omega)} \quad (9.11)$$

where  $b$  is the relative marginal safety investment cost, i.e. normalized to the construction cost ( $C_0$ ), as defined by Eq. (9.12);  $\lambda$  is the failure-instigating event occurrence rate; and  $\xi$  is the relative failure costs, i.e. also normalized to the construction cost. In the case of fire,  $\lambda$  would be the structurally significant fire occurrence rate. For normal design conditions,  $\lambda$  is expressed as one per annum, and the corresponding reliability target is for a 1-year reference period. This formulation is compatible with the traditional formulation underlying Rackwitz [12]:

$$\frac{dC_1}{C_0} = b \frac{dP_f}{P_f} \quad (9.12)$$

Figure 9.8 presents the optimal reliability indices and failure probabilities in function of DII, as proposed by Van Coile et al. [21]. This formulation confirms the scaling of the target failure probability by the occurrence rate  $\lambda$  as proposed conceptually in the NFSC, under the condition however that the ratio of the other



**Fig. 9.8** Optimal failure probability and reliability index in function of the DII [21]

parameters in the *DII* (i.e. the costs of failure and the costs of further safety investments) remains unchanged. Investigation into the costs and benefits of structural fire protection is an area of ongoing research. Target safety levels for structural fire resistance have been derived, e.g. by Fischer [22] for steel structural elements and by Van Coile et al. [23] for concrete slabs.

### 9.3 Uncertainty in Actions

Fire is an uncertain event. Depending upon building use, building size, fire strategy measures, fire safety management, etc., fire occurrence rates differ and so does the likelihood that a fire will develop to an extent that it is structurally significant. Once of an intensity to be considered structurally significant, the manifestation of the fire is uncertain and correspondingly the probability of a fire-induced structural failure. Sections 9.3.1 and 9.3.2 discuss uncertainties that arise in both the fire's occurrence rate and development, alongside what uncertainty arises in mechanical action (load, moment, etc.). Section 9.4 speaks to uncertainty in the response of materials at elevated temperature.

### 9.3.1 Thermal Action

Uncertainty in the thermal action necessitates a separate consideration of the factors leading to a fire’s occurrence and its ability to become fully developed (i.e. fire occurrence rates and interventions), alongside those that influence the fire’s fully developed manifestation (i.e. fire modelling inputs). These are discussed separately in Sects. 9.3.1.1 and 9.3.1.2, respectively.

#### 9.3.1.1 Fire Occurrence Rates and Interventions

Many events can occur between an ignition and a fire becoming fully developed. Jurisdiction-specific statistics are available which, when contrasted to building stock, give an indication of ignition rates. As fire statistics generally relate to reported fires, the thus obtained ignition frequencies should be considered to relate to fires which because of their severity, duration, or operational procedures warrant reporting.

However, subsequent to fire ignition, there will need to be a failure of numerous intervention mechanisms for the fire to become structurally significant. These could include (a) intervention of occupants via first-aid firefighting, (b) activation of automatic fire suppression systems, or (c) fire service operations.

In contributing to the development of Eurocode 1, Part 1.2 [24], the natural fire safety concept (NFSC) project [19] explored some of the probabilistic aspects of structural fire design, with an emphasis on developing design methods that considered the relationships between early fire intervention measures and subsequent demands of the structural fire design. Table 9.5 summarizes some probabilistic factors for fire occurrence rate and differing intervention mechanisms. It should be noted that the values given likely vary significantly between jurisdictions. For sprinklers which are not installed according to standard, Schleich et al. indicate that a lower success rate (below 0.95) may be appropriate.

The NFSC makes further generalizations which are subsequently adopted in EN 1991-1-2:2002, grouping building types into ‘Danger of fire activation’ classifications, ranging from low to ultra-high, as given in Table 9.6. In this table, the probability of fire occurrence is again expressed per unit area but relates to probability of ignition and subsequent unsuccessful intervention by the occupants or fire service. That is, there is no consideration of active systems, such as sprinklers.

**Table 9.5** Fire occurrence rates and intervention factors from NFSC [19]

Input	Building use		
	Dwelling	Office	Industrial
Fire occurrence rate (1/m <sup>2</sup> ·y)	3 × 10 <sup>-5</sup>	1 × 10 <sup>-5</sup>	1 × 10 <sup>-5</sup>
Probability of fire stopped by occupant (-)	0.75	0.60	0.45
Probability of fire stopped by sprinkler (-)	0.995–0.95		
Probability of fire stopped by public fire brigade (-)	0.90–0.95	0.90–0.95	0.80–0.90

**Table 9.6** Influence of danger of fire activation on structurally significant fire occurrence rate [19]

Type of building occupancy	Danger of fire activation	Probability of fire occurring (1/m <sup>2</sup> ·y) <sup>a</sup>
Museum, art gallery	Low	$0.4 \times 10^{-7}$
Hotel, school, office	Normal	$4.0 \times 10^{-7}$
Machine works	High	$40.0 \times 10^{-7}$
Paint workshop, chemistry laboratory	Very high	$400.0 \times 10^{-7}$
Paint factory, fireworks industry	Ultra-high	$4000.0 \times 10^{-7}$

<sup>a</sup>Probability of severe fire including the effect of occupants and standard public fire brigade (per m<sup>2</sup> of floor and per year)

### 9.3.1.2 Fire Modelling Inputs

Once the fire can develop to an extent that it can be considered structurally significant, a fire model will be required to idealize the fire's development/behaviour. Chapter 4 discusses the various fire models that can be employed. Generally, it is found that the following key inputs need to be defined (not in all cases for all models):

- Growth/spread rate.
- Fire load.
- Ventilation conditions.
- Near-field temperature.

#### Fire Growth Rate/Spread Rate

Studies on the variability in fire growth rates are limited in literature. In a residential context, Holborn et al. [25] estimated fire growth rate based on fire investigation data, with 1991 samples, gathered in the Greater London area. Fire damage area was assumed to be consistent with the fire area, for a heat release rate density ( $\dot{Q}''$ ) of 250 kW/m<sup>2</sup>. Holborn et al. [25] proposed that the average fire growth parameter  $\alpha$  (kW/s<sup>2</sup>) could be estimated by assuming a  $t^2$  growth rate based on the area of fire damage when the fire was discovered ( $A_1$ ) compared to when the fire brigade arrived ( $A_2$ ), and the time intervals from ignition to discovery ( $t_1$ ) and ignition to fire brigade arrival ( $t_2$ ). This can be summarised as

$$\alpha = \frac{\dot{Q}''(A_1 t_1^2 + A_2 t_2^2)}{t_1^4 + t_2^4} \quad (9.13)$$

From this it was determined, using assumed log-normal distribution parameters, that dwelling fires had a mean fire growth rate of 0.006 kW/s<sup>2</sup>, a standard deviation of 0.039 kW/s<sup>2</sup>, and a 95th percentile of 0.024 kW/s<sup>2</sup>.



Baker et al. [26] determined a residential growth rate distribution using zone modelling software B-RISK. A residential occupancy based on experiments undertaken in Sweden was modelled using probabilistic inputs for the ‘design fire generator’ (DFG) and by applying the Monte Carlo method. The outcome of the modelling indicated that a fire growth rate distribution could be approximated to a triangular distribution, with a minimum of 0 kW/s<sup>2</sup>, a maximum of 0.412 kW/s<sup>2</sup>, and a mode of 0.033 kW/s<sup>2</sup>.

In a commercial and public building context, Holborn et al. [25] also computed log-normal distribution parameters for the fire growth rate. However, the sample sizes were significantly reduced compared to the residential case. Results are given in Table 9.7.

Nilsson et al. [27] computed fire growth rate distribution parameters for commercial buildings based upon the data in the Swedish fire ‘Indicators, Data and Analysis’ (IDA). The IDA is a national database recording all rescue service responses. Given 2365 commercial fires, excluding arson, Nilsson et al. [27] like Holborn et al. [25] propose a log-normal distribution for the fire growth rate, with mean 0.011 kW/s<sup>2</sup> and 95th percentile of 0.105 kW/s<sup>2</sup>.

Fire spread rates have been subject to further review, albeit no commonly accepted distributions are presented in the literature. Rackauskaite et al. [28] give spread rates which are computed from a range of large-scale fire experiments or real events. These are summarized in Table 9.8. Based upon operational experiences, Grimwood [29] gives faster spread rates, particularly for large open plan offices, as shown in Table 9.9. In the case of the LA Interstate Bank Fire, Grimwood notes that the fire took 66 min to travel 142 m laterally. In comparison, the fire spread laterally 80 m in 46 min at Telstar House, London.

**Table 9.7** Log-normal parameters characterizing the distribution of fire rates for non-residential building fires, Holborn et al. [25]

Occupancy group	Estimated distribution parameters of fire growth rate (kW/s <sup>2</sup> )			
	Fires	Standard deviation	Mean	95th Percentile
Hotels	12	0.035	0.004	0.014
Offices	19	0.019	0.004	0.016
Schools	16	0.037	0.005	0.019
Retail	37	0.159	0.027	0.101

**Table 9.8** Spread rates from Rackauskaite et al. [28]

Fire type/case	Spread rate(s) in (mm/s)
Wood cribs in the open	0.1–2
Lateral or downward spread on thick solids	1
Experiments—natural fires in large-scale compartments	1.5–19.3
Reconstruction of World Trade Center fires (2001)	2.5–16.7
St. Lawrence Burns experiments (1958)	7.5–13
First Interstate Bank Fire (1988)	14.5

**Table 9.9** Spread rates after Grimwood [29]

Fire type/case	Spread rate(s) in (m <sup>2</sup> /min)	Spread rate(s) in (mm/s)
Interstate Bank Fire (1988)	24.6	36
CCAB 67 West Washington fire (2004)	15.3	27
Telstar House fire, London (2004)	24.3	29

**Table 9.10** Fire load densities from EN 1991-1-2:2002

Occupancy type	Mean (MJ/m <sup>2</sup> )	Standard deviation (MJ/m <sup>2</sup> )	80th Percentile (MJ/m <sup>2</sup> )	90th Percentile (MJ/m <sup>2</sup> )	95th Percentile (MJ/m <sup>2</sup> )
Dwelling	780	234	948	1085	1217
Hospital	230	69	280	320	359
Hotel (room)	310	93	377	431	484
Library	1500	450	1824	2087	2340
Office	420	126	511	584	655
School	285	86	347	397	445
Shopping centre	600	180	730	835	936
Theatre (cinema)	300	90	365	417	468
Transport hub (public space)	100	30	122	139	156

## Fire Load Density

Fire load density was subject to extensive surveys within CIB Working Group 14, led by Thomas [30]. Figures within CIB W14 influence the fire load densities adopted within the NFSC [19] and subsequently recommended in EN 1991-1-2:2002. Fire load density distributions within Eurocode 1, Part 1.2, universally adopt a Gumbel type I distribution, with a coefficient of variation (COV) of 0.3. For different occupancy types, corresponding fire load densities are given in Table 9.10.

Zalok et al. [31] present a more contemporary review of fire loadings relative to the NFSC within commercial premises. The study undertook surveys in 168 commercial premises, concluding that fire load density generally followed a log-normal distribution. A summary of findings is given in Table 9.11.

Elhami Khorasani et al. [32] summarize the results of four fire load surveys across different countries. Data from the USA is then adopted to generate a new probabilistic model for fire load density, expressed in function of enclosure area. Equation (9.14) describes a probabilistic model for lightweight occupancies (office and clerical). Equation (9.15) gives a corresponding model for heavyweight occupancies (library, storage, file rooms):

$$q = \exp [6.951 - 0.0047(A_f \times 10.76) + 0.5712\varepsilon] \quad (9.14)$$

**Table 9.11** Fire load densities after Zalok et al. [31]

Occupancy type	No. of samples	Mean (MJ/m <sup>2</sup> )	Standard deviation (MJ/m <sup>2</sup> )	95th Percentile (MJ/m <sup>2</sup> )
All stores	168	747	833	2050
Storage areas	43	1196	1208	4289
Fast-food outlets	18	526	320	881
Clothing stores	14	393	164	661
Restaurants	11	298	190	582
Kitchens	8	314	161	553

$$q = \exp [8.252 - 0.0081(A_f \times 10.76) + 0.5508\varepsilon] \tag{9.15}$$

where  $q$  is in units of MJ/m<sup>2</sup>;  $A_f$  is the room size (m<sup>2</sup>); and  $\varepsilon$  is a random variable that is in accordance with the standard normal distribution.

The proposals of Elhami Khorasani et al. [32] are further developed by Xie et al. [33] who present a fire load density model for office and residential building types. Distributions for both occupancies are said to be log-normal with mean ( $\mu_{qm}$  – MJ/m<sup>2</sup>) and standard deviation ( $\sigma_{qm}$  – MJ/m<sup>2</sup>) varying in function of enclosure area ( $A_f$  – m<sup>2</sup>), as given in Eqs. (9.16) and (9.17) for offices, and Eqs. (9.18) and (9.19) for residential. The maximum enclosure sizes were c. 30 and 120 m<sup>2</sup> for residential and offices, respectively:

$$\mu_{qm} = \frac{568}{\exp(0.00740A_f)} \tag{9.16}$$

$$\sigma_{qm} = \frac{268}{\exp(0.00740A_f)} \tag{9.17}$$

$$\mu_{qm} = \frac{1254}{\exp(0.0441A_f)} \tag{9.18}$$

$$\sigma_{qm} = \frac{268}{\exp(0.0414A_f)} \tag{9.19}$$

### Heat Release Rate

For fuel-controlled burning, the heat release rate density ( $\dot{Q}''$  kW/m<sup>2</sup>) has importance. PD 7974–1:2019 [34], based on the work of Hopkin et al. [35], gives ranges for different occupancies as summarized in Table 9.12.

**Table 9.12** Heat release rate density ( $\dot{Q}''$ ) from PD 7974-1:2019 [34]

Occupancy	$\dot{Q}''$ (kW/m <sup>2</sup> )
Shops	270–1200 (maximum)
Offices	150–650 (maximum)
Hotel rooms	250 (average)
Residential	320–570 (maximum)
Industrial	90–620 (average)
Storage/stacked commodities	400–20,000 (maximum)

For most cases,  $\dot{Q}''$  corresponds with the maximum value estimated over the full duration of a fire. For hotels and industrial buildings,  $\dot{Q}''$  corresponds with the mean value estimated over a defined period of burning.

### Ventilation Conditions

The breakage of openings and associated probabilities has not been subject to extensive research. Studies presented by Hopkin et al. [20] have adopted a uniform distribution between a lower and upper bound of 12.5% and 100% of the total opening area. This ventilation range has no basis other than to introduce some sensitivity to ventilation conditions. Analyses underpinning British Standard BS 9999:2017 by Kirby et al. [36] also adopt a uniform distribution but expressed in function of the opening size relative to the compartment floor area. These range from 5% to 40%, with opening heights varying from 30% to 100% of the compartment height.

The Joint Committee on Structural Safety (JCSS) [37] provides a tentative probabilistic distribution for opening factor ( $O = A_v\sqrt{H/A_f}$ ), where

$$O = O_{\max}(1 - \zeta) \quad (9.20)$$

with  $O_{\max}$  being the maximum opening factor (m<sup>0.5</sup>) assuming the failure of all non-fire-resisting external wall construction and  $\zeta$  a random parameter that is log-normally distributed. The JCSS recommends that  $\zeta$  have a mean of 0.2 and a standard deviation of 0.2, with any values exceeding unity suppressed so as not to generate negative opening factors.

### Near-Field Temperature

Stern-Gottfried [38], in developing a travelling fire methodology, reviewed variability in near-field temperature at different points in time from ‘flashover’ in a limited number of large-scale fire experiments (Dalmarnock and Cardington fire tests). From this, it was determined that spatially resolved near-field temperatures followed a normal distribution. At different points in time, the mean near-field temperature varies. As such, Stern-Gottfried [38] proposes a relationship between average near-

field temperature rise ( $\Delta T_{\text{avg}}$ ) and coefficient of variation ( $\delta$ ). The relationship is defined by Eq. (9.21):

$$\delta = \frac{\sigma}{\Delta T_{\text{avg}}} = 1.939 - 0.266 \ln (\Delta T_{\text{avg}}) \quad (9.21)$$

Stern-Gottfried [38] notes that Eq. (9.21) could be used as a nominal expression of the standard deviation for any temperature-time curve.

In the absence of alternative data, Hopkin et al. [20] used Eq. (9.21) to describe variability in the near-field temperature of travelling fires as part of a probabilistic framework. For travelling fires, Rackauskaite et al. [28] note temperatures of the near field to be in the range of 800–1200 °C. For a conservative case, early applications of the travelling fire method (e.g [39].) adopted a deterministic near-field temperature of 1200 °C. However, structural response is highly sensitive to this input, and therefore a treatment as a stochastic variable in some manner is advocated, e.g. a uniform distribution between 800 and 1200 °C.

## 9.3.2 Mechanical Action

### 9.3.2.1 Introduction

The uncertainty in load and associated actions on structures is discussed widely in the literature, e.g. JCSS [37], Ellingwood [40], and Holicky and Sykora [41]. The study of Ellingwood is specifically focused on fire events. The mechanical actions are traditionally subdivided into permanent actions and imposed (or variable) actions, and their variability with time is an aspect of particular relevance for structural fire engineering. Other mechanical loads include wind load, snow load, and earthquake load. The joint consideration of fire and, for example, earthquake loading may be necessary for exceptional building projects with high consequences of failure, i.e. a requirement for a very high reliability. Ellingwood however adopts a de minimis risk acceptance condition of the order of  $10^{-6}$  for a 1-year reference period, which is subsequently applied as a screening probability for considering combinations of loads.

In design for normal conditions, the load variability is considered by a (characteristic or design) load with a low probability of being exceeded during the lifetime of the structure. Naturally, the day-to-day probability of occurrence of such high (design) load value is low, just as for the day-to-day probability of occurrence of a significant fire. Simultaneously taking into account both events would result in very onerous fire design requirements. Hence, the reduced safety and combination factors in the Eurocode (EN 1990) and in the ASCE design format (load and resistance factor design) (ASCE 7–16) lessen the required load under consideration for structural fire design compared to normal design conditions.

Thus, when directly taking into account the uncertainty in the permanent and imposed load effects, an arbitrary point in time (APIT) load is to be considered. This differs from the stochastic load models commonly considered for normal design conditions, where distribution models for the maximum load in a long (e.g. 50 years) reference period are applied.

A recent literature review by Jovanović et al. [42] of permanent and imposed load models applied in probabilistic structural fire engineering (PSFE) studies has shown that a large variation in models is commonly applied, notably for the imposed load effect. In summary, two distinct families of probabilistic models were discerned. These are revisited in the following Sect. 9.3.2.2, together with a discussion of background studies and recommended distributions to be applied in PSFE applications.

### 9.3.2.2 Permanent Load Model

#### Introduction

The permanent actions result from the self-weight of the structural elements and finishes, and can be considered time invariant [37, 40]. Hence, for the stochastic model of the permanent load, the models applied for normal design qualify as APIT permanent loads. This neglects possible combustion of finishes or structure, as is a standard and conservative approximation.

#### Background

Table 9.13 gives mean values and coefficient of variation for density  $\gamma$  for some common structural framing materials, while Table 9.14 lists standard values for the deviation of structural elements' dimensions from their nominal values. Considering these standard deviations, the mean volume of a structural element exceeds its nominal value. The JCSS Probabilistic Model Code (PMC) however states in a simplifying manner that the mean value of the volume can be calculated directly from the mean value of the dimensions, and that the mean dimensions can be considered equal to their nominal value [37].

With both  $\gamma$  and the volume  $V$  described by a normal distribution, the self-weight  $l$  is in principle not normally distributed. However, when the coefficients of variation

**Table 9.13** Mean and COV for weight density of typical materials [41]

Material	Mean (kN/m <sup>3</sup> )	$\delta_\gamma$	$\delta_l$
Steel	77	<0.01	0.032
Concrete	24	0.04	0.045
Timber	<sup>a</sup>	0.10	0.101

<sup>a</sup>Listed in [37] for 12% moisture content: spruce: 4.4; fir: 4.4; pine: 5.1; larch: 6.6; beech: 6.8; oak: 6.5

**Table 9.14** Mean values and standard deviations for deviations of cross-section dimensions from their nominal values [37]

Material	Mean value	Standard deviation
<b>Rolled steel</b>		
Area of profiles, $A$	$0.01 A_{\text{nom}}$	$0.04 A_{\text{nom}}$
Thickness of plates, $t$	$0.01 t_{\text{nom}}$	$0.02 t_{\text{nom}}$
<b>Concrete members</b>		
Nominal dimension $a < 1000$ mm	$0.003 a_{\text{nom}}$	$4 \text{ mm} + 0.006 a_{\text{nom}}$
Nominal dimension $a > 1000$ mm	3 mm	10 mm
<b>Structural timber</b>		
Sawn beam, $a$	$0.05 a_{\text{nom}}$	2 mm

(COV) of the volume and density are small (which is generally the case), the resulting self-weight loads can nevertheless be assumed to be described by a normal distribution [43]. This has also been adopted in the JCSS PMC [37]. Considering Taylor expansion, the mean value of the self-weight  $\mu_l$  is given by  $\mu_\gamma \cdot \mu_V$ . The coefficient of variation  $\delta_l$  can be estimated from Eq. (9.22), with standard values listed in Table 9.13 [41]:

$$\delta_l^2 = \delta_V^2 + \delta_\gamma^2 + \delta_V^2 \delta_\gamma^2 \tag{9.22}$$

When multiple materials or components contribute with their self-weight to the permanent load effect, this corresponds with an addition of normally distributed variables. When the constituent self-weights  $l_i$  can be considered independent (with mean values  $\mu_{li}$  and standard deviation  $\sigma_{li}$ ), the overall permanent load is described by a normal distribution as well, with mean values  $\mu_G$  and standard deviation  $\sigma_G$  given by

$$\mu_G = \sum_i \mu_{li} \tag{9.23}$$

$$\sigma_G = \sqrt{\sum_i \sigma_{li}^2} \tag{9.24}$$

### Commonly Applied Models in Probabilistic Structural Fire Engineering

When evaluating an existing building, evaluating the load effect through Eqs. (9.23) and (9.24) can be considered reasonable, and may allow a precise assessment of the appropriate probabilistic description of the permanent load. For general reliability studies and code calibration purposes, however, generally applicable models are preferred for generality (thus avoiding assumptions with respect to, e.g., floor build-up and materials).

As elaborated by Jovanović et al. [42], two models are commonly applied for describing the permanent load effect in PSFE. On the one hand, a series of studies (e.g. [44].) and Iqbal and Harichandran [45] model the permanent load effect as a normal distribution with mean value equal to  $1.05 G_{nom}$ , with  $G_{nom}$  as the nominal permanent load, and a coefficient of variation of 0.10. These studies have the 2005 study by Ellingwood as a common point of reference. The other series of studies (e.g. [46, 47].) apply a normal distribution with mean value equal to  $G_{nom}$ , and a COV of 0.10. These studies do not propose a differentiation of permanent load distribution by framing material.

### Recommended Model for the Permanent Load

Considering the above, both commonly applied models agree on describing the permanent load by a normal distribution with a COV of 0.10. The normal distribution is in agreement with the background models. Taking into account Table 9.13, a COV of 0.10 can be considered a (practical) conservative assessment. Considering the discussed background information, the mean permanent load slightly exceeds its nominal value (in the order of 1% for concrete elements). It is considered preferable to neglect a 1% (order of magnitude) exceedance in accordance with the JCSS PMC recommendation than to set  $\mu_G$  equal to  $1.05 G_{nom}$ . This is considered to be compensated by the practical choice for a COV of 0.10.

In conclusion, the permanent load effect  $G$  is recommended to be described by a normal distribution, with mean equal to the nominal permanent load effect  $G_{nom}$ , and COV of 0.10.

### 9.3.2.3 Live Load Model

#### Introduction

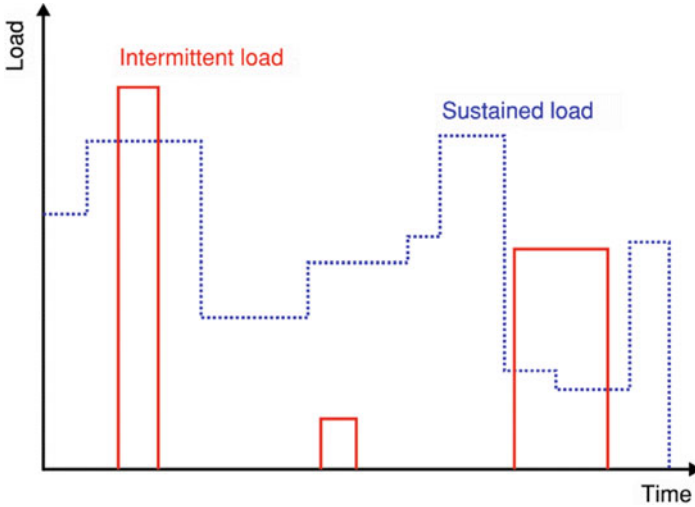
The live (or imposed) loads arise from a range of components, from building occupants to their possessions and movable items, like furniture. The total live load can be broken down into two components: (1) a sustained component and (2) an intermittent or transient component [37, 40, 41].

While both vary with time, by definition, a component of the sustained load is ever present—albeit its magnitude could vary. Figure 9.9 illustrates the difference between the sustained and intermittent live load components, adapted from Ellingwood [40].

Normal people occupancy is generally included in the sustained load, e.g. Chalk and Corotis [48]. The intermittent live load on the other hand relates to exceptional events, such as overcrowding [48] or stacking of objects during refurbishing [37].

For PSFE, the arbitrary point in time (APIT) live load is of interest, and as the occurrence of the intermittent (transient) live load is by its conceptualization rare, it generally does not need to be taken into account simultaneously with fire exposure





**Fig. 9.9** Components of live load—sustained and intermittent, adapted from Ellingwood [40]

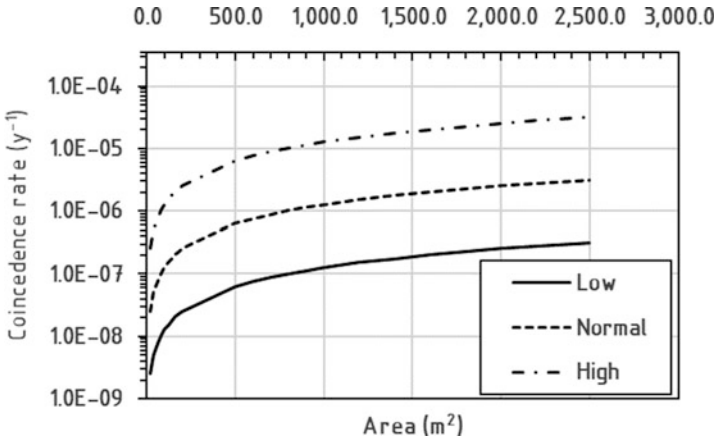
[40]. Ellingwood notes occurrence rates of *c.* 1/y and a duration of 1 day for the intermittent load. For a structurally significant fire occurrence rate of  $10^{-6}$  per annum and duration of 4 h, the coincidence rate of a fire and intermittent live load is significantly below the proposed de minimis limit ( $10^{-6}$ ) leading Ellingwood to propose that the intermittent component be disregarded. While this can be considered sufficient for the general floor area of most buildings (e.g. offices, residential buildings), Jovanović et al. [42] state that care should be taken whenever the live load profile of the building has specific occurrence patterns or particular likelihood of overcrowding (e.g. sports stadia), or when considering buildings with high reliability requirements (e.g. high-rise structures). Figure 9.10 shows the coincidence rates of a 1-year returning intermittent live load and fire, for different compartment sizes and danger of activation (as defined in Table 9.6).

In the following, the APIT model for the sustained live load is discussed.

## Background

The commonly applied live load models have been derived from load surveys conducted in the twentieth century.

Ellingwood and Culver [49] assessed an equivalent uniformly distributed APIT load  $Q$  from a 1974–1975 survey of US office buildings. The mean loads and COV are listed in Table 9.15 and include a nominal personnel load of  $81 \text{ N/m}^2$ . Ellingwood and Culver report that no significant difference with UK data published in the early 1970s could be discerned, and list a gamma distribution as the appropriate distribution model.



**Fig. 9.10** Coincidence rate of intermittent live load (occurrence rate  $y^{-1}$ ) and fire in function of compartment area and ‘danger of activation’

**Table 9.15** Sustained live load in offices, US 1974–1975 survey, as reported by Ellingwood and Culver [49]

Area [m <sup>2</sup> ]	$\mu$ [psf]	$\mu$ [kN/m <sup>2</sup> ]	$\mu/Q_{nom}^a$ [-]	$\mu/Q_{nom}^b$ [-]	COV
18.6	11.6	0.56	0.19	0.23	0.85
37.2	11.6	0.56	0.19	0.23	0.68
92.9	11.6	0.56	0.19	0.23	0.55
185.8	11.6	0.56	0.19	0.23	0.50
464.5	11.6	0.56	0.19	0.23	0.47

<sup>a</sup> $Q_{nom}$  evaluated as 3 kN/m<sup>2</sup>

<sup>b</sup> $Q_{nom}$  evaluated as 2.4 kN/m<sup>2</sup>

**Table 9.16** Sustained live load for different occupancies, as reported by Chalk and Corotis [48]

Occupancy	$\mu$ [psf]	$\mu$ [kN/m <sup>2</sup> ]	$Q_{nom}^a$ [kN/m <sup>2</sup> ]	$\mu/Q_{nom}$ [-]	COV
Office	10.9	0.52	3	0.17	0.70
Residential	6.0	0.29	2	0.14	0.57
Hotel (room)	4.5	0.22	2	0.11	0.33
Retail (first floor)	17.9	0.86	5	0.17	0.31
Retail (upper floors)	12.0	0.57	5	0.11	0.88
Classroom	12.0	0.57	3	0.19	0.25
Warehouse	71.5	3.42	7.5	0.46	0.90

<sup>a</sup>Recommended values in EN 1991-1-1:2002

Chalk and Corotis [48] list APIT sustained live loads for different occupancy types, taking into account data from multiple surveys (Table 9.16). Comparison with the office data listed in Table 9.15 confirms the order of magnitude values. Also Chalk and Corotis applied a gamma distribution in their calculations.

**Table 9.17** Sustained live load parameters, as tabulated in the JCSS Probabilistic Model Code\* [37]

Occupancy	$A_0$	$\mu$	$\sigma_V$	$\sigma_u$	$COV_{inf}^{**}$	$\mu/Q_{nom}$
Office	20	0.5	0.3	0.6	0.60	0.17
Residential	20	0.3	0.15	0.3	0.50	0.15
Hotel (room)	20	0.3	0.05	0.1	0.17	0.15
Retail (first floor)	100	0.9	0.6	1.6	0.67	0.18
Retail (upper floors)	100	0.9	0.6	1.6	0.67	0.18
Classroom	100	0.6	0.15	0.4	0.25	0.20
Warehouse (storage)	100	3.5	2.5	6.9	0.71	0.47

\*Dimensions (m<sup>2</sup>), (kN/m<sup>2</sup>), (-);  $Q_{nom}$  taken as recommended values EN 1991-1-1:2002, as listed in Table 9.16

\*\*COV corresponding with large loaded area A, for which the area-dependent term in (9.25) reduces to zero

The JCSS PMC [37] tabulates live load distribution parameters as listed in Table 9.17 and recommends a gamma distribution for the APIT load. Reference is made to a limited number of documents, amongst which the 1989 CIB report [50] is of particular relevance. This report was drafted by Corotis and Sentler, which can reasonably be considered to imply a close relationship with the work presented in Table 9.16. The CIB report lists multiple surveys dating from 1893 to 1976. Looking into the PMC values for  $\mu/Q_{nom}$ , these are comparable to those listed in Table 9.16, with all categories except warehouses resulting in a value between 0.15 and 0.20.

With respect to the COV, the PMC specifies Eq. (9.25) for the standard deviation of the instantaneous imposed load. In this equation and Table 9.17,  $\sigma_V$  is the standard deviation of the overall load intensity,  $\sigma_U$  the standard deviation associated with the spatial variation of the load,  $A_0$  an occupancy-specific reference area,  $A$  the loaded area, and  $\kappa$  an influence factor (commonly between 1 and 2.4; further taken as 2.2 for agreement with Ellingwood and Culver [49]). The COV for very large loaded areas is listed in Table 9.17 as  $COV_{inf}$ , i.e. where the loaded area-dependent term in Eq. (9.25) reduces to zero. With the exception of the first-floor retail space, these COVs are smaller than those listed in Table 9.16. For small loaded areas, however, the COV resulting from Eq. (9.25) exceeds those in Table 9.16:

$$\sigma^2 = \sigma_V^2 + \sigma_U^2 k \cdot \min \left\{ \frac{A_0}{A}; 1 \right\} \tag{9.25}$$

### Commonly Applied Models in Probabilistic Structural Fire Engineering

With respect to the live load model, a wide variety of distribution models have been applied in PSFE. Not all studies however relate to APIT loads (for example using a load model for the maximum realization in a 50-year reference period instead). Limiting the discussion to APIT models, two families have been discerned in Jovanović et al. [42]:

1. Gamma distribution with mean value  $\mu/Q_{nom}$  equal to 0.24 and COV of 0.60.
2. Gumbel distribution with mean value  $\mu/Q_{nom}$  equal to 0.20 and COV of 1.10.

The first family has the 2005 Ellingwood study as a common point of reference. In this study, Ellingwood specifies  $\mu/Q_{nom}$  as being in the range of 0.24–0.50. In Ellingwood’s study (2005), reference is made to the data in Tables 9.15 and 9.16 and the underlying studies.

The second family models the APIT live load by the distribution for the maximum load in a 5-year reference period (i.e. ‘5y Gumbel distribution’). In essence, it is assumed that the imposed load can be modelled by a rectangular wave renewal process with a 5-year return period [51]. The 5-year return period corresponds with the expected time between renewals (changes in use and users [37]) for office buildings [41]. The specific distribution parameters listed above apply for office buildings designed in accordance with the Eurocode-recommended nominal (characteristic) imposed load of 2–3 kN/m<sup>2</sup>, considering the PMC load values, but can be used as a first approximation for other occupancies as well [41].

While both live load model families seem very distinct at first, the underlying data can reasonably be considered to be comparable, with both families linked to research by amongst others Corotis.

### Recommended Model for the Imposed Load

The background documents agree on the use of a gamma distribution to describe the instantaneous sustained live load. Thus, it is adopted here as a recommendation based on precedent and considering the impossibility of negative values (note that the Gumbel distribution assigns a non-zero probability to negative realizations).

With respect to the distribution parameters, the background documents agree largely on the mean value  $\mu$  for the sustained live load. Thus, for project-specific evaluations it is recommendable to define the mean sustained live load directly from listed data, such as the JCSS PMC [37]. The corresponding ratio  $\mu/Q_{nom}$  depends on the guidance-specific definition of  $Q_{nom}$ . When defining  $Q_{nom}$  through EN 1991-1-1:2002-recommended values, the ratio  $\mu/Q_{nom}$  is largely found to be in the range of 0.10–0.20. A value of 0.20 is considered reasonable for a first assessment for offices, residential areas, retail, hotels, and classrooms. A similar result is obtained for office buildings in accordance with ASCE 7–16, considering a  $Q_{nom}$  recommendation of 65 psf.

The COV for the sustained live load can be considered dependent on the loaded area. For large loaded areas, a COV of 0.60 is found reasonable (see Table 9.17). For smaller loaded areas the COV is higher. Project-specific evaluations are again recommended when applicable. For general reliability assessments, a COV of 0.95 is recommended. This corresponds with the COV for office areas and classrooms at approximately 120 m<sup>2</sup> loaded area. This value also results in a comparable ambient design reliability index compared to the Gumbel model with COV of 1.1 (which was used in the Eurocode background documents, i.e [47].).

In summary, for non-project-specific evaluations, excluding warehouses, the recommended model for the imposed load is given as follows:

- For a large loaded area: Gamma distribution with  $\mu/Q_{nom} = 0.20$ ,  $COV = 0.60$ .
- For a small loaded area: Gamma distribution with  $\mu/Q_{nom} = 0.20$ ,  $COV = 0.95$ .

### 9.3.2.4 Total Load Effect

#### Introduction and Commonly Applied Models

The models for the permanent load  $G$  and imposed load  $Q$  however do not convey the full story on the probabilistic modelling of mechanical actions. Additional stochastic factors are taken into account when combining the permanent and imposed load effects. Again, two distinct formulations are commonly applied: Eq. (9.26) with reference to Ravindra and Galambos [52] and Eq. (9.27) with reference to the JCSS PMC. Standard values for the stochastic variables are listed in Table 9.18:

$$w = E(AG + BQ) \tag{9.26}$$

$$w = K_E(G + Q) \tag{9.27}$$

Ravindra and Galambos [52] refer to Eq. (9.26) as an assumption, and explain that  $A$  and  $B$  are to be interpreted as characterizing the difference between computed and actual internal forces in the structure, while  $E$  is intended to characterize deviations introduced by characterizing a 3D structure into elements or subsystems and other simplifying assumptions (such as boundary conditions). They however do not mention a distribution type for these variables, and indicate that the mean values and COVs (as listed in Table 9.18) were ‘chosen’ and ‘assumed’ as ‘reasonable estimates based on data and judgements’, with further reference to a 1973 Washington University report.

The total load model of Eq. (9.27) is recommended in the JCSS PMC, where a difference is made in the recommended COV for  $K_E$  in function of the considered load effect (axial load, moment). For frames, a COV of 0.1 is the higher value. Only for moments in plates the recommended value is higher at 0.2 [37]. The PMC provides no indication, however, as to the origin of these values. This formulation is nevertheless commonly applied in structural reliability calculations, and has been included in the background documents to the Eurocodes, e.g. Holicky and Sleich [47].

**Table 9.18** Load combination parameters as applied in total load models [42]

Parameter	Distribution	$\mu$	$\delta$
$E$	Normal	1.0	0.05
$A$	Normal	1.0	0.04
$B$	Normal	1.0	0.20
$K_E$	Log-normal	1.0	0.10

Recommended Model for the Total Load Effect

Neither of the above two models has extensive background available, and these are commonly applied based on precedent. The model of Eq. (9.27) is considered to have a greater authority considering its recommendation by the Joint Committee on Structural Safety, which is the common expert group on structural reliability of five international organizations (CEB, DIB, fib, IABSE, and RILEM).

Hence, the recommended total load model is given by Eq. (9.27) with  $K_E$  being the model uncertainty for the total load effect, described by a log-normal distribution with mean 1.0 and COV 0.10.

Taking into account the recommended models for the permanent load  $G$  and the imposed load  $Q$  as defined above, and defining the load ratio  $\chi$  by Eq. (9.28) (with nominal values corresponding with the characteristic values in the Eurocode design format), the total load  $w$  is given in Fig. 9.11 relative to the nominal total load  $P_{nom} = G_{nom} + Q_{nom}$ :

$$\chi = \frac{Q_{nom}}{Q_{nom} + G_{nom}} = \frac{Q_{nom}}{P_{nom}} \tag{9.28}$$

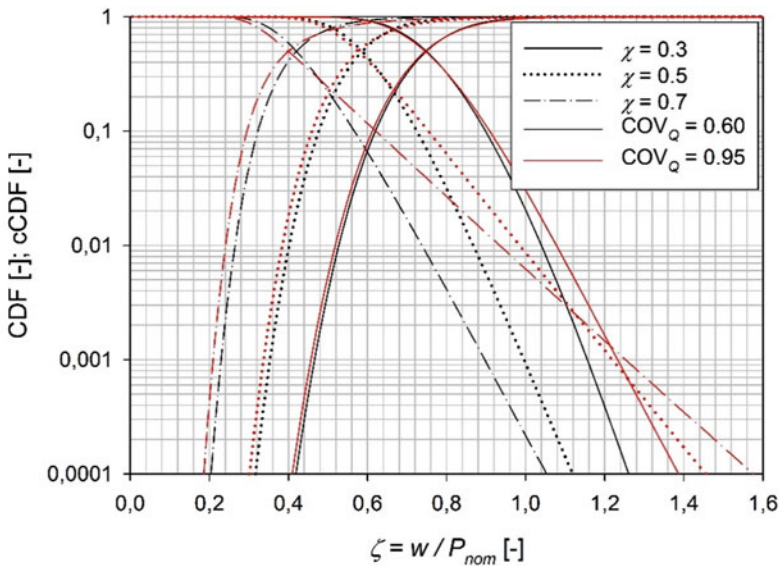


Fig. 9.11 Cumulative density function (CDF) and complementary CDF (cCDF) for the total nominal load  $w$  according to the recommended load models, with  $COV_Q = 0.60$  (black) and  $0.95$  (red), respectively

## 9.4 Materials and Applications

As stated in Sect. 9.1, one of the uncertainties that need to be addressed during structural analysis at high temperatures relates to properties of material during fire. This section provides an overview of existing studies on the subject.

### 9.4.1 Concrete

Strength of concrete is one of the primary properties that are required when analysing and quantifying performance of a concrete structural element (slabs, columns, beams, and walls) at normal or elevated temperatures. This section discusses the available test data on concrete strength retention factor and related temperature-dependent probabilistic models. When analysing reinforced concrete structures, the strength of reinforcement can be modelled following the discussion in the next section on steel material.

Qureshi et al. [53] compiled a database of existing tests on calcareous and siliceous concrete strength at high temperatures, keeping the two concrete types separate following a similar approach in the available deterministic Eurocode (EC) models [54]. A total of 242 data points for siliceous and 162 data points for calcareous concrete were collected. Concrete strength at high temperatures was normalized with respect to the measured strength (or average of multiple measurements) at 20 °C. A relatively large scatter in the data was observed across all temperature ranges. Qureshi et al. [53] followed two approaches to develop probabilistic models for the concrete compressive strength retention factor:

- In the first approach, the data set was divided over different temperature groups with increments of 50 °C. Histograms for each temperature group were then constructed and compared with a number of different probability density functions (PDF) (e.g. log-normal, Weibull). The distribution that fits best over different temperature ranges and has a closed-form solution that can be implemented in computer codes was selected, and temperature-dependent functions for the parameters that would characterize the distribution were proposed.
- In the second approach, the procedure by Elhami Khorasani et al. [55] was followed where a continuous temperature-dependent logistic function is fit to the data set using a Bayesian-based maximum likelihood calculation. In this approach, the logistic function can be a function of any form or defined with an existing deterministic function as the base (such as the EC model) with correction terms added to improve the fit to the data.

One important issue to be considered in developing probabilistic models at elevated temperatures is to ensure continuity and consistency in reliability appraisals in transition between ambient and elevated temperatures; therefore, it is important to note the existing assumptions that are applied at 20 °C. Holicky and Sykora [41]

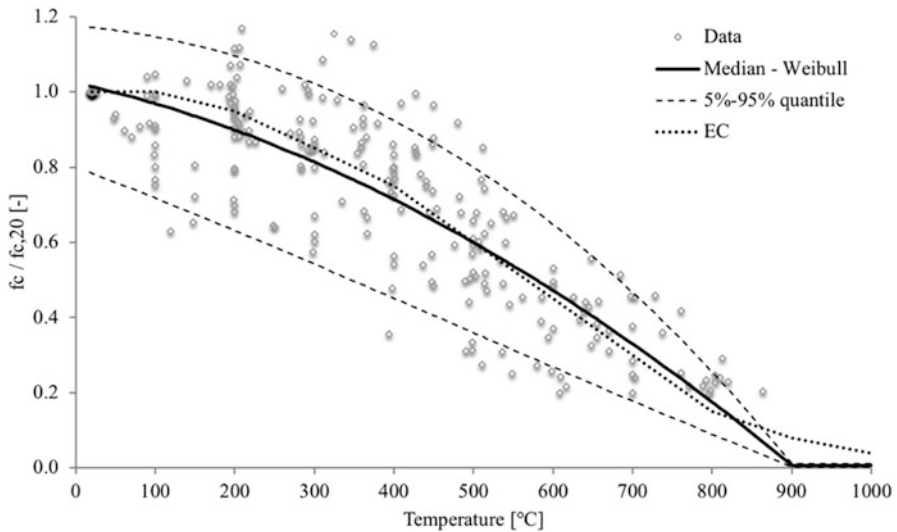
recommended the mean concrete strength at ambient temperature to be defined as the characteristic concrete strength plus two standard deviations, following a log-normal distribution with a coefficient of variation (COV) varying from 0.05 to 0.18 depending on the production procedure.

Using the approaches and considerations explained above, Qureshi et al. [53] proposed a Weibull distribution with parameters  $\lambda$  and  $k$  for calcareous and siliceous concrete strength retention factors, given that closed-form solutions of the Weibull distribution PDF  $f(x; \lambda, k)$  and quantile (i.e. inverse cumulative density function)  $Q(p; \lambda, k)$  are available, shown in Eqs. (9.29) and (9.30). In developing the model, distribution parameters at 20 °C were constrained to closely follow Holicky and Sykora’s recommendation. The size of data points above 700 °C was limited for calcareous concrete; therefore, in order to extend the model beyond 700 °C, it was assumed that the retention factor equals to zero at 1000 °C:

$$f(x; \lambda, k) = \frac{k}{\lambda} \left(\frac{x}{\lambda}\right)^{k-1} e^{-\left(\frac{x}{\lambda}\right)^k} \tag{9.29}$$

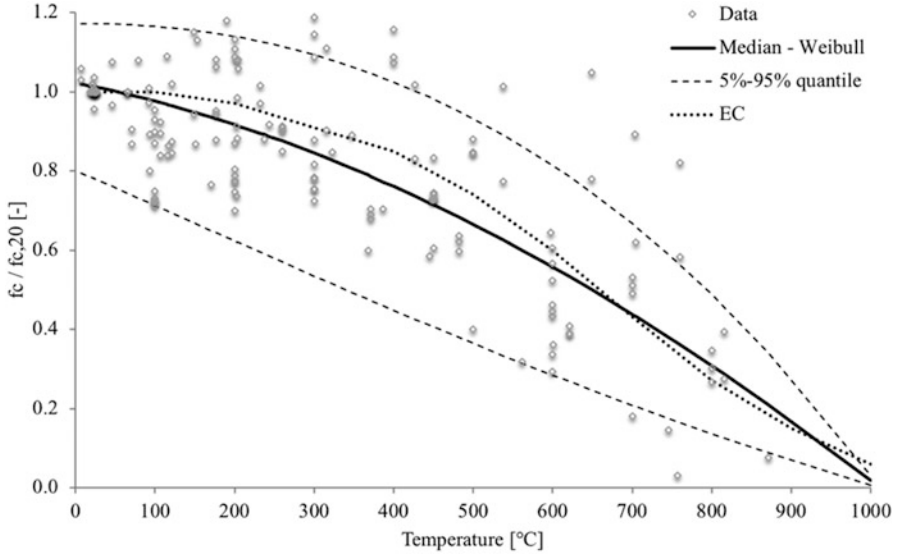
$$Q(p; \lambda, k) = \lambda[-\ln(1 - p)]^{1/k} \tag{9.30}$$

Figures 9.12 and 9.13 show the data set in comparison with the mean, and 5–95% quantiles of the probabilistic models based on the Weibull distribution fit for both calcareous and siliceous concrete. Eqs. (9.31)–(9.34) provide parameters of the Weibull distribution  $\lambda$  and  $k$  as a function of temperature  $T$  in Celsius.



**Fig. 9.12** Siliceous concrete strength retention factor vs. temperature based on Weibull distribution fit





**Fig. 9.13** Calcareous concrete strength retention factor vs. temperature based on Weibull distribution fit

For siliceous concrete:

$$\lambda(T) = -8.4340 \times 10^{-7} \times T^2 - 4.0887 \times 10^{-4} \times T + 1.0598 \tag{9.31}$$

$$K(T) = \frac{9.7348}{0.9231 + 1.9787 \times 10^{-3} \times T} \tag{9.32}$$

For calcareous concrete:

$$\lambda(T) = -7.3849 \times 10^{-7} \times T^2 - 2.9879 \times 10^{-4} \times T + 1.0576 \tag{9.33}$$

$$K(T) = \frac{27.7292}{2.5894 + 7.6323 \times 10^{-3} \times T} \tag{9.34}$$

Using the second approach explained above, Qureshi et al. [53] proposed continuous logistic functions as shown in Eqs. (9.35) and (9.36), where  $T$  is temperature in Celsius and  $\varepsilon$  is the standard normal distribution. A value of zero for  $\varepsilon$  generates the median of the function. Figures 9.14 and 9.15 show the data sets in comparison with the median and two standard deviation envelopes of the logistic functions for both calcareous and siliceous concrete.

For siliceous concrete:

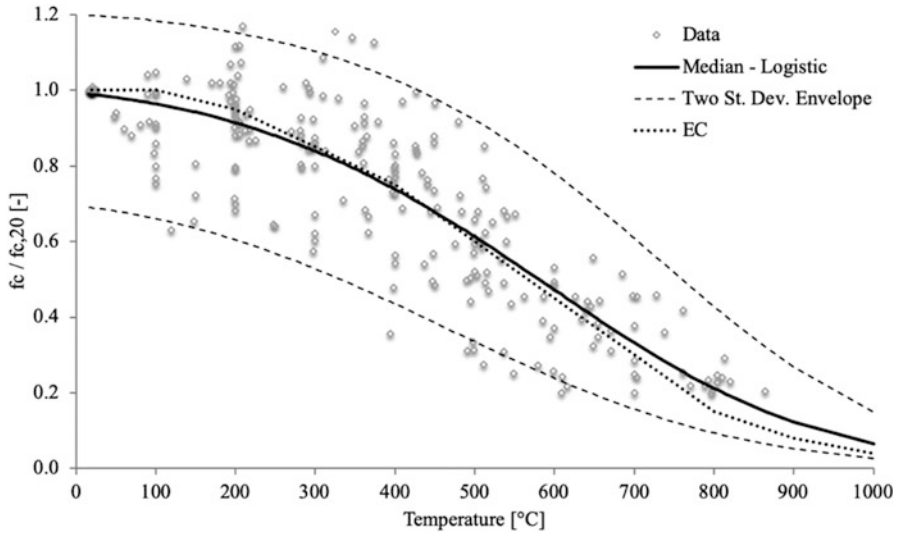


Fig. 9.14 Siliceous concrete strength retention factor vs. temperature based on logistic function

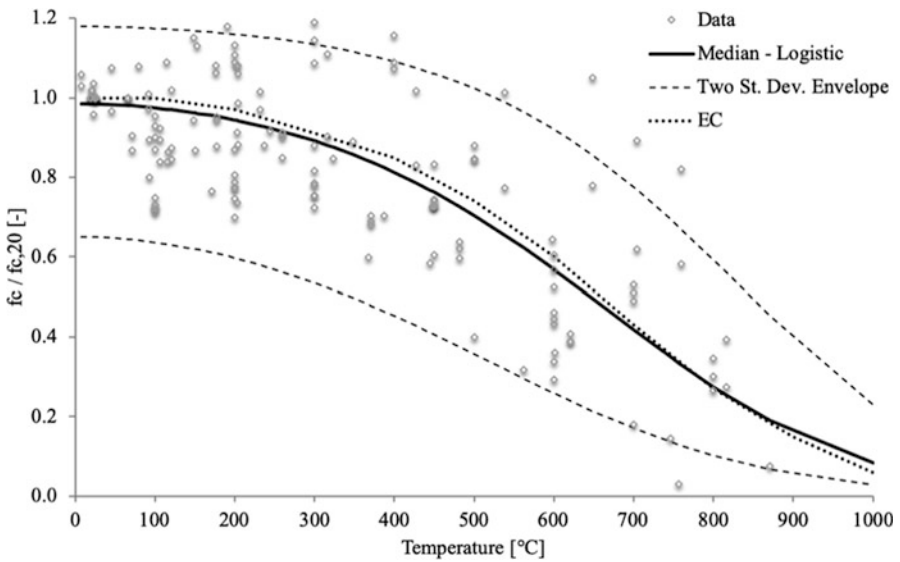


Fig. 9.15 Calcareous concrete strength retention factor vs. temperature based on logistic function

$$\frac{f_c}{f_{c,20}} = \frac{1.4 \times \exp [0.8892 - 0.6319 \times 10^{-3} \times T - 3.295 \times 10^{-6} \times T^2 + 0.45 \times \varepsilon]}{1 + \exp [0.8892 - 0.6319 \times 10^{-3} \times T - 3.295 \times 10^{-6} \times T^2 + 0.45 \times \varepsilon]} \quad (9.35)$$

For calcareous concrete:

$$\frac{f_c}{f_{c,20}} = \frac{1.3 \times \exp [1.142 - 0.0840 \times 10^{-3} \times T - 3.735 \times 10^{-6} \times T^2 + 0.57 \times \varepsilon]}{1 + \exp [1.142 - 0.0840 \times 10^{-3} \times T - 3.735 \times 10^{-6} \times T^2 + 0.57 \times \varepsilon]} \quad (9.36)$$

Qureshi et al. [53] utilized the developed models from two approaches and evaluated probability of failure of reinforced concrete column sections under axial load. It was confirmed that the two models provide similar distribution of failure time and the results are not critically sensitive to the model choice.

## 9.4.2 Steel

For structural steel elements, the primary uncertainties of interest are the material properties and the variability in section profile. The former is discussed within this section, while the latter, as discussed before, carries less uncertainty compared to other random variables involved at elevated temperatures.

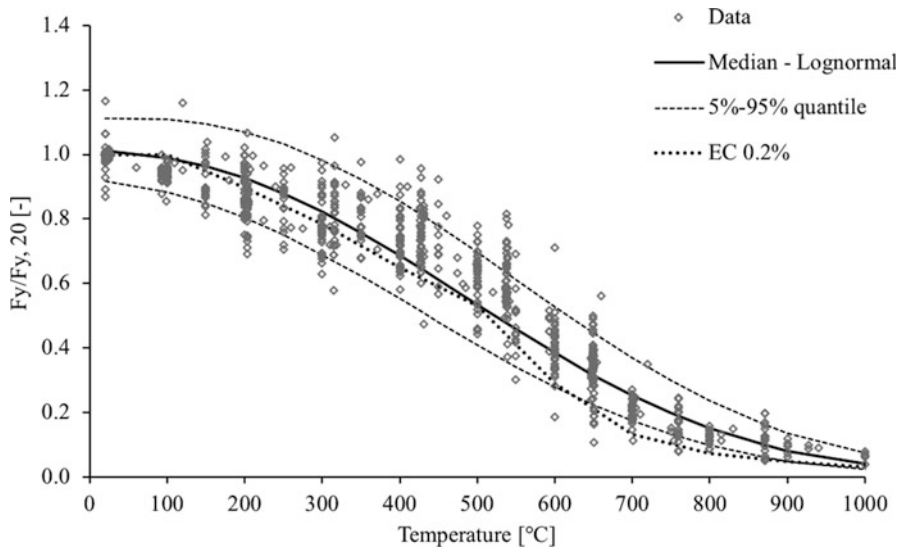
Elhami Khorasani et al. [55], Stephani et al. [56], and Qureshi et al. [53] presented a review of yield strength retention factors and discussed different probabilistic models for this parameter. The data set for the yield strength of steel used in the three studies was based on the data collected by the National Institute of Standards and Technology (NIST) [57]. The NIST study considered the sensitivity of stress-strain behaviour of structural steel to strain rate. Therefore, the data only include tests conducted with a strain rate that comply with the allowed strain rate in testing standards.

Steel yield strength at ambient temperature is typically defined as the 0.2% offset. However, the Eurocode (EC) retention factors at elevated temperatures [58] are based on the strength at a strain equal to 2%, which includes strain-hardening effects at lower temperatures. Such an effect is less significant at higher temperatures, where failure of a steel structure is expected to occur. Therefore, the NIST data set and existing studies, as listed above, considered measured data at both 0.2% offset and 2% strain. A total of 764 data points based on the 0.2% offset, covering a temperature range of 20–1038 °C, and 387 data points based on strain at 2% with a temperature range of 20–940 °C, were used to perform statistical analysis and quantify uncertainty of steel yield strength at elevated temperatures.

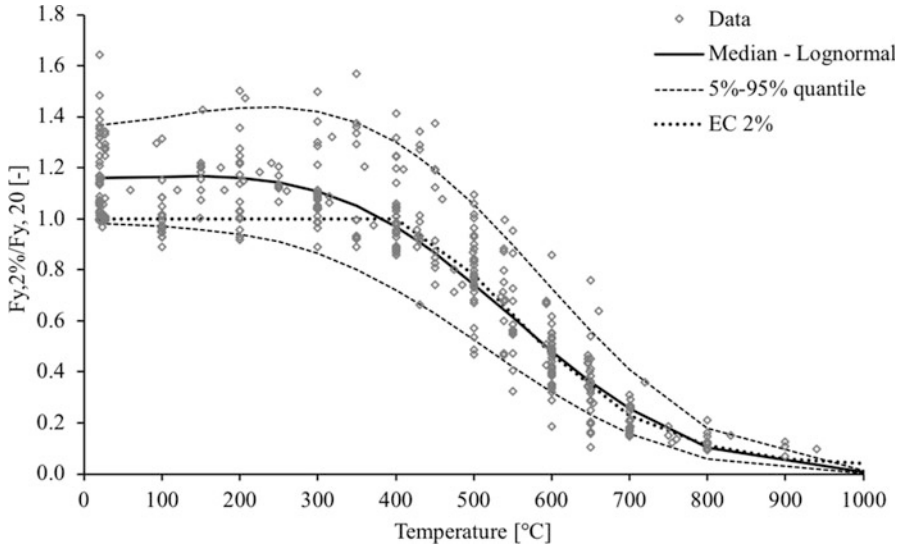
As discussed in the previous section, continuity with reliability appraisals at ambient temperature is important. Holicky and Sykora [41] recommended a

log-normal distribution with mean equal to the characteristic yield strength plus two standard deviations, and COV of 0.07 to quantify uncertainty at ambient temperature. In the collected database, the retention factors were normalized based on the measured yield strength (or average strength in case of multiple measurements) at 20 °C. The majority of data points at 20 °C in the 0.2% data set are close to unity. It is hypothesized that the obtained variability at 20 °C for the 0.2% offset results from very limited intra-batch variability, together with limited inter-batch variability resulting from the different measurement sources. On the other hand, the 2% data set shows a scatter of data at 20 °C, reflecting uncertainty in material performance.

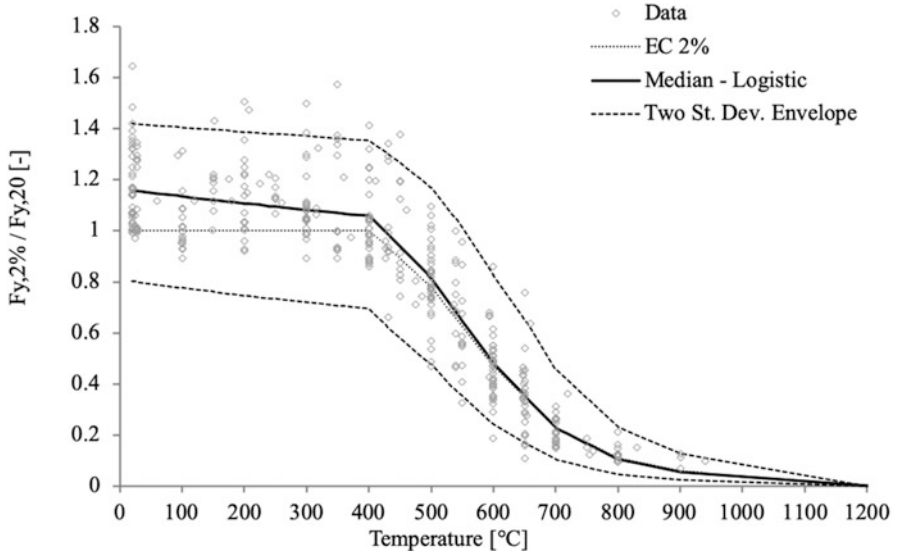
Stephani et al. [56] applied the first approach, based on a series of temperature groups and their histograms (as explained for the case of concrete material in the previous section) on the 0.2% data set. Two different statistical models, namely log-normal and a beta distribution bound by three times the standard deviation on both sides of the mean, were considered with varying means and COVs as a function of temperature. Stephani et al. coupled the proposed models with recommended statistics of steel yield strength at ambient temperature. Qureshi et al. [53] extended the work of Stephani et al. [56] by proposing continuous functions for model parameters varying with temperature where continuity at ambient temperature was also incorporated within the model. Qureshi et al. [53] proposed a log-normal distribution for 0.2% data. Equations (9.37) and (9.38) describe the model parameters; Fig. 9.16 shows the measured data and the model. Qureshi et al. [53] applied the same approach to the 2% data, except in this case the model reflects the scatter in data at 20 °C rather than constraining the model to the recommended distributions for reliability measures at ambient temperature for 0.2% strain offset. Equations



**Fig. 9.16** 0.2% Strain steel yield strength retention factor vs. temperature based on log-normal distribution



**Fig. 9.17** 2% Strain steel yield strength retention factor vs. temperature based on log-normal distribution



**Fig. 9.18** 2% Stain steel yield strength retention factor vs. temperature based on logistic function

(9.39) and (9.40) describe the model parameters, and Fig. 9.17 shows the measured data and the model. In addition, Elhami Khorasani et al. [55] proposed a continuous logistic function for the 2% data. Figure 9.18 and Eq. (9.41) describe the model

where  $T$  is temperature in Celsius,  $k_y, \theta$  is the EC steel retention factor, and  $\varepsilon$  is the standard normal distribution.

Parameters of log-normal distribution for 0.2% data:

$$\mu_{\ln} = -1.45 \times 10^{-9}T^3 - 1.78 \times 10^{-6}T^2 - 2.50 \times 10^{-5}T + 1.19 \times 10^{-2} \quad (9.37)$$

$$\sigma_{\ln} = -1.895 \times 10^{-7}T^2 + 1.15 \times 10^{-4}T + 5.62 \times 10^{-2} \quad (9.38)$$

Parameters of log-normal distribution for 2% data:

$$\mu_{\ln} = -6.89 \times 10^{-9}T^3 + 1.84 \times 10^{-6}T^2 - 8.39 \times 10^{-5}T + 0.148 \quad (9.39)$$

$$\sigma_{\ln} = -2.41 \times 10^{-7}T^2 + 1.07 \times 10^{-4}T + 9.77 \times 10^{-2} \quad (9.40)$$

Logistic function for 2% data:

$$\frac{F_{Y,2\%}}{F_{Y,20}} = \frac{1.7 \times e[r_{\logit} + 0.412 - 0.81 \times 10^{-3} \times T + 0.58 \times 10^{-6} \times T^{1.9} + 0.43 \times \varepsilon]}{1 + e[r_{\logit} + 0.412 - 0.81 \times 10^{-3} \times T + 0.58 \times 10^{-6} \times T^{1.9} + 0.43 \times \varepsilon]} \quad (9.41)$$

$$\text{with } r_{\logit} = \ln \frac{(k_y, \theta + 10^{-6})/1.7}{1 - (k_y, \theta + 10^{-6})/1.7}$$

The models discussed above, when applied to cases of isolated steel column subject to ISO 834 heating, gave comparable distributions of failure temperature for a particular loading condition. The logistic model (derived at 2% strain) implicitly captures the effect of strain hardening at lower temperatures, meaning that the choice of probabilistic model is important for cases where element failure could be expected at low (less than 400 °C) temperatures.

Elhami Khorasani et al. [55] also proposed a logistic function to capture uncertainty in the modulus of elasticity of steel, shown in Fig. 9.19 and Eq. (9.42) where  $T$  is the temperature in Celsius and  $\varepsilon$  is the standard normal distribution. The measured data set is from the National Institute of Standards and Technology (NIST) collected database [57]. The NIST data set can be grouped into three categories based on their measurement method: (1) static, (2) dynamic, and (3) unknown. Elhami Khorasani et al. [55] noted that previous discussions on the measurement method indicated that dynamic testing, in general, results in unconservative predictions of steel modulus. In addition, the analysis of structures under fire is equivalent to static thermal loading, and therefore, the data measured by dynamic testing were disregarded:

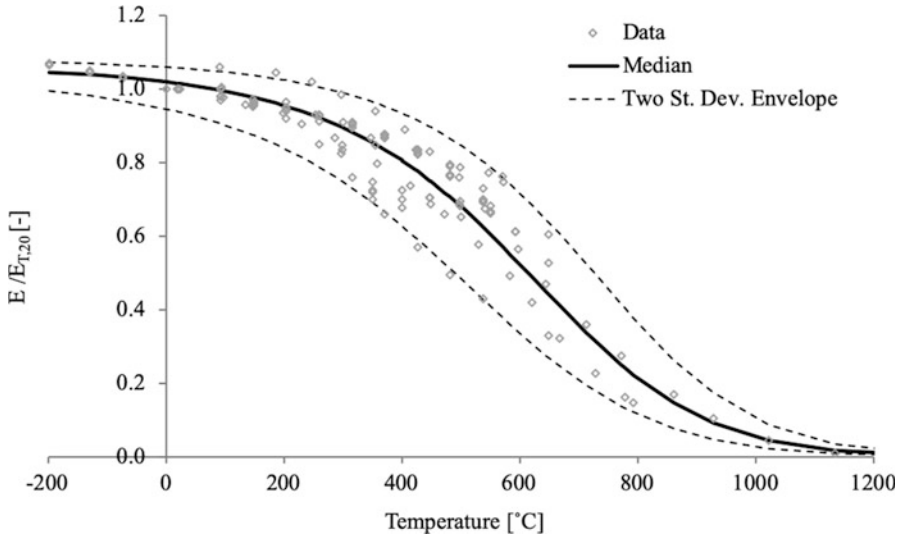


Fig. 9.19 Modulus of elasticity of steel vs. temperature based on logistic function

$$\frac{E}{E_{20}} = \frac{1.1 \times \exp [2.54 - 2.69 \times 10^{-3} \times T - 2.83 \times 10^{-6} \times T^2 + 0.36 \times \varepsilon]}{1 + \exp [2.54 - 2.69 \times 10^{-3} \times T - 2.83 \times 10^{-6} \times T^2 + 0.36 \times \varepsilon]} \tag{9.42}$$

### 9.4.3 Timber

Timber is a graded material with highly variable properties. The material properties can be grouped into reference properties that are considered explicitly, while other properties are only assessed implicitly. Bending strength  $R_m$ , bending modulus of elasticity  $E_m$ , and density  $\rho$  are referred to as the reference material properties. JCSS [16] provides a list of expected values and coefficient of variation of timber properties such as the tension strength parallel or perpendicular to the grain, compression strength parallel or perpendicular to the grain, shear modulus, and shear strength as a function of the reference properties. For European softwood, JCSS [16] specifies a log-normal distribution for bending strength  $R_m$  and bending modulus of elasticity  $E_m$  with COVs of 0.25 and 0.13, respectively, and normal distribution with COV of 0.1 for density  $\rho$ . For glue-laminated timber,  $R_m$  follows a log-normal distribution with COV of 0.15, but  $E_m$  and  $\rho$  have similar distributions as the European softwood. More details can be found in JCSS (2006).

Three methods have been proposed in the literature on how to conduct structural analysis of timber structures at elevated temperatures. Brandon [59] discussed details

of these approaches. One of these methods takes into account the mechanical properties of the material; the other two approaches calculate reduced capacity of a member during fire by reducing the cross section of the element as a function of the char layer. Charring rate is one of the basic quantities of assessment of fire resistance of wooden structural members. Due to the inherent variabilities and uncertainties involved in the fire exposure and the charring process, the charring rate is a factor with substantial uncertainty, which should be taken into account in any assessment of fire resistance of wooden members, in particular in the probabilistic approaches to assess fire resistance. In addition to the reduced dimensions from charring, the reduced cross-section method requires consideration of reduced material properties in a layer ahead of the char front, where timber has lost some strength due to increased temperature but has not charred. This layer is assumed to have zero strength in calculations.

Lange et al. [60] and Lange et al. [61] conducted a total of 32 full-scale fire tests on glulam timber beams and quantified variation in charring rate  $\beta_{n,par}$  as well as depth of zero-strength layer  $d_0$ . The timber beams were exposed to different fire curves including two parametric fire curves and a standard fire curve. The results show that the charring rate and depth of zero-strength layer depend on the heating rate. Following a similar approach to Annex A of EN 1995-1-2 on defining the notional charring rate under parametric fire exposure  $\beta_{n,par}$ , Lange et al. [61] proposed a normal distribution with mean  $\mu$  and standard deviation  $\sigma$  for  $\beta_{n,par}$  as shown in Eqs. (9.43) and (9.44) where  $\beta_n$  is 0.72,  $O$  is the opening factor, and  $k\rho c$  is the thermal inertia of the compartment lining. The mean  $\mu$  and standard deviation  $\sigma$  of the zero-strength layer depth are calculated as a function of the heating rate,  $\Gamma$ , of the parametric fire, shown in Eqs. (9.45) and (9.46). These equations were originally expressed as a function of the opening factor:

$$\mu(\beta_{n,par}) = 1.5 \times \beta_n \frac{0.2\sqrt{\Gamma} - 0.04}{0.16\sqrt{\Gamma} + 0.08} \quad (9.43)$$

$$\text{with } \Gamma = \frac{(O/\sqrt{k\rho c})^2}{(0.04/1160)^2}.$$

$$\sigma(\beta_{n,par}) = 0.06 \times \frac{0.45\sqrt{\Gamma} - 0.2}{0.16\sqrt{\Gamma} + 0.08} \quad (9.44)$$

$$\mu(d_0) = -0.94 \times \Gamma + 16 \quad (9.45)$$

$$\sigma(d_0) = -0.04 \times \Gamma + 1.07 \quad (9.46)$$



In a separate study, Hietaniemi [62] proposed a model for wood charring rate  $\beta$  (mm/min) exposed to time-dependent incident heat flux  $\dot{q}_e''(t)$ , and as a function of wood density  $\rho$ , wood moisture content  $w$ , and ambient oxygen concentration  $\chi_{o_2}$  as

$$\beta = f(\chi_{o_2, t}) \cdot \frac{C \cdot \dot{q}_e''^p(t)}{(\rho + \rho_0)(A + B + w)} \cdot \exp\left(-\frac{t}{\tau}\right) \quad (9.47)$$

where

$$f(\chi_{o_2, t}) = \xi + (1 - \xi) \cdot \left(\frac{\chi_{o_2}(t)}{\chi_{o_2}^{(0)}}\right)^{0.737}$$

$$\chi_{o_2}^{(0)} = 21\%$$

$$\xi \propto U(0.50; 0.65) \text{ (average} = 0.575)$$

$$A \propto U(505; 1095) \text{ kJ/kg (average} = 800)$$

$$B \propto U(2430; 2550) \text{ kJ/kg (average} = 2490)$$

$$C \propto \Delta(2.72; 5.45; 3.93) \text{ kW/m}^2$$

$$p \propto N(0.50; 0.40)$$

$$\rho_0 \propto N(465; 93) \text{ kg m}^{-3}$$

$$\tau \propto \Delta(90; 110; 100) \text{ min}$$

$$\vartheta \propto \Delta(1.026; 1.387; 1.162) \text{ kW/m}^2$$

In the above formulation,  $N(\mu; \sigma)$  is the normal distribution with mean  $\mu$  and standard deviation  $\sigma$ ;  $\Delta(x_{\min}; x_{\max}; x_{\text{peak}})$  is the triangular distribution with minimum value  $x_{\min}$ , maximum value  $x_{\max}$ , and peak value  $x_{\text{peak}}$ ; and  $U(x_{\min}; x_{\max})$  is the uniform distribution with minimum value  $x_{\min}$  and maximum value  $x_{\max}$ .

## 9.5 Uncertainty Quantification Techniques

The acceptance of a design through consideration of reliability or risk acceptance entails explicitly taking into account the design uncertainties discussed in the above sections. A wide range of techniques for uncertainty quantification exist. Uncertainty quantification techniques can be combined as befits the situation. The methods discussed further are:

1. **Event trees:** An intuitive and computationally inexpensive method for quantifying the probability of scenarios.

2. **Analytical solutions:** Exact uncertainty quantification, but only feasible in specific situations.
3. **Monte Carlo techniques:** Uncertainty quantification based on repeated evaluation of the model, considering random sampling of input parameters. Computationally expensive, but easy to implement. Crude Monte Carlo simulations (MCS) and Latin hypercube sampling (LHS) are discussed.
4. **FORM:** Approximate evaluation of the reliability index associated with a limit state equation. Exact in specific cases. The basis of the partial factors applied for Eurocode design in normal conditions.
5. **Maximum entropy methods:** Methodology for estimating the PDF of a scalar model output variable. The ME-MDRM (MaxEnt) method is introduced as a computationally efficient method in case of a limited number of stochastic variables.
6. **Fragility functions:** Fragility functions are, in their general form, a way of representing known probabilities of exceeding a performance threshold (i.e. limit state) in function of one or more defining variables, i.e. not an uncertainty quantification technique, but a useful way of representing uncertainty. With reference to the earthquake engineering field, the concept is often applied with respect to the probability of different ‘damage states’ being exceeded in function of the magnitude of an ‘intensity measure’.
7. **PEER PBEE:** The Pacific Earthquake Engineering Research Center Performance Based Earthquake Engineering framework, or PEER framework for short, is a well-established methodology for quantifying the uncertainty in decision variables (e.g. damage cost) in function of a hazard specification. The methodology applies fragility functions to move stepwise from intensity measures, over engineering demand parameters and damage states, to the decision variables. The framework thus requires uncertainty data (fragility functions) as input, and provides a framework for aggregating these basic uncertainties.

The discussion below starts with event trees as this method is the most intuitive and easily understood. Mathematical rigor is introduced later in order not to hamper the intuitive understanding.

### 9.5.1 Event Trees

An event tree is used to explore the probability of different scenarios, starting from a single common *initiating event*, for example fire ignition. The scenarios diverge every time an additional distinction is made between the scenarios, for example [sprinklers control the fire, yes/no], or [fire load density  $q_F \leq 300 \text{ MJ/m}^2$ ,  $300 \text{ MJ/m}^2 < q_F \leq 700 \text{ MJ/m}^2$ , or  $700 \text{ MJ/m}^2 < q_F$ ]. This creates distinct *branches* of the event tree. By considering the probabilities of the differentiating events, the probability of the overall scenario is calculated.

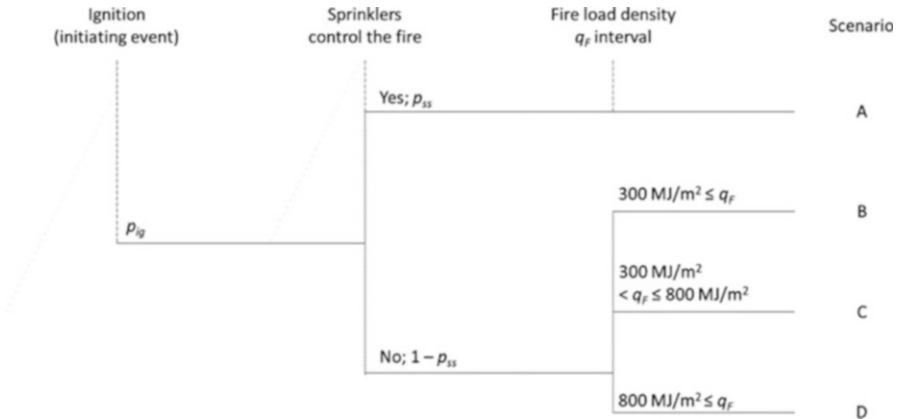
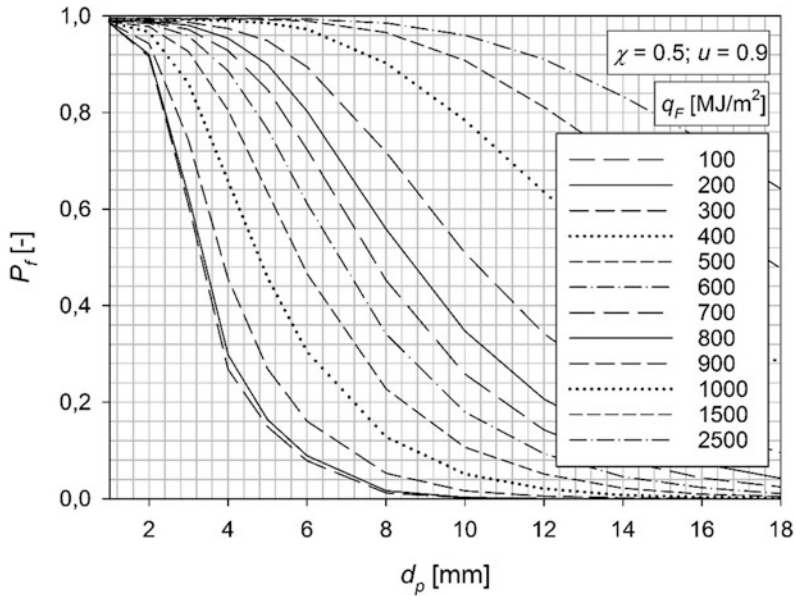


Fig. 9.20 Event tree example

The opposite of an event tree is a *fault tree*, where the different contributions leading to a single *final event* are explored. This approach is most common in fire investigation; see, e.g., Johansson et al. [63].

The application of an event tree is most easily introduced through an example. Consider the event tree of Fig. 9.20, applied to assess the probability of fire-induced failure of a structural element in an office building. Fire-induced failure requires a prior fire ignition, and thus fire ignition has been chosen as the *initiating event*. The probability  $p_{ig}$  of this initiating event can be determined based on fire statistics, expert judgement, or detailed analysis (such as another event tree, or a fault tree). Following the initiating event, the possibility of sprinklers controlling the fire is considered. In case sprinklers control the fire, the steel beam is not in danger of losing its load-bearing capacity (based on analyses or expert judgement). This results in scenario A with a probability of  $p_{ig} \cdot p_{ss}$ , with  $p_{ss}$  being the sprinkler success probability. For this scenario A no further analysis is required, as the beam is not in danger of losing its load-bearing capacity. Sprinkler success probabilities are listed for example in BSI [64]. If sprinklers fail to control the fire, then the ability of the steel beam to maintain its load-bearing capacity till burnout is a function of the fire load density  $q_f$ ; see, e.g., the fragility curves by Hopkin et al. [65] for insulated steel beams (reformatted in Fig. 9.21). Reference is made to the full paper by Hopkin et al. for further details. Based on Fig. 9.21, the failure probability of a steel beam with an intumescent paint thickness  $d_p$  of 12 mm is approximately 0 for fire loads less than 300 MJ/m<sup>2</sup>. Considering the fire load density distribution listed in Table 9.10 in Sect. 9.3.1.2, the probability of actual fire load in the office compartment exceeding 800 MJ/m<sup>2</sup> is approximately 0.01. For this fire load of 800 MJ/m<sup>2</sup> and a  $d_p$  of 12 mm, Fig. 9.21 indicates a failure probability of 0.21. Combining this information in the event tree, three additional scenarios (B, C, and D) are indicated. The probabilities of the respective scenarios have been determined based on the probability density function for the fire load and are listed in Table 9.19, and the constituent probability values are listed in Table 9.20, indicating that—without



**Fig. 9.21** Fragility curves for an insulated steel beam, denoting the probability of structural failure  $P_f$  given a fully developed fire, in function of the intumescent paint thickness  $d_p$ , for different fire load densities  $q_F$

**Table 9.19** Scenario description and probabilities

Scenario	Ignition	Sprinklers control the fire	Fire load density interval	Scenario probability	Steel beam failure probability given scenario
A	$p_{ig}$	Yes: $p_{ss}$	NA	$p_{ig} \cdot p_{ss} = 9.5 \times 10^{-5}$ / year	0
B	$p_{ig}$	No: $1 - p_{ss}$	$q_F \leq 300 \text{ MJ/m}^2$	$p_{ig} \cdot (1 - p_{ss})$ $p_{qF1} = 7.5 \times 10^{-7}$ / year	0
C	$p_{ig}$	No: $1 - p_{ss}$	$300 \text{ MJ/m}^2 \leq q_F \leq 800 \text{ MJ/m}^2$	$p_{ig} \cdot (1 - p_{ss})$ $p_{qF2} = 4.2 \times 10^{-6}$ / year	<0.21
D	$p_{ig}$	No: $1 - p_{ss}$	$800 \text{ MJ/m}^2 \leq q_F$	$p_{ig} \cdot (1 - p_{ss})$ $p_{qF3} = 5 \times 10^{-8}$ / year	<1
Upper bound annual probability fire-induced structural failure				$9.3 \times 10^{-7}$ / year	

further evaluation of scenario C—the annual probability of fire-induced failure is smaller than  $9.3 \times 10^{-7}$ /year. As stated in Sect. 9.2.3.2, the maximum failure probability postulated through the Natural Fire Safety Concept is, in case of no evacuation,  $1.3 \times 10^{-6}$ /year. The event tree analysis (using information from the

**Table 9.20** Probabilities of differentiating events

Symbol	Event	Probability
$p_{ig}$	Fire ignition	$10^{-4}/\text{year}$
$p_{ss}$	Sprinklers control the fire	0.95
$p_{qF}$	Fire load density in range:	<sup>a</sup>
	$q_F \leq 300 \text{ MJ/m}^2$	0.15
	$300 \text{ MJ/m}^2 \leq q_F \leq 800 \text{ MJ/m}^2$	0.84
	$800 \text{ MJ/m}^2 \leq q_F$	0.01

<sup>a</sup>Probabilities calculated considering a Gumbel distribution with a coefficient of variation of 0.3, and mean (nominal) value of  $420 \text{ MJ/m}^2$ ; see Sect. 9.3.1.2

fragility curve of Fig. 9.21) thus indicates that a design with  $d_p = 12 \text{ mm}$  would fulfil this requirement.

An event tree thus allows to pinpoint whether the design or specific situations may need to be considered in further detail. In the example above, a simple analysis was sufficient. While intuitive and easy to use, the creation of an event tree should be done with care. Special consideration should be given to:

- The choice of differentiating events: there is no use in adding distinctions which do not influence the outcome (design decision).
- Probabilities of the differentiating events: these can be evaluated based on statistical data, expert judgement, or a separate uncertainty quantification exercise.
- The probabilities of the differentiating events are conditional probabilities: these probabilities are conditional on the preceding differentiating events. For example, when considering the event [occupants suppress the fire, yes/no], *after* the event [sprinklers fail to suppress the fire], in general different probabilities will apply then when considering [occupants suppress the fire, yes/no] *before* [sprinklers fail to suppress the fire]. In the former situation, the probability of the occupants suppressing the fire will be lower, taking into account that the fire is—for example because of its excessive growth rate—not successfully suppressed by sprinklers.

### 9.5.2 Analytical Solutions

In specific situations uncertainty quantification can be done through closed-form solutions. Consider Eq. (9.48) where  $Y$  is the uncertain response of interest,  $X$  the vector of stochastic input variables  $X_i$ , and  $h$  the modelled relationship. The probability of failure  $P_f$  is then given by the probability of  $Y$  being in the failure domain  $\Omega_f$ , i.e. Eq. (9.49), with  $f_y$  the probability density function (PDF) of  $Y$ :

$$Y = h(X) \quad (9.48)$$

$$P_f = \int_{\Omega_f} f_y(y) dy \quad (9.49)$$

If  $Y$  is a linear combination of independent variables  $X_i$ , i.e. Eq. (9.50), with  $a_i$  coefficients, then the mean value of  $Y$  is given by Eq. (9.51) and its standard deviation by Eq. (9.52). Furthermore, if all  $X_i$  are normally distributed, then  $Y$  is normally distributed as well. This follows from the central limit theorem:

$$Y = \sum_i a_i X_i \quad (9.50)$$

$$\mu_Y = \sum_i a_i \mu_{X_i} \quad (9.51)$$

$$\sigma_Y = \sqrt{\sum_i a_i^2 \sigma_{X_i}^2} \quad (9.52)$$

Similarly, if  $Y$  is a multiplicative combination, i.e. Eq. (9.53), with  $a_i$  exponents, of independent log-normally distributed variables  $X_i$  with parameters  $\mu_{\ln X_i}$  and  $\sigma_{\ln X_i}$  as specified by Eqs. (9.54) and (9.55), then  $Y$  is also log-normally distributed with parameters given by Eqs. (9.56) and (9.57):

$$Y = \prod_i X_i^{a_i} \quad (9.53)$$

$$\mu_{\ln X_i} = \ln(\mu_{X_i}) - \frac{1}{2} \sigma_{\ln X_i}^2 \quad (9.54)$$

$$\sigma_{\ln X_i} = \sqrt{\ln\left(1 + \frac{\sigma_{X_i}^2}{\mu_{X_i}^2}\right)} \quad (9.55)$$

$$\mu_{\ln Y} = \sum_i a_i \mu_{\ln X_i} \quad (9.56)$$

$$\sigma_{\ln Y} = \sqrt{\sum_i a_i^2 \sigma_{\ln X_i}^2} \quad (9.57)$$

The cases of the normal and log-normal distribution of  $Y$  are only two examples out of a wide set of situations for which closed-form solutions exist. The cases above are however the most common.

In cases where  $Y$  relates to an outcome defining the failure of the structure, Eq. (9.49) is to be evaluated. Here  $\Omega_f$  can relate to a fixed limit value (*performance criterion*). For example, when  $Y$  represents the standard fire resistance of a structural

element  $t_R$ , and the failure domain is given by a fixed (equivalent) standard fire duration  $t_E$ , then Eq. (9.49) can be specified to

$$P_f = P[t_R \leq t_E] = \int_0^{t_E} f_{t_R}(t_R) dt_R \quad (9.58)$$

If  $t_R$  is described by a normal distribution, Eq. (9.58) is directly evaluated as Eq. (9.59), with  $\Phi$  the standard cumulative normal distribution function, available in common spreadsheet tools. When  $t_R$  is described by a log-normal distribution, Eq. (9.60) applies. Note that a normally distributed  $t_R$  has a non-zero probability of being negative. When this probability is not negligible, care should be taken with using a normal distribution to describe strictly positive variables:

$$P_f = \Phi\left(\frac{t_E - \mu_{tR}}{\sigma_{tR}}\right) \quad (9.59)$$

$$P_f = \Phi\left(\frac{\ln(t_E) - \mu_{\ln tR}}{\sigma_{\ln tR}}\right) \quad (9.60)$$

Alternatively,  $Y$  can relate to the value of the limit state function as defined in Sect. 9.2.2, and  $\Omega_f$  then corresponds with the limit state being negative. In these situations where  $Y$  represents the limit state,  $P_f$  is given by Eq. (9.61). For  $Y$  described by a normal distribution this specifies to Eq. (9.62). Considering the definition of the reliability index  $\beta$  specified in Eq. (9.8), the ratio  $\mu_Y/\sigma_Y$  directly corresponds with the reliability index. A log-normal distribution on the other hand is strictly positive, and is thus inappropriate for modelling the realization of a limit state function (with failure defined by the limit state being negative):

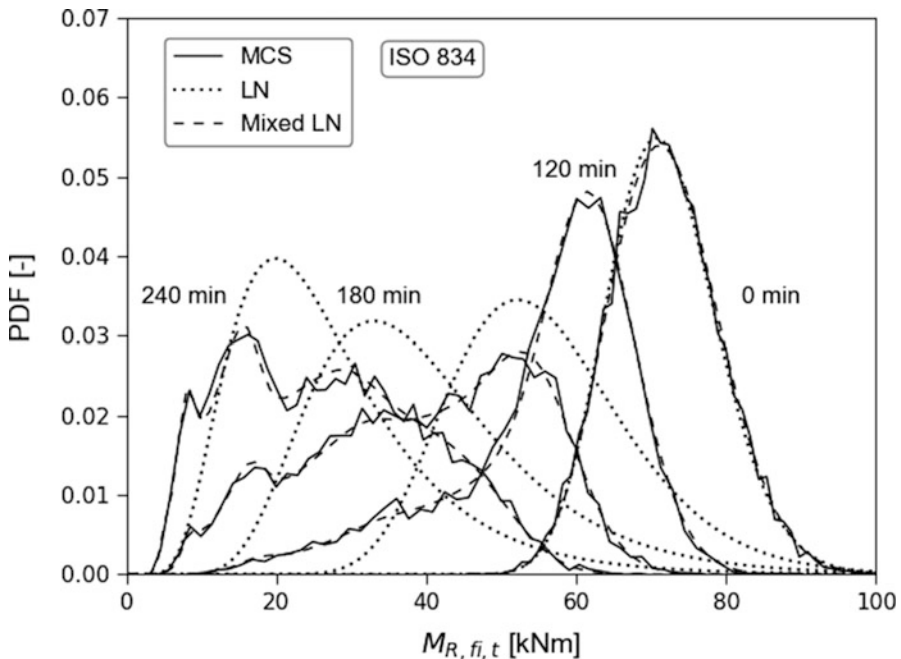
$$P_f = \int_{-\infty}^0 f_Y(y) dy \quad (9.61)$$

$$P_f = \Phi\left(-\frac{\mu_Y}{\sigma_Y}\right) = \Phi(-\beta) \quad (9.62)$$

### 9.5.3 Monte Carlo Techniques

Monte Carlo techniques rely on repeated evaluation of the model for different values (*realizations*) of the input variables. Whereas analytical solutions are feasible in only a limited number of cases, Monte Carlo techniques are generally applicable to any problem. Their drawback is the computational expense of the repeated evaluations, making these techniques infeasible for computationally demanding models.

The resolution of the obtained results in function of the number of model evaluations  $N$  is governed by the input variables' sampling scheme. The most simple sampling scheme is known as crude Monte Carlo simulations (abbreviated MCS), and considers a pure random sampling of the input space [66]. Thus, each model run results in a single random realization of the output variable  $Y$ . The obtained MCS realizations can be visualized in a histogram, revealing the shape of the PDF describing  $Y$ . If sufficient simulations are made (technically if  $N \rightarrow \infty$ ), the full PDF will be perfectly approximated. As an example, Fig. 9.22 represents the histogram obtained from  $10^4$  MCS of the bending moment capacity  $M_{R,fi,t}$  of a concrete slab considering ISO 834 standard fire exposure, as well as log-normal and mixed log-normal approximations. As indicated by the graph, assuming a



**Fig. 9.22** Observed distribution density (MCS,  $10^4$  realizations), log-normal approximation (LN), and mixed log-normal approximation (mixed LN), for concrete slab considering ISO 834 standard fire exposure



specific PDF shape may not always be appropriate. Further details are given in the application example in Sect. 9.6.2.

MCS can also be used to directly evaluate the failure probability, i.e. Eq. (9.49). Every random realization which contributes to failure adds to the count of the number of observed failures  $N_f$ . The estimate of the failure probability is then given by

$$P_f \triangleq \frac{N_f}{N} \quad (9.63)$$

The estimate of  $P_f$  will only be reliable in case sufficient MCS are performed (i.e.  $N$  sufficiently large). This can be clearly observed in Fig. 9.32 further, where the estimated  $P_f$  in function of  $N$  is visualized for the fire-exposed concrete slab. As the repeated observation of failure/no failure results in a binomial distribution, the coefficient of variation of  $P_f$  is given by Eq. (9.64). The coefficient of variation indicates the relative uncertainty in the estimate of  $P_f$  (explicitly: the ratio between the standard deviation and the expected value). In order to obtain meaningful results,  $V_{P_f}$  should be limited to  $V_{lim}$ , e.g. 0.10. This results in the guideline of Eq. (9.65) for the required number of MCS realizations  $N$ . For a failure probability of  $10^{-3}$ , Eq. (9.65) thus recommends  $10^5$  MCS realizations. Note that the number of samples does not depend on the number of random input variables:

$$V_{P_f} = \sqrt{\frac{(1 - P_f)}{P_f N}} \leq V_{lim} \quad (9.64)$$

$$N \geq \frac{(1 - P_f)}{P_f V_{lim}^2} \quad (9.65)$$

A widely used alternative sampling scheme is known as Latin hypercube sampling, or LHS [67]. Whereas in MCS the sampling is done randomly for all input variables, the LHS scheme ensures a balanced sampling across the full input space. Thus, reliable estimates for the moments or distribution parameters of  $Y$  (e.g.  $\mu_Y$  and  $\sigma_Y$ ) can be obtained with a limited number of samples (order of magnitude: 50–200). When using LHS to estimate the output parameters, the evaluation of  $P_f$  through Eq. (9.49) will necessarily rely on an assumed shape of the PDF (e.g. normal, or log-normal). Such an assumption of the distribution type of  $Y$  introduces a bias in the assessment. LHS can however also be applied with a high number of model evaluations, in which case the distinction with MCS diminishes. When using a low number of samples in the LHS scheme, spurious correlation may be introduced (i.e. the sampling scheme may exhibit unintended correlation between the input variables). The sampling scheme can be corrected for the spurious correlation, using the procedure described in, e.g., Olsson et al. [67]. Further information on sampling schemes can be found, e.g., in Bucher [66].

### 9.5.4 FORM

The first-order reliability method introduced by Hasofer and Lind [68], better known as ‘FORM’, provides an efficient way of calculating (failure) probabilities associated with a limit state. The method relies on a linearization of the limit state in standard Gaussian space at the ‘expansion point’  $u^*$  Bucher [66]. This is the point on the limit state where linearization maximizes the probability density mass in the failure domain. Equivalently, this is the point on the limit state which is closest to the origin in the standard Gaussian space (for standard situations where the realization with mean values is not in the failure domain) [68], and thus the point on the limit state with the highest probability density. The reliability index is then given by the distance from this expansion point to the origin. In case the limit state is linear in the standard Gaussian space, and the stochastic variables are independent and normally distributed, the FORM assessment of the failure probability is exact. For non-linear limit states, the linearization introduces an approximation. For stochastic variables  $X$  described by an arbitrary distribution function, a transformation to a standard Gaussian variable  $U$  is required, introducing further approximations. The variable realization  $x^*$  associated with the ‘expansion point’  $u^*$  is called the ‘design point’. This is often referred to as the most probable failure point.

FORM analyses underlie the reliability formats of the Eurocode, see the Appendices of EN 1990 [15], and have been implemented in many readily available software tools. The method is appreciated for its calculation efficiency and its repeatability. The fact that the FORM assessment is invariant to the formulation of the limit state is now taken for granted, but was a major consideration at its introduction [68].

To introduce FORM, and its underlying assumptions and limitations, reference cases with increasing complexity are given in the following. For brevity, the space of the stochastic variables will be denoted the  $X$ -space, and  $U$ -space refers to the standard Gaussian space of the transformed variables.

#### 9.5.4.1 Single Normally Distributed Variable and Failure Criterion of a Deterministic Limiting Value

In the discussion on analytical solutions above, the example was given of a prescribed (deterministic) standard fire duration  $t_E$  and a normally distributed fire resistance time  $t_R$ , with mean  $\mu_{tR}$  and standard deviation  $\sigma_{tR}$ . For a failure criterion specified as  $t_R \leq t_E$ , i.e. a limit state  $Z = t_R - t_E$ , the failure probability  $P_f$  was readily calculated by Eq. (9.59). A graphical representation in the domain of the stochastic fire resistance  $t_R$  is given in Fig. 9.23a, for  $\mu_{tR} = 40$  min,  $\sigma_{tR} = 5$  min, and  $t_E = 30$  min. In this figure, the shaded area corresponds with the failure probability  $P_f$ .

The same assessment can be performed in the  $U$ -space. The transformation of  $t_R$  to its equivalent  $u_{tR}$  in  $U$ -space is given by Eq. (9.66). The limit state equation can be transformed accordingly as shown in Eq. (9.67), and the failure probability is then

given by Eq. (9.68). The expansion point on the limit state ( $Z = 0$ ) is readily determined as Eq. (9.69). Figure 9.23(b) visualizes this point as well as the failure probability in the  $U$ -space. As stated in the general description of FORM above, the distance between the origin and the expansion point now corresponds with the reliability index  $\beta$ . For the considered case,  $\beta$  thus equals 2; see Fig. 9.23 (b) and Eq. (9.70). Taking into account the definition of the reliability index as listed in Eqs. (9.8) and (9.71) holds, demonstrating that the result obtained in accordance with the FORM description is exactly the same as listed in 9.5.2 as an analytical solution. For the values listed above, the failure probability is approximately 0.023; see also Fig. 9.7 for the relationship between  $\beta$  and  $P_f$ :

$$u_{tR} = \frac{t_R - \mu_{tR}}{\sigma_{tR}} \tag{9.66}$$

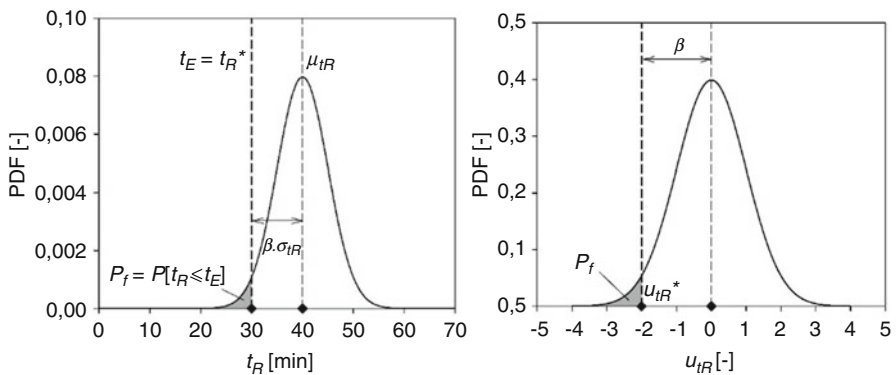
$$Z = t_R - t_E = \mu_{tR} + u_{tR}\sigma_{tR} - t_E \tag{9.67}$$

$$P_f = P[Z < 0] = P\left[u_{tR} < \frac{t_E - \mu_{tR}}{\sigma_{tR}}\right] \tag{9.68}$$

$$u_{tR}^* = \frac{t_E - \mu_{tR}}{\sigma_{tR}} \tag{9.69}$$

$$\beta = |u_{tR}^*| = \left| \frac{t_E - \mu_{tR}}{\sigma_{tR}} \right| = \left| \frac{30 - 40}{5} \right| = 2 \tag{9.70}$$

$$P_f = \Phi(-\beta) = \Phi\left(-\left| \frac{t_E - \mu_{tR}}{\sigma_{tR}} \right|\right) = \Phi\left(\frac{t_E - \mu_{tR}}{\sigma_{tR}}\right) = 0.023 \tag{9.71}$$



**Fig. 9.23** (left) Failure probability and design point in the X-space; (right) failure probability and expansion point in the U-space

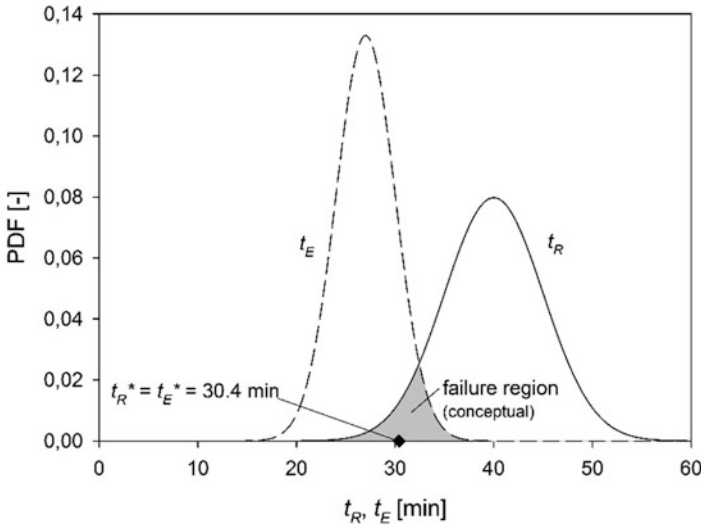
**9.5.4.2 Linear Limit State Equation with Two Normally Distributed Variables**

Expanding the previous example, also the (equivalent) standard fire duration  $t_E$  is now considered stochastic, with a mean value of 27 min and a standard deviation of 3 min. Both probability density functions and (in this case, a conceptual visualization of) failure probability are illustrated in Fig. 9.24, as well as the design point values  $t_R^*$  and  $t_E^*$  as determined below. Taking into account 9.5.2, the limit state output variable  $Z$  is also described by a normal distribution with mean and standard deviation as specified in Eq. (9.72). The failure probability is thus given by Eq. (9.73) and equals 0.013 for this specific example case. Considering the definition of the reliability index,  $\beta$  equals 2.23:

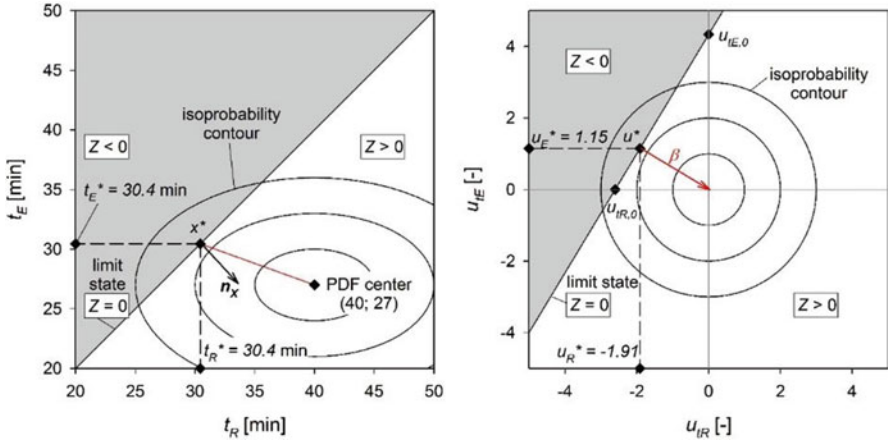
$$\mu_Z = \mu_{tR} - \mu_{tE}; \sigma_Z = \sqrt{\sigma_{tR}^2 + \sigma_{tE}^2} \tag{9.72}$$

$$P_f = P[Z < 0] = \Phi\left(\frac{-\mu_Z}{\sigma_Z}\right) = \Phi\left(-\frac{\mu_{tR} - \mu_{tE}}{\sqrt{\sigma_{tR}^2 + \sigma_{tE}^2}}\right) = \Phi(-2.23) = 0.013 \tag{9.73}$$

The joint probability density function of  $t_R$  and  $t_E$  can be visualized more comprehensively alongside the limit state in a two-dimensional graph (Fig. 9.25 (a)). Note that the different standard deviations of  $t_R$  and  $t_E$  result in an ellipsoid joint PDF in the X-space. The grey zone indicates the failure domain, and integration of the joint PDF over this failure domain is the definition of  $P_f$ . Following the



**Fig. 9.24** Probability density function (PDF) of  $t_R$  and  $t_E$ , and indication of the region associated with failure



**Fig. 9.25** (left) Isoprobability contours, limit state, and design point in the X-space; (right) isoprobability contours, limit state, and expansion point in the U-space

specifications by Hasofer and Lind (see above), both variables as well as the limit state can also be visualized in Gaussian space; see Fig. 9.25(b). The variables  $u_{tR}$  and  $u_{tE}$  are given by Eq. (9.74), while the limit state equation is specified to Eq. (9.75). Contrary to the formulation in the X-space, the considered limit state does not go through the origin in the U-space; it is however still a linear limit state (considering a linear transformation of the variables  $t_R$  and  $t_E$ ). Note that the isoprobability contours of the joint PDF are concentric circles around the origin in the U-space.

From geometric considerations, the expansion point  $u^*$  is readily determined. Consider, for example, that the point  $p$  on a line  $a \cdot x + b \cdot y + c = 0$  closest to the origin (in x-y-coordinate space) has coordinates as specified in Eq. (9.76). Applied to the limit state of Eq. (9.75) in the U-space, this results in the expansion point coordinates of Eq. (9.77), as visualized in Fig. 9.25(b). Alternative procedures can be thought of, for example using trigonometric considerations. The line connecting the expansion point to the origin is—by the definition of distance—perpendicular to the limit state. The distance from the identified expansion point to the origin is equal to  $\sqrt{1.91^2 + 1.15^2} = 2.23$ , demonstrating that the distance from the expansion point to the origin indeed equals the reliability index  $\beta$  as calculated above from analytical considerations. Using trigonometry, it can be shown that the axis through the origin and the expansion point is the axis  $u_Z$ , i.e. the standard Gaussian transformation of the limit state variable  $Z$ . In that case, the one-dimensional case demonstrated above applies, thus proving that the distance between the expansion point and the origin indeed equals the reliability index in this 2D case; see Eq. (9.78). Using the inverse of Eq. (9.74), the design point  $x^*$  in X-space is calculated and visualized in Fig. 9.25(a). The direction  $n_x$  perpendicular to the limit state is also visualized. Note that in the X-space the line connecting the design point to the centre of the joint PDF is not perpendicular to the limit state:

$$u_{tR} = \frac{t_R - \mu_{tR}}{\sigma_{tR}}; u_{tE} = \frac{t_E - \mu_{tE}}{\sigma_{tE}} \quad (9.74)$$

$$Z = t_R - t_E = \sigma_{tR}u_{tR} + (-\sigma_{tE})u_{tE} + (\mu_{tR} - \mu_{tE}) \quad (9.75)$$

$$x_p = \frac{-ac}{a^2 + b^2}; y_p = \frac{-bc}{a^2 + b^2} \quad (9.76)$$

$$u_{tR}^* = \frac{-\sigma_{tR}(\mu_{tR} - \mu_{tE})}{\sigma_{tR}^2 + \sigma_{tE}^2} = -1.91; u_{tE}^* = \frac{\sigma_{tE}(\mu_{tR} - \mu_{tE})}{\sigma_{tR}^2 + \sigma_{tE}^2} = 1.15 \quad (9.77)$$

$$\begin{aligned} P_f &= P[Z < 0] = P[u_Z \sigma_Z + \mu_Z < 0] = P\left[u_Z < -\frac{\mu_Z}{\sigma_Z}\right] = \Phi\left(-\frac{\mu_Z}{\sigma_Z}\right) \\ &= \Phi(-\beta) \end{aligned} \quad (9.78)$$

The above demonstrates how in the U-space the distance between the origin and the (linear) limit state equation corresponds with the reliability index  $\beta$  in case of normally distributed variables. A FORM calculation procedure has, however, not yet been introduced. To this end, observe that:

- (i) The expansion point  $u^*$  is by definition situated on the limit state ( $Z = 0$ ).
- (ii) The vector connecting the expansion point to the origin is by definition perpendicular to the limit state (as  $u^*$  is the point on the limit state closest to the origin). This vector is further denoted as  $\beta$ . The direction of  $\beta$  is specified by the vector  $N_U$  of Eq. (9.79), which results in the normalized directional vector  $n_U$  of Eq. (9.80). For both these equations, the last equality is an application for the considered case  $Z = t_R - t_E$  only. The vector  $n_U$  is the unit vector perpendicular to the limit state, facing outward from the failure region. The components of  $n_U$  are the directional cosines of  $\beta$  and are commonly referred to as the ‘sensitivity factors’  $\alpha_{X_i}$  as they indicate the relative importance of the variability of the underlying variable  $X_i$  in the result for  $\beta$ . For resistance variables, the sensitivity factor is positive, while for load variables the sensitivity factor is negative.
- (iii) The length of  $\beta$  is equal to the reliability index  $\beta$ , as specified by Hasofer and Lind:

$$N_U = \begin{bmatrix} \frac{\partial Z}{\partial u_{tR}} \\ \frac{\partial Z}{\partial u_{tE}} \end{bmatrix} = \begin{bmatrix} \sigma_{tR} \\ -\sigma_{tE} \end{bmatrix} \quad (9.79)$$

$$\mathbf{n}_U = \frac{\mathbf{N}_U}{|\mathbf{N}_U|} = \begin{bmatrix} \alpha_{tR} \\ \alpha_{tE} \end{bmatrix} = \begin{bmatrix} \frac{\sigma_{tR}}{\sqrt{\sigma_{tR}^2 + \sigma_{tE}^2}} \\ -\frac{\sigma_E}{\sqrt{\sigma_{tR}^2 + \sigma_{tE}^2}} \end{bmatrix} \quad (9.80)$$

Considering the above, the vector  $\beta$  is given by  $\beta \cdot \mathbf{n}_u$  and thus the expansion point  $\mathbf{u}^*$  is defined by

$$\mathbf{u}^* = \begin{bmatrix} u_{tR}^* \\ u_{tE}^* \end{bmatrix} = -\beta \cdot \mathbf{n}_U = \begin{bmatrix} -\beta \alpha_{tR} \\ -\beta \alpha_{tE} \end{bmatrix} \quad (9.81)$$

The above allows to specify the following calculation procedure for a general linear limit state of Gaussian variables (can be readily generalized to higher dimensions):

1. Determine the unit vector normal to the limit state  $\mathbf{n}_U$ , i.e. through (the multidimensional equivalent of) Eqs. (9.79) and (9.80).
2. Specify the expansion point  $\mathbf{u}^*$  as  $-\beta \cdot \mathbf{n}_U$ .
3. Substitute  $\mathbf{u}^*$  in the limit state function  $Z$ . As  $\mathbf{u}^*$  is by definition located on the limit state  $Z = 0$ , this results in a linear equation which can be solved for  $\beta$ .

Applying the above for the example case  $Z = t_R - t_E$ ,  $\mathbf{n}_U$  has already been listed above in Eq. (9.80), resulting in the expansion point of Eq. (9.82). Substituting  $u_{tR}^*$  and  $u_{tE}^*$  in Eq. (9.75) gives Eq. (9.83), which is readily simplified to Eq. (9.84), resulting in the same equation for  $\beta$  as derived from analytical considerations in Eq. (9.73):

$$\mathbf{u}^* = \begin{bmatrix} u_{tR}^* \\ u_{tE}^* \end{bmatrix} = \begin{bmatrix} -\beta \frac{\sigma_{tR}}{\sqrt{\sigma_{tR}^2 + \sigma_{tE}^2}} \\ \beta \frac{\sigma_{tE}}{\sqrt{\sigma_{tR}^2 + \sigma_{tE}^2}} \end{bmatrix} \quad (9.82)$$

$$Z(\mathbf{u}^*) = \sigma_{tR} \left( -\beta \frac{\sigma_{tR}}{\sqrt{\sigma_{tR}^2 + \sigma_{tE}^2}} \right) + (-\sigma_{tE}) \beta \frac{\sigma_{tE}}{\sqrt{\sigma_{tR}^2 + \sigma_{tE}^2}} + (\mu_{tR} - \mu_{tE}) = 0 \quad (9.83)$$

$$\beta = \frac{\mu_{tR} - \mu_{tE}}{\frac{\sigma_{tR}^2}{\sqrt{\sigma_{tR}^2 + \sigma_{tE}^2}} + \frac{\sigma_{tE}^2}{\sqrt{\sigma_{tR}^2 + \sigma_{tE}^2}}} = \frac{\mu_{tR} - \mu_{tE}}{\sqrt{\sigma_{tR}^2 + \sigma_{tE}^2}} = 2.23 \quad (9.84)$$

### 9.5.4.3 Generalized Case of a Non-Linear Limit State

The above FORM evaluation of Eqs. (9.82)–(9.84) is very straightforward thanks to the linearity of the limit state eq.  $Z$ . In case of a non-linear limit state, however, the sensitivity factors  $\alpha_{X_i}$  (i.e. the directional cosines of the unit vector  $\mathbf{n}_U$ ) are not

independent of the parameters  $X_i$ . In other words, the unit normal  $\mathbf{n}_U$  to the failure domain is not constant. Consequently, a set of equations are obtained, constituted by Eq. (9.85) for the sensitivity factors  $\alpha_{X_i}$  as evaluated in the expansion point  $\mathbf{u}^*$  and the limit state equation being zero in the expansion point, i.e. Eq. (9.86). Solving this set of equations gives  $\beta$ . As  $\mathbf{n}_U$  is the normal vector to the limit state at the expansion point, the obtained results correspond with the result for the limit state linearized in the expansion point, and it is thus an approximation of the true failure probability:

$$\alpha_{X_i} = \frac{\frac{\partial Z(\mathbf{u}^*)}{\partial X_i}}{\sqrt{\sum_i \left(\frac{\partial Z(\mathbf{u}^*)}{\partial X_i}\right)^2}} \quad \text{for } i = 1..n \quad (9.85)$$

$$Z(\mathbf{u}^*) = Z(-\beta \cdot \mathbf{n}_U) = 0 \quad (9.86)$$

#### 9.5.4.4 Generalized Case with Non-Gaussian Variables

In case of non-Gaussian variables, the transformation to the standard Gaussian space introduces difficulties. A standard approach is the application of the Rackwitz-Fiessler algorithm [69]. This algorithm transforms the distribution of  $X_i$  into a Gaussian distribution with parameters  $\mu_{X_i}^N$  and  $\sigma_{X_i}^N$  which at the design point has the same PDF and CDF values, i.e. Eqs. (9.87) and (9.88). Adding these equations to the set of equations listed above and solving (iteratively) result in an assessment for the reliability index  $\beta$ :

$$F_{X_i}(x_i^*) = \Phi\left(\frac{x_i^* - \mu_{X_i}^N}{\sigma_{X_i}^N}\right) \quad (9.87)$$

$$f_{X_i}(x_i^*) = \frac{1}{\sigma_{X_i}^N} \phi\left(\frac{x_i^* - \mu_{X_i}^N}{\sigma_{X_i}^N}\right) \quad (9.88)$$

#### 9.5.5 Maximum Entropy, and the MaxEnt Method

The *entropy* associated with a random variable gives a measure of the level of uncertainty associated with it [66]. For completeness, Eq. (9.89) gives the definition of the entropy  $H$  associated with a continuous random variable  $Y$ , with  $\Omega_Y$  being the range in which  $Y$  is defined (e.g. from 0 to  $+\infty$  in case  $Y$  is described by a log-normal distribution); see Papoulis and Pillai [70]:



$$H = - \int_{\Omega_Y} f_Y(y) \ln ( f_Y(y) ) dy \quad (9.89)$$

The larger the entropy defined by Eq. (9.89), the larger the uncertainty associated with  $Y$ . Uncertainty quantification methods based on maximum entropy concepts state that, under constraints posed by available information, the PDF  $f_Y$  which maximizes the entropy is the most appropriate, as it does not introduce any subjective information (i.e. it does not introduce a *bias* and thus results in an *unbiased* estimate for  $f_Y$ ).

Consider a positive variable  $Y$  (such as the load bearing capacity) for which a set of  $m$  distribution moments  $\mu_{\alpha_j}$ ,  $j = 1..m$ , are known. The formulation of  $f_Y$  which maximizes the entropy is given by Novi Inverardi and Tagliani [71]

$$\widehat{f}_Y(y) = \exp \left( -\lambda_0 - \sum_{j=1}^m \lambda_j y^{\alpha_j} \right) \quad (9.90)$$

with  $\alpha_j$  being the exponents specifying the distribution moments;  $\lambda_j$  Lagrange multipliers, for  $j$  from 1 to  $m$ ; and  $\lambda_0$  a normalization factor as specified by Eq. (9.91) which ensures that the integral of the PDF over its domain equals unity. The Lagrange multipliers are determined through the boundary conditions of the known moments  $\mu_{\alpha_j}$ . Evaluating the values of  $\lambda_j$  will often require numerical procedures [66]:

$$\lambda_0 = \ln \left( \int_{\Omega_Y} \exp \left( - \sum_{j=1}^m \lambda_j y^{\alpha_j} \right) dy \right) \quad (9.91)$$

When the distribution moments  $\mu_{\alpha_j}$  are assessed from a data sample through the sample moments  $m_{\alpha_j}$ , as calculated by Eq. (9.92), with  $N$  the number of samples and  $y_k$  the  $k^{th}$  realization, Novi Inverardi and Tagliani [71] demonstrated that the Lagrange multipliers  $\lambda_j$  are equivalently determined by the minimization of Eq. (9.93):

$$m_{\alpha_j} = \frac{1}{N} \sum_{k=1}^N y_k^{\alpha_j} \quad (9.92)$$

$$\min_{\lambda_1.. \lambda_j.. \lambda_m} \left[ \lambda_0 + \sum_{j=1}^m \lambda_j m_{\alpha_j} \right] \quad (9.93)$$

When considering sample moments  $m_{\alpha_j}$ , there is no reason why specific values for the exponent  $\alpha_j$  should be preferred. On the other hand, the fact that estimation errors increase with higher exponents introduces a preference for fractional moments  $\alpha_j \in (0,1)$ . Thus the (fractional) sample moments themselves can be part of the (bounded) optimization, resulting in [71]

$$\min_{\alpha_1 \dots \alpha_j \dots \alpha_m} \left[ \min_{\lambda_1 \dots \lambda_j \dots \lambda_m} \left[ \lambda_0 + \sum_{j=1}^m \lambda_j m_{\alpha_j} \right] \right] \quad (9.94)$$

The procedure above is directly applicable in conjunction with MCS or LHS procedures for the estimation of the sample moments in Eq. (9.92). Note that it is not required to re-evaluate the model as part of the optimization of Eq. (9.94): within the optimization, the model realizations  $y_i$  are a given. Having determined the exponents  $\alpha_j$  and coefficient  $\lambda_j$ , the PDF estimate of Eq. (9.90) allows to make an unbiased extrapolation to low probability quantiles of  $Y$ , consistent with the observed realizations.

Using MCS (or to a lesser degree LHS) for the estimation of the sample moments  $m_{\alpha_j}$ , however, still requires a large number of model evaluations. For situations with the number of uncorrelated stochastic input variables  $n \leq 10$  a more efficient calculation scheme has been presented by Van Coile et al. [72], adapted from the work by Zhang [73]. This methodology is denoted as the MaxEnt method, and relies on two approximations: application of the multiplicative dimensional reduction method (MDRM) and Gaussian interpolation.

The MDRM assumes that the model formulation  $h$  of Eq. (9.48), where  $X$  is a multidimensional vector, can be approximated by the product of one-dimensional functions  $h_i$  which isolate the contribution of the different stochastic variables  $X_i$ :

$$Y = h(X) \approx h_0^{1-n} \prod_{i=1}^n h_i(X_i) \quad (9.95)$$

where the one-dimensional functions are defined by Eq. (9.96), i.e. the model evaluation where all  $n - 1$  remaining stochastic variables are set equal to their median value  $\hat{\mu}$ .  $h_0$  then equals the model evaluation where all stochastic variables equal their median value:

$$h_i(x_i) = h(\hat{\mu}_1, \dots, \hat{\mu}_{i-1}, x_i, \hat{\mu}_{i+1}, \dots, \hat{\mu}_n) \quad (9.96)$$

Under the above assumption, the  $\alpha_j^{\text{th}}$  moment of  $Y$  is approximated by

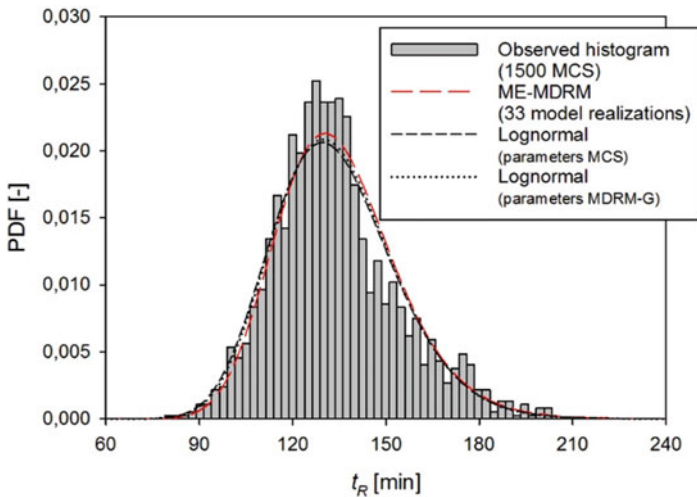
$$\mu_{\alpha_j} \approx h_0^{\alpha_j(1-n)} \prod_{i=1}^n \int_{\Omega_{X_i}} (h_i(x_i))^{\alpha_j} f_{X_i}(x_i) dx_i \tag{9.97}$$

with  $f_{X_i}$  the PDF of  $X_i$ .

Efficiently evaluating the integral of Eq. (9.97) is done through the approximation of Gaussian integration. For each stochastic variable  $X_i$ ,  $L$  Gauss points  $x_{i,l}$  are considered. Together with the associated Gauss weights  $w_l$ , the distribution moment is estimated from the sampled data as

$$\mu_{\alpha_j} \approx h_0^{\alpha_j(1-n)} \prod_{i=1}^n \sum_{l=1}^L w_l h_i(x_{i,l}) \tag{9.98}$$

The obtained estimate for  $m_{\alpha_j}$  can be substituted in the optimization of Eq. (9.94). The above scheme requires  $L$  model realizations per stochastic input variable, as well as one model realization for  $h_0$ . The total number of model realizations is thus limited to  $n \cdot L$ . When  $L$  is odd, one of the Gauss points corresponds with the median value, and thus the number of model realizations is further limited to  $n \cdot (L-1) + 1$ . For a standard scheme with  $L = 5$ ,  $4n + 1$  model realizations are thus required. As long as  $n$  is limited (e.g.  $\leq 10$ ), the total required number of model evaluations will be smaller compared to common alternative sampling schemes such as MCS or LHS. An example application for the fire resistance time of a composite column is visualized in Fig. 9.26. See Gernay et al. [46] for further details and discussion. The approximations introduced by the MDRM and Gaussian interpolation may



**Fig. 9.26** MaxEnt estimate for the fire resistance time of a composite column, together with an MCS validation and log-normal approximations [46]

however introduce errors in the estimate. Further discussion and detailed worked examples are provided by Van Coile et al. [72].

### 9.5.6 Fragility

The fragility of a component or a system is another way of indicating the probability of exceedance of a limit state (i.e. performance threshold). Often this is applied to give a reflection of how likely it is to be in or have exceeded a damage state. It is typically expressed as a cumulative probability distribution, which is dependent on the intensity of some design variable or perturbation. Such curves are widely known as ‘fragility curves’. Seismic fragility, one of the most widely used applications, was first introduced as a concept for the probabilistic assessment of nuclear structures in the energy industry.

Limit states have been introduced in Sect. 9.2.2 and indicate the conditions beyond which the structure no longer fulfils certain criteria for design. Similarly, damage states quantify the damage to components or structures as a result of a perturbation. Damage may take the form of, for example, cosmetic damage, irreversible structural damage, or collapse of the building. They can be considered different from limit states in that they may be related to a description of the physical damage to a component as opposed to a criterion for design verification and therefore are often relatable to the effort required to repair the component and return it to its original state; see Fig. 9.27.

The abbreviation DS is often used to denote damage state. A numerical index associated with the DS may represent consecutively more severe damage states. For example, in earthquake engineering damage state 1 (DS<sub>1</sub>) may represent the smallest amount of damage, and the easiest to repair, requiring only for example taping and repainting of any cracks in the plasterboard. With increasing damage state, the complexity of repair increases. FEMA 273/274/356 defines damage states according to different qualitative performance levels, with DS<sub>1</sub> representing a condition that would not prevent immediate occupancy of a building after an earthquake. DS<sub>2</sub> represents a condition that could represent a risk to life. DS<sub>3</sub> represents a condition whereby the limit state for collapse of the structure is close to being exceeded and the corresponding margin of safety is very low. Often-cited examples of damage states in structural earthquake engineering include damage to beams, columns, or partition walls as a result of inter-storey displacements or internal member forces induced by the perturbation.

Commonly, fragility curves are applied to define the probability of a damage state being exceeded conditional on an intensity measure exceeding a given value associated to the perturbation. For each definition of fragility, the intensity measure, abbreviated IM, is typically one of many possible quantifiable expressions of the intensity of the perturbation. In earthquake engineering, many different intensity measures are used, for example, permanent ground displacement or peak ground

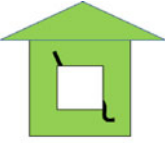



Damage state		Description
	Slight	Small plaster cracks at corners of door and window opening and wall-ceiling intersections; small cracks in masonry chimneys and masonry veneers. Small cracks are assumed to be visible with a maximum width of less than 1/8 inch (cracks wider than 1/8 inch are referred to as “large” cracks).
	Moderate	Large plaster or gypsum board cracks at corners of door and window openings; small diagonal cracks across shear wall panels exhibited by small cracks in stucco and gypsum wall panels; large cracks in brick chimneys.
	Extensive	Large diagonal cracks across shear wall panels or large cracks at plywood joints; permanent lateral movement of floors and roof; toppling of most brick chimneys; cracks in foundations; splitting of wood sill plates and / or slippage of structure over foundations.
	Complete	Structure may have large permanent lateral displacement or be in imminent danger of collapse due to cripple wall failure or failure of the lateral load resisting system; some structures may slip and fall off the foundation; large foundation cracks. Three percent of the total area of buildings with complete damage is expected to be collapsed, on average.

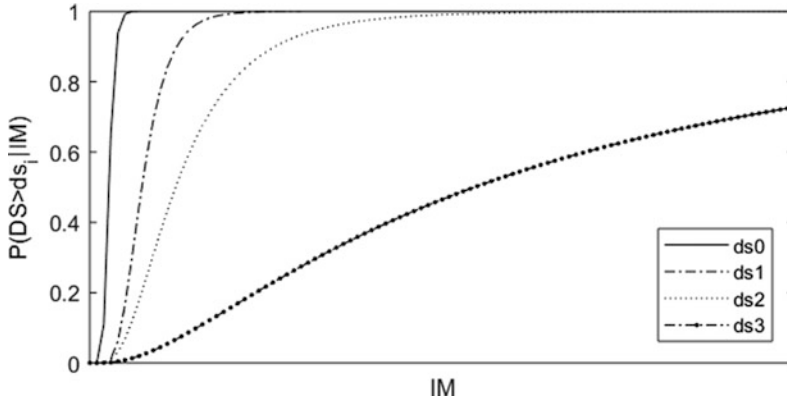
Fig. 9.27 Damage states in earthquake engineering (adapted from [75])

acceleration. The fragility,  $F$ , of a structure representing the probability of exceeding a damage state is thus written as

$$F = P(DS \geq ds_i | IM) \tag{9.99}$$

where  $P(\cdot)$  is the probability operator. An illustrative example of fragility curves for an element with four defined damage states ( $DS_0$ – $DS_4$ ) is shown in Fig. 9.28.

Different classes of methods for creating fragility curves exist [76]. They may be either empirical, i.e. based on observations either from the real world or the lab; analytical, i.e. based on analyses of structural models; or based on expert judgement. The use of fragility curves in structural fire engineering is relatively uncommon, examples including Gernay et al. [77], Van Coile et al. [78], Ioannou et al. [79], and Hopkin et al. [65]. Evaluations for different damage states as in earthquake engineering are however still rare. This can at least partially be attributed to a perceived



**Fig. 9.28** Illustrative example of fragility curves

lack of the required data to generate such curves, and so recent work by Ioannou et al. [80] has relied on the use of expert elicitation, developing fragility curves for concrete exposed to fire. Cooke's method of expert elicitation was used [81], which relies on expert judgement of the results of relatively unknown phenomenon weighted by the same experts' response to a number of questions with known answers, accounting also for their certainty about the answer being given. This study by Ioannou et al. is discussed further in the applications section.

### ***9.5.7 The Pacific Earthquake Engineering Research Center Performance Based Earthquake Engineering Framework***

The PEER (Pacific Earthquake Engineering Research Centre) PBEE (Performance Based Earthquake Engineering) framework has seen application in several different hazards, including fire [82–86]. It is a comprehensive methodology that, in its original application, accounts for seismological, engineering, financial, and societal considerations to the problem of performance-based seismic engineering. The PEER framework disaggregates the problem of linking hazards to decision variables into four models: the hazard model that predicts the intensity measure, the engineering model that predicts the engineering response, the damage model that predicts the damage resulting from the response, and then the loss model that predicts the consequences of that damage from a societal or cost perspective. Each of these models builds upon and is conditional on the previous.

The framework is therefore based across three calculation 'domains': the hazard domain, the structural system domain, and the loss domain. These domains are linked by what may be termed 'pinch variables', against which each of the

subsequent domains is conditioned. The framework is expressed as a triple integral, Eq. (9.100), where intensity measure is denoted as IM; the structural response to the event, the engineering demand parameter, is denoted as EDP; the estimation of damage, the damage measure, is denoted as DM; and resulting losses incurred, decision variable, are denoted as DV. In Eq. (9.100)  $g$  denotes the annual rate of exceeding a given value of one of the pinch variables, and  $P$  denotes the probability of exceeding a given value of one of the pinch variables given a value of the preceding variable:

$$g_{DV} = \iiint \underbrace{P[DV|DM]dP[DM|EDP]}_{\text{Loss Domain}} \underbrace{dP[EDP|IM]}_{\text{Structural System Domain}} \underbrace{dg_{IM}}_{\text{Hazard Domain}} \quad (9.100)$$

Calculation in the hazard domain may be seen as analogous to the development of a ground motion hazard cover as part of a probabilistic seismic hazard analysis (PSHA), with the seismic hazard replaced with a fire hazard, i.e. a PFHA. The output of the PFHA will generally be a single parameter that defines the intensity of the fire and quantifies the rate of exceeding a given value of that intensity, i.e.  $g_{IM} = g(IM > im_i)$  where  $im_i$  is some value of the intensity measure. Extended frameworks which use a combination of intensity measures are however possible, i.e. vector forms of IM exist for earthquake engineering, but are not discussed here in the application to fire engineering.

In PSHA, the intensity measure chosen to represent the hazard is related to the selection of the engineering demand parameter (EDP), with common examples of the former being peak ground acceleration or some spectral response value, and an example of the latter being inter-storey drift. A good selection of the IM will have a strong correlation with the EDP of interest; that is, it will have a high efficiency [87] and therefore the uncertainty of EDP conditional on the IM will be low. Shrivastava et al. [88] explored the efficiency of a range of IMs to structural fire engineering, including maximum fire temperature; time to maximum temperature; the area under the fire curve; the total duration of the fire including cooling phase; and the cumulative incident radiation. They used maximum vertical displacement of an element of structure and showed that cumulative incident radiation was the most efficient IM in this application. Elsewhere, Devaney [82] compared both time to peak compartment temperature and peak compartment temperature as IMs and showed that for the same EDP for an uninsulated composite beam, peak compartment temperature was the most efficient IM.

Ultimately, whichever IM is chosen, the facility definition as well as limitations in either knowledge or model chosen to represent a fire will limit the number of possible scenarios which can occur and which can be modelled. For example, compartment geometry, fuel load composition and total calorific value, possible ventilation conditions, and materials chosen for the compartment boundaries will all influence the dynamics of a fire that can occur in any given volume. These fires could be generated using, e.g., Monte Carlo simulation, as discussed in Sect. 9.5.3, and used to carry out the analysis in the hazard domain.

The analysis in the structural domain requires the generation of records of structural response to a range of different fires that can occur. Additional uncertainties can and should also be incorporated into this analysis, for example, material property uncertainties and geometric uncertainties. As with the hazard analysis, the output from the structural analysis is a probabilistic measure of the response of the structure which will be related to the damage analysis which follows in subsequent stages of the framework. For example, for typical examples of the framework applied to earthquakes, the engineering demand parameter studied is the inter-storey drift and the damage measure evaluated could for example be damage to the non-structural walls. In structural fire engineering, a suitable damage measure could be, e.g., residual deflection. The structural analysis should reflect the response of the structure across the whole vector of the intensity measure.

The engineering demand parameter is expressed as a hazard curve, similar to the intensity measure, which again permits the quantification of the rate of exceedance given the intensity measure hazard curve, i.e.  $g_{EDP} = \int P(EDP > edp_i | IM) dg_{IM}$ .

The calculation in the loss domain requires first the definition of one or more damage states and thus fragilities conditional on the engineering demand parameter. These damage states are denoted  $DS_i$  with  $i$  denoting a specific damage state. For example, three possible damage states may be identified: undamaged ( $DS_0$ ), lightly damaged requiring minor repair work ( $DS_1$ ), and major damage requiring demolition and replacement of the section ( $DS_2$ ).  $P(DM | EDP)$  denotes the probability of a damage measure conditional on the EDP, with the damage measure being the damage states identified.

Finally, the decision variable requires to be conditioned on the damage state. Examples of decision variables include cost to repair or downtime. Devaney in his thesis [82] uses data from the literature to derive cost and downtime distributions for different construction elements damaged by fire. In reference to the damage states identified in the previous paragraph these are shown as normalized against initial construction costs for a beam and for a column in Table 9.21.

The framework is shown schematically in Fig. 9.29. The framework starts with the definition of the facility, including information about its design and location as may be needed for a hazard analysis, and then finishes with a decision-making process where a decision is taken as to whether or not the annual rate of exceedance of one of the decision variables is acceptable.

**Table 9.21** Examples of log-normal distributions of normalized cost consequence functions [82]

	$\mu$	CoV
Monetary cost consequence function, DS1 beam	0.0764	0.414
Monetary cost consequence function, DS2 beam	1.2338	0.694
Monetary cost consequence function, column collapse	1.2918	0.661
Downtime cost consequence function, DS1 beam	1.44	0.2
Downtime cost consequence function, DS2 beam	4.63	0.2
Downtime cost consequence function, column collapse	5.63	0.2



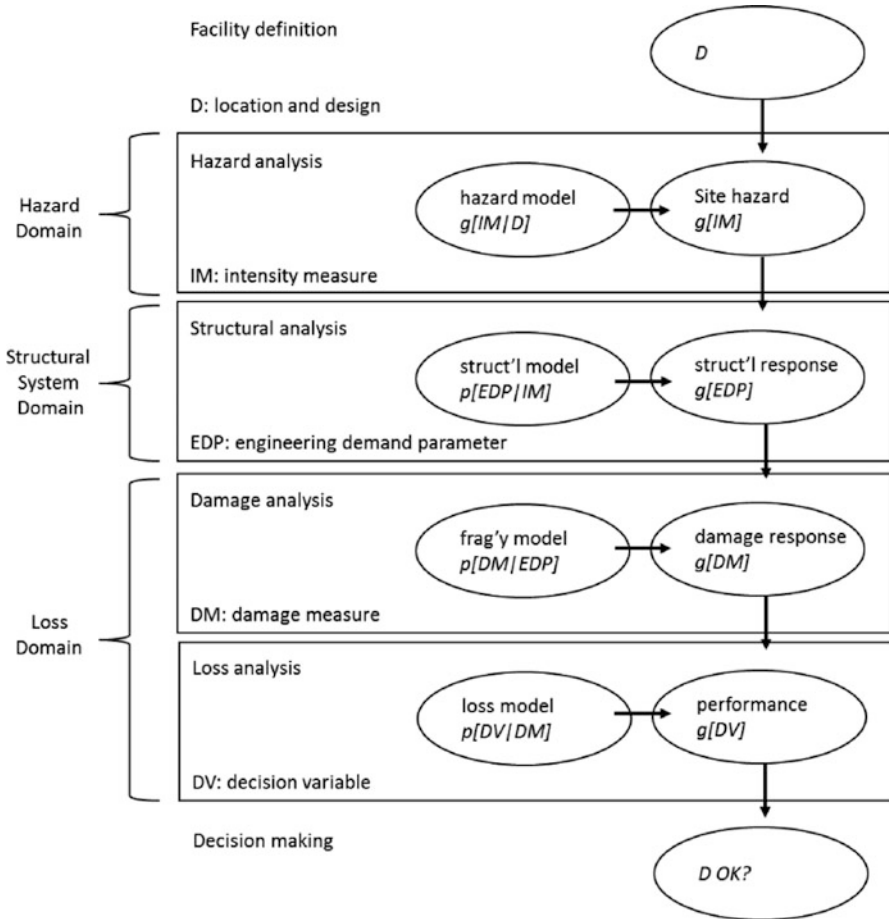


Fig. 9.29 PEER analysis methodology (adapted from ref. [97])

## 9.6 Applications

### 9.6.1 Event Tree

In the aftermath of an earthquake, the likelihood of fire ignition inside a building increases due to ruptured gas lines, electric arcing, toppled furniture, etc. Meanwhile, active and passive fire protections can be damaged due to earthquake shaking. Historically, it is shown that sprinkler systems could be ineffective due to breakage and leakage in the sprinkler piping. The fire compartments could be compromised due to damaged or cracked walls, ceilings, fire doors, and fire-rated linings. Finally, the passive fire protection, such as spray fire-resistant material that is used as fire protection in steel structures, may dislodge during earthquake shaking.

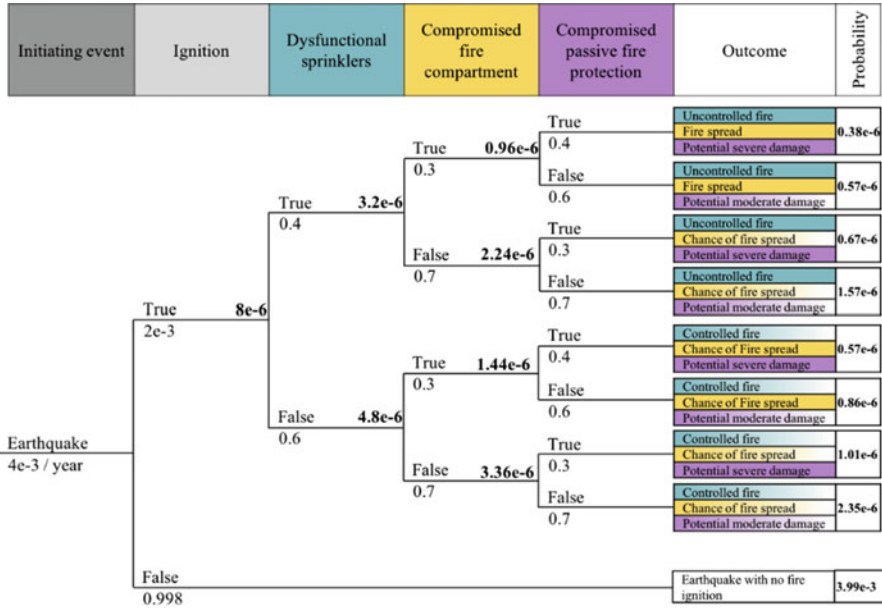


Fig. 9.30 Event tree for post-earthquake fire scenarios inside a building

Figure 9.30 shows an event tree to identify post-earthquake fire scenarios inside a building and quantify the corresponding probabilities. These fire scenarios and the associated occurrence probabilities can be used by the structural engineer to evaluate damage frequency to the structure due to post-earthquake fires.

The initial event, being the earthquake, may lead to a fire ignition. The probability of ignition inside a building can be quantified using the procedure discussed by Elhami Khorasani et al. [89], as a function of earthquake intensity, characteristics of the community, and building construction type. The sprinklers after the earthquake may not be functional leading to an uncontrolled fire. Some statistics of sprinkler performance as a function of ground motion acceleration (earthquake intensity) can be found in the study of LeGrone [90]. The fire can spread across and between floors in a building once it is out of control and the fire compartments are compromised. Historical data can be used to quantify damage to individual elements of fire safety systems, such as fire doors, but the overall probability of damage to the fire compartment is currently being researched and can be assigned by engineering judgement at this time. The final line of defence would be the passive fire protection on steel structural elements in a building. Severe damage to the building could be expected in case of damage to the passive fire protection while an uncontrolled fire spreads inside the building. It should be noted that taking the correlation of damage to fire compartment and passive fire protection into account, the conditional probability of having passive fire protection compromised is assumed to be higher on branches where the compartment is known to be compromised. The event tree

demonstrates the conditional probabilities at different stages within a branch and finally the combined yearly occurrence probability at the end of each branch.

### 9.6.2 Bending Moment Capacity and Bending Failure Probability of a Concrete Slab

#### Introduction and Motivation

Traditionally the fire resistance of solid concrete slabs is defined through tabulated data. For example, EN 1992-1-2:2004 [54] lists minimum concrete cover and slab thicknesses in function of the required (ISO 834) standard fire resistance. For the one-way solid slab specified further in Table 9.22, the fire resistance time listed in Table 5.8 of EN 1992-1-2:2004 is 120 min. The concrete cover realized during construction is however uncertain, as is the realization of other design parameters such as the concrete compressive strength and reinforcement yield stress. The same

**Table 9.22** Model parameters and probabilistic models, as listed by Van Coile [51], based on Holicky and Sykora [41]

Symbol	Property	Distribution	$\mu$	CoV
$f_{c,20}$	Concrete compressive strength at 20 °C	Log-normal	42.9 MPa ( $f_{ck} = 30$ MPa)	0.15
$f_{y,20}$	Reinforcement yield stress $f_{y,20^\circ C}$ at 20 °C	Log-normal	581.4 MPa ( $f_{yk} = 500$ MPa)	0.07
$k_{fy(\theta)}$	Retention factor for the steel yield stress at $\theta$ °C	Beta [ $\mu \pm 3\sigma$ ]	$\theta$ dependent conforming to EN 1992-1-2	$\theta$ dependent
$c$	Concrete cover	Beta [ $\mu \pm 3\sigma$ ]	35 mm	0.14 ( $\sigma = 5$ mm)
$h$	Slab thickness	Normal	200 mm	0.025 ( $\sigma = 5$ mm)
$A_s$	Area bottom reinforcement (for a unit slab width)	Normal	1.02 $A_{s,nom}$ mm <sup>2</sup>	0.02
$\emptyset$	Reinforcement bar diameter	Deterministic	10 mm	–
$b$	Unit slab width	Deterministic	1000 mm	–
$K_R$	Model uncertainty for the resistance effect	Lognormal	1.1	0.1
$M_G$	Bending moment induced by the permanent load effect	Normal	$M_{Gk}$	0.1
$M_{Qk}$	Bending moment induced by the imposed load effect	Gumbel	0.2 $M_{Qk}$	1.1
$K_E$	Model uncertainty for the load effect	Log-normal	1.0	0.1
$M_{Rd}$	Design value for the bending moment capacity in normal design conditions	Deterministic	50.9 kNm	–

applies to the loads acting on the slab during fire exposure. Consequently, there may be situations where the slab bending resistance during fire exposure is insufficient to resist the bending moment induced by the acting loads, and the structure is deemed to 'fail' prematurely.

The above implies amongst others that (i) design solutions in accordance with the tables of EN 1992-1-2 have an (unknown) probability of not meeting their specified fire resistance; (ii) for structures with high requirements for structural integrity in case of fire, the failure probability associated with the tabulated design solutions of EN 1992-1-2 may be too high; (iii) for existing structures which are at first glance not compliant with the tables of EN 1992-1-2, the achieved safety level may nevertheless exceed the safety level associated with the tabulated design solutions, allowing to meet fire resistance requirements without (expensive) refurbishment; and (iv) for designs where the consequences of fire-induced structural failure are low, a higher failure probability may be allowable than as associated with the tabulated data, thus allowing for a less onerous design requirement.

In the following, the failure probability of solid concrete slabs is explored considering standard fire exposure. First the resistance and load models are introduced, as well as the limit state function for bending. These allow a direct evaluation of the failure probability through crude Monte Carlo simulations (MCS). More insight is however obtained by studying the probability density function of the bending moment capacity. This has the further benefit of reducing computational expense when re-evaluating a given slab configuration for, e.g., a different load level and allows the use of approximate and computationally efficient reliability methods such as analytical evaluations or FORM.

Further discussions and background on the case presented here can be found in the works of Van Coile et al. [91] and Thienpont et al. [92]. Applied probabilistic models have been chosen for consistency with these references.

The structure of this section is as follows. First the considered limit state function is introduced together with models for the resistance and load effect in Sect. 9.6.2.1. Subsequently, the failure probability corresponding with the limit state function is evaluated through crude Monte Carlo simulations (MCS) in Sect. 9.6.2.2. In Sect. 9.6.2.3, approximate distributions for the resistance are explored. These approximate distributions allow to make a direct analytical estimate of the failure probability, omitting the computational cost of MCS. This analytical failure probability estimation is demonstrated in Sect. 9.6.2.4.

### 9.6.2.1 The Limit State Function, and Resistance and Load Models

#### Limit State Function

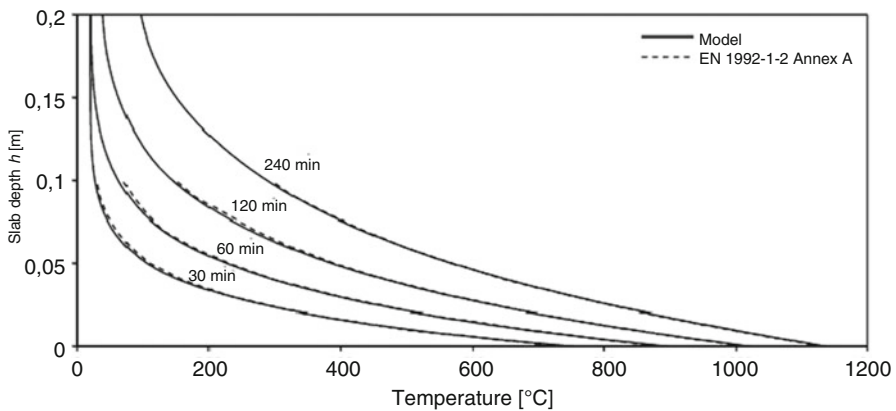
The bending limit state function is given by Eq. (9.101), with  $K_R$  being the model uncertainty for the resistance effect,  $M_{R,fi,t}$  the bending moment capacity of the slab at  $t$  minutes of fire exposure,  $K_E$  the model uncertainty for the load effect,  $M_G$  the bending moment induced by the permanent load, and  $M_Q$  the bending moment induced by the imposed load:

$$g = R - E = K_R M_{R,fi,t} - K_E (M_G + M_Q) \tag{9.101}$$

**Model for the Resistance Effect**

As models are a simplification of reality, the multiplicative model uncertainty  $K_R$  has been introduced in Eq. (9.101). The total resistance effect  $R$  thus equals  $K_R \cdot M_{R,fi,t}$ . The applied probabilistic description of  $K_R$  is given in Table 9.22. While in theory the model uncertainty could be calibrated by a systematic comparison of the model for  $M_{R,fi,t}$  against experimental test results, the difficulty of obtaining experimental data for structural fire engineering implies that  $K_R$  is based on subjective judgement instead, informed by model uncertainties listed for normal design conditions.

In the following, uncertainties with respect to the thermal properties of the reinforced concrete slab are not taken into consideration. This relates to a situation where the performance is evaluated with respect to a standard fire exposure, both regarding the design fire conditions and the concrete thermal properties. Considering one-sided exposure to fire from below, the cross section of the slab is heated non-linearly (see further Fig. 9.31), resulting in a non-linear distribution of free thermal strains across slab depth. The temperature increase furthermore changes the concrete and reinforcing steel mechanical models (stress-strain diagrams). A simplified numerical calculation tool has been applied by Van Coile et al. [91] which evaluates the full moment-curvature diagram for a given slab cross section and fire duration. From this diagram, the bending moment capacity  $M_{R,fi,t}$  is defined as the maximum attainable bending moment. Van Coile et al. [91] then demonstrated that the numerical calculation can be substituted by Eq. (9.102), with parameters as listed in Table 9.22. This equation is more generally applicable for situations where both (i) the slab fails by reinforcement yielding (as is commonly the case in fire conditions as the bottom reinforcement loses its strength) and (ii) the slab is sufficiently thick so that the concrete compressive zone remains relatively cool.



**Fig. 9.31** Temperature distributions in a 200 mm solid concrete slab, exposed at the bottom side to different ISO 834 standard fire durations. Comparison with data listed in EN 1992-1-2:2004 [92]

In Eq. (9.102) only the reinforcement yield stress retention factor  $k_{fy}$  is temperature, and thus time, dependent. The reinforcement temperature depends on the position of the reinforcement (and is thus dependent on the concrete cover realization), and is evaluated through numerical 1D heat transfer analyses [92]. In the absence of numerical evaluation, the temperatures can be directly taken from the temperature distributions for concrete slabs listed in EN 1992-1-2. Both temperatures are compared in Fig. 9.31 for specific ISO 834 standard fire durations. Background and further references for the probabilistic models for the input parameters are listed by Van Coile [51]. Here suffice it to state that the models are based on the review study by Holicky and Sykora [41], and preliminary assessments for the retention factor. Updated models for the retention factor in accordance with Sect. 9.4 of this chapter can be taken into account:

$$M_{R,\bar{f},t} = A_s k_{fy} f_{y,20} \left( h - c - \frac{\varnothing}{2} \right) - 0.5 \frac{(A_s k_{fy} f_{y,20})^2}{b f_{c,20}} \quad (9.102)$$

### Model for the Load Effect

The load effect consists of the bending moment induced by the permanent load and the (equivalent) imposed load. The probabilistic description for both is listed in Table 9.22 in function of their characteristic value. Note that the model for the instantaneous imposed load effect is the model applied by Holicky and Sleich [47] and Gernay et al. [46]; see Sect. 9.3. This has been done for consistency with the results listed by Van Coile [51]. Defining the load ratio  $\chi$  by Eq. (9.103), and considering the Eurocode ambient design criterion of Eq. (9.104), with  $u$  being the ambient design utilization  $\leq 1$  and other parameters as listed in Table 9.23, the bending moments  $M_G$  and  $M_Q$  are fully defined by  $\chi$  and  $u$ , for a given slab configuration.

For a statically determinate slab, the model uncertainty for the load effect included in Eq. (9.101),  $K_E$ , can be considered the same as in normal design conditions (see Table 9.22):

$$\chi = \frac{Q_k}{Q_k + G_k} = \frac{M_{QK}}{M_{QK} + M_{GK}} \quad (9.103)$$

**Table 9.23** Eurocode ambient design parameters Eq. (32), EN 1990 [15]

Symbol	Parameter description	Value
$\gamma_G$	Partial factor for the permanent load	1.35
$\psi_0$	Combination factor	0.70
$\gamma_Q$	Partial factor for the imposed load	1.50
$\xi$	Reduction factor for unfavourable permanent load	0.85

$$M_{Rd} = uM_{GK} \max \left\{ \gamma_G + \psi_0 \gamma_Q \frac{\chi}{1 - \chi}; \xi \gamma_G + \gamma_Q \frac{\chi}{1 - \chi} \right\} \text{ with } u \leq 1 \quad (9.104)$$

### 9.6.2.2 Failure Probability Estimation Through MCS

For a given ISO 834 standard fire duration  $t_E$ , the temperature distribution in the slab is fully defined—as the uncertainty with respect to the thermal properties is not taken into consideration (see Sect. 9.6.2.1). For each Monte Carlo realization, the reinforcement temperature is determined from Fig. 9.31, taking into account the specific realization of the concrete cover.

In Fig. 9.32, the estimated failure probability and corresponding COV are visualized in function of the number of MCS, for  $t_E = 120$  min,  $u = 0.90$ , and  $\chi = 0.40$  (i.e.  $M_{GK} = 21.3$  kNm and  $M_{Qk} = 14.2$  kNm). These results have been obtained through a script, but a spreadsheet evaluation is possible as well (with memory constraints posing a practical limit to the number of MCS in the spreadsheet).

The converged  $P_f$  estimate is  $7.1 \times 10^{-5}$  (for the specified fire exposure). This corresponds with a reliability index  $\beta = 3.8$ , in accordance with Eq. (9.8). This result indicates that for this specific slab—and under the constraints imposed by the model, such as no spalling—structural stability in the bending limit state will be maintained for the 120 min tabulated in EN 1992-1-2:2004 with a very high reliability.

### 9.6.2.3 Probability Density Function Describing the Bending Moment Capacity $M_{R,fi,t}$

#### Introduction

While crude MCS allows to make an assessment of the failure probability, the evaluation requires a large number of model evaluations and is thus no longer feasible when applied with a computationally expensive model. Furthermore, a pure MCS as in Fig. 9.32 requires a full recalculation whenever an aspect of the evaluation is modified (e.g. the load ratio, utilization, or nominal concrete cover).

The difficulty in evaluating the limit state of Eq. (9.101) results first and foremost from the unknown distribution of  $M_{R,fi,t}$ . When the distribution type is known, the parameters of the distribution can be assessed through a more limited number of model evaluations or approximate methods. A commonly assumed distribution type to represent material and cross-sectional strength is the log-normal distribution. As illustrated below however, directly assuming a distribution type without further analysis can result in an inappropriate model choice.

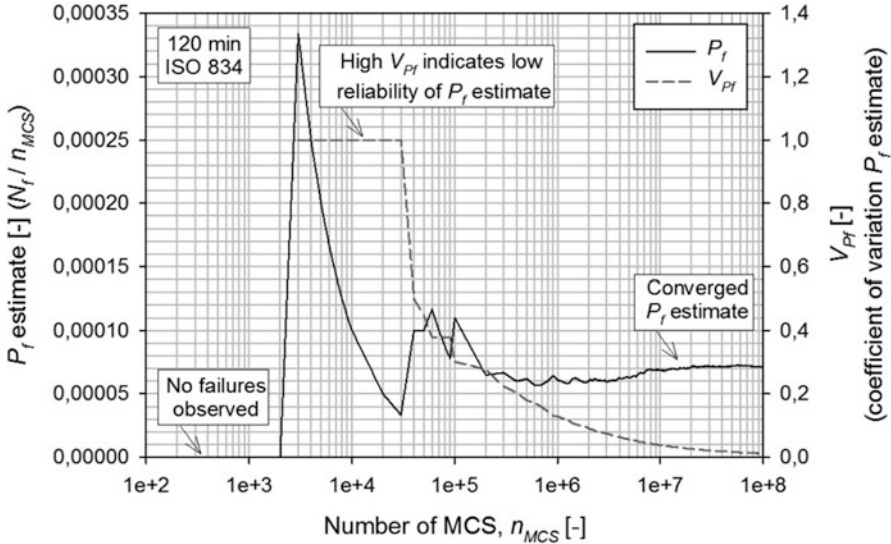


Fig. 9.32 Estimate for  $P_f$  and corresponding  $V_{P_f}$  in function of the number of MCS

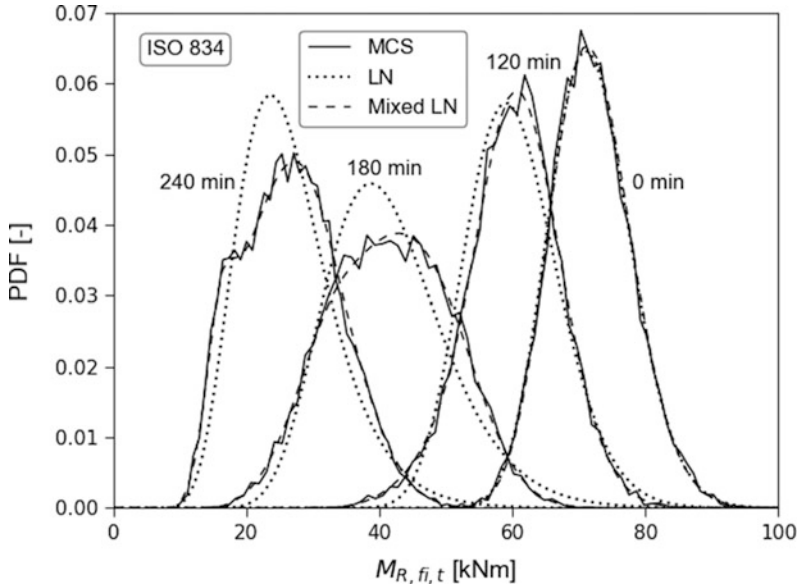
**Observed Density Function Through MCS and Mixed Log-Normal Model**

Statistical tests can be applied to determine appropriate distribution choices; see, e.g., Ang and Tang [93]. In structural engineering applications however, the appropriate description of low strength quantiles and high load quantiles is of great importance, while less importance is assigned to the close description of other quantiles (such as a very high resistance realization or exceptionally low load effect). The Gumbel distribution commonly applied for the imposed load effect for example, see Sect. 9.3.2.3 and Table 9.22, has a non-zero probability of returning a negative load. Clearly this is an inappropriate model for the low quantiles of  $Q$ , but this is of little importance as structural failure is—in reasonable situations—associated with high quantiles of  $Q$ .

Considering the above, the engineer assessing the appropriateness of a distribution model cannot go without a visual comparison of the data against the model. In case of a model for the concrete compressive strength or other experimentally measured parameters, the term data should be understood literally. In the case under consideration here, however, the ‘data’ is the result for  $M_{R,fi,t}$  obtained through MCS.

In Fig. 9.33, the histogram corresponding with  $10^4$  MCS realizations is visualized together with a log-normal approximation for different ISO 834 standard fire durations  $t_E$ , for the slab configuration listed in Table 9.22. Figure 9.34 visualizes similar results for a concrete cover standard deviation of 10 mm (e.g. an existing building with large uncertainty or limited quality control in production).





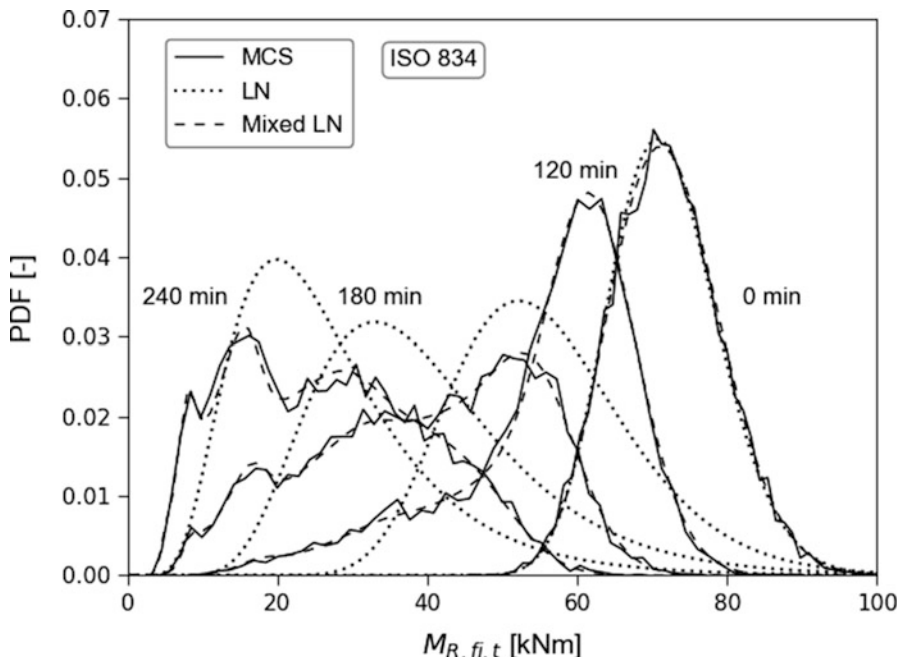
**Fig. 9.33** Observed distribution density (MCS,  $10^4$  realizations), log-normal approximation (LN), and mixed log-normal approximation (mixed LN), for the slab characteristics of Table 9.22, and different ISO 834 standard fire durations  $t_E$

Figures 9.33 and 9.34 suggest that a log-normal distribution is not an appropriate choice for describing  $M_{R,fi,t}$ . Further study indicates that this non-standard PDF shape is the result of the concrete cover variability, and the associated non-linear change in reinforcement temperature, while for a fixed (deterministic) concrete cover  $c_i$ ,  $M_{R,fi,t,c_i}$  is described by the traditional log-normal distribution [91]. Taking this information into account, the distribution for slab bending moment capacity  $M_{R,fi,t}$  is described by a combination of constituent log-normal distributions, whereby each constituent log-normal distribution  $M_{R,fi,t,c_i}$  is valid for a specific fixed concrete cover  $c_i$ , and the combination weights  $P_{c_i}$  correspond with the (lumped) occurrence probabilities for the respective concrete covers:

$$M_{R,fi,t} = \sum_i P_{c_i} M_{R,fi,t,c_i} \tag{9.105}$$

$$P_{c_i} = \int_{c_i - \Delta c / 2}^{c_i + \Delta c / 2} f_c(c) dc \tag{9.106}$$

with  $f_c$  being the PDF for the concrete cover, and  $\Delta c$  the lumping width for the concrete cover realizations (here: 1 mm). In conclusion,  $M_{R,fi,t}$  can be described by a



**Fig. 9.34** Observed distribution density (MCS,  $10^4$  realizations), log-normal approximation (LN), and mixed log-normal approximation (mixed LN), for the slab characteristics of Table 9.22, but with a concrete cover standard deviation of 10 mm instead of 5 mm, and different ISO 834 standard fire durations  $t_E$

mixed log-normal distribution. Note that the summation in Eq. (9.105) represents a combination of log-normal distributions, not a direct summation.

As the constituent distributions  $M_{R,fi,t,ci}$  are known to be described by a log-normal distribution, their parameters can be evaluated using more efficient sampling techniques (such as Latin hypercube sampling; see [67]). In the current case however, the model for  $M_{R,fi,t}$  is given by an equation, i.e. Eq. (9.102), and a direct evaluation of the mean  $\mu$  and standard deviation  $\sigma$  is here also possible through Taylor approximations:

$$\mu_{M_{R,fi,t,ci}} \cong y(\boldsymbol{\mu}) \tag{9.107}$$

$$\sigma_{M_{R,fi,t,ci}}^2 \cong \sum_j \left( \frac{\partial y(\boldsymbol{\mu})}{\partial X_j} \right)^2 \sigma_{X_j}^2 \tag{9.108}$$

where  $\boldsymbol{\mu}$  indicates the vector of mean values for all stochastic variables  $X_j$  in Eq. (9.1), and  $y(\cdot)$  refers to Eq. (9.102) itself.

The evaluation of Eqs. (9.107) and (9.108) can readily be done in a spreadsheet, and so the mixed log-normal distribution for  $M_{R,fi,t}$  is fully specified. This mixed log-normal distribution is compared to the observed MCS histogram in Figs. 9.33 and 9.34, confirming the excellent match.

### 9.6.2.4 Analytical Failure Probability Estimation

Having established the mixed log-normal distribution as an appropriate modelling choice for  $M_{R,fi,t}$ , the failure probability can be evaluated through Eq. (9.109), where  $K_T$  is the total model uncertainty combining both the model uncertainty effects for the load and resistance effect, and the failure probability is separately evaluated for each of the log-normal constituent distributions  $M_{R,fi,t,ci}$  as  $P_{f,i}$ :

$$\begin{aligned} P_f &= P[g < 0] = P\left[M_{R,fi,t} - \frac{K_E}{K_R}(M_G + M_Q) < 0\right] \\ &= \sum_i P_{ci} \cdot P\left[M_{R,fi,t,ci} - K_T(M_G + M_Q) < 0\right] = \sum_i P_{ci} \cdot P_{f,i} \end{aligned} \quad (9.109)$$

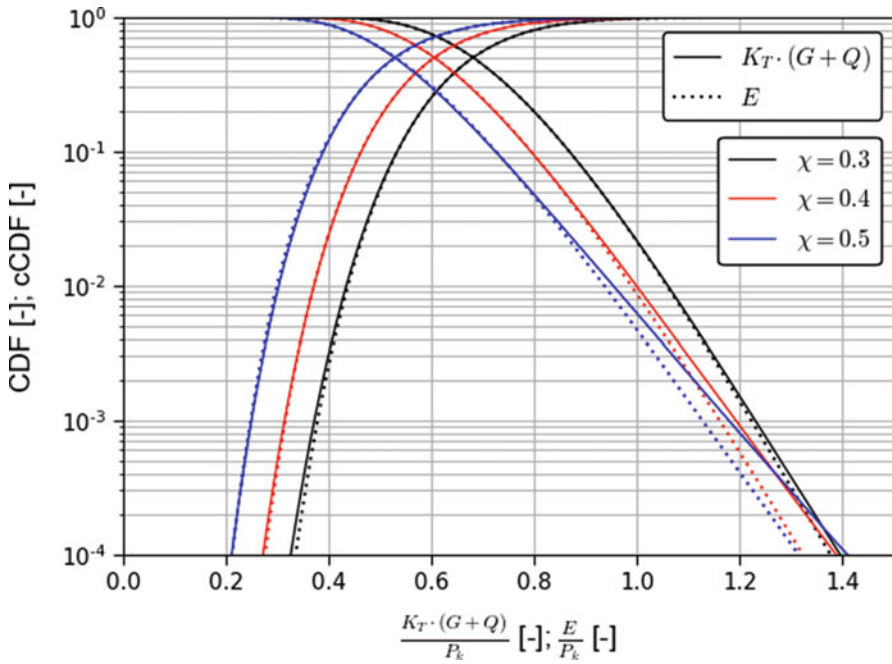
As both  $K_E$  and  $K_R$  are described by a log-normal distribution, also  $K_T$  is log-normal. Furthermore, the total load effect  $E = K_T(M_G + M_Q)$  can be approximated by a log-normal distribution as well, for which the mean and standard deviation can be assessed through Taylor approximations, i.e. Eqs. (9.110) and (9.111).

The appropriateness of the approximation is visualized in Fig. 9.35 (result of  $10^8$  MCS), shown here for the generalized dimensionless case of the load effect divided by the total characteristic load effect  $P_k = G_k + Q_k$ , for different load ratio  $\chi$ . From the figure it is clear that the log-normal approximation is very good for  $\chi = 0.3$ , and becomes less appropriate for higher load ratios. For  $\chi = 0.40$  as in this example, some deviation can thus be expected. As indicated in Fig. 9.35, the log-normal approximation underestimates the occurrence of large realizations of the total load effect, and will thus (for low failure probabilities) underestimate the probability of failure:

$$\mu_E \cong \mu_{K_T} (\mu_G + \mu_Q) \quad (9.110)$$

$$\sigma_E^2 \cong \sigma_{K_T}^2 (\mu_G + \mu_Q)^2 + \mu_{K_T}^2 (\sigma_G^2 + \sigma_Q^2) \quad (9.111)$$

The introduction of an approximate log-normal total load effect  $E$  allows to evaluate Eq. (9.109) analytically. More specifically,  $P_{f,i}$  can be elaborated as Eq. (9.112), where  $Z$  follows a log-normal distribution (considering log-normality of both  $M_{R,fi,t,ci}$  and  $E$ ). The parameters of  $Z$ , i.e.  $\mu_{\ln Z}$  and  $\sigma_{\ln Z}$ , are given by



**Fig. 9.35** Comparison total load model  $K_T(G + Q)$  and log-normal approximation  $E$  (MCS,  $10^8$  realizations), for different load ratio  $\chi$

Eqs. (9.113) and (9.114), which are applications of Eqs. (9.56) and (9.57) in Sect. 9.5.2.

Thus, Eq. (9.115) holds and  $P_{f_i}$  can be evaluated directly. Results for the mean and standard deviation of the constituent log-normal distributions  $M_{R_{f_i,t,c_i}}$  are given in Table 9.24, together with their constituent probability  $P_i$  and failure probability  $P_{f_i}$  (considering  $\mu_E = 22.2$  kNm and  $V_E = 0.21$ , calculated from Sects. 9.6.2.1 and 9.6.2.2). Note that the COV of the constituent  $M_{R_{f_i,t,c_i}}$  is quasi-constant at 0.09.

The resulting estimate for  $P_f$  is  $4.9 \times 10^{-5}$ , which corresponds with a reliability index  $\beta = 3.9$ . Despite the approximations, this result gives a correct order of magnitude evaluation of  $P_f$ , without requiring the application of specialized reliability methods. The calculation can be done in a spreadsheet. Furthermore, Table 9.24 also clearly shows how the largest contribution to the failure probability comes from the lower concrete cover realizations (i.e. the failure probability contributions of the  $c_i$  constituents up to 34.5 mm amount to  $4.8 \times 10^{-5}$ ). This example also illustrates the benefit of communicating small failure probabilities through the reliability index  $\beta$ , as this highlights the comparability of the approximate result with the MCS evaluation:

**Table 9.24** Constituent models (log-normal  $M_{R,fi,t,ci}$ :  $c_i$ ,  $P_i$ , mean, and standard deviation), corresponding failure probability  $P_{fi}$ , and contribution to the overall failure probability  $P_i \cdot P_{fi}$ . Calculation of the overall failure probability  $P_f = 4.9 \times 10^{-5}$

Concrete cover $c_i$ [mm]	$P_i$ [-]	$\mu_{M_{R,fi,t,ci}}$ [kNm]	$\sigma_{M_{R,fi,t,ci}}$ [kNm]	$P_{fi}$ [-]	$P_i \cdot P_{fi}$ [-]
20.5	$4.0 \times 10^{-5}$	35.17	3.31	$1.9 \times 10^{-2}$	$7.4 \times 10^{-7}$
21.5	$5.5 \times 10^{-4}$	37.28	3.51	$9.7 \times 10^{-3}$	$5.3 \times 10^{-6}$
22.5	$2.1 \times 10^{-3}$	39.91	3.75	$4.2 \times 10^{-3}$	$8.9 \times 10^{-6}$
23.5	$5.2 \times 10^{-3}$	42.50	3.99	$1.8 \times 10^{-3}$	$9.3 \times 10^{-6}$
24.5	$9.7 \times 10^{-3}$	44.98	4.23	$7.9 \times 10^{-4}$	$7.7 \times 10^{-6}$
25.5	$1.6 \times 10^{-2}$	47.37	4.45	$3.5 \times 10^{-4}$	$5.6 \times 10^{-6}$
26.5	$2.3 \times 10^{-2}$	49.67	4.66	$1.6 \times 10^{-4}$	$3.7 \times 10^{-6}$
27.5	$3.1 \times 10^{-2}$	51.88	4.87	$7.7 \times 10^{-5}$	$2.4 \times 10^{-6}$
28.5	$3.9 \times 10^{-2}$	54.00	5.07	$3.8 \times 10^{-5}$	$1.5 \times 10^{-6}$
29.5	$4.7 \times 10^{-2}$	56.03	5.25	$1.9 \times 10^{-5}$	$8.9 \times 10^{-7}$
30.5	$5.5 \times 10^{-2}$	57.99	5.44	$9.8 \times 10^{-6}$	$5.4 \times 10^{-7}$
31.5	$6.2 \times 10^{-2}$	58.89	5.49	$7.1 \times 10^{-6}$	$4.3 \times 10^{-7}$
32.5	$6.7 \times 10^{-2}$	59.65	5.53	$5.4 \times 10^{-6}$	$3.6 \times 10^{-7}$
33.5	$7.1 \times 10^{-2}$	60.36	5.57	$4.1 \times 10^{-6}$	$2.9 \times 10^{-7}$
34.5	$7.3 \times 10^{-2}$	61.04	5.60	$3.2 \times 10^{-6}$	$2.3 \times 10^{-7}$
35.5	$7.3 \times 10^{-2}$	61.68	5.63	$2.5 \times 10^{-6}$	$1.8 \times 10^{-7}$
36.5	$7.1 \times 10^{-2}$	62.29	5.66	$2.0 \times 10^{-6}$	$1.4 \times 10^{-7}$
37.5	$6.7 \times 10^{-2}$	62.86	5.68	$1.6 \times 10^{-6}$	$1.1 \times 10^{-7}$
38.5	$6.2 \times 10^{-2}$	63.40	5.71	$1.3 \times 10^{-6}$	$8.3 \times 10^{-8}$
39.5	$5.5 \times 10^{-2}$	63.91	5.73	$1.1 \times 10^{-6}$	$6.1 \times 10^{-8}$
40.5	$4.7 \times 10^{-2}$	64.39	5.75	$9.4 \times 10^{-7}$	$4.4 \times 10^{-8}$
41.5	$3.9 \times 10^{-2}$	64.83	5.76	$7.9 \times 10^{-7}$	$3.1 \times 10^{-8}$
42.5	$3.1 \times 10^{-2}$	64.80	5.74	$7.9 \times 10^{-7}$	$2.4 \times 10^{-8}$
43.5	$2.3 \times 10^{-2}$	64.67	5.71	$8.2 \times 10^{-7}$	$1.9 \times 10^{-8}$
44.5	$1.6 \times 10^{-2}$	64.53	5.68	$8.5 \times 10^{-7}$	$1.3 \times 10^{-8}$
45.5	$9.7 \times 10^{-3}$	64.38	5.65	$8.8 \times 10^{-7}$	$8.6 \times 10^{-9}$
46.5	$5.2 \times 10^{-3}$	64.22	5.62	$9.2 \times 10^{-7}$	$4.8 \times 10^{-9}$
47.5	$2.1 \times 10^{-3}$	64.05	5.59	$9.6 \times 10^{-7}$	$2.1 \times 10^{-9}$
48.5	$5.5 \times 10^{-4}$	63.88	5.56	$1.0 \times 10^{-6}$	$5.6 \times 10^{-10}$
49.5	$4.0 \times 10^{-5}$	63.69	5.53	$1.1 \times 10^{-6}$	$4.3 \times 10^{-11}$
$\sum_i P_i = 1$		$\sum_i P_i \cdot P_{fi} = 4.9 \cdot 10^{-5}$			

$$P_{f,i} = P[M_{R,fi,t,ci} - E < 0] = P\left[\frac{M_{R,fi,t,ci}}{E} < 1\right] = P[Z < 1] \tag{9.112}$$

$$\mu_{\ln Z} = \mu_{\ln M_{R,fi,t,ci}} - \mu_{\ln E} \tag{9.113}$$

$$\sigma_{\ln Z} = \sqrt{\sigma_{\ln M_{R_{f,i,c}}}^2 + \sigma_{\ln E}^2} \tag{9.114}$$

$$P_{f,i} = P[Z < 1] = \Phi\left(\frac{\ln(1) - \mu_{\ln Z}}{\sigma_{\ln Z}}\right) = \Phi\left(-\frac{\mu_{\ln Z}}{\sigma_{\ln Z}}\right) \tag{9.115}$$

### 9.6.3 Application of LHS

A W14x53 steel column section is part of the gravity system in a multistorey frame. Typical floor height is 3.962 m, with column ends constrained from rotation. The fire protection is designed based on the International Building Code guidelines for 2-h fire resistance, with a calculated mean fire protection thickness of 33.4 mm. The column has a characteristic yield strength of 345 MPa.

The question is to evaluate the mean and standard deviation of the column capacity ( $P_n$ ) after exposure to 2 h of ASTM E119 (ISO 834), considering as single stochastic variable the yield strength of steel, in accordance with the model by Elhami Khorasani et al. [55] as presented in Sect. 9.4.2.

#### Solution

The problem is solved using both Monte Carlo simulations (MCS) and Latin hypercube sampling (LHS). The effectiveness of LHS is demonstrated by running both MCS and LHS with different number of samples and tracking the rate of convergence. The final results for the mean and standard deviation of calculated column capacity are presented in Table 9.25 using MCS and Table 9.26 using LHS.

Figure 9.36 shows the cumulative distribution function for the column capacity calculated using MCS and LHS with 10,000 and 500 samplings, respectively.

**Table 9.25** Mean and standard deviation of  $P_n$  using MCS

No. of iterations	50	100	500	1000	2000	3000	4000	5000	7000	10,000
Mean	2469	2505	2486	2482	2473	2470	2480	2476	2467	2475
Standard deviation	295	319	328	339	341	342	336	341	342	340

**Table 9.26** Mean and standard deviation of  $P_n$  using LHS

No. of iterations	10	20	30	40	50	100	150	200	250	500
Mean	2495	2475	2473	2478	2473	2475	2475	2475	2475	2475
Standard deviation	294	360	342	338	346	342	342	340	341	340

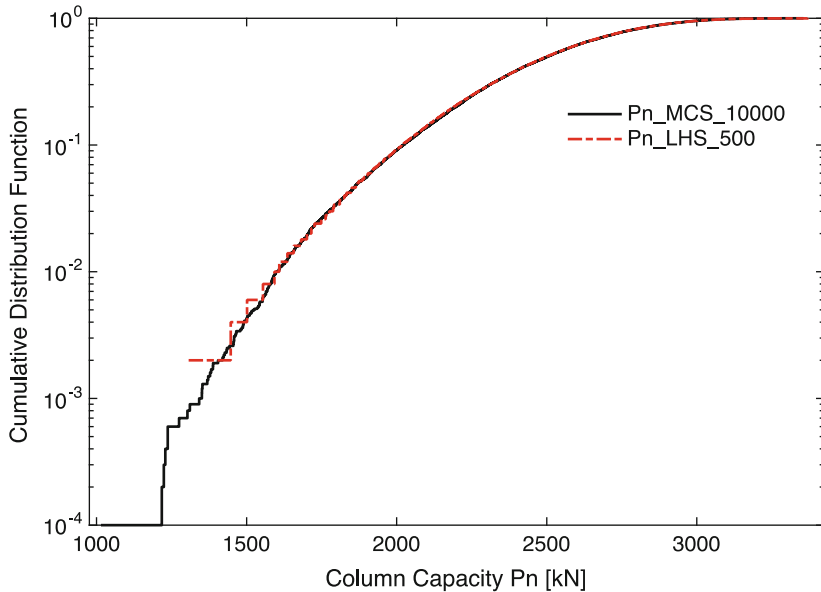


Fig. 9.36 CDF for column capacity calculated using MCS and LHS

### 9.6.4 Application of Fragility Curves

Fragility curves listing the probability of specified damage states in function of an intensity measure, as applied in earthquake engineering, have not yet been extensively developed for structural fire engineering applications. As noted in Sect. 9.5.6, a notable exception is the work by Ioannou et al. [79, 80] where expert elicitation was applied. Details of the procedure can be found in the full reference; the following gives an overview of the damage states specified and results obtained in order to clarify the concept of fragility curves.

Response measures including the presence and extent of spalling, residual capacity, span/deflection ratio, and peak rebar temperature were compared by Ioannou et al. [79, 80] with equivalent duration of standard fire exposure as an intensity measure. These response measures were linked with damage states based on the damage scale proposed by the concrete society [94], Table 9.27, resulting in the development of fragility curves for concrete slabs and concrete columns.

As part of the expert elicitation, 13 experts in structural fire engineering were asked to judge the relationship of these different response measures to the fire intensity, i.e.  $P(RM = y | IM = x)$ , for the fifth percentile, the mean, and the 95th percentile of the distribution. The intensity measure against which the response was conditioned was the time equivalence based on Ingberg’s work [95]. As part of the

**Table 9.27** Visual damage state classification table for reinforced concrete elements [80]

DS	Surface appearance of concrete			Description
	Condition of finish	Colour	Crazing	
$ds_0$	Unaffected or beyond the extent of fire			
$ds_1$	Some peeling	Normal	Slight	Damage primarily cosmetic in nature, which does not impact the design or repair of the structural fabric of RC buildings
$ds_3$	Total loss	Pink/red	Extensive	The element has experienced a significant, but not catastrophic, amount of damage to the effect that, with significant remedial action, it can be reinstated to perform its structural functions
		Whitish grey		
$ds_4$	Destroyed	Whitish grey	Surface lost	The damage caused by the fire is so extensive that it is no longer viable to repair and reuse the element and replacing the element with a new element is the only option. The building has not suffered a disproportionate collapse

same exercise, the same experts were asked to judge the relationship between response thresholds and the different damage states defined in Table 9.27, i.e.  $P(DS \geq ds_i | RM = y)$ , for the fifth, mean, and 95th percentiles of the distributions. Based on  $P(DS \geq ds_i | RM = y)$  a quantified damage scale for slabs and columns was created as shown in Table 9.28, accounting also for the uncertainty of the experts' judgement.

Fragility functions were then created through a random sampling technique which couples the relationships of response measure (RM) to intensity measure (IM) and damage state (DS) to response measure (RM). The procedure for this is described in both Ioannou et al. [80] and in more detail in Porter and Kiremidjian [96]. In summary however this involves drawing a random sample from the unit interval, which is used to select a value of RM conditioned on IM that has cumulative probability equal to this random number. Then the probability that each damage state will be reached or exceeded is determined by drawing another random sample on the unit interval to select a value of DS conditional on the RM. A large number of iterations of this is then performed to determine the probability that a building or component will sustain a damage level  $DS \geq ds_i$ . Figure 9.37 shows the resulting fragility curves derived using this method by Ioannou et al. [80].

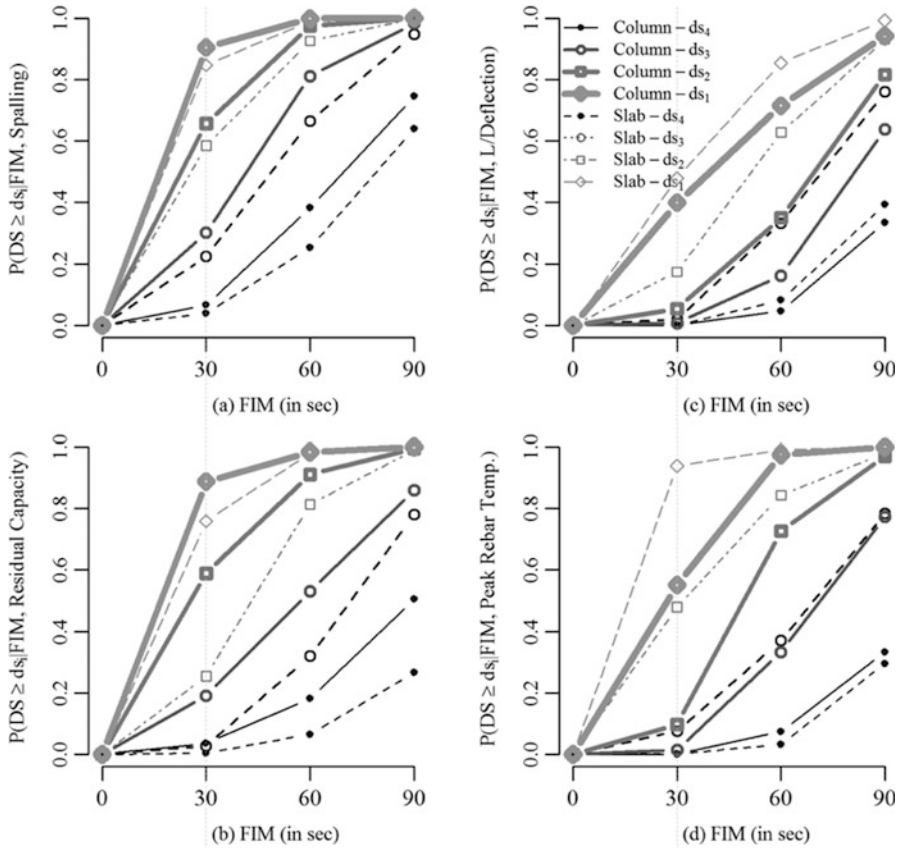
This same technique can be used to derive fragility functions based on relationships of DS, RM, and IM which are obtained through other means.

**Acknowledgement** The support of Inzienghe Inerhunwa in reviewing the text is gratefully acknowledged.



**Table 9.28** Quantified damage states for reinforced concrete slabs and columns

C	Element	Spalling			L/deflection			Residual capacity			Peak rebar temperature			
		5%	95%	Mean	5%	95%	Mean	5%	95%	Mean	5%	95%	Mean	
$d_{s0}$	-													
$d_{s1}$	Slab	0.38	13.06	4.75	722.13	24068.88	7357.69	90.16	99.92	97	15.28	157.91	63.2	
	Column	0.24	13.11	4.48	134.05	25956.29	6716.82	91.54	99.91	97	15.93	147.68	60.99	
$d_{s2}$	Slab	3.42	30.91	14.62	121.74	9109.59	2489.4	75.26	96.62	88	77.82	391.55	196.93	
	Column	2.83	2.62	14.68	84.95	934.54	367.5	82.67	97.26	91	77.17	348.3	182.08	
$d_{s3}$	Slab	13.64	63.55	36.87	31.15	1650.29	469.61	40.71	87.55	66	190.21	730.63	405.32	
	Column	12.02	61.82	34.88	63.07	222.46	127.47	35.08	95.33	70	169.87	615.82	349.2	
$d_{s4}$	Slab	36.38	92.79	68.07	7.07	221.93	68.57	4.87	73.77	35	434.97	1037.84	695.77	
	Column	31.27	91.9	64.78	13.6	97.46	43.55	4.12	83.42	39	335.76	986.07	607.09	



**Fig. 9.37** Fragility curves corresponding to three damage states for (a) spalling, (b) deflection, (c) residual capacity, and (d) pear rebar temperature constructed for slabs and columns, from Ioannou et al. [80]. Note: the horizontal axis is in minutes

## References

1. The Stationery Office. (2010). *Schedule 1, Part 2 of building and buildings*. The Building Regulations, UK.
2. SFPE. (2007) *SFPE Engineering guide to performance-based fire protection* (2nd ed.).
3. Van Coile, R., Hopkin, D., Lange, D., Jomaas, G., & Bisby, L. (2019). The need for hierarchies of acceptance criteria for probabilistic risk assessments in fire engineering. *Fire Technology*, 55 (4), 1111–1146. <https://doi.org/10.1007/s10694-018-0746-7>
4. Fröderberg, M., & Thelandersson, S. (2015). Uncertainty caused variability in preliminary structural design of buildings. *Structural Safety*, 52, 183–193. <https://doi.org/10.1016/j.strusafe.2014.02.001>
5. Lange, D., & Boström, L. (2017). A round robin study on modelling the fire resistance of a loaded steel beam. *Fire Safety Journal*, 92, 64–76. <https://doi.org/10.1016/j.firesaf.2017.05.013>

6. Buchanan, A. H., & Abu, A. (2017). *Structural design for fire safety* (2nd ed.). John Wiley & Sons.
7. Hopkin, D., Van Coile, R. & Lange, D. (2017) *Certain uncertainty – Demonstrating safety in fire engineering design and the need for safety targets*. SFPE Europe 7.
8. ISO. (2015). *ISO 2394:2015—General principles on reliability for structures*. International Organization for Standardization (ISO).
9. Holicky, M. (2009). *Reliability analysis for structural design* (1st ed.). SUN Media.
10. ISO. (2019). *ISO 24679-1:2019—Fire safety engineering—Performance of structures in fire Part 1: General*. International Organization for Standardization (ISO).
11. Van Coile, R., Hopkin, D., Bisby, L., & Caspeele, R. (2017). The meaning of Beta: background and applicability of the target reliability index for normal conditions to structural fire engineering. *Procedia Engineering*, 210, 528–536. <https://doi.org/10.1016/j.proeng.2017.11.110>
12. Rackwitz, R. (2000). Optimization—The basis of code-making and reliability verification. *Structural Safety*, 22(1), 27–60. [https://doi.org/10.1016/S0167-4730\(99\)00037-5](https://doi.org/10.1016/S0167-4730(99)00037-5)
13. Fischer, K., Viljoen, C., Köhler, J., & Faber, M. H. (2019). Optimal and acceptable reliabilities for structural design. *Structural Safety*, 76, 149–161. <https://doi.org/10.1016/j.strusafe.2018.09.002>
14. ISO. (1998). *ISO 2394:1998—General principles on reliability for structures*. International Organization for Standardization (ISO).
15. CEN. (2002). *EN 1990:2002—Eurocode 0. Basis of structural design*. CEN: European Committee for Standardization.
16. JCSS. (2001). Probabilistic model code. Part 1 – Basis of Design. Joint Committee on Structural Safety.
17. Fischer, K., Barnardo-Viljoen, C. & Faber, M. (2012) Deriving Target Reliabilities from the LQI. *LQI Symposium*. Kgs. Lyngby, Denmark.
18. Van Coile, R., Jomaas, G., & Bisby, L. (2019). Defining ALARP for fire safety engineering design via the Life Quality Index. *Fire Safety Journal*, 107, 1–14. <https://doi.org/10.1016/j.firesaf.2019.04.015>
19. Sleich, J. B., Cajot, L. G., Pierre, M., Joyeux, D., Aurtenetxe, G., Unanua, J., Pustorino, S., Heise, F. J., Salomon, R., Twilt, L., & Van Oerle, J. (2002). *Valorisation project: Natural fire safety concept: Final report*. Directorate-General for Research, European Commission.
20. Hopkin, D., Van Coile, R., Hopkin, C., Fu, I. & Spearpoint, M. (2018) Transient reliability evaluation of a stochastic structural system in fire. In *Proceedings of the 16th International Probabilistic Workshop., 2018 Vienna*.
21. Van Coile, R., Gernay, T., Hopkin, D. & Elhami Khorasani, N. (2019) Resilience targets for structural fire design: An exploratory study. *International Probabilistic Workshop (IPW 2019)*. Edinburgh.
22. Fischer, K. (2014). *Societal decision-making for optimal fire safety*. Doctoral dissertation, ETH Zurich, Switzerland.
23. Van Coile, R., Caspeele, R., & Taerwe, L. (2014). Lifetime cost optimization for the structural fire resistance of concrete slabs. *Fire Technology*, 50(5), 1201–1227. <https://doi.org/10.1007/s10694-013-0350-9>
24. CEN. (2002). *EN 1991-1-2:2002—Eurocode 1. Actions on structures. General actions. Actions on structures exposed to fire*. CEN: European Committee for Standardization.
25. Holborn, P. G., Nolan, P. F., & Golt, J. (2004). An analysis of fire sizes, fire growth rates and times between events using data from fire investigations. *Fire Safety Journal*, 39(6), 481–524. <https://doi.org/10.1016/j.firesaf.2004.05.002>
26. Baker, G., Wade, C., Spearpoint, M., & Fleischmann, C. (2013). Developing probabilistic design fires for performance-based fire safety engineering. *Procedia Engineering*, 62, 639–647.
27. Nilsson, M., Johansson, N., & Van Hees, P. (2014). A new method for quantifying fire growth rates using statistical and empirical data – Applied to determine the effect of Arson. In *11th International Symposium on Fire Safety Science 2014*. Christchurch, New Zealand.

28. Rackauskaite, E., Hamel, C., Law, A., & Rein, G. (2015). Improved formulation of travelling fires and application to concrete and steel structures. *Structure*, 3, 250–260. <https://doi.org/10.1016/j.istruc.2015.06.001>
29. Grimwood, P. (2018). Structural fire engineering: realistic ‘travelling fires’ in large office compartments. *International fire professional*, Issue 25.
30. Thomas, P. H. (1986). Design guide: Structure fire safety CIB W14 Workshop report. *Fire Safety Journal*, 10(2), 77–137. [https://doi.org/10.1016/0379-7112\(86\)90041-X](https://doi.org/10.1016/0379-7112(86)90041-X)
31. Zalok, E., Hadjisophocleous, G. V., & Mehaffey, J. R. (2009). Fire loads in commercial premises. *Fire and Materials*, 33(2), 63–78. <https://doi.org/10.1002/fam.984>
32. Elhami Khorasani, N., Garlock, M., & Gardoni, P. (2014). Fire load: Survey data, recent standards, and probabilistic models for office buildings. *Engineering Structures*, 58, 152–165. <https://doi.org/10.1016/j.engstruct.2013.07.042>
33. Xie, Q., Xiao, J., Gardoni, P., & Hu, K. (2019). Probabilistic analysis of building fire severity based on fire load density models. *Fire Technology*, 55(4), 1349–1375. <https://doi.org/10.1007/s10694-018-0716-0>
34. BSI. (2019). *PD 7974-1:2019—Application of fire safety engineering principles to the design of buildings. Initiation and development of fire within the enclosure of origin (Sub-system 1)*. British Standards Institution.
35. Hopkin, C., Spearpoint, M., & Hopkin, D. (2019). A review of design values adopted for heat release rate per unit area. *Fire Technology*, 55(5), 1599–1618. <https://doi.org/10.1007/s10694-019-00834-8>
36. Kirby, B. R., Newman, G. M., Butterworth, N., Pagan, J., & English, C. (2004). A new approach to specifying fire resistance periods. *Structural Engineer*, 82(19).
37. JCSS. (2001) *Probabilistic model code, Part II: Load models*. Joint Committee on Structural Safety (JCSS).
38. Stern-Gottfried, J. (2011). *Travelling fires for structural design*. PhD Thesis, The University of Edinburgh.
39. Law, A., Stern-Gottfried, J., Gillie, M., & Rein, G. (2011). The influence of travelling fires on a concrete frame. *Engineering Structures*, 33(5), 1635–1642. <https://doi.org/10.1016/j.engstruct.2011.01.034>
40. Ellingwood, B. R. (2005). Load combination requirements for fire-resistant structural design. *Journal of Fire Protection Engineering*, 15(1), 43–61.
41. Holicky, M. & Sykora, M. (2010) Stochastic models in analysis of structural reliability. In *International symposium on stochastic models in reliability engineering, life sciences and operation management*. Beer Sheva, Israel.
42. Jovanović, B., Van Coile, R., Hopkin, D., Elhami Khorasani, N., Lange, D., & Gernay, T. (2020). Review of current practice in probabilistic structural fire engineering: Permanent and live load modelling. *Fire Technology*. <https://doi.org/10.1007/s10694-020-01005-w>
43. CIB. (1989) *Actions on structures: Self-weight loads*. CIB Report No. 115.
44. Guo, Q., & Jeffers, A. E. (2014). Finite-element reliability analysis of structures subjected to fire. *Journal of Structural Engineering*, 141(4), 04014129. [https://doi.org/10.1061/\(ASCE\)ST.1943-541X.0001082](https://doi.org/10.1061/(ASCE)ST.1943-541X.0001082)
45. Iqbal, S., & Harichandran, R. (2010). Capacity reduction and fire load factors for design of steel members exposed to fire. *Journal of Structural Engineering*, 136(12), 1554–1562. [https://doi.org/10.1061/\(ASCE\)ST.1943-541X.0000256](https://doi.org/10.1061/(ASCE)ST.1943-541X.0000256)
46. Gernay, T., Van Coile, R., Elhami Khorasani, N., & Hopkin, D. (2019). Efficient uncertainty quantification method applied to structural fire engineering computations. *Engineering Structures*, 183, 1–17. <https://doi.org/10.1016/j.engstruct.2019.01.002>
47. Holicky, M. & Sleich, J. B. (2005) Accidental combinations in case of fire. In *Implementation of Eurocodes: Handbook 5*. [Online] Available: [eurocodes.jrc.ec.europa.eu](http://eurocodes.jrc.ec.europa.eu).
48. Chalk, P. L., & Corotis, R. B. (1980). Probability model for design live loads. *Journal of the Structural Division*, 106(10), 2017–2033.

49. Ellingwood, B. R., & Culver, C. G. (1977). Analysis of live loads in office buildings. *Journal of the Structural Division*, 103(8), 1551–1560.
50. CIB. (1989) *Actions on structures, live loads in buildings*. CIB Report No. 116.
51. Van Coile, R. (2015). *Reliability-based decision making for concrete elements exposed to fire*. Doctoral dissertation, Ghent University, Belgium.
52. Ravindra, M. K., & Galambos, T. V. (1978). Load and resistance factor design for steel. *Journal of the Structural Division*, 104(9), 1337–1353.
53. Qureshi, R., Ni, S., Van Coile, R., Elhami Khorasani, N., Hopkin, D., & Gernay, T. (2020). Probabilistic models for temperature dependent strength of steel and concrete. *ASCE Journal of Structural Engineering*, 146(6), 04020102.
54. CEN. (2004) EN 1992-1-2 Eurocode 2 – Design of concrete structures – Part 1-2: General rules – Structural fire design.
55. Elhami Khorasani, N., Gardoni, P., & Garlock, M. (2015). Probabilistic fire analysis: Material models and evaluation of steel structural members. *Journal of Structural Engineering*, 141(12), 04015050. [https://doi.org/10.1061/\(ASCE\)ST.1943-541X.0001285](https://doi.org/10.1061/(ASCE)ST.1943-541X.0001285)
56. Stephani, A., Van Coile, R., Elhami Khorasani, N., Gernay, T., & Hopkin, D. (2018). Probabilistic model for steel yield strength retention factor at elevated temperatures, influence of model choice on structural failure fragility curve. In *Proceedings of the 16th International Probabilistic Workshop (IPW), September 12–14 2018 Vienna, Austria*.
57. Luecke, W. E. (2011). High- temperature tensile constitutive data and models for structural steels in fire. *NIST Technical Note 1714*. Gaithersburg, MD.
58. CEN. (2005). *EN 1993-1-2:2005 - Eurocode 3. Design of steel structures. General rules. Structural fire design*. Brussels, Belgium, CEN: European Committee for Standardization.
59. Brandon, D. (2018). Engineering methods for structural fire design of wood buildings— structural integrity during a full natural fire. *Brandforsk Technical Report, 2018, 2*.
60. Lange, D., Bostrom, L., Schmid, J. & Albrektsson, J. (2014) The influence of parametric fire scenarios on structural timber performance and reliability. *Project 303–121. SP Report 2014:35*. Sweden.
61. Lange, D., Bostrom, L., & Schmid, J. (2016). Reliability of timber elements exposed to fire. In *Proceedings of World Conference on Timber Engineering, August 22–25, 2016 Vienna, Austria*.
62. Hietaniemi, J. (2005) A probabilistic approach to wood charring rate. *Espoo: VTT; 2005* [Online] (VTT Working Papers 31). Available: <http://www.vtt.fi/inf/pdf/workingpapers/2005/W31.pdf>.
63. Johansson, N., van Hees, P., & Sårdqvist, S. (2012). Combining Statistics and Case Studies to Identify and Understand Deficiencies in Fire Protection. *Fire Technology*, 48(4), 945–960. <https://doi.org/10.1007/s10694-012-0255-z>
64. BSI. (2019) PD 7974–7:2019—Application of fire safety engineering principles to the design of buildings. Probabilistic risk assessment.
65. Hopkin, D., Van Coile, R. & Fu, I. (2018) Developing fragility curves and estimating failure probabilities for protected steel structural elements subject to fully developed fires. In *Proceedings of the 10th International Conference on Structures in Fire*. Belfast.
66. Bucher, C. (2009). *Computational analysis of randomness in structural mechanics: Structures and infrastructures book series* (Vol. 3, 1st ed.). CRC Press. <https://doi.org/10.1201/9780203876534>
67. Olsson, A., Sandberg, G., & Dahlblom, O. (2003). On Latin hypercube sampling for structural reliability analysis. *Structural Safety*, 25(1), 47–68. [https://doi.org/10.1016/S0167-4730\(02\)00039-5](https://doi.org/10.1016/S0167-4730(02)00039-5)
68. Hasofer, A. M., & Lind, N. C. (1974). Exact and invariant second-moment code format. *Journal of the Engineering Mechanics Division*, 100(1), 111–121.
69. Rackwitz, R., & Fiessler, B. (1978). Structural reliability under combined random load sequences. *Computers & Structures*, 9(5), 489–494.

70. Papoulis, A., & Pillai, U. (2001). *Probability, random variables and stochastic processes* (4th ed.). McGraw-Hill.
71. Novi Inverardi, P. L., & Tagliani, A. (2003). Maximum entropy density estimation from fractional moments. *Communications in Statistics: Theory and Methods*, 32(2), 327–345. <https://doi.org/10.1081/STA-120018189>
72. Van Coile, R., Balomenos, G., Pandey, M., & Caspeepe, R. (2017). An unbiased method for probabilistic fire safety engineering, requiring a limited number of model evaluations. *Fire Technology*, 53(5), 1705–1744. <https://doi.org/10.1007/s10694-017-0660-4>
73. Zhang, X. (2013) *Efficient computational methods for structural reliability and global sensitivity analyses*. Doctoral dissertation. University of Waterloo, Waterloo, Canada.
74. Gernay, T., Elhami Khorasani, N., & Garlock, M. (2019). Fire fragility functions for steel frame buildings: Sensitivity analysis and reliability framework. *Fire Technology*, 55(4), 1175–1210. <https://doi.org/10.1007/s10694-018-0764-5>
75. FEMA. (2019). HAZUS. <https://www.fema.gov/hazus> (accessed 12/7/2019).
76. Porter, K., Kennedy, R., & Bachman, R. (2007). Creating fragility functions for performance-based earthquake engineering. *Earthquake Spectra*, 23(2), 471–489.
77. Gernay, T., Khorasani, N. E., & Garlock, M. (2016). Fire fragility curves for steel buildings in a community context: A methodology. *Engineering Structures*, 113, 259–276. <https://doi.org/10.1016/j.engstruct.2016.01.043>
78. Van Coile, R., Bisby, L., Rush, D., & Manes, M. (2017). Design for post-fire use: a case study in fire resilience design. In Y. Lu, A. Usmani, K. Cashell, & P. Das (Eds.), *Second International conference on structural safety under fire and blast loading – CONFAB 2017. London*.
79. Ioannou, I., Aspinall, W., Rush, D., Bisby, L., & Rossetto, T. (2017). Expert judgment-based fragility assessment of reinforced concrete buildings exposed to fire. *Reliability Engineering & System Safety*, 167, 105–127. <https://doi.org/10.1016/j.res.2017.05.011>
80. Ioannou, I., Rush, D., Bisby, L., Aspinall, W. & Rossetto, T. (2015) Application of expert judgment to the quantification of a damage scale for reinforced concrete buildings exposed to fire. In: *2015. 12th International Conference on Applications of Statistics and Probability*.
81. Cooke, R. (1991) *Experts in uncertainty: Opinion and subjective probability in science*: Oxford University Press on Demand.
82. Devaney, S. (2015) *Development of software for reliability based design of steel framed structures in fire*. PhD Thesis, University of Edinburgh.
83. Devaney, S., Lange, D., Usmani, A. & Manohar, C. S. (2012) Development of a performance-based structural fire engineering framework for implementation as a software design tool. In *Proceedings of the 6th International Asranet Conference, 2012 Croydon*.
84. Devaney, S., Usmani, A. & Manohar, C. S. (2014) Software firelab for probabilistic analysis of steel-framed structures in fire. In: Li, G.-Q., Kodur, V., Jiang, S.-C., Jiang, J., Chen, S.-W. & Lou, G.-B. (Eds.) *Proceedings of the 8th International Conference on Structures in Fire, 2014 Shanghai* (pp. 919–926). Tongji University Press.
85. Hamilton, S. (2011) *Performance-based fire engineering for steel framed structures: a probabilistic methodology*. PhD Thesis, Stanford University.
86. Lange, D., Devaney, S., & Usmani, A. (2014). An application of the PEER performance based earthquake engineering framework to structures in fire. *Engineering Structures*, 66, 100–115. <https://doi.org/10.1016/j.engstruct.2014.01.052>
87. Baker, J. W., & Cornell, C. A. (2008). Vector-valued Intensity Measures Incorporating Spectral Shape for Prediction of Structural Response. *Journal of Earthquake Engineering*, 12(4), 534–554. <https://doi.org/10.1080/13632460701673076>
88. Shrivastava, M., Abu, A. K., Dhakal, R. P., & Moss, P. J. (2019). Severity measures and stripe analysis for probabilistic structural fire engineering. *Fire Technology*, 55(4), 1147–1173. <https://doi.org/10.1007/s10694-018-0799-7>
89. Elhami Khorasani, N., Gernay, T., & Garlock, M. (2017). Data-driven probabilistic post-earthquake fire ignition model for a community. *Fire Safety Journal*, 94, 33–44. <https://doi.org/10.1016/j.firesaf.2017.09.005>

90. LeGrone, P. D. (2004) An analysis of fire sprinkler system failures during the Northridge earthquake and comparison with the seismic design standard for these systems. In *Proceedings of the 13th World Conference on Earthquake Engineering Conference*. Vancouver, Canada.
91. Van Coile, R., Caspeele, R. & Taerwe, L. (2013) The mixed lognormal distribution for a more precise assessment of the reliability of concrete slabs exposed to fire. In *Proceedings of ESREL* (Vol. 2013, No. 29/09), 2013. pp. 2–10.
92. Thienpont, T., Van Coile, R., De Corte, W. & Caspeele, R. (2019) Determining a global resistance factor for simply supported fire exposed RC slabs. In *Fib Symposium 2019 concrete-innovations in materials, design and structures*.
93. Ang, A. H.-S., & Tang, W. H. (2007). *Probability concepts in engineering planning and design: Emphasis on application to civil and environmental engineering*. Wiley.
94. The Concrete Society. (2008) Assessment, design and repair of fire-damaged concrete structures. *Technical report no. 68*. Camberley, UK: The Concrete Society.
95. Ingberg, S. H. (1928). Tests of the severity of building fires. *NFPA Quarterly*, 22(1), 43–61.
96. Porter, K. A. & Kiremidjian, A. S. (2000) *Assembly-based vulnerability of buildings and its uses in seismic performance evaluation and risk-management decision-making*: SPA Risk LLC.
97. Porter, K. A. (2003) An overview of PEER's performance-based earthquake engineering methodology. In *Ninth International Conference on Applications of Statistics and Probability in Civil Engineering (ICASP9)*, San-Francisco, USA.

# Chapter 10

## Advanced Analysis



Thomas Gernay and Panos Kotsovinos

### 10.1 Basics of Advanced Analysis

#### 10.1.1 Context and Purpose

##### 10.1.1.1 Definition of Advanced Analysis in Structural Fire Engineering

The behavior of structures under fire is generally complex and highly nonlinear. It involves, first, establishing the development and distribution of the temperature within structural members, with transient thermal conduction in the sections leading to nonlinear temperature gradients. Second, it requires assessing the mechanical behavior of the structure (or of some part of it), which is affected by a complex combination of changes of mechanical properties with temperature and effects of thermally induced strains and stresses. As a result, the use of analytical methods leading to closed-form solutions is only possible in the field for models of limited sophistication. For instance, analytical methods are mainly developed for analyzing structural members under thermal actions generated by a nominal (standard) fire. For other thermal actions, the temperature profiles are different and simple methods are generally not available. Furthermore, analytical methods have mostly been developed for the analysis of isolated members, and cannot account for the indirect fire actions resulting from the interaction with the rest of the structure (or if they do, it is in a very simplified manner).

---

T. Gernay (✉)  
Johns Hopkins University, Baltimore, MD, USA  
e-mail: [tjernay@jhu.edu](mailto:tgernay@jhu.edu)

P. Kotsovinos  
Arup, Manchester, UK  
e-mail: [Panos.Kotsovinos@arup.com](mailto:Panos.Kotsovinos@arup.com)



In this context, the development of advanced analysis aims at providing methods in which engineering principles are applied and the fundamental physical behavior is considered in order to lead to a realistic approximation of the expected behavior of structures exposed to fire. As with any method of analysis, the fundamental relations of equilibrium, compatibility, and constitutive material laws are considered. However, the system of partial differential equations obtained from these relations is generally handled through an approximate solution that is solved numerically, for instance using the finite element method, rather than through the search for closed-form solutions. Because advanced analysis is based on the fundamental physical behavior, it can be used to model the response of entire structures of any shape or material under any fire exposure. This statement must be tempered, however, by the fact that the model inputs, such as the material properties, must be known with sufficient reliability and properly incorporated in the model.

Advanced analysis is thus a powerful and versatile method at the service of structural fire engineers. It is particularly useful to those who wish to adopt a performance-based approach, although it can also be used in a prescriptive framework. It allows dealing with nonlinearities and large displacements; see Sect. 10.1.3. Yet, a solid understanding of the assumptions and limitations of the method is essential to its proper use. Results of advanced analysis are directly dependent on the quality of the model and reliability of the input data. These results may be significantly affected by engineering decisions on the type of finite element that is used, the boundary conditions, the material constitutive models, or the imperfections, amongst others. Most importantly, structural fire engineers should be aware of any potential failure modes not covered by their advanced analysis and should exclude these failure modes by appropriate means. Examples may include spalling, shear and bond failure in concrete members, or local buckling in steel members. Some of these failure modes can be captured by advanced analysis but this requires adopting the proper modeling assumptions (for instance, local buckling can be captured using shell finite elements but is usually not captured by beam finite elements). Others are currently beyond the capabilities of the models, such as spalling which remains very difficult to predict. The modeling process is discussed in detail in Sect. 10.2, while the main capabilities and limitations of advanced analysis are the focus of Sect. 10.3.

#### 10.1.1.2 Purpose of Advanced Analysis

There are two main reasons to adopt an advanced analysis method for determination of the behavior of a structure in the fire situation:

1. Simplified methods are not applicable to the case under study, given the complexity or sophistication, so that advanced analysis is the only option. Indeed, the scope of simplified methods is limited in terms of fire representation and structural model. Simplified methods are primarily developed for nominal fires; very few models have been proposed to account for more realistic fire exposure. As a

**Table 10.1** Alternative methods for determination of fire resistance under a nominal fire (adapted from Eurocode)

Nominal Fire			
	Tabulated data	Simplified methods	Advanced methods
Member analysis	YES	YES	YES
Analysis of parts of the structure	–	YES (if available)	YES
Global structural analysis	–	–	YES

**Table 10.2** Alternative methods for determination of fire resistance under a fire evaluated in a performance-based approach (adapted from Eurocode)

Physically based thermal actions			
	Tabulated data	Simplified methods	Advanced methods
Member analysis	–	YES (if available)	YES
Analysis of parts of the structure	–	–	YES
Global structural analysis	–	–	YES

result, the consideration of physically based thermal actions generally leads to the need for advanced analysis (Table 10.2). This will be the case, for instance, when analyzing structures under heating and cooling-down phases, or when analyzing large structures (stadiums, train stations, open-space office buildings, etc.) in which localized or traveling fires are expected. Similarly, simplified methods apply mainly to individual members. In few cases, they can be applied to the analysis of parts of a structure, where the indirect fire actions within the subassembly are considered in a simplified manner, but no time-dependent interaction with other parts of the structure is accounted for. In any case, for performing a global structural analysis where indirect fire actions are considered throughout the entire structure, it is necessary to adopt an advanced analysis (Tables 10.1 and 10.2). Advanced methods may also be necessary, even for member analysis, if the section shape is complex or irregular. Finally, advanced methods are needed if one wants to get an understanding of the actual fire response of a structure (beyond a simple fire resistance design check). This is relevant, for example, to evaluate different degrees of damage as part of a fire resilience assessment, or to evaluate the reliability level of a design.

2. Simplified methods are applicable but do not allow the justification of a sufficient fire resistance and, since these methods are based on conservative assumptions, it is expected that the use of advanced analysis may lead to evaluation of an improved fire resistance. Indeed, as a general rule, methods of a higher degree of sophistication aim at capturing more accurately the real behavior, whereas simplified methods provide more crude estimates which should be on the conservative side. In certain cases, it might be esteemed that simplified methods would lead to an overly conservative fire design, so that it is desirable to shift to an advanced analysis. This may be the case, for instance, when a nominal fire appears as an excessively severe thermal action because flashover is very unlikely to occur, or when the interaction between structural members is expected to

provide a significant beneficial effect on the fire behavior as is the case for instance with the development of tensile membrane action in steel-concrete floors.

In Europe, the Eurocodes permit the use of advanced analysis for structural design. It is specified that advanced calculation methods should include calculation models for the determination of the temperature distributions within structural members (thermal response model) and the mechanical behavior of the structure (mechanical response model).

In the USA, ASCE/SEI 7 Appendix E [1] was recently introduced that allows the use of advanced analysis along with the use of natural fires for the performance-based design of structures. A manual of practice has also been developed by ASCE [2] to assist structural fire engineers.

Other countries also have their codes for fire design, which may allow for the use of advanced methods such as in New Zealand and Australia.

### **10.1.1.3 Thermal Response**

Advanced analysis of the thermal response of structural members in fire is based on the well-established theory of heat transfer. The thermal actions generated by the fire are input in the analysis. The determination of the temperature evolution and distribution within structural members should consider the variation of the thermal properties of the materials with temperature. The effects of heat transfer to adjacent building components may be included where appropriate, such as in the case of a beam supporting a concrete slab.

### **10.1.1.4 Mechanical Response**

Advanced analysis of the mechanical behavior of structures in fire is based on the well-established principles and assumptions of the theory of structural mechanics. The analysis should take into account the combined effects of mechanical actions, geometrical imperfections, and thermal actions. In particular, geometrical nonlinear effects can play a significant role in the mechanical response under fire due to thermally induced strains. The effects of thermally induced stresses both due to temperature rise and due to temperature gradients need also to be included in the model. Finally, the analysis should take into account the changes of mechanical properties of the materials with temperature, as well as the material nonlinear effects.

Advanced analysis can be performed without pre-embedded failure criterion, and therefore be run until it fails to converge to a state of equilibrium for the structure or it encounters numerical problems at the material level. It must be verified that the deformations predicted by the analysis remain acceptable with respect to adequate

support at the boundaries and compatibility with the remainder of the structure (not present in the model). The assessment of failure is discussed further in Sect. 10.4.

### 10.1.1.5 Validation of Advanced Analysis Method

The numerical software used for advanced analysis typically use relevant test results for validation. Use of sensitivity analysis to verify the physical sense of the model is also good practice. The Eurocode states: “The critical parameters should be checked to ensure that the model complies with sound engineering principles, by means of a sensitivity analysis. Critical parameters may refer, for example to the buckling length, the size of the elements, the load level.” Verification, validation, and review process are discussed in Sect. 10.5.

### 10.1.1.6 Scope of the Chapter

The objective of this chapter is to describe the main principles and assumptions of advanced analysis in the field of structures in fire. It covers the different steps of the analysis, from the definition of the conceptual model to the modeling of elements and materials. Being aimed at structural fire engineers, it focuses on the typical construction members that are the beams, columns, walls, and slabs, while also providing information about trusses, bracings, and connections. In terms of materials, it deals mainly with steel and concrete, while briefly describing the case of timber. Rather than providing an exhaustive guidance, this chapter is designed to highlight the most important aspects of advanced analysis and to discuss issues that, while being often overlooked, are critical to the practitioners, such as the assessment of failure and the validation process. A whole section is also dedicated to defining the main capabilities and limitations of current advanced analysis models used in the field. Indeed, the problem of capturing the effect of fire on structures remains a very challenging one, which requires dealing with multiple physics, scales, and uncertainties; therefore it is deemed essential to explicitly highlight the types of problems that still remain beyond the predictive capabilities of the current state of knowledge. Finally, the chapter briefly presents different software that are typically used in the field.

The chapter is structured as follows. Section 10.1 discusses important aspects of advanced analysis including the nonlinearity, discretization process, and computational aspects. Section 10.2 examines the modeling process when conducting an advanced analysis, from the conceptual definition of the model to the representation of elements, connections, materials, imperfections, and boundary conditions. Section 10.3 presents the main capabilities and limitations of advanced analysis. Section 10.4 discusses the assessment of failure. Section 10.5 presents the verification, validation, and review process. Finally, Sect. 10.6 gives an overview of the different types of software.

### ***10.1.2 Discretization***

Multiple computational strategies can be adopted for the discretization of the structures for the purposes of advanced analysis. The most common approaches are finite element analysis (FEA), finite difference (FD), finite volume method (FVM), and boundary element method (BEM).

For structures in fire, it is common to adopt the use of finite element analysis (nonlinear) for both the thermal and mechanical response assessment of structures or alternatively the use of finite difference (or an empirical calculation method) for the assessment of the thermal response and the use of finite element analysis (nonlinear) for the mechanical response assessment. As a result, this chapter subsequently only focuses on the latter types of analysis that are commonly used in the context of structural fire engineering. More information is given in Sect. 10.2.3 on the different types of elements used to model the structural members.

### ***10.1.3 Nonlinearity***

There are two main types of nonlinearities affecting the behavior of structures. Material nonlinearities are related to processes taking place at the material level, such as yielding in steel or cracking in concrete, when the strains exceed the linear elastic range. Geometrical nonlinearities stem from large deformations of the structure, which lead to additional internal actions and consequently even larger deformations. Both types of nonlinearities may be even more important in the fire situation than at ambient temperature, as explained below. Advanced analysis is the most appropriate method to account for these nonlinearities.

#### **10.1.3.1 Material Nonlinearity**

The occurrence and significance of material nonlinearities may be amplified by the fire loading. As properties degrade with temperature, the heated material can enter in yielding or cracking even if the loads are kept constant. Besides, the stress-strain behavior of several materials becomes more nonlinear with increasing temperature. For steel, for instance, the proportional limit, giving the maximum stress up to which the behavior is linear elastic, is reduced faster with temperature than the yield strength [3]. For concrete, it is typical to have cracking develop in the central part of the section as a result of internal (auto-equilibrated) thermal stresses developing due to the nonlinear thermal gradient.

### 10.1.3.2 Geometrical Nonlinearity

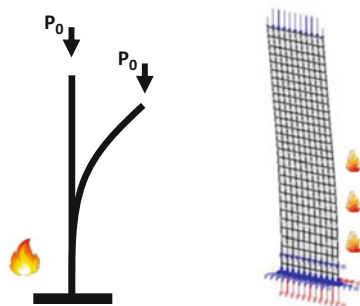
The deformations of a heated structure are generally amplified due to thermal expansion. This can increase the effects of geometrical nonlinearities. For instance, the behavior of a structural wall heated on one face is highly influenced by its thermal curvature (Fig. 10.1). The resulting P- $\Delta$  effect, i.e., the effect of the increasing eccentricity of a load applied at the top of the element, may generate significant internal forces leading to failure. As an example, experimental tests at Notre Dame University [4] have shown the effects of one-sided fire exposure on the out-of-plane deflections and failure of reinforced concrete walls, while finite element modeling of these experiments [5] has shown that this behavior can be captured with advanced analysis using shell elements and a plasticity-damage concrete model.

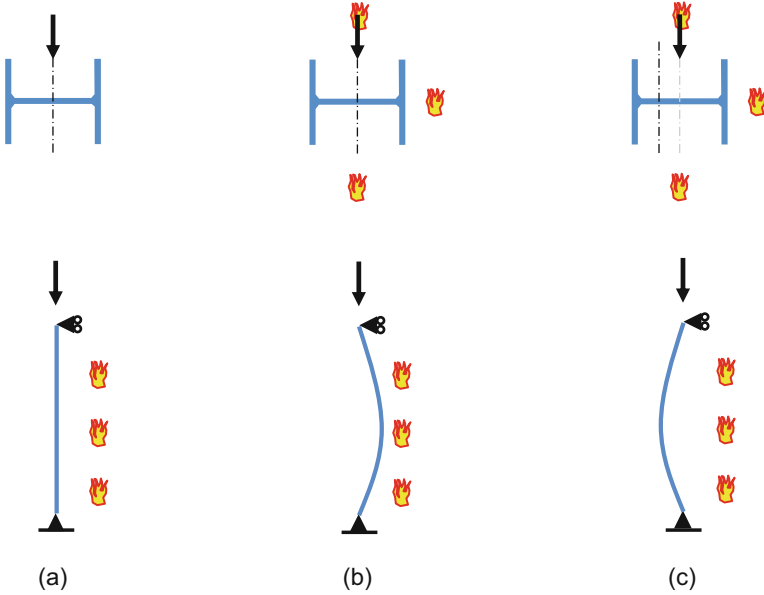
The second-order effects produced by fire in structures are complex because of the combination of the effects of thermal strain and material degradation. For instance, consider a column that is simply supported, axially loaded, and exposed to fire on three sides (Fig. 10.2). The thermal gradient generates two effects. On the one hand, the differential thermal elongation between the hot right part and the cold left part produces a thermal curvature where the column bends toward the fire (Fig. 10.2b). On the other hand, the same thermal gradient leads to a shift to the left of the neutral axis position. This results in an eccentricity of the applied load that tends to bend the column opposite to the fire (Fig. 10.2c). At any moment during the fire, these two effects compete. The tendency of the column to bend in one direction or the other will depend on many parameters including the cross-section geometry, heating rate, magnitude of the applied load, etc., and the direction of bending may change over the course of the fire. Advanced analysis can trace these effects by accounting for geometrically nonlinear effects and thermal gradients in the cross section (e.g., using fiber-based beam finite elements).

### 10.1.3.3 Whole-Building Behavior

As discussed in Sect. 10.1.1, advanced calculation methods are the only option for the analysis of structural systems. They allow taking into account the effects of the

**Fig. 10.1** Deflection of a cantilever wall subjected to fire on one face





**Fig. 10.2** (a) Column subjected to axial compression and three-sided fire exposure. (b) The effects of thermal bowing and (c) the effects of the shift of the neutral axis position produce complex second-order effects



**Fig. 10.3** Shear failure of a column outside the fire compartments due to thermal expansion of a floor

surrounding structure on the elements or structural assemblies subjected to fire. Generally, these effects are nonlinear. Due to thermal expansion, restraints at the boundaries of the fire-affected structure can lead to significant forces building up. These forces can be either detrimental or beneficial to the fire-affected structure. For instance, a vertical axial restraint on a column can lead to premature failure in buckling. On the other hand, for reinforced or prestressed concrete slabs or beams, a horizontal axial restraint force may have a positive effect on the fire behavior, provided that the line of thrust is below the compressive stress block. Meanwhile, these restraint forces may also jeopardize the surrounding structure. For instance, thermal expansion of a concrete floor can lead to shear failure of a stiff column (Fig. 10.3). It is therefore important to carefully consider the effects of thermally induced forces both on the fire-affected elements and on the surrounding structure.

Nonlinear advanced analysis is also able to account for redundancies in a structure. It may be used to simulate the load redistributions that occur in a structure following failure of one or a few elements. This capability has been used by several researchers to study alternative failure mechanisms and progressive collapse. In this case, the analysis should account for large displacements. Also, a dynamic solver is recommended for numerical convergence as explained in Sect. 10.1.4.

### ***10.1.4 Computational Aspects***

#### **10.1.4.1 Thermal-Structural Model**

Several software packages allow performing advanced structural fire analysis. An important aspect of any such software lies in the way the thermal and structural analyses are coupled. In particular, the mapping of the temperatures obtained from the thermal analysis to the members of the structural analysis is a critical aspect.

For instance, some software packages use a fiber discretization of the section for the thermal analysis of beam elements. The section is discretized with 2D finite elements (fibers), each one made of its own material. The temperatures are calculated during the thermal analysis. Then, in the subsequent mechanical analysis, which uses beam-type elements, the determination of forces and stiffness in the section are based on the temperatures in each fiber. More specifically, at any time step each fiber is associated with its own constitutive model and its own thermal strain based on its current temperature. The strains and stresses are evaluated in each fiber and then integrated over the cross section. This method has proven to be versatile and efficient to capture the effects of nonlinear temperature gradients in cross sections of any shape and materials.

Shell elements are typically used to model planar members (e.g., floors, walls) as well as the plates of steel sections prone to local instabilities. In shell elements, a typical assumption is that the temperature varies across the thickness of the plate but not in the plane of the element. Unidirectional heat transfer is assumed. When the thermal boundary conditions are not uniform, such as with localized fire exposures, it may be required to capture differences in temperatures in the plane of the element as well.

When using solid 3D elements, the same discretization is typically used for the thermal and the structural analysis. This allows a direct mapping of the outcome of the thermal analysis into the structural analysis. However, this leads to more computationally expensive models. Also fully 3D constitutive models are needed that capture the tridimensional stress-strain behavior of materials at elevated temperature.



#### 10.1.4.2 Static vs. Dynamic and Implicit vs. Explicit Models

Finite element solvers are generally categorized into static and dynamic and implicit or explicit which can all be used for the analysis of structures in fire. There can be any type of combination; that is, solvers can be implicit static, implicit dynamic, explicit static, or explicit dynamic. It should be however noted that the majority of commercial explicit solvers are primarily dynamic and it is not common to have an explicit static solver. Some software may offer all types of solvers (typically generic finite element software) while other software may only offer the possibility of a single type of solver (typically specialist software or developed as part of research projects).

Depending on the type of solver, as expected a different solution algorithm may be adopted. In a strongly nonlinear analysis such as that of structures in fire, the chosen solution algorithm and the numerical parameters selected can have a significant impact on the convergence of the model and on the final accuracy of the results. Multiple solution algorithms have been proposed in the finite element literature. For the analysis of structures in fire, it is common to adopt Newton-Raphson for implicit static analysis, Newmark for implicit dynamic analysis, and central difference for explicit dynamic analysis. It is outside the scope of this chapter to numerically describe these solution algorithms in detail since these can be found in standard finite element textbooks.

Dynamic solvers are based on the equation of motion and therefore take into account inertia effects while for static solvers, time is only a computational expression for factoring the loads and/or varying the temperature during an analysis. Due to its application time, fire when applied to structures is not necessarily a dynamic phenomenon. However, a dynamic approach is often employed when considering redundant structures as a numerical tool to go beyond limit points and account for temporary dynamic motion which is not present during the whole duration of a fire. Indeed, consideration of the inertia effects during sudden local failure in a structure stabilizes the numerical solver and therefore may allow for more robust numerical integration enabling the continuation of the simulation beyond this local failure.

Table 10.3 notes the characteristic differences between running an implicit or an explicit analysis.

## 10.2 Modeling Process

### 10.2.1 *Definition of the Conceptual Model and the Modeling Criteria*

Depending on the goals of a project after a fire scenario has been established, three types of advanced analysis can be considered: structural/stress, thermal, or coupled structural-thermal. The selection of the properties of a numerical model (solver,

**Table 10.3** Different types of finite element solvers

	Explicit	Implicit
Matrix inversion	No	Yes
Time step size	Small	Can be large
Convergence	No convergence required	Convergence required
What limits the time step?	Stability	Accuracy
Cost per time step	Small	Large
What dominates the cost?	Element processing	Matrix inversion
Acceleration	Acceleration is constant for each time step	Varies linearly over one time step
	Velocity is linear for each time step	

elements, materials, etc.) in a nonlinear structural fire analysis will be dependent on a number of factors such as:

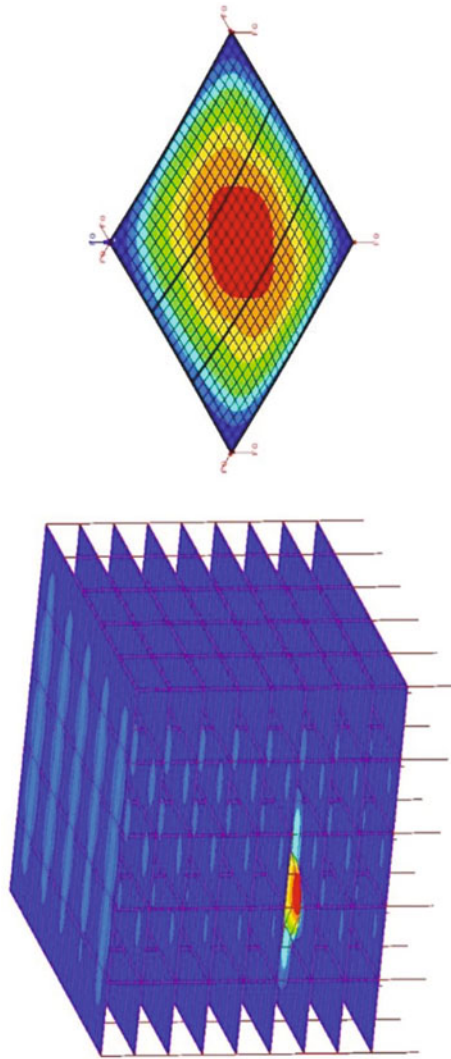
- The objectives of the analysis.
- The type and accuracy of the response required (e.g., analysis of global vs. local response).
- The “cost” in the development of the numerical model.
- The “cost” in running a numerical model and the interpretation of results (considering that often several parametric studies need to be performed).
- The experience of the user.

As a result, there can be a variety of approaches that can be adopted on a case-by-case basis.

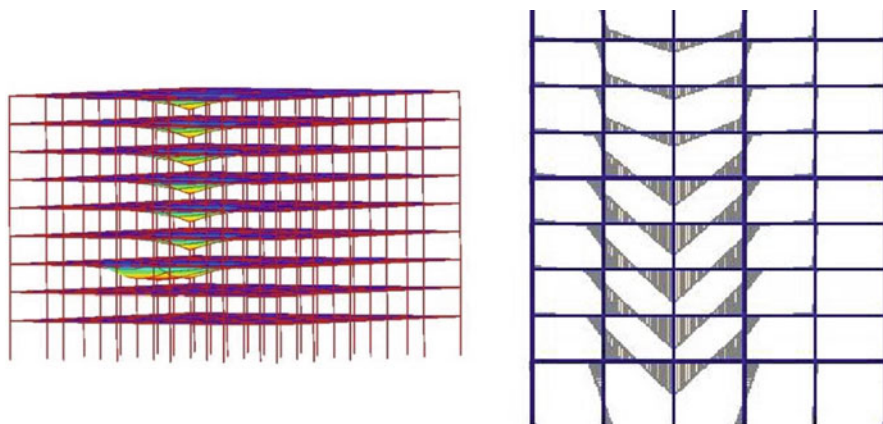
### 10.2.1.1 Extent of Finite Element Models

The extent and boundaries of a finite element model for structural fire analysis can depend on the intent of the analysis, extent of the fire-affected zone, and potential symmetries in the geometry and need to be strategically selected by modelers in advance of progressing with the development of the model.

On the one end global finite element models (which could include for example the whole floor plate of a building) can be used when the interest is on understanding the overall structural response of a structural frame (Fig. 10.4). Global models are also needed when studying the response to a global scenario, such as when studying a multi-compartment fire spread within a multistory steel-concrete building [6]. Local models on the other hand could focus on specific structural assemblies or components. These can range from models of a floor system acting in tensile membrane action [7] to simulations of beam-column members [8] to detailed modeling of a bolted steel connection [9]. Local models are commonly used when the interest is in the detailed response of a member or component which would otherwise be too numerically expensive or repetitive to be undertaken in a global model. Additionally,



**Fig. 10.4** Model of the full building versus the floor system in the fire compartment [6]



**Fig. 10.5** A full building model in 3D [6] versus in 2D [10]

local models can be used for obtaining more efficiently than global models an estimate of the global structural response and for undertaking extensive parametric studies.

Additionally, symmetry can often be employed by modelers in order to reduce the extent of a finite element model. In certain instances, this could also lead to the representation of a structure in two-dimensional form instead of its three-dimensional form. The two-dimensional representation results in omitting certain structural responses (Fig. 10.5). Notably, in steel-concrete composite buildings, it neglects the possible beneficial effect of tensile membrane action developing in the floor systems, which may lead to an overconservative assessment of the structural fire response. In other cases, omitting certain three-dimensional structural effects may not be conservative, for example due to disregarded thermally induced forces in the orthogonal plane [11]. A careful assessment of the implications is thus needed.

The areas of the structure not included in a structural fire analysis need to be considered as boundary conditions in the finite element model. These boundary conditions are typically achieved in the simplest form by restraining the appropriate (translational and rotational) degrees of freedom of nodes in the boundaries of the model. Alternatively, spring elements with linear or nonlinear properties can also be utilized to more realistically represent the axial and bending stiffness of the surrounding structure not included in the finite element model. Boundary conditions are described in more detail in Sect. 10.2.6.

### **10.2.2 General Procedure for a SFE Advanced Analysis**

The analysis of the performance of a structure in fire requires completing the following steps:

- (a) Selection of the relevant design fire scenarios.
- (b) Evaluation of the fire development in the vicinity of the structure.
- (c) Evaluation of the temperature evolution within the structural members.
- (d) Evaluation of the structural response of the heated structure.

### **10.2.2.1 Selection of the Relevant Design Fire Scenarios**

The identification of the relevant design fire scenarios and the associated design fires for the considered structure should be determined on the basis of a fire risk assessment. More information is given in Chap. 4.

### **10.2.2.2 Evaluation of the Fire Development in the Vicinity of the Structure**

The development and growth of the fire depend on many parameters including ventilation, fire load, geometry of the compartment, etc. For instance, open-air fires exhibit a distinct behavior compared to fires in small enclosed area because of the ventilation conditions and the absence of flashover. Different types of models can be used for the evaluation of the fire development in the vicinity of the structure [12]. The simplest models are nominal time-temperature curves giving the evolution of the gas temperature. These models assume that the gas temperature is continuously increasing (i.e., no cooling phase) and is spatially uniform. Examples are the Eurocode standard fire [13] and the ASTM standard fire [14]. On the other hand, natural fire models can be used to account for the cooling phase of the fire. Natural fire models may assume a uniform temperature distribution as a function of time (post-flashover fires in a compartment) or a spatially nonuniform temperature distribution as a function of time (localized fires). Simplified and advanced natural fire models have been proposed in the literature, including the parametric temperature-time curves of Eurocode [15], localized fire models [15], traveling fire models [16], zone models [17], and computational fluid dynamics models [18]. More information about design fires is given in Chap. 4.

### **10.2.2.3 Evaluation of the Temperature Evolution Within the Structural Members**

The results of the design fire scenarios and design fire evaluation (steps a–b) represent boundary conditions for the heat transfer analysis within the structural members (step c). Generally, the boundary conditions take the form of prescribed time-temperature relationships for the hot gases that surround the section of the structural member (e.g., for standard fire curves defined in the codes), or prescribed heat fluxes at the boundary as a function of time. The thermal actions determined from these boundary conditions, i.e., the net heat fluxes to the surface of the member,

must consider heat transfer by convection and radiation between the environment and the surfaces of the members.

The relative position of the design fire and the structural member must be taken into account. When natural fire models are adopted, the temperature analysis of the structural members needs to be made for the full duration of the fire including the cooling phase [19]. Within the member, heat transfer by conduction according to Fourier law is generally assumed. More information about heat transfer is given in Chap. 5. In advanced analyses, the heat transfer problem is usually solved using numerical methods with a discretization of the domain (e.g., finite element method) and a time integration procedure.

#### **10.2.2.4 Evaluation of the Structural Response of the Heated Structure**

As a last step, the calculation of the mechanical behavior of the structure is performed to determine the stresses, strains, and displacements in the structure exposed to fire. This calculation must account for the temperature distribution in the members determined in the previous steps. As a result of the temperature changes due to fire exposure, the mechanical properties of the materials are affected; hence the analysis must consider the temperature dependency of the properties. Besides, imposed and constrained expansions and deformations generally result in effects of actions which also need to be considered in the analysis. In advanced analyses, the mechanical problem is usually solved using numerical methods with a discretization of the domain (e.g., FEM) and a time integration procedure. A quasi-static formulation can be used as long as the structure remains relatively stable, but a dynamic formulation provides a better insight into the failure mode, by enabling to find equilibrium even after the structure or part of it becomes statically unstable.

#### **10.2.2.5 Representation of Thermal Boundary Conditions**

The thermal boundary conditions model the action of the fire on structural members. These conditions are used as an input for the heat transfer analysis within the structural members. From the user point of view, the thermal boundary conditions may take several forms. The most common forms consist of inputting prescribed time-temperature relationships for the hot gases enveloping the structure, or prescribed heat fluxes at the boundary as a function of time.

However, more sophisticated approaches are also possible. This is an advantage of advanced analysis methods over simplified methods, which allows for instance representing the attack of spatially nonuniform fires on the structural members. For instance, heat fluxes can be imported from one or several localized fire models, such as the Hasemi model [20] or the LOCAFI model [21]. As another possibility, gas temperatures can be imported from a traveling fire model such as the iTFM [22]. Finally, the fire information can be imported from a computational fluid dynamics (CFD) analysis. The CFD software fire dynamics simulator (FDS),

developed by NIST [23], is the most commonly used in the field. These advanced options are discussed more in detail in Sect. 10.3.5.

Note that, in most software, the convention when no boundary condition is applied on a surface is to assume that there is no heat exchange through this surface (i.e., it is an adiabatic boundary condition). This can be used to model an axis of symmetry. In this case, the isotherms are perpendicular to this boundary. However, for a surface that is in contact with a cold environment (for instance the upper face of a slab), a boundary condition should be applied to allow heat transfer. For instance, a gas temperature-time relationship is prescribed on the surface with a gas temperature remaining at 20 °C.

#### **10.2.2.6 Weak Coupling Strategy for Thermomechanical Analysis**

The strategy commonly adopted to deal with the coupled physics in advanced analyses of structural fire engineering is a weak coupling from the thermal problem to the mechanical problem. As discussed above, the temperature field is evaluated in the different parts of the structure up to the end of the fire prior to the mechanical analysis. The calculated temperatures are then taken into account in the subsequent mechanical analysis. However, the results of the mechanical analysis have no influence on the temperature distribution. A few FE software allow performing the thermomechanical analysis of structures with an automatic transfer of results from the thermal to the mechanical analyses (e.g., SAFIR). This strategy is valid in most cases because temperatures affect strongly the mechanical response of structures, whereas the opposite influence is negligible except in very specific situations.

#### **10.2.2.7 Sequence and Application of Loads**

In advanced analyses, verification of the fire resistance is commonly made in the time domain. The structure is mechanically loaded at room temperature to be heated thereafter with the applied loads being kept constant. The time in the mechanical simulation thus corresponds to the fire duration. This type of analysis is referred to as transient state. In practice, it is recommended to perform first an analysis at room temperature to determine the load-bearing capacity of the structure in normal conditions. This can be done by increasing the loads proportionally as a function of time at constant temperature. This exercise is highly recommended before modeling the fire behavior. First, this allows verifying the model (type of supports, of connections) in a situation that is more familiar to many users than the fire situation and, also, this gives an idea of the load level during the fire situation and, hence, of the fire resistance time that can be expected.

### 10.2.2.8 Failure

Definition of failure for structures in fire is a complex matter. Generally, advanced analysis tools do not have any failure criterion embedded as such. The time integration procedure continues until the time specified by the user is reached or until it cannot converge to a state of equilibrium for the structure or it encounters numerical problems at the material level. It is then the responsibility of the user to judge whether the last converged step corresponds to the fire resistance time or to a premature numerical failure. Conversely, excessively ductile behavior must also be detected in which cases user-defined deflection criteria have to be applied. A typical case is a beam that exhibits such horizontal displacement at its extremity that it would lose its support in a real application. More detailed discussion on the assessment of failure is given in Sect. 10.4.

## 10.2.3 Representation of Structural Members

### 10.2.3.1 Selection of Finite Elements

The selection of finite elements for representing structural members can depend on the following key parameters:

- The failure mechanisms of the structural members that are intended to be captured (bending, local instabilities, shear, lateral torsional buckling, etc.): For example, steel frame members can be modeled by beam-type finite elements when the failure modes are either global instabilities or section capacity. However these steel frame members are modeled by shell-type elements when studying local instabilities of the flanges or the web [24].
- The load-bearing mode that is intended to be captured: For example, concrete and composite steel-concrete floors can develop tensile membrane action in fire [5]; however capturing this behavior requires the use of planar elements (such as shells) rather than uniaxial elements (beams).
- The computational cost and size of the model: For example, representing a single beam using shell finite elements increases the computation cost compared with a representation using beam finite elements. The decision to adopt the latter or the former is then also influenced by whether one wants to model an entire multistory frame structure or a small subset of a structure.
- The structural form: For example, a steel beam may require a different modeling approach to a CLT beam. It should be noted that, in practice, most finite element modeling of structures in fire involves steel and steel-concrete composite structures, while concrete and timber structures are currently less frequently considered for advanced thermomechanical modelling.
- The complexity required in assessing material response: Multiaxial material models are needed for certain type of elements, yet these material models might



not be available for certain materials at elevated temperature (e.g., cross-laminated timber response in fire), hereby limiting the availability to use multiaxial elements with these materials in the current state of research.

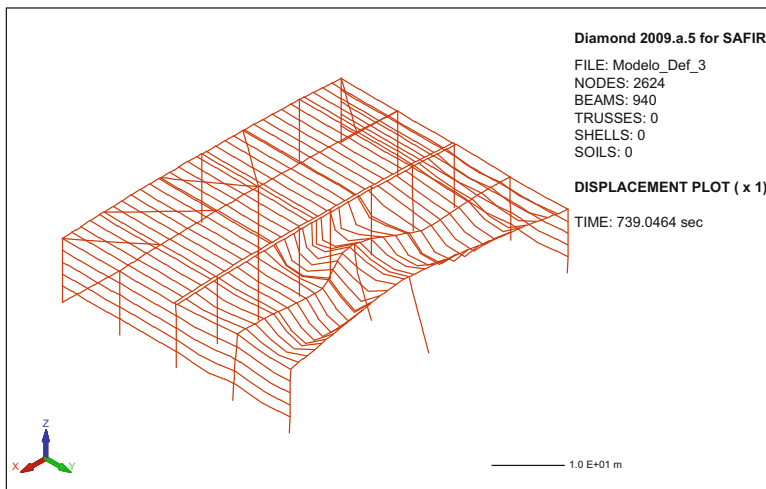
- For the thermal part, the directions of the heat transfer across the structure: For example, the heat transfer problem in frame members can generally be simplified as a 2D problem across the section, while the longitudinal heat transfer is negligible. However, the situation is different in the zone of a joint between a column and a floor, where the temperature field can be expected to be 3D.
- The required accuracy of the model.
- The availability and constraints of a given finite element software.

### 10.2.3.2 Steel or Concrete Beams/Columns

Line (also known as “beam-column” elements) elements are generally selected for representing steel or concrete beam and columns when developing global finite element models of structures in fire. It should be noted that line elements can be based on different assumptions and formulations such as Euler-Bernoulli or Timoshenko, displacement or force based, and distributed or concentrated plasticity. Independent of their formulation, beam-column elements can capture through depth cross-sectional plasticity in the structural members through the discretization of the cross section into smaller layers (also known as “fibers”). Each fiber can have its own material properties and therefore reinforced concrete or composite sections can also be represented using a single element with different layers (noting that this approach has inherent assumptions about the contact of the materials and does not allow for a potential slip). In order to capture the second-order effects and large deflections of a structural member, multiple line elements will typically be required for each structural member. The number of these line elements depends on their formulation (a fewer number of elements may be required if each element has multiple integration points along its length) and the intended accuracy of the model.

Line elements can capture global and member failure mechanisms (such as bending, buckling); see Fig. 10.6. However they cannot capture local failure mechanisms such as local buckling (Fig. 10.7), lateral-torsional buckling, and shear failure. As a result, 2D/3D elements such as shell elements and brick elements are to be used when such failure mechanisms are required to be captured. Some common examples where 2D or 3D elements may be required are:

- Slender steel sections that experience the potential of lateral-torsional buckling in particular when they are not constrained by a concrete slab [26].
- Steel cellular beams that can have specific local failure modes such as web-post buckling [27]; see Fig. 10.8.
- Steel elements that are nonuniformly heated resulting in the potential of a local failure arising in the directly heated zone [29].
- Large and deep structural members are more likely to experience local failure modes.

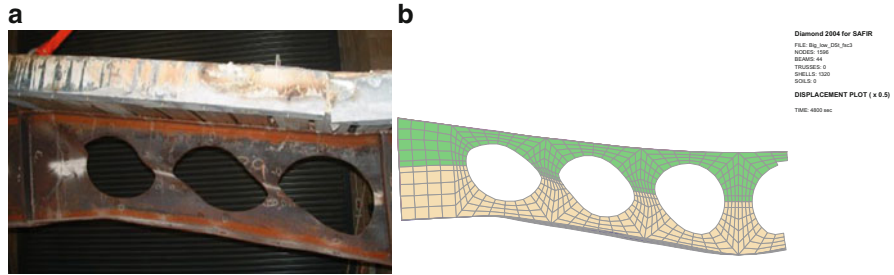


**Fig. 10.6** Global failure mechanisms of a steel frame structure in fire: finite element model using beam elements in SAFIR

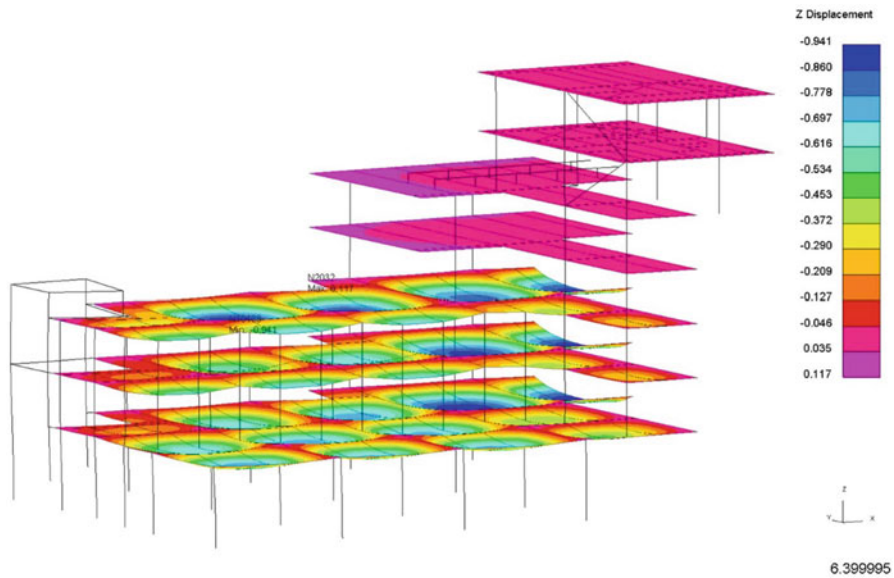
**Fig. 10.7** Local instabilities in the flanges and in the web of a slender steel column in fire: (a) FIDESC4 RFCS test and (b) finite element model using shell elements in SAFIR [25]



To take advantage of the efficiency of beam-type finite elements when dealing with slender members, effective stress approaches have been proposed to capture local instabilities through a reduction of the constitutive material law in compression [30, 31]. These approaches are convenient to enable modeling of large frame structures (e.g., Fig. 10.9) (which require an efficient computational approach for the frame members) where local buckling needs to be accounted for, as exemplified in practical applications (e.g., [32]).



**Fig. 10.8** Web-post buckling of a cellular steel beam in fire: (a) FICEB RFCS test and (b) finite element model using shell elements in SAFIR [28]



**Fig. 10.9** A concrete slab modeled with shell elements

### 10.2.3.3 Concrete Slabs

Concrete slabs are commonly considered in structural fire models (of for example composite floors). Slabs have two dimensions that are much greater compared to their third dimension. As a result, 2D/3D elements such as shell elements and brick elements can be used to represent concrete slabs. Shell elements are more commonly used for the concrete slab in combination with beam or shell elements for the steel beams when modeling composite steel and concrete slabs [33].

It should be noted that researchers have also used beam elements for modeling the global mechanical performance of concrete slabs in fire. This approach is less accurate and ignores potential localized failures and the beneficial tensile membrane action mechanism that is of primary importance for composite floors.

### 10.2.3.4 Concrete Walls

Similarly to the slabs, walls generally have two dimensions that are much greater compared to their third dimension (EN1992 definition of a wall for example is an aspect rate of breadth/width of 4). As a result, 2D/3D elements such as shell elements and brick elements can be used to represent concrete walls (Fig. 10.1).

### 10.2.3.5 Steel Trusses/Bracing

Trusses and bracing are predominantly subjected to axial forces and therefore it is common to utilize beam-column elements when modeling these members (Fig. 10.10). For slender members that are not restrained and for which the potential

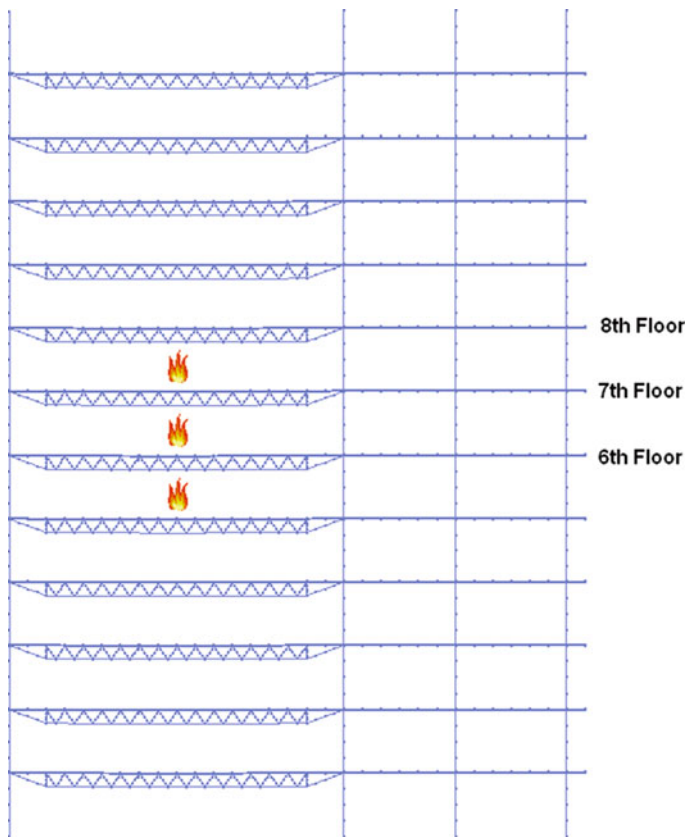


Fig. 10.10 Steel trusses modeled with beam finite elements

for lateral torsional buckling exists, 2D/3D elements such as shell elements and brick elements are required.

## ***10.2.4 Representation of Materials***

Appropriate models for the materials are needed for the evaluation of the temperature evolution within the structural members (heat transfer analysis) and the evaluation of the structural response of the heated structure (mechanical analysis).

### **10.2.4.1 Material Models for Thermal Analysis**

The material models for the heat transfer analysis should include the temperature-dependent thermal properties of the materials. Coefficient of heat transfer by convection  $\alpha_c$  and emissivity  $\varepsilon_m$  is needed for solving the heat transfer equation at the surface of the member. Different values of the coefficient of heat transfer by convection are usually assumed for the exposed and the unexposed sides of separating members. Besides, thermal conductivity, specific heat, and density are needed for finding the material temperature considering transient conduction in the solid. Temperature-dependent values for these properties are given in the literature and in design codes (e.g., Eurocode) for different materials. For materials in which water plays a role (e.g., concrete, gypsum, wood), the moisture content at the beginning of the fire should also be specified as it influences the propagation of heat through the section. Computation of the thermal solution using the enthalpy formulation, instead of the specific heat, increases stability of the time integration process in cases where the specific heat curve shows sudden and severe variations as is the case, for example, in gypsum, in carbon steel, or with the evaporation of moisture.

Wood is a combustible material which, under the action of fire, is subject to pyrolysis. Pyrolysis leads to a reduction of the thickness of timber members exposed to fire, but at the same time, a char layer is generated which provides thermal insulation to the rest of the section. In advanced analysis, a common approach consists of adopting apparent values of the thermal properties that implicitly take into account the complex phenomena at stake, such as increased heat transfer due to mass transport, e.g., due to the vaporization of moisture; increased heat transfer due to shrinkage cracks of the char layer above 500 °C; and consumption of the char layer at about 1000 °C. Using these apparent values, the thermal analysis in wood is based on Fourier conduction without an explicit modeling of the charring process.

For natural fire exposures, the thermal properties have to be defined also for the cooling-down phase. They should not necessarily be taken as reversible, in particular for materials in which water plays a role since there is generally no re-condensation of the water that was evaporated during the heating phase.

### 10.2.4.2 Material Models for Mechanical Analysis

The material models for the mechanical analysis should include the temperature-dependent mechanical properties of the materials, the thermal elongation, as well as the use of appropriate constitutive (stress-strain) relationships. Small deformations are usually assumed (but large displacements). The dimension of the constitutive relationship is dictated by the representation of the structural member. In all generality, the constitutive relationships are based on the strain decomposition of Eq. (10.1). In this equation,  $\epsilon_{tot}$  is the total strain, obtained from spatial derivatives of the displacement field;  $\epsilon_{th}$  is the thermal elongation;  $\epsilon_{\sigma}$  is the stress-related strain that contains the elastic and plastic parts of the strain;  $\epsilon_{tr}$  is the transient creep, a particular term that appears in concrete during first heating under load;  $\epsilon_{cr}$  is the basic creep, a term that develops when only time is changing with all other conditions such as stress and temperature being constant; and  $\epsilon_i$  is an initial strain representing for instance the strain that exists in in situ concrete when it hardens at a moment when loads already exist in the structure:

$$\epsilon_{tot} = \epsilon_{th} + \epsilon_{\sigma} + \epsilon_{tr} + \epsilon_{cr} + \epsilon_i \quad (10.1)$$

Beam and truss finite elements require uniaxial stress-strain relationships. An explicit equation relating the uniaxial stress  $\sigma$  to  $\epsilon_{\sigma}$  can be used. For steel, an elastoplastic relationship symmetric in tension and compression is typically assumed [3]. It is important to set a limit to the value of the strain, i.e., define an ultimate strain at which the stress falls to zero, because, physically, the material does not have infinite ductility and, mathematically, the assumption of small strains is usually made. For concrete, typical constitutive relationships include a nonlinear plastic behavior in compression and a fragile damage behavior in tension. For advanced analysis, a descending branch is required in the model. For wood, a linear relation between stress and strain until failure is usually assumed.

Shell finite elements require plane stress laws. For steel, elastoplastic models are commonly adopted, for instance with a von Mises yield function and isotropic nonlinear hardening. For concrete, various types of temperature-dependent models have been proposed, e.g., damage models [34], plastic-damage models [35], and microplane models [36]. In plastic-damage models, plasticity is for instance based on a Drucker-Prager yield function in compression and a Rankine cutoff in tension. Damage can be assumed as isotropic or anisotropic, but it should capture the different damage processes in tension and compression and the effect of stress reversal on the concrete stiffness (crack closure).

3D solid elements require triaxial laws with six independent stress components (Cauchy stress tensor). The types of models used for steel and concrete are similar to the ones described for plane stress states.

### 10.2.4.3 Steel

For steel, Young modulus and yield strength are reduced with temperature. In Eurocode, the limiting strain at effective yield stress is assumed to be independent of temperature for structural carbon steel and for reinforcing steel. The effects of transient thermal creep and basic creep in steel are generally neglected for heating rates between 2 and 50 K/min and characteristic fire durations [3]. Yet for steel members heated above approximately 400 °C for prolonged time periods, the creep effects may adversely influence the fire behavior by leading to additional second-order effects [37]. During cooling, thermal expansion is fully recovered. However, research indicates that steel heated beyond 600 °C does not fully recover its strength; a loss of residual yield strength of 0.3 MPa/°C has been proposed for steel once heated beyond 600 °C [38].

### 10.2.4.4 Concrete

For concrete, the evolution of the mechanical properties with temperature depends on the type of aggregate (siliceous or calcareous). Transient creep has a significant influence on the behavior of structural concrete in fire and therefore needs to be considered in the constitutive model [39]. Transient creep strain depends on the stress-temperature history and is irrecoverable. In a heated concrete section, the stress-temperature history is complex and involves unloading. Indeed, even with a standard fire and constant external applied loads, the stresses vary over time across the section due to differential thermal expansion. More complex stress-temperature histories are experienced in case of structural restraint or heating-cooling sequence. Models that incorporate an explicit term for tracking the evolution of transient creep (as in Eq. 10.1) should be preferred over implicit models, because only explicit models can take into account the non-reversibility of the transient creep strain component when the stress and/or the temperature is decreasing [40]. The impact of using an implicit model on the predicted structural response during cooling or unloading is a significant underestimation of the permanent strains developed in the concrete [41], which can for instance lead to an underestimation of the loads redistributed to members adjacent to the heated member [42]. Basic creep is usually neglected for typical fire durations. During cooling, the mechanical properties of strength and strain at peak stress are not reversible [43]. Extensive research has shown an additional loss of the concrete compressive strength with respect to the value at maximum reached temperature during cooling [44]. Besides, a residual thermal expansion or shrinkage is observed when the concrete is back to ambient temperature [45].

#### 10.2.4.5 Wood

For wood, the strength and stiffness start to decrease as soon as the temperature exceeds 20 °C and they reduce to zero at 300 °C (temperature of charring). In the range of 20–300 °C, different reduction factors apply to tension and compression for the strength and modulus of elasticity. The effects of transient creep should be taken into account; they are typically included implicitly in the mechanical material properties. The behavior is not reversible during cooling. The thermal strain is null.

#### 10.2.4.6 Multi-hazard

Fire can occur as a secondary event in a multi-hazard scenario. Typical primary events triggering a fire include earthquake or blast. Advanced analysis can be used to study the response of structures to a fire following earthquake [46] or fire following blast [47], but adequate material models are required to capture the behavior of the materials under these loadings. In addition to the effects of temperature, which are described above, it may be necessary to include in the models other effects at the material level such as strain rate effects.

### 10.2.5 Representation of Structural Connections

The forensic analyses of the collapses of the World Trade Center complex [48], and the Cardington steel frame fire tests [49], have highlighted that structural connections play an important role in the performance of structures in fire. Failure of connections can lead to subsequent structural failures. When structures are subjected to fire, large deformations/forces are often expected which can severely test the capacity of structural connections in particular when these have not been explicitly designed for a fire event. In a fire event, the connections are initially subjected to compression forces due to the restrained thermal expansion of the adjacent beams. These forces can change to tension, later in the fire, when the adjacent beams experience catenary action.

When undertaking advanced structural fire analysis, the structural connections can be represented in a number of different ways depending on the level of sophistication required. The most common modeling approaches can be grouped into i) use of springs to represent translational and rotational continuity; ii) suitably developed multi-spring connection elements (component-based models); iii) high-fidelity 3D connection models built from shell or brick finite elements. Recent research has also proposed the use of finite elements with additional degrees of freedom and condensation/de-condensation technique to relax the DoFs through specifying a connection behavior that can be semirigid and temperature dependent.



The selection of the appropriate modeling approach relies on the scope of the analysis as well as on the objectives and experience of the user.

### **10.2.5.1 Spring Representation of Translational and Rotational Continuity**

The representation of connections through translational and rotational springs when undertaking finite element analysis is the simplest approach. These connection elements assume total independence of the moment–rotation and force–displacement relationships of a connection. This approach has limitations since the moment–rotation relationship of the connection of a structural member will not be influenced by the axial force within the member and vice versa. A shear failure of the connection is also not considered.

### **10.2.5.2 Multi-spring Connection Elements (Component-Based Models)**

To address the limitations of the simplistic representation of translational and rotational continuity, multi-spring connection elements (component-based models) can be utilized. While these models are more advanced in comparison to the simpler spring representation, they are still simplified enough so that they can be utilized in global structural fire analyses (unlike 3D connection models).

Multi-spring connection elements can more accurately represent the role of connections during an advanced analysis. Multi-spring connection elements that have been developed in particular for structural fire engineering applications [50, 51] have multiple components in order to capture the tension, compression, bending, and shear characteristics in different parts of the connections. The approach proposed by Block et al. uses force–displacement–temperature models for the individual connection components such that the combined connection element is able to deal with moment–rotation–thrust–temperature.

Depending on their formulation, limitations are applicable to multi-spring connection elements as well. As an example, for the model proposed by Block et al., the following limitations are noted: automatic consideration of group effects between bolt rows in the tension zone, consideration of the shear deformations in the column web, beam-end and bottom-flange buckling of the beams, and behavior of heat-treated bolts in fire situations.

Additionally when component-based models are adopted in a static structural analysis, a failure of a single component (spring) could lead to non-convergence of the analysis due to numerical instability associated with the stiffness matrix of the connection element. In reality, a failure of an individual spring does not necessarily imply that the whole connection has failed. A dynamic analysis would likely overcome this constraint.

### 10.2.5.3 3D Connection Models

Advanced fire element models can be adopted to explicitly represent the nonlinear 3D response of a structural connection in fire [52, 53]. This modeling approach is computationally expensive and would therefore be less suited for global structural modeling, but rather when localized models (of a portion of a floor system for example) are considered. These models are less frequently used in engineering practice.

3D connection models could explicitly consider the potential instabilities and failure modes such as beam web and flange buckling, and bolt shear and bolt bearing. Careful consideration is required by the user on the modeling representation of individual components and the boundary conditions used. It is suggested that the model is appropriately validated against a similar connection experiment.

## 10.2.6 Representation of Mechanical Boundary Conditions

The mechanical boundary conditions in a finite element model can be represented in one or a combination of the following forms:

- Using single-point constraints (i.e., by constraining the relevant degrees of freedom at a node): The prescribed constraint pertaining to a given degree of freedom can be either a displacement (e.g., displacement is set to zero at a support) or a force (e.g., a force of 1000 N is applied). Any combination of displacement and force constraints can be applied to different DoFs of a given node. However, for a given DoF it is impossible to control simultaneously the displacement and the force.
- By representing the stiffness from the surrounding structure through the inclusion of connections: This can be realized using a range of techniques from specifying a partial restraint, buttress restraint, or same relationship (i.e., master-slave) between nodes to modeling the connection using beam-column elements, shell elements, and spring elements.

## 10.2.7 Representation of Imperfections

The models used in advanced analysis, e.g., finite element models, are mathematical approximations for the actual structures under study. In a model, columns can be represented as perfectly straight; loads can be applied exactly at the centroid of the section. In actual structures though, the members are not perfect: they have geometrical imperfections and residual stresses. Besides, eccentricities are present in joints and applied loads. Such imperfections can have a large impact on the results of advanced analyses, in particular when instability phenomena are at stake (e.g., global

buckling of a column; local buckling of a plate in a slender steel beam). Indeed, numerical models of perfectly straight member would overestimate the critical load compared to the one of an actual imperfect member. Without any imperfection in the models to initiate the second-order effects, instability occurs by bifurcation, whereas in experimental testing and actual structures a more progressive process is observed.

The topic of imperfections is general to structural engineering. It has been extensively studied in the literature and recommendations have been formulated in design codes for structures at ambient temperature, e.g., Eurocode. Yet due to its complexity, this topic is still under investigation and many questions remain open.

Fire action generally amplifies the second-order effects and risk of instabilities by reducing the stiffness of the members and generating thermally induced displacements and forces. Therefore, adequate consideration of the instability phenomena is crucial when evaluating members under fire conditions in which all or part of the section is in compression. Where the fire is symmetrically applied, for instance on four faces of a column, initial imperfections are of particular importance; advanced analysis results can be very sensitive to this parameter. Where the fire is non-symmetrically applied, for instance on one side of a wall, the thermally induced curvature introduces an asymmetry in the problem which may make the structure less sensitive to the magnitude of the initial imperfection.

In advanced analysis, the members which will be subject to compression should therefore be modeled with initial geometric imperfections (for both global and local imperfections). The shape of these imperfections should be based on the most unfavorable critical buckling shape. Regarding the amplitude of the imperfections, some recommendations can be found in the design codes or in the literature (e.g., [30, 52, 54, 55]). For instance, the Eurocode recommends using a sinusoidal initial imperfection with a maximum value of  $h/1000$  at mid-height for the analysis of isolated vertical steel members [3]. The consideration of residual stresses in steel members, on the other hand, does not seem to influence significantly the structural behavior in fire, according to recent research [25].

### **10.3 Capabilities and Limitations of Advanced Analysis Methods**

As discussed throughout this chapter, advanced analysis methods are a powerful tool at the service of structural fire engineers. They allow approaching the real behavior of a structural system under fire exposure, by enabling the consideration of structural assemblies rather than isolated structural members, and the modeling of realistic fire conditions rather than nominal fire curves. They provide many advantages to the designer in favor of a performance-based design approach. One of the objectives of this section is to present such advantages and capabilities, which are proper to advanced analysis methods and cannot be obtained with more simplified approaches.

However, advanced analysis methods cannot solve all engineering problems. They have limitations, which should be carefully considered and kept in mind by the user. These limitations may stem from the theoretical simplifications behind the methods, from the assumptions underlying the models built by the users, or from the inherent complexity of some processes that make them still out of reach of our modeling capabilities. In any case, it is essential to acknowledge that advanced models are still models, hence imperfect representation of the reality. Therefore the other objective of this section, perhaps the most important one, is to alert the reader to the limits of advanced methods by discussing some important limitations and assumptions of the methods most commonly used.

### **10.3.1 Material Behavior**

#### **10.3.1.1 Capabilities**

Materials exhibit a complex behavior in the fire situation. They are subject to thermal expansion and to different processes leading to a deterioration of their mechanical properties. They may be subject to additional creep effects, such as transient creep strain in concrete. As thermal gradients develop, the stress state varies throughout the section in a complex manner; in a concrete column section, for instance, thermal gradients may lead to cracking of the inner core. As a result, from a phenomenological perspective, materials have a highly nonlinear behavior. Advanced analysis methods are able to compute the stresses and strains in any point in a structure. They can account for the effects of the stress-temperature history, including loading-unloading and heating-cooling sequences. The material models used in the analysis can incorporate full nonlinear stress-strain behavior of all materials with, amongst others, plasticity, damage, creep, and non-recoverable mechanical properties with temperature. This is an advantage over simplified calculation methods which rely on basic material models.

#### **10.3.1.2 Limitations**

A potential difficulty with the modeling of materials in advanced methods lies with the identification of the material properties and their evolution with temperature. As is obvious, models can only be as good as their modeling inputs. Some material properties, such as the steel yield strength, have been extensively studied at elevated temperature. Therefore, the use of steel yield strength in a high-temperature model does not raise any specific difficulty. However, for some other material properties, there is a lack of experimental data. Material properties that are not sufficiently well characterized at elevated temperature include the thermal properties of some

insulation materials and the transient creep strain of concrete in multiaxial stress states. It is important for the user of advanced analysis methods to be well aware of the models used for the material behavior and for the evolution of the material properties with temperature.

The vast majority of the experimental tests conducted to establish material properties in the fire situation have focused on the effects of a heating phase. Material specimens were tested either under an increasing temperature (transient test) or at a constant elevated temperature (steady-state test). Yet, real fires are characterized by a heating phase followed by a cooling phase. The structural behavior during and after the cooling phase is also of interest in a performance-based approach. Advanced methods are the only option to analyze the behavior of structures under realistic fires, but they require reliable models for the material properties throughout the entire course of the fire. Some experiments have been conducted on material specimens that had been heated and then cooled down to ambient temperature (residual properties test), but research is still ongoing to improve the characterization of the material behavior under realistic fire exposure. From the user perspective, it is important to ensure that the material models that are adopted in the analysis are suitable for the heating and the cooling phases; for instance, concrete experiences an additional reduction in compressive strength during cooling, and does not recover transient creep strain. In some cases, a limitation to the application of advanced methods to realistic fire exposures is raised by the lack of knowledge about the material behavior in cooling.

In materials such as concrete, timber, or gypsum, the behavior is influenced by moisture content. An example is the phenomenon of spalling in concrete, which is caused by a combination of thermal stresses and pore pressure. In theory, the effects of moisture can be considered through coupled hydro-thermo-mechanical models. Yet in practice, such models are rarely used for analyzing structures in fire, due to their level of complexity and the difficulty to calibrate the parameters. Therefore, traditionally, the effects of moisture are either included implicitly (for instance, vaporization is accounted for in the specific heat of the material) or neglected. Spalling remains very difficult to predict at the structural level. The preferred approach consists of avoiding the occurrence of spalling, when necessary, through the application of polypropylene fibers in the mix, rather than trying to predict it and to evaluate its influence on the performance of the structure.

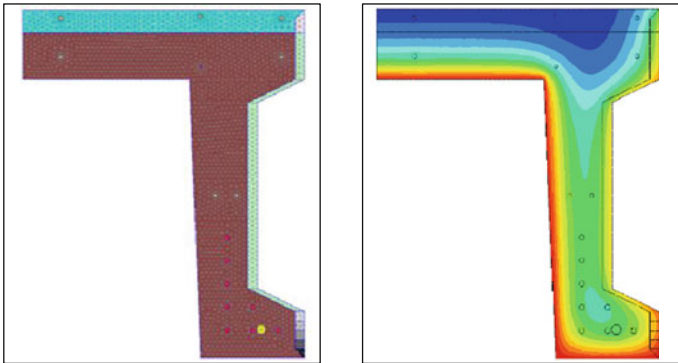
Advanced analysis methods are focused on, and performant for, evaluating the stability of structures (traditionally called the fire resistance criterion). They are also used to assess the heat transfer through compartmentalization elements such as walls and slabs (insulation criterion). Yet, they are not well adapted to the evaluation of flame spread (integrity criterion). This is because the methods typically rely on continuum mechanics models which do not allow estimation of crack width. Evaluation of the integrity of a member, with respect to flame spread, is currently beyond the capabilities of the methods used in advanced structural fire engineering analysis.

## 10.3.2 Structural Behavior

### 10.3.2.1 Capabilities

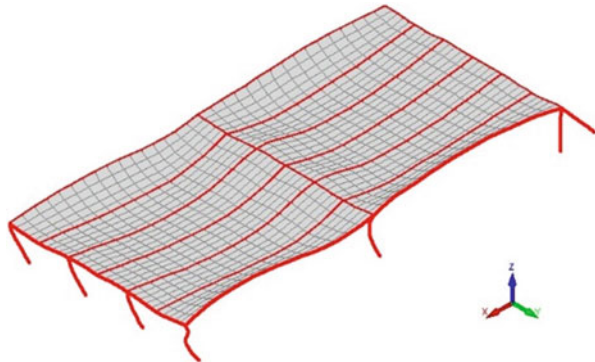
An advantage of advanced methods is that they can be used to analyze the behavior of complex sections and structural shapes. Finite element models allow considering virtually any section geometry, with different constituting materials combined (Fig. 10.11).

Advanced methods are also the only option for analyzing the behavior of structural assemblies (Fig. 10.12). They can take into account the effect of structural interactions with the surrounding structure. Due to thermal expansion effects, restraint forces build up in structural systems subjected to fire. Advanced analysis allows computing the evolution of these restraint forces and considering their effects on the structural response. It is also the only way to assess the robustness of a structure under a local failure or to perform progressive collapse analysis of an entire building.



**Fig. 10.11** Thermal analysis of a prestressed concrete girder consisting of a  $\pi$ -shape cross section and different materials (half of the section is modeled)

**Fig. 10.12** Mechanical analysis of a steel-concrete structure subjected to fire



Under realistic fire exposure, the heating-cooling sequences generate significant redistribution of forces in a structure. Advanced methods are also able to account for the force redistributions and effects of thermal deformations under any fire exposure scenario. This requires, however, the use of proper material models, as discussed above.

### **10.3.2.2 Limitations**

As is the case at ambient temperature, the types of finite elements used in the analysis influence the types of phenomena that can be captured. For instance, local (section) buckling of a steel beam cannot be captured with a Bernoulli beam finite element. Hence, an advanced analysis may overlook important phenomena if the models are not suitable. It is therefore essential to select properly the types of finite elements as a function of the objectives of the analysis; this aspect is discussed in more details in Sect. 10.2.

Connections are important components of structural assemblies. Connections join different structural elements (e.g., a beam to a column), or different materials in a composite element (e.g., a shear connector). The behavior of connections may, in certain cases, play a significant role in the behavior of the structure. Yet, modeling of connections in a structural model is not an easy task. Two approaches are typically adopted: the use of a detailed 3D model of the connection with solid brick elements, or the use of uniaxial spring elements. The former approach is difficult to combine with a model of a large structure due to the different scales. The latter approach has been preferred by several researchers. The spring elements are generally defined as zero-length elements with axial and/or rotational stiffness. Several springs can be combined based on a component method. This approach can be powerful [56]. Yet, the level of model sophistication required for incorporating connections in the analysis cannot necessarily be achieved in all analyses due to project constraints. An engineering decision is needed to discern the cases where connections should be explicitly modeled. Nevertheless, when connections are idealized as perfectly rigid, it is important to verify a posteriori that the forces transmitted between the elements can be transferred by the connections.

### **10.3.3 Failure Modes**

Advanced analysis methods are, in theory, able to capture virtually any structural failure modes. In practice, however, the capabilities are limited by modeling assumptions, uncertainties, or limitations in the current understanding of complex phenomena.

Limitations can be due to modeling assumptions. For instance, the selection of the type of finite element has an influence on the failure modes that can be captured. Local buckling in steel beams can properly be predicted using shell finite elements,

but is neglected when using Bernoulli-type beam finite elements. Models made of three-dimensional brick finite elements could capture shear punching in a concrete slab owing to the use of fully multiaxial stress-strain models (although modeling of this failure mode remains very challenging). Yet, concrete slabs are most commonly modeled using shell finite elements for practical reasons such as limitation of the number of elements and CPU time. In shell elements, plane stress material models are used. Therefore, shear transversal to the plane of the slab cannot be captured.

Modeling simplifications are notably motivated by the complexity of the multi-scale character of the problem. For instance, accounting for the connections in a large structural model is challenging, as discussed above. Processes that take place at the microscale level, in the materials, are generally accounted for using phenomenological approaches. The latter are powerful methods that allow studying entire structural systems; however they limit our ability to capture some failure modes such as spalling or loss of integrity due to crack opening.

Failure modes that deserve special attention, because they may not be captured by a classical advanced structural fire analysis and therefore may require a specific verification, include amongst others in steel, local buckling and failure in shear and in concrete, insufficient rotational capacity, spalling, local buckling of compressed reinforcement, shear and bond failure, and damage to anchorage devices. In some cases, the verification can be made on the basis of results obtained from the advanced analysis (e.g., check the maximum rotation at a support).

### ***10.3.4 Large Displacements and Progressive Collapse***

Large displacements and second-order effects take a particular importance in fire conditions. Advanced analysis methods developed for structural fire engineering can incorporate geometric nonlinearities, through the use of suitable finite element formulations. They are also the only option for studying structural assemblies until failure, accounting for complex load redistributions due to thermal restraint effects and/or local plasticity/failure. Advanced analysis can be used to study post-critical behavior, robustness, and progressive collapse.

The main limitation associated with the aforementioned behavior is the need for numerical robustness of the models and software packages that are used. Modeling the behavior of structures under extreme solicitation and large displacements raises some difficulties for convergence of implicit numerical models. Materials may develop a softening behavior and the stiffness matrix of the system may become negative. Dynamic equations have been proposed to replace the static formulation of the problem in some structural fire analysis software such as SAFIR, which leads to much improved numerical stability. However, it remains necessary to critically analyze the results of the analyses to assess whether the end of the computation corresponds to a physical failure or to a numerical one caused by a lack of convergence. At the other end of the spectrum, engineering judgment is also required to detect abnormally ductile results, where numerical convergence was obtained but the



level of deformations would not be realistically admissible in a structure. These aspects are discussed further in Sect. 10.4 on failure.

### ***10.3.5 Nonstandard Fire Exposure***

#### **10.3.5.1 Capabilities**

Another advantage of advanced analysis with respect to simplified method is the versatility with respect to the ways the fire attack can be considered. Indeed, simplified methods are mostly limited to nominal fire curves. In contrast, advanced analysis can consider more complex and physically based representations of the fire scenarios. They can account for the effects of the cooling-down phase and of a localized fire exposure on the structures.

The most common methods to consider the fire attack on the structure in advanced analysis are listed here below.

- (a) Prescribed time-temperature relationships at the nodes or elements of the section: This option implies that the user already knows the temperature within the structural member (or at least in some parts of it). It is particularly useful for benchmark purposes, or when the temperatures have been recorded during a furnace test and the user wants to follow these temperatures in the mechanical model as closely as possible because the focus of the analysis is on the mechanical response.
- (b) Prescribed time-temperature relationships for the hot gases enveloping the structure: This option is equivalent to time-temperature curves that result from fire resistance testing. It is mainly used when the gas temperature is assumed as spatially uniform, e.g., for standard fires (such as ISO 834) or for post-flashover compartment fires.
- (c) Prescribed heat fluxes at the boundary as a function of time: This option implies that the user already knows these heat fluxes from a separate analysis. When prescribing a constant incoming flux to a member, it is necessary to allow energy reemission to the far field. If not, a continuous incoming flux will increase the temperature continuously to infinite values.

In addition to the relatively simple thermal boundary conditions (a)–(c), more sophisticated approaches can be used to represent the attack of spatially nonuniform fires on the structural members. In this case, the attack of the fire (be it represented by heat fluxes, gas temperature, adiabatic surface temperature, etc.) will depend on the relative position of the fire and the surface of the member (possibly including shadow effects). Some FE software have developed dedicated strategies to automatically interface the information from spatially nonuniform natural fire models with the thermomechanical FE models. Several particular cases are discussed here below.

- (d) Heat fluxes imported from one or several localized fire models: Different models are available to represent localized fires and evaluate the resulting heat fluxes. These fluxes can then be transferred in a thermomechanical FE software where they are applied on the members in a thermal analysis.

For instance, the Hasemi model gives the thermal flux from a local fire to a beam or a ceiling slab [20]. The Hasemi model, given in Annex C of EN1991-1-2 [15], assumes that the flame touches the ceiling. With this model, the heat flux received by the section is isotropic, which means that the direction from the fire to the section is not considered.

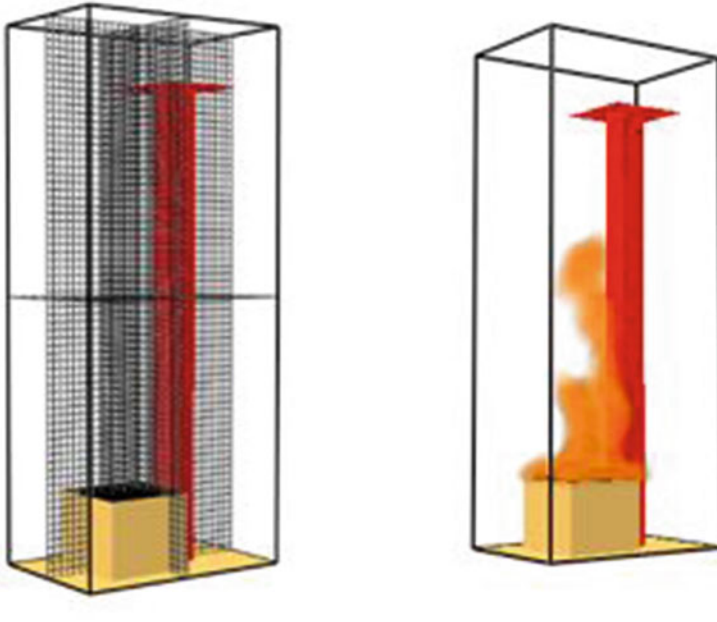
As another example, the LOCAFI model gives the thermal flux from a local fire to a column [21]. The length of the flame is calculated at each time step and the model is valid whether the flame touches the ceiling or not. The thermal attack from the fire to the section is anisotropic: the boundaries that are facing the fire receive the highest flux while the boundaries on the opposite side receive no flux at all.

In the latter fire models, the fire source is described by the 3D position of the source in the structure (where the flame originates), the vertical elevation of the ceiling (used to check whether the flame touches the ceiling or not), and, as a function of time, the diameter of the circular fire source and the rate of heat release of the fire. In case of multiple fires, the input fluxes from each fire are simply added. The generated heat fluxes can be calculated using a spreadsheet. In SAFIR, a dedicated interface allows evaluating the heat fluxes and using them as inputs in the thermal analysis.

Localized fire models have been used in recent structural fire analyses, for instance by Lelli et al. [57] where the Hasemi fire model was used in the study of a composite slab. In the latter, the generated heat fluxes, the resulting member temperatures, and the structural response were evaluated using SAFIR.

- (e) Gas temperatures imported from a traveling fire model (TFM): TFM has been proposed to capture the dynamic behavior of fires in large open-plan compartments [16, 58]. In a TFM, the fire source location varies with time to represent the progressive burning of the fuel and spread of the fire. The generated spatially nonuniform temperatures can be imported as boundary conditions in a FE software.

For instance, the iTFM [22] yields the gas temperature-time relationships at the ceiling of a medium-height compartment at any location in the compartment. The fire is assumed to be composed of two moving regions: the near field (flames) and the far field (smoke). The temperature field depends on one spatial dimension (the horizontal dimension, at the level of the ceiling, in a 2D model) and on time, accounting for the movement of the location of the fire front. The latter is determined over time using the fire spread rate. Temperature in the near field is based on the peak flame temperature, assuming that the flame touches the ceiling. Temperature in the far field is estimated using Alpert's ceiling jet correlation [59]. The fire is assumed to be fuel controlled. The iTFM is based on uniform fuel load distribution along the fire path and constant fire spread rate.



**Fig. 10.13** Numerical model of a fire test on a steel column using FDS

Traveling fire models have been used in recent structural fire analyses, for instance by Rackauskaite et al. [60, 61] where the iTFM was used in the study of a multistory steel frame building. In the latter, the temperature fields and the member thermal analyses were conducted in MATLAB and then the member temperatures were imported in a structural model in the software LS-DYNA.

- (f) Information imported from a computational fluid dynamics (CFD) analysis: CFD can be used to create advanced fire models that capture the fire development over time in any point of the defined space. For instance, the CFD software Fire Dynamics Simulator (FDS), developed by NIST [23], is widely used in fire engineering (Fig. 10.13).

The results of a CFD analysis can be output in different manners for interfacing with a thermomechanical FE software. In all cases, these results have to be recorded at selected grid points of the CFD model and at selected time steps. Spatial and temporal interpolations are then required when inputting the CFD results into the FE model. A weak coupling strategy is commonly used; that is, the CFD calculation does not depend on the mechanical response of the structure. Structural elements need to be incorporated in the CFD model if they influence significantly the flow of mass or of energy (for instance, when the structural elements also form the boundary of the compartment, or for deep

concrete beams). However, they may be omitted if their influence is negligible (for instance, a steel column situated far from the fire source).

One option is to transfer from the CFD model to the FE model the temperature of the gas and radiant intensities from various directions. Convection factors can also be transferred, but more typically a uniform value for the convection factor is introduced by the user in the FE software performing the thermal analysis (as suggested in the Eurocode for instance). Radiant intensities from different directions are preferable to impinging radiant fluxes on predefined surfaces because, generally, the structural elements are not included in the CFD model, and thus no information is available yet about the shape of the cross sections. The fluxes at the surface of the structural elements can be computed within the FE software by integrating the radiant intensities, which allow taking into account possible shadow effects in concave sections. This option is the one implemented in the automatic FDS-SAFIR interface [62].

Another option is to use the so-called adiabatic surface temperature (AST) concept [63]. The AST is a fictitious temperature of an element assumed as a perfect insulator, which can then be considered as an equivalent fire temperature for calculating the heat flux to an exposed structure. This concept allows using a simple single parameter to describe the complex convective and radiative conditions to which the surface of a structural element is exposed during fire. This parameter is a convenient interface between fire and thermal/structural models [64]. However, since the information is condensed into a single parameter (for a given point in space and time), the directionality information is lost; therefore it does not allow accounting for possible shadow effects in sections not present in the CFD model. As an example of application, the AST has been used for interfacing FDS with Abaqus by Alos-Moya [65] or with SAFIR [66] in bridge fire applications.

### 10.3.5.2 Limitations

As illustrated by the above discussion, the capabilities of advanced analysis for modeling the fire exposure are numerous and go well beyond the consideration of standard fire curves. The main limitations stem from the lack of physically based fire models to be used in structural fire engineering analyses. Indeed, despite the research progress in the field, the most commonly used fire models remain either oversimplified (e.g., to account for the traveling nature of the fire in large compartments) or too computationally expensive (e.g., CFD-based models). Few data are available and there is generally a lack of validation of the models employed in the field. As a result, the general recommendation is to consider several fire scenarios to cover the range of possible fire severities and include some sensitivity analysis.

### ***10.3.6 Thermal-Mechanical Weak Coupling Assumption***

Several software packages allow performing the thermal analysis followed by the mechanical analysis with an easy transfer of information between the two. The strategy most commonly adopted is based on a weak coupling assumption from the thermal analysis to the mechanical analysis. This means that the temperatures influence the mechanical behavior but the results of the mechanical analysis have no influence on the temperature distribution. This strategy has implications in terms of the phenomena that can and cannot be accounted for in a structure subjected to fire.

#### **10.3.6.1 Capabilities**

The weak coupling assumption is valid in most cases because temperatures affect strongly the mechanical response of structures, whereas the opposite influence is negligible except in very specific situations. Examples of effects of the temperatures on the mechanical response, which are taken into account, include:

- Reduction of the mechanical properties of material with temperature.
- Development of free thermal strain.
- Development of transient creep strain.
- Development of thermal gradient-induced stresses in a section.
- Development of thermally induced restraint forces in a member.

#### **10.3.6.2 Limitations**

Due to the weak coupling assumption, any influence of the mechanical response on the thermal behavior is neglected. Although this influence is generally negligible, in some cases, nevertheless, the mechanical response may affect the temperature distributions in the members. An obvious example is the occurrence of spalling in a concrete section, which may reduce the cover and hence lead to a faster increase of temperature in the steel reinforcement. It is thus essential for the user of advanced analysis methods to be aware that, under a weak coupling assumption, no influence of the mechanical response on the temperatures is taken into account. Examples of potential effects of the mechanical response on the temperatures, which are not taken into account, include:

- Plasticity-generated heat.
- Anisotropy of conductivity in cracked materials.
- Contact resistance between two adjacent materials that have separated.
- Stress-induced change of geometry modifying the fire-exposed surface (e.g., spalling, local buckling in a concrete-filled hollow steel section).
- Large displacements of the structure influencing its position relative to the fire source.

- Effects of the loss of stability, insulation performance, or integrity of a separating member on the fire scenario.

As these effects cannot be accounted for with a weak coupling assumption, it should be checked that they would not significantly influence the structural fire response for the considered analysis.

## 10.4 Assessment of Failure

### 10.4.1 *Definition of Failure in a Prescriptive vs. Performance-Based Environment*

In a prescriptive environment, well-defined failure criteria are adopted to allow objective evaluation of the failure time of the considered specimens. This is the case, for instance, in laboratory fire testing of structural members. For load-bearing members, deflection and deflection rate are monitored throughout the tests; failure is assessed by comparing these measures to predefined thresholds [67]. It must be stressed that these criteria are not necessarily correlated to any actual failure that would occur if the specimen were part of a structural assembly subjected to a real fire. The main purpose of the prescriptive criteria is to be, as much as possible, not subject to interpretation in order to allow standardization.

In contrast, assessment of failure in a performance-based environment is usually a more complex problem. Failure is deemed to occur when the structure is not able to meet the performance requirement, i.e., generally, when it cannot ensure its load-bearing function. Hence, there is no unique, predefined set of criteria to be checked. Different criteria apply to different structures, situations, and objectives. Failure can only be defined by interpretation of the results of a predictive model. As performance-based design is interested in the real performance of a structure, the behavior at the system level is considered. Local failure may be acceptable if the loads can be redistributed and the local damage does not impair the stability of the structural assembly. Therefore, there is not much sense in adopting deflection thresholds in a performance-based environment. Changes in load-bearing modes, such as the shift from bending to tensile membrane action in composite steel-concrete floors, require large deformations to develop. For convenience, or due to lack of a better solution, deflection criteria or other simplified thresholds are sometimes adopted as proxy for failure in advanced analyses, but it is important to understand the limits of such criteria.

The engineer who performs an advanced analysis to assess the behavior of a structure in fire needs to take special care in interpreting the results of the analysis. Particularly, the assessment of failure requires careful consideration. Finite element software do not have any failure criterion embedded as such. This is because, as mentioned above, the notion of failure is arbitrary and depends on the performance requirements for the specific situation. Therefore, a simulation will run until the time

specified by the user is reached, or until it cannot converge to a state of equilibrium for the structure, or until it encounters numerical problems, whichever occurs first. Engineering judgement is then required to assess whether the last converged step corresponds to the time of failure. A procedure is suggested in the next section.

## **10.4.2 Procedure to Assess Structural Failure**

Different cases must be distinguished when processing the results of an advanced numerical analysis. These are listed here below and discussed in more details next.

- Case 1: The software does not run.
- Case 2: The software runs, until the end time specified by the user.
- Case 3: The software runs, but stops before the specified end time.

### **10.4.2.1 Case 1: The Software Does Not Run**

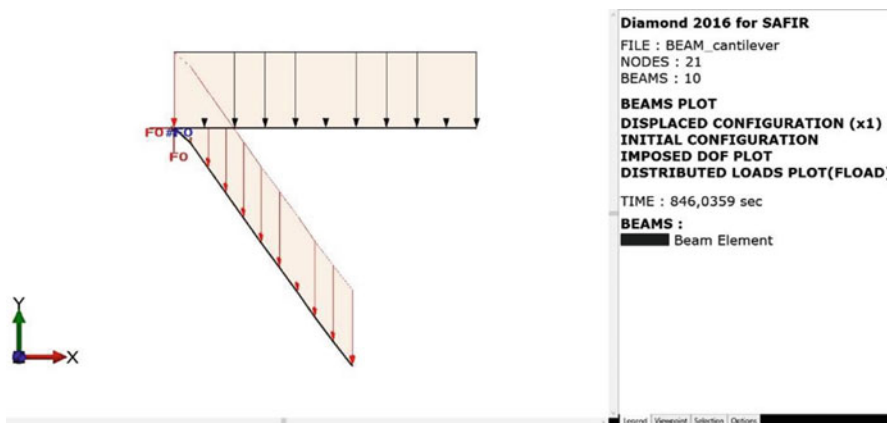
If the computation fails to start, this results either from an error in the definition of the engineering problem or from an error in the numerical model.

The engineering problem may be ill designed. For instance, the section size of the structural members may be insufficient to carry the applied loads. The boundary conditions may be such that the structure is unstable, i.e., it is a mechanism. Therefore, the structural analysis and design need to be carefully checked. In any case, it is recommended to have a clear understanding of the structure's response under the applied loads at ambient temperature prior to conducting the structural fire analysis.

If the structure is properly designed, but the software computation does not start, the error lies in the numerical model. The model needs to be checked for the inputs and assumptions such as material properties, boundary conditions, load level, presence of mechanism (e.g., unconstrained axial rotation in a diagonal), or isolated nodes (nodes not linked to any element and hence without any stiffness). Numerical parameters such as the initial time step, integration strategy, and convergence criterion should also be considered as potential source of issues.

### **10.4.2.2 Case 2: The Software Runs, Until the End Time Specified by the User**

As the numerical analysis has reached the end time specified by the user, it is likely that no failure has occurred. Yet, a verification of the results still needs to be conducted. Indeed, in some cases, a numerical analysis can continue to run, and generate results, despite the fact that the structure has reached an unacceptable response which, by all reasonable engineering judgment, corresponds to failure. A



**Fig. 10.14** Horizontal cantilever beam subjected to uniformly distributed load and ISO fire: initial configuration and displaced configuration at the last converged time step. Excessively ductile behavior, for which a loss of integrity is likely in practice, may in some instances be predicted by advanced analysis. In such cases, the structural failure time precedes the last converged time step

careful interpretation of the structural response is thus required to assess whether the computation has reached the end time *in a satisfactory manner* or not.

One variable that deserves particular attention is the displacement. Although the adoption of a one-size-fits-all deflection criteria (as is done in a prescriptive approach) is not relevant to advanced numerical analysis, computed displacements could be considered as excessive in certain situations and a specific threshold could be applied to determine a meaningful failure time. This would be the case if the simulation develops excessively ductile behavior. Examples of verifications that should be conducted include the horizontal displacement at beam extremities, which could result in the loss of support for the beam. Another example is excessive displacements that would lead to interpenetration of different members, or deflection of a member into the ground. Excessive deflections can also be obtained numerically with cantilever beams, which may be transformed into a cable hanging on the support. For instance, Fig. 10.14 shows the displaced structure at the last converged time step for a cantilever HEB 200 steel beam subjected to a uniformly distributed mechanical load and to ISO fire on three sides. The displacements shown are not amplified. The cantilever beam was in the process of shifting its behavior toward that of a cable. The simulation stopped because the steel material law incorporates a descending branch that limits the yield plateau and that descending branch was reached in the beam finite element at the support. In the absence of a material descending branch, the numerical simulation could have continued until the end time. In situations such as the ones exemplified here above, it is clear that the structure should be deemed to have failed even if the numerical analysis was able to continue converging toward a solution. The use of a user-defined deflection criterion appears justified in this type of situations.



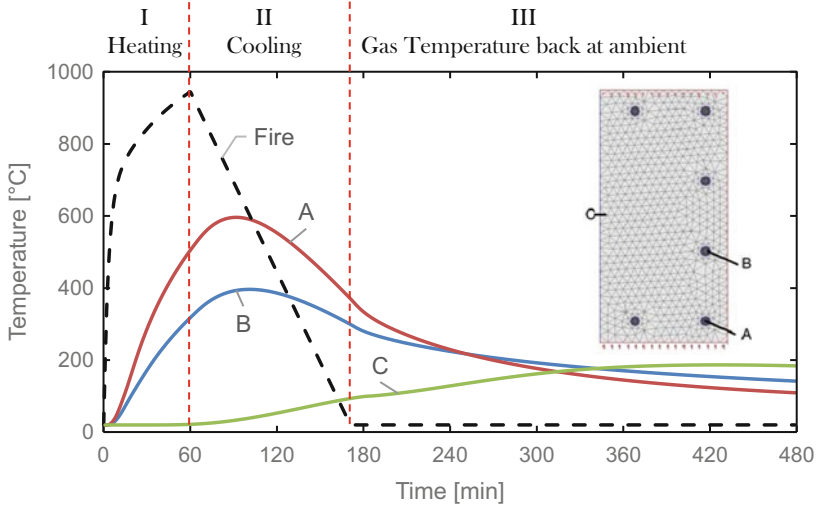
Other variables should also be looked at to identify potential failure modes that could occur yet did not lead to termination of the computation. In particular, the user should be careful to consider the failure modes not explicitly captured by the simulation. For instance, connections are rarely explicitly modeled. The numerical analysis will provide the effects of action that need to be transferred by the connections. A separate check of the connections is then required to assess the possibility of failure in these elements, which cannot be detected by the numerical analysis. Similar considerations should be made about local buckling of steel members modeled with beam FE, or shear punching in concrete slabs modeled with shell FE, for instance. Excessive strain in the materials should also be detected (for instance, a strain of 0.10 in steel is probably excessive in a FE analysis based on the small strain assumption). Detecting excessive material strains is particularly important if the material laws in the software do not incorporate any descending branch. Additional information is given in Sect. 10.3.3.

The end time specified by the user has different meanings depending on the situation. When a standard fire (e.g., ISO 834 time-temperature curve) is used, the end time input for the simulation is generally the requested fire resistance. For instance, a user may only be interested in proving compliance with the prescribed fire resistance of 2 h for a given structure. In this case, he/she runs the simulation for 2 h. If the simulation reaches this end time, and the structure is still standing, the objective of demonstrating the requested fire resistance is reached. However, nothing is learned about the failure mode, which could have been accessed by pursuing the simulation to a later time.

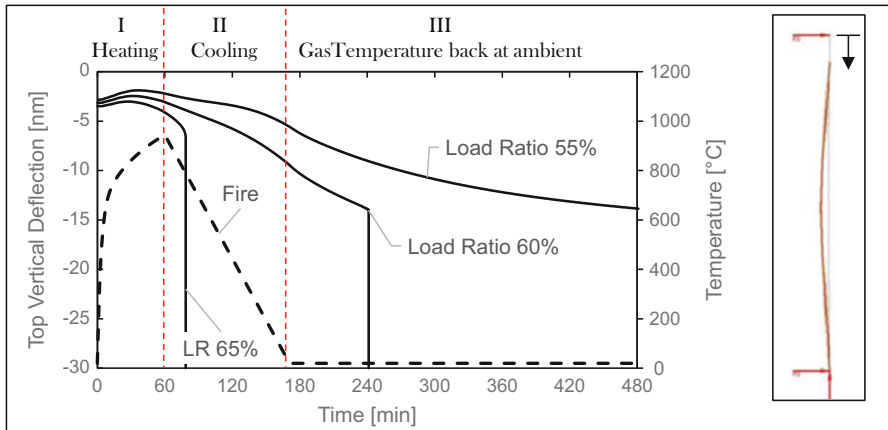
In contrast, when a natural fire is used, the objective is usually to check whether the structure can survive until full burnout [19]. It is of foremost importance to specify a simulation end time which is significantly later than the end of the fire. Indeed, due to thermal inertia, the heating of structural members continues long after the gas temperature reaches their maximum in a compartment, and high temperatures remain in these members long after the gas temperatures are back to 20 °C (Fig. 10.15). This effect, coupled with a number of other factors (such as the additional loss of strength in some materials during cooling and the effects of thermally induced forces), can lead to failure of structures during or even after the cooling phase of a natural fire; see Fig. 10.16 [35, 68, 69]. Therefore, to verify that a structure can survive until full burnout, the numerical analysis should be conducted for a time sufficient to guarantee that the effects of high temperatures have completely dissipated in the members.

#### **10.4.2.3 Case 3: The Software Runs, but Stops Before the Specified End Time**

This case requires a careful examination of the results to determine whether the termination of the simulation is due to the impossibility to converge to a state of equilibrium for the structure, or due to numerical problems encountered by the simulation. Indeed, the last converged step may correspond to the occurrence of an

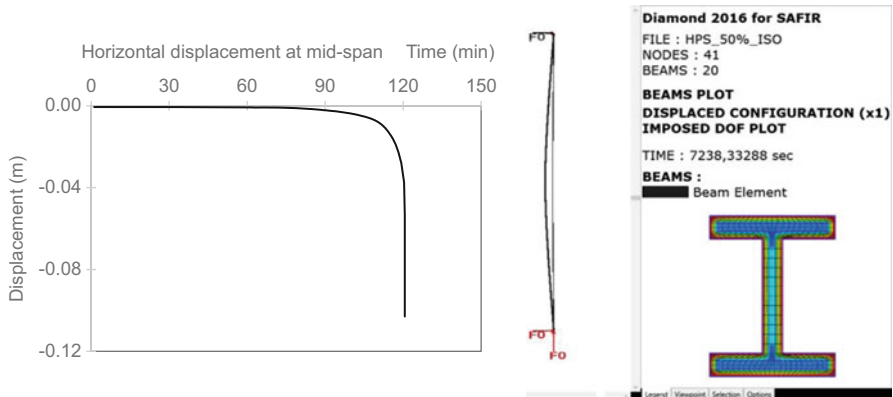


**Fig. 10.15** Evolution of temperature in the section of a reinforced concrete column exposed to a 60-min heating-phase natural fire. Temperatures continue to increase in parts of the section long after the end of the fire. Consequently, the numerical simulation end time must be defined long enough after the end of the fire when considering natural fires



**Fig. 10.16** Time evolution of top vertical displacement for a reinforced concrete column exposed to a 60-min heating-phase natural fire, for different levels of applied compressive load. Structural failure may occur during or after the cooling phase of the fire

actual failure of the structure. But it may also be earlier than the time of failure, as happens in the case of premature numerical failure. Finally, the possibility exists that the last converged step is later than the time of failure; this happens in the case where the code has converged to a solution that is not physically acceptable, as discussed in *Case 2*.

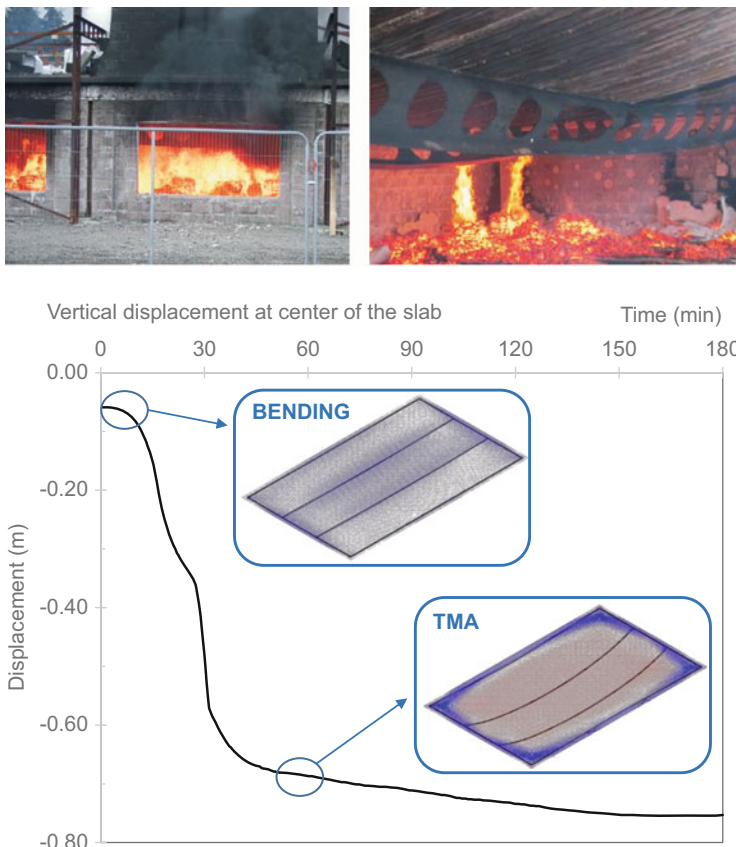


**Fig. 10.17** Behavior of a fire-exposed steel column. The evolution of the horizontal displacement at mid-span shows an accelerating trend (asymptote) which is typical of a buckling failure. Here, the last converged time step coincides with structural failure

Here, examination of the displacements and deflected shape may provide important insights. These displacements may be assessed as excessive for the structural stability and lead to the decision that failure has occurred. Possibly, the time of failure is earlier than the last converged step, if the displacements have exceeded a meaningful threshold; this situation has been discussed in *Case 2* above (Fig. 10.14).

Alternatively, examination of the results leads to the conclusion that the final displacements are not excessive. In this case, it is recommended to look for the initiation of a runaway-type failure in one of the degrees of freedom (DoF) of the structure. A vertical asymptote in the evolution of displacement of one DoF is a good indicator of a runaway failure, or failure by instability. For instance, Fig. 10.17 shows the behavior of a protected HEB400 steel profile under a vertical load applied at the top and subjected to ISO fire on its four sides. The column height is 4 m and it has a sinusoidal geometric imperfection with a maximum amplitude  $L/300$ . At the last converged time step, the maximum vertical displacement is of the order of 1 cm, whereas the maximum horizontal displacement reaches 10 cm. These values are not excessive, but examination of the evolution of the horizontal displacement shows a clear asymptote, indicating that the column is buckling. Hence, last converged time step and structural failure coincide in this case.

When a structural instability is detected, engineering judgment is required to assess whether this instability would lead to structural failure or the development of a post-critical behavior is possible. Indeed, a simulation may terminate while displaying a vertical asymptote in displacements, although the structure could actually survive longer by developing a post-critical behavior. An example is the analysis of a steel truss structure subjected to localized fire in which the analysis stops at the time of buckling of one bar. A vertical asymptote is observed in the out-of-plane displacement evolution of the central node of the bar. Yet in some cases, the structure is able to bridge over the failed element and withstand the fire for a longer time. As it is numerically challenging to find convergence at the time of buckling,



**Fig. 10.18** Numerical simulation of a steel-concrete composite structure with unprotected secondary steel beams under natural fire. The structure behavior transitions to a tensile membrane action mode in the fire situation. This transition is accompanied by important and sudden displacements (vertical asymptote) which should not be mistaken for a failure

this member buckling may result in the termination of the simulation. Software that include a dynamic formulation are better suited to provide an insight into the structural behavior in the post-critical phase as they can better deal with local failure and load redistributions. Other examples of situations where post-critical behavior may occur include the shift from bending mode to tensile membrane action in concrete and composite slabs, or from bending to catenary action in steel beams. For instance, Fig. 10.18 shows the numerical simulation of the large-scale Ulster fire test on a steel-concrete composite floor with cellular steel beams acting in membrane action [5, 70]. At ambient temperature, the composite floor acts in bending mode, with support from the intermediate cellular steel beams. The vertical displacement at the center of the slab is limited. The membrane forces in the shell finite elements are mainly compression (due to the composite action between the concrete shells and the

steel beams). Yet in the fire situation, the intermediate beams, which are not thermally protected, quickly and suddenly fail by web-post buckling. As a result, the floor transitions from a bending mode to a tensile membrane action mode. This transition is accompanied by large displacements and large rates of displacements (akin to an asymptote), as can be seen between minutes 12 and 35. Yet this does not correspond to the ultimate capacity of the structure. A post-critical behavior is possible in the structure. Here, tensile membrane action develops in the composite slab. Observation of the membrane forces shows that the whole central part of the slab is in tension (owing to the steel reinforcement bars) whereas a compression ring develops in the concrete. However for developing this tensile membrane behavior, large displacements were needed and it could have been incorrectly concluded that, in that stage between minutes 12 and 35, the structure was collapsing. In such cases, a numerical simulation that stops before the structure could transition to its post-critical behavior should be treated as a premature failure due to numerical lack of convergence, rather than an actual “physical” failure of the structure.

If the displacements are not excessive and do not exhibit any asymptotic behavior, a numerical failure is to be suspected. Numerical problems are often at the material level when sophisticated nonlinear constitutive equations have to be integrated [43]. However, the simulation termination could still correspond to an actual failure when the failure mode is particularly fragile. It is recommended to look for material failure by examining the distributions of stresses and strains in key sections. Changing the calculation parameters (time step, integration strategy, etc.) and using a dynamic solver may help overcome potential convergence issue.

### ***10.4.3 Assessing Specific Failure Modes***

Particular consideration is required for the failure modes not captured by the advanced analysis model. As discussed in Sect. 10.3.3, limitations exist in the failure modes that are captured by an advanced analysis model. In general, these limitations may be due to modeling assumptions, uncertainties, or limitations in the current understanding of complex phenomena. For any relevant failure mode that is not explicitly modeled, a separate verification is required. Some examples are briefly discussed here.

Spalling in fire-exposed concrete remains very hard to predict. Structural concrete models typically do not incorporate the water transport phenomena necessary to model the occurrence and effects of spalling. This results in a quasi-impossibility to explicitly and reliably account for the influence of spalling on the structural performance. Since spalling is an undesirable phenomenon which cannot be reliably predicted, the commonly accepted approach is to take measures to avoid its occurrence. These include the use of additives (polypropylene fibers) in the concrete mix

or the limitation of moisture content. Absent such measures, a simplified conservative approach is adopted to check the influence of an arbitrary amount of spalling on the structural fire performance. For instance, the Eurocode states that the influence of explosive spalling on the load-bearing capacity of a beam or a slab can be assessed by assuming local loss of cover to some of the steel reinforcement in the cross section and then checking the reduced load-bearing capacity of the section. Similar simplified approaches based on limiting temperature in high-strength concrete have been proposed in the literature [71].

In reinforced concrete, another potential failure mode is by rupture of the steel reinforcement. Advanced analysis models typically capture this failure mode by reaching the ultimate strain in the steel material. It must be stressed that this requires the use of a material constitutive law that includes a descending branch. Further, the value of the limiting strain for yield strength (i.e., the threshold of the yielding plateau) must be limited to a realistic value. As most advanced analysis methods used for reinforced concrete subjected to fire are based on continuum mechanics with a smeared crack approach, a conservative value of the limiting strain should be selected to account for possible local fracture.

Connections are rarely modeled explicitly in (large) numerical models of structures in fire. Yet real events have demonstrated that connections can be critical elements in the structural response in fire. Notably, force reversal due to heating-cooling sequences can lead to tensile failure. Advanced analysis without explicit connection modeling can be used to assess the evolution of forces in the connections (demand), followed by a separate verification of the connection design. The reduction of capacity due to temperature needs to be accounted for in the calculation. The temperature evolution can also be extracted from the advanced analysis. This topic is discussed in detail in Sect. 10.2.5.

For connections in fire, the scale of the structural members is important as it governs the magnitude of the thermal expansion effects. There is currently a knowledge gap about the behavior of very large structural members and assemblies in fire, due to the practical challenges and cost associated with conducting full-scale tests for large structures. A recent test campaign at the National Institute of Standards and Technology (NIST) focused on the fire response of long-span composite beams [72]. The 12.8 m long beams were made of  $W18 \times 35$  steel profiles with a 1.83 m wide concrete slab cast over a steel deck. These tests shed light on the significant role of steel shear studs and shear connections on the fire response of long-span composite beams.

## 10.5 Verification, Validation, and Review Process

### 10.5.1 Software Verification and Benchmarking

Benchmarking procedures are relevant not only when developing new codes but also when using already developed software to ensure that the modeling intent is

appropriately captured. Additionally, even for commercial software, when different versions are released a suite of appropriate benchmarks need to be tested by the modeler to ensure that the outcomes are not affected. Verification and validation exercises and benchmarks have been presented by Zaharia et al. [73], Rackauskaite et al. [60, 61], and Ferreira et al. [74]. However, generally speaking, there is a lack of guidance and norms to conduct validation exercises of advanced methods for structures in fire. It is also not in the culture of the community to invest major efforts in validating advanced methods and software, contrary to what has been traditionally done in other disciplines such as nuclear engineering. As these tools become more and more adopted by structural fire engineers, notably to design real buildings, one can hope that more emphasis will be put on the benchmarking and validation.

When conducting benchmarking studies, not only one parameter but also a range of output need to be compared between the benchmark cases and the models, in order to ensure that all appropriate phenomena are captured in a holistic way. Such outputs may include (i) maximum temperature at selected nodes across the section, (ii) mid-span deflection of key beams and slab bays, (iii) lateral deflection of key columns, (iv) forces in key connections, (v) axial forces in beams and columns, (vi) overall vertical reaction force, and (vii) strain in the slab/rebar in key bays particularly over protected beams.

Benchmarking examples should ideally include sensitivity analyses. Indeed, the results of a code should be proven not to be disproportionately sensitive to input parameters such as the size of the elements or the time step [74]. Also, if any software would require extremely small elements and/or extremely short time steps to achieve satisfactory results, this should be put to the attention of the users.

The assumptions made in calculating the reference solutions should be mentioned to allow determining the reasons of eventual deviations between the tests and the simulations. Notably, failure criteria should be clearly mentioned when a mechanical calculation must be compared with the results of an experimental test of other software, if the ultimate resistance or fire resistance is being considered.

Meta-analyses of comparisons of results with real-world structures offer a great way to provide additional validation to a software, by delivering insight about the quality of the results obtained and the typology of the comparisons made.

Any software should not be used for purposes that are outside of those that they have been originally verified and validated. For example, if an in-house code has been developed for the analysis of steel structures in fire, it should not be used for the analysis of concrete or timber structures in fire without a prior verification and validation for this purpose. Likewise, if the implemented material models have been derived from standard testing under standard fire (i.e., heating phase only), these material models should not be used in an analysis that involves the cooling-down phase.

### ***10.5.2 Sensitivity/Confidence Assessment and Q&A Procedures***

After a finite element software has been verified and validated for certain structural fire engineering applications, a further degree of assessment is required for the generated models to ensure confidence in the outcomes of the model. A number of round robin studies have shown that even with verified and validated software, different users could often end up with different outcomes even for the same simple model [75].

A sensitivity/confidence assessment of finite element models of structures in fire would generally involve the following steps:

1. Establishing the model outputs that are of interest (such as temperatures, deflections, plastic strains).
2. Establishing the model inputs (such as mesh density, material properties, and models) that could influence the model outputs and therefore the conclusions of the assessment.
3. Assessing the sensitivity of the model outputs to the model inputs (for different potential inputs).
4. Selecting appropriate model inputs based on the undertaken sensitivity assessment such that there is an adequately low sensitivity and sufficient confidence in the results.

To increase confidence in the model, it is also good practice to have someone other than the modeler check the model.

### ***10.5.3 Reporting of the Analyses***

Once a numerical assessment of structural performance in fire has been conducted for a commercial project it is typical to produce a report describing the assessment for review by the approval bodies and potentially by a third-party reviewer (similarly for a research project, a technical report or paper may be written which may also be peer reviewed by the scientific community). When reporting such analyses, sufficient information needs to be provided such that any potential reader/reviewer can repeat independently the analyses that were conducted.

The final report should therefore contain all the necessary information such as:

1. The software used and the solver (static vs. dynamic and implicit vs. static) adopted in the study: Details of the numerical strategy should also be provided, such as if dynamic analysis was used and whether damping/mass scaling was used.
2. The thermal exposure assumed and how it was idealized in the finite element model, including how many through-depth sectional points are considered.



3. How the gravity loads were applied.
4. Type of elements used (including ID for commercial software), mesh characteristics, and number and location of sectional integration points considered.
5. Type of materials used (including ID for commercial software) and mesh characteristics.
6. Assumed boundary conditions.

The essential point is to provide sufficient details to allow independent reproducibility of the results.

#### ***10.5.4 Agreement with Approval Bodies***

The intent to undertake a structural fire engineering assessment should be communicated to the approval authorities in advance of the initiation of the analyses. The engineer should arrange a meeting with the approval bodies to discuss the modeling approach (such as which areas of the structure will be modeled) and the performance criteria that will be adopted for the study (for example deflection-based criteria). The relation between the expected performance of the structure and the performance criteria that will be assessed from the numerical analysis needs to be explicitly defined at the onset.

### **10.6 Overview of the Different Types of Software**

The advanced analysis methods discussed in this chapter are implemented in different numerical codes and software. These software can be divided into three types.

The first type are large multipurpose software packages that can be particularized for structural fire engineering applications. These are commercial finite element analysis programs such as Abaqus, Ansys, Nastran, or LS-DYNA. These programs are widely distributed, used, and validated. They offer a wide field of capabilities. Documentation and validation are usually at a high level given their commercial purpose. The graphic user interfaces are effective. As these programs were not primarily developed for the fire situation, there may be increased complexity, or convoluted strategies, to interface the thermal and mechanical problems. Particular care must be taken in defining the parameters of the model, such as the material laws, because of the multiple options not fire-related offered by these programs for each input. The price can also be hefty. Many examples of applications can be found in the literature [29, 53, 60, 61].

The second type are software specifically developed for structures in fire. These dedicated software have emerged over the last two decades from research groups at universities active in structural fire engineering. The most established structural fire engineering software are SAFIR, created at the University of Liege and now

developed at Liege and Johns Hopkins University [76, 77], and Vulcan developed at the University of Sheffield [78, 79]. Another software is OpenSees, which was originally developed for seismic engineering at the University of Berkeley and the PEER Center [80], but has been extended in recent years to accommodate structural fire analyses [81, 82]. These software are versatile within the specific application of structures in fire, offering different types of elements, materials, and interfaces with fire models. Their main advantage is that, being developed specifically for the fire purpose, they handle both the thermal and structural analyses with an efficient transfer of information from the former to the latter. Also, they may provide more advanced elevated temperature features (such as material models, bond behavior) than general-purpose software. As a result, they have been increasingly adopted beyond their group of origin within the SFE community, including for design projects (e.g., [32, 57]). Challenges exist however to compete with large commercial software, including in developing the documentation and user-friendly interfaces which must accompany a software when it becomes largely disseminated.

Finally, the third type are numerical codes developed for a specific application. These typically stem from the works of one researcher investigating the behavior of a specific member type subjected to fire, for example within the framework of a PhD thesis. A number of such codes have also been generated by research teams as part of a dedicated research project, such as the software MACS+ for composite slabs at high temperatures [83]. As a result, these codes can be state of the art to capture the phenomena involved in the fire response of the member under consideration, but have a limited field of application. A challenge lies in making these codes durable after the author leaves the research group or the project expires.

**Declaration of Interest** Under a license agreement between Gesval S.A. and the Johns Hopkins University, Dr. Gernay and the University are entitled to royalty distributions related to the technology SAFIR discussed in this publication. This arrangement has been reviewed and approved by the Johns Hopkins University in accordance with its conflict of interest policies.

## References

1. ASCE/SEI 7. (2016). *Minimum design loads and associated criteria for buildings and other structures*. American Society of Civil Engineers: Structural Engineering Institute.
2. ASCE/SEI Manual of Practice No. 138. (2018). *Structural fire engineering*, American Society of Civil Engineers. Structural Engineering Institute.
3. CEN. (2005). *Eurocode 3: Design of steel structures – Part 1–2: General rules – structural fire design, EN 1993-1-2*. CEN.
4. Mueller, K. A., & Kurama, Y. C. (2015). Out-of-plane behavior and stability of five planar reinforced concrete bearing wall specimens under fire. *ACI Structural Journal*, 112(6).
5. Gernay, T., & Franssen, J. M. (2015a). A plastic-damage model for concrete in fire: Applications in structural fire engineering. *Fire Safety Journal*, 71, 268–278.
6. Gernay, T., & Khorasani, N. E. (2020). Recommendations for performance-based fire design of composite steel buildings using computational analysis. *Journal of Constructional Steel Research*, 166, 105906.

7. Khorasani, N. E., Gernay, T., & Fang, C. (2019). Parametric study for performance-based fire design of US prototype composite floor systems. *Journal of Structural Engineering*, *145*(5), 04019030.
8. Lopes, N., Manuel, M., Sousa, A. R., & Real, P. V. (2019). Parametric study on austenitic stainless steel beam-columns with hollow sections under fire. *Journal of Constructional Steel Research*, *152*, 274–283.
9. Yu, H., Burgess, I. W., Davison, J. B., & Plank, R. J. (2008). Numerical simulation of bolted steel connections in fire using explicit dynamic analysis. *Journal of Constructional Steel Research*, *64*(5), 515–525.
10. Gernay, T., & Gamba, A. (2018). Progressive collapse triggered by fire induced column loss: Detrimental effect of thermal forces. *Engineering Structures*, *172*, 483–496.
11. Ni, S., & Gernay, T. (2020). Predicting residual deformations in a reinforced concrete building structure after a fire event. *Engineering Structures*, *202*, 109853.
12. Khan, A. A., Usmani, A., & Torero, J. L. (2021). Evolution of fire models for estimating structural fire-resistance. *Fire Safety Journal*, 103367.
13. ISO834. (1975). *Fire resistance tests – Elements of building construction*. International Organization for Standardization.
14. ASTM E119-00. (2007). *Standard methods of fire test of building construction and materials*. American Society for Testing and Materials.
15. CEN. (2002). *Eurocode 1: Actions on structures – Part 1-2: General actions – Actions on structure exposed to fire, EN 1991-1-2*. CEN.
16. Stern-Gottfried, J., & Rein, G. (2012). Travelling fires for structural design – Part I: Literature review. *Fire Safety Journal*, *54*, 74–85.
17. Cadorn, J.-F., & Franssen, J.-M. (2003). A tool to design steel elements submitted to compartment fires—OZone V2. Part 1: Pre- and post-flashover compartment fire model. *Fire Safety Journal*, *38*(5), 395–427.
18. NIST. (2017). *Fire dynamics simulator user's guide* (6th ed.). NIST. <https://doi.org/10.6028/NIST.SP.1019>
19. Gernay, T. (2019). Fire resistance and burnout resistance of reinforced concrete columns. *Fire Safety Journal*, *104*, 67–78.
20. Hasemi, Y., & Tokunaga, T. (1984). Some experimental aspects of turbulent diffusion flames and buoyant plumes from fire sources against a wall and in a corner of walls. *Combustion Science and Technology*, *40*(1–4), 1–18.
21. Vassart, O., Hanus, F., et al. (2016). Temperature assessment of a vertical steel member subjected to LOCALised Fire. In *Acronym LOCAFI, Report RFSR-CT-2012-00023, European Commission Research Programme of the Research Fund for Coal and Steel*. Luxembourg.
22. Rackauskaite, E., Hamel, C., Law, A., & Rein, G. (2015). Improved formulation of travelling fires and application to concrete and steel structures. *Structure*, *3*, 250–260.
23. McGrattan, K., Klein, B., Hostikka, S., & Floyd, J. (2007). Fire dynamics simulator (version 5): User's guide. *National Institute of Standards and Technology (NIST)*.
24. Couto, C., Real, P. V., Lopes, N., & Zhao, B. (2015). Resistance of steel cross-sections with local buckling at elevated temperatures. *Journal of Constructional Steel Research*, *109*, 101–114.
25. FIDESC4. (2015). *Fire design of steel members with welded or hot-rolled class 4 cross-sections*, Final report, Research program of the Research Fund for Coal and Steel.
26. Couto, C., Real, P. V., Lopes, N., & Zhao, B. (2016). Numerical investigation of the lateral-torsional buckling of beams with slender cross sections for the case of fire. *Engineering Structures*, *106*, 410–421.
27. Nadjai, A., Vassart, O., Ali, F., Talamona, D., Allam, A., & Hawes, M. (2007). Performance of cellular composite floor beams at elevated temperatures. *Fire Safety Journal*, *42*(6-7), 489–497.
28. FICEB. (2012). Fire resistance of long span cellular beam made of rolled profiles, Final report, Research program of the Research Fund for Coal and Steel

29. Zhang, C., Li, G. Q., & Usmani, A. (2013). Simulating the behavior of restrained steel beams to flame impingement from localized-fires. *Journal of Constructional Steel Research*, 83, 156–165.
30. Franssen, J. M., Cowez, B., & Gernay, T. (2014). Effective stress method to be used in beam finite elements to take local instabilities into account. *Fire Safety Science*, 11, 544–557. <https://doi.org/10.3801/IAFSS.FSS.11-544>
31. Maraveas, C., Gernay, T., & Franssen, J.-M. (2019). An equivalent stress method to account for local buckling in beam finite elements subjected to fire. *Journal of Structural Fire Engineering*, 10(3), 340–353.
32. Hopkin, D., et al. (2018). A structural fire strategy for an exposed weathering steel-framed building. *The Structural Engineer: Journal of the Institution of Structural Engineer*, 96(1), 60–66.
33. Drury, M. M., Kordosky, A. N., & Quiel, S. E. (2020). Structural fire resistance of partially restrained, partially composite floor beams, II: Modeling. *Journal of Constructional Steel Research*, 167, 105946.
34. Baker, G., & de Borst, R. (2005). An anisotropic thermomechanical damage model for concrete at transient elevated temperatures. *Philosophical Transactions of the Royal Society B*, 363, 2603–2628.
35. Gernay, T., Millard, A., & Franssen, J. M. (2013). A multiaxial constitutive model for concrete in the fire situation: Theoretical formulation. *International Journal of Solids Structure*, 50(22–23), 3659–3673.
36. Ožbolt, J., Bošnjak, J., Periškić, G., & Sharma, A. (2014). 3D numerical analysis of reinforced concrete beams exposed to elevated temperature. *Engineering Structures*, 58, 166–174.
37. Toric, N., Harapin, A., & Boko, I. (2013). Experimental verification of a newly developed implicit creep model for steel structures exposed to fire. *Engineering Structure*, 57, 116–124.
38. Kirby, B. R., Lapwood, D. G., & Thomson, G. (1986). *The reinstatement of fire damaged steel and iron framed structures*. B.S.C., Swinden Laboratories. 0 900206 46 2.
39. Li, L., & Purkiss, J. (2005). Stress–strain constitutive equations of concrete material at elevated temperatures. *Fire Safety Journal*, 40, 669–686.
40. Gernay, T., & Franssen, J. M. (2012). A formulation of the Eurocode 2 concrete model at elevated temperature that includes an explicit term for transient creep. *Fire Safety Journal*, 51, 1–9.
41. Law, A., & Gillie, M. (2008). Load induced thermal strain: implications for structural behavior. In *in: Proceedings of the Fifth International Conference – Structures in Fire, SIF2008, Singapore* (pp. 488–496).
42. Gernay, T. (2012). Effect of transient creep strain model on the behavior of concrete columns subjected to heating and cooling. *Fire Technology*, 48(2), 313–329.
43. Ni, S., & Gernay, T. (2021). Considerations on computational modeling of concrete structures in fire. *Fire Safety Journal*, 120, 103065.
44. Yi-Hai, L., & Franssen, J. M. (2011). Test results and model for the residual compressive strength of concrete after a fire. *Journal of Structural Fire Engineering*, 2(1), 29–44.
45. Franssen, J. M. (1993). *Thermal elongation of concrete during heating up to 700 °C and cooling*. University of Liege.
46. Behnam, B., & Ronagh, H. (2013). Performance of reinforced concrete structures subjected to fire following earthquake. *European Journal of Environmental and Civil Engineering*, 17(4), 270–292.
47. Quiel, S. E., & Marjanishvili, S. M. (2012). Fire resistance of a damaged steel building frame designed to resist progressive collapse. *Journal of Performance of Constructed Facilities*, 26(4), 402–409.
48. Gann Richard G. (2008). Final Report on the Collapse of World Trade Center Building 7, Federal Building and Fire Safety Investigation of the World Trade Center Disaster (NIST NCSTAR 1A). No. National Construction Safety Team Act Reports (NIST NCSTAR).

49. Al-Jabri, K. S., Davison, J. B., & Burgess, I. W. (2008). Performance of beam-to-column joints in fire—A review. *Fire Safety Journal*, 43(1), 50–62.
50. Block, F. M., Davison, J. B., Burgess, I. W., & Plank, R. J. (2013). Principles of a component-based connection element for the analysis of steel frames in fire. *Engineering Structures*, 49, 1059–1067.
51. Huang, Z. (2011). A simplified model for analysis of end-plate connections subjected to fire.. *Journal of Structural Fire Engineering*.
52. Quiel, S. E., & Garlock, M. E. M. (2010). Calculating the buckling strength of steel plates exposed to fire. *Thin-Walled Structures*, 48, 684–695.
53. Sarraj, M., Burgess, I. W., Davison, J. B., & Plank, R. J. (2007). Finite element modelling of steel fin plate connections in fire. *Fire Safety Journal*, 42(6–7), 408–415.
54. Couto, C., Real, P. V., Lopes, N., & Zhao, B. (2014). Effective width method to account for the local buckling of steel thin plates at elevated temperatures. *Thin-Walled Structures*, 84, 134–149.
55. Maraveas, C., Gernay, T., & Franssen, J. M. (2017). Buckling of steel plates at elevated temperatures: Theory of perfect plates vs finite element analysis. In *2nd International Conference on Structural Safety Under Fire and Blast Loading – CONFAB, London, UK*.
56. Block, F. M., Burgess, I. W., Davison, J. B., & Plank, R. J. (2007). The development of a component-based connection element for endplate connections in fire. *Fire Safety Journal*, 42 (6-7), 498–506.
57. Lelli, L., & Loutan, J. (2017). Advanced analyses of the membrane action of composite slabs under natural fire scenarios: A case study of the JTI headquarters. *Journal of Structural Fire Engineering*. <https://doi.org/10.1108/JSFE-12-2016-0020>
58. Bailey, C. G., Burgess, I. W., & Plank, R. J. (1996). Analyses of the effects of cooling and fire spread on steel-framed buildings. *Fire Safety Journal*, 26(4), 273–293.
59. Alpert, R. L. (1972). Calculation of response time of ceiling-mounted fire detectors. *Fire Technology*, 8, 181–195.
60. Rackauskaite, E., Kotsovinos, P., & Rein, G. (2017a). Structural response of a steel-frame building to horizontal and vertical travelling fires in multiple floors. *Fire Safety Journal*.
61. Rackauskaite, E., Kotsovinos, P., & Rein, G. (2017b). Model parameter sensitivity and benchmarking of the explicit dynamic solver of LS-DYNA for structural analysis in case of fire. *Fire Safety Journal*, 90, 123–138.
62. Tondini, N., Morbioli, A., Vassart, O., Lechêne, S., & Franssen, J.-M. (2016). An integrated modelling strategy between a CFD and an FE software. *Journal of Structural Fire Engineering*, 7(3), 217–233.
63. Wickström, U., Duthinh, D., & McGrattan, K. B. (2007). Adiabatic surface temperature for calculating heat transfer to fire exposed structures. In *Proceedings of the Eleventh International Interflam Conference* (Vol. 167). Interscience Communications.
64. Wickström, U. L. F., Robbins, A., & Baker, G. (2011). The use of adiabatic surface temperature to design structures for fire exposure. *Journal of Structural Fire Engineering*, 2(1), 21–28.
65. Alos-Moya, J., Paya-Zaforteza, I., Garlock, M. E. M., Loma-Ossorio, E., Schiffner, D., & Hospitaler, A. (2014). Analysis of a bridge failure due to fire using computational fluid dynamics and finite element models. *Engineering Structures*, 68, 96–110.
66. Tonicello, E., Desanghere, S., Vassart, O., & Franssen, J. M. (2012). Fire analysis of a new steel bridge. In *Proceedings of the 7th International Conference on Structures in Fire* (pp. 815–822). ETH Zürich.
67. Dumont, F., Wellens, E., Gernay, T., & Franssen, J. M. (2016). Loadbearing capacity criteria in fire resistance testing. *Materials and Structures*, 49(11), 4565–4581.
68. Bamonte, P., Kalaba, N., & Felicetti, R. (2018). Computational study on prestressed concrete members exposed to natural fires. *Fire Safety Journal*, 97, 54–65.
69. Gernay, T., & Franssen, J. M. (2015b). A performance indicator for structures under natural fire. *Engineering Structures*, 100, 94–103.

70. Vassart, O., Bailey, C. G., Hawes, M., Nadjai, A., Simms, W. I., Zhao, B., Gernay, T., & Franssen, J. M. (2012). Large-scale fire test of unprotected cellular beam acting in membrane action. *Proceedings of the Institution of Civil Engineers-Structures and Buildings*, 165(7), 327–334.
71. Kodur, V. K. R., Wang, T. C., & Cheng, F. P. (2004). Predicting the fire resistance behaviour of high strength concrete columns. *Cement and Concrete Composites*, 26(2), 141–153.
72. Ramesh, S., Choe, L., Hoehler, M., Grosshandler, W., & Gross, J. (2018). *Design and construction of long-span composite beam specimens for large structural-fire tests*. NIST.
73. Zaharia, R., & Gernay, T. (2012). Validation of the advanced calculation model SAFIR through DIN EN 1991-1-2 procedure. In *Proceedings of the 10th International Conference ASCCS 2012* (pp. 841–848). Research Publishing Services.
74. Ferreira, J., Gernay, T., & Franssen, J.M. (2018). Discussion on a systematic approach to validation of software for structures in fire. In *Structures in fire (Proc. of the 10th Int. Conf.)*. Ulster University, UK, Jun 6–8.
75. Lange, D., & Bostrom, L. (2017). A round robin study on modelling the fire resistance of a loaded steel beam. *Fire Safety Journal*, 92, 64–76.
76. Franssen, J. M. (2005). SAFIR: A thermal/structural program for modeling structures under fire. *Engineering Journal-American Institute of Steel Construction Inc.*, 42(3), 143–158.
77. Franssen, J. M., & Gernay, T. (2017). Modeling structures in fire with SAFIR<sup>®</sup>: Theoretical background and capabilities. *Journal of Structural Fire Engineering*, 8(3).
78. Huang, Z., Burgess, I. W., & Plank, R. J. (2009). Three-dimensional analysis of reinforced concrete beam-column structures in fire. *Journal of Structural Engineering*, 135(10), 1201–1212.
79. Sun, R., Huang, Z., & Burgess, I. W. (2012). The collapse behaviour of braced steel frames exposed to fire. *Journal of Constructional Steel Research*, 72, 130–142.
80. McKenna, F., Scott, M. H., & Fenves, G. L. (2010). Nonlinear finite-element analysis software architecture using object composition. *Journal of Computing in Civil Engineering*, 24(1), 95–107.
81. Khorasani, N. E., Garlock, M. E., & Quiel, S. E. (2015). Modeling steel structures in OpenSees: Enhancements for fire and multi-hazard probabilistic analyses. *Computers & Structures*, 157, 218–231.
82. Jiang, J., Jiang, L., Kotsovinos, P., Zhang, J., Usmani, A., McKenna, F., & Li, G. Q. (2015). OpenSees software architecture for the analysis of structures in fire. *Journal of Computing in Civil Engineering*, 29(1), 04014030.
83. Vassart, O., & Zhao, B. (2012). *MACS+ for membrane action of composite structures in case of fire. Design guide*. ArcelorMittal.

# Chapter 11

## Reinstatement of Fire-Damaged Structures



Tom Lennon and Octavian Lalu

### 11.1 Principles of Inspecting and Assessing Structural Damage Arising from a Fire

Following a fire there is often a need for an initial inspection generally by a structural engineer to evaluate the integrity of the building. Depending on the circumstances this may even be requested by the Fire and Rescue Service (FRS) during an incident to provide information on whether it is safe to enter the building to fight the fire or, if not, to establish a safe distance to proceed with defensive firefighting activities.

If there is any obvious sign of a loss of structural integrity then the initial inspection by a structural engineer may even precede any forensic investigation to establish the nature and cause of the fire. Depending on the circumstances a number of parties may wish to visit the scene as soon as possible following a fire. Such parties may include the FRS Fire Investigation team, the police, representatives from the company responsible for insuring the building and the owners of the building.

In the first instance it is important to ensure that any detailed investigation can be undertaken safely. An early expert opinion on the potential for wall or floor collapse following a fire may be the initial priority. Depending on the nature of the damage it may be that raking shores to maintain the stability of damaged walls may be required or props to provide temporary support to damaged floors are needed. The initial inspection in such circumstances will be a visual inspection sometimes without actually entering the damaged structure and will be based on the experience of the assessor and an understanding of the effects of fire on material degradation and structural integrity. At each stage those responsible for assessing, inspecting and

---

T. Lennon (✉) · O. Lalu  
Fire Safety Department, Building Research Establishment, Watford, UK  
e-mail: [Thomas.Lennon@bre.co.uk](mailto:Thomas.Lennon@bre.co.uk); [Octavian.Lalu@bre.co.uk](mailto:Octavian.Lalu@bre.co.uk)

surveying the aftermath of a fire incident should be considering the following questions:

- Is the damage so severe that the only option is demolition?
- Are any temporary works required to ensure stability during repair or reinstatement?
- Does the structural damage to the building warrant further investigation?
- Are there any further investigations/tests/experiments that could be undertaken to quantify the nature and extent of the structural damage?

Undertaking repairs and reinstating a fire-damaged building incorporate risks that are generally not present during construction under normal conditions. It is important that sufficient information is provided to those involved in reinstatement operations on the potential issues due to permanent reduction in strength or potential issues with connections between structural elements to enable the works to be undertaken safely.

Broadly speaking there are two main strands to an assessment of structural damage following a fire. Firstly a detailed visual inspection to determine the nature and extent of damage to the building: In many cases, this will be sufficient to identify what needs to be done based on the experience and a knowledge of the impact of elevated temperatures both on the structure itself and on other parts of the building that will provide an indication of the severity of the fire. If questions still remain as to the adequacy of the load-bearing elements of structure then a number of options are available ranging from small-scale non-destructive tests (see in particular the section covering fire-damaged concrete buildings) through laboratory tests on samples taken from the scene to large-scale load tests (Fig. 11.1).

### ***11.1.1 Preliminary Investigation***

Wherever possible the first step in a preliminary investigation should be to collate all available information on the building and the fire. This may include accessing any available plans and drawings for the building to establish the nature of the load-bearing elements, the location of the fire and the potential implications for the stability of the building. If possible, speaking to eyewitnesses and particularly firefighters involved in the incident can be very helpful in providing general information on the likely severity and duration of the fire. Nowadays many incidents are captured on video cameras by either individual onlookers, firefighters or CCTV cameras.

Once data on the building and the fire has been collated and the structure has been assessed as safe to enter the preliminary investigation can begin. Following a fire the primary objective is to ensure public safety. The Fire and Rescue Service (FRS) will usually secure the building. If there are any concerns regarding structural stability they will normally involve the local authority building control office to make a preliminary assessment.



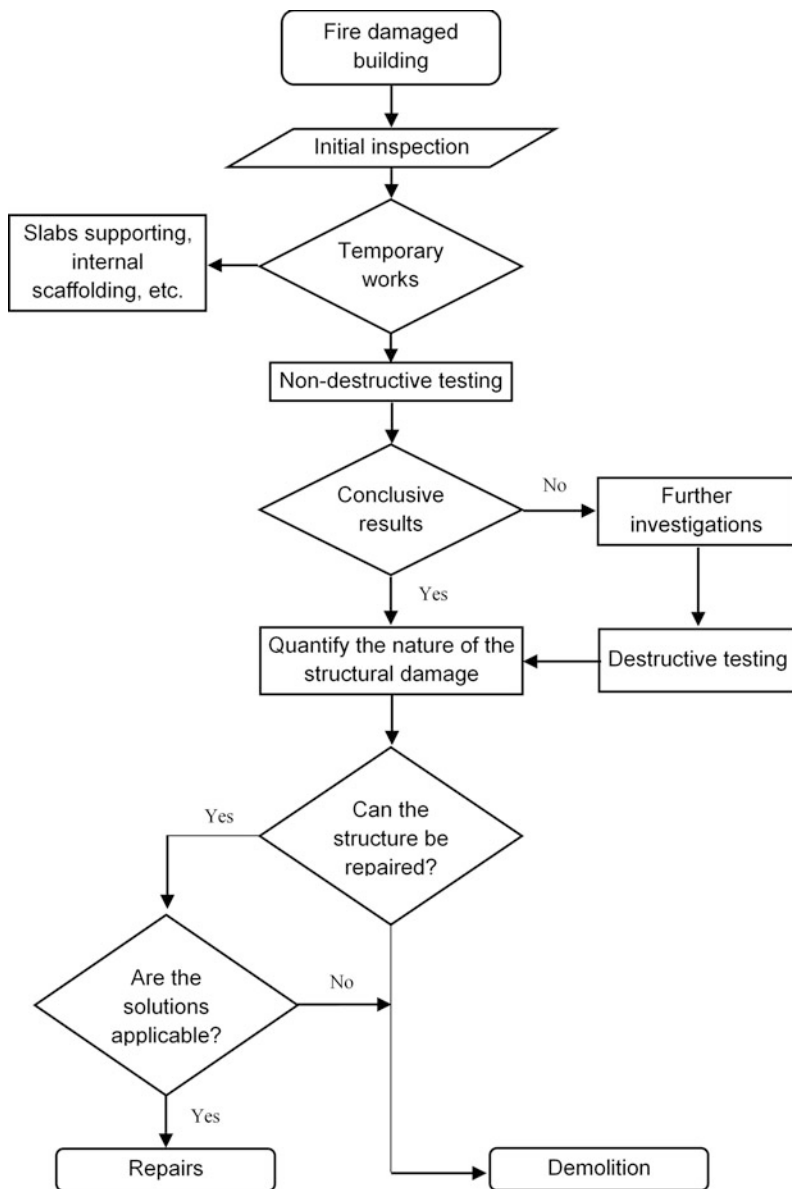


Fig. 11.1 Flow chart related to the process of assessment of structural damage due to fire

It is important that the appraisal process starts as soon as the safety of the structure has been assessed and before the removal of debris to preserve what might be crucial evidence. Often the first impression is one of complete devastation (Fig. 11.2) but

**Fig. 11.2** Accumulated debris following a fire



**Fig. 11.3** Accumulated debris covering fire floor



once non-structural debris and removal of soot deposits have taken place the extent of the damage can be properly evaluated.

Conversely accumulated debris may mask areas where the damage is particularly significant particularly on floors (Fig. 11.3). Depending on the nature and extent of the fire and the consequent damage the preliminary investigation may be sufficient to

draw firm conclusions and provide recommendations for the most appropriate form of action in relation to reinstatement (or demolition). The objectives of the preliminary investigation are to provide information on the condition of the structure, to identify the nature and extent of any defects and to collate evidence that will support a recommendation in relation to the potential to reinstate the building. In many cases this may involve a more detailed investigation. Often the residue from the products of combustion may preclude a detailed visual inspection. In such cases it will first be necessary to clean all exposed surfaces of soot to reveal any cracks, fissures, areas of spalled material, etc. Depending on the nature and extent of the building and the fire damage, cleaning may involve sand or grit blasting, water blasting or chemical cleaning or simply the removal of debris from affected areas. One of the most obvious signs of structural distress in all materials is the presence of large deflections, rotations or misalignment of structural members. The type of damage and its severity should be documented to identify the principal locations requiring further investigation.

Specific information is provided in the sections dealing with the main construction framing materials but in general discoloration can provide some clues to the temperatures attained in a fire. The presence of a hot smoke layer causing soot layering on walls and doors (Figs. 11.4 and 11.5) is indicative of a two-zone fire development where flashover has not occurred. Temperatures in these areas are unlikely to have exceeded 600 °C. One of the most important indicators of temperatures attained in specific areas of the fire-damaged structure is the impact the fire has had on materials other than the main load-bearing elements. Aluminium which has maintained its shape and structure would be indicative of a fire where temperatures had not exceeded approximately 650 °C. Conversely evidence that glazing had softened and/or liquefied would indicate a more severe fire where temperatures had exceeded approximately 850 °C. It should be borne in mind that at times a study of undamaged items can provide as much information as those items that have been damaged or have suffered an obvious change in physical appearance.

Table 11.1 provides information on the effects of temperature on materials commonly found in buildings which can be used to help map out likely temperatures

**Fig. 11.4** Soot layer on oriented strand board indicative of stratification of hot smoke layer



**Fig. 11.5** Soot damage to flat entrance door due to hot smoke layer



at different locations within the fire-damaged area [1, 2]. Figures given are approximate for general guidance and such values should never be used in isolation to evaluate the nature and extent of damage to load-bearing elements.

An alternative publication providing general guidance on the performance of existing structures after a fire is the Institution of Structural Engineers publication *Appraisal of existing structures* [3]. Appendix 6 of this publication is particularly useful and provides general information as well as guidance relevant to specific forms of construction (concrete (reinforced and prestressed), timber, brickwork, steelwork, cast iron and wrought iron). Further information of a general nature is provided in BRE Information Paper 24/81 [4] which considers an assessment of temperatures reached by selected materials and components in a fire based on an examination of post-fire debris and specific information related to concrete, brickwork, timber, steel reinforcement, hollow clay tiles and woodwool cement slabs, plaster and tiles and slates.

Charring of timber provides an indication of the severity of fire even in structures other than timber frame. Figure 11.6 shows charred timber battens within a concrete and masonry framed structure where a knowledge of the original section size and the nature of the exposure could be used to estimate the peak temperatures experienced by the precast concrete floor slabs. The ignition temperature of timber is dependent on a number of factors but timber can ignite once its temperature exceeds 200 °C. The charring rate of timber is variable depending on the species but is generally around 0.6–0.7 mm/min for softwoods based on exposure to the standard fire curve [5].

**Table 11.1** Temperature effects for materials

Material	Examples of their use	Change in structure	Approximate indicative temperature (°C)
Aluminium	Fixtures, brackets, cooking utensils	Drops formed flowing material	650
Brass	Furniture on doors and windows; fixtures and fittings	Softened or drops formed	900–1000
Bronze	Frames, artefacts	Softened or drops formed	1000
Cast iron	Radiators, pipes	Melts	1100–1200
		Drop formation	1150–1250
Cellulose	Wood, cotton	Darkens	200–300
Copper	Wiring, cables	Melts	1000–1100
Lead	Plumbing pipes, roof flashing	Softened or drops formed	300–350
Moulded glass	Jars and bottles	Softened	700–750
		Rounded	750
		Flowing	800
Paint	Surface treatment of linings	Deteriorates	100
		Destroyed	150
Polyethylene	Bottles, bags, buckets	Shrivels	49
		Melts	66
HD polyethylene	Pipes, guttering	Melts, flows	190
Polystyrene	Insulation, packaging	Softens	50–60
		Melts and flows	120
Polymethyl methacrylate	Handles, skylights	Softens	130–200
		Bubbles	250
PVC	Cables, pipes, ducts	Degrades	100
		Fumes	150
		Browns	200
		Chars	400–500
Sheet glass	Windows	Softened	700–750
		Rounded	800
		Flowing	850
Silver	Jewellery, cutlery, coins	Droplets	950
Solder	Plumbing joints	Melts	250
Steel	Structure, fittings	Melts	1400
Vinyl-based paints	Covering to steelwork	Melts, flows	120
Wood	Structure, furniture	Ignites	240
Zinc	Plumbing fittings, galvanized surfaces	Drops formed	400

**Fig. 11.6** Charring of timber battens (and localized spalling of concrete soffit)



**Table 11.2** Ignition and auto-ignition temperatures for commonly used materials

Material	Ignition temperature (°C)	Auto-ignition temperature (°C)
Cotton	230–266	254
Paper/newsprint	230	230
Phenolic resins	520–540	570–580
Polyamide	421	424
Polyester	346–399	483–488
Polyethylene	341	349
Polymethyl methacrylate	280–300	450–462
Polystyrene	345–360	488–496
Polyvinyl chloride	391	454
Rigid polyurethane foam	310	416
Wood	280–310	525
Wool	200	–

Table 11.2, based on the information from Kirby et al. [6], provides information on the ignition temperature and auto-ignition temperature of various commonly used materials. The ignition temperature is defined as the temperature to which the material has to be heated for sustained combustion to be initiated from a pilot source. The auto-ignition temperature is defined as the temperature at which the heat evolved by a material decomposing under the influence of heat is sufficient to bring about combustion without the application of an external source of ignition and tends to be higher than the piloted ignition temperature.

The Concrete Society Report sets out the assessment and repair process as a series of steps which would cover most incidents whether involving concrete structures or not. The number of steps required and the degree of detail involved in each step will vary from case to case. The process is summarized below.

- 1. Preliminary inspection:** Secure public safety and safety of the structure, prop members requiring additional support.

2. **Assessment of damage:** Carry out on-site assessment to determine the extent of damage. This may involve a combination of visual inspection and non-destructive testing.
3. **Testing and detailed assessment:** Carry out laboratory testing of samples taken from site. Carry out dimensional surveys and calculations to determine likely fire severity and residual structural capacity.
4. **Design of repairs to structural elements:** Decide on the nature and extent of any demolition required. Design repair system to reinstate original capacity. Produce drawings and specifications for repair.
5. **Implement structural repairs:** Select suitable contractor to carry out structural repairs. Agree method statements and sequence of working. Undertake repairs.

Following completion of the preliminary investigation/inspection the detail involved in the subsequent steps will be dependent on the severity of the fire and the specific materials providing the structural support to the building.

### ***11.1.2 Assessment by Calculation***

While the process of design to withstand a fire is not the same as that used to assess the condition of a structure following a fire, many of the techniques used to undertake a performance-based structural fire engineering design can be used to support an assessment of the structure following a fire. Such techniques should be used in combination with the visual inspection and test processes described earlier to provide a more reliable picture of the likely temperature distribution within the structure during both the heating and cooling phases of a fire. Simple worked examples are presented under the sections dealing with inspection, assessment and repair for the various structural materials considered in this chapter that illustrate how structural fire engineering design procedures may be modified to provide an estimation of the temperature experienced by the structure and an evaluation of the residual load-bearing capacity.

## **11.2 Inspection, Assessment and Reinstatement of Fire-Damaged Steel-Framed Buildings**

Although the behaviour of structural steel at elevated temperatures is well understood and predictable there is a great deal of uncertainty regarding the reuse and repair of fire-damaged steel structures. The most difficult question is whether steel exposed to high temperatures and not obviously deformed or visibly damaged can be reused and, if so, will it be capable of providing the full design capacity. Steel strength and stiffness reduce with increasing temperature and this reduction is particularly significant at temperatures in excess of 550 °C. For this reason in

many cases structural steelwork will be protected by an insulating material which may be in the form of boards, spray or applied reactive coating (intumescent). The purpose of such materials may be partly aesthetic but is principally to protect the steel element in the event of a fire. Fire protection is designed to provide the required level of performance during a single fire exposure. Therefore following a site visit the protection material may be damaged due to a combination of the effects of the fire often exacerbated by firefighting operations. One of the principal areas of investigation is to establish if the steelwork was fire protected and, if so, what sort of material was used. The condition of the fire protection may provide some indication of the severity of the fire and the nature and duration of the exposure of the steelwork.

For steel structures the primary purpose of the initial site investigation is to identify those elements most seriously affected by the fire and to use this information to determine the extent to which structural elements should be replaced. There are two ways in which the steel may be damaged: permanent strain due to excessive deformation or rotation and chemical metallurgical changes that have an impact on the residual strength of the material. The former are generally easier to identify than the latter but this is not always the case. Where beams or columns are subject to excessive deflections such as in Figs. 11.7 and 11.8 then it is evident that these members will need to be replaced. However, even where the structural member appears to be dimensionally straight and notionally undamaged particular care should be taken to investigate the connections and the area around the connections for signs of distress, local buckling (Fig. 11.9) and damaged, loose or stripped bolts (Fig. 11.10).

During a fire, steel structures, particularly exposed steel structures, will experience deformation as a consequence of thermal expansion and material degradation. Depending on the degree of elastic or plastic deformation, on cooling the steel members will contract. Where thermal expansion and subsequent contraction are restrained by the adjacent structure and by the stiffness of the connections then very

**Fig. 11.7** Steel beam and composite floor slab subject to significant deformation due to fire





**Fig. 11.8** Deformed column (damage due to explosion)



**Fig. 11.9** Local buckling of beam lower flange



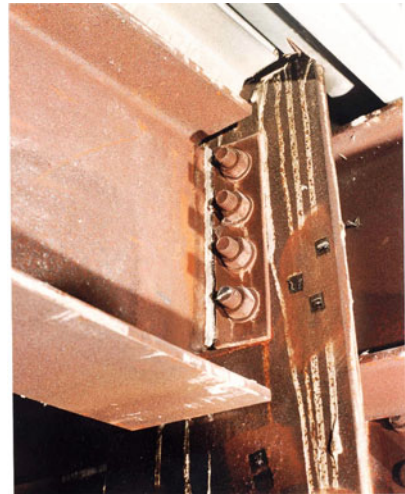
large tensile forces can develop leading to rupture of welds, end plates (Fig. 11.11) or even beam web (Fig. 11.12).

In relation to assessing the residual strength of fire-damaged steel structures the most comprehensive guidance is that provided by Kirby et al. [6]. The document provides residual mechanical properties for different types of structural and reinforcing steels, iron and bolts following exposure to a range of high temperatures. Metallurgical evaluation of fire-damaged structural steelwork is described along with case studies from real fire incidents.

**Fig. 11.10** Elongation of bolt and thread stripping of bolts in tension



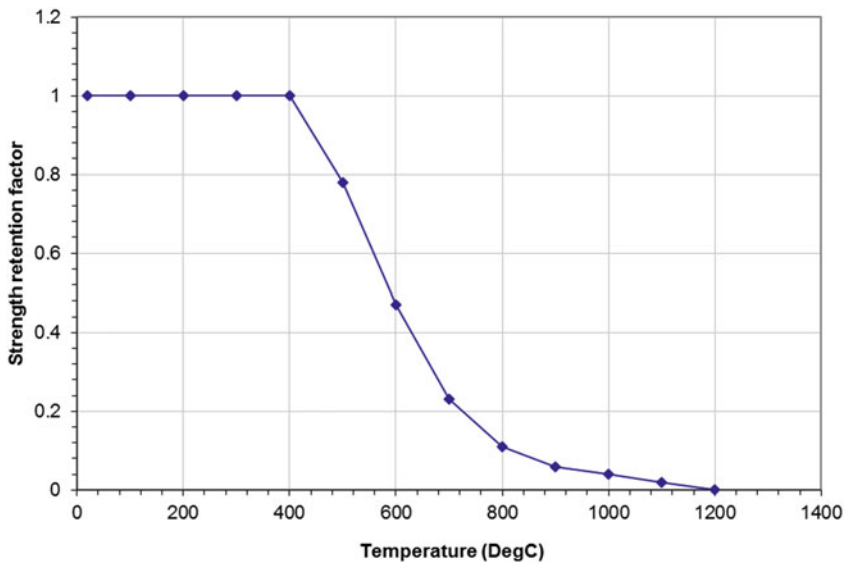
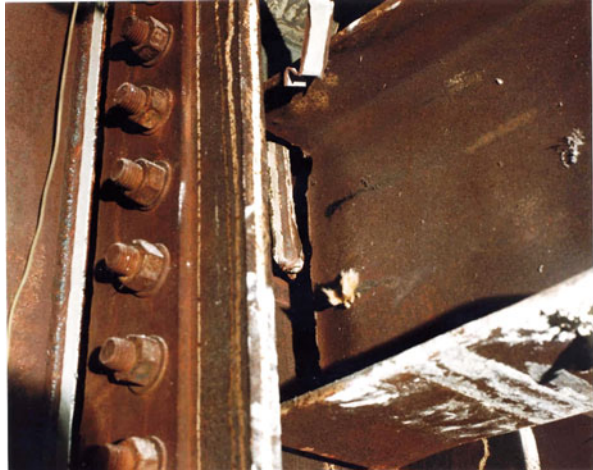
**Fig. 11.11** Fracture of end plate



### ***11.2.1 Material Properties***

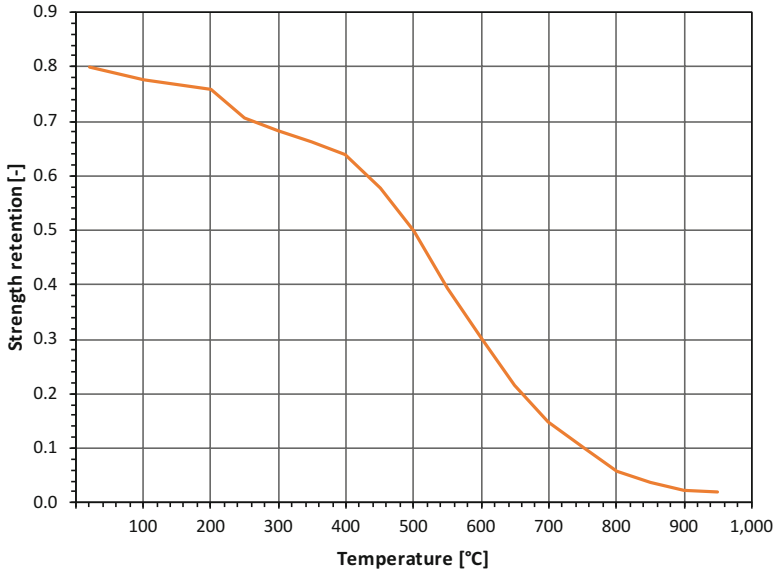
In recent years a great deal of work has been undertaken to derive reliable relationships between steel strength and temperature. This information has been essential in the development of structural fire engineering design as a recognized academic discipline. The fire parts of the structural Eurocodes [7–12] set out the detailed relationship between temperature and strength for a wide range of structural materials. The relationship between temperature and strength for hot-rolled carbon steel is summarized in Fig. 11.13.

**Fig. 11.12** Fracture of beam due to large tensile forces on cooling



**Fig. 11.13** Relationship between temperature and strength for hot-rolled structural steel

Work reported by Kirby et al. [6] has shown that the mechanical properties of structural steelwork (residual strength) do not significantly deteriorate when exposed to fires up to 600 °C. Above 600 °C the residual mechanical properties of structural steelwork are affected. The reduction in yield stress and tensile strength is dependent on the grade of steel and the temperature and duration of exposure. In certain cases an assumed reduction of 10% of the nominal values would be justified in



**Fig. 11.14** Strength reduction factors for Grade 8.8 bolts (from [13])

determining residual capacity. If there is any doubt recourse should be made to methods of non-destructive testing (NDT) or samples of the steelwork should be taken from the worst-affected zones, machined into tensile coupons and tested to determine tensile strength and yield stress.

Kirby [13] has derived strength reduction factors for Grade 8.8 bolts at various temperatures. The results are summarized in Fig. 11.14. As with structural steels the residual strength properties are high, provided that excessive temperatures are not encountered. In general, bolts will not be found in the hottest part of the fire compartment and will be partially protected in some form or other by the mass of the steel members forming the connection. However, as already highlighted, an assessment of the performance of connections needs to take into account more than just the temperature to which the fixings have been exposed. The expansion and movement of the connected structural members are generally of more importance as such deformations may generate stress levels (in shear, tension and bending) which are far in excess of normal design requirements.

High strength friction grip bolts, even if they appear undamaged, may have lost a degree of the tension grip on which they rely. In such cases the bolts need to be replaced. If there is any doubt about the adequacy of bolted connections or if there is evidence that the steelwork in the vicinity of the connections has been heated to very high temperatures, then bolts and ancillary components should be removed and replaced. Connections are an essential part of ensuring structural integrity and robustness and therefore must be capable of transferring the design loads for the structure. In general, heating a welded joint during a fire is likely to be more

beneficial than detrimental due to the increased ductility at the cost of a minor drop in resistance. However, all welds should be carefully inspected for signs of cracking or distress in the heat-affected zone.

Cold-formed galvanized steel products are widely used in modern structures. Such members would typically be found in industrial buildings as purlins or roof beams and in residential buildings as wall panels and floor cassettes (studs and floor joists). An example of a steel-framed floor system following a severe fire is shown in Fig. 11.15. A cold-formed wall panel subject to the same fire exposure is shown in Fig. 11.16. The elevated temperature strength of cold-formed steel is illustrated in Fig. 11.17 based on the information provided in a Steel Construction Institute report [14].

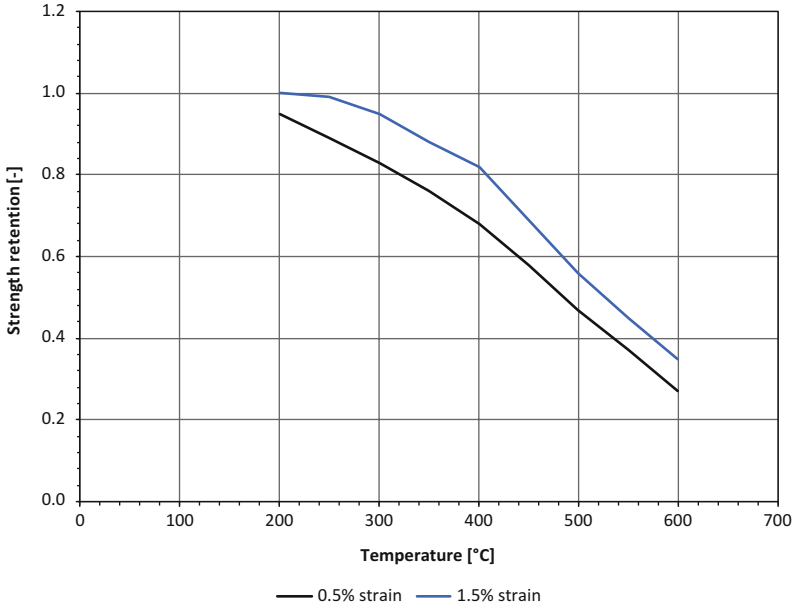
Although the strength reduction for cold-formed steel is not markedly different to hot-rolled steel over the temperature range considered, cold-formed steel products are thin and the thermal capacity is therefore low with material temperatures closely

**Fig. 11.15** Cold-formed steel floor following a fire



**Fig. 11.16** Cold-formed steel wall panel following a fire





**Fig. 11.17** Strength reduction factors for cold-formed steel at different strain rates (from [14])

following the gas temperature of the environment. It is relatively easy therefore to cause irreparable damage to purlins, cladding rails, steel sheeting, etc. The galvanized coating providing the protective layer is composed of zinc which has a melting point of approximately 420 °C. Surface damage (bubbling) is usually observed on heating to approximately 275–300 °C which again can provide some indication of fire intensity in specific locations.

### 11.2.2 Testing of Fire-Damaged Steel

Two techniques are available to estimate the residual strength of fire-damaged steel without recourse to destructive methods. The first involves the use of a hardness tester to establish the Brinell hardness number which will provide an indication of the tensile strength of the material. The tensile strength can then be used to estimate the minimum yield stress based on known values of the ratio between the two values for specific grades of steel (yield stress generally in the region  $0.55\text{--}0.75 \times$  the tensile strength). The other technique requires specialist equipment and specialist metallurgical expertise to carry out an on-site microscopic examination of the steel microstructure.

Where visual inspection and non-destructive testing are insufficient to assess the residual strength of damaged steel structures then recourse may be made to

destructive testing by cutting and machining tensile test specimens for laboratory assessment of ultimate strength and yield stress. This is the only way to effectively guarantee that the material conforms to the required specification.

As with other forms of construction if resources are available and the specific conditions warrant it then the damaged area or the entire structure could be assessed through a full-scale loading test to evaluate response and measure deflections.

### ***11.2.3 Assessment by Calculation***

In addition to visual inspection and testing it is possible to calculate fire temperatures and to use this information and principles of heat transfer to determine the temperature distribution within the structural members. This information can be vitally important in determining whether individual beams and columns can be reused or whether they should be replaced. Where information is available on the specific characteristics of a fire compartment then calculation procedures can be used to determine the severity of the fire. The most commonly used procedure is the parametric approach set out in the fire part of the Eurocode for Actions [15]. Once the anticipated fire behaviour has been calculated then this is used as the basis to determine the temperature rise of the structural elements which can inform decisions on whether to demolish or repair and reinstate. The procedure is illustrated by a worked example to establish the likely maximum temperature of a protected load-bearing steel beam.

#### **11.2.3.1 Worked Example**

This example aims to show the Eurocode procedure for estimating the time temperature development based on parametric calculations [15] and the steel temperature rise for unprotected and protected members [8]. Once the peak temperature reached has been determined the information is used to assess the reduction in strength and the residual capacity for steel structural elements. In this case there was no noticeable damage to the steel section. The assessment process is based on the information on strength reduction with temperature and residual strength of heated steel covered in Sect. 11.2.1. Based on the information on the loads applied to the beam, if it can be shown that the temperature of the steel member had not exceeded a critical value of 550 °C, then it can safely be assumed that the beam can be reused and will have sufficient strength to carry the design loads required. However, any residual damage due to restrained thermal expansion/contraction should be carefully inspected and evaluated separately.

The layout for the fire compartment is shown in Fig. 11.18. All input data for the parametric time-temperature development is presented in Table 11.3.

The time-temperature curve in the heating regime can be calculated using the equation below. The calculation procedure is described in EN 1991-1-2 [15]:

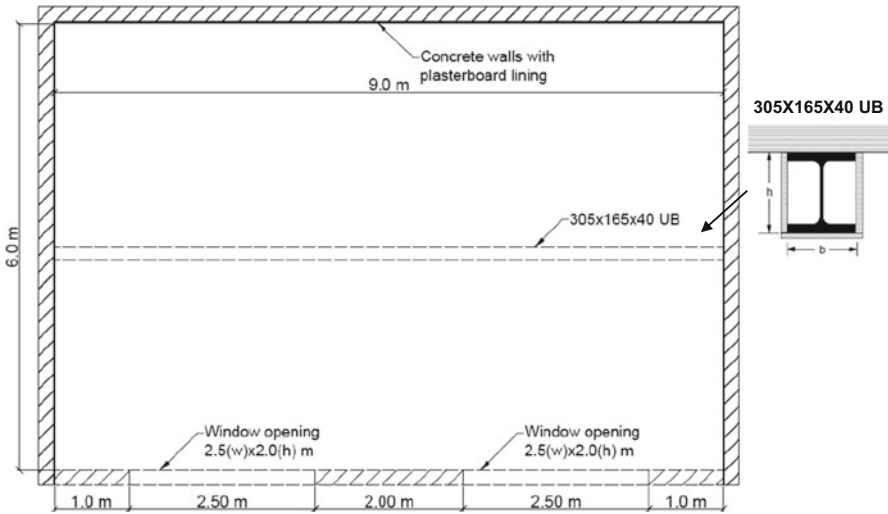


Fig. 11.18 Plan showing the fire compartment and location of central protected beam

Table 11.3 Input data for parametric time-temperature calculation

Occupancy	$q_{f,d}$ (MJ/m <sup>2</sup> )	$A_r$ (m <sup>2</sup> )	$A_v$ (m <sup>2</sup> )	$h_v$ (m)	$O$ (m <sup>-1</sup> )	$b$ (J/m <sup>2</sup> s <sup>1/2</sup> K)	Fire growth rate
Office	570	228	10	2.8	0.073	1190	Medium

$$\theta_g = \theta_0 + 1325 \cdot (1 - 0.324 \cdot e^{-0.2t^*} - 0.204 \cdot e^{-1.7t^*} - 0.472 \cdot e^{-19t^*}) \quad (11.1)$$

where  $\theta_g$  represents the gas temperature (°C), and  $t^*$  represents the parametric time as a function of opening factor (O) and thermal absorptivity (b). The calculation procedure considers a linear regression curve for the cooling phase.

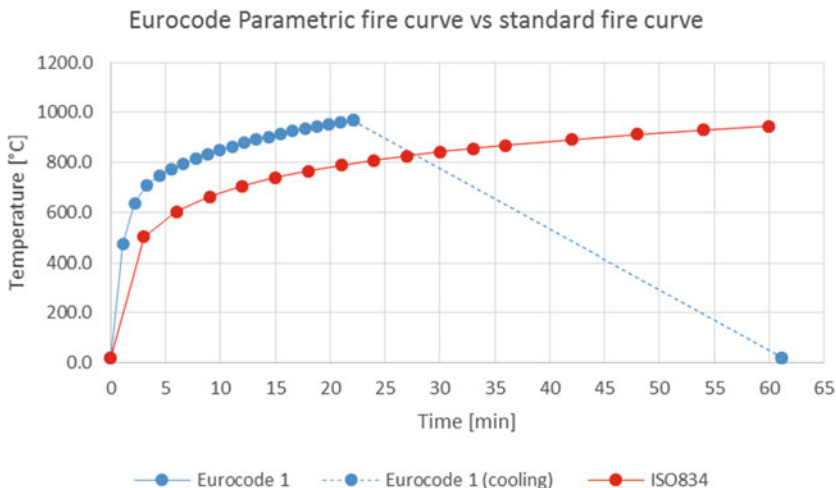
A comparison between the standard fire exposure (ISO834) and the time-temperature curve based on the parametric approach is presented in Fig. 11.19:

The purpose of the exercise is to determine the temperature to which the central beam running down the middle of the compartment has been exposed. This beam is a 305 × 165 × 40 UB, exposed to fire on three faces, as shown in Fig. 11.18. EN 1993-1-2 [8] offers a simplified procedure for estimating an equivalent uniform temperature distribution in the cross section with and without protection.

In this case the beam was protected with a single layer of gypsum board. Following the fire, the beam appeared to be undamaged although much of the board had been removed. It is believed that this was a result of intervention from the fire service rather than a failure of the board system.

The first calculation assumes that the beam is unprotected and the calculated steel temperature is very close to the gas temperatures derived using the parametric approach.





**Fig. 11.19** Parametric fire exposure used to represent the atmosphere temperatures within the fire compartment

In the first case it will be considered that the steel section is exposed to fire without any protection. The increase in temperature ( $\Delta\theta_{a,t}$ ) in an unprotected steel member during a time interval  $\Delta t$  is calculated using Eq. (11.2), as described in EN 1993-1-2 [6]:

$$\Delta\theta_{a,t} = k_{sh} \frac{A_m/V}{c_a \rho_a} \dot{h}_{net} \cdot \Delta t \tag{11.2}$$

It can be observed that the critical temperature ( $\theta_{cr}$ ) of 550 °C is reached shortly after 5 min of fire exposure. Based on observations the more likely scenario is that the board remained intact for the entire exposure period and provided protection to the beam.

For a steel member insulated with fire protection material, the uniform temperature distribution in the cross section can be estimated using Eq. (11.3):

$$\Delta\theta_{a,t} = \frac{\lambda_p \cdot A_p/V \cdot (\theta_{g,t} - \theta_{a,t})}{d_p c_a \rho_a \cdot (1 + \frac{\phi}{3})} \Delta t - (e^{\phi/10} - 1) \Delta\theta_{g,t} \tag{11.3}$$

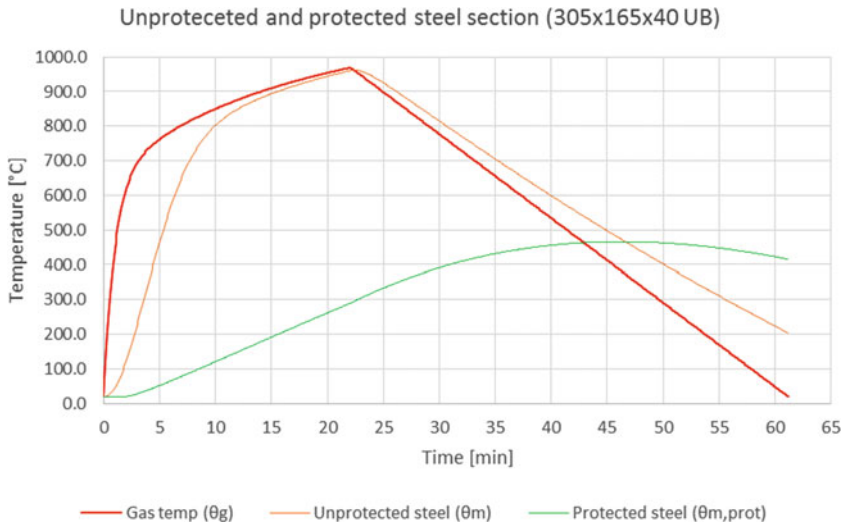
with

$$\phi = \frac{c_p \rho_p}{c_a \rho_a} d_p \cdot A_p/V \tag{11.4}$$

The properties of protection material are presented in Table 11.4.

**Table 11.4** Fire protection properties assumed in calculation

Fire protection	$d_p$ (m)	$\lambda_p$ (W/mK)	$c_p$ (J/kg K)	$\rho_p$ (kg/m <sup>3</sup> )	Exposure	Ap/V (m <sup>-1</sup> )	$\varphi$ (-)
Plasterboard	0.015	0.2	1700	840	3 Sides	150	0.682



**Fig. 11.20** Temperature calculation for steel beam

It can be observed that after 46 min of fire exposure the maximum temperature of steel section is 466 °C, which is less than the critical temperature considered ( $\theta_{cr}$ ) of 550 °C, and therefore the beam can be retained and reused. A comparison between the temperature distribution on the unprotected and protected steel section considered is shown in Fig. 11.20.

### 11.2.4 Repair of Fire-Damaged Steel Buildings

Kirby et al. [6] produced a flow chart for reinstatement of fire-damaged steel (or iron)-framed buildings. They classified the level of damage as either none, slight or extensive. Where no visible damage was apparent the repair would consist of a simple check of the bolted connections particularly where a heated member was connected to an unheated member, and the replacement of bolts if required. Where the damage is classified as slight, repair may consist of reuse with a reduced load-bearing capacity, repair and reinforcement to reinstate the required load-bearing capacity, or if repairs prove to be uneconomic then steel members from the area affected should be scrapped. Where the damage is extensive with steelwork twisted

and distorted beyond acceptable levels then the only option is to scrap all such sections and either replace with new members or completely demolish depending on the relative cost of each option. Examples are presented of the various options available ranging from reuse with no significant changes to replacement of fire-damaged steel sections. The choice of the repair option was dictated by tests on the fire-damaged steelwork.

### **11.3 Inspection, Assessment and Reinstatement of Fire-Damaged Concrete-Framed Buildings**

Concrete is a non-combustible material and is traditionally regarded as a construction material that performs particularly well in the event of a fire. For many years concrete has been used to provide protection to other materials (e.g. structural steel) in a fire situation. Concrete structures are generally capable of being repaired following a fire, even a severe fire. Tovey and Crook [16] summarized the information from over 100 fires. Most of the buildings were repaired and returned to service. When structures were demolished and replaced it was generally for reasons other than structural damage. However, anticipated performance is dependent on an appropriate design specification and construction process.

Readers should consult the Concrete Society report [1] for detailed guidance in relation to the assessment, design and repair of fire-damaged concrete structures. Further guidance is available in FIB Bulletin 46 [17] dealing with design, structural behaviour and assessment. Following the initial visual inspection two methodologies are presented for evaluation of the residual strength. The first is to test the fire-damaged concrete to directly assess the concrete quality and strength. The second is to estimate the fire severity and calculate the temperature profiles through the concrete to determine residual strength. For concrete structures there are a number of non-destructive techniques, petrographic analysis and intrusive investigations available that will provide information on the condition of the material. The second is really a general technique applicable to all types of material.

#### ***11.3.1 Material Properties***

The relationship between concrete compressive strength and temperature is dependent on the type of aggregate used. The relationship for siliceous, calcareous and lightweight concrete is shown in Fig. 11.21. The same relation is shown in Fig. 11.22 for various types of reinforcement. The reduction in strength with temperature for concrete and indeed for “normal” reinforcement is similar to that for steel with approximately 50% of the ambient temperature strength available at a temperature of approximately 550 °C. However, there are two main differences between steel and

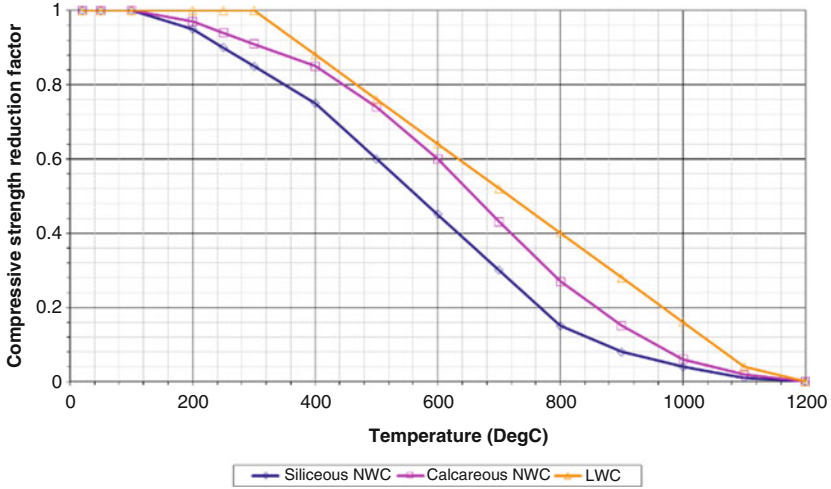


Fig. 11.21 Relationship between concrete strength and temperature (from [7, 9])

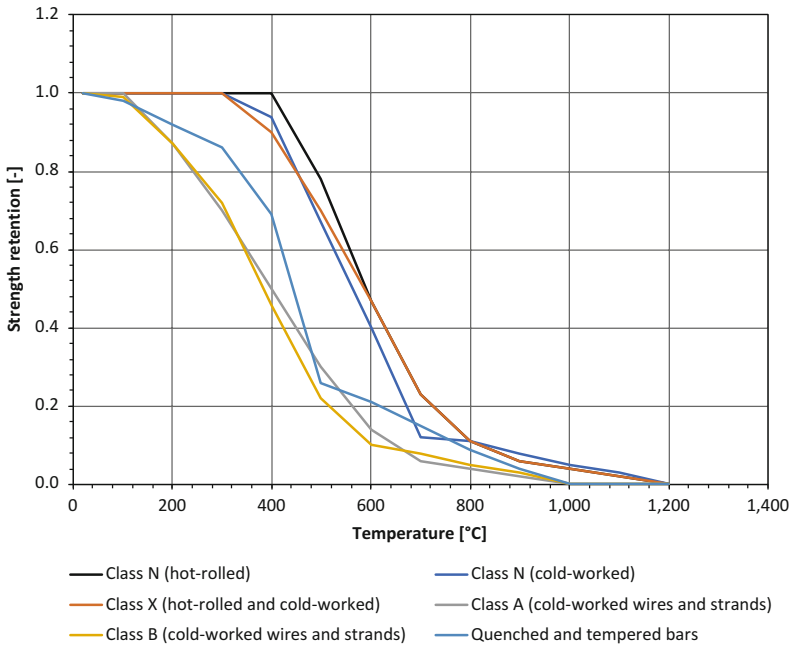


Fig. 11.22 Strength reduction factors for different types of reinforcement and prestressing steel (from [7])

concrete structures when considering exposed element temperatures. The first is that damaged concrete is unlikely to recover much, if any, of the ambient temperature strength on cooling while we have seen that steel is capable of recovering almost all of its capacity as long as the temperatures remain below approximately 600 °C.

Indeed strength based on the peak temperatures during the fire exposure may overestimate the concrete residual strength due to further losses occurring during the cooling phase. More detailed guidance on the residual material characteristics may be found in FIB Bulletin 46 [17]. The extent of deterioration in the microstructure is dependent not only on the maximum temperature but also on the duration of the fire exposure. Secondly concrete structural elements tend to have a very high thermal mass and therefore, unlike exposed steel, the vast majority of the section may not have experienced a significant rise in temperature. For this reason it is often possible to remove the damaged concrete from the surface and repair by spraying fresh concrete (or other cementitious spray) to the exposed surface. For assessing the stability of concrete structures immediately following a fire the Eurocode approach of discounting the strength of concrete exposed to temperatures greater than 500 °C may be appropriate. However, industry guidance [1] recommends discounting the residual strength for concrete exposed to temperatures greater than 300 °C when carrying out an appraisal of a fire-damaged structure.

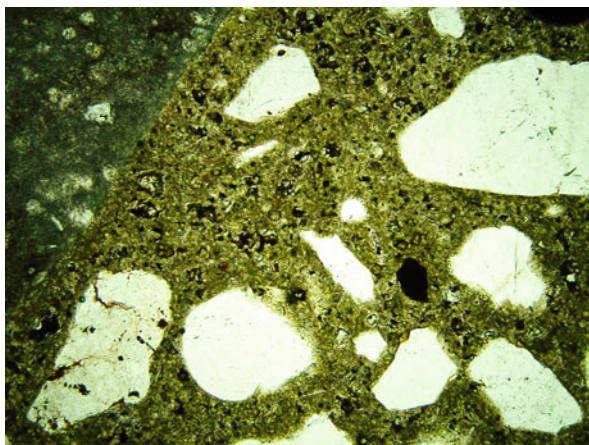
Although the temperature/strength relationship for normal concrete reinforcement is similar to that of structural steel it should be borne in mind that steel used for prestressed structures has a significantly inferior relationship. Cold-worked Class B wires and strands retain only approximately 20% of the ambient temperature strength when heated to 500 °C. Concrete structures are designed, whether implicitly or explicitly, to limit the temperature of the reinforcement to specified limits for the requisite fire resistance period. Cover to the reinforcement is required both to prevent corrosion and to provide the necessary level of protection in the event of a fire. Different critical temperatures are used for ordinary reinforcement and prestressing strands and cables that reflect the differences highlighted in Fig. 11.22. Stainless steel reinforcing bars perform much better than either cold-worked or hot-worked bars and in terms of residual strength are capable of recovering their entire ambient temperature strength on cooling even when heated to 850–900 °C [17].

As with steel heated to high temperatures, changes in the chemical microstructure of the concrete occur at high temperature which has a significant impact on the resistance of the structure.

The mineralogical changes that occur can be investigated by petrographic examination to determine maximum temperatures attained and to evaluate the depth to which the concrete member has been damaged (Fig. 11.23).

One of the simplest methods of assessing the temperature to which concrete elements have been exposed is to identify the colour of the section through the depth. The colour of concrete can change on heating. Depending on the type of aggregate used, a pink/red discolouration occurs above 300 °C which coincides with the temperature at which a significant loss of strength occurs. Any concrete exhibiting such a colour change should be regarded as weakened. Colour changes are most pronounced for siliceous aggregates. A summary of the mineralogical changes of ordinary Portland cement concrete as it is heated is presented in Table 11.5 based on the information in [1].

**Fig. 11.23** Petrographic analysis of cement paste matrix (magnification  $\times 100$  in plane polarized light)



**Table 11.5** Mineralogical and strength changes to concrete due to heating (from [1])

Temperature (°C)	Mineralogical changes	Strength changes
105	Loss of physically bound water, increasing porosity and micro-cracking	Minor loss of strength (<10%)
250–350	Pink/red discolouration of aggregate. Loss of chemically bound water	Significant loss of strength from 300 °C
450–500	Red discoloration of aggregate may deepen up to 600 °C. Flint aggregates may exhibit grey/white colour between 250 and 450 °C	
600–800	Volume contraction due to decarbonation leading to severe micro-cracking	Concrete not structurally sound when heated to temperatures in excess of 550–600 °C (Fig. 11.20)
800–1200	Limestone aggregate particles become white. Disintegration of cement matrix leading to a white/grey powder	Figure 11.21
1200		Concrete starts to melt
1300–1400		Concrete melted (Fig. 11.22)

The nature and extent of the damage observed are largely dependent on the nature of the thermal exposure. Figures 11.24–11.26 are examples where concrete elements or samples have been exposed to a fire exposure over and above what would normally be encountered in a building. Figure 11.24 shows severe cracking of a reinforced concrete slab when exposed to a hydrocarbon fire exposure with temperatures held at 1200 °C for some time. Figure 11.25 shows a white discoloration of the limestone aggregate where the surface material has degraded and fallen away when subject to a similar hydrocarbon exposure. Figure 11.26 shows the extreme chemical transformation where the samples have been heated to 1300 °C and the concrete has vitrified and melted and solidified on cooling.

**Fig. 11.24** Severe cracking of loaded slab exposed to hydrocarbon fire exposure (1200 °C)



**Fig. 11.25** White discoloration of limestone aggregate following exposure to hydrocarbon curve (1200 °C)



### ***11.3.2 Spalling***

Spalling of concrete in fire involves layers or pieces of concrete breaking off from the surface of the structure as it is heated (or sometimes as it cools). Although spalling of concrete is often observed during or following a fire it is important to understand the conditions where it may pose a problem in relation to residual strength and repair of fire-damaged structures. As already mentioned concrete structures generally perform very well in the event of a fire due to the incombustible nature and low thermal diffusivity of the material. The loss of concrete cover due to spalling increases the rate of heating to the inner layers of the structure providing a greater risk of significant structural damage.

**Fig. 11.26** Concrete cubes melted due to exposure to modified hydrocarbon curve (1300 °C)



**Fig. 11.27** Explosive spalling of loaded slab subject to hydrocarbon fire exposure



There are three main types of spalling—explosive spalling, aggregate spalling and sloughing off or corner spalling. The first two generally occur in the early stages of fire exposure while corner spalling typically occurs in the later stages of fire exposure. Explosive spalling is the most significant in relation to the robustness of the structure as very large sections can be removed instantly exposing the reinforcement during the peak burning phase of the fire. Figure 11.27 is a loaded slab where extensive spalling has occurred significantly reducing the depth of the element while Fig. 11.28 shows a similar section where explosive spalling has exposed the reinforcement. In both cases the elements were subject to a hydrocarbon fire exposure. Spalling of concrete is a complex subject and arises from the interaction of a number of different parameters. For further details readers are advised to consult FIB Bulletin 38 [18].



**Fig. 11.28** Explosive spalling of loaded slab subject to hydrocarbon fire exposure exposing reinforcement



**Fig. 11.29** Extensive aggregate spalling of the underside of concrete floor slab exposing tensile reinforcement



Figure 11.29 shows extensive aggregate spalling of the underside of a concrete floor slab following a large-scale fire test on a concrete building. Figure 11.30 shows extensive spalling of an edge column following a fire incident. Figure 11.31 shows how spalling of a concrete beam has exposed the reinforcement. The figure also illustrates the pinkish discoloration of the aggregate.

Design procedures should ensure that for normal-strength concrete with typical moisture content (<3% by weight) spalling of concrete in fire is not an issue for structural stability.

**Fig. 11.30** Extensive spalling of edge column following a fire



**Fig. 11.31** Beam reinforcement exposed due to spalling (note: pinkish discoloration of aggregate)



### ***11.3.3 Testing of Fire-Damaged Concrete***

In addition to a visual inspection, a number of on-site and laboratory-based techniques are available to assist the engineer in the assessment of fire-damaged structures.

In many cases it may be sufficient to take soundings of the potentially damaged concrete using a hammer and chisel. Damaged concrete tends to produce a dull thud if not sufficiently damaged to break away on impact whereas sound concrete produces a ringing sound when struck. If required cores can be taken from fire-damaged areas to allow for a more detailed visual inspection (Fig. 11.32) or subsequent laboratory testing if required. Coring itself can provide some indication on the depth of damage if it is possible to measure both the coring depth and the energy

**Fig. 11.32** Core taken from fire-damaged area



involved in extracting the core. Apart from laboratory strength tests (typically compression testing of “slices” cut and prepared from a long core) cores can be used as the basis for subsequent colorimetry, analysis of porosity and permeability and chemical and mineralogical investigation.

Non-destructive testing techniques include the Schmidt hammer test, the ultrasonic pulse velocity test, the Windsor probe, the BRE internal fracture test, the CAPO test and techniques based on drilling resistance. More detailed information may be found in FIB Bulletin 46 [17].

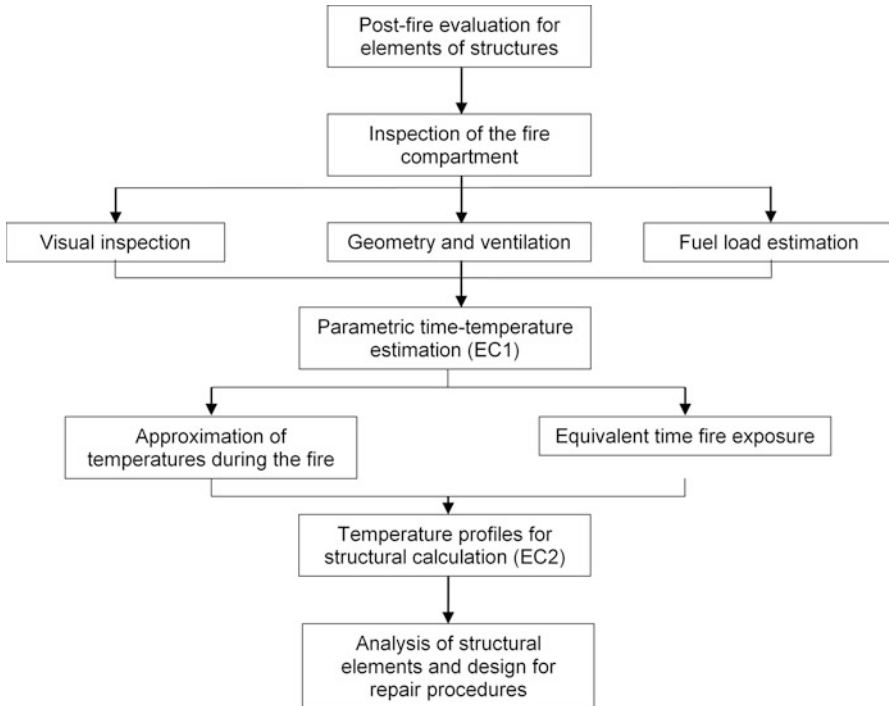
### ***11.3.4 Assessment by Calculation***

The calculation of compartment time-temperature response covered above with respect to the assessment of fire-damaged steel structures is material independent and, provided that all relevant parameters are known, (fire load, ventilation conditions, compartment geometry and thermal properties of compartment linings), calculation procedures can be used to estimate the temperature to which the structural elements have been exposed.

#### **11.3.4.1 Worked Example**

This worked example shows how Eurocode design procedures can be used to assist in the assessment of fire-damaged concrete structures and how the results may be used to inform decisions concerning the repair and reinstatement options. The schematic procedure in Fig. 11.33 summarizes the process adopted.

In this example we will consider a compartment with the following parameters (Table 11.6). The layout of the fire compartment and the structural elements is



**Fig. 11.33** Schematic procedure for post-fire evaluation of concrete structural elements

**Table 11.6** Input data for parametric time-temperature calculation

Occupancy	$q_{f,d}$ (MJ/m <sup>2</sup> )	$A_r$ (m <sup>2</sup> )	$A_f$ (m <sup>2</sup> )	$A_v$ (m <sup>2</sup> )	$h_v$ (m)	$O$ (m <sup>-1</sup> )	$b$ (W s <sup>1/2</sup> /m <sup>2</sup> °C)	Fire growth rate
Office	720	705	225	27.2	4.25	0.0795	1104	Medium

presented in Fig. 11.34. The walls are built from blockwork lined with one layer of plasterboard. The ceiling is also covered with one layer of plasterboard and the floor is made from reinforced concrete. An assessment is made of the central beam and the central column.

The reinforced concrete central column has a section of  $h \times b = 400 \text{ mm} \times 400 \text{ mm}$ , exposed to fire on four sides. The section is provided with four 32 mm diameter reinforcement bars connected with 8 mm diameter links, with a cover to the links of 20 mm. The central beam has a section of  $h \times b = 600 \text{ mm} \times 250 \text{ mm}$ , exposed to fire on three sides. The beam section is reinforced with two 20 mm diameter bars on top and two 32 mm diameter bars on the bottom, connected with 12 mm diameter links, with a cover to the links of 20 mm. A summary of the structural elements considered is presented in Table 11.7.

A comparison between the standard fire exposure (ISO834) and the time-temperature curve based on parametric approach is presented in Fig. 11.35:

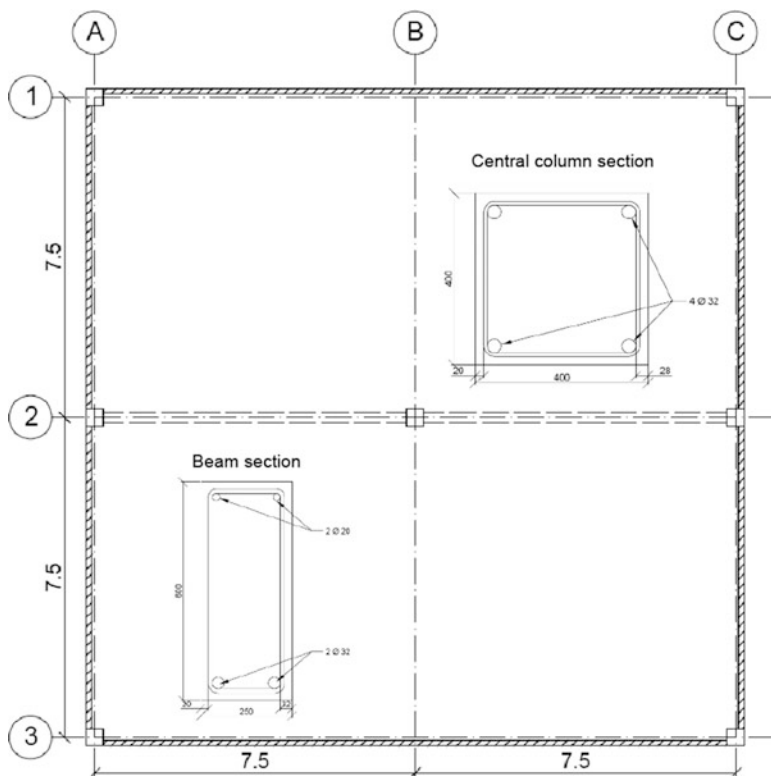


Fig. 11.34 Compartment geometry and sections of the structural elements that are evaluated

Table 11.7 Structural elements considered

Type of element	Dimensions (mm)	Length (mm)	Rebars (mm)	Links (mm)	Cover to links (mm)	Axis distance for main bars (mm)	Faces exposed to fire
Beam	600 × 250	7500	2φ20 top 2φ32 bottom	φ12	20	42 top 48 bottom	3
Column	400 × 400	3650	4φ32	φ8	20	44	4

In order to use the temperature profiles that are presented in EN 1992-1-2 [7] it is necessary to relate the calculated fire exposure to the standard fire curve. The concept of equivalent time of fire exposure is used based on the calculation procedure set out in Annex F of EN 1991-1-2.

The equivalent time of standard fire exposure is defined by following equation:

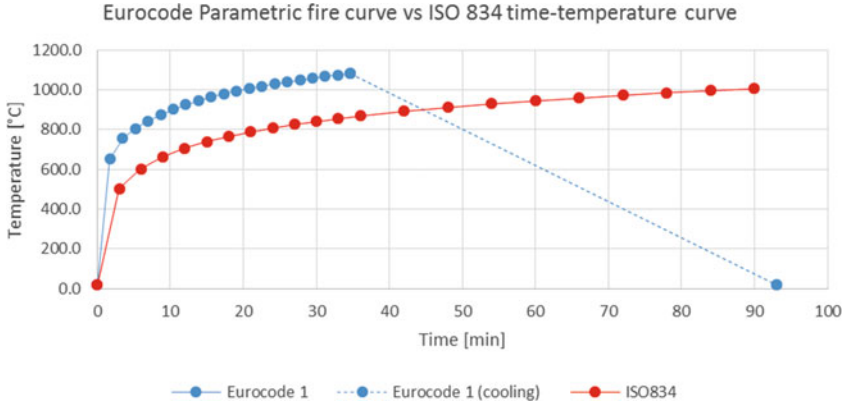


Fig. 11.35 Time-temperature parametric curve and comparison with ISO834 fire exposure

$$t_{e,d} = (q_{f,d} \cdot k_b \cdot w_f) \cdot k_c \text{ [min]} \tag{11.5}$$

where  $q_{f,d}$  represents the design fire load density;  $k_b$  and  $k_c$  are conversion and correction factors dependent on the nature of the linings and the nature of the form of construction, respectively (Annex F); and  $w_f$  represents a ventilation factor which can, in the absence of horizontal openings, be calculated with the following equation:

$$w_f = \left(\frac{6.0}{H}\right)^{0.3} \cdot \left[0.62 + 90 \cdot (0.4 - \alpha_v)^4\right] \text{ [-]} \tag{11.6}$$

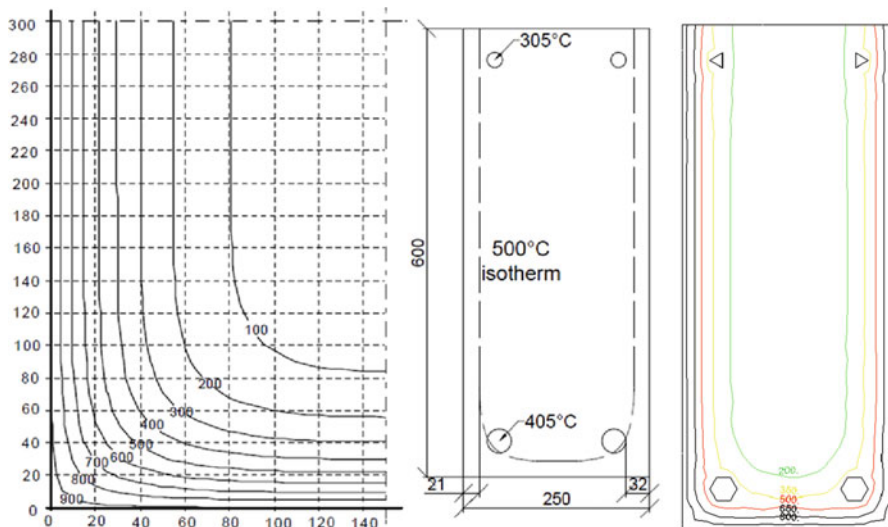
where  $H$  is the height of the compartment, and  $\alpha_v$  is the parameter to account for the opening area as a ratio of the compartment floor area.

For small compartments ( $A_f < 100 \text{ m}^2$ ), without openings in the roof, a simplification can be made for the ventilation factor as follows:

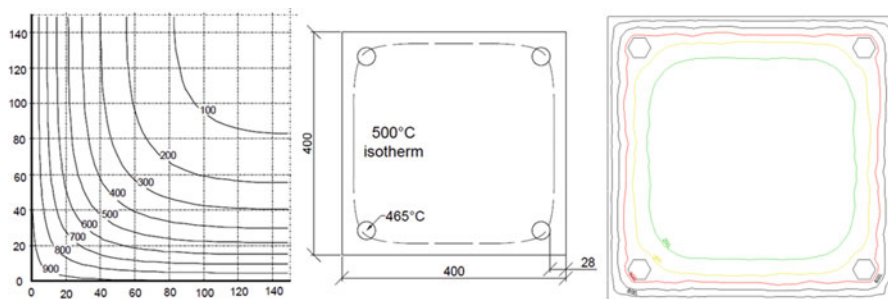
$$w_f = O^{-0.5} \cdot \frac{A_f}{A_t} \text{ [-]} \tag{11.7}$$

Based on the equations above and using  $k_b = 0.07 \text{ [min m}^2/\text{MJ]}$  (UK annex) and  $k_c = 1.0$ , an equivalent time exposure  $t_{e,d}$  of 65 min is obtained.

Eurocode 1992-1-2 [7] (Annex A) presents the temperature profiles for different structural components (i.e. slabs, beams and columns with various profiles dimensions), for standard fire exposure time between R 30 and R 240. The temperature profiles can be used to estimate the position of the 500 °C isotherm and the temperature of the main reinforcement.



**Fig. 11.36** Temperature profiles for a beam section at 60 min of standard fire exposure, position of 500 °C isotherm and output from an advanced model



**Fig. 11.37** Temperature profiles for a column section at 60 min of standard exposure, position of 500 °C isotherm and output from an advanced model

Figure 11.36 is the temperature profile from EN 1992-1-2, for a beam section  $h \times b = 600 \times 300$  mm and for a standard exposure of 60 min, and shows the position of the 500 °C isotherm for the 600 × 250 mm beam section. The figures from Annex A represent a conservative estimate of the heat transfer through the member. A more precise determination can be achieved using advanced calculation methods. The figure also illustrates the results from an advanced model.

Figure 11.37 shows the temperature profile from EN 1992-1-2, for a column  $h \times b = 300 \times 300$  mm and for a standard exposure of 60 min together with the position of the 500 °C isotherm, and the output from an advanced model for the 400 × 400 mm column section.

From Fig. 11.36, we can conclude that the lower reinforcement bars ( $\phi 32$ ) have a temperature at the midpoint of 405 °C and the upper reinforcing bars ( $\phi 20$ ) have a temperature of 305 °C. From the stress-strain relationship given in EN 1992-1-2 a reduction coefficient  $k_s(400) = 1.00$  will be applied to the lower reinforcement and in the same manner  $k_s(300) = 1.00$  will be applied to the upper bars (for hot-rolled reinforcing steel).

From Fig. 11.37 it can be observed that the temperature of the reinforcement bars ( $\phi 32$ ) is approximately 465 °C which gives a reduction factor from EN 1992-1-2  $k_s(465) = 0.85$ .

The stress-strain relationship for steel reinforcement (hot rolled, cold rolled and prestressed) is presented in Chapter 8 of ASCE/SEI Manual of Practice No. 138 [19].

In conclusion, the capacity of the beam and column is reduced due to the concrete degradation outside the 500 °C. No strength reduction factors are applied to the reinforcement bars from the beam and a reduction factor of 0.85 is applied for the reinforcement bars from the column. Based on the calculated capacity of the reduced section in line with observations of the scene and non-destructive testing it is considered that the structural elements were not seriously damaged during the fire and only concrete repair works will be required to reinstate the cover to the reinforcement.

However, before finally deciding on the appropriate remedial measures a thorough inspection should be carried out to look for signs of spalling, unusual deflections and reinforcement bars that have been directly exposed to fire. A significant reduction in strength for the reinforcement bars occurs when the estimated temperature is over 700 °C ( $k_s = 0.23$ ). In this situation calculations should be carried out in order to determine the load ratio in actual conditions. Depending on the residual strength of the section new reinforcing bars may be required to achieve the specified level of performance.

### ***11.3.5 Repair of Fire-Damaged Concrete Buildings***

The nature and extent of the repairs required will follow from the results of the assessment and investigation process. Depending on the nature of the damage some members may need only cosmetic repairs and others may have to be strengthened. In some cases the repair will consist of a combination of repair of damaged elements and integration of new replacement construction. In the worst cases the only option may be a complete demolition and rebuilding. There is extensive guidance on repair techniques in the Concrete Society report [1]. The main processes identified are:

- Removal of damaged or weakened concrete.
- Replacement of weakened reinforcement.
- Replacement of concrete both to reinstate the original form and to provide the required level of structural performance: This may include reinstatement of special finishes for aesthetic reasons.



## 11.4 Inspection, Assessment and Reinstatement of Fire-Damaged Timber-Framed Buildings

Timber is a combustible material and widely used as a source of fuel. There is therefore an understandable perception that timber structures will not perform well in the event of a fire. However, in many cases, where timber sections are adequately designed and detailed and when small-section timber studs and joists are adequately protected by non-combustible linings there is no reason why timber buildings cannot survive even a severe fire exposure with minimal structural damage.

The initial conditions following a fire (see for example Fig. 11.3) may suggest that repair and reinstatement are not a practical option. The presence of fire-damaged plasterboard and insulation materials coupled with the remains of the consumables within the fire compartment mixed with water from firefighting operations often produces a compressed deposit on the floor that may give the impression of the floor being unsafe. Debris may hide the true nature of the supporting structure and should be cleared away as soon as reasonably practicable once the overall safety of the building has been assessed and any necessary forensic examination has been completed.

### 11.4.1 *Material Properties*

The rate of combustion of timber is influenced by a number of properties including density, timber species, moisture content and surface area-to-volume ratio. Once ignited timber chars to produce an extremely effective insulating layer which, for a certain period, will protect the unburnt material below the charred surface. The thermal conductivity of charred timber is approximately one-sixth of solid timber [20]. Immediately beneath the charred layer is a pyrolysis zone where the chemical composition of the timber gradually changes and releases combustible gases.

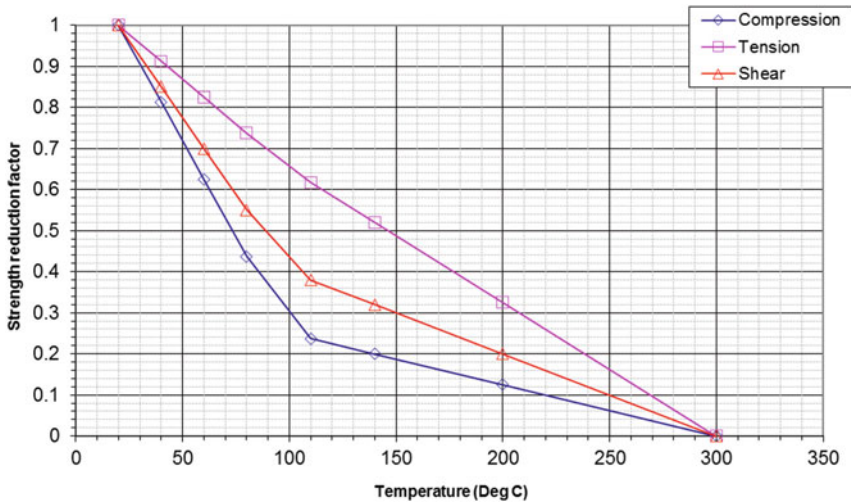
The predictable rate of charring and the unaffected properties of the residual section below the pyrolysis zone means that the structural response of timber to fire can be easily assessed.

Although light timber framing requires protection from the effects of heat from a fire large-section timber can perform exceptionally well in a fire scenario. Charring rates are set out in design standards [8]. Both notional (taking into account rounding at corners from two-dimensional heat exposure) and one-dimensional charring rates are summarized in Table 11.8.

The relationship between strength and temperature for timber is illustrated in Fig. 11.38.

**Table 11.8** Charring rates from [10]

Material	Charring rate (mm/min)		Depth of charring after fire exposure of:			
	One-dimensional ( $\beta_0$ )	Notional ( $\beta_n$ )	30 min		60 min	
Solid softwood and beech	0.65	0.7	19.5	21	39	42
Glue-laminated softwood and beech	0.65	0.8	19.5	24	39	48
Solid or glue-laminated hardwood density $\geq 290 \text{ kg/m}^3$	0.65	0.7	19.5	21	39	42
Solid or glue-laminated hardwood density $\geq 450 \text{ kg/m}^3$	0.5	0.55	15	16.5	30	33



**Fig. 11.38** Strength reduction factors for timber from [10]

### 11.4.2 Assessment by Calculation

In this example we will use the Eurocode simplified calculation procedure in order to assess the load-bearing capacity of a glulam beam, after fire exposure.

The glulam beam has a span of 7500 mm with section dimensions 440 × 180 mm ( $h \times b$ ), as presented in Fig. 11.39. The reduced load, in fire situation, applied on the beam is  $P_{fi} = 6.1 \text{ kN/m}$ .

The initial design data are summarized in Table 11.9, as follows:

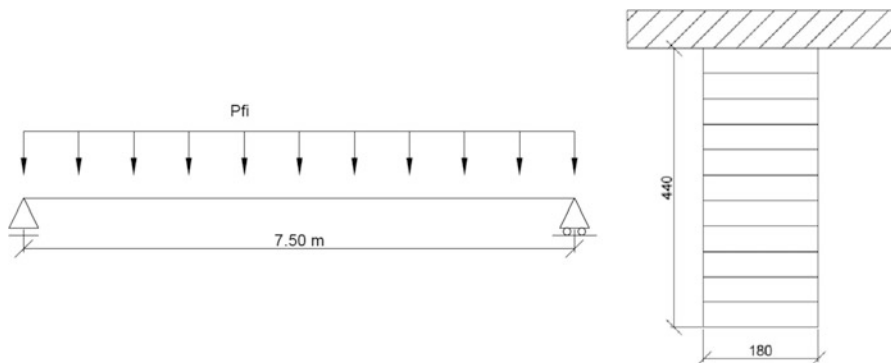


Fig. 11.39 Static scheme of glulam wooden beam, with sectional details

Table 11.9 Initial design data

$h \times b$ (mm)	$P_{fi}$ (kN/m)	$L$ (mm)	$f_{m,k}$ (N/mm <sup>2</sup> )	$E$ (N/mm <sup>2</sup> )	$M_{Ed,fi}$ (kN/m)	$M_{Rd}$ (kN/m)	$\eta_{fi}$ (%)
440 × 180	6.10	7500	24	11,600	42.90	139.40	31



Fig. 11.40 Residual section after investigation procedure for a three-side-exposed beam (post-fire)

After the element has been exposed to fire, an investigation procedure *in situ* should be undertaken, in order to find the residual section dimensions. This would involve scraping away the char to reveal the solid timber beneath. The residual section after fire exposure is presented in Fig. 11.40.

From Fig. 11.40, it can be observed that the residual section is 391 × 82 mm ( $h_{eff} \times b_{eff}$ ).

EN 1995-1-2 (Table 3.1) provides a series of design charring rates for different types of wood species, with different densities, under standard fire exposure. For the glulam GL24H beam a value for the notional charring rate ( $\beta_n$ ) of 0.7 mm/min is appropriate. The notional charring rate defined in the Eurocode represents a simplification to take into account the effect of corner roundings and fissures.

Based on this assumption we can determine an approximate time equivalent value for the fire exposure of the element, using the equation below:

$$t_{\text{equiv}} = \frac{d_{\text{eff}} - k_0 \cdot d_0}{\beta_n} = \frac{0.5(180 - 82) - 1.0 \cdot 7}{0.7} = 60 \text{ [min]} \quad (11.8)$$

where  $k_0 d_0$  takes into account that the thickness of the material close to the char layer has zero strength and stiffness. The coefficient  $k_0$  has a linear variation in the first 20 min of fire exposure and after it is considered with a constant value of 1.0, and for the zero-strength layer  $d_0$  a value of 7 mm is specified.

The calculation of the equivalent time represents an important indicator of the fire severity that occurred and potential damage to other structural elements present in the same compartment.

The bending stress in fire situation is determined as

$$\sigma_{fi} = \frac{M_{Ed}}{W_{fi}} = \frac{6 \cdot M_{Ed}}{(b_{\text{eff}} \cdot h_{\text{eff}}^2)} = \frac{6 \cdot 42.90 \cdot 10^6}{(82 \cdot 391^2)} 20.53 \text{ [N/mm}^2\text{]} \quad (11.9)$$

$$\sigma_{fi} \leq f_{m,d} \Rightarrow 20.53 < 24.0 \text{ Verification OK}$$

The load ratio at 60 min of fire exposure, based on the residual section bending moment capacity, can be determined as

$$\eta_{fi,60 \text{ min}} = \frac{M_{Ed,fi}}{M_{Rd,fi,60 \text{ min}}} = \frac{42.90}{57.67} = 74\% \quad (11.10)$$

From Eq. (11.10) we can observe that the residual section is not fully loaded and is providing a value of approximately 48% of the bending moment capacity reserve.

After fire exposure, visible deflections of the structural elements should be taken into account. The maximum deflection of the residual section, illustrated in Fig. 11.41, can be determined with Eq. (11.15).

$$\delta_{\text{max}} = \frac{5P \cdot L^4}{384 \cdot EI} = 52.90 \text{ [mm]} \quad (11.11)$$

It can be observed that the maximum deflection of the beam is approximately 41% higher than the limit considered for this situation of  $L/200$ . Consequently a series of repairs are required to return the element to its original position.

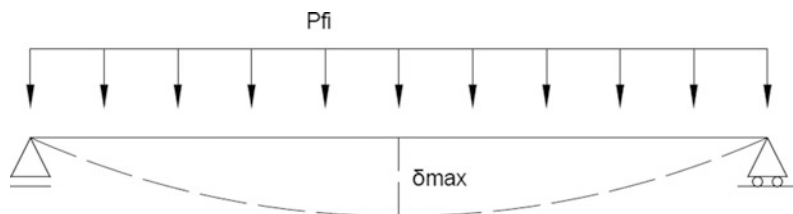


Fig. 11.41 Maximum deflection for a simply supported beam

### 11.4.3 Repair of Fire-Damaged Timber Buildings

Reinstating the fire-damaged structure of a timber-frame building requires a different engineering approach and alternative details to the original design as the same details cannot be precisely replicated. Structural elements at intermediate storeys cannot be refitted as originally designed as it would be necessary to dismantle the floors above. The alternative details need to be designed and approved to ensure the structural safety of the building following a fire. Timber structures are very flexible and there is scope to locally reinforce damaged elements without having to remove large sections of the building.

Localized inspection of a fire-damaged floor is possible from below by removing ceiling boards which avoids the risk of collapse while working on a damaged floor. In certain cases damaged timber elements can be replaced by alternative materials such as steel plates or steel reinforcing elements. One important aspect which needs to be taken into account is the impact of residual odours from the fire-damaged structures on building occupants.

## 11.5 Inspection, Assessment and Reinstatement of Fire-Damaged Masonry-Framed Buildings

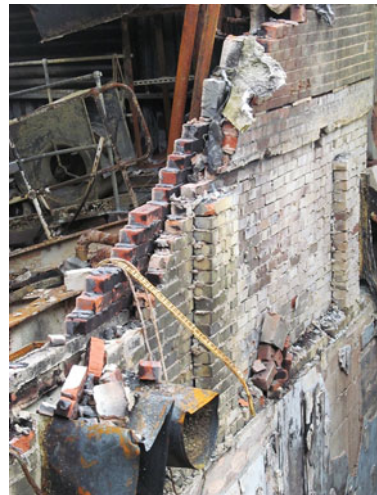
Masonry is inherently fire resistant and refractory (i.e. heat resistant) due to the nature of the manufacture of bricks and blocks. It is often used to provide insulation to other structural materials such as timber and steel which do not possess the requisite qualities to remain unprotected in the event of a fire.

It is important in relation to the assessment of fire-damaged structure that masonry structural elements (principally walls) are not monolithic structural elements but a collection of individual components acting compositely to perform specified functions. A masonry wall is an assemblage of discrete units of natural stone, clay, concrete, calcium silicate, gypsum, etc. stabilized and sealed with mortar [21]. The post-fire resistance of the wall will depend heavily on the nature of the principal constituent material of the masonry units as the strength of concrete and

calcium silicate blocks reduces significantly on exposure to the temperatures characteristic of a compartment fire while the strength of clay bricks is unlikely to be reduced to any great extent. The mortar is an inorganic setting mastic usually containing sand and a hydraulic binder. Often the masonry units may remain unaffected when exposed to heat but the mortar joints may have softened on the face exposed directly to fire. Available evidence [22] suggests that weakened mortar has little effect on the axial load-carrying capacity of masonry walls. For high walls resistance is limited by the slenderness of the wall and the tendency to buckle. Fire exposure increases the tendency to buckling as differential expansion between the hot and cold surfaces causes the wall to bow towards the fire [23]. If the deflection exceeds a critical value the wall will become unstable and may collapse suddenly. Guidance suggests that critical point occurs as the mid-height deflection of the wall reaches approximately 80% of the wall thickness [24]. Although failure of masonry walls may occur due to thermal bowing the most common failure mode is walls being pushed out of plane by thermal expansion of the surrounding structure.

In many cases a visual inspection of the wall is sufficient to assess the extent of damage particularly if the damage is significant (Fig. 11.42). Signs of deflection, cracking, deformation and surface defects such as spalling should be noted and documented. If a more detailed investigation is required then the strength can be determined by taking samples from the scene and carrying out compressive strength tests. Results from standard fire tests [22] suggest that (concrete) masonry walls can survive one severe fire without replacement and still be able to perform structurally in the event of a second severe fire. This is borne out from laboratory-scale natural fire tests where concrete masonry compartments have been used for a complete experimental series with only minor repairs required in between tests [25].

**Fig. 11.42** Fire-damaged masonry separating wall



Clay masonry walls exhibit a very good performance at elevated temperatures and also have an ability to retain strength on cooling. However, mortars begin to lose strength at temperatures above 300–400 °C and have virtually no strength at temperatures characteristic of a fully developed fire (approximately 1000 °C) although damage is usually confined to a depth of approximately 12–19 mm from the surface [22].

### 11.5.1 *Material Properties*

As a composite material combining refractory products with a binding medium it is difficult to define precisely a material strength reduction at elevated temperature for masonry structures in the manner that has been done for other materials covered in this chapter. Information has already been provided on the reduction in strength of lightweight concrete [9], a principal constituent in many masonry units. In many cases the controlling factor will be the strength of the mortar which, as mentioned above, deteriorates rapidly at temperatures above 300 °C. The extent of damage to mortar beds will be a function not only of the peak temperatures experienced but also of the duration of the fire exposure. The moisture plateau will delay the onset of temperatures above 100 °C for a limited period of time dependent on the moisture content and the severity of the fire exposure. Damage to the mortar beds through either material degradation or thermal differential thermal movements or a combination of both may lead to the formation of inclined cracks (Fig. 11.43) leading to a collapse of the wall.

**Fig. 11.43** Inclined cracks in masonry façade following a fire



### 11.5.2 Assessment by Calculation

In this example the calculation procedure will be applied to an aerated autoclaved concrete (AAC) masonry wall system after a fire exposure.

The initial design data are summarized in Table 11.10:

The characteristic compressive strength can be determined with the following relation:

$$f_k = K \cdot f_b^\alpha \cdot f_m^\beta = 0.6 \cdot 2.5^{0.7} \cdot 5^{0.3} = 1.84 \text{ (N/mm}^2\text{)} \quad (11.12)$$

with  $K$  and  $\alpha, \beta$  being the coefficients given in EN 1996-1-1. For AAC masonry type and general-purpose mortar the relevant values are given in Table 11.10.

In case of masonry walls subjected to mainly vertical loadings, the axial capacity can be calculated with the following equation:

$$N_{Rd} = \Phi \cdot t \cdot f_k = 0.7 \cdot 100 \cdot 1.84 = 128.8 \text{ (kN/m)} \quad (11.13)$$

where  $\Phi$  represents a capacity reduction coefficient taking into account the slenderness and loading eccentricity (defined in the national annex).

The load ratio at the fire limit state can be determined as follows (before fire exposure):

$$\alpha_{fi} = \frac{N_{Ed,fi}}{N_{Rd}} = \frac{0.7 \cdot 55}{128.8} = 0.29 \approx 0.3 \quad (11.14)$$

Based on the load ratio, we can determine the initial fire performance of the masonry wall. Tabulated data are provided in the Eurocode for different performance criteria combinations (EI, REI, REI-M, EI-M and R). In this case ( $\alpha < 0.6$ ), based on the tabulated data the AAC masonry wall can provide a fire resistance (REI) up to 120 min of standard fire exposure.

In Annex C of EN 1996-1-2 there is a simplified calculation method for the load-bearing capacity which is determined by boundary conditions on the residual cross section of the masonry for different fire exposure times.

However, at the limit state for the fire situation, the design values of the vertical load applied to the AAC wall ( $N_{Ed,fi}$ ) should be less than or equal to the design value of the vertical resistance at a specific time ( $N_{Rd,fi}(\theta_i)$ ):

$$N_{Ed,fi} \leq N_{Rd,fi}(\theta_i) \quad (11.15)$$

The design value for the vertical resistance of the wall at a specific time of fire exposure can be determined as follows:



**Table 11.10** Design data for masonry (AAC) wall

Height (mm)	Thickness (mm)	Density (kg/m <sup>3</sup> )	Load $N_{ed}$ (kN/m)	$f_b$ (N/mm <sup>2</sup> )	$f_m$ (N/mm <sup>2</sup> )	Fire exposure	$\alpha$	$\beta$	$K$	$\Phi$
3000	100	400 ± 50	55	2.5	5	60 min	0.7	0.3	0.6	0.7

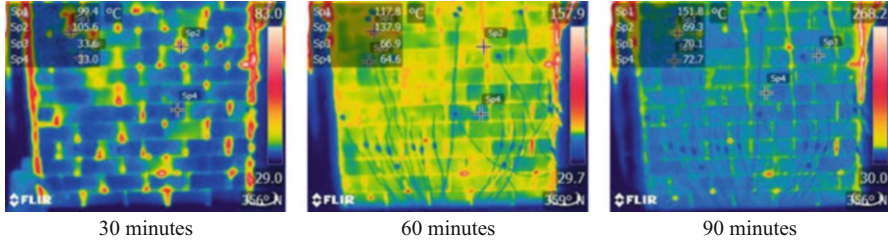


Fig. 11.44 Thermal imagery of AAC wall for various periods of standard fire exposure

$$N_{Rd,fi}(\theta_i) = \Phi \cdot [(f_{d\theta_1} \cdot (t - t_{\text{damaged},\theta_i}) + f_{d\theta_2} \cdot t_{\text{damaged},\theta_i}] \tag{11.16}$$

where  $\theta_1$  represents the temperature for which the cold strength of masonry can be used (200 °C for AAC) and  $\theta_2$  represents the temperature above which the material has no residual strength. However, between  $\theta_1$  and  $\theta_2$  a reduction factor ( $c_{\text{aac}} = 0.5$ ) should be used.

In Fig. 11.44 the temperature distribution is presented for 100 mm AAC, in standard fire exposure for 30, 60 and 90 min. We can observe some localized thermal bridges due to installation imperfections. However, they do not have a significant influence on the overall performance of the AAC wall.

The damaged area of the masonry wall can be measured on-site. An example is presented in Fig. 11.45:

Based on the heat transfer curves provided in Annex E of EN 1996-1-2 (Fig. 11.46), the residual section can be determined. From Fig. 11.45 we can conclude that the residual section after 60 min is approximately 87 mm.

The vertical resistance of the residual section of the masonry wall can be expressed as follows:

$$N_{Rd,fi}(\theta_i) = 0.7 \cdot (1.84 \cdot 47 + 40 \cdot 1.84 \cdot 0.5 + 0 \cdot 13) = 86.2 \text{ (kN/m)} \tag{11.17}$$

We can conclude that the fire-damaged AAC masonry wall is able to provide its separation function after a fire exposure of 60 min.

### 11.5.3 Repair of Fire-Damaged Masonry Buildings

Guidance is provided on the options for repair of fire-damaged masonry structures in a fire protection planning report [26]. The report highlights the inherent fire resistance of concrete and masonry structures and provides general guidance on preliminary inspection procedures following a fire starting with a visual inspection to determine the nature and extent of any cracking, spalling, deflections, distortions and misalignment. The presence of any of these may suggest that the load-bearing

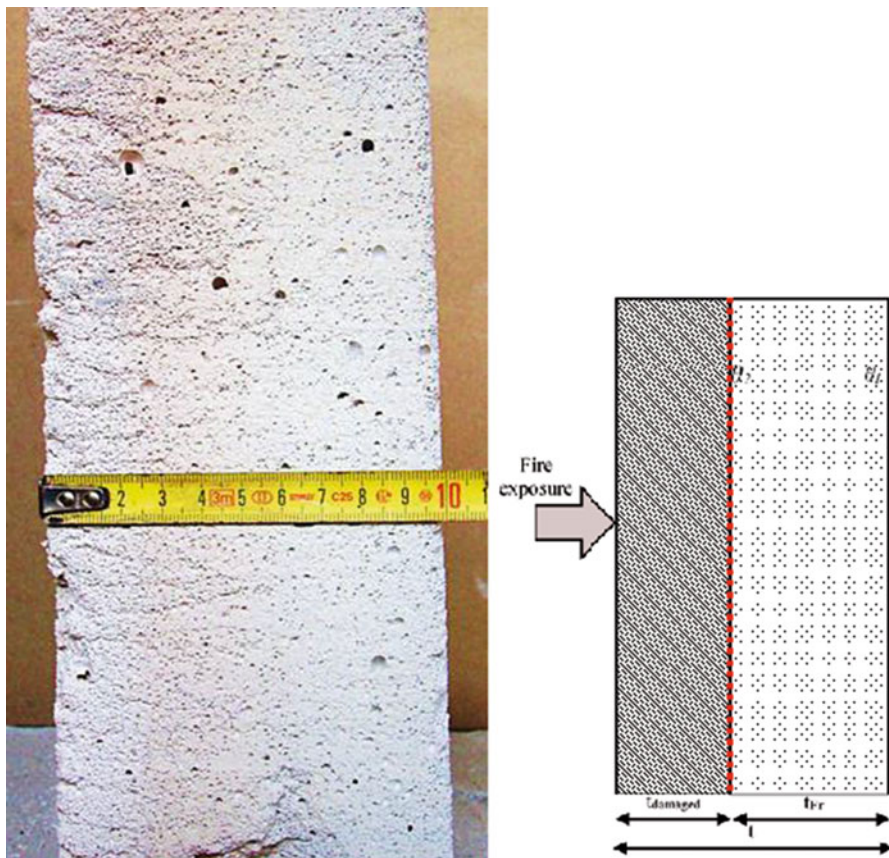


Fig. 11.45 Damage on the AAC masonry block after 220 min of fire exposure

capacity has been compromised. In the absence of any of these physical phenomena it is likely that the structural element can be retained or repaired.

Masonry can exhibit distress similar to that of concrete structures discussed above. Small hairline cracks, pitting of aggregates and shallow surface spalling indicate a need for purely aesthetic repairs. Larger cracks ( $>1.6$  mm) or softened mortar joints are indicative of more serious damage but this may be restricted to localized areas.

In general if concrete or clay masonry does not exhibit excessive deformations or large cracks then in situ repairs are normally the best way to proceed. Conversely any large deformations or dilations would necessitate demolition and replacement of the affected areas.

Non-destructive techniques such as a hammer and chisel to determine the soundness of the construction can prove useful. A screwdriver or chisel can be used to probe mortar joints for softened areas.

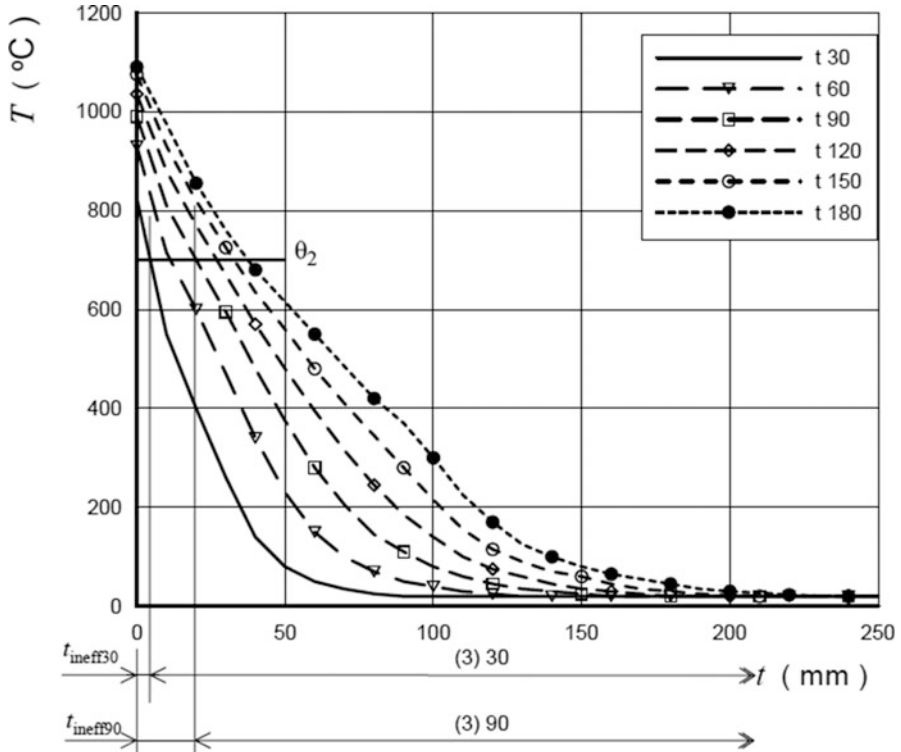


Fig. 11.46 Temperature distribution inside the masonry wall for different fire exposure times

Unlike the evaluation process for fire-damaged concrete construction non-destructive field testing is not generally used for masonry structures. Where appropriate saw cutting and removal of sections of a fire-damaged wall can be used to provide samples for compressive strength tests.

### References

1. Technical Report No. 68 (2008, December), Assessment, Design and Repair of Fire Damaged Concrete Structures, Report of a Concrete Society Working Group, Published by the Concrete Society.
2. Narendra, K., Gosain, K., Ray, F., Drexler, P. E., & Choudhuri, D. (2008, September). *Structure magazine*, pp. 18–22.
3. The Institution of Structural Engineers (2010, October). Appraisal of existing structures (3rd ed.).
4. Tucker, D. M., & Read, R. E. H. (1981, November). Assessment of fire damaged structures, BRE Information Paper IP 24/81, Building Research Establishment.

5. British Standards Institution. (2012). BS EN 1363–1:2012, Fire resistance tests Part 1: General requirements, BSI, Chiswick.
6. Kirby, B. R., Lapwood, D. G., & Thomson, G. (1986). *The reinstatement of fire damaged steel and iron framed structures*. British Steel Corporation, Swinden Laboratories.
7. British Standards Institution. (2005). BS EN 1992-1-2:2004 Eurocode 2: Design of concrete structures – Part 1–2: General rules – Structural fire design, BSI, Chiswick.
8. British Standards Institution. (2005). BS EN 1993-1-2:2005 Eurocode 3 Design of steel structures – Part 1–2: General rules – Structural fire design, BSI, Chiswick.
9. British Standards Institution. (2005). BS EN 1994-1-2:2005 Eurocode 4 Design of composite steel and concrete structures – Part 1–2: General rules – Structural fire design, BSI, Chiswick.
10. British Standards Institution (2009). BS EN 1995-1-2:2004 Eurocode 5 Design of timber structures – Part 1–2: General – Structural fire design, BSI, Chiswick.
11. British Standards Institution. (2005). BS EN 1996-1-2:2005 Eurocode 6 Design of masonry structures – Part 1–2: General rules – Structural fire design, BSI, Chiswick.
12. British Standards Institution. (2009). BS EN 1999-1-2:2007 Eurocode 9 Design of aluminium structures – Part 1–2: Structural fire design, BSI, Chiswick.
13. Kirby, B. R. (1992). *The behaviour of high strength grade 8.8 bolts in fire*. British Steel Technical Swinden Laboratories, British Steel.
14. Lawson, R. M., Burgan, B., & Newman, G. M. (1993). Building design using cold formed steel sections: Fire protection, Steel Construction Institute Publication P129, SCI, Ascot.
15. British Standards Institution (2002). BS EN 1991-1-2:2002 Eurocode 1: Actions on structures – Part 1–2: Actions on structures exposed to fire, BSI, Chiswick.
16. Tovey, A. K., & Crook, R. N. (1986). Experience of fires in concrete structures. *Concrete*, 20 (8), 19–22.
17. Bulletin 46, fib Task Group 4.3 Fire design of concrete structures – Structural behavior and assessment, federation international du beton (fib), 2008.
18. Bulletin 38, fib Task Group.
19. ASCE/SEI Manual of Practice No. 138: Structural Fire Engineering, American Society of Civil Engineers: Structural Engineering Institute, Reston, VA, USA, 2018.
20. Bregulla, J., & Enjily, V. (2004). *Structural fire engineering design: Materials behavior – Timber*, BRE Digest 487 Part 4, BRE.
21. de Vekey R. (2004). *Structural fire engineering design: materials behavior – Masonry*. BRE Digest 487 Part 3, BRE.
22. Menzel, C. A. (1934). *Tests of the fire resistance and strength of walls of concrete masonry units*. Portland Cement Association.
23. Cooke, G. M. E. (1988). *Thermal bowing in fire and how it affects building design*. BRE Information Paper IP 21/88, BRE Bookshop.
24. Gnanakrishnan, N., & Lawther, R. (1990). Performance of Masonry Walls exposed to fire. In *Proceedings Fifth North American Masonry Conference, Vol III, University of Illinois at Champaign/Urbana, June 3–6*, pp. 901–914.
25. Lennon, T., & Moore, D. (2003). The natural fire safety concept – Full-scale tests at Cardington. *Fire Safety Journal*, 38(2003), 623–643.
26. Fire Protection Planning Report, assessing the Condition and Repair Alternatives of Fire-Exposed Concrete and Masonry Members, August 1994.

# Index

## A

Acceptable failure probability, 331, 336  
Acceptance criteria  
    SFE design, 65  
AAC masonry wall system, 510  
Accumulated debris, 472  
Adiabatic surface temperature (AST), 119, 449  
Advanced analysis method  
    agreement with approval bodies, 462  
    aims, 414  
    ASCE/SEI 2016, 416  
    benchmarking, 459, 460  
    capabilities and limitations (*see* SFE  
        advanced analysis, capabilities and  
        limitations)  
    computational aspects, 421  
    definition, 414  
    discretization, 418  
    Eurocodes, 416  
    failure assessment (*see* Failure assessment,  
        advanced analysis)  
    failure modes, 414  
    fundamental physical behavior, 414  
    mechanical response, 416  
    modeling process (*see* Modeling process,  
        advanced analysis)  
    model quality and data reliability, 414  
    nonlinearities, 418  
    performance-based approach, 440  
    pre-embedded failure criterion, 416  
    purpose, 414–416  
    reporting, 461, 462  
    sensitivity/confidence assessment, 461  
    software, 462, 463

    structural system, 440  
    thermal response, 416  
    validation, 417  
    verification and validation, 460  
    whole-building behavior, 419, 420  
Advanced fire element models, 439  
Aerated autoclaved concrete (AAC), 510  
ALARP evaluation, 331, 333  
Aleatory uncertainty, 326–328  
Aleatory variability, 326  
American Institute of Steel Construction  
    (AISC), 19  
American Society of Testing of Materials  
    (ASTM), 14  
Applied passive fire protection material,  
    136, 137  
Arbitrary point in time (APIT), 346, 348–351  
Asymptotic behavior, 458  
Authority having jurisdiction (AHJ), 76  
Auto-ignition temperature, 476  
Automatic system, 79  
Available Safe Egress Time (ASET), 51

## B

Bailey-BRE method, 210, 214  
Beams  
    elements, 421  
    finite elements, 431  
    lateral torsional buckling, 199  
    moment resistance, 198, 199  
    shear resistance, 199  
Benchmarking, 459  
Bending limit state function, 392

- Bending moment capacity, 372, 391–393, 397
- Bernoulli beam finite element, 444
- Bernoulli formula, 81
- Bernoulli-type beam finite elements, 445
- Biot number, 120–122
- Boundary element method (BEM), 418
- Broadgate fire, 202
- Building codes, 51, 55, 65
- Building Research Establishment (BRE), 203
- Buoyancy-driven inflow, 98
- C**
- Calculation methods, 39  
   standard fire curve, 38  
   structural fire design, 39
- Cantilever HEB 200 steel beam, 453
- Cell-bound water, 236
- Cellulose, 236
- Charring, 240, 241  
   rates, 474, 503, 504, 506  
   of timber, 134  
   of timber battens, 476
- Clay masonry walls, 509
- Cold-formed galvanized steel, 483
- Collapse mechanism, 204, 210
- Compartmentalization elements, 442
- Compartment boundary component, 93
- Component-based method, 220
- Composite systems  
   broadgate fire, 202  
   cardington tests, 202–205  
   hand calculations *vs.* finite element analyses, 211–213  
   key design parameters, 214  
   key failure modes, 210, 211  
   tensile membrane action, 205
- Compressive membrane action (CMA), 179, 180
- Compressive stress block, 420
- Computational fire modelling  
   zone model, 107
- Computational fluid dynamics (CFD), 108, 427, 448, 449  
   benefit, 109  
   fire and smoke modelling tools, 109, 110  
   non-laminar flow, 109  
   structural fire engineering, 109
- Concrete, 489  
   advantage, 145  
   calcareous concrete, 357, 359  
   calcareous concrete strength retention factor *vs.* temperature, 357, 358  
   compositions, 146  
   compressive strength retention factor, 355  
   as construction material, 145  
   density, 133  
   heat flow, 147  
   HSC (*see* High-strength concrete (HSC))  
   LWC, 149, 150  
   man-made material, 145  
   moisture, 132, 134  
   NSC (*see* Normal-strength concrete (NSC))  
   PFRC, 150  
   probabilistic models, 356  
   SFRC, 150, 166  
   siliceous concrete, 357  
   siliceous concrete strength retention factor *vs.* temperature, 356, 358  
   strength, 355  
   superior fire resistance, 145  
   thermal behavior, 146  
   thermal conductivity, 133  
   thermal properties, 132
- Concrete cubes, 494
- Concrete slabs, 432  
   and columns, 405  
   and concrete columns, 403  
   fire-exposed, 373  
   ISO 834 standard, 372
- Concrete Society report, 489, 502
- Concrete structural elements, 491
- Concrete structures  
   catastrophic failure, 146  
   cooling phase after fire, 182  
   design of hollow core concrete slabs, 176  
   design of two-way slabs against fire, 176  
   effects of fire, 146  
   fire-induced collapse, 146  
   fire-loading case, 146  
   fire resistance  
     for continuous beams, 176  
     for continuous flexural members, 175  
     for continuous slabs, 175  
     failure modes and full structure response, 156, 157  
     mechanical properties, 151  
     prestressed concrete, 153, 154  
     reinforced concrete members, 152, 153  
     for simply supported members, 174  
     spalling, 155, 156  
     temperature profile in members, 154, 155  
     thermal deformations, 151  
   joints between precast concrete slabs, 179

- joints between precast concrete wall panels, 178
    - material properties at elevated temperatures (*see* Material properties, concrete)
    - postfire evaluation, 183
    - prestressed concrete members, 178
    - properties influencing fire resistance
      - compressive strength, 158, 159
      - creep, 160
      - deformation properties, 158, 160
      - density, 159
      - mechanical properties, 158, 159
      - spalling, 158
      - specific heat, 159
      - tensile strength, 159
      - thermal conductivity, 158
      - thermal expansion, 160
      - thermal properties, 158
      - transient strain, 160
  - Concrete temperature/strength relationship, 490, 491
  - Concrete walls, 433
  - Conductive heat transfer, 100
  - Connections, 482
  - Continuum mechanics models, 442
  - Convective heat transfer coefficient, 327
  - Conventional steel reinforcement, 171
  - Cooling-phase regime, 95
  - Cooling-phase temperature, 96
  - Cracking, 483, 492, 493, 508, 512
  - Creep
    - in concrete, 170
    - deformations of steel, 174
    - and micro-cracking, 169
    - tests, 174
  - Creep effects, 441
  - Creep strain, 160, 169, 182
  - Critical temperature, 487, 491
  - Cross-laminated timber (CLT), 235, 244, 245
    - cross-section method, 301
    - European, 302
    - USA, 303, 305
    - zero-strength layer, 302
  - Cumulative probability distribution, 384
  - Curving-fitting method, 220
- D**
- Damage states, 366, 384, 385, 388, 403–405
  - Decay phase, 84
  - Degrees of freedom (DoF), 456
  - Demand/capacity-based design, 325
  - Denver equitable building, 10
  - Design approach/solution, 3
  - Design brief document, 30, 58, 59
  - Design implementation, SFE design
    - acceptance criteria, 65
    - design team, 61–63
    - FEA, computational resources, 63–64
    - stakeholder briefings, 65–66
  - Design philosophies
    - definition, 222
    - limit stand design, 223
    - member utilisation
      - default critical temperature, 226–229
      - tension members, 226
      - uniform temperature distribution, 225
    - structural system response, simulation, 223–225
  - Differential expansion, 508
  - Discoloration, 473, 492, 495
  - Discretionary performance objectives, 51
  - Discretization, 418, 421
  - Displacements, 456
  - Drucker-Prager yield function, 435
  - Dynamic approach, 422
  - Dynamic equations, 445
  - Dynamic formulation, 457
  - Dynamic solvers, 422
- E**
- Earthquake intensity, 390
  - Elastic/plastic deformation, 478
  - Empirical calculation methods
    - International Building Code, 22
    - standard fire tests, 22
  - Engineering judgment, 452, 456
  - ENV formulation, 103
  - Epistemic uncertainties, 326–329
  - Equivalence methods, 22
    - qualitative approaches, 22
  - Equivalency formulas, 97
  - Euler-Bernoulli/Timoshenko, 430
  - Eurocode (EC), 33, 329, 331, 333, 335–337, 339, 342, 345, 352–355, 359, 366, 374, 394, 416, 436, 440, 485, 500
  - Eurocode design procedures, 497
  - Eurocode framework, 111
  - Eurocode parametric fire curve, 90, 94, 102, 106
  - Eurocode parametric fire format, 101
  - Eurocode parametric time curve, 106
  - European/international equivalent, 84
  - “Eutectoid reaction”, 171
  - Event tree, 366–369



- Explicit creep models, 190  
 Explosive spalling, 494, 495  
 Extensive aggregate spalling, 495
- F**
- Failure assessment, advanced analysis  
 criteria, 451  
 finite element software, 451, 452  
 performance-based environment, 451  
 specific modes, 458–459  
 structural assembly, 451  
 structural procedures (*see* Structural failure assessment procedure)
- Failure criterion, 17  
 Failure modes, 53  
 Failure probability, 331–335, 337, 338, 367, 373, 374, 376, 392, 395, 399–401  
 FDS-SAFIR interface, 449  
 FE software, 446  
 Fiber discretization, 421  
 Fibers, 430  
 Finite difference (FD) method, 124–127, 418  
 Finite element analysis (FEA), 63, 64, 212, 418  
 Finite element methods/model (FEMs), 127, 414  
 beam elements, 431  
 boundary conditions, 439  
 determination, temperature profile, 128  
 extent and boundaries, 423  
 formulations, 127  
 fundamental equations, 127  
 global and local, 423  
 heat transfer assessment, 128  
 mathematical approximations, 439  
 nodes and “finite” elements, 127  
 numerical methods, 127  
 section geometry, 443  
 sensitivity/confidence assessment, 461  
 shell elements, 431, 432  
 structural fire analysis, 425, 430  
 Finite element solvers, 422, 423  
 Finite volume method (FVM), 418  
 Fire and Rescue Service (FRS), 469, 470  
 Fire attack, 446  
 Fire burnout, 51, 52  
 Fire compartment plan, 485, 486  
 Fire-damaged building, 470  
 Fire-damaged concrete construction  
 non-destructive field testing, 514  
 Fire-damaged concrete-framed buildings  
 assessment by calculation, 497–502  
 Concrete Society report, 489  
 material properties, 489, 491, 492  
 repairing, 502  
 spalling, 493  
 structures, 489  
 testing, 496, 497  
 Fire-damaged masonry-framed buildings  
 assemblage, 507  
 assessment by calculation, 510, 512  
 fire exposure, 508  
 material properties, 509  
 mortar joints, 508  
 repairing, 512, 514  
 structural materials, 507  
 temperatures, 509  
 visual inspection, 508  
 Fire-damaged steel-framed buildings  
 assessment by calculation, 485–488  
 bolt and thread stripping, 480  
 deformed column, 479  
 elevated temperatures, 477  
 fire protection, 478  
 investigation areas, 478  
 local buckling, 479  
 material properties, 480–484  
 repairing, 488, 489  
 residual strength, 479  
 steel beam and composite, 478  
 steel structures, 478  
 testing, 484, 485  
 Fire-damaged timber-framed buildings  
 assessment by calculation, 504–506  
 initial conditions, 503  
 material properties, 503  
 non-combustible linings, 503  
 repairing, 507  
 Fire dynamics  
 combustion reaction, 81  
 fire growth, 81  
 ventilation-controlled fires, 81  
 ventilation-controlled heat release, 82  
 zone model, 80  
 Fire dynamics simulator (FDS), 427, 448  
 Fire-exposed steel column, 456  
 Fire exposure, 77  
 Fire growth phase, 81  
 Fire hazard, 53–56, 62, 65  
 Fire ignition, 339, 366, 367, 389, 390  
 Fire-induced collapse, 146, 158  
 Fire load density, 342, 343  
 Fire models, 447  
 Fireproof, 10  
 Fire resistance, 4  
 ad hoc testing, 10

- criterion, 442
  - ASTM standards, 15
  - design, 9
  - directories, 9
  - evaluation, 10
  - fire testing, 9
  - gas-phase temperature, 12
  - origins, 10
  - solid concrete slabs, 391
  - standard fire testing, 16
- Fire safety, 5
- Fire safety engineers, 61, 63
- Fire severity, 477, 489, 506
- Fire ventilation, 55, 56, 62, 72, 73
- First-order reliability method (FORM), 374
- Flame extension, 86, 87
- Fourier equation, 99
- Fracture, 480
- Fragility, 384–386
- Fragility curves, 367–369, 384–386, 403, 404, 406
- Fragility functions, 366, 404
- Franssen's proposals, 104
- FRS Fire Investigation team, 469
- Fuel-controlled fires, 82, 83
- Full-frame model, 42
- Fuel load, 54–56, 70, 329, 387
  
- G**
- Gas temperature, 118–120, 123, 486
- Generalized FEA packages, 64
- Geometrical nonlinearities, 419
- Global models, 423
- Global structural analysis, 415
- Glue-laminated lumber, 244, 270
  
- H**
- Hadvig's method, 282
- Harmathy's Rules, 22–24
- Hasemi model, 447
- Heat fluxes, 116, 446, 447
- Heating curve, 95
- Heating-phase gas temperature, 96
- Heat transfer, 327, 329
  - Biot number, 120–122
  - example problems, 128–130
  - FEMs (*see* Finite element methods (FEMs))
  - finite difference method, 124–127
  - fundamentals, 116
  - heat fluxes, 116
  - lumped mass method, 122–124
  - material properties, 117
  - materials thermal properties (*see* Thermal properties of materials)
  - via radiation, 116
  - structural elements, special design
    - phase change, 138
  - structural performance, 117
  - thermal boundary conditions, 117–119
  - thermal conductivity, 116
  - variable properties, 117
- Heat transfer coefficients, 329
- Heat transfer model, 329
- Heavy timber construction
  - elements, 290
  - fire performance, 290
  - fire resistance test, 291
  - integrity criterion, 291
- Hemicellulose, 236
- High-strength concrete (HSC)
  - combined factors, 149
  - compressive strength, 148
  - experimental research, 149
  - vs.* normal-strength concrete members, 149
  - UHPC, 149
  - water-to-cement ratio, 149
- Hollow core slabs, 154, 156, 176, 177
- Horizontal displacement, 456
- Hot-rolled carbon steel, 480, 481
- Hydrocarbon, 85
- Hydro-thermo-mechanical models, 442
- Hypothetical steel structures, 48
  
- I**
- iBMB parametric fire curve, 106
- Ignition, 78
- Ignition temperature, 476
- Implicit *vs.* explicit analysis, 422
- Implicit numerical models, 445
- Industrial by-products, 149
- Intermediate cellular steel beams, 457
- International Building Code (IBC), 244
- Ira Woolson's tests, 12
- iTFM (traveling fire model), 447
  
- J**
- JCSS Probabilistic Model Code (PMC), 346, 351
- Joint Committee on Structural Safety (JCSS), 335, 344–348, 352, 353, 363

**L**

Laminated veneer lumber (LVL), 244  
 Latin hypercube sampling (LHS), 366, 373, 382, 383, 398, 402, 403  
 Life quality index (LQI), 336  
 Light timber frame (LTF), 273, 274, 503  
 Lightweight aggregates, 149, 150  
 Lightweight concrete (LWC), 149, 150, 158, 163, 167  
 Lignin, 236  
 Limit states, 332, 384  
 Line elements, 430  
 Linear elastic response, 325  
 Linear regression curve, 486  
 Linear time-temperature relationships, 102  
 Load combinations, 111  
 Load effect, 332, 346–348, 353, 354, 391, 392, 394, 396, 399  
 LOCAFI model, 447  
 Local models, 423  
 Localized fire models, 427, 447  
 Localized fires, 85  
 Localized inspection, 507  
 Loss of structural integrity, 469  
 Lumped capacitance formulation, 121  
 Lumped mass method, 122–124

**M**

Masonry, 507, 513  
 Mass loss, 158, 159, 161, 164  
 Material behavior, 442  
 Material experiments, 442  
 Material models  
   concrete, 436  
   heat transfer analysis, 434  
   mechanical analysis, 435  
   multi-hazard, 437  
   properties identification, 441  
   steel, 436  
   wood, 437  
 Material nonlinearities, 418  
 Material properties, concrete, 442  
   deformation properties, 169  
     creep and transient strains, 170  
     thermal expansion, 169, 170  
   mechanical properties  
     compressive strength, 164–166  
     elasticity, 167  
     high-temperature tests, 164  
     stress-strain response, 167, 168  
     tensile strength, 166  
   thermal conductivity, 162

thermal properties

  mass loss, 163, 164  
   specific heat, 162, 163  
   thermal conductivity, 161, 162

Maximum entropy, 380–383

Mechanical calculation, 460

Mechanical integrity

  changes in thermal properties, 138  
   definition, 138  
   dimensional scaling, 141  
   failures, 138  
   protective insulation, 140, 141  
   standard fire testing, 142

Medium-density fiber board (MDF), 246

Membrane forces, 179

ME-MDRM (MaxEnt) method, 366, 380–383

Meta-analyses, 460

Modeling process, advanced analysis

  conceptual model and criteria, 423, 425  
   general procedure, 425  
   imperfections representation, 439, 440  
   materials representation, 434  
   mechanical boundary conditions, 439  
   representing structural members, 429  
   structural connections representations, 437

Modeling simplifications, 445

Model parameters, 360, 361, 391

Modulus of elasticity (MOE), 259, 326, 362, 363

Monte Carlo simulations (MCS), 366, 372, 373, 382, 383, 392, 395–400, 402, 403

Monte Carlo techniques, 372, 373

Mortar, 508

Multiaxial stress states, 442

Multi-compartment computer zone models, 82

Multi-hazard, 437

Multipurpose software packages, 462

Multi-spring connection elements (component-based models), 438

Multi-temperature analysis (MTA), 228, 229

**N**

National Institute of Standards and Technology (NIST), 20, 459

Natural fire exposures, 434

Natural Fire Safety Concept (NFSC), 336, 337, 339, 342

Near-field temperature, 344, 345

New York Fire Tests, 13

Newton-Raphson, 422

Noncombustible material, 146, 151

- Non-destructive testing (NDT), 482, 484, 489, 513
- Nonlinear advanced analysis, 421
- Nonlinear analysis, 422
- Nonlinear stress-strain behavior, 441
- Nonlinear structural fire analysis, 423
- Nonlinear temperature gradients, 421
- Nonstructural systems, 53
- Non-uniform temperature distribution, 201
- Normal reinforcement, 489
- Normal-strength concrete (NSC)
  - coarse aggregates, 147
  - compressive strength, 147
  - density, 148
  - moisture content, 148
  - Portland cement, 147
  - in reinforced concrete, 148
  - water-to-cement ratio, 148
- Numerical analysis
  - cantilever beam, 453
  - excessive deflections, 453
  - excessive strain, 454
  - failure modes, 454
  - gas temperatures, 454
  - natural fire, 454, 455
  - one-size-fits-all deflection criteria, 453
  - prescribed fire resistance, 454
  - steel-concrete composite structure, 457
  - structural response, 453
  - user-defined deflection criterion, 453
  - user specified end time, 452
- Numerical 1D heat transfer analyses, 394
- Numerical codes, 463
  
- O**
- Occupant egress, 29
- Occupant evacuation, 50–52
- One-dimensional charring rates, 503
- One-size-fits-all deflection criteria, 453
- Oriented strand board (OSB), 246, 261
  
- P**
- Parametric fire curves, 90, 103, 105
  - BFD curve, 106
  - iBMB parametric fire curve, 106
- Parametric fire exposure, 486, 487
- Parametric fire formulation, 105
- Parametric time-temperature calculation, 498
- Passive fire protection (PFP), 137, 261, 389, 390
- PBEE (Performance Based Earthquake Engineering) framework, 386
- PEER (Pacific Earthquake Engineering Research Centre), 386, 389
- Performance-based approach, 415
- Performance-based design, 3, 53, 324, 325, 330, 440
- Performance-based structural fire engineering design, 477
- Performance expectations, 34
- Petrographic analysis, 492
- Phase change, 138
- Phenol-formaldehyde (PF), 246
- Phenol-resorcinol-formaldehyde (PRF), 246
- Physical failure, 458
- Physically based fire models, 449
- Physically based thermal actions, 415
- Plasticity-damage concrete model, 419, 435
- Polymer fiber-reinforced concrete (PFRC), 150
- Polypropylene fibers, 151, 442
- Post-critical behavior, 456
- Post-earthquake fire scenarios, 390
- Postfire evaluation, 183
- Post-flashover fire curve, 90
- Post-flashover fire exposure, 118
- Preliminary assessments, 394
- Preliminary investigation, structural damage
  - accumulated debris, 472
  - alternative publication, 474
  - building and fire, 470
  - Concrete Society Report, 476
  - eyewitnesses, 470
  - fire severity, 474
  - incidents, captured videos, 470
  - non-structural debris, 472
  - objectives, 473
  - primary objective, 470
  - process steps, 476
  - temperatures, 473, 475, 476
- Prescribed time-temperature relationships, 446
- Prestressed concrete, 153
  - design principles, 153
  - mechanical properties, 153
  - shear resistance, 154
  - spalling, 154
  - steel tendons, 148, 153
  - structural members, 153
  - temperature profile, 155
  - thermal calculations, 155
- Pretensioned hollow core slabs, 154, 156
- Probabilistic methods, 323, 329
- Probabilistic Model Code, 335

Probabilistic models, 342, 346  
 Probabilistic risk assessment (PRA), 330  
 Probabilistic structural fire engineering (PSFE),  
 346–348, 351  
 Probability density functions (PDF), 355, 367,  
 369, 376, 392, 395  
 Pyrolysis, 236, 237, 239–241, 251, 269, 434

## Q

Qualification tests, 16  
 ASTM standard, 16  
 furnace size limitations, 17  
 goal, 16  
 limitations, 17  
 standard time-temperature curve, 17  
 Quantitative approaches, 24  
 Quasi-static formulation, 427

## R

Real fires, 157, 442  
 Realistic fire exposure, 444  
 Reed's tests, 11  
 Reinforced concrete (RC), 152, 153, 498  
 axial restraint, 152  
 CMA, 180  
 columns, 177  
 fire performance, 160  
 fire response, 158  
 FRC, 158  
 PFRC, 150  
 steel reinforcement, 152  
 SFRC, 150  
 shear failures, 181  
 steel reinforcement bars, 148  
 thermal conductivity, 162  
 TMA, 179  
 unloaded beam section, 153  
 walls, 177, 178  
 Reinforcing and prestressing steel  
 applications, 170  
 creep and prestress loss, 174  
 stress-strain properties, 171, 172  
 thermal properties, 171  
 yield strength and elastic modulus, 172–174  
 Reinforcing steel, 147, 151, 152, 155, 158, 172  
 Relevant standards  
 ASCE/SEI 7, 28  
 ASCE/SEI 7-16, 29, 32, 33  
 Eurocode, 31  
 fire resistance design, 28  
 NFPA 557 standard, 30, 31

structural components, 32  
 survey-based method, 31  
 time-dependent thermal boundary, 31  
 Reliability  
 conceptual visualization, 332  
 definition, 331  
 Eurocodes, 331  
 functional requirement, 332  
 limit states, 332  
 performance criterion, 332  
 Reliability-based design, 333  
 Reliability-based methodologies, 183  
 Reliability index, 333–338, 352, 366, 371,  
 374–378, 380, 395, 400  
 Required Safe Egress Time (RSET), 51  
 Resistance effect, 391, 393, 399  
 Restrained vs. unrestrained classification, 34  
 ASCE/SEI 7 standard, 20  
 ASTM, 18  
 industry consensus, 21  
 organizations, 20  
 standard fire testing, 20  
 thermal restraint, 19  
 Risk acceptance  
 in structural fire design, 330, 331  
 Risk-based technique, 324  
 Runaway-type failure, 456

## S

Safety factors, 323, 333, 335  
 Safety margin, 332, 333  
 SAFIR (Software Architecture For Information  
 and Realtime systems), 445,  
 449, 462  
 Scaled time, 98  
 Scope creep, 59–61  
 Seismic fragility, 384  
 SFE advanced analysis, capabilities and  
 limitations  
 failure modes, 444, 445  
 large displacements, 445  
 material behavior, 441  
 nonstandard fire exposure, 446, 449  
 structural behavior, 443, 444  
 weak coupling assumption, 450, 451  
 SFE advanced analysis procedure  
 failure, 429  
 fire development evaluation, 426  
 loads sequence and application, 428  
 relevant design selection, 426  
 structural response evaluation, 427  
 temperature evolution evaluation, 426, 427

- thermal boundary conditions representation, 427, 428
  - weak coupling strategy, 428
- Shear failures, 156, 157, 181
- Shear punching, 156, 181
- Shell elements, 421, 432
- Shell finite elements, 435
- Simple system under axial load, 325
- Simplified methods, 414, 415
- Single-member analyses, 40
- Single-point constraints, 439
- Slab panel method (SPM), 176, 209
- Small-scaled models, 220
- Solid concrete slabs
  - failure probability, 392
  - fire resistance, 391
  - temperature distributions, 393, 394
- Soot damage, 474
- Soot layer, 473
- Sophistication, 415
- Spalling, 139, 141, 155, 156, 493
  - heating rates, 155
  - in HSC members, 149, 155
  - lower ratios, 148
  - prestressed members, 154
  - stresses and pore pressure, 155
- Specific failure modes assessment
  - additives, 459
  - connections, 459
  - consideration, 458
  - Eurocodes, 459
  - reinforced concrete, 459
  - spalling, 458
  - verification, 458
- Specific heat, 159
  - aggregate type, 163
  - concrete, 134, 159
  - concrete at room temperature, 162
  - DTA, 159
  - material properties, 117
  - normal-strength concrete, 162
  - for NSC, 162
  - protective insulation, 123
  - steel, 123, 130, 131, 133
- Specific volumetric enthalpy, 138
- Spray fire-resistive materials (SFRM), 136, 139, 140, 142
- Spring elements, 444
- Stainless steel reinforcing, 491
- Standard fire curves, 449
- Standard fire resistance design (SFRD), 46, 49
  - framework, 84
  - insulation protection, 49
  - requirements for applied insulation, 48
  - vs. SFE, 47
  - standards and guidelines, 63
  - structural performance indeterminacy, 48
- Steel, 436
  - capture uncertainty, 362
  - conductor of heat, 131
  - density, 130
  - EC steel retention factor, 362
  - emissivity, 130, 131
  - modulus of elasticity of steel vs. temperature, 363
  - specific heat, 131, 133
  - statistical models, 360
  - strain steel yield strength retention factor vs. temperature, 360, 361
  - thermal conductivity, 132
  - thermal properties, 130
  - yield strength, 359, 360
- Steel and composite structures
  - connections
    - classifications, 215, 216
    - fire effects, 216–218
    - performance, 219, 220
    - structural members, 215
  - design philosophies, 222
  - elements
    - beams, 197
    - columns, 195–197
    - member performance, 194
    - prescriptive/performance-based models, 194
    - tension members, 200
    - trusses, 201
  - mechanical properties
    - steel enforcement, 192, 193
    - steel shear studs, 193
    - structural steel, 189–191
- Steel-concrete composite buildings, 425
- Steel fiber-reinforced concrete (SFRC), 150, 166
- Steel reinforcement, 160
- Steel strength and stiffness, 477
- Steel trusses/bracing, 433
- Stefan-Boltzmann constant, 118, 123
- Strength domain
  - ASCE/SEI 7, 27
  - ASD, 26
  - DCR calculations, 27
  - LRFD criteria, 26
  - structural insulation, 25
- Strength reduction factors, 502
  - Grade 8.8 bolts, 482

- Stress-strain relationship, 327, 502
  - Stress-temperature history, 441
  - Structural assemblies, 420, 443, 444
  - Structural connections, 437, 439
  - Structural connections failures, 437
  - Structural connections representations
    - multi-spring connection elements, 438
    - sophistication levels, 437
    - 3D connection models, 439
    - translational and rotational springs, 438
  - Structural damage assessment
    - assessment by calculation, 477
    - preliminary investigation (*see* Preliminary investigation, structural damage)
    - small-scale non-destructive tests, 470
    - visual inspection, 469, 470
  - Structural design fire, 53, 56, 61, 62, 73
  - Structural elements, 499
  - Structural engineering, 25
    - observed density function, 396
  - Structural Eurocodes, 480
  - Structural failure assessment procedure, 452–458
  - Structural fire analysis software, 445
  - Structural fire design, 179, 180, 291
    - ambient reliability targets, 336
    - ASCE design format, 345
    - failure modes, 53
    - intervention measures, 339
    - nonstructural components, 52, 53
    - performance, 332
    - primary structural system, 52, 53
    - risk acceptance, 330, 331
    - secondary structural systems, 52, 53
    - structural stability, 332
  - Structural fire engineering (SFE), 5, 25, 46, 75, 118, 128, 130, 138, 141, 142, 147, 171, 323
    - applications, 76
    - approach to project stakeholders, 45
    - for building authority, 46
    - changes in occupancy/use, 69–71
    - confirmation, design assumptions, 66–69
    - design brief documentation, 58–59
    - design implementation (*see* Design implementation, SFE design)
    - design metrics and assumptions, 57–58
    - design process, 76
    - fire hazard, 53–57
    - furnace heating exposure, 48
    - hypothetical steel structures, 48
    - modification/extension of existing building, 71–73
    - performance objectives, 51–52
    - scope creep, 59–61
    - simple and convincing image, 46
    - simple and straightforward imagery, 46
    - software, 462
    - stakeholder presentations, 46
    - stakeholders design goals
      - building authorities, 50
      - building owner, 50
      - project architect, 50
      - safety metrics, 50
    - vs.* standard fire resistance design, 47
    - value-added benefits, 46
  - Structural fire FEA simulations, 64
  - Structural fire protection, 60, 61, 71
  - Structural fire safety, 46–48, 50, 51
  - Structural instability, 456
  - Structural insulated panels (SIPs), 243, 262
  - Structural integrity, 469, 482
  - Structural lightweight concrete, 149
  - Structural members representation
    - concrete slabs, 432
    - concrete walls, 433
    - parameters, 429, 430
    - steel/concrete beams/columns, 430, 431
    - steel trusses/bracing, 433
  - Structural welds, 479, 482
  - Sub-frame analyses, 40
  - Surface temperature, 239
  - Swedish curves, 98
- T**
- Temperature-dependent values, 434
  - Temperature profile, 413, 501
  - Tensile membrane action (TMA), 179, 180, 458
    - advantage, 206
    - application, 205
    - calculation method, 206, 208
    - definition, 205
    - SPM, 209
  - Tension properties, 258
  - Thermal analysis, 443
  - Thermal boundary conditions, 116–119, 427, 446
  - Thermal conductivity, 116, 117, 122, 123, 130–133, 137, 161, 162
  - Thermal expansion effects, 443
  - Thermal gradients, 121, 152–154, 419
  - Thermally induced strains and stresses, 413
  - Thermal-mechanical weak coupling
    - assumption, 450, 451

- Thermal properties of materials
  - applied passive fire protection material, 136, 137
  - concrete, 132–134
  - key thermal properties, 130
  - steel, 130–133
  - term emissivity, 130
  - timber, 134, 135
- Thermal response, 121, 125
- Thermal-structural model, 421
- Thermocouples, 269
- Thermomechanical analysis, 428
- Thermomechanical FE models
  - AST, 449
  - CFD, 448, 449
  - heat fluxes, 447
  - TFM, 447, 448
- Thermo-mechanical properties, 78
- 3D connection models, 439
- 3D solid elements, 435
- Thin skin calorimeters (TSC), 275
- Timber, 134, 135, 503
  - beams, 364
  - for European softwood, 363
  - glue-laminated, 363
  - material properties, 363
- Timber construction
  - board products, 246
  - categories, 243
  - CLT, 245
  - connections, 247
  - engineered mass timber, 244
  - glulam, 244
  - grading process, 243
  - heavy, 244
  - light timber frame, 245, 246
  - LVL, 244
  - nonhomogeneous material, 243
- Timber structures
  - B-RISK model, 288
  - calculation methods
    - fire conditions/temperatures, 289
    - fire safety requirements, 290
    - holistic approach, 290
    - natural fires, 290
    - performance-based requirement, 290
    - traditional approach, 290
  - char layer conductivity, 288
  - compartment fire experiments, 270–272
  - composition, 236
  - constant heat flux, 279
  - construction material, 235
  - construction products, 235
  - debonding, 277, 278
  - effective cross-section method, 308–310
    - Australian, 300
    - beam, 292
    - Canadian method, 291, 298, 299
    - capacity, 291
    - char depth, 293
    - char layer, 292
    - char models, 294, 295
    - charring models, 295
    - fire resistance tests, 294
    - gypsum plasterboards, 297
    - k-coefficients, 293
    - load-bearing capacity, 291
    - mechanical properties, 291
    - New Zealand, 300, 301
    - one-dimensional and notional charring rates, 294
    - passive fire protection, 294
    - temperature measurements, 296
    - USA, 296, 298
    - zero-strength layer, 292
  - enclosure time-temperature relationship, 287
  - engineered timber, 277, 278
  - engineered wood products, 235
  - European method, 312
  - exposed CLT, 274–276
  - fiber-based insulation products, 262, 265, 266
  - flaming combustion
    - charring, 240, 241
    - ignition, 239, 240
    - pyrolysis, 239
    - self-extinction, 241, 242
    - smoldering combustion, 243
  - gypsum plasterboard
    - bentonite, 261
    - calcium sulfate anhydrite, 262
    - calcium sulfate hemihydrate, 262
    - density, 263
    - energy, 262
    - fire resistance characteristics, 262
    - heat, 263
    - heat capacitance, 262
    - heat transfer characteristics, 262
    - light timber frame construction, 261
    - temperature, 262
    - thermal boundary conditions, 262
    - vermiculite, 261
  - heat and mass transfer
    - boundary layer, 239
    - external heat flux, 237



- Timber structures (*cont.*)
  - physical processes, 237
  - solid, 237, 238
  - temperature zones, 237, 238
  - thermal and mechanical changes, 237
  - loaded and unloaded assemblies, 311–313
  - LTF, 273, 274, 311
  - natural fire exposure
    - combustion energy, 284
    - cooling phases, 284
    - development, 284
    - “effective” relationships, 283
    - effective thermal properties, 284
    - heating phase, 284, 286
    - influence of combustion, 284
    - thermal exposure condition, 284
    - timber behavior, 284
    - time vs. temperature development, 285, 286
  - nominal time-temperature curves, 279, 280
  - numerical method, 311
  - parametric fire exposure, 307, 308, 313
  - protection materials
    - critical falloff temperatures, 266
    - fire performance, 264
    - fire resistance test conditions, 267
    - floor assemblies, 268
    - linear regression, 266
    - temperatures, 268
    - thermophysical properties, 264
  - pyrolysis process, 236
  - reduced load-bearing capacity, 306, 307
  - self-extinction, 269, 289
  - simplified post-flashover fire models, 280–283
  - stepwise process, 287
  - structural response, 269, 270
  - tabulated data, 305, 306
  - wood combustion model, 287, 288
- Timber thermophysical properties
  - conductivity, 248
  - density, 251, 252
  - high temperature, 257–259
  - kinetic properties, 252–254
  - mechanical properties
    - constitutive behavior, 255
    - design purposes, 255
    - EN 338: 2003, 255
    - fracture energy and tension-softening, 256
    - natural unmodified timber, 255
    - strain energy, 256
    - stress-strain behavior of wood, 256, 257
    - tensile strength, 255
    - timber-specific heat, 249, 250
  - Time-dependent incident heat flux, 365
  - Time-equivalent fires, 39
  - Time-temperature curve, 80, 485
  - Time temperature development, 485
  - Time-temperature parametric curve, 498–500
  - Total load effect, 354, 399
  - Traditional fire safety design, 330
  - Transient creep strain, 151, 157, 182, 436
  - Transient thermal conduction, 413
  - Travelling fire, 79, 87
    - ceiling point, 89
    - decay phase, 88
  - Travelling fire method (TFM), 88, 447, 448
  - 2D thermal model, 25
  - 2D/3D elements, 430, 432, 434
  - Two-zone enclosure model, 108
- U**
  - Ultrahigh-performance concrete (UHPC), 149
  - Uncertainty in mechanical actions, 345
    - imposed load, 353
    - live load model, 348–352
    - load variability, 345
    - permanent actions, 346, 347
    - permanent load, 348
    - PSFE, 347, 348
    - total load effect, 353, 354
  - Uncertainty in structural fire engineering, 327
    - element geometry, 329
    - fire characteristics, 329
    - fuel load, 329
    - probability distributions, 329
    - sources, 328
  - Uncertainty in thermal action
    - fire modelling
      - fire growth rate/spread rate, 340–342
      - fire load density, 342, 343
      - heat release rate density, 343, 344
      - inputs, 340
      - near-field temperature, 344, 345
      - ventilation conditions, 344
    - fire occurrence rates and interventions, 339, 340
  - Uncertainty quantification techniques
    - analytical solutions, 366, 369–371
    - event tree, 365–369
    - failure criterion, 374
    - failure probability, 376
    - FORM, 366, 374
    - fragility, 366, 384–386

Gaussian variables, 379  
maximum entropy and MaxEnt method,  
366, 380–383  
Monte Carlo techniques, 366, 372, 373  
non-linear limit state, 379, 380  
PEER framework, 366, 386–388  
Unidirectional heat transfer, 421  
Uniform temperature distribution, 200, 487  
Unrestrained classification, 18  
User-defined deflection criteria, 429  
US National Design Specification (NDS), 303

**V**

Ventilation, 340, 344, 387  
Ventilation-controlled fire, 104  
Ventilation-controlled heat, 82  
Ventilation-controlled regime, 79

Verification, 324  
Visual inspection, 469, 484

**W**

Water-to-cement ratio, 148  
Web-post buckling, 458  
Whilst fire resistance, 4  
White discoloration, 493  
Whole-building behavior, 419, 420  
Wickström's formulation, 97  
Wood, 434, 437

**Z**

Zero-failure probability, 331  
Zone fire model, 77, 108